



VNIVERSITAT DE VALÈNCIA

Membrane-based technologies for recovery of dissolved methane and phosphorous from liquid effluents: membrane surface modification and performance enhancement

Ph.D. Thesis

Ramón Jiménez Robles

Supervisors:

Vicente Martínez Soria

Marta Izquierdo Sanchis

Doctoral Program in Chemical,
Environmental and Process Engineering

July 2023



VNIVERSITAT Đ VALÈNCIA

(Ğ) Escola Tècnica Superior d'Enginyeria

Department of Chemical Engineering



**Membrane-based technologies for
recovery of dissolved methane and
phosphorous from liquid effluents:
membrane surface modification and
performance enhancement**

Doctoral Program in Chemical, Environmental and Process
Engineering

A thesis submitted to the University
of Valencia in fulfilment of the
requirement for the degree of Doctor
by
RAMÓN JIMÉNEZ ROBLES

Thesis supervisors:
Dr. **VICENTE MARTÍNEZ SORIA**
Dra. **MARTA IZQUIERDO SANCHIS**

Valencia, July 2023

Dr. Vicente Martínez Soria, catedrático del Departamento de Ingeniería Química de la Universitat de València, y

Dra. Marta Izquierdo Sanchis, profesora titular del Departamento de Ingeniería Química de la Universitat de València,

certifican que,

D. Ramón Jiménez Robles, graduado en Ingeniería Química y con título de Máster en Ingeniería Química, ha realizado bajo su dirección el trabajo que bajo el título de “**Membrane-based technologies for recovery of dissolved methane and phosphorous from liquid effluents: membrane surface modification and performance enhancement**” presenta en esta Memoria y que constituye su Tesis para optar al Título de Doctor con Mención Internacional por la Universitat de València en el Programa de Doctorado en Ingeniería Química, Ambiental y de Procesos.

Y para que conste a los efectos oportunos, firman el presente certificado en Valencia a julio de 2023.

Dr. Vicente Martínez Soria

Dra. Marta Izquierdo Sanchis

TABLE OF CONTENT

Acknowledgments	vii
Abstract	xi
Resumen	xv
Structure of the thesis	xix
Contributions of this thesis	xxi
Journal articles	xxi
Conference contributions	xxii
1 Introduction	1
1.1 Environmental concern and sustainability.	1
1.1.1 Climate change and greenhouse gas emissions.	1
1.1.1.1 Methane emissions.	5
1.1.1.2 Methane applications and sources.	7
1.1.2 Phosphorus applications and sources.	9
1.1.2.1 Depletion of conventional phosphorus sources.	9
1.1.2.2 Waste to phosphorus: renewable phosphorus sources.	10
1.2 Polymeric membrane contactor technology for the recovery of dissolved methane.....	13
1.2.1 Technologies for the recovery, removal and reuse of dissolved methane.....	15
1.2.2 Membrane contactors for dissolved methane recovery.	19
1.2.3 Challenges of gas-liquid membrane contactors.	26
1.3 Membrane-assisted crystallisation technology for the recovery of phosphorus.....	31
1.3.1 Conventional phosphorus recovery technologies from wastewaters. ..	31
1.3.2 Membrane-assisted crystallisation technology for phosphorus recovery as vivianite.....	35
1.4 Membrane functionalisation.	40
1.4.1 Classification of membrane activation methodologies.	42
1.4.1.1 Wet methods.	43
1.4.1.2 Dry methods.....	44
1.4.2 Classification of membrane functionalisation methodologies.....	47

1.4.2.1 Physical treatments.....	47
1.4.2.2 Chemical treatments.....	50
1.4.3 Challenges in the membrane functionalisation.....	53
2 Objectives.....	57
3 Materials and Methods.....	61
3.1 Membrane modules and materials.....	61
3.1.1 Flat-sheet membranes.....	61
3.1.1.1 Flat-sheet modules.....	61
3.1.1.2 Flat-sheet membrane materials.....	63
3.1.2 Hollow fibre membrane contactor.....	65
3.2 Experimental setups and procedures.....	67
3.2.1 Degasification tests for dissolved methane recovery.....	67
3.2.1.1 Degasification tests with a flat-sheet membrane module.....	68
3.2.1.2 Degasification tests with a hollow fibre membrane contactor.....	71
3.2.2 Long-term operation tests.....	74
3.2.2.1 Stability tests.....	74
3.2.2.2 Fouling tests.....	75
3.2.3 Membrane-assisted reactive crystallisation tests for phosphorus recovery.....	76
3.3 Membrane functionalisation methodologies.....	80
3.3.1 Membrane activation methods.....	82
3.3.1.1 Membrane activation with alkali solution.....	82
3.3.1.2 Membrane activation with oxygen plasma treatment.....	83
3.3.2 Membrane functionalisation protocol.....	83
3.3.2.1 Chemical reactions of the functionalisation step.....	84
3.4 Analytical techniques and calculation methods.....	86
3.4.1 Evaluation of the membrane performance in degasification tests.....	86
3.4.1.1 Analysis of dissolved methane in liquid samples.....	86
3.4.1.2 Analysis of methane in the recovered gas stream.....	88
3.4.1.3 Mass transfer evaluation in the flat-sheet membrane contactor.....	88
3.4.1.4 Mass transfer evaluation in the hollow fibre membrane contactor.....	92
3.4.2 Evaluation of the membrane-assisted reactive crystallisation tests.....	95

3.4.2.1 Determination of the bulk and scaling induction time.	95
3.4.2.2 Supersaturation analysis.	96
3.4.2.3 Crystallisation kinetic analysis.	100
3.4.3 Membrane characterisation.	101
3.4.3.1 Hydrophobicity.....	101
3.4.3.2 Surface and cross-section morphology.....	102
3.4.3.3 Roughness.	102
3.4.3.4 Thickness.....	103
3.4.3.5 Porosity.....	103
3.4.3.6 Elemental distribution and functional groups.....	104
3.4.3.7 Liquid entry pressure.	104
3.4.3.8 Thermal properties.	105
3.4.4 Crystal characterisation.	106
3.4.4.1 Shape and size distribution.....	106
3.4.4.2 Chemical composition.....	106
3.4.5 Fouling characterisation.	107
3.4.5.1 Morphology and chemical characterisation of the fouling cake.	107
3.4.5.2 Protein and polysaccharide content in the fouling cake.	108
3.4.5.3 Extraction and characterisation of the foulants from the membrane.....	109
3.4.6 Characterisation of the anaerobic effluents.	110
3.4.7 Design of experiments and statistical analysis.	111
4 Results and Discussion.	113
4.1 Recovery of dissolved methane through a flat-sheet module with PDMS, PP, and PVDF membranes.	113
4.1.1 Motivation, aim and overview.....	113
4.1.2 Results and discussion.....	114
4.1.3 Conclusions.....	117
4.2 Flat PVDF membrane with enhanced hydrophobicity through alkali activation and organofluorosilanisation for dissolved methane recovery.....	119
4.2.1 Motivation, aim and overview.....	120
4.2.2 Results and discussion.....	121
4.2.3 Conclusions.....	123

4.3 Fouling characterisation in PVDF membrane contactors for dissolved methane recovery from anaerobic effluents: effect of surface organofluorosilanisation.....	125
4.3.1 Motivation, aim and overview.....	125
4.3.2 Results and discussion.....	127
4.3.3 Conclusions.....	128
4.4 Stability of superhydrophobicity and structure of PVDF membranes treated by vacuum oxygen plasma and organofluorosilanisation.	130
4.4.1 Motivation, aim and overview.....	131
4.4.2 Results and discussion.....	133
4.4.3 Conclusions.....	135
4.5 Simultaneous application of vacuum and sweep gas in a polypropylene membrane contactor for the recovery of dissolved methane from water.	136
4.5.1 Motivation, aim and overview.....	137
4.5.2 Results and discussion.....	138
4.5.3 Conclusions.....	140
4.6 Membrane-assisted reactive crystallisation for the recovery of dissolved phosphorus in vivianite form from liquid effluents.....	141
4.6.1 Motivation, aim and overview.....	142
4.6.2 Results and discussion.....	144
4.6.3 Conclusions.....	146
5 Conclusions and Future Prospect.....	147
5.1 Main conclusions of this thesis.....	147
5.2 Future prospect.	152
6 References.....	155
7 Nomenclature.....	187
8 Resumen extendido.....	195
8.1 Recuperación de metano disuelto usando un módulo plano con membranas de PDMS, PP y PVDF.	196
8.2 Mejora de la hidrofobicidad de una membrana plana de PVDF mediante activación alcalina y organofluorosilanización para la recuperación de metano disuelto.	200
8.3 Caracterización del ensuciamiento en contactores de membranas de PVDF para la recuperación de metano disuelto en efluentes anaerobios: efecto de la organofluorosilanización superficial.....	204

8.4 Estabilidad de la superhidrofobicidad y estructura de membranas de PVDF tratadas por plasma de oxígeno a vacío y organofluorosilanicación.	207
8.5 Aplicación simultánea de vacío y gas de arrastre en un contactor de membrana de fibra hueca de polipropileno para la recuperación de metano disuelto en agua.....	211
8.6 Cristalización reactiva asistida por membrana para la recuperación de fósforo disuelto en efluentes líquidos en forma de vivianita.....	214
8.7 Conclusiones.....	218
Appendix I: Contribution I.....	223
Appendix II: Contribution II.....	251
Appendix III: Contribution III.	285
Appendix IV: Contribution IV.	315
Appendix V: Contribution V.....	341
Appendix VI: Contribution VI.	357

ACKNOWLEDGMENTS

GRACIAS

A mis padres: Papi y Mami, siempre seréis los primeros de mi lista de agradecimientos ya que, si yo estoy aquí hoy, no cabe ninguna duda de que es gracias a vosotros. Siempre me habéis dado todo lo necesario e incluso más para poder avanzar hacia adelante en la vida sin cuestionarme ya que siempre habéis creído en mí. Pero la lección más importante que he aprendido durante los años que viví bajo vuestro techo es que el dinero no lo es todo, sino que lo único necesario para conseguir la felicidad es la humildad y la honradez para conseguir la paz interior con toda la gente que te rodea. Así mismo también debo mencionar el carácter trabajador que ambos poseéis, siempre habéis hecho todo lo posible para que ni a mis hermanas ni a mi nos faltase un plato de comida en tiempos difíciles, y especialmente os doy gracias por eso, porque habéis conseguido traer al mundo un hijo con ese mismo carácter trabajador, aprovechando cada segundo para hacer de este mundo un lugar mejor sin desperdicio de esta vida tan fugaz que nos ha tocado.

A mis hermanas: a mis queridas hermanas mayores, Tata y María Isabel, también tengo que agradecerles todo, especialmente agradecerles que siempre siempre siempre hayan creído en mí y me hayan apoyado allá a donde fuera. También me llena de mucha honra que os sintáis tan orgullosas de vuestro hermano pequeño y que transmitáis ese sentimiento a tod@s vuestr@s amig@s, lo cual demuestra que me queréis tantísimo como yo os quiero a vosotras. Finalmente, me gustaría haceros ver que al igual que yo estoy cumpliendo mis sueños profesionales y personales vosotras también tenéis esa capacidad para lograr todo lo que os propongáis desde cualquier lugar del mundo.

A mis directores de tesis Marta y Vicente: me refiero a vosotros como directores porque es la denominación técnica, aunque para mí, esa relación alumno-profesor ha ido más allá, y estoy muy orgulloso de poder consideraros mis amigos. Especialmente agradecer todo el apoyo que me habéis brindado y la gran confianza depositada en mí desde mucho antes del inicio de esta tesis doctoral. Desde entonces apostasteis por mí, y gracias a ello todos hemos podido conseguir muchos logros a través de ese trabajo en equipo. También agradecer el trato que me habéis dado siempre, ya que en ningún momento me habéis tratado como un simple becario sino todo lo contrario: siempre estáis ahí para ayudarme y escuchar abiertamente mi ideas, propuestas y opiniones. En definitiva, gracias a vosotros he podido recorrer el sendero directo, aunque en ocasiones tortuoso, que me ha llevado hasta una de mis metas personales y profesionales: la mención de Doctor Internacional. Espero que sean muchos más los años que podamos seguir trabajando en el mismo laboratorio y que nuestros nombres continúen apareciendo juntos en los futuros proyectos y contribuciones científicas.

Al grupo de investigación GI2AM: por ser el primer grupo que me acogió en la Universitat y por las oportunidades que me ha brindado. Gracias en primer lugar a su directora Carmen Gabaldón, la primera persona con quien establecí contacto y me mostró el camino a seguir, y, en segundo lugar, pero sin ser menos importantes, al resto de sus miembros Javier Álvarez, Josep Manuel Peñarrocha, Paula Marzal y Pau San Valero por toda la ayuda prestada siempre que la he necesitado para el desarrollo de esta tesis. Siempre habéis mostrado interés por mi tesis, la cual no hubiera llegado hasta este alto nivel de desarrollo sin ese apoyo. Estoy muy agradecido de todos los conocimientos que me habéis transmitido durante este período formativo, y que sin duda alguna han favorecido mi formación profesional y que me ayudarán en el correcto desarrollo de mi carrera científica.

Al grupo de investigación MATS: a José David Badia, Amparo Cháfer y Josep Pasqual, quienes recientemente me han acogido en MATS creando un

nuevo proyecto de futuro a largo plazo en conjunto. Esto me demuestra que vosotros también habéis depositado vuestra confianza en mí, lo cual agradezco enormemente. Gracias a toda la formación y habilidades que he adquirido durante esta ardua etapa predoctoral, me siento totalmente capacitado para cumplir con esas expectativas que tenéis sobre mí y asumir las responsabilidades que me corresponden como nuevo miembro de MATS. Pero los aspectos que considero más importantes en agradecimiento son dos: la ilusión y motivación que volví a sentir para seguir siendo parte del mundo científico y académico, que en una época agria había perdido parcialmente, y por otro lado vuestro constante apoyo a todos y cada uno de los diferentes miembros del grupo, sin importar su rango profesional, promoviendo la salud mental, que en mi opinión es la base para establecer un entorno de trabajo en equipo productivo y eficaz a la vez que genera una sonrisa en la persona que cada día está presente en el laboratorio.

A tod@s aquellos con los que alguna vez he compartido laboratorio: contando en esta lista interminable con Alejo, Bea, Carlos, Mario, Miguel, Stalin y Rosa. A tod@s vosotros muchas gracias por ayudarme dentro del laboratorio y por todos esos momentos vividos tanto dentro como fuera de la Escuela. Espero que nuestros futuros profesionales sigan manteniendo algún punto en común.

Al Departamento de Ingeniería Química: a todos los profesores, técnicos y personal administrativo, muchas gracias también por vuestra acogida y apoyo para hacer realidad este proyecto de tesis. Me gusta ver que este Departamento trabaja como una colonia de abejas, es decir, como una familia, en la que la función de cada miembro es esencial para el éxito del propio Departamento y, por tanto, de cada uno de sus integrantes. Y al igual que las abejas son de vital importancia para la vida, este Departamento también, ya que constituye un pilar esencial en el campo académico y de investigación: tenemos la capacidad intelectual y la obligación moral de conducir la sociedad hacia un estado **real** de bienestar.

Al Servicio Central de Soporte a la Investigación Experimental (SCSIE) de la Universitat de València: a los técnicos de la sección de microscopía Enrique, Javi, Mari Tere y Pilar. Gran parte de esta tesis se ha basado en análisis microscópicos, que no habrían sido posibles sin vuestras innumerables horas de dedicación para transmitirme todos vuestros conocimientos y resolver todos los problemas a los que tuve que enfrentarme.

I would like to thank Ewan McAdam and his great Membrane Processes group from Cranfield University in United Kingdom, for offering me the chance to learn with them and welcoming me into their research group for 3 months. I learned a lot in such a brief time and sincerely hope to collaborate in a near future. I really appreciate all the time you spent on me during that short stay and the following months for the writing of a fascinating paper. Now, the crystallisation world has caught my attention.

También me gustaría agradecer al Ministerio de Universidades la beca concedida (FPU19/02478) para la realización de la presente tesis doctoral, y al Ministerio de Educación y Formación Profesional por la concesión de una ayuda complementaria para estancias breves (EST22/00167).

Aunque te dejo para la última, no es porque seas la menos importante sino todo lo contrario porque, el último lugar siempre está reservado para aquella persona especialmente importante. **Marta, mi pareja de viaje**, agradecerte todo lo que me has ayudado para mantener la cabeza alta en los momentos difíciles y tener un motivo por el que querer ir a casa todos los días. Hemos apostado por una vida juntos lejos de nuestras casas, lo cual quiere decir que estamos construyendo una nueva vida partiendo de cero y por ello tengo un gran sentimiento de que esta vida es totalmente nuestra y de nadie más. Hemos conseguido empezar esta vida bastante jóvenes, así que espero que aprovechemos esta juventud para seguir disfrutando desde los placeres más pequeños hasta los más grandes que nos ofrece el mundo.

ABSTRACT

The current situation of the environment regarding climate change, pollution and raw material depletion is being aggravated due to the population growth and improved living standards. Hence, there is an imperative need to develop robust technologies which allow the exploitation of new renewable sources and satisfy the concept of process intensification and rationalisation of raw materials. In this regard, membrane contactors have been presented as an alternative over conventional separation units due to their attractive features, especially the higher achievable overall productivity and the potential cost savings during operation. For these reasons, membrane contactors at lab-scale for the valorisation of residual liquid effluents by means of the separation and recovery of dissolved methane (CH_4) and phosphorus (P) were investigated in this thesis. Thus, this thesis aims to: i) elucidate the effects of the operational conditions and membrane properties in the CH_4 recovery performance using flat-sheet membrane contactors under simulated and real conditions, ii) optimise the dissolved CH_4 recovery process using a hollow fibre membrane contactor working in combination mode (simultaneous application of vacuum and sweep gas), and iii) integrate a membrane crystallisation process for the recovery of dissolved P as vivianite.

On the one hand, the recovery of dissolved CH_4 from anaerobic effluents were evaluated with a gas-liquid flat-sheet membrane contactor using different common membrane materials (PDMS, PP and PVDF). The use of a flat-sheet membrane module presented great advantages for investigation purposes such as versatility and easy membrane extraction, replacement, and analysis. The effects of the membrane properties in the CH_4 removal efficiency and mass transport were investigated. Additionally, a membrane functionalisation method based on the grafting of fluoroalkylsilanes was evaluated for increasing the wetting resistance of PVDF membranes. Two membranes activation methods (alkali and plasma treatments) previous to the grafting were

evaluated, and the modification conditions were optimised. Stability of the membranes and functionalisation layers were evaluated in long-term operation using deionised water and a real anaerobic effluent to determine their useful lifetime. The composition and mechanisms of the fouling developed on PVDF membranes when treating a real anaerobic effluent were characterised. Finally, the dissolved CH₄ recovery process was optimised using a PP hollow fibre membrane contactor in combination mode to minimise the energy and sweep gas consumption.

On the other hand, the recovery of dissolved P from liquid streams in vivianite form by means of a membrane-assisted reactive crystallisation was evaluated for the first time in the literature, as far as we know. The vivianite crystallisation was evaluated in a flat-sheet membrane contactor at lab-scale under different hydraulic conditions and membranes (PP, PVDF and PTFE) to elucidate how the boundary layer and membrane properties can be used to regulate the nucleation kinetic.

Regarding the results of dissolved CH₄ recovery with the polymeric flat-sheet membrane contactor, the dissolved CH₄ removal efficiency was mainly influenced by the hydraulic conditions in the liquid phase. Moreover, the mass transfer resistance of the membrane and gas phase was negligible, except for PVDF membranes which suffered from wetting. Therefore, a surface functionalisation with alkali activation was applied to increase the antiwetting properties of PVDF, and the results showed an increase in the removal efficiency. However, all the membranes tended to suffer from a surface deterioration and/or deformation at moderate-high liquid velocities, affecting their properties and efficiency. In this regard, a new surface functionalisation with a vacuum oxygen plasma activation was investigated to obtain more stable PVDF membranes over time. As result, superhydrophobic membranes were obtained with a pillared-like surface and a higher surface porosity and roughness. In addition, superhydrophobic PVDF presented a more stable

hydrophobicity in long-term operation than that of the functionalised PVDF with alkali activation.

After evaluating operational conditions and membrane wetting mitigation methodologies for the dissolved CH₄ recovery from synthetic effluents, PVDF membranes were tested under real operational conditions to evaluate another critical issue regarding membrane operations: membrane fouling. Despite the higher fouling experienced by the functionalised PVDF with alkali activation, this membrane showed a greater chemical and/or mechanical resistance and stability than the non-modified PVDF when treating a real anaerobic effluent during >800 h. The fouling developed on the membranes showed a stratified composition: a first layer mainly of proteins and polysaccharides, the fouling cake bulk composed of calcium, carbonate, and phosphate salts, and the cake top composed mainly of organic matter including biomass. This fouling characterisation will ease the selection of the appropriate cleaning protocols.

The final step regarding the evaluation of the dissolved CH₄ recovery was the optimisation of the energy and input consumption using hollow fibre membrane contactors as most representative configuration in industrial processes. In this regard, the use of the combination mode was evaluated, showing significantly greater removal efficiencies, mass transfer coefficients and net energy productions than independent operational modes (vacuum and sweep gas). Additionally, the combination mode mitigated the membrane wetting. In conclusion, setting the appropriate hydraulic conditions, grafting of fluoroalkylsilanes, and combination mode can enhance the performance of the membrane contactor to recover dissolved CH₄ from anaerobic effluents, reducing the operational costs and carbon footprint of an anaerobic wastewater treatment plant.

In the search of new applications for integrating membrane technology, a membrane crystallisation process was investigated for the P recovery as vivianite. As result, nanoparticles of ~35 nm with a relatively narrow

distribution were always obtained. Crystal nucleation was strongly influenced by the boundary layer inside the membrane module, in which nucleation rate increased as the liquid velocity decreased. In addition, a porous membrane facilitated the micromixing of the reactants and lowered the energy barrier for nucleation. An ion-dependent collision mechanism for the nucleation kinetic was inferred, in which the higher supersaturation rates promote greater mixing and a higher ion collision probability for nucleation. Moreover, the previous surface functionalisation was elucidated as a useful methodology to increase nucleation rate as the hydrophobicity increases. Thus, the membrane-assisted reactive crystallisation offered a high control over nucleation compared to conventional crystallisers with a somewhat inefficient mixing of reactants.

RESUMEN

La situación medioambiental actual en relación con el cambio climático, la contaminación y el agotamiento de las materias primas se está agravando debido al crecimiento de la población y los cambios en los estándares de vida. Por ello, existe una necesidad imperiosa de desarrollar tecnologías robustas que permitan la explotación de nuevas fuentes renovables y satisfagan el concepto de intensificación de procesos y racionalización de materias primas. En este sentido, los contactores de membrana se presentan como una alternativa a las unidades de separación convencionales debido a sus atractivas características, especialmente la mayor productividad y el potencial ahorro de costes de operación. Por ello, en esta tesis se utilizaron contactores de membrana a escala de laboratorio para la valorización de efluentes líquidos residuales mediante la separación y recuperación de metano (CH_4) y fósforo (P) disueltos. Por lo tanto, esta tesis tiene como objetivo: i) estudiar los efectos de las condiciones de operación y las propiedades de la membrana en el rendimiento de recuperación de CH_4 utilizando contactores de membrana plana en condiciones simuladas y reales, ii) optimizar el proceso de recuperación de CH_4 disuelto utilizando un contactor de membrana de fibra hueca trabajando en modo combinado (aplicación simultánea de vacío y gas de arrastre), y iii) integrar un proceso de cristalización asistida por membrana para la recuperación de P disuelto en forma de vivianita.

Por un lado, se evaluó la recuperación de CH_4 disuelto de efluentes anaerobios con un contactor de membrana plana gas-líquido utilizando diferentes materiales de membrana (PDMS, PP y PVDF). El uso de un módulo de membrana plana presentó importantes ventajas para fines de investigación, como la versatilidad y fácil extracción, reemplazo y análisis de la membrana. Se investigaron los efectos de las propiedades de membrana sobre la eficacia de eliminación de CH_4 y el transporte de materia. Además, se evaluó un método de funcionalización superficial de membranas basado en la incorporación de

fluoroalquilsilanos para aumentar la resistencia a la humectación de los poros de las membranas de PVDF. Se evaluaron dos métodos para la activación de la membrana (tratamiento alcalino y de plasma) previa a la incorporación de los agentes de funcionalización, y las condiciones de modificación fueron optimizadas. Se evaluó la estabilidad de las membranas y capas de funcionalización en operación a largo plazo utilizando agua desionizada y un efluente anaeróbico real para determinar su vida útil. Se caracterizó la composición y mecanismos del ensuciamiento desarrollado sobre membranas de PVDF al tratar un efluente anaeróbico real. Finalmente, se optimizó el proceso de recuperación de CH_4 disuelto utilizando un contactor de membrana de fibra hueca de PP en modo combinado para minimizar el consumo de energía y gas de arrastre.

Por otro lado, y por lo que hasta la fecha conocemos, este trabajo ha supuesto la primera vez que se ha evaluado en la literatura científica la recuperación de P disuelto en corrientes líquidas en forma de vivianita mediante una cristalización reactiva asistida por membrana. La cristalización de vivianita se evaluó usando un contactor de membrana plano a escala de laboratorio aplicando diferentes condiciones hidráulicas y membranas (PP, PVDF y PTFE) para estudiar cómo la capa límite y las propiedades de membrana pueden regular la cinética de nucleación.

Respecto a los resultados de la recuperación de CH_4 disuelto con contactores de membrana plana, la eficacia de eliminación de CH_4 disuelto estuvo influenciada principalmente por las condiciones hidráulicas de la fase líquida debido a la resistencia despreciable a la transferencia de materia de la membrana y la fase gaseosa, a excepción de las membranas de PVDF que experimentaron humectación de los poros (*wetting* del término en inglés). Por ello, se aplicó una funcionalización superficial con activación alcalina para aumentar la resistencia a la humectación de los poros de la membrana de PVDF, cuyos resultados mostraron un incremento en la eficacia de eliminación. Sin embargo, todas las membranas eran propensas a sufrir una degradación y/o

deterioro superficial a velocidades de líquido moderadas-altas, afectando a sus propiedades y rendimiento. En este sentido, se evaluó una nueva funcionalización superficial con una activación por plasma de oxígeno en vacío para conseguir membranas de PVDF más estables con el tiempo. Como resultado, se obtuvieron membranas superhidrofóbicas con una estructura superficial en forma de pilares y una mayor porosidad superficial y rugosidad. Además, las membranas de PVDF superhidrofóbico presentaron una hidrofobicidad más estable en operaciones a largo plazo en comparación con las membranas funcionalizadas con activación alcalina.

Después de evaluar las condiciones de operación y las metodologías de mitigación de la humectación de los poros de membranas para la recuperación de CH_4 disuelto de efluentes sintéticos, las membranas de PVDF se probaron en condiciones de operación reales para evaluar otro problema crítico relacionado con las operaciones con membranas: el ensuciamiento. A pesar del mayor ensuciamiento experimentado por la membrana funcionalizada de PVDF con activación alcalina, esta membrana mostró una mayor resistencia química y/o mecánica y estabilidad que la membrana no modificada al tratar un efluente anaerobio real durante más de 800 h de operación. El ensuciamiento desarrollado sobre las membranas mostró una composición estratificada: una primera capa principalmente de proteínas y polisacáridos, el interior de la torta de ensuciamiento compuesta por sales de calcio, carbonato y fosfato, y la parte superior de la torta compuesta principalmente por materia orgánica, incluida la biomasa. Esta caracterización del ensuciamiento puede servir para facilitar la selección de los protocolos de limpieza de membrana más adecuados.

El paso final en cuanto a la evaluación de la recuperación de CH_4 disuelto fue la optimización del consumo de energía e insumos del proceso utilizando un contactor de membrana de fibra hueca, como la configuración más representativa en procesos industriales. En este sentido, se evaluó el uso del modo combinado en el contactor de fibra hueca para la recuperación de CH_4 disuelto, que mostró eficacias de eliminación, coeficientes de transferencia de

materia y producciones netas de energía significativamente mayores que los modos de operación independientes (vacío y gas de arrastre). Además, el modo combinado mitigó la humectación de los poros. En conclusión, la selección de las condiciones hidráulicas más apropiadas, la incorporación de fluoroalquilsilanos y el modo combinado pueden mejorar el rendimiento del contactor de membrana para recuperar el CH₄ disuelto de los efluentes anaerobios, lo que reduciría los costes de operación y la huella de carbono de una planta de tratamiento anaerobio de aguas residuales.

En la búsqueda de nuevas aplicaciones dónde integrar la tecnología de membranas, se evaluó un proceso de cristalización asistido por membrana para la recuperación de fósforo en forma de vivianita. Como resultado, se obtuvieron nanopartículas de ~35 nm con una distribución relativamente pequeña. La nucleación de cristales estuvo muy influenciada por la capa límite dentro del módulo de membrana, en la que la velocidad de nucleación aumentó a medida que disminuyó la velocidad del líquido. Además, las membranas porosas facilitaron la micromezcla de los reactivos y redujo la barrera energética para la nucleación. El análisis de la cinética de nucleación sugirió un mecanismo dependiente de la colisión de iones, en el que una mayor velocidad de supersaturación da lugar a un mejor mezclado de los reactivos y a una mayor probabilidad de colisión de iones para la nucleación. Además, la funcionalización superficial anteriormente estudiada se mostró como una metodología útil para aumentar la velocidad de nucleación, favorecida por el aumento de la hidrofobicidad. Por lo tanto, la cristalización reactiva asistida por membrana permitió ofrecer un alto control sobre la nucleación en comparación con los cristalizadores convencionales que presentan un nivel de mezclado de reactivos menos eficiente.

STRUCTURE OF THE THESIS

The thesis starts with the section *1 Introduction* composed of four background subsections. The subsection *1.1 Environmental concern and sustainability* exposes an overview of the main environmental challenges in what this thesis is focused on; the subsection *1.2 Polymeric membrane contactor technology for the recovery of dissolved methane* shows a description of membrane contactors technologies focused on the methane recovery from liquid streams, as well as on the current challenges that should be overcome for the full large-scale application; the subsection *1.3 Membrane-assisted crystallisation technology for the recovery of phosphorus* is focused on the description of the membrane crystallisation process and the recovery of dissolved phosphorus in vivianite form; and the section *1.4 Membrane functionalisation* discusses about the available membrane functionalisation techniques for tailoring the membrane properties in order to enhance the membrane performance.

The different aims of this thesis are exposed in section *2 Objectives* followed by the detailed description of the materials and methodologies applied in this thesis in section *3 Materials and Methods*. The materials and methods section is divided into four subsections: the subsection *3.1 Membrane modules and materials* details the different membranes evaluated in this work, the subsection *3.2 Experimental setups and procedures* shows the different experimental setups and procedures conducted for the different studies, the subsection *3.3 Membrane functionalisation methodologies* describes the modification techniques for tailoring the membrane properties, and the subsection *3.4 Analytical techniques and calculation methods* is focused on the different analytical methods needed for evaluating the performance of the different tests and characterising the membrane, fouling and crystals.

This thesis is presented as a compendium of five scientific published papers and one paper under review. Thus, section *4 Results and Discussion* is

divided into six subsections: 4.1 *Flat PVDF membrane with enhanced hydrophobicity through alkali activation and organofluorosilanisation for dissolved methane recovery*, 4.2 *Flat PVDF membrane with enhanced hydrophobicity through alkali activation and organofluorosilanisation for dissolved methane recovery*, 4.3 *Fouling characterisation in PVDF membrane contactors for dissolved methane recovery from anaerobic effluents: effect of surface organofluorosilanisation*, 4.4 *Stability of superhydrophobicity and structure of PVDF membranes treated by vacuum oxygen plasma and organofluorosilanisation*, 4.5 *Simultaneous application of vacuum and sweep gas in a polypropylene membrane contactor for the recovery of dissolved methane from water*, and 4.6 *Membrane-assisted reactive crystallisation for the recovery of dissolved phosphorus in vivianite form from liquid effluents*. In these subsections, the motivation, aim and overview as well as the main results and conclusions of each study are summarised and discussed. The reader can find the five published scientific papers and the preprint version of one paper (not peer reviewed) in the Appendix section.

Then, the section 5 *Conclusions and Future Prospect* is presented, where the main conclusions of this thesis are gathered, and the main results are highlighted. As well, several future lines of work are suggested.

Then the reader can find the list of the references as well the description of the nomenclature and abbreviations used in this thesis document in sections 6 *References* and 7 *Nomenclature*, respectively.

Finally, section 8 *Resumen extendido* shows an extended abstract in Spanish.

The five scientific publications and the preprint version of the paper under review are presented in the Appendix, following the same order as exposed in section 4 *Results and Discussion*.

CONTRIBUTIONS OF THIS THESIS

The results obtained during the execution of this thesis have been published in five journal articles and one article is under review at the moment of the thesis deposit. As well, four works were presented in conferences as oral or poster communication and one work has been accepted for a forthcoming conference. All these contributions are gathered as follows.

JOURNAL ARTICLES

The original scientific papers are the following:

Contribution I: R. Jiménez-Robles, C. Gabaldón, J.D. Badia, M. Izquierdo, V. Martínez-Soria, Recovery of dissolved methane through a flat sheet module with PDMS, PP, and PVDF membranes, *Sep. Purif. Technol.* 282 (2022) 120057. <https://doi.org/10.1016/j.seppur.2021.120057>.

Contribution II: R. Jiménez-Robles, B.M. Moreno-Torrallbo, J.D. Badia, V. Martínez-Soria, M. Izquierdo, Flat PVDF membrane with enhanced hydrophobicity through alkali activation and organofluorosilanisation for dissolved methane recovery, *Membranes*. 12 (2022) 426. <https://doi.org/10.3390/membranes12040426>.

Contribution III: R. Jiménez-Robles, V. Martínez-Soria, M. Izquierdo, Fouling characterisation in PVDF membrane contactors for dissolved methane recovery from anaerobic effluents: effect of surface organofluorosilanisation, *Environmental Science and Pollution Research*. 30 (2023) 29164–29179. <https://doi.org/10.1007/s11356-022-24019-z>.

Contribution IV: R. Jiménez-Robles, M. Izquierdo, V. Martínez-Soria, L. Martí, A. Monleón, J.D. Badia, Stability of superhydrophobicity and structure of PVDF membranes treated by vacuum oxygen plasma and

organofluorosilanisation, Membranes. 13 (2023) 314.
<https://doi.org/10.3390/membranes13030314>.

Contribution V: R. Jiménez-Robles, C. Gabaldón, V. Martínez-Soria, M. Izquierdo, Simultaneous application of vacuum and sweep gas in a polypropylene membrane contactor for the recovery of dissolved methane from water, J. Memb. Sci. 617 (2021) 118560.
<https://doi.org/10.1016/j.memsci.2020.118560>.

Contribution VI: R. Jiménez-Robles, M. Izquierdo, V. Martínez-Soria, Lo-I Chen, K. Le Corre Pidou, E.J. McAdam, Membrane-assisted reactive crystallisation for the recovery of dissolved phosphorous in vivianite form from liquid effluents. Under review in Sep. Purif. Technol. Pre-print available at <http://dx.doi.org/10.2139/ssrn.4481071>.

CONFERENCE CONTRIBUTIONS

Four different works were presented in international chemical engineering conferences and one work has been accepted for a forthcoming national conference. These works are listed as follows:

R. Jiménez-Robles, C. Gabaldón, V. Martínez-Soria, M. Izquierdo, Evaluation of the combo mode operation of a PP membrane module for methane degassing of anaerobic effluents, 14th Mediterranean Congress of Chemical Engineering (MECCE2020), Barcelona, Spain (16/11/2020 – 20/11/2020).

R. Jiménez-Robles, J. D. Badia, C. Gabaldón, V. Martínez-Soria, M. Izquierdo, Surface modification of membranes for methane degassing from water: preliminary study on hydrophobicity and performance, 14th Mediterranean Congress of Chemical Engineering (MECCE2020), Barcelona, Spain (16/11/2020 – 20/11/2020).

R. Jiménez-Robles, M. Izquierdo, V. Martínez-Soria, L. Martí, A. Monleón, J.D. Badia, Surface chemical modification of PVDF membrane by

oxygen plasma and organofluorosilanisation: stability of the superhydrophobicity and structure, 15th Mediterranean Congress of Chemical Engineering (MECCE2023), Barcelona, Spain (30/05/2023 – 02/06/2023).

R. Jiménez-Robles, M. Izquierdo, V. Martínez-Soria, J.D. Badia, Corona treatment activation for the organofluorosilanisation of PVDF membrane. Effect of the long-term operation in the hydrophobicity, 15th Mediterranean Congress of Chemical Engineering (MECCE2023), Barcelona, Spain (30/05/2023 – 02/06/2023).

R. Jiménez-Robles, V. Martínez-Soria, M. Izquierdo, L. Chen, E.J. McAdam, Evaluación de la cristalización reactiva asistida por membrana para la recuperación de fósforo disuelto en aguas residuales en forma de vivianita. Accepted as oral presentation in XXXVII Jornadas Nacionales de Ingeniería Química, Castellón, Spain, which will be held on 13/09/2023.

1 INTRODUCTION.

1.1 ENVIRONMENTAL CONCERN AND SUSTAINABILITY.

1.1.1 Climate change and greenhouse gas emissions.

According to the Intergovernmental Panel on Climate Change (IPCC), the climate change is defined as “a change in the state of the climate that can be identified by changes in the mean and/ or the variability of its properties and that persists for an extended period, typically decades or longer. Climate change may be due to natural internal processes or external forces such as modulations of the solar cycles, volcanic eruptions, and persistent anthropogenic changes in the composition of the atmosphere or in land use” [1]. Nonetheless, a different definition is made by the United Nations Framework Convention on Climate Change (UNFCCC), which defines climate change as “a change of climate which is attributed directly or indirectly to human activity that alters the composition of the global atmosphere and which is in addition to natural climate variability observed over comparable time periods”. This definition makes a distinction between climate change attributable to human activities altering the atmospheric composition and climate variability attributable to natural causes.

Climate change is leading to extreme climatology effects and a global warming all over the planet. The warming of the climate system is a fact, as can be deduced from the increase in air and ocean temperatures, decrease in the volume of arctic ice, and the rise in sea level. Most of the global warming recorded since the mid-20th century is due to the increase in greenhouse gas (GHG) concentrations, as a consequence of emissions from human activity. The global temperature has increased by approximately 1.1 °C in the last 150 years, and it is expected to continue risen [2]. Scientific evidence and, therefore, organizations such as the UNFCCC, have recognized the objective of limiting

the increase in global average temperature to less than 2 °C with respect to pre-industrial levels. In fact, in December 2015, the Paris Agreement was established with the aim of preventing global warming from exceeding 1.5 °C, promoting additional efforts to do so.

Climate change is mainly attributed to the exacerbated emissions of GHGs from anthropogenic activities. GHGs are gaseous constituents of the atmosphere, both natural and anthropogenic, that absorb and emit radiation at specific wavelengths, causing the greenhouse effect. Water vapour (H₂O), carbon dioxide (CO₂), nitrous oxide (N₂O), methane (CH₄) and ozone (O₃) are the primary GHGs in the Earth's atmosphere. Currently, humanmade GHGs include mainly sulphur hexafluoride (SF₆), hydrofluorocarbons (HFCs), perfluorocarbons (PFCs), and nitrogen trifluoride (NF₃) [1]. The main GHGs emitted to atmosphere and their sources are gathered in Table 1.1.

Long-life GHGs, such as CO₂ and N₂O, present a chemical stability and persistence in the atmosphere for several decades and centuries, and thereby, they affect the climate in the long-term. The most long-life GHGs are those related with the PFCs, whose use is being restricted by stricter regulations and substituted by HFCs with a shorter lifetime. The relatively short-life GHGs, such as CH₄, sulphur dioxide (SO₂) and carbon monoxide (CO), are more reactive, and therefore, they are removed by means of a natural oxidation into the atmosphere or through the rains. The lifetime of the main GHGs emitted are listed in Table 1.1.

The global warming potential (GWP) of each GHG is used a measurement of its contribution to the global warming and can be defined as “an index of the radiative forcing following an emission of a unit mass of a given substance, accumulated over a chosen time horizon (usually 100 years, GWP100), relative to that of the reference substance, CO₂” [1]. Thus, the GWP represents the combined effect of the differing times in which these substances remain in the atmosphere, and their effectiveness in causing radiative forcing. The GWP100 of the main emitted GHGs is shown in Table 1.1. Despite the

anthropogenic gases HFCs, PFCs, SF₆, and NF₃ represent less than 3% of the total GHG emissions (Figure 1.1), the highest GWP100 values correspond to these gases, which highlights the importance in the reduction of these emissions.

Table 1.1. Main emission sources, Global Warming Potential at 100 years horizon (GWP100), and atmospheric lifetime for the main greenhouse gases emitted to the atmosphere [3–5].

Gas	Emission sources	GWP100	Lifetime, years
Carbon dioxide (CO₂)	Natural: oceans, lands, plants, animals. Anthropogenic: fossil fuel combustion, industry, deforestation.	1	N/A
Methane (CH₄)	Natural: anaerobic bacterial decomposition of organic matter, volcanoes, vents in the ocean floor. Anthropogenic: livestock, fugitive emissions, waste management.	27 – 30	12
Nitrous oxide (N₂O)	Natural: oceans and lands. Anthropogenic: fossil fuel combustion, use of fertilisers, production of nitric and adipic acid, wastewater management and combustion of waste and biomass.	273	109
Hydrofluorocarbons (HFCs)	Anthropogenic: refrigerant gases, aluminium and semiconductor industry.	164 – 14590	2 – 228
Perfluorocarbons (PFCs)	Anthropogenic: aluminium and semiconductor industry.	7379 – 13902	2600 – 50000
Sulphur hexafluoride (SF₆)	Anthropogenic: electrical insulating of fluid in power distribution equipment and analysis of atmospheric and oceanic transport processes	25184	3200
Nitrogen trifluoride (NF₃)	Anthropogenic: semiconductor industry.	17423	569

N/A: not available

CO₂ is the main GHG emitted through anthropogenic activities representing around the 80% of the total anthropogenic GHG emissions (Figure 1.1), followed by CH₄ (12%) and N₂O (5%). Anthropogenic emissions are the greatest responsible for the increase in atmospheric CO₂ concentration since the

industrial revolution. The main human activity that emits CO₂ is the burning of fossil fuels (coal, natural gas, and oil) for energy production and transport. CO₂ is also emitted from industrial processes in lower extent, such as in the production and consumption of mineral products, the production of metals, and the production of chemical products. In addition, changes in the land uses and deforestation causes significant CO₂ emissions, influencing the carbon cycle and contributing to the climate change and loss of biodiversity and ecosystems.

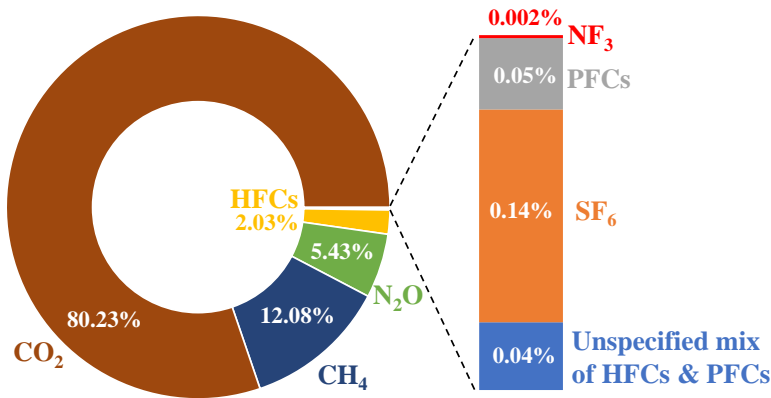


Figure 1.1. Distribution in the anthropogenic emissions of the different greenhouse gases in European Union during 2021. Own figure based on data from [6].

CH₄ is the second (12%) most relevant GHG emitted to the atmosphere from human activities (Figure 1.1) with a significant lifetime of 12 years (Table 1.1). Moreover, CH₄ emission rate has been increasing in the past decades due to the rise in the human activities. Thus, CH₄ emissions management is a critical issue in order to mitigate the effects of the climate change. Since the high relevance of CH₄ as a GHG, the CH₄ emissions to the atmosphere, the sources and the environmental concern will be discussed in the next sections.

1.1.1.1 Methane emissions.

Methane is a simple hydrocarbon, which constitutes the main component of natural gas. CH₄ is the second most important GHG contributor to climate change following CO₂. Although CH₄ is emitted into the atmosphere in smaller amounts than CO₂, its GWP100 is ~28 times higher than that of CO₂ (Table 1.1). Therefore, CH₄ is a powerful and abundant GHG, which makes it a significant contributor to climate change, especially in the medium term. Moreover, CH₄ is a potent local air contaminant and contributor to O₃ formation, which itself causes serious health problems [7]. Therefore, CH₄ emissions are highly relevant to 2050 climate objectives of the European Green Deal to reinforce the global leadership of the European Union (EU) in the fight against climate change.

On the one hand, CH₄ is emitted by natural sources such as wetlands, as a consequence of natural anaerobic fermentation processes. On the other hand, CH₄ is also released into the atmosphere through human activities, such as agriculture and waste management (Table 1.1). Figure 1.2 shows the CH₄ emissions in 2021 in the EU by activity sectors [6]. Agriculture and farming sector are the main source of CH₄ emissions, representing an almost 56% of the total emissions, mainly due to the enteric fermentation of ruminant animals, which produce large amounts of CH₄ as part of their digestive process. Likewise, the waste management sector (including all wastes from industries, population, and agricultural sector) constitutes an anthropogenic source of relevance in terms of CH₄ emissions, representing a near 24%. These emissions are consequence of the organic matter decomposition under anaerobic conditions that occurs in rice fields and landfills among other poor oxygen environments. Wastewater management subsector is highlighted since this activity emitted a 4% of the total CH₄ emission due to the anaerobic processes during conveying in sewers and in anaerobic digesters which could involve further diffuse or fugitive emissions [8,9]. The exploitation of fossil fuels for energy production and distribution is also an important CH₄ source, representing a 11%. These

emissions include frequent leaks from natural gas systems during production, processing, storage, and distribution. Additionally, industrial, residential, and commercial activities, changes in the land use and deforestation, and the combustion of fossil fuels for commercial and domestic transport represent significant CH₄ sources, even though in a lesser extent (<10%).

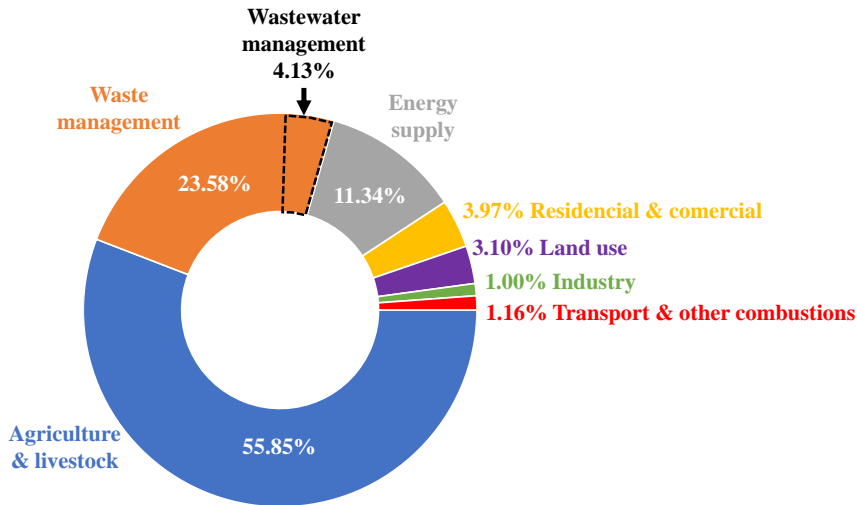


Figure 1.2. Distribution of the methane emissions by sectors in EU-27 zone in 2021. Own figure based on data from [6].

Although the net amount of CH₄ in the atmosphere has increased over the past 30 years, the CH₄ concentration in the atmosphere has been decreased during certain periods, likely due to its high reactivity [10]. Most of the CH₄ is removed from the atmosphere through the oxidation induced by the hydroxyl free radicals in the troposphere, which were produced photochemically by natural processes. This leads to the formation of formaldehyde (CH₂O), CO and O₃ in the presence of sufficiently high N₂O levels. Therefore, CH₄ acts as a regulator of hydroxyl free radicals in the atmosphere. Other less important CH₄ sinks are related to its reactivity with free chlorine, its destruction in the stratosphere, and its dissipation in soils. In addition, CH₄ emissions present a large interannual variability that has not been explained to date, but which may be due to variations in emissions from burning biomass and wetlands [10]. However, the general trend of the CH₄ concentration shows a continuous

increase, and therefore, the mean atmospheric CH₄ concentration has more than doubled since preindustrial times (697 ppb in 1751), reaching 1842 ppb in 2021 [11].

Reducing CH₄ emissions is a priority initiative in the European Green Deal and the EU's methane strategy, published in October 2020 [12]. The strategy aims to curb temperature pathways to 2050, improve air quality and reinforce the EU's global leadership in the fight against climate change. The focus of this strategy is on reducing CH₄ emissions in the energy, agriculture, and waste sectors, as these areas account for almost all anthropogenic CH₄ emissions. Reducing CH₄ emissions is not only important for mitigating climate change, but brings many other energy, health, and safety related benefits such as the reduction in tropospheric O₃, production of energy from the recovered/captured CH₄, and protection of water resources and ecosystems. The production of energy from recovered CH₄ provides a clean renewable energy source that can stimulate local economic development by replacing fossil fuel-based energy sources. In this context, the main scope of this thesis is the recovery of the dissolved CH₄ from liquid waste effluents by means of membrane-based technologies since their intrinsic characteristics of efficiency.

1.1.1.2 Methane applications and sources.

Methane is a hydrocarbon lighter than air which produces more energy per unit weight than coal and oil [13]. In addition, CH₄ combustion leads to a very limited carbonaceous deposits. Hence, CH₄ is preferred over coal and oil as fuel for electricity and heat production at domestic, commercial, and industrial level [13]. Also, CH₄ gas is used to run and power engines in factories. This produced energy is used in industries such as petroleum refineries, food processors, pulp and paper, and companies that work with glass, clay, and stone. Furthermore, methane-based combustion is applied for drying, dehumidifying, melting, and sanitizing industrial products. Besides the energy

sector, CH₄ is used as a raw material in the chemical industry for the production of valuable compounds [13]. For example, CH₄ is an important source of syngas, which is essential for the ammonia production [13,14]. Other valuable compounds derived from CH₄ include methanol (CH₃OH), chloroform (CHCl₃), carbon tetrachloride (CCl₄), and nitromethane (CH₃NO₂) [13]. Moreover, the incomplete combustion of CH₄ yields carbon deposits known as carbon black, which is mainly used as a reinforcing agent in rubbers for vehicle tire manufacture [13].

Currently, the main source of CH₄ is fossil-based, leading to a positive net CH₄ emission and a threat of depletion. In this regard, **biogas has been considered the main renewable source for a sustainable supply of CH₄ in long-term.** Biogas is the name given to the gas produced in an anaerobic treatment process consisting of a mixture of methane (between 50 and 75%_v of CH₄) and carbon dioxide (between 50 and 25%_v of CO₂) and other elements in low concentrations such as oxygen (O₂), nitrogen (N₂), H₂O, ammonia (NH₃), and hydrogen sulphide (SH₂) [15]. Biogas can be used as direct fuel for the production of electricity and heating or upgraded to obtain biomethane which complies with the quality standards imposed by national legal regulations and can be further injected into the natural gas network.

Biogas is being the focus of different initiatives to promote renewable energy in EU. Thus, biogas production in EU is expected to increase from 3.5 billion cubic meters registered in 2021 to 35 billion cubic meters in 2030 [16]. Around 19000 biogas and biomethane plants operated in EU in 2021 producing 196 TWh of energy, and they are dedicated to both the anaerobic digestion of solid waste and the anaerobic degradation of wastewater [16]. These biogas plants are mainly located in Germany, Italy, United Kingdom, and France. In general, countries with large industries in the agricultural, agri-food and waste management sectors like Spain present a great potential for biogas production [17], so that new regulations, roadmaps, and frameworks are emerging to promote these treatment plants. In Spain there are only 146 plants of this type

with a total energy production of 2.74 TWh [18], but the Spanish Biogas Roadmap [17] pretends to multiply by 3.8 the sustainable production of biogas by 2030, which can quickly activate the market. In this context, the continuous increase in the biogas plants may induce a higher global CH₄ emission due to the dissolved methane in the anaerobic effluents, which is discussed in the next section. Therefore, the dissolved CH₄ recovery from such effluents is imperative to avoid GHGs emissions and release a renewable source for CH₄. In this context, the application of membrane contactors for recovering dissolved CH₄ is the main scope of this thesis.

1.1.2 Phosphorus applications and sources.

1.1.2.1 Depletion of conventional phosphorus sources.

World population is continuously increasing and will reach 9.7 billion by 2050, a 34% more than the current population [19,20]. The crop production yield and the request for animal protein are expected to rise by 30% in 2050 [20] and 14% in 2030 [21], respectively, in order to provide enough food for the larger, richer and more urban population. This global increase in crop production involves an increase in the demand for fertilisers, whose current consumption is 200 Mt, and the supply-demand balance will decline progressively [22]. Additionally, the increase in the agricultural activity must be developed under the sustainable principles to avoid negative impacts in the environment related to the GHG emissions and water pollution. Implementing a sustainable intensification of farming following the circular economy principles, minimising nutrient losses and release of chemicals and GHG into the environment will aid in the sustainable food production [20,23].

Nitrogen (N), phosphorus (P), and potassium (K), are the main elements of inorganic fossil-based fertilisers [24], which are the most used fertilisers in agriculture. Thus, the non-renewable origin of these conventional fertilisers makes the supply of nutrients unsustainable, leading to a concern in the nutrient availability over long-term [25]. In the case of P, the natural sources

are expected to be used up by the end of this century, being the fertiliser industry one of the major consumers of P [26].

P-based fertilisers are obtained from mineral phosphate rocks, mainly as impure calcium phosphate which is further processed and refined. Because of the non-renewable origin of phosphate rocks and the fast depletion of reserves, the demand for phosphoric fertilisers is estimated to be higher than their availability by 2033 [25]. Furthermore, 90% of the P reserves are located in few countries such as China, Morocco, Algeria, Syria and Iraq, making uncertain the mineral availability due to instable geopolitical relationships. Regarding the environmental impact of P-based fertilisers, the production of ammonium phosphate and triple-super phosphate involves the emission of 1.3 – 8.9 and 0.4 – 1.6 kg CO₂ kg⁻¹ P₂O₅ [27], respectively, and requires a high energy demand of around 7700 kJ kg⁻¹ of phosphate [23]. Thus, manufacture of these fertilisers contributes significantly to the GHG emissions, aggravating the effects of the climate change.

Around 133.9 million hectares of farmland with requirements of fertilisation are present in EU [28], and most of this farmland is intensively cultivated. Thus, 11.2 Mt of inorganic fossil-based fertilisers were consumed in EU in 2020, which involved an increase of 6.9% and 21.9% in the consumption of N and P elements, respectively, compared to 2010 [29]. Furthermore, most of the nutrients consumed in EU were imported mainly from Belarus and Russia [30], which makes nutrients, especially P, critical and strategical raw materials for the EU [31].

1.1.2.2 Waste to phosphorus: renewable phosphorus sources.

Natural P cycle has been substantially broken due to anthropogenic activities, especially the agricultural sector. In fact, the estimations show that half of the worldwide food production is based on mineral non-renewable fertilisers [26]. In addition, the P present in wastewater effluents is responsible of eutrophication, causing an environmental damage and even dead zones in

aquatic systems. Thus, an urgent global action for a sustainable and secure P supply is imperative. Valorisation of waste effluents for P-based fertilisers should be the milestone for a sustainable supply of P in the context of circular economy, closing the anthropogenic cycle of P which also release benefits such as the reduction of environmental damage, and therefore costs.

P has been recently well recognised as an essential element for society. Therefore, industrial and investigation sectors have paid great attention to sustainable P management systems, contributing to the development of a new green and circular P industry [32,33]. Three different types of waste can be considered from where P could be potentially recycled: agricultural and livestock waste, wastewater, and industrial waste. However, current P recycling technologies is not always a feasible business opportunity for most companies since the still cheaper price of conventional mineral fertilisers. Therefore, **the critical challenge for a sustainable P management is the implementation of an economical, reliable, and predictable P recycling technology** which ensures a safety P supply.

Anthropogenic P flows in wastewaters involve more than 4.6 Mt P per year, which means more than 2% of the total phosphate rock production [32]. The P content in wastewaters comes from the human metabolism (30 – 50%), phosphate detergents (50 – 70%) and industrial activities (2 – 20%) [34]. Therefore, wastewaters could be an important source of P through effective recycling techniques coupled in wastewater treatment plants. However, there is a clear lack of guidance for P recycling in wastewater treatment plants due to the technological challenge in implementing feasible technologies which allow the economic recovery of P products whilst they keep free of pollutants such as heavy metals or pathogens. Consequently, the global P recycling from wastewaters is on low scale [26] and much more efforts are needed to implement a sustainable P source globally which requires the cooperation of many stakeholders [34].

In Central Europe countries, the P content in municipal wastewaters could replace around 50% of the non-renewable P-based fertilisers used annually if P is effectively recovered [33]. In the case of Switzerland, the amount of P in sewage sludge has been estimated to be similar to the total P imported for agriculture [32]. Therefore, the effective P recycling could provide almost the total quantity of fertilisers needed per year. In this context, Germany has been one of the first countries in imposing the P recovery in wastewater treatment plants. Thus, the German sludge ordinance makes mandatory the recovery of more than 50% of the total P from the wastewater that enters the treatment plant [35].

Although the P recovery from waste effluents for its reuse as input for the P cycle is not a common practice because of technical limitations, the P removal from municipal wastewater is widely applied and well established globally due to the current wastewater discharge regulations. In conventional wastewater treatment plants, the 80 – 90% of influent P ends up in the sludge due to the chemical precipitation induced by Al^{3+} and Fe^{3+} salts or is biologically metabolised [36]. However, the precipitates are insoluble salts of P located in the sludge bulk, hindering the ulterior P recovery. Only the dissolved P present in the liquid phase of the sludge and in the effluent can be easily recovered through struvite precipitation, which is the most common and feasible current technique. Therefore, the P recovery in existing treatment plants is limited to around 30% [32] of the total P contained in the wastewater.

1.2 POLYMERIC MEMBRANE CONTACTOR TECHNOLOGY FOR THE RECOVERY OF DISSOLVED METHANE.

CH₄ emissions during the handling and treatment of municipal and industrial wastewaters are expected to increase by approximately 19% from 2010 to 2030 due to the continuous human population growth [37]. Thus, the development and implementation of methodologies that lead to the reduction in these CH₄ emissions from wastewaters could be of special interest. In this regard, anaerobic treatment of sludge and wastes involves the production of a large amount of CH₄ in form of biogas, which is considered a second-generation biofuel. Nevertheless, these processes could involve potential diffuse and fugitive CH₄ emissions, especially from the anaerobic effluents, which contain large amounts of dissolved CH₄, being released into the atmosphere after the discharge of the liquid effluent into the environment. Despite the low CH₄ solubility in water (~23 mg L⁻¹ at 25 °C [38]), several studies have shown that dissolved CH₄ concentrations in the anaerobic effluents could be much higher than equilibrium concentration. The CH₄ supersaturation grade is affected mainly by the: i) organic load of the treated waste in which a higher substrate and active biomass concentration lead to higher CH₄ production rates, favouring the supersaturation, and ii) the CH₄ mass transfer towards the headspace of the reactor, which is limited in reactors based on gravity settling due to a poor mixing and low liquid velocities, such as what it occurs in an Upflow Anaerobic Sludge Blanket (UASB) reactor [39]. The work of Crone et al. [39] compiles some domestic wastewater treatment and low organic load systems, where supersaturation grades ranging from 1.0 to 6.9 were reported, and the estimated dissolved CH₄ losses ranged between 11 and 88% of the total produced CH₄ (Table 1.2).

Table 1.2. Supersaturation grade and estimated losses of dissolved methane in the effluents from some anaerobic wastewater treatments. Adapted from [39]. UASB: Upflow Anaerobic Sludge Blanket; EGSB: Expanded Granular Sludge Bed; AnMBR: Anaerobic Membrane Bioreactor; SAnMBR: Submerged Anaerobic Membrane Bioreactor.

Reference	Reactor	Scale	Temperature, °C	CH ₄ supersaturation	Lost CH ₄ in effluent, %
[40]	EGSB	Pilot	16	1.57	45
[41]	UASB	Pilot	28	6.9	85
[42]	UASB	Laboratory	35	1.67 – 1.53	11 – 13
[43]	UASB	Pilot	25	1.64	41
[44]	UASB	Laboratory	25	1.3	45
	AnMBR	Laboratory	25	1.0	88
[45]	AnMBR	Laboratory	15	1.5	40 – 50
[46]	SAnMBR	Pilot	33	1.009	43
	SAnMBR	Pilot	21	1.007	46

Besides the negative environmental effects of the CH₄ emissions, the degassing of effluents from anaerobic processes or from any liquid effluent with a high dissolved CH₄ concentration is of great importance for several reasons. On the one hand, the discharge of these effluents leads to a loss of a potential energy source. The recovered dissolved CH₄ could be added to the main biogas line for a further use as biofuel. On the other hand, explosive atmospheres can be generated when the effluent is discharged into sewers or other closed spaces or conduits. A CH₄ concentration below 5%_v (lower explosive limit) must be ensured in the air to comply with the safety requirements [44].

For all the reasons abovementioned concerning CH₄ emissions from anaerobic wastewater treatment plants, the recovery and further use of the dissolved CH₄ is imperative for a sustainable development.

1.2.1 Technologies for the recovery, removal and reuse of dissolved methane.

Several technologies have been developed to recover or remove dissolved CH₄ from liquid effluents, ranging from the conventional aeration and gas stripping to the relatively recent processes including biological oxidation and membrane contactors. These main technologies used for the CH₄ removal and recovery from liquid streams are shown in Table 1.3, as well as the main advantages and disadvantages of each technique.

Degasification of anaerobic effluents has been usually conducted by conventional desorption techniques such as aeration and gas stripping using gas-liquid columns. **Aerators** are easily operated by means of the gas bubbling in the liquid bulk. They also offer high mass transfer area for CH₄ uptake and allows the sulphide control [47]. However, aeration units lead to critical issues, such as dilution of recovered CH₄, difficulty in operation, scaling and quality control of the recovered gas, and potential explosion hazards due to the mixture CH₄/O₂ [47]. Moreover, this technique usually presents a quite low efficiency.

Gas stripping processes are commonly used for the removal of volatile organic compounds from several water sources [50–52] due to the facile scale up and operation of these units [47]. Despite the ease of operation and effectiveness of these techniques, gas stripping has scarcely been used for dissolved CH₄ removal from anaerobic effluents [53,54]. On the one hand, the highly diluted CH₄-containing gas makes difficult the further upgrading and reuse of the CH₄ [53]. On the other hand, if the waste gas is going to be directly discharge to atmosphere, a large air flow is needed to ensure a CH₄ concentration below the lower explosion limit, which makes the process energy intensive and contributes to the GHG emissions. Additionally, flooding, foaming, and channelling may occur during the operation. Despite these shortcomings, the simplicity of the process makes gas stripping the most suitable technique for degassing effluents with a low dissolved CH₄ concentration when CH₄ removal is imperative [55].

Table 1.3. Different techniques for methane removal and/or recovery from liquid effluents [47–49].

Technique	Description	Advantages	Shortcomings
Aeration	Bubbling of a carrier gas, usually air, into solution	Simplicity. High mass transfer area.	Phase mixing. Difficult scaling and operation. Difficult control quality. Dilution of recovered gases. Potential explosion hazards. Foaming.
Gas stripping	Distribution of liquid phase into the gas phase (liquid-in-gas) or vice versa (gas-in-liquid) through packing materials or trays in columns	Ease of scaling and operation.	Low efficiency. Low mass transfer area. Flooding, channelling, and foaming. High gas-to-liquid flow rate ratios.
Biological treatments	Methane oxidation by the metabolism of bacteria	Low energy consumption. Simultaneous energy production. Suitable in presence of foaming agents. Simultaneous consumption of nutrients. High removal efficiencies. Methane to value-added products conversion. Ease of scaling.	Conversion of CH ₄ to CO ₂ . Sludge generation. Low mature technology.
Membrane contactor	Mass transfer of the solutes through a selective membrane	Low energy consumption. High compactness. Avoid phase mixing. Ease of operation and scaling. High purity of recovered gases.	Additional mass transfer resistance. Periodical replacement of membranes. Fouling and wetting.

Biological treatments involve the conversion of the dissolved CH₄ into CO₂, energy, or value-added products. Thus, different biological treatments have been investigated in the literature. Microbiological oxidation of CH₄ into CO₂ is conducted by the methanotrophic bacteria metabolism which use dissolved CH₄ as the sole energy and carbon source in engineering bioreactors [56,57]. Although the biological oxidation of dissolved CH₄ requires aeration, the process presents significantly lower energy requirements than gas stripping, which makes aerobic CH₄ oxidation a suitable approach for dissolved CH₄ control [48,49]. Indeed, CH₄ oxidation can be coupled to denitrification process for the simultaneous removal of dissolved CH₄ and nutrients with considerable operational cost savings [47]. An emerging biological treatment is the CH₄ oxidation in microbial fuel cells (MFCs). MFC is a bioelectrochemical system which uses the dissolved CH₄ as the organic substrate, producing electricity. Despite high CH₄ removal efficiencies can be achieved by MFC (>80%), the CH₄-to-energy conversion is quite low (<20%) with small power densities (<200 mW m⁻²) [47,49]. Another biological treatment is the synthesis of value-added products such as methanol, biopolymers, proteins, and organic acid from the biological conversion of dissolved CH₄ by methanotrophs. However, separation and purification processes are required for harvesting these products, which may considerably rise the operational costs especially when the yield is low and the dissolved CH₄ and the final products are very diluted [49]. All these technologies have been demonstrated mainly at lab-scale with very limited information at large-scale. Biological treatments for dissolved CH₄ removal and reuse are in an early stage of development, so that a deeper insight into the biological processes and several issues must be addressed before the implementation at full scale to maximise the CH₄ conversion and determine the feasibility of the process at full scale.

Membrane contactor represent the most reliable and effective unit for wastewater treatment application due to the easier operation and higher mass transfer area than the previous aeration and gas stripping units [47,58,59]. Membrane systems can be integrated into anaerobic treatments as a post

treatment removing the dissolved CH_4 from the effluent, or in-situ, removing dissolved CH_4 from the liquid bulk by means of submerged membranes. This technology has the potential to recover dissolved CH_4 in a suitable form for its further use as a biofuel, with minimal plant upgrading [39,59,60]. In addition, membrane units alleviate operating issues such as flooding and foaming. However, some disadvantages are present when using membranes systems, mainly related to wetting and fouling which lowers the efficiency of the process and leads to an increase of the operational and maintenance costs [47] attributed mainly to the periodical membrane cleaning or replacement. Additionally, a post-treatment of the recovered gas would be needed when using a sweep gas in the permeate side for the collection of the CH_4 due to the dilution effect. Therefore, the CH_4 should be concentrated to enable the use of this gas in heat or electrical generators.

In general terms, the recovery of dissolved CH_4 from anaerobic effluents through gas-liquid membrane contactors yields a higher performance than the conventional separation units due to several advantages:

- No dispersion of the gas phase into the liquid effluent.
- High CH_4 purity in the recovered gas can be obtained when applying vacuum in the permeate side, which enables the direct use of that gas as fuel.
- Low energy cost with no temperature requirements.
- Low maintenance.
- Easy cleaning of membranes with appropriate cleaning protocols.
- Ease of scaling up and operation.
- Compact systems.

Membrane contactor technology will be deeply detailed in the next section.

1.2.2 Membrane contactors for dissolved methane recovery.

Membranes, with their intrinsic characteristics of efficiency and operational simplicity, high permeability and selectivity for the mass transport of specific components, low energetic requirement, compatibility between different membrane operations in integrated systems, easy control and scale-up, good stability under operating conditions, environmental compatibility, and large operational flexibility, represent a technology that satisfies the concept of the intensification and rationalization of chemical productions [61].

A **membrane contactor**, also commonly referred as membrane module or membrane cell, is a compact device that allows the selective separation and purification of two different phases by applying a driving force based on partial pressure, temperature, concentration, or electric potential gradients [62]. The main distinct feature of membrane contactors respect to conventional technologies is that the separation takes place without dispersing one phase into another since the membrane itself separate both phases and provides the contact surface for the mass transfer of the solute (Figure 1.3). Depending on the physical state of the phases involved in the process, the contacting system is referred as liquid-gas, gas-gas, or liquid-liquid membrane contactor. Currently, membrane contactors are widely used in several industrial applications such as in gas separation, wastewater treatment, and preparation of beverages, as well as in more recent applications of forward and reverse osmosis, osmotic evaporation, membrane distillation, and membrane crystallization processes [62]. In the past decade, gas-liquid membrane contactors have been demonstrated as a very useful and promising technology for the dissolved CH₄ separation from anaerobic effluents at lab-scale [59,63,64]. However, the full-scale implementation of this process is still hindered by some issues related to the membrane wetting and fouling. Thus, a deeper insight into the mechanisms that govern the separation process and especially the wetting and fouling phenomena is required as well as the techniques for increasing the membrane antiwetting and antifouling properties.

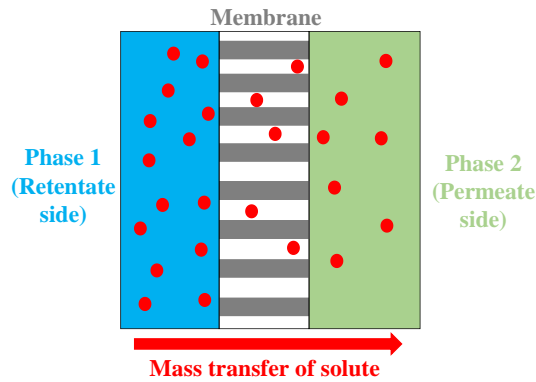


Figure 1.3. Scheme of a membrane separation process.

Membranes can be classified depending on their microscopy structure and morphology [65] (Figure 1.4). **Symmetrical membranes** present the same properties along the membrane, and they are usually composed of a single phase. These membranes can be porous and non-porous (dense) and, often, they are very thin and therefore quite fragile. The mass transfer across the porous membrane takes place by means of the sieve effect or molecular diffusion mechanism, whilst the dilution-diffusion mechanism governs the mass transport in dense membranes, leading to a larger mass transfer resistance. The **asymmetric membranes** are composed of two or more phases of the same or different material, leading to different properties along the membrane cross section. These membranes typically consist in a thin surface layer with a few microns composed of the selective material for the separation which is supported in a secondary porous layer (50 – 150 μm) to provide a higher mechanical resistance. These membranes are classified into anisotropic porous membranes when the surface layer is porous, and thin film composite membranes when the surface layer presents a dense structure.

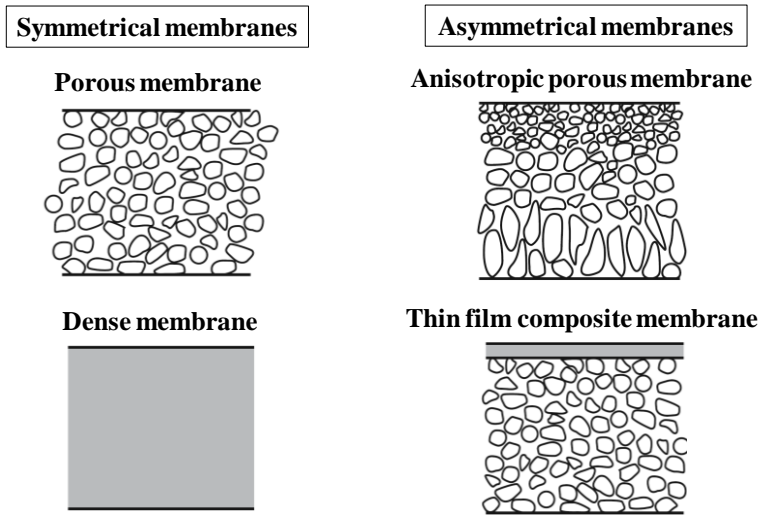


Figure 1.4. Different types of membranes based on their morphology. Adapted from [65].

Several **materials** are used for the synthesis of membranes [65], being the **organic polymers** the most widely materials used for membranes since it is possible to manufacture polymeric membranes with tailored properties in order to adapt them to a specific application. Polymeric materials range from natural and bioinspired materials such as cellulose and chitosan to all kinds of synthetic materials. The selection of the suitable membrane material depends on the application and the operational conditions related mainly to the temperature and pressure requirements, presence of acids, alkalis, solvent or other aggressive chemicals, and the membrane cost. On the other hand, there is a growing interest in inorganic membranes (metallic, glass and ceramic membranes) since they are characterized by a greater chemical, mechanical and thermal stability than polymeric materials. However, inorganic membranes are not usually applied for industrial separations mainly due to their high cost [62,66].

Regarding the **wettability behaviour of the membranes**, their surface hydrophobicity grade plays a crucial role in selecting the membrane for a specific application [65,67]. The **hydrophobicity** is the main parameter that determines the wetting resistance of the membrane. The terms hydrophobicity

and hydrophilicity relate to the ability of surfaces to attract or repel water, respectively, by means of the control of the surface tension at the solid-liquid-gas interface. In this regard, wettability is defined as the ability of a liquid to wet a surface and is determined by the measurement of **contact angle**, which is defined as the three-phase contact point of the solid-liquid-air interface, as shown in Figure 1.5. The contact angle value can vary from one surface material to another, and it is affected by several surface properties such as surface free energy, roughness, chemical composition, porosity, surface tension, surface chemistry and surface load. Hydrophilic surfaces are often used to increase the affinity with water, which makes hydrophilic membranes suitable for pressure-driven membrane processes like micro, ultra and nanofiltration [68]. On the contrary hydrophobic surfaces are often used to reduce wetting of surfaces by water, which is particularly interesting in applications with gas-liquid membrane contactors [69] such as dissolved CH₄ recovery from anaerobic effluents and desalination of seawater through membrane distillation.

In hydrophobic membranes, the adhesion forces between the membrane and the liquid molecules are weaker than the cohesive forces of the liquid molecules, so the membrane present no affinity for the liquid which is repelled from the membrane surface. On the contrary situation, the liquid molecules present affinity for the membrane and the liquid phase is adsorbed, resulting in a hydrophilic membrane. Thus, hydrophobic membranes with a water contact angle higher than 90° repels water whilst hydrophilic membranes present a great affinity for water with a water contact angle lower than 90° (Figure 1.5). Thus, hydrophilic membranes are spontaneously wetted with the aqueous phase, even though hydrophobic membranes can be also wetted when a critical transmembrane pressure is surpassed.

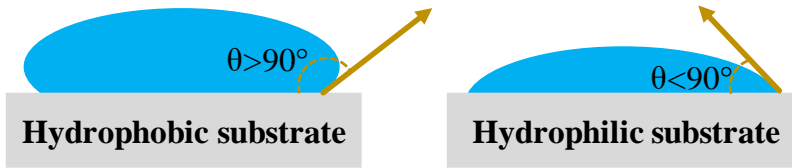


Figure 1.5. Schematic representation of the contact angle of a liquid on a hydrophobic and hydrophilic substrate. θ : contact angle.

Different hydrophobic porous and dense membranes have been used for the dissolved CH_4 recovery from liquid streams [70]. Porous membranes are always preferred in first instance due to the lower mass transfer resistance that they offer for the CH_4 transport through the membrane, and consequently, a higher performance. These membranes are typically composed of polypropylene (PP), polytetrafluoroethylene (PTFE) and polyvinylidene fluoride (PVDF). However, porous membranes are prone to suffer from a severe fouling when treating waste liquids like anaerobic effluents due to pore clogging and deposition of foulants on the porous surface, causing a decline in the membrane performance [71–73]. Therefore, dense and thin film composite membranes could be used when a high fouling is expected on the membranes, since the smoother surface of dense membranes are less prone to suffer from fouling. The most common dense membrane used for dissolved CH_4 recovery is composed of polydimethylsiloxane (PDMS) due to its high CH_4 permeability.

Different **membrane modules** have been developed, which present different geometries and configurations [65]. The most common membrane modules commercially available and their main properties are listed and compared in Table 1.4.

The **plate-and-frame membrane modules** or flat-sheet membrane modules (FMs) consist of different flat-sheet membranes parallel placed, and spacers were placed between them to allow the flux of the liquid or gas phase (Figure 1.6a). The packing factor of the membranes is relatively small, which makes these modules more expensive compared to the rest, although the flat-sheet membranes are easier to maintain, clean and replace.

Table 1.4. Characteristics of the different membrane modules. Adapted from [65].

	Plate-and-frame	Tubular	Spiral-wound	Hollow fibres
Specific area ($\text{m}^2 \text{m}^{-3}$)	400 – 500	25 – 100	500 – 2000	1500 – 3000
Cost (€ m^{-2})	46 – 187	46 – 187	6 – 92	6 – 18
Pressure drop	Low	Low	Moderate	High
Operation at high pressure	Yes	Marginal	Yes	Yes
Limitation in membrane material	No	No	No	Yes

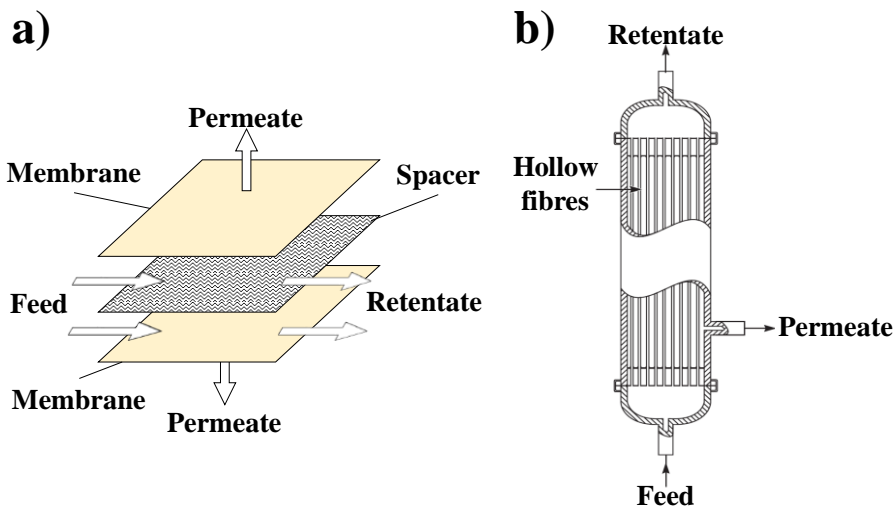


Figure 1.6. Scheme of a) plate-and-frame membrane module, and b) hollow fibre membrane contactor. Adapted from [65]. Both configurations were used in the present thesis.

In the **tubular membrane modules**, the membranes present a tubular configuration. Thus, the module consists of several of these tubular membranes nested inside a single, large tube known as shell. The typical inner tube diameter is between 0.5 and 1.0 cm. These membranes can have the selective separation layer inside the tubes or on the outside, depending on whether the feed stream flows inside the tubes or through the shell side, respectively. The drawback of this module is that it has one of the lowest packing factors of all

the modules, so a very large equipment is required. The main advantages are a higher resistance to fouling than most of the other configurations and an easy cleaning.

Spiral-wound membrane modules consist of two flat-sheet membranes and spacer between them, leaving the active layer to the outside, and they are sealed on three of their four sides. The free side is connected to a collecting tube and the membranes are rolled onto that tube. Thus, the feed stream always flows axially between the membranes and the permeate flows radially towards the central collecting tube. This multi-layer cylindrical structure offers a much higher packing factor than plate-and-frame and tubular modules.

The **hollow fibre membrane contactors (HFMCs)** are similar to tubular modules, but in this case the diameter of the tubes is less than 1.25 mm. Hence, a hollow fibre contactor consists of a bundle of fibres of up to several thousand packed inside a shell (Figure 1.6b), leading to extremely compact membrane modules with very high membrane surfaces in a very small space and at a very low cost. But due to the small diameter of the fibres, these membranes are more susceptible to fouling and clogging and more difficult to clean.

Membrane contactors typically operate in sweep gas or vacuum mode for the recovery of dissolved CH_4 , in order to generate a partial pressure gradient of CH_4 as the driving force. When only vacuum is applied in the permeate side, high purity gas CH_4 can be obtained, which can be directly used for thermal and electricity production without previous concentration [74]. On the contrary, CH_4 is diluted at sweep gas mode, in which N_2 is the most common gas applied at atmospheric pressure. As an alternative to overcome the shortcomings of each operation mode, sweep gas and vacuum can be applied simultaneously. Also, the use of O_2 as sweep gas could allow the direct combustion of the recovered CH_4 without further concentration, reducing operational costs.

In the present thesis, a flat-sheet membrane module configuration has been used for the dissolved CH₄ recovery from liquid streams since this configuration allows an easy extraction, analysis, cleaning, and replacement of the membranes during operation, allowing considerable time and cost savings. In addition, the dissolved CH₄ recovery process was optimised by means of a hollow fibre membrane contactor since this membrane configuration is the most common in this kind of applications (gas-liquid separations).

1.2.3 Challenges of gas-liquid membrane contactors.

The full implementation of polymeric membrane contactors at industrial scale is still hindered by two major drawbacks: **wetting and fouling phenomena** in the membrane (Figure 1.7). In hydrophobic membranes commonly used for gas-liquid and liquid-liquid separations, membrane wetting takes place in porous membranes when the liquid phase fills the membrane pores total or partially. This liquid intrusion in the membrane creates a stagnant liquid phase resulting in an additional mass transfer resistance which lowers the separation efficiency as the filled pore fraction increases. The two main causes of wetting are the exceeding of the critical transmembrane pressure and the capillary condensation.

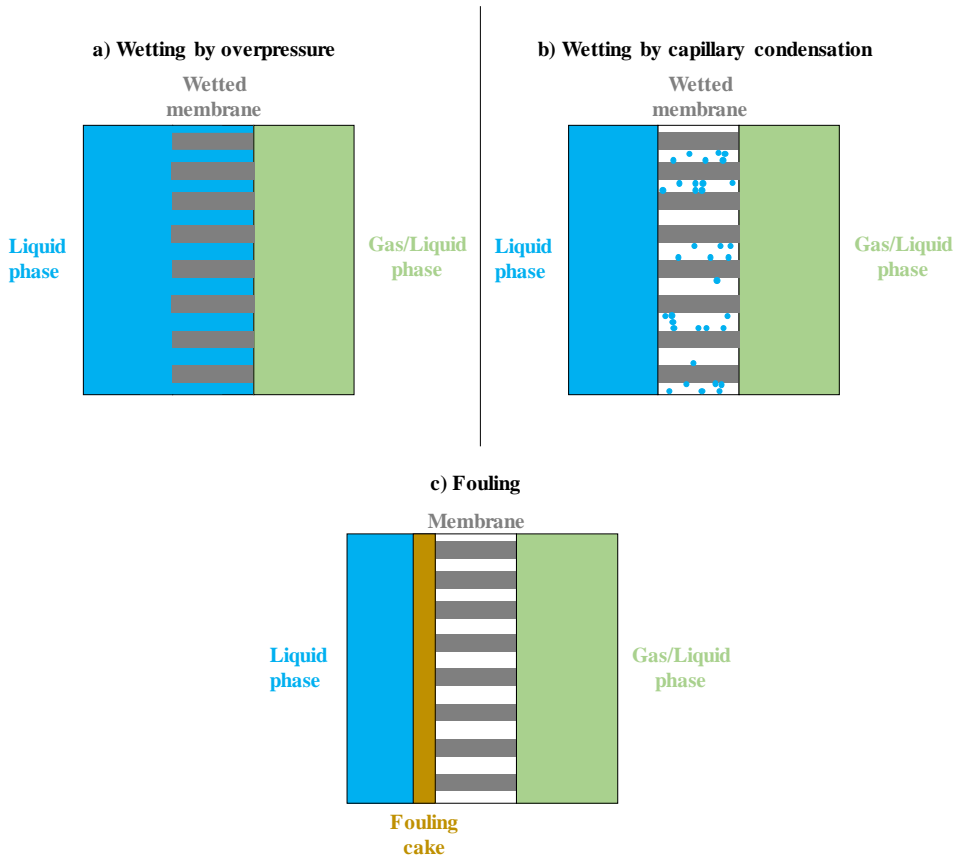


Figure 1.7. Scheme of the membrane wetting by a) exceeding the critical transmembrane pressure (overpressure) and b) capillary condensation, and c) membrane fouling phenomenon.

The critical transmembrane pressure of the membrane, also known as the liquid entry pressure (LEP), defines the pressure at which a specified liquid starts to penetrate the membrane pore structure. Hence, the liquid pressure is able to overcome the hydrophobic forces and can flow across the membrane (Figure 1.7a). The liquid entry pressure is well described by the Young-Laplace equation (Eq. (1)), which shows that LEP is a function of the liquid surface tension (γ , N m^{-1}), the maximum membrane pore size ($r_{p,\text{max}}$, m), the contact angle (θ , $^\circ$) of the membrane with the liquid and the geometric pore coefficient (β) which is 1 for cylindrical pores [75,76]. Thus, the membrane wetting relies not only on the operational conditions (liquid velocity and pressure) but also on

membrane properties (contact angle, pore size and microstructure) and liquid characteristics (surface tension).

$$\text{LEP} = -\frac{\gamma \beta \cos \theta}{r_{p,\max}} \quad (1)$$

From Eq. (1), hydrophobic membranes present a high LEP whilst only a slight pressure would be needed for pushing the liquid through a hydrophilic membrane. Additionally, membranes with a larger pore size are more prone to suffer from wetting due to the lower external force required to overcome the hydrophobic forces [77,78]. Therefore, both **hydrophobicity and pore size** should be carefully considered when selecting or synthesising membranes for gas-liquid or liquid-liquid applications. In this regard, membrane functionalisation appears as an alternative approach to tailor the membrane properties, and thereby, increasing the antiwetting properties of the membrane by enhancing its hydrophobicity. Different membrane functionalisation techniques are discussed in further sections.

The **physical properties of the liquid phase** such as surface tension and viscosity also influence on membrane wettability. In this regard, the wetting resistance of the membrane decreases as the liquid surface tension and viscosity decrease. Most of the absorbent and organic solvents have a lower surface tension than water, which could lead to membrane wetting during operation with such liquids [79]. Additionally, the presence of some compounds in the liquid such as surfactants can decrease the solution surface tension aggravating the membrane wetting. The compatibility between the liquid streams and membrane material is also of importance. In this regard, long-term operation may alter the membrane surface properties and morphology, reducing its hydrophobicity and the mass transfer rates [80].

Regarding the **operational parameters**, the vacuum applied in the gas side, the pressurisation of the liquid phase, high liquid velocities and the pressure drop along the membrane module increase the transmembrane pressure and induce wetting [77,81–83]. For example, the work of Henares et

al. [84] showed that mass transfer resistance for the dissolved CH₄ recovery remarkably increased as feed liquid velocity rose through the lumen side in vacuum mode, which was attributed to membrane wetting. A wet pore fraction between 0.25 and 0.53 was estimated, and no wetting was observed in sweep gas mode. Thus, operational conditions of the membrane modules are limited to avoid wetting or failure due to exceeding pressures and stress.

Membrane wetting can be also a consequence of the capillary condensation phenomenon (Figure 1.7b), even in membranes with a high hydrophobicity, since the driving force for capillary condensation is the vapour pressure difference [85]. The vapour molecules transported across the membrane may be adsorb on the pore wall, and eventually the adsorbed molecules lead to the formation of a liquid meniscus inside the pore when sufficient vapour is adsorbed [86]. Thus, pores can be locally filled with the liquid phase. This type of wetting is more difficult to control than the previous wetting associated to a high transmembrane pressure, since capillary condensation can occur at any instance during the operation. The effects of the capillary condensation are more noticeable in membranes with a smaller pore size than in larger pore sizes [87–89].

Besides wetting, another anticipated long-term operational issue concerning membrane contactors is the **membrane fouling** onto the membrane surface when treating wastewaters such as anaerobic effluents. The resultant fouling cake involves an additional mass transfer which can produce a decrease in system performance (Figure 1.7c), needing frequent cleanings that can reduce membrane lifespan and increase costs [68,90–92].

The membrane fouling when treating wastewaters results from the interaction of the membrane material and the fouling agents [93]. Based on the reversibility of the fouling, membrane fouling is classified into reversible and irreversible. According to Meng et al. [94], there are two types of reversible fouling: the external deposition of fouling agents on the membrane, which can be removed by physical means such as backwashing, and the pore blockage and

strong attraction between fouling agents and membrane, which generally needs to be removed by chemical washing. In contrast, irreversible fouling is a permanent phenomenon, which cannot be eliminated with any cleaning strategy.

Fouling can be also classified depending on the nature of the fouling agents. Hence, inorganic, organic and biological fouling can be distinguished [95,96]. Biofouling is mainly related to the biomass present in the effluent which can be adhered to the membrane surface with a further growing and formation of biofilms. This biofilm involves the secretion of extracellular polymeric substances (EPS) and soluble microbial products (SMP) which will be adsorbed and accumulated on the membrane surface and pores [90,97]. The organic fouling refers to the deposition of organic matter mainly related to biopolymers such as proteins and polysaccharides present in the effluent [97]. Regarding inorganic fouling, the deposition and precipitation of salts also takes place simultaneously to biological and organic fouling. Struvite, calcium carbonates and other phosphate and ammonium salts have been considered as the major inorganic foulants on membranes which treated wastewaters [96,97].

The extent of the fouling on a membrane depends on the membrane properties, nature of the treated effluent and operational conditions. Thus, strategies for the control of the fouling and membrane cleaning are needed to prevent and mitigate the fouling effects on the membrane performance. These strategies can be based on the pretreatment of the effluent (filtration, disinfection), optimisation of the operational conditions (reduce the probability for the membrane-fouling agent interaction), optimisation of the module configuration (increase turbulence on membrane surface), cleaning of the membrane (periodical cleaning with water, acids, alkalis and/or organic solvents) and membrane modification (increase the fouling resistance).

1.3 MEMBRANE-ASSISTED CRYSTALLISATION TECHNOLOGY FOR THE RECOVERY OF PHOSPHORUS.

Municipal wastewaters typically contain from 4 to 16 mg L⁻¹ of total P [98–100], which can reach concentrations up to 2000 mg L⁻¹ in industrial wastewaters such as in effluents from electronic industry [101], making them a potential source of sustainable P. According with environmental regulations, the total P concentration in the effluent from wastewater treatments plants should be usually lower than 1 mg L⁻¹ [98,100]. Therefore, the removal of P from wastewaters is mandatory. Chemical (flocculation and sedimentation) and biological (active sludge) processes are widely implemented in wastewaters treatment plants for removing the P [98]. However, these processes are not usually focused on the further recovery and reuse of P, which is concentrated in the sludge. Thus, P could end up in landfills or in cements as additive from the ash generated in the incineration of the sludge if P recycling methodologies are not implemented. Currently, only a few wastewater treatment plants have implemented P recovery processes worldwide, and they are mainly focused on the struvite precipitation [102]. Different technologies for P recovery from wastewater are discussed in the next section.

1.3.1 Conventional phosphorus recovery technologies from wastewaters.

In general, three different approaches to recover and reuse the P from wastewater are commonly considered: i) the direct use of the sludge as fertilisers, being the most common of the three options; ii) the use of the ash from the incineration of the sludge; and, iii) the P extraction from sludge by chemical or biological precipitation [32].

Sewage sludge is composed of a complex matrix of organic and inorganic compounds, which makes difficult the recovery of the P accumulated in that sludge. Hence, sewage sludge has been used for the direct application on soils

as fertiliser and conditioner. However, the inadequate management of this technique, mainly related to the nutrient surplus leaching, can lead to severe pollution issues such as eutrophication of surface waters, accumulation of nitrates, phosphates and heavy metals in soils and groundwaters, and GHG emissions, especially NH_3 and N_2O [103].

Currently, there are some **technologies for recovering P from sewage sludge** which has substituted unsustainable pathways such as the waste disposing in landfills or incineration processes [26,34]. Sewage sludge and other solid residues from farming and livestock are often treated by anaerobic digestion. In the anaerobic digestion, the digestate generated as a subproduct is rich in nutrient compounds. In addition, anaerobic digestion favours the P release accumulated by microorganisms, which makes P bioavailable and eases the P recovery [32]. Thus, the remaining P contained in the digestate could be recycled.

The first step for P recovery from digestate is usually the separation of the liquid and solid fractions, which is conducted typically by using centrifuges, screw-presses, and belt filters. The separated solid fraction is characterised by a high amount of organic N and P [23] whilst the liquid fraction is richer in NH_3 [104]. The resulting solid fraction can be directly used as a soil conditioner or further treated by means of drying or composting for commercial fertiliser production [24]. Both liquid and solid fraction can be further processed to recover, separate, and concentrate the P compounds, which are mainly in the form of phosphates. Most of P recovery methodologies are focused on the liquid phase since the presence of hazardous organic contaminants and complex heavy metals in the solid phase of the sludge may hinder the P recovery [105]. The available technologies are discussed below.

Struvite precipitation. Struvite ($\text{MgNH}_4\text{PO}_4 \cdot 6 \text{H}_2\text{O}$) can be obtained by means of precipitation, which is favoured in environments with a high concentration of phosphate and ammonium compounds. Therefore, struvite can be produced and recovered from the digestate. To induce struvite precipitation,

magnesium salts are added, mainly in form of magnesium oxide (MgO) and magnesium chloride (MgCl₂), and pH is increased to 8.3 – 10 with sodium hydroxide (NaOH) [104]. This methodology presents high P removal efficiencies (up to 80 – 90%), even though it can require a high consumption of chemicals because of the addition of magnesium salts and alkalis, depending on the nature of the digestate [106]. Therefore, the process cost for struvite precipitation varies from 270 to 2000 € t⁻¹ of P removed [106], depending mainly on the reagent cost. This process is also limited to a minimum P concentration of 100 mg P L⁻¹, so that this technique is commonly applied for the treatment of sewage sludge and digestate which have high P concentrations, with only a few pilot and full scale plants implemented world-wide [23,107].

Vivianite precipitation. Vivianite (Fe₃(PO₄)₂ · 8 H₂O) is a phosphate mineral that is naturally present in iron (Fe) and P rich environments under reducing conditions [108]. Vivianite presents an extremely low solubility in water [108,109], thereby, it could be easily obtained by precipitation of phosphates contained in a liquid matrix after the addition of a ferrous ion (Fe²⁺) salt [105,110]. The lower solubility of vivianite also implies that higher removal efficiencies can be achieved and may be viable for a broader range of effluent concentrations. Compared with struvite, vivianite precipitation could reduce operational costs of P recovery mainly due to a lower consumption of chemicals [102,105,109], even though relevant studies on vivianite precipitation are very scarce [102]. Process cost for vivianite precipitation has only been reported for electrochemical crystallisation processes which consume electricity. These processes showed a P removal up to 100% with a cost of 700 – 2900 € t⁻¹ of removed P [105].

Pressure-driven membrane filtration. The digestate is separated in a solid fraction (retentate) and a liquid fraction (permeate) through the application of a membrane filtration process. Initially, the digestate is subjected to a rough liquid-solid separation as mentioned above. Then, the liquid fraction is first treated in a microfiltration system (pore size >100 nm), followed by an

ultrafiltration step (pore size 1 – 100 nm), and a final nanofiltration or reverse osmosis step (pore size <1 nm). The retentate from the final step constitutes a nutrient rich solid fraction, and pure water free of particles, dissolved compounds and pathogens is obtained as the permeate. In addition, the retentate from the ultrafiltration system contains significant amounts of ammonium and potassium, which could be used as a liquid fertiliser. This membrane technology allows P removal efficiencies up to 98% with a cost ranging from 4 to 12 € m⁻³ of liquid feed [111,112]. Membrane fouling is the main drawback of this process, which involves the periodical cleaning and replacement of membranes to maintain the membrane performance [23].

Ion exchange and adsorption. In these processes, a solid matrix usually suspended in a packed-bed adsorption column is used to adsorb ions or nutrient compounds. Such solids include clays, resins, and zeolites [104] which can be regenerated after their saturation. Metal oxide, zirconium, and red mud could be used as sorbents for P recovery [23], achieving a high P recovery without pH adjusting unlike the struvite precipitation. Nevertheless, the ion competition, decline of the adsorption capacity over time, and fouling of the packed bed are the main shortcomings of ion exchange and adsorption processes [113,114].

Evaporation. This technique consists of the evaporation of the liquid fraction volume of the digestate by applying heat in order to concentrate and recover a nutrient-rich digestate. This evaporation requires a high thermal energy demand, ranging from 300 to 350 kWh t⁻¹ of water evaporated [24]. This high energy demand hinders the industrial implementation of this process, making it feasible only in the case of an excess heat is available, for example, the energy produced from the biogas combustion in a combined heat and power unit.

Freeze concentration. In this process, P compounds are separated from the solution by a selective freezing and crystallisation [115], and high P recoveries of up to 90% can be achieved. In addition, freeze concentration

requires a lower energy consumption (335 kJ g^{-1}) than the evaporation process (2500 kJ g^{-1}) [116]. However, this technique is in an early stage of development, being the main shortcomings related to the crystal formation control and their further separation from the solution.

Electrodialysis. Electrodialysis is also a membrane-based technology for separation applications. In this case, the liquid fraction of the digestate is placed in an electric field where cations move toward the cathode and anions towards the anode. A mono-selective membrane for PO_4^{3-} is located between the electrodes which allows the selective separation of phosphates ions. The concentration of PO_4^{3-} in solution can favour a further precipitation of struvite [117]. However, electrodialysis leads to high energetic costs for the nutrient recovery, and membrane fouling has also a huge impact in the operational costs.

1.3.2 Membrane-assisted crystallisation technology for phosphorus recovery as vivianite.

Despite the struvite crystallisation is one of the main P recovery methods implemented from wastewaters, this approach may not be the optimal solution due to low the value of struvite, overweighing costs, complex operational conditions, and relatively low recovery efficiencies (<50%) [102]. Therefore, developing other economic and efficient approaches for P recovery seems necessary. In this regard, the crystallisation of P in form of vivianite appears as a promising alternative since its attractive economic value as fertiliser due to an easy accessibility, high P content, and slow release [102]. In fact, the market price of vivianite is considerably higher than those of the recovered struvite ($\sim 10000 \text{ € t}^{-1}$ against $\sim 500 \text{ € t}^{-1}$) [102]. In addition, vivianite formation does not require complex operational conditions, basification, and high chemical dosing, unlike struvite crystallisation, which will lower operational costs [102].

The optimal pH value for vivianite formation varies from 6 to 8, similar to the typical wastewater pH. Moreover, the presence of iron in wastewaters

and the further addition of iron salts as flocculants reduce the dosing requirements of external iron salts for vivianite formation. Hence, vivianite is present and spontaneously formed in sewers and wastewater treatment plants since the reaction between ferrous and phosphate ions is favoured, leading to vivianite crystals which is the predominant iron phosphate in wastewater sludge [102]. The high presence of organic matter which release P in phosphate form and reducing conditions which reduce Fe^{3+} to Fe^{2+} , especially in anaerobic environment, promote the vivianite formation [102]. Thus, vivianite has been detected in different sludge, including activated sludge and digestate from anaerobic reactors, in which vivianite represent >50% of the Fe-P fraction, being up to >90% in digestate from anaerobic reactors [102]. The paramagnetic nature of vivianite may ease the further separation of vivianite from sludge [105].

Therefore, **P recovery in vivianite form from wastewaters** can be considered as a competitive approach compared with other P recovery techniques due to all its considerable advantages abovementioned. Although, P recovery as vivianite has caught worldwide attention in recent years, only a few studies have been published. In these studies, different approaches for vivianite formation have been evaluated such as chemical precipitation [118], electrochemical crystallisation [101], and biomineralization [119–121]. For example, a fluidized bed crystalliser has been optimised to achieve a P removal efficiency of 95% by means of the addition of iron (II) salts, showing a great potential for P removal [118]. Despite the optimisation of some of these processes with P removal efficiencies up to 100% [101,105], the control of the crystallisation kinetics remains challenging, leading to a poor downstream crystal quality [122]. The poor mixing level in conventional crystallisers, namely stirred tanks, lead to a high dispersion in the crystal size distribution, with vivianite crystals between 50 and 700 μm [105]. In addition, conventional crystallisers often require large equipment and relatively high operation times which increase costs. Thus, a novel membrane crystallisation process is proposed in this thesis as a promising approach to recover P in vivianite form with a well-controlled crystallisation kinetic leading to vivianite nanoparticles

with a narrow crystal size distribution. Up to our knowledge, the work included in this PhD thesis represents the first attempt in integrating a membrane crystallisation process for the P recovery as vivianite.

Membrane technology have been proposed to enhance the performance and intensify the crystallisation processes because of the intrinsic features of the membrane contactors previously mentioned [123]. Thus, membrane-assisted crystallisation (MAC) has emerged in recent years in an effort to optimise and control the nucleation and crystal growth [61,122,123]. The application of MAC has primarily focused on evaporative crystallisation of high soluble aqueous salts, and antisolvent crystallisation for the production of high value but poorly soluble active pharmaceutical ingredients [124–126]. **Membrane-assisted reactive crystallisation (MARC)** is physically analogous to antisolvent crystallisation, as the membrane regulates the inclusion of liquid reactant into the reaction zone through an overpressure within the pores. Thus, this technique consists in the dosing of a reactant through a porous membrane into the solution that contains the target solute for the crystallisation, generating supersaturation (Figure 1.8). In this method, both sides of the membrane are in liquid phase. However, the mechanisms of crystallisation in the MAC and MARC process are distinct since the reactant is used to raise supersaturation in MARC rather than to reduce the solubility limit in MAC [61]. In spite of the concept has been proposed, MARC has been rarely studied. In principle, the membrane can provide a high level of micromixing [126–129], allowing high supersaturation indices and low induction times [122], since all the surface pores of the membrane could act as mixing points at a microscopic and molecular level [122,126,130]. The membrane has also been proposed to promote heterogeneous nucleation [61,123,131], by reducing the free energy barrier through advancing solute-membrane interactions [122,124], which lower the supersaturation required for starting crystallisation. Hence, the quality of the final crystals could be adjusted by the selection of the appropriate membrane properties and hydraulic conditions [61,132–134]. For example, Jia et al. [130,135] evaluated for first time a MARC integrated with a

stirred tank as a crystalliser for the synthesis of nanoparticles of BaSO_4 and CaCO_3 , and they reported a high influence of the membrane pore size, reactant concentration, transmembrane pressure and temperature in the crystallisation. Thereby, the crystal size distribution and morphology rely on the dominance of the nucleation, crystal growth or agglomeration step at the different operational conditions.

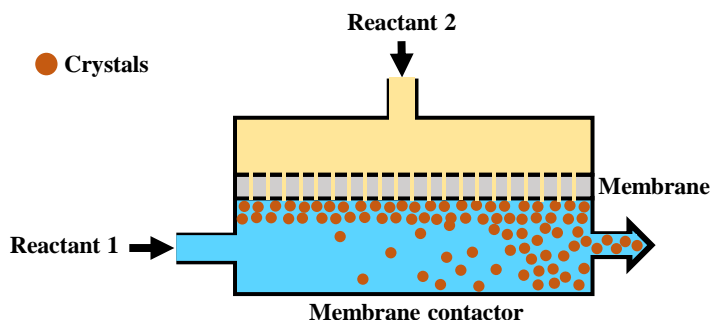


Figure 1.8. Scheme of a membrane-assisted reactive crystallisation process.

Supersaturation is the driving force for nucleation and crystal growth in membrane crystallisation. Sparingly soluble salts such as vivianite require significant supersaturation to develop before induction. Mixing is also important as the increased likelihood for molecular collision can reduce the activation energy requirement for nucleation [136,137]. However, the regulation of supersaturation in existing conventional crystallisers is extremely challenging due to the poorly defined hydrodynamic conditions, leading to an inefficient mixing of reactants [123,124,138]. This can result in overdosing of reactants and inconsistent crystal product quality which can be important for downstream applications. Membrane contactors offer a constant interfacial area to foster the homogeneous regulation of supersaturation by tuning the mass transfer through the membrane [61], while the formation of a well-defined laminar boundary layer also creates a region of elevated supersaturation which is thought to enable the independent control of nucleation from crystal growth in separate compartments [61,123,139]. Additionally, a MARC operation offers the ability to affect crystal features such as shape, size, polymorphic form, and

purity, allowing a high uniformity in the crystal morphology and habit [61]. Consequently, membrane contactors offer greater control over nucleation, and their high interfacial area creates a more scalable and lower cost alternative to conventional equipment for separation and reactions processes [61,140–142]. In this regard, a MARC process could provide a potential feasible technology for the P recovery as vivianite from wastewaters.

MARC process can operate with different membrane module configurations, being the flat-sheet and hollow fibre membrane modules the most common used. These membrane module configurations are similar those exposed in the previous section *1.2.2 Membrane contactors for dissolved methane recovery*, being hydrophilic porous polymeric membranes the most used [61]. Hydrophobic membranes could be also used for the MARC operation in order to avoid the convective flux of reactant A solution toward reactant B solution (Figure 1.8), even though the higher transmembrane pressure needed for dosing of reactant will increase the energy cost. Physico-chemical properties of membrane such as the hydrophobic/hydrophilic nature will determine the crystallisation mechanisms and kinetic [122,123], as well as the potential fouling and scaling that the membrane may suffer in most long-term membrane processes. As an emerging technology, many issues and fundamental investigations on MARC operations need to be addressed before the full implementation at large-scale for a specific application.

1.4 MEMBRANE FUNCTIONALISATION.

Surface functionalisation (also referred as surface modification) of polymeric membranes is a relatively simple and cost-effective approach to tailor and enhance the membrane properties (such as hydrophobicity, hydrophilicity, anti-fouling, biocompatibility, surface unpleasantness, antibacterial and antistatic properties, and conductivity) without altering the internal chemistry and morphological structure of the membrane [143,144]. In general, polymeric materials that have outstanding physical bulk and chemical properties, such as mechanical and high-temperature resistance, lack of the required surface properties for being used in particular applications. In this context, different strategies of surface modification for polymeric membranes have been proposed, e.g. coating, self-assembly, chemical treatment, plasma treatment, and surface graft polymerization [145–147]. Remarkably, the use of organic macromolecules for modifying polymeric membranes applied in water treatment has attracted a wide interest in recent years due to the potential improvement induced in the membrane antiwetting, antifouling, and performance [148].

In this sense, main challenges of gas-liquid and liquid-liquid membrane contactors, i.e., **wetting and fouling phenomena, could be overcome by means of surface functionalisation techniques**, improving their antiwetting and antifouling properties. For the prevention or mitigation of membrane wetting and fouling, surface modification related methods are extensively reported, even though optimisation of operational parameters and selection of the proper liquids and absorbents are also useful methodologies to prevent both phenomena.

According to the Young-Laplace equation (Eq. (1)), the LEP of a membrane can improve at a higher contact angle and smaller pore sizes of the membrane, which infers a higher membrane wetting resistance. In this context, **hydrophobic-based modifications (hydrophobisation) have been usually reported to increase the wetting resistance of the membrane**. Thus, surface fluorination and roughening are the most reported methods for

enhancing hydrophobicity [149]. Fluorinated substances present a strong C-F bond, thereby they exhibit a low polarity and surface energy that could contribute to increase the membrane surface hydrophobicity [150]. The roughening or texturing of the membrane surface leads to the formation of an extremely rough surface at the nanoscale, which also greatly contributes to the hydrophobicity enhancement. Composite and mixed-matrices membranes have also appeared as useful approach to prevent membrane wetting. These membranes are basically composed of a porous support with a surface thin dense layer, which is permeable to selected components and limits the liquid penetration into the membrane. However, these composite membranes may suffer from partial wetting due to the capillary condensation, and the dense layer could involve a non-negligible mass transfer resistance [85,151–153].

In contrast, hydrophobic surfaces can present different effects in the fouling experienced on the membrane, depending on the hydrophobic and hydrophilic nature of the foulants and the tendency to suffer from scaling. Additionally, contradictory results have been reported for the effects of the membrane roughness in the fouling [68]. However, in general terms a hydrophobic and rough membrane surfaces are generally more prone to organic fouling due to its hydrophobic nature and particulate matter [68,154]. Therefore, in case of organic fouling prevention, a hydrophilic-based modification (hydrophilisation) would be needed instead of hydrophobisation. In hydrophilic membranes, a hydration layer is easily form on the membrane surface via hydrogen bonds, which restrains the adsorption of hydrophobic foulants such as protein and polysaccharides due to the higher energy barrier between the membrane surface and the foulant [155]. Different techniques for introducing polar functional groups onto the membrane surface have been successfully implemented for lowering the hydrophobicity. For example, the grafting or coating with amphiphilic copolymers with both hydrophobic and hydrophilic segments, such as polyethylene glycol (PEG) segmented fluoropolymers, are widely experimented [156–158]. These compounds provide

antiadhesion properties due to the non-polar fluorinated segments and fouling resistance to hydrophilic substances due to PEG segments [156].

The incorporation of functional agents at the surface of polymer membranes usually requires a previous activation stage, especially in those membranes that present a high inertness and chemical stability, such as PVDF and PTFE. This activation is usually based on the generation of active sites on the membrane surface by means of the addition of functional groups with a high chemical reactivity or generation of radicals in the backbones of the polymeric chains. Typically, the addition of oxygen-containing functional groups such as hydroxyls (-O-H), peroxides (-O-O-) and carbonyls (-C=O) is conducted to provide active sites for the subsequent grafting [145,159,160]. Furthermore, the activation is also applied for initiating the polymerisation of the functional agents in the chemically induced grafting or for cross-linking purposes.

In the present thesis work, different chemical surface functionalisation methodologies were conducted in PVDF membranes in order to increase their hydrophobicity, and therefore antiwetting properties. A fluoroalkylsilane (FAS) was used as modifying agent, and two different activation techniques prior to the grafting of the FAS were evaluated. First, a wet alkali activation with NaOH was evaluated to increase the antiwetting properties of the membrane. Then, a dry activation by means of a vacuum oxygen plasma treatment was evaluated as a method to obtain superhydrophobic surfaces leading to membranes with antiwetting and even, antifouling properties. The different activation and surface functionalisation methods are described in the next sections.

1.4.1 Classification of membrane activation methodologies.

Activation methods can be divided into **wet and dry methods**. Wet methods involve the use of acid or alkaline solutions for the membrane treatment, and consequently, the whole membrane is impregnated including the bulk. Wet methods require simple equipment, although the generation of hazardous waste and the potential degradation of the inner membrane

structure by the active agent attack are the main disadvantages. On the other hand, dry methods involve the use of the active agents in gas form or energy radiation. Hence, dry methods usually act only at surface level, keeping the internal membrane mechanical properties. However, severe treatment conditions and/or long-time exposure can reach the inner membrane structure, which may negatively affect the membrane integrity due to chain scission, branching or cross-linking reactions and membrane may become brittle. Activation methods could be applied for generating active sites and for initiating the grafting of monomers, but also they could be used to induce hydrophilicity on the membrane surface without further functionalisation.

1.4.1.1 Wet methods.

Wet methods are a type of functionalisation by surface chemical reactions. Thus, wet methods are based on direct chemical reactions between the membrane surface and reactants to endow the membrane with new functional groups. These treatments include hydrolysis, oxidation, addition, and substitution reactions, in which the oxidation is the dominant mean for the formation of oxygen-rich functional groups onto the membrane, inducing hydrophilicity on the membrane surface. Different active reagents can be used relying on the membrane material and the purpose of the treatment. Thus, inorganic acids (HCl, HF, H₂SO₄, etc.), inorganic bases (NaOH, KOH, LiOH, etc.), and organic acids (alkyl phosphoric acid, fluorosilicic acid, etc.) are commonly used [68,145,161–165], and sometimes in combination with other additives such as hydrogen peroxide, alcohols, formaldehyde, permanganates, transition metal nitrates, etc.

Alkali treatment is often used for the activation of PVDF membranes, especially using NaOH solutions [166,167]. This process is known as defluorination since the fluorine atoms from the polymer chains are substituted by hydroxyl groups. These new oxygen-based groups are naturally hydrophilic and can act as active sites for a subsequent grafting. Additionally, the negative

charge ascribed to the hydroxyl group endows the membrane with those negative charges, which can be advantageous for mitigating organic fouling [161]. However, the small added oxygen-containing functional groups usually present a low chemical stability and can be easily oxidised in the air [161].

1.4.1.2 Dry methods.

Different techniques for dry activation can be distinguished based on the application of active reagents in gas form (ozonation, corona and plasma treatment) or an energy radiation without chemicals (UV irradiation and high energy irradiation).

Ozonation. The exposure of polymer membranes to a source of ozone provokes the formation of mainly peroxides groups onto the membrane surface [145]. These new functional groups lower the hydrophobicity of the membrane and can be used for a subsequent grafting. Moreover, the fast decomposition of the peroxide groups, because of their low chemical stability, allows to initiate a radical polymerisation from the surface. Functional layers of poly(methyl methacrylate) and polyacrylamide were grafted by the radical polymerisation on PP and polyurethane (PU) membranes [168,169], respectively. However, ozonation is not capable to activate membranes composed of fluorine-based polymers, such as PTFE and poly(hexafluoropropylene) (PFP) films [168].

Plasma treatment. Plasma treatment is considered as an environmentally friendly, versatile, reproducible and inexpensive method for activating and texturing polymer surfaces [170–172]. This technique consists in a high energy discharge that ionizes the gas near the electrodes and produces a complex gas mixture of excited ions, atoms, molecule fragments, free radicals and so on [167,173]. The plasma discharge is commonly conducted in a controlled environment at low pressure, i.e., inside a vacuum chamber while a certain fresh gas is steadily supplied, and the contaminated gas from inside the chamber is taken out. The effect of the plasma discharge in the treated membrane relies on the type and conditions of the supplied gas, pressure, the

power of the discharge, the duration of the treatment and the configuration of the chamber and electrodes [174,175]. Thus, chemical and/or physical modifications can be induced on the membrane surface [174], since the ion and electron bombardment and interaction with the different reactive species contained in the plasma can produce sputtering of the membrane material (etching), substitution reactions, atom abstraction, free radicals and unsaturated bond in the polymer chains, removal of volatile substances, scission of polymeric chains, and/or cross-linking [173,176]. Such effects only take place at the top-most nanometers of the membrane, keeping unaffected the bulk properties [167,177], even though the mechanism governing the plasma treatment over the membrane surface are not fully understood [145]. Additionally, the use of oxidative gases such as O₂, CO₂ and H₂O for the plasma treatment create a more reactive environment capable to add oxygen-containing functional groups on the membrane such as hydroxyls, peroxides and carbonyls that could act as active sites for subsequent grafting from the backbone [145,159]. However, this hydrophilisation is usually quite labile, losing the effect of the plasma treatment in short times. Thus, a further grafting would be required for a permanent modification [145].

Plasma systems allow the use of several process gases, and therefore, monomers in gas phase can be used during the plasma discharge to induce simultaneously the generation of active sites and the polymerisation. In this regard, the use of tetrafluoromethane (CF₄) gas has gain a lot of interest for the fluorination of membrane surfaces [178–180]. Another great advantage that plasma discharges offer is the modification of materials that are difficult to surface-modify by other chemical treatments, especially PTFE membranes which present a high inertness and chemical stability because of the C-F bonds. Application of argon (Ar) plasma over PTFE films causes oxidation and defluorination of the surface, leading to the formation of mainly peroxides groups, whose decomposition trigger the subsequent polymerisation of monomers such as acrylic acid and acrylamide [181]. Cross-linking and formation of radicals on PTFE chain have been also reported [181].

Corona treatment. Also known as glow discharge treatment, the corona treatment is the most common physical method in industrial application for activating surfaces [182]. The corona treatment consists of the ionisation of the air near a pair of electrodes by the application of a high-frequency discharge at atmospheric pressure, even though this corona discharge can be also conducted in a controlled environment with inert or active gases. The membrane is placed between two asymmetrical electrodes: the high-voltage and the grounded electrode, in which the discharge is generated near the high-voltage one and is spread towards the grounded one. The corona discharge in air generates ozone, oxygen atoms, and oxygen-free radicals which interact with the polymeric membrane surface creating hydroxy, peroxide, carboxyl, carbonyl, and ester groups [182]. This process can also induce the roughening of the surface [182]. Comparing with plasma discharge, the surface treatment is less homogeneous by corona treatments due to the filamentary discharge [182]. Similar to the ozonation, radical polymerisation can be conducted on corona treated membranes as the peroxides decompose [145]. The main advantages of corona treatment are the low investment cost and energy consumption, and the ease of operation [182].

Photochemical treatment. This treatment is based on the tendency of some chemical groups to be excited when they are exposed to a source of light. This excitation may generate reactive radicals which can act as active sites and trigger the polymerisation [183]. The UV irradiation is widely used as photochemical treatment. The exposure of polymeric membranes to UV light can induce chain scission with a subsequent formation of radicals, and carboxylic groups. The generation of oxygen-containing functional groups contribute to lower the hydrophobicity. This treatment is usually conducted at ambient temperature and pressure and needs no specialised equipment, which make UV irradiation an easy and low-cost technique [145].

High-energy radiation. Besides UV irradiation, other sources of high-energy radiation such as electron beam, X-rays and γ -rays can be efficiently applied for membrane activation and initiate the grafting polymerisation. This method is also based on the formation of radicals on the polymer structure [145]. High-energy radiation is a very versatile method since it can operate under different operational conditions which allows a high control over the grafting degree. In addition, high-energy radiation is able to penetrate deeper in the membrane than plasma discharge or UV irradiation, which may be advantageous to produce a more homogeneous modified surface.

1.4.2 Classification of membrane functionalisation methodologies.

Membrane functionalisation methodologies can be classified attending to the type of bond established between the membrane surface and the functionalisation agents. Thus, physical, and chemical treatments can be distinguished, in which physical interactions and covalent bonds are established, respectively. Most typical physical treatments usually lead to coating layers whilst chemical treatments involve the grafting of new molecules into the chemical structure of the membrane surface (Figure 1.9).

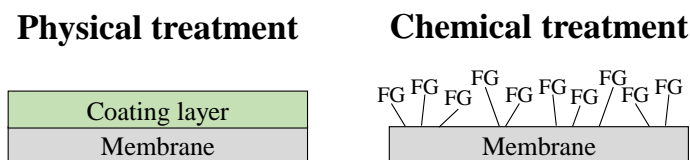


Figure 1.9. Schematic representation of different membrane surface functionalisation methods: a coating as a physical treatment and a grafting of new functional groups (FG) by covalent bonding as chemical treatments.

1.4.2.1 Physical treatments.

The membrane functionalisation by means of physical treatments involves only physical interactions between the functionalisation agents (also referred as modifiers and functional agents or materials) and the membrane surface, such as electrostatic and mechanical interactions, and weak Van der

Waals forces. Thus, the chemical composition of the membrane bulk and surface keeps unchanged, also due to the absence of covalent bonding. Therefore, despite these techniques are very effective and simple to apply, the functionalised surface layer may be easily washed away along the operation or during cleaning processes due to the relatively weak physical interactions [161]. Different physical treatments are discussed below.

Coatings. The principles and applications of coatings techniques are very simple. The functionalisation agents are physically deposited onto the membrane surface by means of one or more of the following mechanisms: i) adsorption and adhesion, in which multiple secondary interactions between functional groups from the functional layer and the solid surface (e.g. electrostatic or van der Waals interactions) determine the binding strength; ii) interpenetration by mixing between the membrane and the functional layer in an interphase located in the membrane surface; and iii) macroscopic entanglement (mechanical interpenetration) of the functional layer and the surface pore structure of the membrane. The nature of the membrane and functional layer surfaces determine the strength of these interactions, in which electrostatically adsorbed modifiers present a more robust adhesion. Coatings can be applied by means of different techniques, which mainly account for dip-coating [184,185], spray-deposition [186,187] [187], cold-plasma treatment [178,188,189], and self-assembly [190,191] [191]. As result, the membrane will be covered by the coating layer, which will define the surface properties of the modified membrane. Thus, a hydrophobic and non-biocompatible membrane can be covered by a hydrophilic and biocompatible layer. Also, a rough surface could be converted to a smoother surface after the coating application. Nevertheless, the resultant coating layers do not usually present sufficient stability since the functional layer absorbed on the membrane may be run away easily [192].

Etching, roughening, sputtering, or texturing. Etching consists in the application of physical treatments to develop scratches by removing material from the surface of a substrate, usually at a nanoscale, which induces a rougher surface (Figure 1.10). The absence of an additional layer on the membrane top makes these modified surfaces more stable under long-term operation compared with coatings. Membrane etching is technologically produced by the removal of material from the surface by the application of a high energy source, such as electron beam [193], deep reactive ion etching [194] or plasma [176]. Etching is widely developed for the texturing of silicon-based semiconductor processing, in order to transfer accurate patterns [195]. Plasma discharge is the most common technique used for increasing the membrane roughness. During the plasma process, inert gases (argon, neon, helium, etc.) are activated and accelerated towards the membrane surface. The high energy content of these species in the formed plasma is transferred to the surface atoms in the membrane via elastic and inelastic collisions. Therefore, surface atoms which acquire enough energy can escape from the membrane. Plasma sputtering has been useful for texturing different polymeric membranes of PDMS [170,196,197], PP [159,198] and PTFE [174] among others.

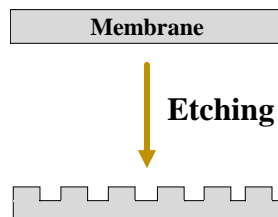


Figure 1.10. Schematic representation of the etching effect on the membrane surface.

Surface patterning. The principles of the surface patterning are the same that those of the etching, in which the scratches are made orderly to create a specific pattern. Generation of various patterns, such as line-, prism-, and pyramid-shape, on the membrane surface has been also reported as an effective method to tailor the flux patterns as well as to prevent membrane fouling by adding turbulence [60,69]. The patterns on the membranes can be created by

the etching techniques in which a mask with the desired pattern is placed on the membrane, thereby, only the surface areas exposed to the high energy source suffer from the material sputtering [176]. Also, the use of molds has been used for patterning by applying heat and pressure [199]. In addition, the nanoimprint lithography technique has been used for patterning polymeric membranes [200,201]. These techniques have been scarcely applied to membrane contactors, so further research would be needed to optimise the patterning of the membrane surfaces.

1.4.2.2 Chemical treatments.

Chemical treatments for membrane functionalisation involve the covalent attachment between the functionalisation agents and the molecular structure of the membrane, unlike the physical treatments. Hence, the functional molecules, chains, brushes, or layers are immobilised on the membrane surface, achieving a greater functional stability along the operation [68,161] since the stronger covalent bonding which avoids the desorption of the functional agents. However, chemical treatments usually are conducted under hazardous conditions since toxic chemicals are sometimes required [68]. Chemical treatments can be classified in chemical coating, grafting and surface chemical reactions.

Chemical coating. Besides physical interactions, coatings can be also attached to the membrane surface via strong chemical bonding. In this sense, the functionalisation solution is composed of the functional agent (polymers, monomers, etc.), co-reactants with low molecular weight (amines, hydroxy compounds, etc.), and additives (cross-linking agents, surfactants, etc.). Thus, in a typical chemical coating process, the membrane is first submerged in this functionalisation solution to form the coating on the surface, and then the membrane is cured to promote addition reactions for the chemical bonding between the functional components and the membrane [202,203]. In this sense, hydrophobic PVDF membranes have been coated by this technique with a

hydrophilic cellulose polymer using aromatic co-reactants like hydroxycompounds, amines and epoxides for enhancing the membrane performance and reducing fouling in ultrafiltration processes [202,203].

Surface grafting. Grafting is a popular and promising method for membrane surface functionalisation through covalent bonding between functional agents and membrane since membrane surface can be modified and tailored to gain specific properties depending on the choice of different functional agents. In some cases, the grafting is conducted without adding significant additional layers, and therefore, avoiding an additional mass transfer resistance, unlike the coating techniques. Two different surface grafting mechanisms can be distinguished: “grafting to” and “grafting from”. “Grafting to” reactions involve the direct immobilisation of preformed molecules on the membrane surface through coupling reactions such as condensation. The main advantage of this method is that the graft molecules are synthesised, purified and characterised before grafting, which allows reproducibility and a precise control of the graft chain structure [161]. Nevertheless, the grafting degree and densities can be limited by a poor diffusion of the graft molecules, which is hindered as the functional layer is built up or active sites on membrane are consumed [204]. In addition, graft molecules may not be sufficiently reactive for coupling reactions [161], so they must contain appropriate reactive groups in their molecular structure [145]. On the other hand, “grafting from” is conducted through a polymer chain growth from the membrane surface towards the outside bulk phase. Hence, one or two different monomers can be used for the polymerisation using different initiation processes (activation) [161]. “Grafting from” techniques offer a greater control over the process than “grafting to” technique [161,205]. Hence, a wide range of grafting densities, chain lengths and structure could be obtained by varying the monomers and their concentrations, initiating means, solvent, temperature, additives, and other reaction conditions [161]. Nonetheless, initiators are needed for the “grafting from”, and controlling the final chain length may be more difficult than in “grafting to” [145], leading to a non-uniform chain length

over the membrane. Based on these two mechanisms, the surface grafting approach can be divided into two different methods: small molecule coupling (“grafting to”) and chemically induced grafting (“grafting from”).

The small molecule coupling process commonly involve the grafting of organic-based compounds with low molecular weight (FASs, propylene oxide ($\text{CH}_3\text{CHCH}_2\text{O}$), propane sultone ($(\text{CH}_2)_3\text{SO}_3$), etc.) which add new chemical moieties (functional groups) on the membrane surface. To graft these molecules, both membrane and functional molecules must present reactive groups. For example, propane sultone has been used for introducing hydrophilic moieties on the surface of polysulfone (PS) membranes [206–208]. Also, silanes and FASs have been extensively used for increasing hydrophobicity of membranes contactors, leading even to superhydrophobic and omniphobic surfaces [209].

The chemically induced grafting process, or polymerisation/copolymerisation, also requires active functional groups such as double bonds in the membrane surface, which will further react with the monomers [209]. Different chemical or physical methods can be used for the initiation/activation of polymerisation reactions, which has been detailed in section 1.4.1 *Classification of membrane activation methodologies*.

Surface chemical reactions. This methodology for chemical treatment is based on direct chemical reactions between the membrane surface and reactants to endow the membrane with new functional groups such as hydroxyls, peroxides and carbonyls. Surface chemical treatments do not involve the grafting of the modifying agents. In this regard, the wet activation methods previously discussed are a kind of surface chemical reactions. These techniques can also induce a roughening of the membrane surface, especially under severe acid and alkali treatments since they can alter the surface microstructure [161,210]. For example, PVDF membranes can experience a significant change in its surface microstructure after the alkali treatment with a NaOH solutions, leading to a higher roughness [166,211].

Once the main methodologies for surface activation and functionalisation of membranes have been exposed, the reader can consult several reviews published in recent years for more information about the different functional agents for a wide range of membrane materials. For example, the review from Rana and Matsuura [68] compiles a lot of functionalisation methodologies focused on membrane fouling prevention. The review from Liu et al. [161] is focused exclusively in the hydrophilisation of PVDF membranes to increase their wettability, and consequently the water flux in pressure-driven membrane separations. Xu et al. [71] published a review in which shows different functionalisation methodologies for enhancing the wetting and fouling resistance of gas-liquid membrane contactors. Miller et al [145] review the available functionalisation techniques of the most common membranes used for water purification. Finally, Nguyen et al. [209] compile a series of functional agents as alternatives to the conventional FASs since the high cost and potential toxicity of these organofluoride compounds.

1.4.3 Challenges in the membrane functionalisation.

The previous discussion has shown that surface functionalisation of membranes has been extensively studied and is a current active area of research. However, the fundamental principles of the functionalisation as well as the relations between the membrane surface and the functional material are not fully developed, which is challenging despite the wide knowledge regarding the different functionalisation strategies [212]. A deeper insight into the **mechanisms** behind the membrane functionalisation will aid in producing membrane with long-lasting functional properties since the poor stability and leachability of the functional layer and grafted molecules are the main concern. Also, there is a lack of studies addressing the **scaling-up of the functionalisation** protocols and testing modified membranes with real process streams. Hence, this limited information makes difficult to determine the applicability of the functionalisation methodologies at industrial scale,

especially for plasma, UV, and high energy radiation treatments which involve some difficulties at large scale [68].

Functionalisation processes are sometimes environmentally unfriendly since the very **hazardous chemicals** involve in the process, especially in the chemical treatments [68]. Thus, significant volumes of hazardous waste containing halogenated, aromatic, and persistent compounds could be generated, representing a potential source of pollution. Regarding the FASs as the most widely used functional agents for enhancing wetting resistance, there is a growing concern related to their toxicity [209]. These substances are precursors of perfluoroalkyl carboxylic acids, which are a threat for environment and human health [213]. Additionally, these substances are usually very expensive which can hinder the full implementation at industrial scale. Therefore, the development of functionalisation methodologies which ensure the fixation of FAS molecules onto the membrane should be addressed. In this regard, a deeper insight into the functionalisation mechanisms and the evaluation of the functional layer stability represents critical issues. In addition, the investigation in the use of biocompatible functional agents and green solvents constitutes another alternative for the sustainable development of the membrane functionalisation technology.

Numerous wetting and fouling prevention techniques for gas-liquid and liquid-liquid membrane contactors are reported in the literature, even though most of them are not valid for the **simultaneous enhancement of antiwetting and antifouling properties**. Therefore, increasing membrane hydrophobicity enhances the wetting resistance, but usually worsen the fouling resistance against organic matter. Thus, the methodologies to enhance the wetting and fouling resistance of the membranes should address both issues simultaneously, which could be very challenging. In this sense, superhydrophobic and omniphobic membranes have recently emerged as quite interesting alternatives for suppressing both wetting and fouling effects at once. However, there is still a limited number of relevant studies.

Superhydrophobic surfaces have attracted great technical interest due to its many potential properties, such as self-cleaning [214,215], or anti-icing [216,217], among other [218]. Superhydrophobicity is related to the decrease of the adhesion/non-stick and roll-off behaviour of droplets on the surface. A surface is considered as superhydrophobic when its static contact angle is higher than 150° and the dynamic contact angle hysteresis is less than 10° , which minimises the solid-liquid contact [219]. In the nature of the lotus leaf (*Nelumbo nucifera*), it can be found that the natural surface has the superhydrophobic characteristic of rolling off. The well-known lotus effect phenomenon is responsible for the self-cleaning properties (dropping behaviour) of these leaves. It has been shown that this behaviour is due to the combination of a surface wax with a very low surface energy and micro-nano layered structure. Nonetheless, superhydrophobicity can be also found in other natural systems, such as the gecko feet, at the rose petals, or at the butterflies' wings [220], and therefore the design challenge is related to the biomimetics' approach.

This thesis aims to contribute to the generation of knowledge in the surface functionalisation insight. In this regard, the hydrophobisation of PVDF membranes was conducted by means of alkali activation and a further grafting of FAS in order to increase the antiwetting properties of the membrane. The functionalised membrane was deeply characterised by means of spectroscopy, microscopy and, also evaluated in operation for the dissolved CH_4 recovery. This membrane operated using a real anaerobic effluent in long-term operation to elucidate the potential benefits of the membrane functionalisation in the membrane performance and fouling. Furthermore, plasma activation was evaluated as a method to obtain superhydrophobic and more stable surfaces in long-term, which could also enhance the fouling resistance of the membrane. The comparison between coated membranes and membranes treated by alkali and plasma activation was conducted to elucidate the most suitable technique for obtaining stable functionalised membranes.

2 OBJECTIVES.

The global aim of this thesis is the evaluation of membrane technology in the valorisation of residual liquid effluents by means of the separation and recovery of two valuable chemicals, CH₄ and P, dissolved in anaerobic effluents and wastewaters. Different membrane contactors, materials, configurations, and operational conditions were tested with synthetic and real anaerobic effluents. Furthermore, different membrane surface functionalisation methodologies were proposed and applied to increase the wetting resistance and useful lifetime of PVDF membranes. This global aim is divided into **three partial objectives**:

- 1) Evaluation of the membrane performance in the dissolved CH₄ recovery from liquid effluents using gas-liquid membrane contactors with a flat-sheet configuration. Different membrane materials (porous, dense, and functionalised) and operational conditions were tested with synthetic water and a real anaerobic effluent in short and long-term operation. The **specific objectives** are to:
 - Validate an experimental setup including the flat-sheet membrane contactor (FM-SS) as a versatile and feasible methodology for studying the membrane performance, stability and fouling of commercial and functionalised membranes at different operational conditions. This objective was fulfilled in *Contribution I*.
 - Analyse the influence of the membrane properties in the dissolved CH₄ removal efficiency by evaluating a dense (PDMS) and different porous (PP-1E, PP-2E, PVDF-Ds) membranes. This objective was fulfilled in *Contribution I*.
 - Maximise the hydrophobicity of the PVDF membranes (PVDF-Ds and PVDF-Dp) by optimising the selected membrane surface modification procedures. Membranes were functionalised with a

FAS, and two different techniques for the membrane activation were tested: a wet treatment with an alkali solution (NaOH), and a dry treatment by means of a vacuum oxygen plasma discharge. This objective was fulfilled in *Contributions II and IV*.

- Characterise the morphology and chemical composition of the modified membranes to investigate how the functionalisation procedure changed the membrane properties. This objective was fulfilled in *Contributions II and IV*.
- Evaluate the stability of the modified membrane properties under long-term operation conditions using synthetic and real anaerobic effluents, and benchmark with non-modified membranes. This objective was fulfilled in *Contributions II and IV*.
- Determine the effect of the functionalisation in the membrane performance to investigate the potential enhancement of the CH₄ removal efficiency. This objective was fulfilled in *Contribution II*.
- Characterise the mechanisms and composition of the fouling developed on the membrane surface when using an anaerobic effluent in order to provide a deep insight into the fouling phenomena for establishing preventive and cleaning strategies. This objective was fulfilled in *Contribution III*.

2) Compare the operation mode, vacuum, sweep gas or both (combination mode), in the performance of the dissolved CH₄ recovery from liquid effluents with a PP HFMC. A synthetic water stream saturated with CH₄ was used as liquid effluent and applied through the lumen side of a commercial HFMC, working in continuous operation. This work corresponds to *Contribution V*. The **specific objectives** are to:

- Study the effect of operational and hydraulic conditions in the CH₄ removal efficiency by varying the liquid velocity, vacuum pressure and sweep gas flow rate in short-term experiments.

- Study the CH₄ mass transfer in the HFMC under the combination mode at different operational and hydraulic conditions.
 - Estimate the energy balance in the experiments to establish the operational conditions that maximised the net energy production by the degasification process.
 - Benchmark the combination mode performance with vacuum and sweep gas modes used independently in terms of CH₄ removal efficiency, mass transfer and net energy production.
- 3) Integration of membrane crystallisation in the recovery of dissolved P in form of vivianite. Thus, a membrane-assisted reactive crystallisation process was proposed for treating a phosphate-rich solution with a continuous dosing of a ferrous ion solution in order to obtain vivianite crystals. A flat-sheet membrane module (FM-MA) was used for this work, which corresponds to *Contribution VI*. The **specific objectives** are to:
- Assess membrane integration for vivianite crystallisation in a batch system using a synthetic liquid effluent rich in phosphates and benchmark with conventional stirred tank crystallisers.
 - Identify how boundary layer conditions can be used to modify supersaturation leading to the advancement in regulation of nucleation kinetics by applying different hydrodynamic conditions inside the membrane module.
 - Study the effects of membrane properties on the nucleation kinetics, through their role in micromixing, and reducing critical surface free energy requirement for nucleation.
 - Develop a framework that can describe how nucleation kinetics can be modified by using a membrane-assisted reactive crystallisation.
 - Determine the size distribution and chemical composition of the solid particles synthesised at the end of the crystallisation process.

3 MATERIALS AND METHODS.

All the experimental setups, methodologies and materials used in this thesis work are detailed in this section. It should be mentioned that all the relevant information shown here can be found in the different contributions derived from this thesis and compiled in the appendix.

3.1 MEMBRANE MODULES AND MATERIALS.

3.1.1 Flat-sheet membranes.

3.1.1.1 Flat-sheet modules.

A total of three different flat-sheet modules (FMs) were used for the different types of tests. These modules are identified as FM-SS, FM-PLA and FM-MA which are detailed below:

- **FM-SS:** corresponds with a circular FM made of stainless steel based on our design (Figure 3.1). The module was designed to be operated at similar liquid velocities to that usually applied in hollow fibre contactors [84], which favoured comparison purposes. A plastic spacer was coupled inside the FM to support the membrane and avoid its deformation or breakage. The main characteristics and dimensions of the FM are shown in Table 3.1. This module was used in CH₄ degasification, long-term stability, and fouling tests of *Contributions I, II, and III*.

Table 3.1. Characteristics of the flat-sheet membrane modules.

Property	FM-SS	FM-PLA	FM-MA
Effective size, cm	Ø 4.7	6.6 × 3.8	10.0 × 4.0
Liquid channel gap, cm	0.1	0.2	0.2
Gas channel gap, cm	0.8	0.1	0.2
Effective contact area, cm ²	17.3	25.0	40.0

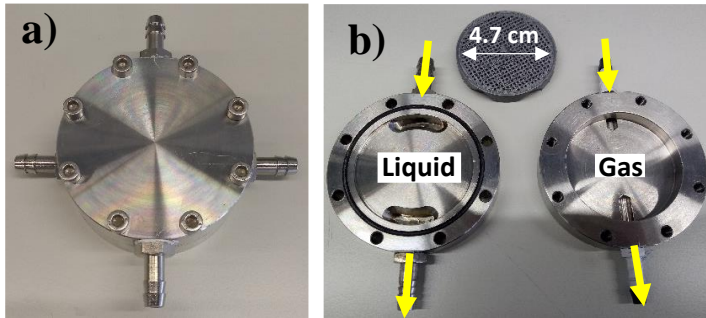


Figure 3.1. a) External and b) internal view of the flat-sheet membrane module FM-SS.

- **FM-PLA:** corresponds with a 3D printed FM build in polylactic acid (PLA) (Figure 3.2) with a plastic spacer. This FM was own-designed for being used in long-term stability tests in *Contribution IV*. The characteristics of the FM-PLA were similar to those of the FM-SS (Table 3.1). Several FM-PLA were built which allowed to conduct several stability tests simultaneously.

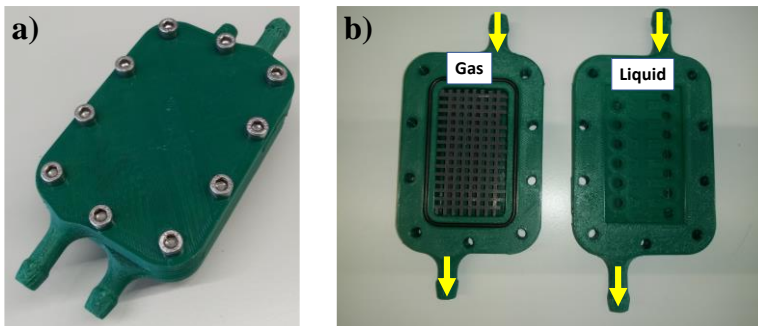


Figure 3.2. a) External and b) internal view of the flat-sheet membrane module FM-PLA.

- **FM-MA:** is a FM build in methacrylate (MA) with a rectangular section and a metallic spacer (Figure 3.3). This module was provided by the School of Water, Energy and Environment (Cranfield University). The characteristics of the FM-MA are listed in Table 3.1. The two sides of FM-MA were identical unlike the previous FMs described. This FM was

designed for being used in crystallisation tests of *Contribution VI* since the transparent walls allowed the visualisation and recording of the membrane surface during operation.

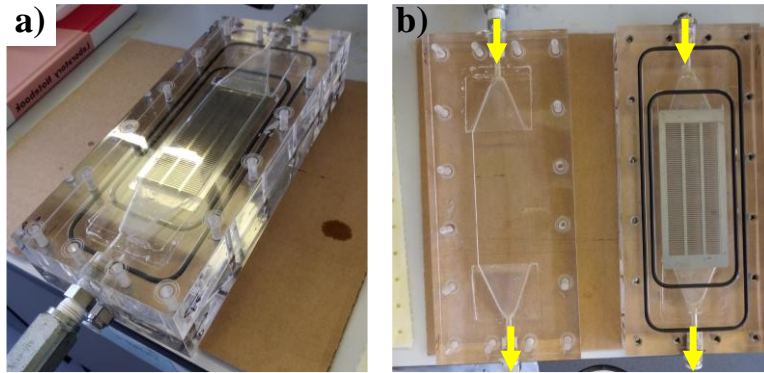


Figure 3.3. a) External and b) internal view of the flat-sheet membrane module FM-MA.

3.1.1.2 *Flat-sheet membrane materials.*

Eight commercial flat-sheet membranes were used and described below, whose properties are listed in Table 3.2:

- **PDMS:** hydrophobic membrane of polydimethylsiloxane (Pervatech, The Netherlands). The PDMS membrane consisted of a support of porous polyester (PET) and polyimide (PI) and a superficial dense layer of PDMS. The thickness of the dense layer (active layer) was 2.5 μm . The CH_4 permeability of PDMS was $7.13 \cdot 10^{-15} \text{ m}^2 \text{ Pa}^{-1} \text{ s}^{-1}$ [221]. This membrane was used in *Contribution I*.
- **PP-1E:** polypropylene membrane unsupported with pore size of $<0.06 \mu\text{m}$ (Accurel® PP-1E, 3M Liqui-Cel, MN, USA). This membrane was used in *Contribution I*.

- **PP-2E:** polypropylene membrane unsupported with pore size of 0.24 μm (Accurel® PP-2EHF, 3M Liqui-Cel, MN, USA). This membrane was used in *Contribution I* and *VI*.
- **PVDF-Ds:** hydrophobic polyvinylidene fluoride membrane supported on PET (Dorsan Filtration S.L., Barcelona, Spain). This membrane was used in *Contribution I, II, III* and *VI*.
- **PVDF-Dp:** hydrophobic unsupported polyvinylidene fluoride membrane (Durapore, Merck KGaA, Darmstadt, Germany). This membrane was used in *Contribution IV* and *VI*.
- **PVDF-St:** hydrophilic polyvinylidene fluoride membrane supported on PET (Trisep UB70, Microdyn-Nadir, Hessen, Germany). This membrane was used in *Contribution VI*.
- **PTFE-1:** hydrophobic unsupported polytetrafluoroethylene membrane with pore size of 1 μm (PF-1F, Cobetter Filtration Equipment Co., Ltd., Hangzhou, China). This membrane was used in *Contribution VI*.
- **PTFE-3:** hydrophobic unsupported polytetrafluoroethylene membrane with pore size of 3 μm (PF-3W, Cobetter Filtration Equipment Co., Ltd., Hangzhou, China). This membrane was used in *Contribution VI*.

Table 3.2. Properties of the flat-sheet membranes: water contact angle (WCA), pore size (r_p), overall thickness (δ), overall porosity (ϵ), and liquid entry pressure (LEP).

Membrane	WCA ^b , °	δ , μm	r_p , μm	ϵ ^b , %	LEP ^b , bar
PDMS	101 ± 1	175 ± 5 ^a	-	-	-
PP-1E	157 ± 3	100 ± 15 ^a	<0.06 ^b	81 ± 5	>5.00
PP-2E	154 ± 3	170 ± 15 ^a	0.24 ^b	79 ± 5	2.67 ± 0.10
PVDF-Ds	103 ± 2	159 ± 2 ^b	0.20 ^a	62 ± 3	2.79 ± 0.28
PVDF-Dp	119 ± 2	125 ^a	0.22 ^a	69 ± 1	2.27 ± 0.02
PVDF-St	36 ± 3	160 – 200 ^a	0.03 ^a	63 ± 2	0.13 ± 0.04
PTFE-1	148 ± 2	88 ± 16 ^b	1.00 ^a	90 ± 5	0.58 ± 0.13
PTFE-3	148 ± 2	66 ± 9 ^b	3.00 ^a	91 ± 5	0.57 ± 0.02

^a Provided by the manufacturer

^b Measured in this work

3.1.2 Hollow fibre membrane contactor.

A commercial polypropylene (PP) HFMC (1x5.5 MiniModule, Liqui-Cel, Membrane GmbH, Germany) with a microporous and hydrophobic structure was selected in *Contribution V* (Figure 3.4), and the main features of the membrane are summarised in Table 3.3. This HFMC was considered to be representative of the membranes in real industrial applications and it had been used in previous studies [63,84].



Figure 3.4. Polypropylene hollow fibre membrane contactor used in this thesis.

Table 3.3. Characteristics of the polypropylene (PP) hollow fibre membrane contactor (provided by the manufacturer).

Property	Value
Structure	Microporous
Shell tube inner diameter, m	0.025
Module length, m	0.176
Number of fibres	2300
Membrane length (l), m	0.1397
Effective membrane length (l_{ef}), m	0.1132
Inner diameter (d_i), μm	220
Outer diameter (d_o), μm	300
Effective internal area (A_i), m^2	0.180
Effective external area (A_e), m^2	0.245
Pore size (r_p), μm	0.04
Porosity (ϵ), %	40
Tortuosity (τ)	1.4
Packing fraction	0.33
Maximum liquid flow rate, L h^{-1}	30
Maximum sweep gas flow rate, L h^{-1}	800

3.2 EXPERIMENTAL SETUPS AND PROCEDURES.

3.2.1 Degasification tests for dissolved methane recovery.

Different membrane contactors and materials were evaluated in the dissolved CH₄ recovery process from liquid streams by means of degasification tests. Two types of liquid streams were used for these tests:

- A **synthetic water stream** of de-ionised water (**DW**) ($<1 \mu\text{S cm}^{-1}$) was used to simulate an anaerobic reactor effluent rich in dissolved CH₄, preventing the potential interferences of soluble or suspended compounds presented in this type of effluents. DW was used in *Contributions I, II, IV* and *V*.
- An **anaerobic reactor effluent (AE)** for evaluating the membrane performance under real operational conditions and conducting fouling tests (detailed in section 3.2.2.2 *Fouling tests*). AE was collected from the anaerobic reactor of the urban Quart-Benager II wastewater treatment plant (Valencia, Spain), filtered with a 10 – 20 μm filter, and store in the fridge ($<4 \text{ }^\circ\text{C}$) before use in the tests. The characteristics of the filtered AE were measured, and they are listed in Table 3.4. AE was used in *Contributions II* and *III*.

Table 3.4. Characteristics of the filtered anaerobic reactor effluent. TSS and VSS: total and volatile suspended solids, respectively; COD: chemical oxygen demand, VFA: volatile fatty acids.

Parameter	Value
pH	7.84
Conductivity, mS cm ⁻¹	8.61
Turbidity, NTU	6.7
Alkalinity, mg CaCO ₃ L ⁻¹	2102
TSS, mg L ⁻¹	75.75
VSS, mg L ⁻¹	67.50
COD, mg O ₂ L ⁻¹	414
VFA, mg CH ₃ COOH L ⁻¹	<5.0 ^a
Proteins, mg L ⁻¹	125.06
Polysaccharides, mg L ⁻¹	79.19
NH ₄ ⁺ , mg L ⁻¹	1500
NO ₃ ⁻ , mg L ⁻¹	2500
NO ₂ ⁻ , mg L ⁻¹	400
PO ₄ ³⁻ , mg L ⁻¹	74
SO ₄ ²⁻ , mg L ⁻¹	<200 ^a
Ca ⁺ , mg L ⁻¹	50
Fe ²⁺ , mg L ⁻¹	0
Live cells, L ⁻¹	3.15 · 10 ¹⁰
Dead cells, L ⁻¹	0.40 · 10 ¹⁰

^a Below detection limit

3.2.1.1 *Degasification tests with a flat-sheet membrane module.*

A lab scale system (Figure 3.5) was assembled including the FM-SS for the non-steady-state degasification tests using a water stream with dissolved CH₄ (D-CH₄) in *Contributions I* and *II*. Initially, circular membrane samples were prepared with a diameter of 6.5 cm. They were clamped into the FM-SS by means of a rubber O-ring for leak-proof-seal, so the membrane edge was fixed. Then, the different elements of the system were fully filled with DW or AE, the gas bubbles were purged, and a leak checking was carried out.

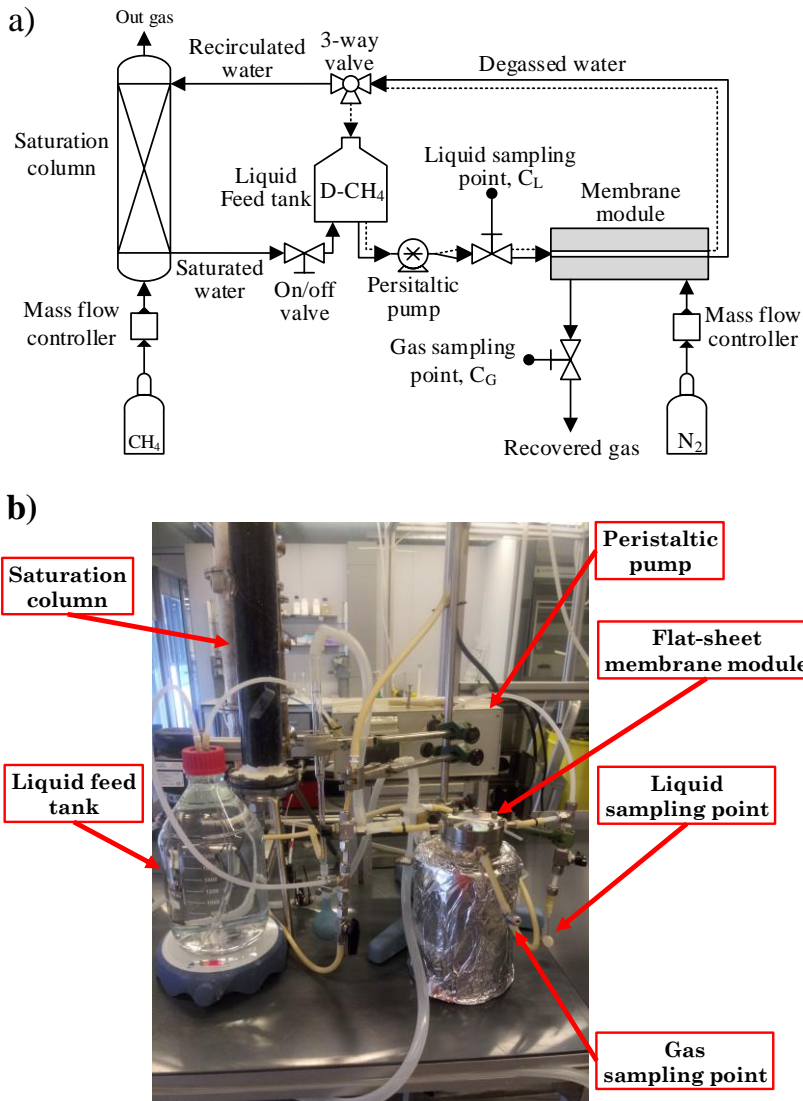


Figure 3.5. a) Scheme and b) picture of the experimental system for dissolved methane recovery from water with a flat-sheet membrane module.

In the first step of a degasification test, the water was saturated in a packed-bed absorption column with 99.5%_v CH₄ (Carbueros Metálicos, Spain) in a counter-current flux at atmospheric pressure in the outlet. The column was built of methacrylate with an inner diameter of 6.5 cm, an effective height of 50.0 cm, and filled with 1" pall rings (Refilltech, Germany). The CH₄ flow rate was fixed at 1000 mL min⁻¹ using a mass flow controller (Bronkhorst Hi-Tec,

The Netherlands) with a manometric pressure in the bottom of the column <0.1 bar. During the saturation step, the on/off valve was kept opened and water was pumped from the bottom of the column to the liquid feed tank in order to fill it with saturated water. The liquid feed tank consisted of a 2 L glass bottle with a magnetic stirrer fixed at 500 rpm. The outlet water from the tank was pumped to the FM-SS, keeping its gas ports closed. Finally, the water from the FM-SS was discharged at the top of the column by means of the 3-way valve connecting the FM-SS with the column. Thus, the water was continuously recirculated in every part of the system with a peristaltic pump (Watson-Marlow Fluid Technology Solutions, UK) operating in a closed loop (continuous line in Figure 3.5a). The liquid flow rate ranged from 21 to 27 L h⁻¹ for the saturation step. The water saturation was conducted at room temperature (23 ± 1 °C). A stable behaviour was observed after 1 h of saturation, reaching a CH₄ concentration of 23.2 ± 3.4 mg L⁻¹, which is comparable to the CH₄ saturation in water, with a value of 23.8 mg L⁻¹ at 23 °C [38]. Similar CH₄ concentration values were reported by other authors for degasification tests with synthetic liquid streams [44,222].

Once the saturation with CH₄ was reached, the saturation column was disconnected from the rest of the system by closing the on/off valve and 3-way valve connecting the FM-SS with the liquid tank (loop in dotted line, Figure 3.5a). Then, water saturated with CH₄ was stored in the liquid feed tank. All experiments were carried out at the sweep gas mode using N₂ to generate a partial pressure gradient for CH₄ and to recover the D-CH₄ in the gas form. For the degasification test, the gas ports of the FM-SS were opened and the N₂ mass flow controller was switched on. The tested N₂ flow rates (Q_{N_2}) ranged from 0.05 to 15.00 L h⁻¹ supplied at atmospheric pressure (gas velocity ranging from 0.0043 to 1.3 cm s⁻¹). No significant pressure drop (<0.01 bar) was observed across the gas side of the FM-SS. The liquid stream was pumped from the liquid feed tank to the FM-SS and then continuously recirculated to the tank operating in a closed loop (dotted line in Figure 3.5a). The liquid flow rates (Q_L) were fixed in values ranging from 3.5 to 40.5 L h⁻¹ (liquid velocity ranging from 2.8 to 32.5

cm s⁻¹). The tests were carried out at room temperature (23 ± 1 °C). The duration of the unsteady experiments was usually 5 h, although some tests were extended up to 22 h.

All the results shown in this work were obtained with liquid and sweep gas flowing in a cross flow configuration, as shown in Figure 3.1a. Remarkably, the experiments carried out with counter-current flow showed no significant differences with respect to the cross flow configuration, showing that the flow configuration was not crucial in these experiments.

Liquid and gas samples were periodically collected to analyse the evolution of the CH₄ concentration and to evaluate the performance of the system. Duplicates of liquid samples were collected at the outlet of the liquid feed tank. Gas samples were taken from the outlet gas port of the FM-SS, which contained the recovered CH₄ (R-CH₄). A total of 3 – 6 samples were taken for liquid and gas in each experiment.

The flat-sheet membranes were reused, and their water contact angle was measured after 2 – 5 experiments. Membranes could suffer from surface alteration, deformation, or degradation. Hence, membrane hydrophobicity was checked with the time of use as an easy and fast technique to determine the membrane operational lifetime.

3.2.1.2 *Degasification tests with a hollow fibre membrane contactor.*

Degasification or demethanisation tests in steady state with the PP HFMC were conducted with a synthetic D-CH₄ water stream. Figure 3.6 shows the flowchart and a picture of the experimental system used to carry out the degassing tests and evaluate the membrane performance in *Contribution V*. Synthetic D-CH₄ water stream was obtained using the former saturation system with the packed-bed absorption column detailed in the previous section. In the experiments with the HFMC, the mean concentration of CH₄ in the liquid effluent was 21.65 ± 0.62 mg L⁻¹, near the CH₄ saturation value. The total

volume of the system was 1.5 L of water, and the total operation time of each experiment was 1 hour, until a steady-state condition was reached.

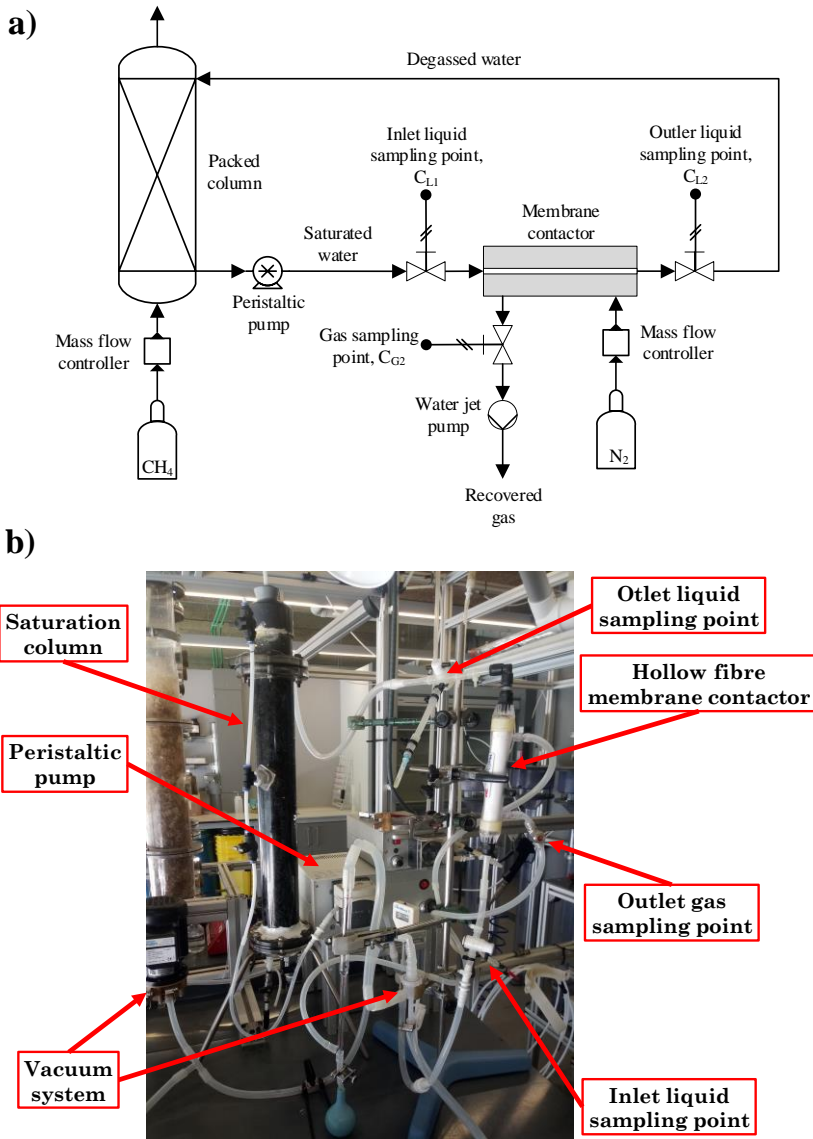


Figure 3.6. a) Flowchart and b) picture of the degassing system with the hollow fibre membrane contactor, including the packed column for the saturation, sweep gas and vacuum generation equipment, and sampling points.

Experiments were carried out at room temperature (23 ± 3 °C). Only synthetic water was used in these tests in order to prevent the potential interference of suspended or soluble compounds in the performance of the system. Long-term performance of the same PP membrane contactor treating the anaerobic effluent of an EGSB reactor was reported in a previous work [84], in which a continuous fouling of the membrane was detected that negatively affected the membrane performance.

In this experimental setup, water operated in a closed loop (Figure 3.6a). Thus, water was recirculated in the system by using a peristaltic pump (Watson-Marlow Fluid Technology Solutions, UK). Initially, the system was filled with DW, and the water inside the column was saturated with a continuous CH₄ flux. In a typical test, after the saturation of the water with CH₄, the system was run without the operation of the HFMC (gas ports were closed) in an initial pre-start period, to ensure that the effluent from the column reached a stable value near saturation. After this, membrane gas ports were opened, and the N₂ mass flow controller and the vacuum system were simultaneously switched on. The desired N₂ flow rate and vacuum pressure stabilized in less than one minute and the degassing process started.

The HFMC was operated in lumen side mode, where experiments were carried out with the liquid flowing in the lumen side and vacuum or sweep gas applied in the shell side, and in counter-current flow. Liquid flow rate (Q_L) was varied between 5.0 and 28.0 L h⁻¹, with a pressure drop ranging from 40 to 60 mbar. N₂ (99.9%_v, Carbueros Metálicos, Spain) was used as sweep gas, with a Q_{N_2} ranging from 0.5 to 1.5 L h⁻¹ adjusted by means of a mass flow controller (Bronkhorst Hi-Tec, The Netherlands). Under these operational conditions, the gas-to-liquid ratio (G/L) varied from 0.012 to 0.302. Vacuum was generated by using a water jet pump (VWR, Spain). The applied vacuum pressure (P_{vac}) ranged from 0 to 480 mbar (manometric pressure was from 0 to -480 mbar) and it was measured with a digital manometer (Kimo MP112, Kimo Instruments, France) at the inlet and outlet of the membrane contactor to ensure stable vacuum along the module.

In HFMC, duplicate liquid samples were collected at the inlet and outlet ports and gas samples were taken from the outlet gas port, which contained the R-CH₄. All samples were collected without the samples being exposed to the atmosphere. The evaluation of the membrane performance was carried out when the steady state performance was reached after 20 – 30 minutes of operation.

3.2.2 Long-term operation tests.

3.2.2.1 Stability tests.

Tests in long-term operation with FMs were carried out to evaluate the stability of the morphological and chemical structures and hydrophobicity of the membranes under a continuous liquid flux of DW in the lab-scale system depicted in Figure 3.7, which was used in *Contributions I, II, and IV*. Initially, the membrane was coupled inside the FM, and a 2-L liquid feed tank was filled with DW. A constant water flux was applied through the liquid side of the FM, in a closed loop, by using a peristaltic pump (Watson-Marlow Fluid Technology Solutions, UK). Modules FM-SS and FM-PLA were used for this type of tests. For comparison purposes and based on previous studies [223,224], the stability tests were operated at the moderate-high liquid flow rate of 21 L h⁻¹ for a period of 160 h or until a constant WCA was achieved. The membrane was extracted periodically to measure its WCA in order to monitor the surface hydrophobicity as a function of time of use [225,226]. The morphology, thickness, chemical composition, surface porosity and thermal stability of the tested membranes were evaluated after the stability test.

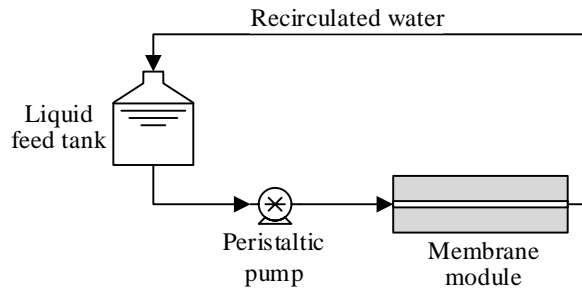


Figure 3.7. Scheme of the experimental system for the long-term stability tests with a flat-sheet membrane module using de-ionised water.

3.2.2.2 *Fouling tests.*

Fouling tests were carried out in order to evaluate: i) the tendency of the membranes to suffer from fouling, ii) evaluate the effects of the membrane functionalisation on the fouling resistance, iii) the effects of the fouling in the membrane performance and useful lifetime, and iv) the fouling mechanisms in hydrophobic PVDF membranes using a real anaerobic effluent. Thus, fouling tests were conducted under long-term operation (>800 h) using the lab-scale system depicted in Figure 3.8, which was used in *Contribution II* and *III*. Initially, a membrane sample was placed inside the flat-sheet module FM-SS and a 2-L liquid feed tank was filled with AE. Then, a constant Q_L of 3.5 L h⁻¹ was pumped in a closed loop through the liquid side of the FM-SS using a peristaltic pump (Watson-Marlow Fluid Technology Solutions, UK) for up to around 830 h. Q_L was set based on our previous works (*Contributions I* and *II*) and to promote the fouling deposition on the membrane because high fluxes increase the turbulence and may favour the fouling mitigation [227]. The anaerobic water inside the system was replaced up to three times with fresh AE to ensure availability of foulants. The membrane was extracted periodically to measure its WCA in order to monitor the surface hydrophobicity with time of use, as reported in the literature [225,226]. Also, the membrane performance for D-CH₄ recovery was evaluated at different times of use using that AE saturated with CH₄ as the liquid stream in degasification tests (see section

3.2.1.1. *Degasification tests with a flat-sheet membrane module*). At the end of the fouling tests, the membranes were extracted from the FM-SS and subjected to different analysis techniques and methodologies (FESEM-EDX, FTIR, staining, and fouling extraction). In addition, liquid samples were taken from the liquid sampling point at different times of operation to measure the concentration of proteins and polysaccharides and the chemical oxygen demand (COD).

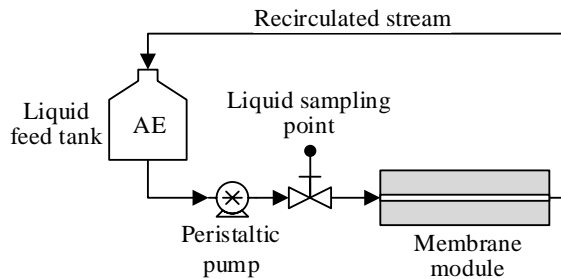


Figure 3.8. Scheme of the experimental setup for the fouling tests with the flat-sheet membrane module FM-SS using an anaerobic reactor effluent (AE).

3.2.3 Membrane-assisted reactive crystallisation tests for phosphorus recovery.

The crystallisation tests for the P recovery in vivianite form by means of a membrane-assisted reactive crystallisation were conducted in the laboratory-scale system shown in Figure 3.9 with the FM-MA module. This experimental setup was used in *Contribution VI* in the facilities of the School of Water, Energy and Environment (Cranfield University). First, a phosphate stock solution at a concentration of 1.1 mM was prepared with sodium phosphate dibasic heptahydrate ($\text{Na}_2\text{HPO}_4 \cdot 7\text{H}_2\text{O}$, $\geq 99\%$, Acros Organics, Geel, Belgium), and a ferrous stock solution (Fe^{2+}) at a concentration of 1.6 mM was prepared with iron (II) chloride tetrahydrate ($\text{FeCl}_2 \cdot 4\text{H}_2\text{O}$, $\geq 99\%$, Sigma-Aldrich, USA). MilliQ water was used as the solvent for both solutions, and flushed with N_2 prior to use in order to remove the residual dissolved oxygen and avoid the oxidation of the ferrous ion [108,109].

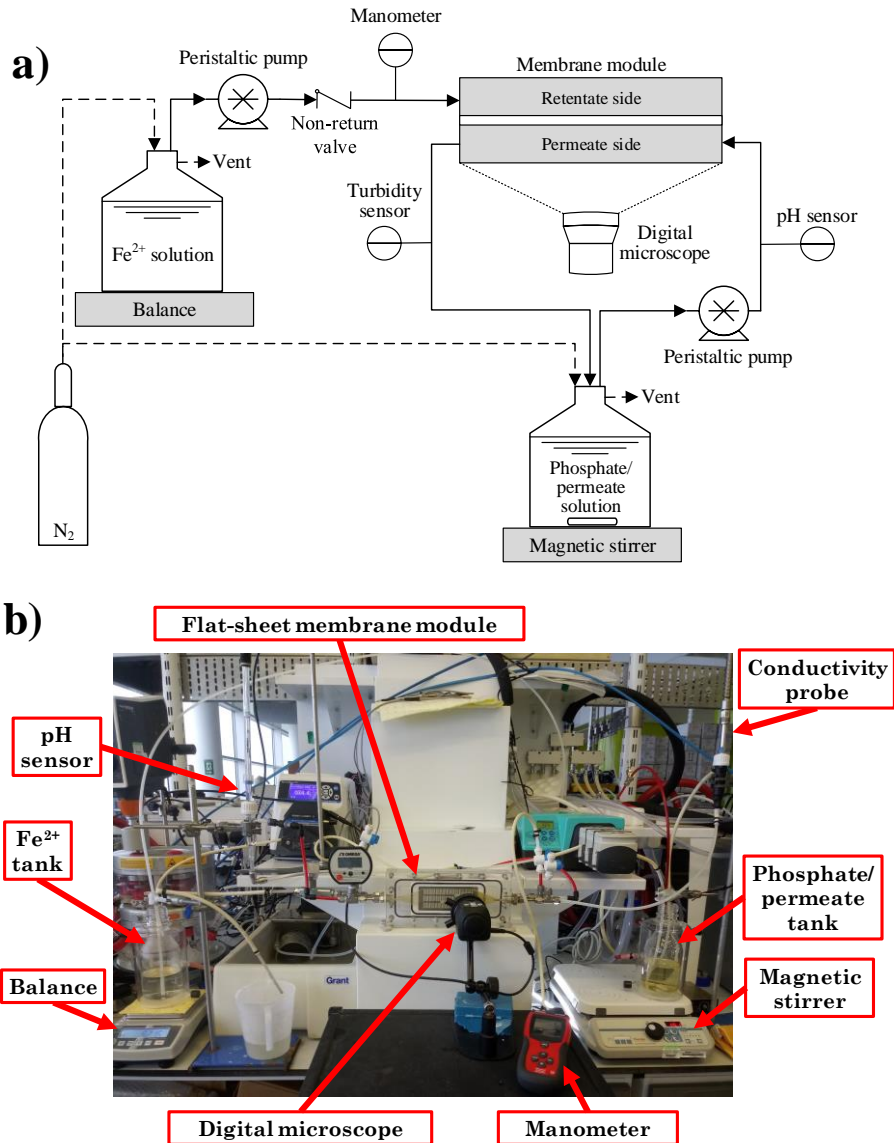


Figure 3.9. a) Flowchart and b) picture of the membrane-assisted reactive crystallisation for the phosphorus recovery in vivianite form.

A 500 mL glass bottle was initially filled with 250 mL of the phosphate stock solution, and it was placed on a magnetic stirrer (Super-nuova multi-place, Thermo Scientific, USA) at 300 rpm with a 2 cm magnetic bar for the continuous agitation of the solution. Also, another 500 mL glass bottle was initially filled with 250 mL of the Fe^{2+} stock solution and placed on a precision balance (PCB, Kern & Sohn GmbH, Balinge, Germany) in order to carry out a

mass balance. The headspace of both bottles was kept under a continuous N₂ flow to avoid the inclusion of oxygen into the solutions during the crystallisation tests [109,118].

A flat-sheet membrane sample was coupled inside the FM-MA, and the permeate and retentate side of the module were connected to the phosphate and Fe²⁺ solutions, respectively. Initially, the phosphate solution was recirculated through the permeate side at a Q_L ranging from 8 to 30 L h⁻¹ using a peristaltic pump (323, Watson-Marlow, UK), which resulted in liquid velocities between 2.8 and 10.4 cm s⁻¹ and Reynold numbers (Re_p) from 105 to 395 inside the FM-MA. The liquid velocity inside the FM-MA was set based on a previous work (*Contribution I*). Also, the Fe²⁺ solution was driven to the retentate side of the FM-MA at a flow rate of 4.66 ± 0.12 mL min⁻¹ with a peristaltic pump (Easy-Load Masterflex L/S, USA), keeping the outlet port of the retentate side closed. The pressure increased in the retentate side of the FM-MA as consequence of the continuous Fe²⁺ solution pumping, and the pressure was monitored with a digital manometer (RS-8890G, RS Group, UK). The beginning of the crystallisation tests (t_c = 0) was set at the time in which the pressure of the retentate side reached the liquid entry pressure (LEP) of the membrane (see Table 3.2 for LEP values of each membrane), thereby, the dosing of Fe²⁺ into the permeate side started. The crystallisation test was stopped after the dosing of 250 mL of Fe²⁺ solution, resulting in an iron-to-phosphorus atomic ratio (Fe/P) of 1.5 in the phosphate/permeate solution. This Fe/P ratio satisfied the stoichiometry of the overall chemical reaction between Fe²⁺ and PO₄³⁻ for the vivianite formation (Eq. (2)), and it has been reported as the optimal value for the vivianite formation [105]. Crystallisation tests were conducted at room temperature without additional control (21.3 ± 1.3 °C), since the temperature has a negligible effect on the solubility product of vivianite in this range of values [108,109].



Vivianite crystallisation was monitored based on the turbidity of the phosphate/permeate solution by means of a twin-axial turbidity probe (InPro 8200/Epoxy/120, Mettler Toledo, UK) mounted at the outlet of the permeate side of the FM-MA, which provides sensitive detection for the onset of nucleation. In addition, the pH of the phosphate/permeate solution was monitored with a pH probe (Easy Ferm PlusPHI Arc 325, Hamilton Company, Switzerland) and maintained at pH 7, at which vivianite formation is believed to dominate the Fe-P reactions [102,109]. The pH was adjusted [109] with the addition of 1M sodium hydroxide (NaOH pellets, Fisher Chemicals, UK) and 1 M hydrochloric acid (HCl, 37%_{wt}, Fisher Scientific, UK) solutions. The total added volume of pH adjusting solutions during a test was always lower than 0.5 mL, thus this extra volume was neglected for the further calculations. In order to analyse the scaling/deposition of solid particles onto the membrane, the membrane surface facing the permeate side was recorded throughout the crystallisation test using a digital microscope (Kopa, Ostec, Guangzhou, China). Each crystallisation test was conducted in duplicate at the different experimental conditions tested in this work.

Immediately after the end of the test, a 5 mL sample of the phosphate/permeate solution was filtered in a vacuum filtration system using mixed cellulose esters filters with a pore size of 0.025 μm (MF-Millipore®, Merck KGaA, Darmstadt, Germany) for the collection of crystals. After the filtration, the filters were dried under a N_2 flow of 0.1 L min^{-1} overnight, and then, the obtained crystals were stored in zip bags inside a desiccator until further analysis.

3.3 MEMBRANE FUNCTIONALISATION METHODOLOGIES.

The tailoring of the membrane surface hydrophobicity and its effects on the membrane performance in degasification, long-term and crystallisation tests were evaluated by means of different surface functionalisation protocols. Only hydrophobic PVDF membranes were tested. The surface functionalisation of the membranes was carried out in a two-step procedure as depicted in Figure 3.10: (1) activation, and (2) functionalisation. Firstly, the original hydrophobic PVDF membrane was activated to promote the formation of oxygen-rich functional groups onto the membrane such as hydroxyls (-OH), which led to the reduction of WCA. Afterwards, modifying agents reacted with those oxygen-rich functional groups promoting the grafting of that modifiers (functionalisation step). The different activation protocols and the functionalisation step are deeply detailed in the next sections.

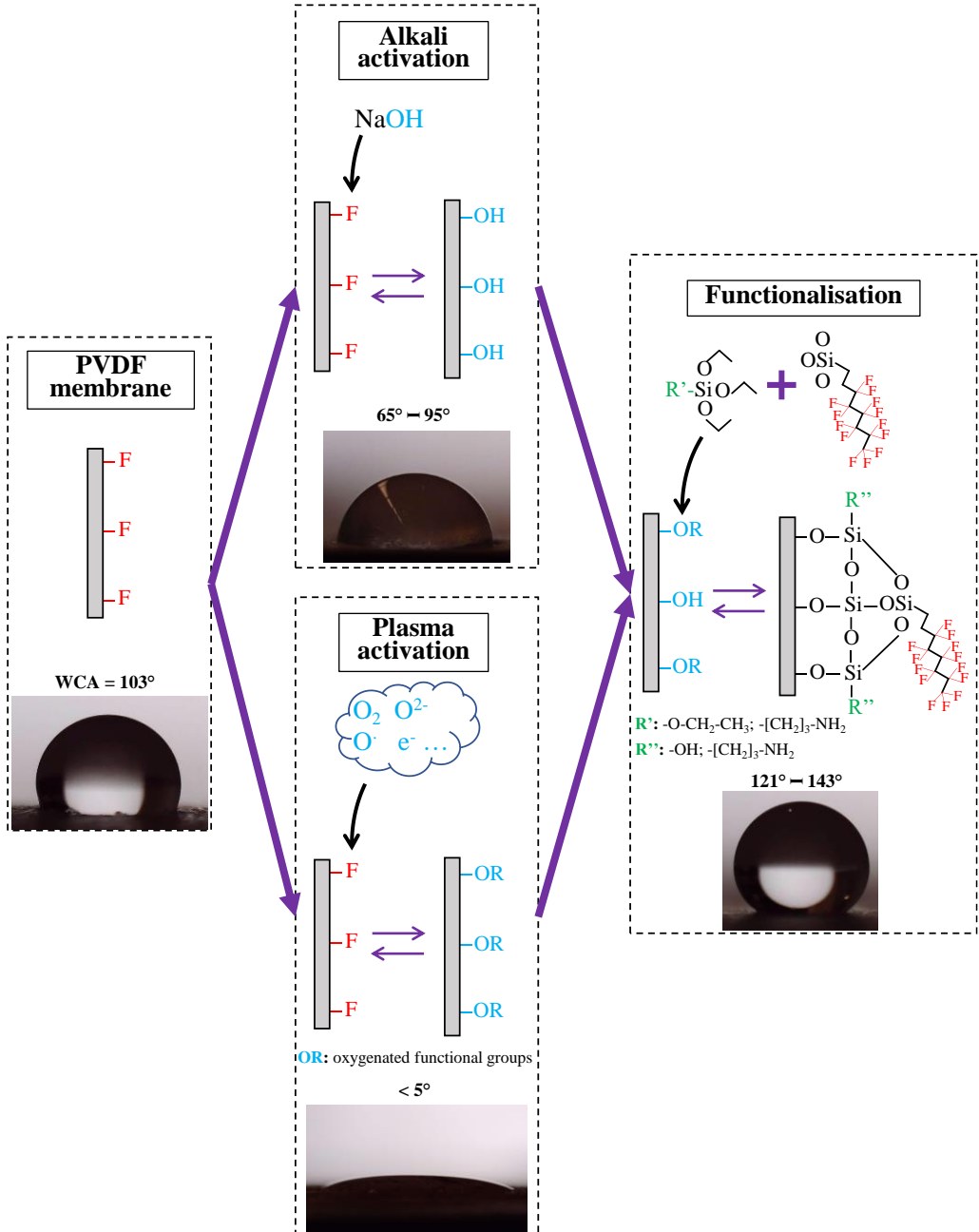


Figure 3.10. Scheme of the functionalisation protocol for the PVDF membranes.

3.3.1 Membrane activation methods.

An activation step prior to the grafting of the modifying agents is frequently needed in membranes that present a high inertness and chemical stability, such as PVDF [228,229]. In this thesis, a wet alkali treatment with NaOH and a dry oxygen plasma treatment were evaluated as activation techniques.

3.3.1.1 Membrane activation with alkali solution.

In the alkali activation conducted in *Contribution II* and *III*, the PVDF was hydroxylated with 2.5 mL of NaOH solution per cm² of membrane in an orbital shaker at 150 rpm. According to preliminary experiments, the temperature and time of the activation step were fixed at 50 °C and 1 h, respectively, and the NaOH concentration (NaOH%_{w/v}) ranged from 1 to 6%, as suitable for the purposes of activation. Afterwards, the activated membranes were immediately rinsed with milliQ water to stop the reaction and the excess of water on the sample surface gently removed. In the hydroxylation reaction (Figure 3.11), the OH⁻ ions replaced the F atoms from the PVDF chains, which promoted a decrease in its hydrophobicity, mainly by a defluorination mechanism [166]. Secondary reactions could occur involving the formation of carbonyl (C=O) when severe conditions of the activation step, i.e. high temperature, time and NaOH concentration, are used or when a not homogeneous NaOH attack is produced [166]. C-O-F groups can also be formed since the total defluorination does not occur [166].

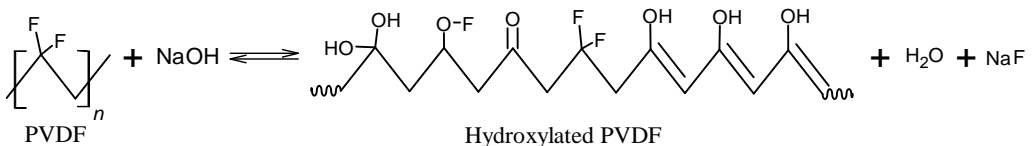


Figure 3.11. Hydroxylation reaction of the poly(vinylidene fluoride) (PVDF) with sodium hydroxide in the activation step.

3.3.1.2 *Membrane activation with oxygen plasma treatment.*

A dry technique for activating the surface PVDF membranes was also evaluated in *Contribution IV*. Thus, an oxygen plasma treatment was conducted and evaluated with a vacuum plasma system (Femto, Diener electronic GmbH & Co., Germany) equipped with a generator frequency of 40 kHz and a stainless-steel vacuum chamber of 100 mm diameter and 278 mm length, belonging to the Technological Institute of Plastic AIMPLAS (Valencia, Spain). Initially, each membrane sample was placed in the middle of the chamber with the target surface upward, and O₂ was flowed at 1.5 sccm during the plasma treatment, maintaining a constant absolute pressure of 0.4 mbar inside the chamber. The power and time of the plasma treatment ranged from 3 to 17 W and 3 to 17 min, respectively. The plasma treated membranes were immediately immersed in the functionalisation solution as detailed in the next section.

3.3.2 *Membrane functionalisation protocol.*

In order to graft additional fluoride chains onto the PVDF in the functionalisation step, the fluoroalkylsilane (FAS) 1H,1H,2H,2H-perfluorooctyltriethoxysilane (Dynasylan® F8261, Evonik GmbH, Germany) was used as the modifying agent, and two different silica precursors (SiP), tetraethyl orthosilicate (TEOS, ≥99%, Sigma-Aldrich, USA) and 3-(triethoxysilyl)-propylamine (APTES, Sigma-Aldrich, USA), were evaluated. A mixture of 2-propanol (IPA; HPLC grade, VWR Chemicals) and milliQ water in a molar ratio of 57:1 was used as solvent (labelled as IPA/H₂O). For the preparation of the functionalisation solution (FS), an initial mixture of the FAS and SiP was prepared and then the IPA/H₂O solvent added dropwise [225]. The presence of water in the FS was needed in order to hydrolyse the SiP, as reported by several authors [225,226,230,231]. Once the solvent was fully added, the pH of the FS was adjusted with concentrated HCl (37%_{wt}, reagent grade, VWR Chemicals) to a value of 2 – 3 in order to promote the hydrolysis of the TEOS and APTES [225,230]. Finally, the FS remained under magnetic

stirring at 200 rpm at room temperature for 24 h in order to achieve the complete hydrolysis of the SiP. The mixture of FAS and SiP in the FS was labelled 'FSi_x', where 'F' denotes the fluorine modifying agent and 'Si_x' the silica precursor (with 'x' = T or A for TEOS and APTES, respectively). The volumetric ratio of the modifying agent in the FSi_x mixture (FSi_x ratio = FAS volume/FSi_x mixture volume) ranged from 0.17 to 0.94, and the FSi_x volumetric percentage in the solvent (FSi_x%_v) ranged from 0.8 to 9.2%. The ranges of both parameters were set from preliminary experiments. In the functionalisation step, the membrane samples were immersed in 2 mL of the FS per cm² of the membrane for 1 h at 100 rpm and room temperature and then rinsed with IPA. Finally, the membrane was cured in an oven at 60 °C overnight on a Petri dish. Functionalisation and curing times were also established based on the preliminary experiments. The reactions involved in the functionalisation are detailed in the next section.

For comparison purposes, coated membranes were prepared without activation in *Contribution IV*. Through the dip-coating technique, membranes were immersed in the functionalisation solution and cured in an oven at 60 °C overnight without any activation treatment. Therefore, no chemical bonding between membranes and FAS or SiP was anticipated due to the high inertness of PVDF.

3.3.2.1 Chemical reactions of the functionalisation step.

For the functionalisation step, the ethoxy groups of the SiP were hydrolysed to silanols during the preparation of the functionalisation solution [225,226,230,231] (Figure 3.12). The silanol molecules coordinate with the hydroxyl group on the activated PVDF, grafting the silica precursor [30,34]. In addition, silanols are chemically reactive and they can condensate forming oxane bonds between Si atoms [167,232,233]. Thus, the proposed chemical reaction and structure is shown in Figure 3.13.

Finally, the FAS is grafted on the membrane by coordinating with the silanols groups [231], as proposed in Figure 3.14. The secondary reactions involved in the activation step, the residual fluorine, and the non-homogeneous condensation of the silanols can lead to a heterogeneous surface.

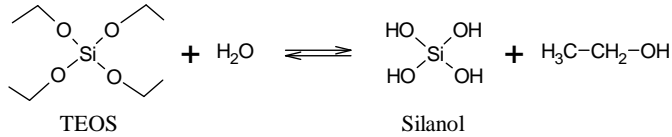


Figure 3.12. Example of the hydrolysis reaction of the tetraethyl orthosilicate (TEOS).

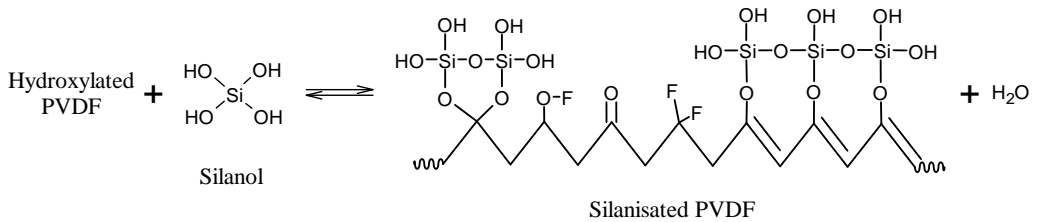


Figure 3.13. Condensation reaction of the silanols from TEOS on the hydroxylated PVDF in the functionalisation step.

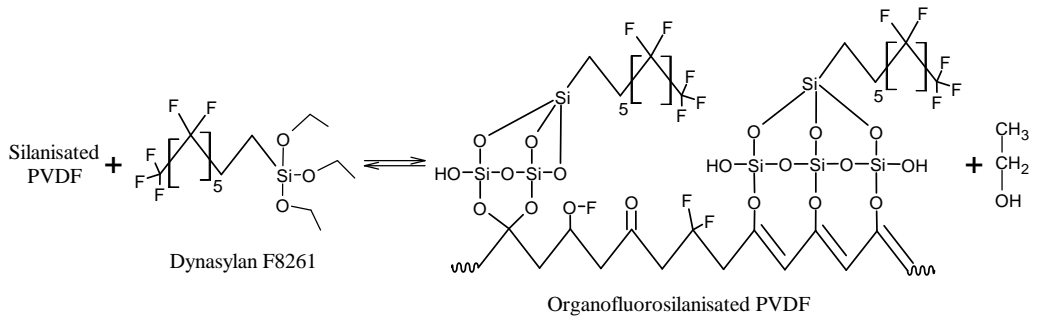


Figure 3.14. Condensation reaction of the 1H,1H,2H,2H-perfluorooctyltriethoxysilane (Dynasylan F8261®) onto the membrane surface in the functionalisation step.

3.4 ANALYTICAL TECHNIQUES AND CALCULATION METHODS.

3.4.1 Evaluation of the membrane performance in degasification tests.

The performance of the D-CH₄ recovery process was evaluated by means of the removal efficiency of D-CH₄ (RE, %) and the CH₄ flux (J_{CH_4} , g s⁻¹ m⁻²) through the membrane which are defined as follows:

$$\text{For degasification tests with HFMC: RE} = \frac{C_{L1} - C_{L2}}{C_{L1}} \cdot 100 \quad (3)$$

$$\text{For degasification tests with FM:} \left\{ \begin{array}{l} \text{RE} = \frac{C_{L0} - C_{L,t_d}}{C_{L0}} \cdot 100 \quad (4) \\ J_{CH_4} = \frac{V_T \cdot 10}{A \cdot 10000} \cdot \frac{dC_L}{dt_d} \quad (5) \end{array} \right.$$

where C_{L1} and C_{L2} (mg L⁻¹) are the D-CH₄ concentration in the inlet and outlet liquid from the HFMC, respectively, C_{L0} and C_{L,t_d} (mg L⁻¹) are the D-CH₄ concentrations in the liquid feed tank at initial time ($t_d = 0$) and at time on stream (t_d) of the degassing test with the FM, respectively, V_T is the total liquid volume in the system (2.35 L for the experimental setup using the FM), and A (m²) is the effective membrane area. The variation in liquid volume flow rate was assumed to be negligible for the application of equations (3) – (5).

3.4.1.1 Analysis of dissolved methane in liquid samples.

The liquid samples collected from degasification tests using the PP HFMC in *Contribution V* were analysed by using the head-space method described elsewhere [40,42,63]. 50 mL of liquid samples were collected and injected in sealed vials of 125 mL, prefilled with air. These vials were kept in an orbital shaker at 150 rpm and 25 °C for 1.5 hours (to ensure gas-liquid

equilibrium). After this, 0.5 mL of the head-space gas was injected into a gas chromatograph (GC 7820A, Agilent Technologies S.L., Spain) equipped with Agilent HP-PLOT/U and Agilent HP-MOLESIEVE and a thermal conductivity detector.

In studies with the FM-SS (*Contributions I and II*), the head-space method was optimised to minimise the volume of sample and equilibration time needed for the analysis. As result of this optimisation, 5 mL of the liquid samples were collected in sealed vials of 16.0 mL prefilled with air for the CH₄ concentration determination. These vials were placed in an orbital shaker at 200 rpm and 25 °C for 30 min. After this, 0.5 mL of the head-space gas was injected into the former gas chromatograph.

In order to determine the CH₄ concentration in the liquid sample, it was necessary to apply Henry's Law:

$$H^{cp} = \frac{C_{L,eq}}{P^{p,eq} \cdot M_{CH_4}} \quad (6)$$

where $C_{L,eq}$ ($\text{mg L}^{-1} \equiv \text{g m}^{-3}$) is the methane concentration in the liquid in equilibrium with the head-space gas, $P^{p,eq}$ (Pa) is the partial pressure of the CH₄ in the head-space in equilibrium with the liquid phase, M_{CH_4} is the molecular weight of the CH₄ (16 g mol^{-1}) and H^{cp} is the Henry's Law constant, expressed in $\text{mol m}^{-3} \text{ Pa}^{-1}$. The value of H^{cp} is $1.4 \cdot 10^{-5} \text{ mol m}^{-3} \text{ Pa}^{-1}$ at 25 °C [38]. So, the CH₄ concentration in the original liquid sample was determined from:

$$C_L = \frac{C_{G,eq} \cdot V_G + C_{L,eq} \cdot V_L}{V_L} \quad (7)$$

where C_L and $C_{G,eq}$ (mg L^{-1}) is the CH₄ concentration in the original sample and in the head-space of the analysis vials, respectively, and V_G and V_L (L) is the gas and liquid volume inside the analysis vials, respectively.

3.4.1.2 Analysis of methane in the recovered gas stream.

Gas samples of the recovered gas were taken from the sampling points located at the outlet of the membrane modules during the degasification tests. For the determination of CH₄ concentration in the recovered gas (C_{G2}, mg L⁻¹), 0.5 mL were directly taken from the sampling points by means of a gas chromatography syringe, and then the sample were injected into the gas chromatograph described in section 3.4.1.1 *Analysis of dissolved methane in liquid samples*. The CH₄ content in the recovered gas (y_{CH₄}, %_v) was also calculated by the following equation:

$$y_{\text{CH}_4} = \frac{C_{\text{G2}}}{\rho_{\text{CH}_4}} \cdot 100 \quad (8)$$

where ρ_{CH_4} (mg L⁻¹) is the CH₄ density.

Moisture content of the recovered gas was measured using a hygrometer (model HygroPalm-HP21, Rotronic Instruments, Switzerland) mounted in-line. The moisture of the recovered gas was usually >90% at the most severe condition tested, i.e., when vacuum and high N₂ flow rates were applied as driving force. That moisture content corresponded to a H₂O content always lower than 3% at standard conditions, therefore, the presence of water in the recovered gas could be neglected for further calculations.

3.4.1.3 Mass transfer evaluation in the flat-sheet membrane contactor.

The CH₄ mass transfer of the separation process using the FM-SS in non-steady-state was evaluated in the liquid-membrane-gas system (*Contribution I*). From the mass balance and Fick's First Law, the experimental overall mass transfer coefficient (K^{FM}_{L,exp}, m s⁻¹) based on the liquid phase was calculated with the following expression [234,235]:

$$K_{\text{L,exp}}^{\text{FM}} = \frac{M_{\text{T}}}{A \cdot \rho_{\text{L}} \cdot t_{\text{d}}} \ln \left(\frac{C_{\text{L},0} - C_{\text{L},0}^*}{C_{\text{L},t_{\text{d}}} - C_{\text{L},t_{\text{d}}}^*} \right) \quad (9)$$

where M_T is the total liquid mass in the system (2.35 kg), A is the effective membrane area (0.00173 m²), ρ_L (kg m⁻³) is the liquid density, t_d (s) is the time on stream, and $C_{L,0}^*$ and C_{L,t_d}^* (mg L⁻¹) are the CH₄ concentrations in the liquid in equilibrium with the CH₄ content in the outlet gas (C_{G2} , mg L⁻¹) at initial time ($t_d = 0$) and time t_d , respectively, calculated from Henry's Law ($C_L^* = C_{G2}/H$, H being the dimensionless Henry's constant with a value of 29.55 at 25 °C [38]). Some assumptions were taken for using equation (9): (i) a constant membrane permeability coefficient, and (ii) M_T was assumed constant due to the small quantity of CH₄ recovered (<52 mg) [234].

The overall mass transfer coefficient based on the liquid phase can be estimated using the resistance in series model for compounds transferring from the bulk liquid phase to the bulk gas phase ($K_{L,est}^{FM}$, m s⁻¹) for a flat-sheet membrane module [236]:

$$R_{ov}^{FM} = \frac{1}{K_{L,est}^{FM}} = \frac{1}{k_L^{FM}} + \frac{1}{H \cdot k_m} + \frac{1}{k_G^{FM}} = R_L^{FM} + R_m^{FM} + R_G^{FM} \quad (10)$$

where k_L^{FM} , k_m , and k_G^{FM} (m s⁻¹) are the individual mass transfer coefficients of the liquid phase, membrane, and gas phase in the FM-SS, respectively, R_{ov}^{FM} (s m⁻¹) is the overall mass transfer resistance in the FM-SS, and R_L^{FM} , R_m , and R_G^{FM} (s m⁻¹) are the individual mass transfer resistances of the liquid phase, membrane, and gas phase in the FM-SS, respectively. The liquid mass transfer coefficient has been estimated from the following empirical equation obtained for a FM with similar characteristics [236]:

$$Sh_L = \frac{k_L^{FM} \cdot d_{hL}}{D_{L,CH_4}} = 0.823 \cdot Re_L^{0.39} \cdot Sc_L^{1/3} \cdot \left(\frac{d_{hL}}{l_{ef}}\right)^{0.075} \quad (11)$$

where Sh_L , Re_L , and Sc_L are the Sherwood, Reynolds, and Schmidt numbers of the liquid phase, respectively, d_{hL} (m) is the hydraulic diameter of the liquid side of the module, D_{L,CH_4} is the molecular diffusion coefficient of CH₄ in the liquid phase (1.76 · 10⁻⁹ m² s⁻¹ at 25 °C and 1 bar [237]), and l_{ef} is the effective length of the module (m).

The gas mass transfer coefficient was also estimated with empirical equations obtained for similar flat-sheet membrane modules [238,239]:

$$k_G^{FM} = \frac{Sh_G \cdot D_{G,CH_4}}{d_{hG}} \quad (12)$$

$$Sh_G = (Sh_0^4 + Sh_\infty^4)^{1/4} \quad (13)$$

$$Sh_0 = 2.52 \quad (14)$$

$$Sh_\infty = 0.808 \cdot Re_G^{0.405} \cdot Sc_G^{1/3} \quad (15)$$

where Sh_G , Re_G , and Sc_G are the Sherwood, Reynold, and Schmidt numbers of the gas phase, respectively, D_{G,CH_4} ($m^2 s^{-1}$) is the molecular diffusion coefficient of CH_4 in the gas phase, d_{hG} is the hydraulic diameter of the gas side (m), and Sh_0 and Sh_∞ are the limiting Sherwood numbers. In the gas side of the module, only N_2 as the sweep gas was applied; thus, molecular diffusion of CH_4 in the gas can be estimated as follows [240]:

$$D_{G,CH_4} = \frac{0.01013 \cdot T^{1.75} \cdot \left(\frac{1}{M_{N_2}} + \frac{1}{M_{CH_4}} \right)^{1/2}}{P \cdot \left[(\sum v)_{N_2}^{1/3} + (\sum v)_{CH_4}^{1/3} \right]^2} \quad (16)$$

where T (K) is the temperature of the test, M ($g mol^{-1}$) is the molar mass, P (Pa) is the pressure in the gas phase, and $(\sum v)$ is the especial atomic diffusion volume (17.90 for N_2 and 24.42 for CH_4 [241]).

The membrane mass transfer coefficient can be estimated for both porous and dense membranes. For porous structures, it was estimated based on the diffusion of the solutes through the pores without convection as follows [238,242]:

$$k_{m,porous} = \frac{D_{G,eff} \cdot \left(\frac{\epsilon}{100} \right)}{\tau \cdot \delta} \quad (17)$$

where ε (%), τ , and δ (m) are the porosity, tortuosity, and thickness of the membrane or layer and $D_{G,eff}$ is the effective diffusion of the transferred species in the gas phase inside the pores, which was estimated as follows [243]:

$$\frac{1}{D_{G,eff}} = \frac{1}{D_{G,CH_4}} + \frac{1}{D_{G,Kn}} \quad (18)$$

where $D_{G,Kn}$ ($m^2 s^{-1}$) is the Knudsen diffusion coefficient of CH_4 through the pores, which can be calculated by equation (19) [244]:

$$D_{G,Kn} = 48.5 \cdot r_p \cdot \left(\frac{T}{M_{CH_4}} \right)^{1/2} \quad (19)$$

where r_p (m) is the pore diameter (equivalent to the membrane pore size). The pores were assumed to be completely filled only with the sweep gas, N_2 .

For the dense membrane, the following equation can be used to estimate the membrane mass transfer coefficient [153]:

$$k_{m,dense} = \frac{P_{m,CH_4} \cdot R \cdot T}{\delta \cdot V_{m,CH_4}} \quad (20)$$

where P_{m,CH_4} is the permeability of CH_4 through the dense membrane ($7.1256 \cdot 10^{-15} m^2 Pa^{-1} s^{-1}$ at $25^\circ C$ for PDMS [221]), R is the ideal gas constant ($8.314 m^3 Pa mol^{-1} K^{-1}$), and V_{m,CH_4} ($m^3 mol^{-1}$) is the molar volume of CH_4 .

The membranes can be composed of more than one layer of different materials, as the PDMS and PVFD tested in this study. The total membrane mass transfer coefficient can be estimated by means of the resistance in series model with equation (21) [238].

$$\frac{1}{k_m} = \sum_n \frac{1}{k_{m,layer n}} \quad (21)$$

3.4.1.4 Mass transfer evaluation in the hollow fibre membrane contactor.

Analogous to the mass transfer analysis conducted in the FM-SS, the mass transfer of the separation process using the PP HFMC in steady state was also evaluated in *Contribution V*. For this purpose, the overall experimental mass transfer coefficient using the PP HFMC ($K_{L,\text{exp}}^{\text{HF}}$, m s^{-1}) was calculated from the following differential mass balance applied to the liquid phase [245]:

$$Q_l \cdot \frac{dC}{dA} = -K_{L,\text{exp}}^{\text{HF}} \cdot (\Delta C_{\text{lm}}) \quad (22)$$

The integration resulting from equation (22) is as follows [246]:

$$K_{L,\text{exp}}^{\text{HF}} = \frac{Q_l}{A_L} \frac{C_{L2} - C_{L1}}{\Delta C_{\text{lm}}} \quad (23)$$

ΔC_{lm} is defined as [246]:

$$\Delta C_{\text{lm}} = \frac{(C_{L2}^* - C_{L2}) - (C_{L1}^* - C_{L1})}{\ln \left(\frac{C_{L2}^* - C_{L2}}{C_{L1}^* - C_{L1}} \right)} \quad (24)$$

where A_L (m^2) is the interfacial area in contact with the liquid phase, Q_l ($\text{m}^3 \text{s}^{-1}$) is the liquid flow rate and C_{L1}^* and C_{L2}^* (mg L^{-1}) are the CH_4 concentration in the liquid in equilibrium with the CH_4 content in the outlet gas (C_{G2} , mg L^{-1}) and inlet gas ($C_{G1} = 0 \text{ mg L}^{-1}$), respectively, calculated from Henry's Law ($C_L^* = C_G/H$). With the liquid flowing in lumen side mode, A_L is the membrane's internal area (A_i). The mass transfer can also be evaluated through the overall experimental mass transfer resistance ($R_{\text{ov,exp}}^{\text{HF}}$, s m^{-3}):

$$R_{\text{ov,exp}}^{\text{HF}} = \frac{1}{K_{L,\text{exp}}^{\text{HF}} \cdot A_L} \quad (25)$$

The overall resistance for a hydrophobic, microporous HFMC with gas filled pores consists of three resistances in series: the liquid phase boundary

layer ($R_{L,est}^{HF}$), the membrane ($R_{m,est}^{HF}$), and the gaseous phase boundary layer ($R_{G,est}^{HF}$). The estimated overall mass transfer resistance with a HFMC ($R_{ov,est}^{HF}$) can be obtained by adding the partial resistances in series. Thus, in a cylindrical geometry like in the HFMC, the overall resistance can be described by means of the equation:

$$\begin{aligned} R_{ov,est}^{HF} &= R_{L,est}^{HF} + R_{m,est}^{HF} + R_{G,est}^{HF} = \frac{1}{k_L^{HF} \cdot A_L} + \frac{1}{H \cdot k_m \cdot A_{ml}} + \frac{1}{H \cdot k_G^{HF} \cdot A_G} = \\ &= \frac{1}{K_{L,est}^{HF} \cdot A_L} \end{aligned} \quad (26)$$

where k_G^{HF} , k_m and k_L^{HF} ($m \text{ s}^{-1}$) stand for the individual mass transfer coefficients in the gas, membrane and liquid, respectively, $K_{L,est}^{HF}$ ($m \text{ s}^{-1}$) is the estimated overall mass transfer coefficient when using a HFMC, A_G and A_L (m^2) are the membrane surfaces in contact with gas and liquid, respectively, and A_{ml} (m^2) is the logarithmic mean membrane surface.

The k_L^{HF} value can be estimated from the L ev eque equation [247] when using a HFMC with the liquid flowing in the lumen side:

$$k_L^{HF} = 1.62 \cdot \frac{D_{L,CH_4}}{d_i} \cdot \left(\frac{d_i^2 \cdot v_L}{D_{L,CH_4} \cdot l} \right)^{1/3} \quad (27)$$

where v_L ($m \text{ s}^{-1}$) is the liquid velocity and D_{L,CH_4} ($m^2 \text{ s}^{-1}$) is the diffusion coefficient of CH_4 in water ($1.76 \cdot 10^{-9} \text{ m}^2 \text{ s}^{-1}$ at $25 \text{ }^\circ\text{C}$ and 1 bar [237]). Equation (27) is adequate for the Graetz Number (Gz) > 4 .

For the gas phase, k_G^{HF} is estimated for a stripping process with a shell side and parallel flow of the gas [248]:

$$k_G^{HF} = 1.25 \cdot \left(\frac{\mu_G}{D_{G,CH_4} \cdot \rho_G} \right)^{0.33} \cdot \left(Re_G \frac{d_o}{l} \right)^{0.93} \quad (28)$$

where D_{G,CH_4} ($m^2 \text{ s}^{-1}$) is the diffusion coefficient of CH_4 through the gas (nitrogen and water vapour mixture), ρ_G ($kg \text{ m}^{-3}$) is the gas density, μ_G ($kg \text{ m}^{-1} \text{ s}^{-1}$) is the

gas viscosity and Re_G is the Reynold number in the gas phase. It should be note that water vapour was also considered in the gas for the mass transfer analysis with the PP HFMC since the application of vacuum provoked the desorption of water until values of relative humidity >90%. The water vapour was not considered in the mass transfer analysis of the FM-SS because no vacuum was applied in those degasification tests.

The value of k_m for the porous PP membrane can be estimated by mean of the previous equation (17). For the calculation of the $D_{G,eff}$, the gas mixture of N_2 and water must be taken into account, therefore, D_{G,CH_4} must be recalculated by equations (29) to (31) [240,241]:

$$D_{G,CH_4} = \frac{1}{\sum_i \frac{y'_i}{D_{CH_4-i}}} \quad (29)$$

$$y'_i = \frac{y_i}{1 - y_{CH_4}} \quad (30)$$

$$D_{CH_4-i} = \frac{0.01013 \cdot T^{1.75} \cdot \left(\frac{1}{M_i} + \frac{1}{M_{CH_4}} \right)^{1/2}}{P \cdot \left[(\sum v)_i^{1/3} + (\sum v)_{CH_4}^{1/3} \right]^2} \quad (31)$$

where i correspond to N_2 or H_2O molecules, y'_i is the mole fraction of specie i evaluated on CH_4 -free basis, D_{CH_4-i} is the binary diffusion coefficient of CH_4 trough specie i , T (K) is the temperature, M is the molecular weight, P (Pa) is the pressure in the gas phase and $(\sum v)$ is the special atomic diffusion volume (17.90 for N_2 , 12.70 for H_2O and 24.42 for CH_4).

Finally, $K_{L,est}^{HF}$ can be calculated as follows [245]:

$$\frac{1}{K_{L,est}} = \frac{1}{k_L} + \frac{d_i}{H \cdot k_m \cdot d_{lm}} + \frac{d_i}{H \cdot k_G \cdot d_o} \quad (32)$$

where d_{lm} (m) is the logarithmic mean fibre diameter.

3.4.2 Evaluation of the membrane-assisted reactive crystallisation tests.

3.4.2.1 Determination of the bulk and scaling induction time.

The bulk and scaling induction times are defined as the time in which the solid particles were detected for first time in the phosphate/permeate solution and in the membrane surface, respectively, during a crystallisation test. The turbidity profiles were used for the determination of the bulk induction time in *Contribution VI*. Hence, the bulk induction time was set at the time in which the turbidity increased to 1 NTU.

The scaling induction time was determined from the recordings obtained with the coupled digital microscope and focused on the membrane surface during the crystallisation tests in *Contribution VI*. Frames were taken at different times of the tests from the recordings and processed with the ImageJ software (National Institutes of Health, USA) [131]. The determination of scaling or presence of particles on the membrane was based on an image segmentation. First, a blank was analysed, which corresponded with the frames taken at the beginning of the test ($t_c = 0$). A membrane area of around $250 \times 50 \mu\text{m}$ were cropped from the image and the colour threshold adjusted, establishing the black and white as the threshold colour and the default thresholding method. Then, the saturation was set at the maximum value which allowed a clear white image while keeping the hue and brightness at 0. This image corresponded with the original membrane without scaling or depositions (blank). The following images of that sample at $t_c > 0$ were taken from the same membrane location and analysed at the saturation value set with the blank. The onset (scaling induction time) and advancing of the scaling were noted in the images as black areas, which could be quantified for determining the scaling extent.

3.4.2.2 Supersaturation analysis.

The supersaturation index (SI) of the produced vivianite was estimated in *Contribution VI* using the Visual MINTEQ 3.1 software (Swedish University of Agricultural Sciences, Sweden) based on the ratio of the ionic activity product (IAP) to the vivianite solubility product constant in water ($K_{sp} = 1.82 \cdot 10^{-41}$ at 25 °C [109]) as $SI = \log (IAP / K_{sp})$. Thus, SI was estimated in the bulk of the phosphate/permeate solution (SI^b) at the different PO_4^{3-} and Fe^{2+} concentrations with the test time (t_c). The estimation of the mean concentrations of the different components (phosphate, iron, sodium, and chloride) present in the system with the time were calculated based on a mass balance applied in the overall system (Figure 3.15). There was only one inlet in the system which corresponded with the dosed stream of the Fe^{2+} solution.

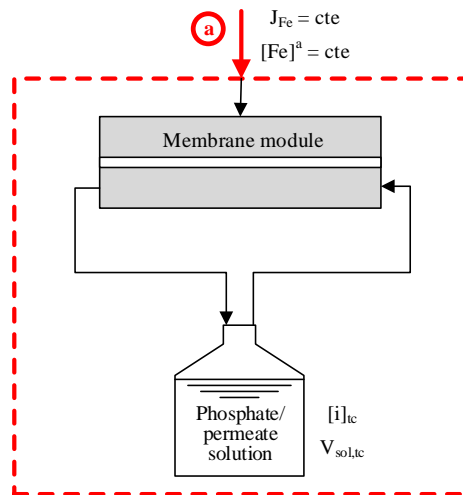


Figure 3.15. Scheme of the mass balance applied in the overall system. Red dashed line denotes the limits for the mass balance. J_{Fe} : dosing rate of Fe^{2+} solution ($mL \cdot min^{-1}$); $[Fe]^a$ denotes the Fe^{2+} concentration at the inlet of the retentate side of the module; $[i]_{tc}$: concentration of component i (M) at a time t_c minutes; $V_{sol,tc}$: liquid volume of the solution in the tank (mL) at a time t_c minutes.

The mean concentrations of each component in the system were calculated as follows:

$$V_{\text{sol},t_c} = V_{\text{sol},0} + t_c \cdot J_{\text{Fe}} \quad (33)$$

$$[\text{PO}_4]_{t_c} = [\text{PO}_4]_0 \cdot \frac{V_{\text{sol},0}}{V_{\text{sol},t_c}} \quad (34)$$

$$[\text{Fe}]_{t_c} = \frac{[\text{Fe}]^a \cdot t_c \cdot J_{\text{Fe}}}{V_{\text{sol},t_c}} \quad (35)$$

$$[\text{Na}]_{t_c} = [\text{PO}_4]_{t_c} \quad (36)$$

$$[\text{Cl}]_{t_c} = 2 \cdot [\text{Fe}]_{t_c} \quad (37)$$

where $V_{\text{sol},0}$ and V_{sol,t_c} (mL) are the total volume of the solution inside the phosphate/permeate tank at the beginning of the crystallisation tests ($t_c = 0$) and at a time t_c (min), J_{Fe} (mL min^{-1}) is the dosing rate of the Fe^{2+} solution, and $[i]_0$ and $[i]_{t_c}$ (M) are the mean concentrations of the component i in the system at the beginning of the tests ($t_c = 0$) and at a time t_c , with i being phosphate, iron, sodium and chloride. According with the results of the chemical speciation calculations from Visual MINTEQ software, the phosphate components inside the phosphate/permeate solution were mainly present in the form of HPO_4^{2-} , H_2PO_4^- , FeHPO_4 (aq), and $\text{FeH}_2\text{PO}_4^+$ (being HPO_4^{2-} , H_2PO_4^- the major species), the iron components in the form of Fe^{2+} , and FeHPO_4 (aq) (being Fe^{2+} the major specie), the sodium components in the form of Na^+ , and chloride components in form of Cl^- .

Also, the SI inside the FM (SI^m) was estimated using mean PO_4^{3-} and Fe^{2+} concentrations values inside the membrane module, relying on the time and Q_L . The estimation of the mean concentrations of the different components (phosphate, iron, sodium, and chloride) inside the permeate side of the flat-sheet membrane module were calculated based on a mass balance applied in the membrane module (Figure 3.16). There were two inlets in the considered

system: the constant dosing of the Fe^{2+} solution, and the inlet of the phosphate/permeate solution into the membrane module, and one exit from the system which returned to the phosphate/permeate tank.

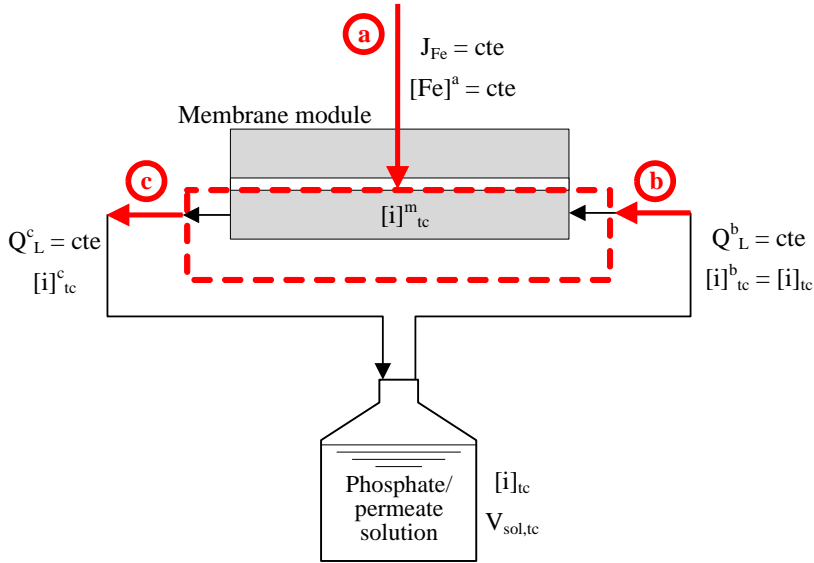


Figure 3.16. Scheme of the mass balance applied in the permeate side of the membrane module. Red dashed line denotes the limits for the mass balance. J_{Fe} : dosing rate of Fe^{2+} solution (mL min^{-1}); $[i]_{t_c}$: concentration of component i (M) at a time t_c minutes; Q_L : liquid flow rate (L h^{-1}); V_{sol,t_c} : liquid volume of the solution in the tank (mL) at a time t_c minutes; and superscript “a”, “b”, “c”, and “m” denote the inlets “a” and “b”, outlet “c” and the inside of the membrane module where the mass balance was applied, respectively.

The volume of the solution and concentration of each component i inside the phosphate/permeate tank at a time t_c (V_{sol,t_c} and C_{i,t_c} , respectively) were determined using equations (33) – (37). The mean concentrations of the different components inside the membrane module ($[i]_{t_c}^m$, M) were calculated as follows:

$$Q_L^c = Q_L^b + \frac{J_{\text{Fe}} \cdot 60}{1000} \quad (38)$$

$$[\text{PO}_4]_{t_c}^c = \frac{[\text{PO}_4]_{t_c}^b \cdot Q_L^b}{Q_L^c} \quad (39)$$

$$[\text{Fe}]_{t_c}^c = \frac{[\text{Fe}]_{t_c}^b \cdot Q_L^b + \frac{J_{\text{Fe}} \cdot 60}{1000} \cdot [\text{Fe}]^a}{Q_L^c} \quad (40)$$

$$[\text{Na}]_{t_c}^c = [\text{PO}_4]_{t_c}^c \quad (41)$$

$$[\text{Cl}]_{t_c}^c = 2 \cdot [\text{Fe}]_{t_c}^c \quad (42)$$

$$[i]_{t_c}^m = \frac{[i]_{t_c}^b + [i]_{t_c}^c}{2} \quad (43)$$

where superscripts “a”, “b”, “c”, and “m” denote the point corresponding to the inlet of the Fe^{2+} solution dosing, the inlet of the permeate side, the outlet of the permeate side and the inside of the membrane module, respectively.

In addition, the mean concentration of vivianite inside the membrane module with the time of operation t_c ($[\text{viv}]_{t_c}^m$, M) was estimated assuming a complete reaction between Fe^{2+} and PO_4^{3-} towards vivianite and no secondary reactions:

$$[\text{viv}]_{t_c}^m = \frac{[\text{Fe}]_{t_c}^m}{3} \quad (44)$$

This mass balances are intended only to illustrate the overall concentration gradient, since a complete description of mass transport within the boundary layer requires significant numerical analysis and validation to describe the relative role of local mixing.

3.4.2.3 Crystallisation kinetic analysis.

Nucleation kinetic was characterised for the crystallisation of vivianite in *Contribution VI*. The nucleation rate of vivianite expressed in mass basis (r' , $\text{mg L}^{-1} \text{min}^{-1}$) was assumed to be the rate of supersaturation at the bulk induction time [249]:

$$r' = \frac{[\text{viv}]_{\text{ind}}^{\text{m}}}{t_{\text{c}}^{\text{ind}}} \cdot M_{\text{viv}} \cdot 1000 \quad (45)$$

where $[\text{viv}]_{\text{ind}}^{\text{m}}$ (M) is the mean concentration of vivianite inside the FM-MA at bulk induction time, $t_{\text{c}}^{\text{ind}}$ (min) is the bulk induction time and M_{viv} is the molar mass of vivianite ($501.61 \text{ g mol}^{-1}$). For the estimation of $[\text{viv}]_{\text{ind}}^{\text{m}}$ shown in the previous section, a complete reaction between Fe^{2+} and PO_4^{3-} towards vivianite, and no secondary reactions were assumed.

The empirical power-law relationship between the nucleation rate and supersaturation (S) developed by Sangwal (2009) [250] was used to determine whether the primary nucleation kinetic inside the FM-MA was in accordance with the classical nucleation theory (CNT) principles [250]:

$$r' = k'(\ln S_{\text{ind}}^{\text{m}})^{m'} \quad (46)$$

where m' is the so-called the apparent nucleation order, k' is the nucleation constant related with the number of stable nuclei forming per unit volume per unit time, and $S_{\text{ind}}^{\text{m}}$ is the supersaturation of the vivianite inside the FM-MA at bulk induction time calculated as follows:

$$S_{\text{ind}}^{\text{m}} = \frac{[\text{viv}]_{\text{ind}}^{\text{m}}}{[\text{viv}]^*} \quad (47)$$

where $[\text{Viv}]^*$ is the solubility of the vivianite calculated from the K_{sp} ($[\text{Viv}]^* = 3.47 \cdot 10^{-9} \text{ M}$). The linearization of Sangwal's power-law yields:

$$\ln(r') = \ln(k') + m' \cdot \ln(\ln(S_{\text{ind}}^{\text{m}})) \quad (48)$$

3.4.3 Membrane characterisation.

3.4.3.1 Hydrophobicity.

The surface hydrophobicity of the membranes was evaluated by means of the static water contact angle (WCA). WCA measurements were conducted by the sessile drop technique [251] using a homemade device (Figure 3.17). A water drop of $5.5 \pm 0.1 \mu\text{L}$ was placed onto the membrane surface using a syringe pump (KF Technology s.r.l., Italy) at room temperature ($\sim 25^\circ\text{C}$). An image of the water drop profile was captured at 15 s with a digital microscope (Handheld Digital Microscope Pro, Celestron LLC., USA) under white light (Philips HUE Lamp, Koninklijke Philips NV, The Netherlands). ImageJ software (National Institutes of Health, USA) was used for image processing using the *Contact Angle Plug-in* based on the ellipse approximation. The WCA was evaluated at different locations on the membrane surface, and a mean value was obtained from at least four measurements, using the standard deviation as a measure of the associated error. Wet membranes from degasification or long-term tests were dried prior to the WCA measurements by removing the excess water and evaporation of moisture with forced aeration at room temperature for more than 1 h.

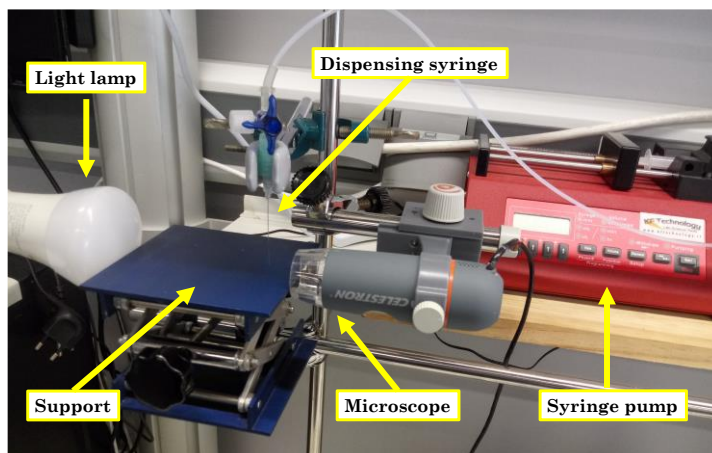


Figure 3.17. Water contact angle measurement device.

For the study of the membrane-assisted reactive crystallisation for the P recovery, as part of the research stay of this thesis, the OCA25 Goniometer (DataPhysics, Filderstadt, Germany) was used for the WCA measurements. This measurement was also based on the sessile drop technique in which a water droplet of 5 μL was placed onto the membrane surface at room temperature. An image of the water droplet was taken at 3 s and the WCA was determined with the SCA20 software (DataPhysics, Filderstadt, Germany). A mean WCA value was obtained from different locations.

3.4.3.2 Surface and cross-section morphology.

The inspection and visualisation of the membrane surface and cross-section was conducted by a field emission scanning electron microscope (FESEM) equipped with an energy dispersive X-ray (EDX) spectrometer with an accelerating voltage of 10 – 20 kV (Hitachi S4800, Hitachi Ltd., Japan). Previous to the image acquisition, the membrane coupons were dried at 45 °C overnight. Afterwards, the coupons were placed on an aluminium holder, and then coated with a fine layer of Au/Pd by sputtering in vacuum for 45 – 60 min. For the analysis of the membrane cross section, the membrane coupons were cut in cryogenic conditions using an ion miller (Ion milling 1010, E.A. Fischione instruments, INC., USA) before placing them in the holder.

3.4.3.3 Roughness.

Surface membrane roughness was determined by using an atomic force microscope (AFM) operating in tapping mode (Digital Instruments, Dimension 3100 SPM with Nanoscope V controller, Veeco Instruments, Inc., USA) and using AFM probes with a force constant and length of 42 N/m and 125 μm , respectively (PPP-NCHR, NanosensorsTM, Switzerland). Images of the membrane topography were taken with a size scan of 25 \times 25 μm , and Gwyddion data analysis software (Department of Nanometrology, Czech Metrology Institute, Czech Republic) was used for image processing and determination of

the root mean square roughness (R_q , nm). A mean value of R_q was determined from at least three different locations of the surface.

3.4.3.4 Thickness.

The thickness of the membranes was determined by the FESEM images obtained from the analysis of the membrane cross section (see section 3.4.3.2. *Surface and cross-section morphology*). At least four different locations were analysed, and a mean value was obtained.

3.4.3.5 Porosity.

The overall porosity (ϵ , %) of the membranes was gravimetrically measured with 1-octanol (99%, Acros Organics, Geel, Belgium) [177]. 2×2 cm samples were weighed and immersed in vials with 10 mL of 1-octanol. The vials were kept in an orbital shaker for 2 hours at room temperature. Finally, the membranes samples were surface dried with absorbent paper and weighed. At least five samples of each membrane were analysed or until obtaining a standard deviation lower than 5%.

The porosity was also evaluated at surface level. Thus, the surface porosity (%) is defined as the ratio of the pore area in the surface respect to the total membrane surface:

$$\text{Surface porosity (\%)} = \frac{\text{Surface pore area}}{\text{Total surface membrane area}} \cdot 100 \quad (49)$$

The surface porosity was determined from the surface FESEM images, which were further processed with the ImageJ software [252–254]. The image processing was based on a segmentation of the image. First, the area to determine the surface porosity was selected, cropped, and quantified, and then the threshold was adjusted until the whole pore area was completely separated from the membrane surface. Afterwards, the image is converted to a binary

image of black and white (pores and membrane surface, respectively). Finally, the black area was quantified, corresponding to the pore area.

3.4.3.6 *Elemental distribution and functional groups.*

The composition of the membranes was analysed by two different techniques:

- **Energy Dispersive X-ray spectroscopy (EDX):** this device was coupled into the FESEM previously described. This analysis provided information regarding the chemical composition and distribution of the different elements on the membrane surface and cross section. At least three different locations were analysed, and a mean value was obtained in order to determine the chemical composition of a sample.
- **Fourier Transform-Infrared spectroscopy (FTIR):** the infrared spectra of the membranes were obtained to determine the functional groups presented in the membrane surface. The infrared spectra were obtained by means of a FTIR analysis in attenuated total reflectance (ATR) mode (Cary 630 FTIR Spectrometer, Agilent Technologies, Inc., USA). The infrared spectra were recorded in the range of 4000 – 650 cm^{-1} and a resolution of 4 cm^{-1} , and processed with the Agilent MicroLab FTIR software. For the infrared spectra acquisition, the membrane coupons were previously dried at 45 °C overnight.

3.4.3.7 *Liquid entry pressure.*

The liquid entry pressure (LEP) of the membranes was evaluated using the configuration of the experimental setup detailed previously for the crystallisation tests (Figure 3.9). A membrane sample was placed inside the FM-MA contactor, the outlet port of the retentate side was kept closed, and the ports of the permeate side were open to the atmosphere. De-ionised water was pumped inside the retentate side at a flow rate of 5 mL min^{-1} in order to increase the pressure slowly and gradually, and the membrane surface of the permeate

side was continuously monitored with the digital microscope. The pressure at which the first drop appeared on the membrane surface was established as the LEP. At least five measurements were conducted for each membrane.

3.4.3.8 *Thermal properties.*

Thermal analysis of the PVDF-Ds membranes were conducted to evaluate their thermal characteristics and crystalline nature. To determine the thermal stability of the membranes under different environments, thermogravimetric analysis (TGA) measurements were conducted in nitrogen and air atmospheres with a TGA Q5000 IR analyser (TA Instruments, USA) using high-temperature platinum pans. A 10 mg sample was placed in the holder, and the heating rate and gas flow rate were set at 10 °C min⁻¹ and 50 mL min⁻¹, respectively. The specimens were heated from room temperature to 800 °C. Moreover, differential scanning calorimetry (DSC) was conducted with samples of 5 mg under a flowing nitrogen atmosphere (50 mL min⁻¹) at a heating rate of 10 °C min⁻¹ from room temperature to 200 °C. The DSC measurements were performed with a DSC 214 Polyma (NETZSCH-Gerätebau GmbH, Germany) using aluminium pans.

The degree of crystallinity, χ (%), of the membranes was determined by using equation (50) [160]:

$$\chi = \frac{\Delta h_m}{x\Delta h_\alpha + y\Delta h_\beta} \cdot 100 \quad (50)$$

where Δh_m (J g⁻¹) is the experimental melting enthalpy of the sample, Δh_α (93.07 J g⁻¹) and Δh_β (103.40 J g⁻¹) are the melting enthalpies of a 100% crystalline PVDF in the α and β phases [255], and x and y are the molar fractions of the α and β phases in the sample, respectively, which were assumed to be the predominant phases ($x + y = 1$). The fraction of the β phase in a sample containing both phases can be estimated using equation (51) [256]:

$$y = \frac{a_{\beta}}{\left(\frac{K_{\beta}}{K_{\alpha}}\right)a_{\alpha} + a_{\beta}} \cdot 100 \quad (51)$$

where a_{α} and a_{β} represent the absorbance at the wavelengths of 766 cm^{-1} and 840 cm^{-1} , respectively, from the infrared spectra, and K_{α} ($6.1 \cdot 10^4 \text{ cm}^2 \text{ mol}^{-1}$) and K_{β} ($7.7 \cdot 10^4 \text{ cm}^2 \text{ mol}^{-1}$) are the absorption coefficients of the α and β phases, respectively [257]. The measured absorbance at the wavelengths of 766 cm^{-1} and 840 cm^{-1} were 0.167 and 0.187, respectively, for all the tested membranes. The fraction values of the α and β phases were 0.53 and 0.47, respectively.

3.4.4 Crystal characterisation.

3.4.4.1 *Shape and size distribution.*

The crystals collected on the filters at the end of the vivianite crystallisation tests were analysed by microscopy to determine the crystal shape and size. Thus, crystals were analysed by means of a FESEM with an accelerating voltage of 10 kV (Tescan Vega 4, Tescan Orsay Holding, a.s., Czech Republic). For image acquisition, the filter samples with the collected crystals were previously placed on a metal holder and then coated with a fine layer of Au. The mean crystal size and distribution were obtained by measuring the diameter of at least 300 particles from three FESEM images with the abovementioned ImageJ software.

3.4.4.2 *Chemical composition.*

The chemical composition of the crystals collected at the end of a crystallisation test were determined by spectroscopy techniques. The previous FESEM used for the crystal shape and size determination was equipped with an EDX spectrometer, which was used for the atomic content determination of different elements. A mean value of the atomic content was obtained from at least three measurements in different locations.

Additionally, X-ray diffraction (XRD) analysis was carried out for the identification of crystalline phases in the crystals formed during the crystallisation tests. The crystals collected on the filter were analysed with an XRD system (AXS D8 ADVANCE A25, Bruker, MA, USA) and the diffractograms were processed with QualX2.0 software (Software IC, Institute of Crystallography-CNR, Bari, Italy).

3.4.5 Fouling characterisation.

3.4.5.1 Morphology and chemical characterisation of the fouling cake.

Analogous to the characterisation of the membranes by microscopy, the surface and cross section of the fouling cake deposited on them was also analysed using the FESEM equipped with an energy EDX spectrometer with an accelerating voltage of 20 kV (Hitachi S4800, Hitachi Ltd., Japan). For the image acquisition, the membrane coupons were softly dehydrated in an ethanol series in a sequence of 50, 80, 100, and 100% for 3 min each and then air-dried overnight. Afterwards, the coupons were placed on an aluminium holder and then coated with a fine layer of Au/Pd by sputtering in vacuum for 1 min. For the analysis of the fouling cake cross section, the membrane coupons were cut in cryogenic conditions using an ion miller (Ion milling 1010, E.A. Fischione instruments, INC., USA) before placing them in the holder. The FESEM-EDX technique was used to analyse the surface and cross section morphology, thickness, and chemical composition of the membrane and the fouling cake.

The surface composition of the fouling cake was also studied by means of FTIR in the ATR mode as detailed in section *3.4.3.6 Elemental distribution and functional groups*. For the infrared spectra acquisition, the membrane coupons were previously dehydrated with ethanol, as previously detailed.

3.4.5.2 Protein and polysaccharide content in the fouling cake.

The identification and quantification of protein and polysaccharides attached on the membrane surface and fouling cake were carried out by means of staining techniques and imaging with a confocal laser scanning microscope (CLSM) (Olympus FV1000, Olympus Corporation, Japan) equipped with a 10× magnification objective. The SYPRO Orange Dye and the Concanavalin A conjugates to Alexa Fluor 633 (Molecular Probes, Inc., USA) were applied to stain proteins and polysaccharides, respectively.

The protein staining solution was prepared by diluting the SYPRO Orange Dye with 7.5%_v acetic acid (acetic acid 100%, VWR Chemicals, USA) until a volume ratio of 1:5000 was achieved. The polysaccharide staining solution was prepared at a concentration of 100 µg of Concanavalin A mL⁻¹ using a phosphate-buffered saline solution (PBS) as the solvent.

For the staining technique, a 1 × 1 cm membrane coupon was first immersed in 1 mL of the protein staining solution and placed in a rotary shaker in the dark for 1 h at 75 rpm and room temperature. Then, the membrane was rinsed in 7.5%_v acetic acid to remove the excess staining solution (<1 min) and then immersed in a PBS solution to remove the residual acetic acid (<1 min). Afterwards, the membrane coupon was immersed in 1 mL of the polysaccharide staining solution and shaken for 1 h at 75 rpm at room temperature in the dark. Then, the membrane was rinsed in the PBS solution (<1 min). Finally, the stained membrane coupon was air-dried with force aeration for ~2 h and stored in the dark at 4 °C.

The stained samples were observed with the CLSM, and at least two different series of images were taken at different depths with an imaged surface size of 1300 × 1300 µm. Each series of the CLSM images was processed with the *Imaris* software (Oxford Instruments, UK) to reconstruct a 3D image [258,259]. In order to quantify the volume of the stained proteins and polysaccharides on the membrane, a 3D model was generated from the CLSM images also using the *Imaris* software [259]. Thus, the specific volume of the foulant (proteins or

polysaccharides) is defined as the total volume per unit of membrane area ($\mu\text{m}^3 \mu\text{m}^{-2}$) [259].

3.4.5.3 Extraction and characterisation of the foulants from the membrane.

The fouling agents adhered to the membrane in form of a fouling cake after a fouling test were extracted for an ulterior characterisation. Hence, the fouling cake was detached from a membrane coupon of 8.7 cm² using a sonication bath (Bransonic® 1510E-MT, Branson Ultrasonic Corporation, USA) with different solutions: a soft cleaning with 20-mL milliQ water for 60 min followed by an alkaline cleaning with 20 mL of 0.01 M NaOH solution for 60 min. Then, the membrane coupon was dried in an oven at 45 °C overnight. Both water and NaOH extraction solutions were analysed to measure the concentration of proteins, polysaccharides, phosphates, alkalinity, COD, total suspended solids (TSS), volatile suspended solids (VSS), and the metabolic status of the bacteria.

The determination of TSS and VSS was carried out according to standard methods [260]. Alkalinity was determined by means of the 5 pH point titration procedure [261] using the 848 Titrino Plus (Metrohm, Switzerland). The polysaccharide content was analysed by the phenol-sulphuric acid method proposed by Dubois et al. [262] with glucose as the standard [263,264]. The protein content was determined according to the modified Lowry methods by Onishi and Bar (Total protein kit, micro Lowry, Onishi & Bar modification, Sigma-Aldrich, USA) using bovine serum albumin as the standard. The COD and phosphate content were determined using colorimetric analysis kits (COD Cell Test 0 – 150 mg L⁻¹ and PO₄³⁻ Cell Test 1.5 – 76.7 mg L⁻¹, respectively, Merck Chemicals, Germany).

The metabolic status of the bacteria contained in the fouling extraction solutions was evaluated to investigate the influence of the biofouling on the fouling cake development. The quantification of the live and dead cells was

conducted by means of a flow cytometry using the LIVE/DEAD BacLight™ Bacterial Viability Kit L7012 (Molecular Probes Inc., USA) for the bacteria staining in the liquid samples. The viability kit is composed of the SYTO 9 and propidium iodide (PI) dyes to stain the live and dead cells, respectively. A staining solution was firstly prepared with a volume ratio of 1:1 (SYTO 9:PI) according to the specifications. 3 µL of the staining solution was added to 1 mL of the liquid sample. The sample was vigorously shaken and incubated in the dark for 15 min at 200 rpm. Afterwards, the stained samples were filtered with a 50 µm filter and analysed in a flow cytometer (FACSVerse 3L 8C, Becton, Dickinson and Company, USA) equipped with a 488 nm laser and using BD Trucount™ Tubes (Becton, Dickinson and Company, USA) for the quantification of live and dead cells. Data acquisition and treatment were carried out with the FACSSuite software.

3.4.6 Characterisation of the anaerobic effluents.

The parameters of the AE used in the degasification and fouling tests were determined. The TSS, VSS, alkalinity, protein and polysaccharide content, COD, phosphate content and the metabolic status of the bacteria were determined by the protocols previously detailed in section *3.4.5.3 Extraction and characterisation of the foulants from the membrane*. The turbidity was measured with a turbidimeter (Merck Turbiquant 1500IR, Germany), volatile fatty acids (VFA) were determined using potentiometer titration (848 Titrino Plus, Metrohm, Switzerland), and a pH and conductivity meter was used (pH/Cond 340i WTW, Germany) for measurements of pH and conductivity. The concentration of sulphates (SO_4^{2-}), ammonium (NH_4^+), nitrates (NO_3^-), nitrites (NO_2^-), calcium (Ca^+) and iron (Fe^{2+}) were determined by means of colorimetric methods using test strips (commercial kits from Merck-Quant, Germany).

3.4.7 Design of experiments and statistical analysis.

The effects of the different parameters of the membrane modification procedure on the membrane hydrophobicity were evaluated by means of the design of experiment (DOE) methodology in *Contributions II* and *IV*. Hence, statistical experimental designs were conducted to determine the main variables (factors) involved in the modification procedures and the values of that factors that maximise the hydrophobicity. 2×2 cm membrane specimens were used for the experimental runs, measuring their WCA (response variable) after the functionalisation. Firstly, factorial, and central composite designs for the analysis of variance (ANOVA) were conducted with an alpha (α) value of 1.41 and a level of confidence of 95% to identify the significant effects of the factors and their interactions on the response variable. Then, a surface response analysis based on a multiple linear regression was conducted to determine the maximum and/or optimum values of the factors leading to the maximum response. The different experimental runs were conducted randomly in duplicate to avoid systematic errors. The statistical software Minitab® (Lead Technologies, Inc., Charlotte, NC, USA) was used to aid in the design of experiments and the statistical analysis.

4 RESULTS AND DISCUSSION.

4.1 RECOVERY OF DISSOLVED METHANE THROUGH A FLAT-SHEET MODULE WITH PDMS, PP, AND PVDF MEMBRANES.

This section shows the overview and main results and conclusions derived from the work entitled “*R. Jiménez-Robles, C. Gabaldón, J.D. Badia, M. Izquierdo, V. Martínez-Soria, Recovery of dissolved methane through a flat sheet module with PDMS, PP, and PVDF membranes, Sep. Purif. Technol. 282 (2022) 120057. <https://doi.org/10.1016/j.seppur.2021.120057>*”. The details of the publication and the full paper can be found in *Appendix I: Contribution I*.

This work was the first of a series of four studies focused on hydrophobic flat-sheet membranes for the D-CH₄ recovery from liquid effluents using the gas-liquid membrane contactor FM-SS. In this first stage, an experimental system was proposed at lab-scale system working in non-steady-state. The validation of this system allowed its use in further studies for the evaluation of the stability, wetting and fouling resistance of new and functionalised membranes (*Contributions II – IV*). As well, the insight into this technology was also useful for exploring new and novel applications in the wastewater treatment, such as the P recovery via membrane-assisted reactive crystallisation, which was the focus of the *Contribution VI* of this thesis.

4.1.1 Motivation, aim and overview.

Comparing with hollow fibre membrane contactors (HFMCs), flat-sheet membrane modules (FMs) can present several advantages related to their simplicity and versatility. The flat-sheet membrane can easily be extracted, analysed, and cleaned during operation and/or replaced, allowing considerable time and cost savings. This makes the FMs especially useful where the fouling

and wetting resistance or membrane stability are the focus of the research or to facilitate the performance comparison of different membrane materials.

In this context, the first aim of this work was to determine the applicability and versatility (and also limitations) of the gas-liquid flat-sheet membrane system using the FM-SS contactor for the recovery of D-CH₄ from water. For this purpose, the effect of the hydraulic operational conditions on the efficiency in CH₄ recovery was determined, and different types of membranes were tested. Additionally, the CH₄ mass transfer was modelled for the system under study and the stability of membranes were evaluated in this application.

In order to elucidate the effect of the operational parameters in the membrane performance and D-CH₄ recovery, degasification tests with the FM-SS contactor were carried out with PDMS, PVDF-Ds, PP-1E and PP-2E membranes. FM-SS operated in non-steady state and in sweep gas mode with N₂ flow rates (Q_{N_2}) ranging from 0.05 to 15.00 L h⁻¹ (gas velocity from 0.0043 to 1.3 cm s⁻¹). The liquid flowed in recirculating mode with flow rates (Q_L) ranging from 3.5 to 40.5 L h⁻¹ (liquid velocity from 2.8 to 32.5 cm s⁻¹). The profiles of the D-CH₄ removal efficiency (RE) and CH₄ content (y_{CH_4}) versus time on stream were determined at the different operational conditions. Furthermore, the CH₄ mass transport was modelled based on the resistances in series model, which was validated based on the experimental results. Finally, the membrane stability with the time of use was also determined by monitoring the membrane hydrophobicity and imaging the surface and cross section in search of potential degradation using the electron microscope (FESEM).

4.1.2 Results and discussion.

The effects of the operational parameters (liquid and N₂ flow rates) in the RE and in the y_{CH_4} during a degasification test was initially studied with a PDMS membrane. The RE increased with the operation time due to the continuous degassing of the water from the tank and the non-steady state condition of the tests, reaching values up to 95% at 22 h. The outcomes showed

that the RE at a fixed time increased with the liquid flow rate, since the total liquid volume inside the feed tank was degassed at a higher rate and the mass transfer was improved. For example, a RE of 24% and 55% were obtained at 5 h of operation at the liquid flow rates of 3.5 and 40.5 L h⁻¹, respectively. Higher liquid velocities inside the FM-SS led to a higher turbulence which favoured the CH₄ mass transfer, with estimated liquid phase mass transfer coefficients of $2.25 \cdot 10^{-5}$ and $5.85 \cdot 10^{-5}$ m s⁻¹ at 3.5 and 40.5 L h⁻¹, respectively. The effect of the N₂ sweep gas flow rate was not so remarkable. RE only increased slightly from a N₂ flow rate of 0.05 to 0.5 L h⁻¹ (RE of 40% and 45%, respectively, at 5 h of operation), and then RE stayed almost constant, which is consistent with the negligible mass transfer resistance estimated for the gas phase, which only represented less than 0.05% of the overall resistance.

Regarding the composition of the recovered gas, the CH₄ content was strongly influenced by the liquid and N₂ flow rates. Higher CH₄ content was obtained as the liquid flow rate increased, since higher CH₄ fluxes were determined. Thus, for the maximum CH₄ flux obtained of 118 g s⁻¹ m⁻² at the highest liquid flow rate, the CH₄ content was near to 5%. On the contrary, the CH₄ content drastically declined with increasing the N₂ flow rate due to the dilution effect, with values always lower than 0.4% for N₂ flow rates ≥ 4.0 L h⁻¹. In addition, the CH₄ flux and content decreased with the operation time up to values of <11 g s⁻¹ m⁻² and $<0.5\%$, respectively, at 22 h of operation. This observation was in accordance with the lower driving force inferred as the D-CH₄ concentration in the liquid declined.

Membrane properties such as the hydrophobicity, permeability, porous structure, and thickness could play an important role in the performance of a separation process, since those properties could affect the membrane resistance for the mass transport. Thus, different dense and porous membranes were tested. Both porous PP membranes tested showed similar RE and CH₄ content than the dense PDMS membrane, attributed to a negligible membrane mass transfer resistance. In fact, the estimated membrane resistance represented

lower than 0.5% of the overall resistance. Despite the dense layer of the PDMS, the low mass transfer resistance estimated was attributed to the small thickness of that dense layer (2.5 μm) which led to a similar overall performance than the porous membranes.

Regarding the PVDF-Ds membrane, a plastic deformation of its surface was observed when used at liquid flow rates $\geq 21 \text{ L h}^{-1}$ during at least 5 h likely due to the stress induced by the liquid flow on the membrane. Thus, this altered membrane (aPVDF-Ds) presented a surface with a lower porosity and a higher hydrophobicity. The unaltered membrane (uPVDF-Ds) showed a slightly lower RE than the PDMS and PP membranes, whilst the aPVDF-Ds showed quite similar results to PDMS and PP membranes. This performance increase of the PVDF-Ds was attributed to a higher wetting resistance inferred by the lower surface porosity and higher hydrophobicity which constrained the intrusion of water in the membrane pores.

The stability and useful lifetime of the membranes are essential issues that limit the operational conditions of the process. In this sense, the surface stability of the membranes was tested based mainly on the hydrophobicity. Thus, the water contact angle (WCA) of the different membranes was measured at different times of use and liquid flow rates. A moderate-high liquid flow rate of 21.0 L h^{-1} provoked a relatively fast degradation of the membranes, especially in PP membranes whose WCA declined more than a 14% in only 5 h of use due to a deformation of the entire membrane. PDMS experienced a slight decline in the WCA from 101° to 94° at 0 and 95 h of use, respectively, even though cleavages and delamination of the top dense layer were detected in the FESEM. This degradation provoked a water breakthrough, indicating the end of the useful lifetime of that PDMS membrane. In the case of PVDF-Ds, the WCA increased until a stable value of $\sim 115^\circ$ at 90 h of use, due to the deformation previously discussed. In contrast, PDMS and PVDF-Ds membranes showed a higher stability at the lowest liquid flow rate of 3.5 L h^{-1} , since their original WCA kept almost unchanged during more than 175 h of use, and no deformation

or water breakthrough were observed on their surfaces. Thus, these membranes could be used for long-term operations at soft liquid flow rates.

Finally, the experimental mass transfer coefficients (Eq. (9)) were compared with the estimated coefficients based on empirical equations (Eq. (10) – (21)). The experimental coefficients obtained with the PDMS, PP-2E and aPVDF-Ds were in agreement with those estimated with the model, indicating that empirical equations used for the mass transfer analysis seemed suitable for the prediction of the mass transfer resistance of the system with these membranes. However, the estimated overall mass transfer coefficient with uPVDF-Ds and PP-1E were slightly higher than the experimental values. The experimental overall mass transfer coefficients ranged from $1.66 \cdot 10^{-5}$ to $6.28 \cdot 10^{-5}$ m s^{-1} at the operational condition and the membranes tested and showed that the main resistance was located in the liquid phase. Thus, the performance in the D-CH₄ using FMs is mainly governed by the hydraulic conditions of the liquid feed side.

4.1.3 Conclusions.

The applicability and versatility of a gas-liquid flat-sheet membrane module have been demonstrated for the dissolved CH₄ recovery. PDMS, two types of PP, and PVDF membranes were tested and compared at different hydraulic and driving force conditions. As result, the CH₄ removal efficiency was mainly controlled by the hydraulic conditions of the liquid feed stream, obtaining higher removal efficiencies as the liquid flow rate increased. In contrast, the removal efficiency was not significantly influenced by N₂ flow rates due to the negligible mass transfer resistance of the gas phase. A maximum removal efficiency of 95% was observed at 22 h of time on stream with the highest liquid flow rate of 40.5 L h⁻¹ with PDMS.

Similar removal efficiencies were observed with dense PDMS and microporous PP membranes and when a microporous PVDF membrane was

altered at a moderate-high liquid flow rate (21 L h^{-1}) since the membrane mass transfer resistance was always negligible.

The mass transfer model for CH_4 transport based on empirical equations agreed with most of the experimental results and showed that the main transfer resistance was located in the liquid phase.

Membranes showed a considerable degradation, especially at surface level, when operated at moderate-high flow rates ($\geq 21.0 \text{ L h}^{-1}$). Hydrophobicity decrease, plastic deformations, cleavages, and delamination were detected on the membrane surface. In contrast, no degradation was observed under low liquid flow rates. These results suggest that contact angle measurements could be a useful and low-cost methodological approach to determine the stability of membranes during operation.

4.2 FLAT PVDF MEMBRANE WITH ENHANCED HYDROPHOBICITY THROUGH ALKALI ACTIVATION AND ORGANOFLUOROSILANISATION FOR DISSOLVED METHANE RECOVERY.

This section shows the overview and main results and conclusions derived from the work entitled “*R. Jiménez-Robles, B.M. Moreno-Torralbo, J.D. Badia, V. Martínez-Soria, M. Izquierdo, Flat PVDF membrane with enhanced hydrophobicity through alkali activation and organofluorosilanisation for dissolved methane recovery, Membranes. 12 (2022) 426. <https://doi.org/10.3390/membranes12040426>*”. The details of the publication and the full paper can be found in *Appendix II: Contribution II*.

This work was the second of a series of studies focused on hydrophobic flat-sheet membranes for the D-CH₄ recovery from liquid effluents using the gas-liquid membrane contactor FM-SS. In a first stage, an experimental lab-scale system was validated as a useful and versatile approach to characterise the membrane performance and stability under operation (*Contribution I*). In this second stage, the former experimental system was used for the testing of functionalised membranes with enhanced hydrophobicity in order to increase the wetting resistance. Thus, a lower membrane mass transfer resistance and a higher membrane stability were expected due to the higher rejection of water from the membrane as the hydrophobicity increased. Moreover, the effluent from an anaerobic digester was used for testing the membranes under actual operational conditions in the degasification and stability tests. This work was furtherly extended in order to characterise the fouling experienced on functionalised membranes when using a real anaerobic effluent (*Contribution III*).

4.2.1 Motivation, aim and overview.

As was experienced in our previous work (*Contribution I*), FM presents several advantages related to its simplicity, versatility and ease of cleaning and replacement for the recovery of D-CH₄ from anaerobic waters. As membrane material, PVDF has been intensively studied in recent years [161] due to its outstanding properties [71,228] as well as a good thermodynamic affinity with various fluoropolymers [211] which can enhance its hydrophobic characteristics.

Two major shortcomings are apparent when operating with membranes: wetting and fouling. In microporous membranes, the liquid pressure over the membrane surface can induce the filling of the membrane pores [71,84]. This membrane wetting can induce an increase of ~20% in the mass transfer resistance with only the 5% of membrane pores occupied by the liquid [91], which reduces the separation efficiency. On the other hand, the fouling agents contained in an anaerobic effluent can adhere to the membrane surface [90], which causes restrictions for mass transfer and membrane degradation [68].

In order to overcome these shortcomings, membranes can be enhanced by adding new functionalities on the surface [68,265]. The surface membrane modification has gained a great deal of attention in recent years due to the versatility offered by the different techniques [68,228]. Chemical treatments commonly involve grafting of modifying agents onto the membrane by means of covalent bonding, achieving a strong adhesion force. In this sense, fluorinated organic compounds and siloxanes have been developed and evaluated as modifying agents, since they are well known to reduce surface free energy and, consequently, to increase hydrophobicity and wetting resistance [71].

The stress and dragging effect of a continuous liquid flux over the modified membranes in long-term operations can remove the functionalisation layer or alter the surface morphology, producing a change in the surface properties such as the hydrophobicity [73,225] and reducing the membrane lifetime. Reports into the evaluation of the structural and chemical stability of modified membranes after long-term operations for D-CH₄ recovery are very

scarce but would provide useful preview information about the economic viability of applying membrane modification procedures at the industrial scale.

In this context, the aim of this work was to evaluate the effect of a chemical surface modification applied over a PVDF membrane for the recovery of D-CH₄ from aqueous streams. Firstly, a modification procedure based on an alkali activation followed by a functionalisation was proposed, and the membrane hydrophobicity was maximised. Then, the stability and the membrane performance in D-CH₄ recovery by modified PVDF membranes were evaluated and benchmarked with non-modified PVDF. These membranes were tested in the FM-SS module under several operational conditions with deionised water (DW) and real anaerobic reactor effluent (AE).

In order to increase the membrane hydrophobicity, PVDF-Ds was activated via wet alkali activation with a NaOH solution followed by a functionalisation with the fluoroalkylsilane (FAS) 1H,1H,2H,2H-perfluorooctyltriethoxysilane, using TEOS as silica precursor (SiP). The hydrophobicity, expressed as WCA, was maximised by means of a statistical design of experiments to optimise the reactant concentrations. The surface and cross section of modified membranes were characterised by microscopy and spectroscopy. Furthermore, the membrane performance and stability in the D-CH₄ recovery operation were also evaluated by means of degasification, long-term stability, and fouling tests.

4.2.2 Results and discussion.

The modified PVDF-Ds membranes (mPVDF) always presented WCA values higher than that of the non-modified PVDF-Ds (nmPVDF, $103.4 \pm 1.6^\circ$), indicating that the proposed functionalisation procedure was suitable to increase the PVDF-Ds hydrophobicity. Hence, a statistical experimental design and a response surface analysis evaluating the main parameters that affect the membrane surface hydrophobicity were conducted to maximise the WCA of the modified membranes. These main variables involved in the functionalisation

method were the NaOH concentration (NaOH%_{wt}) for the membrane activation and the FAS/TEOS ratio (FSi_T) and concentration (FSi_T%_v) in the functionalisation solution. As result, the individual factors presented the highest effects on the response, especially the factors involved in the functionalisation step (FSi_T%_v and FSi_T), since the FSi_T ratio and FSi_T%_v determined the number of O–Si bonds on the PVDF chains and the total F content at the end of the functionalisation process. Therefore, the resulting WCA was higher as the F content increased. A maximum WCA of $143.2 \pm 2.5^\circ$ was obtained for the optimal modification conditions, which were established at the values of 5%, 7.2% and 0.55 for NaOH%_{wt}, FSi_T%_v and FSi_T, respectively.

An inspection of the surface and cross-section of nmPVDF and modified PVDF-Ds with the maximum WCA (mPVDF_{max}) was carried out by means of a FESEM. The effect of membrane modification resulted in a heterogeneous surface with porous zones and zones with dense and smooth clusters, and less surface porosity than the nmPVDF. This can be attributed mainly to a coating-like effect of the polymerisation/condensation of the FAS and TEOS, and consequently, a dense and thick top layer was observed for mPVDF_{max} with a thickness between 15 and 37 μm . Furthermore, the mPVDF_{max} showed a slightly higher F content than that obtained for nmPVDF (55% and 53%, respectively) indicating that the FAS had been grafted on the surface. These results were probably responsible for the increase in hydrophobicity and likely to improve the wetting resistance of the membrane.

The potential improvement of the modified membrane stability was evaluated under long-term stability tests. The mPVDF_{max} was tested under a moderate-high DW flux (21 L h⁻¹), showing that its WCA decreased continuously to a value of $105.4 \pm 2.5^\circ$ at 47 h and then stayed almost constant in $\sim 100^\circ$, similar to the nmPVDF ($103.4 \pm 1.6^\circ$). The WCA decrease could be due to the reduction of F content detected in the EDX analysis from 55% to 53%. This F loss was attributed to the stress and dragging effect of the liquid flux removing the functionalisation layer. This effect was confirmed by the reduction of the

membrane thickness from 164 ± 1 to 148 ± 12 μm at 0 and 160 h, respectively. Regarding the hydrophobicity results with the AE at a softer liquid flux (3.5 L h^{-1}), the WCA of both nmPVDF and mPVDF_{max} decreased a 54% after >800 h of use. This result corroborated that the membrane was covered by a fouling cake, obscuring the hydrophobic nature of the membrane. In addition, a water breakthrough was detected on the nmPVDF at 816 h, indicating mechanical or chemical deterioration.

Regarding the performance of the modified and non-modified membranes in the D-CH₄ recovery operation with a synthetic DW stream, the mPVDF_{max} showed a greater mass transport of CH₄ than did nmPVDF under the same liquid and gas hydraulic conditions and at the highest Q_L (21.0 L h^{-1}), since the obtained RE was slightly higher with mPVDF_{max} (RE of 39% and 42% for nmPVDF and mPVDF_{max}, respectively). This could be attributed to the increase in the wetting resistance.

The effect of membrane fouling on D-CH₄ removal efficiency was evaluated with experiments at 3.5 and 21.0 L h^{-1} with an AE. At low liquid flow rate (3.5 L h^{-1}), the effect of fouling could be considered negligible for both membranes. In contrast, RE declined a 13% and 52% for the used nmPVDF and mPVDF_{max}, respectively, at >650 h and at the highest liquid flow rate (21.0 L h^{-1}). Thus, a lower fouling resistance was inferred for the modified PVDF-Ds.

4.2.3 Conclusions.

The hydrophobicity of a PVDF-Ds membrane surface has been maximised by chemical grafting of a fluoroalkylsilane in order to increase the membrane performance in the recovery of dissolved CH₄ from aqueous streams. The alkali activation and the further functionalisation step was optimised, and a maximum increase of a 36% in the water contact angle was achieved. In addition, a higher removal efficiency and CH₄ fluxes were obtained with that modified membrane due to the pore wetting prevention.

The effect of the functionalisation layer in the membrane hydrophobicity was lost in short times of operation at moderate-high liquid flow rates. In addition, the results allowed the conclusion that the modification of PVDF promoted a higher additional mass transfer resistance due to the deposition of foulants contained in the anaerobic effluent hindering D-CH₄ recovery. However, a longer useful lifetime was achieved for modified membranes, since no water breakthrough was observed at >800 h with an anaerobic effluent, unlike the non-modified PVDF. Thus, the modification procedure seemed to improve the stability of the PVDF in long-term operations with real effluents. In this regard, the surface modification should be taken into account as a strategy to increase the useful lifetime of the membrane since a greater chemical or mechanical resistance could be induced.

4.3 FOULING CHARACTERISATION IN PVDF MEMBRANE CONTACTORS FOR DISSOLVED METHANE RECOVERY FROM ANAEROBIC EFFLUENTS: EFFECT OF SURFACE ORGANOFLUOROSILANISATION.

This section shows the overview and main results and conclusions derived from the work entitled “*R. Jiménez-Robles, V. Martínez-Soria, M. Izquierdo, Fouling characterisation in PVDF membrane contactors for dissolved methane recovery from anaerobic effluents: effect of surface organofluorosilanisation, Environmental Science and Pollution Research. 30 (2023) 29164–29179. <https://doi.org/10.1007/s11356-022-24019-z>*”. The details of the publication and the full paper can be found in *Appendix III: Contribution III*.

This work was the third of a series of studies focused on hydrophobic flat-sheet membranes for the D-CH₄ recovery from liquid effluents using the gas-liquid membrane contactor FM-SS. In the first stage, an experimental lab-scale system was validated as a useful and versatile approach to characterise the membrane performance and stability under operation (*Contribution I*). In the second stage, the former experimental system was used for the testing of functionalised membranes with enhanced hydrophobicity in order to improve the membrane performance and stability (*Contribution II*). This third work is complementary and in continuity with this previous contribution since the fouling tests conducted in that study were further evaluated to elucidate the fouling mechanisms on non-modified and modified PVDF-Ds membranes.

4.3.1 Motivation, aim and overview.

In the last years, membrane contactors for D-CH₄ recovery from AEs have been successfully implemented at the bench scale and at the prototype scale [42,44,59,63,64,266]. Nevertheless, the main challenge related to the full implementation of this technology is the prevention of both fouling and wetting

of the membranes. In this regard, the elucidation of fouling mechanisms in the membrane contactor has recently been identified as a critical issue that needs to be overcome [267].

The fouling cake on the membrane can induce an additional mass transfer resistance and/or a reduction in its useful lifetime [68,69,268]. The fouling grade relies on several factors related to membrane characteristics, hydrodynamic conditions, and nature of the treated water [68,90,92]. For hydrophobic membranes such as PVDF, a strong interaction with organic matter is the main cause of fouling due to the hydrophobic nature of most organic compounds [268]. Therefore, proteins and polysaccharides are the major foulants when treating wastewaters or residual effluents [266,269]. Furthermore, these organic foulants could hydrophilise the membrane surface, reducing the wetting resistance and promoting scaling and pore clogging [73,268,270].

Different strategies have been proposed in order to prevent or minimize the negative effect of the fouling on the membrane performance, such as membrane cleaning procedures [90,97,271]. Nonetheless, potential degradation of the membrane due to the attack of the residual foulants and aggressive chemical cleaners limit the useful lifetime of the membrane [268,271,272]. To overcome such limitations, the membrane surface modification has appeared as a useful approach to enhance fouling resistance, in which both a hydrophilic and superhydrophobic surfaces tends to suffer from lesser fouling [268,273,274]. However, research works tackling the fouling effects and the characterisation of the fouling mechanisms on hydrophobic membranes treating AEs have been scarcely studied [267].

In this context, the main objective of this work was the determination of the fouling composition and potential mechanisms on flat-sheet PVDF-Ds membranes with different hydrophobicity grades used for the degassing of an anaerobic reactor effluent. For this purpose, fouling tests under a long-term operation were conducted with the FM-SS module using a commercial PVDF-

Ds (WCA = $103.4 \pm 1.6^\circ$) and a functionalised PVDF-Ds with enhanced hydrophobicity (mPVDF, WCA = $140.9 \pm 2.5^\circ$). PVDF-Ds was modified by means of the organofluorosilanisation exposed in *Contribution II*. Then, the fouling cake was deeply analysed by means of different microscopy and spectroscopy techniques (FESEM-EDX and FTIR) in order to identify the different elements and compounds. Staining techniques were also used for the identification and quantification of proteins and polysaccharides and for the sensing of the metabolic status of the bacteria. In addition, a fouling extraction from the membrane was carried out with water and a NaOH solution in order to analyse the composition of the reversible and irreversible fouling. Finally, the influence of the fouling on the membrane stability was also elucidated.

4.3.2 Results and discussion.

Both PVDF-Ds and mPVDF membranes were susceptible to fouling when treating an AE for D-CH₄ recovery, though mPVDF suffered from a more severe fouling due to its higher hydrophobicity. The fouling content increased with the time of operation owing to a continuous deposition of foulants from the anaerobic water and/or biofilm growth [259]. The resultant fouling cake presented a dense-like structure, which reduced the membrane surface porosity and created an additional mass transfer resistance for CH₄ diffusion.

The decrease in more than 50% of the WCA at the end of the fouling test agreed with the fouling cake development. This surface hydrophilisation can be especially favoured by the deposition of amphiphilic proteins and polysaccharides [97,269,270,275] detected in the fouling cake. Also, the biofilms, metal oxides, and aluminosilicates presented in the fouling contributed to the hydrophilization [73,97]. In addition, the potential loss of F atoms from the membrane surface owing to the degradation observed in the FESEM images and EDX results was especially severe on the non-modified PVDF-Ds, contributing to the decrease in the WCA.

Both organic and inorganic fouling were found on the membrane, being proteins and polysaccharides the major organic foulants, and the inorganic fouling was composed mainly of Ca, P and Mg salts. Clear differences were determined between the surface and bulk composition of the fouling cake, denoting a clear stratification of foulants. Thus, the outcomes persuaded to conclude that protein and polysaccharide deposition was more dominant in the first stage of the fouling formation according to the large hydrophobic interaction forces with the membrane surface. Then, this deposition led to a conditioning layer that promoted the adherence of inorganic compounds and microorganisms [90,259], even though the organic matter dominated the most external parts of the fouling cake.

Irreversible fouling was always observed, which was mainly attributed to a strong hydrophobic-hydrophobic interaction of the proteins and polysaccharides with the membrane [259], especially with the mPVDF with a higher hydrophobicity. Nonetheless, the absence of polysaccharides in the irreversible fouling cake on the mPVDF suggests lower adhesion forces between polysaccharides and the modified surface and/or an improvement in the cleaning efficiency. In addition, the functionalisation layer led to a membrane with a greater stability under long-term operation because no significant degradation was observed, unlike the non-modified PVDF-Ds which suffer from a severe structural degradation, losing partially the active layer and appearing a water breakthrough. Moreover, the functionalisation layer hindered the extent of biofouling since a much lower presence of microorganism was determined in the fouling cake on the mPVDF.

4.3.3 Conclusions.

The commercial PVDF-Ds membrane and the organofluorisilanised PVDF-Ds membrane with enhanced hydrophobicity experienced a similar heterogeneous fouling cake formation on their surfaces when treating an anaerobic effluent for dissolved CH₄ recovery during a long-term operation

(>800 h). Proteins and polysaccharides were the major organic foulants and were mainly located at the surface of the membrane and of the fouling cake. Inorganic fouling was composed mainly of carbonate, calcium, and phosphate salts and was especially located in the centre bulk of the fouling cake, which indicates a stratification of the foulants. Hence, a proper cleaning strategy of membranes would be required to preserve the membrane integrity and performance, avoiding early membrane deterioration and exacerbated maintenance costs.

Regarding the effects of the organofluorosilanisation of PVDF-Ds, the functionalisation layer promoted the fouling deposition due to a stronger foulant-membrane interaction. However, this layer favoured the polysaccharides removal from the mPVDF surface, a lower fouling related to biomass, and a higher membrane stability against damaging attack by foulants and cleaning agents.

4.4 STABILITY OF SUPERHYDROPHOBICITY AND STRUCTURE OF PVDF MEMBRANES TREATED BY VACUUM OXYGEN PLASMA AND ORGANOFLUOROSILANISATION.

This section shows the overview and main results and conclusions derived from the work entitled “*R. Jiménez-Robles, M. Izquierdo, V. Martínez-Soria, L. Martí, A. Monleón, J.D. Badia, Stability of superhydrophobicity and structure of PVDF membranes treated by vacuum oxygen plasma and organofluorosilanisation, Membranes. 13 (2023) 314. <https://doi.org/10.3390/membranes13030314>*”. The details of the publication and the full paper can be found in *Appendix IV: Contribution IV*.

This work was the last of a series of four studies focused on hydrophobic flat-sheet membranes for the D-CH₄ recovery from liquid effluents using the gas-liquid flat-sheet membrane contactors. The previous works were focused on the validation of an experimental system for the versatile evaluation of flat-sheet membranes which allowed a useful approach for comparing different membranes and operational conditions, and for characterising the fouling under real anaerobic effluents in long-term operation (*Contributions I and III*). In addition, a membrane functionalisation methodology was validated by means of a wet alkali activation with a further grafting of a fluoroalkylsilane to enhance the wetting resistance, even though the stability of the functionalisation layer could not be guaranteed under long-term operation under a moderate-high liquid flow rate (*Contribution II*). This fourth work pretends to explore an alternative membrane functionalisation approach by using a dry activation which led to superhydrophobic membranes and avoid the generation of hazardous waste, unlike the residual NaOH solution at the end of the wet alkali activation step. As well, the potential increase in the functionalisation layer stability in long-term was investigated for this new

approach. Thus, a plasma treatment prior to the functionalisation step was evaluated on PVDF-Dp membranes.

4.4.1 Motivation, aim and overview.

As stated previously, membranes tend to suffer from wetting and fouling, especially in those applications that involve highly contaminated or quite complex liquid feeds, such as AEs [268,272,273], reducing the separation efficiency and involving additional cleaning processes [84]. Up to now, these issues are not completely resolved, hindering the large-scale application of membrane technology in such areas as desalination or dissolved CH₄ recovery [70,254,276].

Different techniques for tailoring membranes have been successfully implemented to improve their wetting resistance [68,277]. In this regard, superhydrophobic membranes (WCA $\geq 150^\circ$) [278] have been reported to significantly mitigate the wetting and fouling which was attributed to the low contact area between the liquid phase and the membrane [188]. The application of a dry plasma treatment offers an interesting methodology to induce superhydrophobicity on polymeric membrane surfaces by means of a chemical surface functionalisation. Plasma treatment is considered a versatile, reproducible, easily scalable and inexpensive method for activating and texturing polymer surfaces [170–172,279–281]. Chemical and/or physical modifications can be induced on the membrane surface depending on the plasma conditions [174,282], since the ion bombardment and interaction with the different reactive species contained in the plasma can produce sputtering of the membrane material (etching), substitution reactions, atom abstraction, removal of volatile substances and/or scission of polymer chains [173,176,179,283]. Additionally, the use of oxidative gases, such as O₂, CO₂, and H₂O, for the plasma treatment creates a more reactive environment capable of adding oxygen-containing functional groups onto the membrane surface which will act as active sites for a further grafting of functional agents.

The published works that have evaluated the effects of the long-term operation on the chemical properties, morphology and the stability of the hydrophobicity of the modified membranes are still very scarce [159]. Therefore, it is an area of interest requiring further studies into the effects of the combination of plasma activation and surface grafting on the long-term stability of membrane properties.

In this context, the aim of this work was to evaluate the effect of the vacuum oxygen plasma treatment for the surface modification of a flat-sheet PVDF-Dp membrane and the evaluation of different SiPs for the further grafting of a FAS in order to produce superhydrophobic membranes. First, membrane hydrophobicity was maximised by optimising the plasma conditions. Second, the membrane stability of the modified PVDF-Dp was evaluated and benchmarked against the pristine PVDF-Dp in terms of hydrophobicity, thermal properties, morphology, and chemical composition.

In order to elucidate the effect of an oxygen plasma treatment in the membrane hydrophobicity, a statistical design of experiment was conducted varying the plasma power and time from 3 to 17 W and from 3 to 17 min, respectively, and using two different SiPs, TEOS and APTES. Hence, a central composite design and a surface response analysis were used to optimise the power and time of the plasma discharge and maximise the membrane WCA. Afterwards, the modified membrane with the highest WCA was subjected to stability tests with the FM-PLA module using DW. Further analysis of this modified membrane before and after the stability test was conducted to determine the thermal properties (TGA and DSC), morphology (FESEM) and chemical composition (EDX). These results were benchmarked with those obtained for the pristine and coated PVDF-Dp. Coated PVDF-Dp was obtained by immersion of the membrane into the functionalisation solution without prior activation, so that only physical interactions are expected between the membrane and functional agents.

4.4.2 Results and discussion.

After the plasma treatment and functionalisation of the membranes, a WCA higher than that of the pristine PVDF-Dp ($119.4 \pm 1.7^\circ$) was obtained for all the modified membranes, with an overall mean value of 153.3° . This demonstrated that the modification procedure with the oxygen plasma activation proposed in this work was suitable to obtain superhydrophobic PVDF membranes. The incorporation of oxygen functional groups after the plasma discharge was confirmed by the hydrophilic behaviour of the membrane (WCA $<10^\circ$). The statistical design of experiments showed that SiP presented the highest standardised effect, indicating that the WCA was mainly influenced by the use of TEOS or APTES. The highest WCA values of the plasma-treated membranes were obtained with APTES, with an overall mean value of 155° , compared to those membranes modified with TEOS, with a significantly lower overall mean value of 151° . At a plasma power and time of 15% and 15 min, respectively, the fluorine-to-carbon ratio (F/C) of the pristine PVDF-Dp (0.92) increased to 0.99 and 0.95 when using APTES and TEOS, respectively. Thereby, the grafting of the FAS moieties was confirmed from the higher F/C determined for the modified membranes. Moreover, the higher F/C of the membrane treated with APTES explained its higher WCA compared with that of the membrane treated with TEOS.

The plasma power also significantly affected the WCA in the tested conditions. According to the power effect results, it seemed that the increase in the plasma power at values higher than 3 W did not create additional active sites, limiting the grafting of the SiP and FAS. However, the etching effect was observed for a power >10 W which significantly increased the WCA. Finally, from the analysis of variance and response surface, the optimal plasma conditions were set at a plasma and time of 15 W and 15 min, respectively, which maximised the WCA up to values of $\sim 157^\circ$. WCA did not increase significantly at a higher power and time, and the membrane became brittle.

Further stability tests were conducted for the membranes modified at the optimal conditions with TEOS and APTES (PO₂-TEOS and PO₂-APTES, respectively). Although the WCA of PO₂-TEOS and PO₂-APTES decreased to ~130° at 75 h, the WCA stayed almost constant and slightly higher than those of the pristine PVDF-Dp after 75 h. Thus, the effect of the functionalisation was partially lost, likely due to the dragging of grafted molecules. However, stronger chemical bonding and interactions could be inferred between the SiP, FAS and plasma activated PVDF-Dp than those shown by the coated and alkali activated membranes, whose WCAs decreased up to similar values of the original membrane in <50 h (see 4.2 *Flat PVDF membrane with enhanced hydrophobicity through alkali activation and organofluorosilanisation for dissolved methane recovery* for alkali activation results). Additionally, PO₂-APTES always showed slightly higher WCAs than PO₂-TEOS with the time of use, which was mainly attributed to the higher F content with a F/C of 0.85 and 0.80 for PO₂-APTES and PO₂-TEOS, respectively, after the stability test.

From the thermal analysis, similar findings and trends were observed for all membranes, regardless of the membrane treatment and operation, which highlights the stability of the bulk PVDF-Dp toward surface modification technologies and long-term operations. As result, a melting and decomposition temperature of ~163 °C and ~475 °C and a crystallinity of 55 – 60% were observed for all membranes.

The surface morphology of the plasma-treated membranes was similar to that of the pristine PVDF-Dp, when a low plasma power and time of 5 W and 5 min were applied, respectively. In contrast, at a higher plasma power and time of 15 W and 15 min, respectively, the surface became a pillar-like structure with a higher porosity of 15% for both PO₂-TEOS and PO₂-APTES (surface porosity of pristine membrane = 11%). Thus, a rougher surface was obtained which contributed to the increase of the WCA, leading to superhydrophobic membranes in which the droplets easily rolled off. Nonetheless, after the

stability tests, all the membranes experienced a reduction in the surface porosity to a value of ~5%, due to a plastic deformation.

4.4.3 Conclusions.

Superhydrophobic PVDF membranes were prepared by means of a surface treatment based on an initial oxygen plasma activation followed by a functionalisation with a fluoroalkylsilane and silica precursors. Thus, a maximum water contact angle of $>155^\circ$ was obtained for membranes treated at the optimal plasma conditions. Moreover, at these plasma conditions, the membrane surface showed a pillar-like morphology, with a higher porosity and roughness which favoured the superhydrophobicity and self-cleaning properties. Additionally, the use of APTES as silica precursor always led to membranes with a higher hydrophobicity than those obtained by using TEOS, which was ascribed mainly to a higher fluorine content.

Under long-term operation with a continuous liquid flux, the hydrophobic effect of the functionalisation layer was partially lost, which was attributed mainly to the removal of fluoroalkylsilane molecules. However, the functionalisation layer of the oxygen plasma-activated membranes showed the highest stability of all the membranes tested (coated membranes and alkali activated membranes). Further research should focus on the improvement of the anchoring of the modifying agents onto the PVDF substrate, and the feasibility and scalability of the functionalization methodologies for its implementation at industrial scale.

4.5 SIMULTANEOUS APPLICATION OF VACUUM AND SWEEP GAS IN A POLYPROPYLENE MEMBRANE CONTACTOR FOR THE RECOVERY OF DISSOLVED METHANE FROM WATER.

This section shows the overview and main results and conclusions derived from the work “R. Jiménez-Robles, C. Gabaldón, V. Martínez-Soria, M. Izquierdo, *Simultaneous application of vacuum and sweep gas in a polypropylene membrane contactor for the recovery of dissolved methane from water*, *Journal of Membrane Science* 617 (2021) 118560. <https://doi.org/10.1016/j.memsci.2020.118560>”. The details of the publication and the full paper can be found in *Appendix V: Contribution V*.

The potential feasibility of membrane technology in degasification of liquids, especially in the D-CH₄ recovery from AEs, makes the energy optimisation of the process a mandatory task for the full implementation of this technology at industrial scale. For that reason, the optimisation of the D-CH₄ recovery process from an energetic point of view was investigated. The main novelty of this study was the simultaneous application of a sweep gas and vacuum for creating a partial pressure gradient for the CH₄ degassing. This combination mode avoided the shortcomings of each operation mode working individually, leading to a minimum energy and sweep gas consumption. This study was focused on the operational parameters of the process and analysed some of the practical aspects involved in the potential application and implementation, and therefore it could be considered as a suitable complement to the four previous contributions. In fact, and in contrast to all the previous studies presented in this thesis, this work evaluated a commercial hollow fibre membrane contactor (HFMC) at lab-scale. A microporous PP HFMC was selected for this purpose by the results of previous studies of the research group [63].

4.5.1 Motivation, aim and overview.

The AE from biogas plants has high amounts of D-CH₄, resulting in diffuse and fugitive emissions [48]. These CH₄ emissions involve the loss of a potential energy source, environmental problems, and an explosive atmosphere. As stated previously, HFMC have emerged as a promising alternative for degasification of liquid streams since they are able to achieve high removal efficiencies with very compact units. In this regard, the CH₄ degassing in AEs with HFMC have received increasing research attention [39], and studies showing the viability of this technology [40,42,44,222,284] have recently been reported.

HFMC can operate in vacuum or sweep gas mode, in order to generate a partial pressure gradient of the solute as the driving force. On the one hand, when only vacuum is applied, high purity gas CH₄ can be obtained whilst CH₄ is diluted at sweep gas mode. On the other hand, vacuum mode shows the greatest energy consumption, even though the recovered gas CH₄ can be directly used for thermal and electricity production without previous upgrading [74]. As an alternative to overcome the drawbacks of each operation mode, vacuum and sweep gas can be used simultaneously. Nevertheless, only a few studies have reported results for this combination mode [285,286]. Considering this scarce information, it seems that studies on the combination mode are needed to enhance and deepen the knowledge of this technology, which could be especially suitable in cases of CH₄ degassing applications.

In this context, the main aim of this work was to evaluate the performance of a microporous PP HFMC operating by means of both vacuum and sweep gas simultaneously for CH₄ recovery. For this purpose, degasification tests with a synthetic water stream containing D-CH₄ were conducted, and the CH₄ removal efficiency was analysed under different operational and hydraulic conditions in short-term operation. The HFMC was operated in counter-current flow with the liquid flowing in the lumen side and vacuum and sweep gas applied in the shell side. The tested liquid flow rate ranged from 5 to 28 L h⁻¹

(liquid velocity from 1.59 to 8.90 cm s⁻¹), vacuum pressure (P_{vac}) ranged from 0 to 480 mbar, and sweep gas (N₂) flow rate ranged from 0.5 to 1.5 L h⁻¹ (gas velocity from 0.04 to 0.13 cm s⁻¹). To elucidate the effect of the combination mode on the CH₄ mass transport and feasibility for energy production from the recovered CH₄, a mass transfer and energy analysis were also carried out.

4.5.2 Results and discussion.

When operating with the PP HFMC under combination mode, the RE tended to increase with the vacuum and N₂ flow rate, due to the increase of the driving force for the CH₄ transport. The highest REs obtained in this work (~90%) were achieved for the minimum Q_L (5.0 L h⁻¹), and values of P_{vac} and Q_{N_2} higher than 100 mbar and 0.5 L h⁻¹, respectively. However, the increase in P_{vac} or Q_{N_2} at values higher than 200 mbar and 1.0 L h⁻¹, respectively, did not improve the efficiency of the process, significantly. This shows that, from a practical point of view, a combination of intermediate values of P_{vac} and Q_{N_2} would be the most suitable operational conditions.

In general, the highest RE values have been reported in sweep gas operations, and these values of RE can only be obtained with high vacuum values (800 to 950 mbar) [42,84,287,288]. A comparison of the results of this work with those obtained in a previous work [84], carried out with exactly the same HFMC under similar operational conditions in vacuum mode operation, is exposed. Similar RE values can be obtained with a combination of low vacuum and sweep gas flow rate, rather than using only a high vacuum at any Q_L values. For example, at Q_L of 5.0 L h⁻¹, RE was 84% in combination mode (with P_{vac} of 100 mbar and Q_{N_2} of 0.5 L h⁻¹) whilst a P_{vac} of 500 mbar was necessary to obtain a similar RE (82%) when only using vacuum at Q_L of 4.1 L h⁻¹. These results demonstrate the potential enhancement of the driving force caused by the additive effect of the combination of vacuum and sweep gas.

CH₄ content in the recovered gas (y_{CH_4}) played an important role when using that gas stream in microturbines for energy production, in which a

minimum CH₄ content of a 35% is required. In this sense, the gas-to-liquid flow rate ratio ($G/L = Q_{N_2}/Q_L$) appeared as a useful parameter to determine the CH₄ content. The decrease of the y_{CH_4} with G/L followed a power regression equation, indicating the high sensitivity of the y_{CH_4} in the recovered gas at low values of G/L , especially between 0.010 and 0.050, independently of the vacuum. Thus, a y_{CH_4} higher than 35% were obtained for $G/L < 0.030$, which corresponded with REs between 50% and 55%, and a maximum y_{CH_4} of 45% was obtained for the minimum G/L tested (0.012) with a RE of ~40%. A compromise between the final y_{CH_4} and RE achieved should be required for a proper optimisation of the process, from an energetic point of view.

From the mass transfer analysis, the experimental overall mass transfer coefficient ranged from $1.65 \cdot 10^{-5}$ to $3.67 \cdot 10^{-5}$ m s⁻¹, which was quite similar to those estimated by the proposed model. The mass transfer resistance of the liquid phase represented more than 98% of the overall resistance since the membrane and gas phase resistance were always below 1%. Therefore, the resistance to the CH₄ mass transport was mainly located in the liquid phase. In this sense, the efficiency of the process can be mainly controlled by the hydraulic conditions of the liquid feed, i.e., the liquid velocity. On the other hand, lower overall mass transfer resistances were usually obtained in combination mode than in vacuum mode, attributed to the absence of wetting [84]. Wetting presented a severe negative impact in the mass transfer [84] in vacuum mode, but this phenomenon was not observed in combination mode. Thus, the presence of sweep gas seemed to involve a synergic effect on the membrane surface, avoiding the overcoming of the critical transmembrane pressure [63,85,289].

In order to determine the feasibility of the operation in terms of its energy requirements, an energy analysis was carried out, assuming that the main energy consumption was related to the pumps (vacuum and liquid), and the net recovered energy was obtained from the difference between the energy produced in a microturbine using the recovered CH₄ and total energy consumption. A positive net energy was obtained under all operating conditions.

The maximum net energy was 270 kJ m⁻³, at Q_{N₂} of 1.5 L h⁻¹, Q_L of 5.0 L h⁻¹ and vacuum of 200 mbar. At these conditions, y_{CH₄} is lower than 35%, thus the recovered gas should be mixed with the main biogas stream from the anaerobic process to recover the maximum energy for electricity production. In the case of the direct use of the recovered gas in a microturbine (y_{CH₄} ≥ 35%), the actual maximum net energy was 145 kJ m⁻³ when Q_{N₂} and Q_L were 0.5 and 13.7 L h⁻¹, respectively, without vacuum.

4.5.3 Conclusions.

The recovery of dissolved methane from water by means of a microporous polypropylene hollow fibre membrane contactor, operating in combination mode (vacuum and nitrogen as sweep gas, simultaneously), showed significantly greater removal efficiencies of CH₄ and lower mass transfer resistances than independent operational modes. The maximum removal efficiency observed was higher than 90% in soft operational conditions (low nitrogen flow rate and vacuum) and a G/L ratio from 0.20. In addition, a CH₄ content of ≥ 35% was achieved at the lowest G/L ratios (<0.03) and moderate vacuum (<200 mbar).

The mass transfer analysis showed that wetting phenomenon did not take place in combination mode and the main mass transfer resistance was located in the liquid phase. On the other hand, the energy balance showed that the energy production from recovered CH₄ was greater than the energy consumption by the degasification process, allowing a self-sufficient process and reducing the carbon footprint of an anaerobic wastewater treatment plant by using this CH₄ for electricity or heat production.

4.6 MEMBRANE-ASSISTED REACTIVE CRYSTALLISATION FOR THE RECOVERY OF DISSOLVED PHOSPHORUS IN VIVIANITE FORM FROM LIQUID EFFLUENTS.

This section shows the overview and main results and conclusions derived from the work “*R. Jiménez-Robles, M. Izquierdo, V. Martínez-Soria, Lo-I Chen, K. Le Corre Pidou, E.J. McAdam, Membrane-assisted reactive crystallisation for the recovery of dissolved phosphorus in vivianite form from liquid effluents. Under review in Sep. Purif. Technol. Pre-print available at <http://dx.doi.org/10.2139/ssrn.4481071>*”. The details of the publication and the full manuscript can be found in *Appendix VI: Contribution VI*.

This work explored a new and novel application for the nutrient recovery from wastewaters. Optimisation of existing technologies and development of new technologies for nutrient recovery (P and N) are considered an essential task to be addressed for the safety nutrient supply. Thus, this work aimed to study a membrane-assisted reactive crystallisation process for the P recovery in form of vivianite using different types of flat-sheet membranes at lab-scale. This new approach could enhance the prospect of P recovery to realise benefits to cost and yield at large-scale processes, while also taking advantage of downstream value due to a homogeneous quality of the product.

In addition, the characterisation and evaluation methods of the process studied have been rarely reported. Thus, this work presents the development of new knowledge in the crystallisation of vivianite, and the development of membrane-assisted crystallisation as a platform technology for reactive systems. This meant a broadening of the thesis scope by including an additional membrane-based technology application for the resource recovery.

4.6.1 Motivation, aim and overview.

As stated in the introduction section, P is an essential element for life in Earth [102,105,290], and an important component of the most used fertilizers [290]. In addition, P compounds are valuable chemicals for the electronic industry [118] and immobilization of heavy metals [291,292], among others applications. However, the available P in nature is depleting at an accelerated rate due to the rising global demand [102,109,293]. Therefore, the search and exploitation of new and renewable P sources seem of vital importance to ensure the feasible supply of this element [118,294]. In this regard, the wastewaters rich in phosphates appear as a potential source of renewable P, which also will aid in the compliance of the environmental regulations. The main process for P recovery is the crystallisation of struvite by the addition of Mg salts [23], even though the high cost in chemicals and the relative low efficiency of the process hinder the application and feasibility at large-scale [102,105,140]. Thus, the optimization of current techniques and the development of new processes that enable lower cost and higher efficiency with greater control are imperative.

Vivianite ($\text{Fe}_3(\text{PO}_4)_2 \cdot 8\text{H}_2\text{O}$) is considered a valuable chemical for its use as a slow-release fertilizer, for the production of lithium-ion batteries and in the electronic industry [102,108,118]. Vivianite presents an extremely low solubility in water [108,109], thereby, it could be easily obtained by precipitation of phosphates contained in a liquid matrix after the addition of Fe^{2+} salts [105,110], which are cheaper than Mg salts. However, only a few studies regarding the synthesis of vivianite has been published [102,109,118]. Thus, the crystallisation processes of the vivianite need a comprehensive and deeper understanding in order to develop a feasible and scalable process [109].

The main drawback of traditional crystallisers (stirred tanks) is the difficult control of the crystallisation due to low mixing level of the reactants which leads to the poor regulation of supersaturation, which is the driving force for crystal nucleation [123,124,138]. In contrast, membrane contactors can provide a fixed and huge interfacial area which provides a homogeneous

regulation of supersaturation, while the formation of a well-defined boundary layer also creates a region of elevated supersaturation [123,139]. As well, the membrane can provide a high level of micromixing [126–129], allowing high supersaturation indices and low induction times [122]. Consequently, membrane-assisted reactive crystallisation (MARC) process has emerged in recent years in an effort to optimise and control both nucleation and crystal growth [61,122,123]. However, this process has been rarely studied. In this sense, MARC could provide strict control over nucleation kinetics that can enhance the prospect of P recovery.

In this context, a MARC process for the P recovery in the form of vivianite by means of a FM at lab-scale was proposed. The MARC was applied in treating a phosphate-rich solution as a synthetic effluent for the continuous crystallisation of vivianite by the dosing of a Fe^{2+} solution through the membrane. Main specific objectives were therefore to: (i) investigate how boundary layer conditions can be used to regulate supersaturation and nucleation kinetics by applying different hydrodynamic conditions; (ii) study the effects of membrane properties to determine how they might influence in the nucleation kinetic, and; (iii) develop a framework that can relate boundary layer conditions to nucleation kinetics by direct determination of induction time in the bulk solution and at the membrane.

For the evaluation of the MARC process in the P recovery, crystallisation tests were conducted with the FM-MA module under different hydraulic conditions, varying the liquid flow rate from 8 to 30 L h^{-1} (liquid velocities from 2.8 to 10.4 cm s^{-1} and Reynolds [Re_p] from 105 to 395). In order to elucidate the effects of the membrane properties in the crystallisation process, different membranes were evaluated: PVDF-St, PVDF-Ds, alkali activated and functionalised PVDF-Ds, PVDF-Dp, PP-2E, PTFE-1 and PTFE-3. The synthesised crystals from the crystallisation tests were further analysed by means of electron microscopy (FESEM) and spectroscopy (EDX, XRD) techniques in order to determine its morphology, crystal size and chemical

composition. Also, the supersaturation was estimated, and the kinetic of the crystallisation process was analysed based on the principles of the classical nucleation theory.

4.6.2 Results and discussion.

Crystallisation tests for the P recovery were conducted with the PVDF-St membrane at different Re_p inside the FM to evaluate the role of the boundary layer at different hydrodynamic conditions in modifying the nucleation rate of vivianite. Turbidity profiles evidenced the onset of nucleation, in which the first solid particles were detected in the solution bulk (bulk induction time). The time at which turbidity commenced was delayed when Re_p was increased from 105 to 395 (10.5 ± 0.7 y 26.0 ± 5.7 min, respectively). Following nucleation, the turbidity continued to increase, reaching higher values as Re_p decreased. This indicates that a higher nucleation rate can be achieved at lower liquid velocities inside the membrane module.

Supersaturation index (SI) values ranging from 8.0 to 8.7 at bulk induction times of 10.5 and 26.0 min were estimated, respectively. Although the supersaturation is the main driving force for nucleation, the estimated SI of vivianite was independent of the hydrodynamics conditions tested, which was attributed to the low solubility of vivianite [295]. However, two aspects should be considered: (i) the liquid velocity decreased may result in a relatively higher local supersaturation in the boundary layer, which would increase the nucleation rate [124], and (ii) the high level of micromixing provided by the porous membrane [122,132] may increase the collision frequency of the reactive ions, lowering the activation energy for nucleation [136,137]. Thus, longer residence times at low Re_p would increase the probability for mixing and ion collision inside the membrane module, accelerating the nucleation. This effect was in accordance with the experimental tendency obtained.

In order to elucidate the influence of the supersaturation in the nucleation rate, a crystallisation kinetic analysis was conducted using the

empirical power-law model proposed by Sangwal [250] based on the CNT. Although CNT postulates that higher nucleation rates are ordinarily facilitated within a region of elevated supersaturation, higher nucleation rates were associated to a lower vivianite supersaturation in this study. Thus, nucleation rates from 3.40 to 5.69 mg L⁻¹ min⁻¹ were estimated as the bulk induction time decreased from 26.0 to 4.0 min. Therefore, other factors such as micromixing effects, ion collision probability, ion diffusion, and local supersaturation seemed to exert a dominant effect in the nucleation rate at the operational condition tested. Nonetheless, the empirical power-law model could predict the nucleation rate as a function of the supersaturation with a high level of confidence ($R^2 = 0.98$). In conclusion, mixing effects and boundary layer conditions should be considered in the crystallisation kinetics, especially for the scaling up of the technology.

Membrane materials also presented an important influence in determining the free energy requirement of nucleation, and/or in modifying local mixing conditions to shorten induction times. In general terms, the induction times were especially conditioned by the WCA and ϵ of the membrane. WCA and ϵ values higher than 119° and 65%, respectively, considerably shortened the induction time, suggesting that the activation energy requirement for nucleation was lowered, and leading to higher nucleation rates. This tendency was attributed to a preferential heterogeneous primary nucleation and the promotion of mixing effects. Hence, this analysis indicated that nucleation kinetics can be controlled also by setting the membrane properties.

The solid particles formed during the crystallisation tests corresponded with spherical and glassy-like nanoparticles of ~35 nm, and no conglomerates were observed. The characteristics of this type of particles/crystals suggested that high nucleation rates were achieved, and the nucleation region was limited to the membrane module whilst the crystal growth was hindered. Finally, the chemical composition and structure of the particles were determined. The

particles were composed of amorphous and partially oxidised vivianite-based compounds with significant amount of iron hydroxides.

4.6.3 Conclusions.

The membrane-assisted reactive crystallisation has been demonstrated as a useful approach for controlling and modifying the vivianite nucleation process in the P recovery from a liquid effluent by the dosing of an iron (II) solution. The crystal nucleation was strongly influenced by the boundary layer and membrane properties; therefore, the nucleation could be controlled by means of the hydrodynamic conditions and changing or tailoring the membrane properties.

The nucleation process aided by a membrane module did not agree the principles of the classical nucleation theory, since nucleation was strongly influenced by local mixing effects. A higher local supersaturation, the enhanced mixing and ion collision probability favoured the nucleation even at lower supersaturation degrees. These effects were enhanced at low liquid velocities which provided a higher residence time inside the membrane module, and at higher membrane hydrophobicity and porosity which promoted the micromixing and lowered the energy barrier for nucleation.

In conclusion, the integration of the membrane technology and the modelling of the nucleation kinetic can ease the prospect of P recovery in vivianite to release benefits to cost and yield at large-scale processes, while also taking advantage of downstream value due to a homogeneous quality of crystals.

5 CONCLUSIONS AND FUTURE PROSPECT.

5.1 MAIN CONCLUSIONS OF THIS THESIS.

Membrane technology has been demonstrated to be a useful approach for separation and reactive systems in the recent decades, due to its intrinsic characteristic of efficiency, satisfying the concept of process intensification. Nevertheless, wetting, and fouling phenomena stay as the main issues unsolved which hinder the full implementation of membrane contactors at large-scale. Therefore, the optimisation of operational conditions, and the search of suitable prevention techniques such as membrane functionalisation or cleaning protocols are imperative to avoid or mitigate the wetting and fouling effects, ensuring a high membrane performance in long-term operation. As well, the integration of membrane technology might resolve some of the challenges that Chemical Engineering is currently facing such as the difficult control of the mixing level of the reactants in conventional stirred tanks or the rationalisation of raw materials.

In this sense, this thesis has focused on the applicability of membrane contactors in the recovery of dissolved CH_4 and P from liquid effluents for their valorisation. As well, surface functionalisation methods were evaluated in order to increase the wetting resistance, performance and useful lifetime of PVDF membranes. In general terms, membrane contactors always provided high removal efficiencies and an easy control of the process. Moreover, membrane surface functionalisation with fluoroalkylsilanes increased the wetting resistance, and especially the membrane useful lifetime, which could lower considerably the OPEX at industrial scale.

The significant conclusions of the whole work are divided into three sections according to the three partial objectives of this thesis and summarised below.

Objective 1. Evaluation of the membrane performance in the dissolved methane recovery from liquid effluents using gas-liquid flat-sheet membrane contactors.

The applicability and versatility of a gas-liquid flat-sheet membrane contactor has been demonstrated for the dissolved CH₄ recovery from liquid effluents. The removal efficiency was mainly influenced by the hydraulic conditions since the negligible mass transfer resistance of the membrane and gas phase. However, commercial PVDF membranes showed a lower removal efficiency at moderate-high liquid velocities attributed to the membrane wetting, which was avoided after the membrane functionalisation with an alkali activation, leading to an increase in the removal efficiency.

The water contact angle measurements were a useful indicator of the membrane stability during their operations. Thus, the commercial PDMS and PVDF membranes presented a good stability (no significant changes in their hydrophobicity) after 150 h at low liquid velocities (2.8 cm s⁻¹). On the contrary, their hydrophobicity was altered with the time at moderate-high liquid velocities (16.9 cm s⁻¹), according to the surface deformation and degradation observed, limiting their useful lifetime.

The surface modification of PVDF-Ds membranes with alkali activation followed by the functionalisation with a fluoroalkylsilane led to a maximum water contact angle of ~143° at the optimal conditions, representing an increase of 39% respect to the initial value of the non-modified membrane (nmPVDF). This modified membrane (mPVDF_{max}) presented a heterogeneous surface with dense-like clusters and a higher fluorine content than nmPVDF which led to a reduction of the surface porosity, and an increase in the hydrophobicity.

The mPVDF_{max} showed a slightly higher CH₄ removal efficiency in short-term experiments attributed to the higher wetting resistance than the nmPVDF. In long-term operation with a real anaerobic effluent, the removal efficiency declined with the time due to the fouling cake formation, and consequently, to the additional resistance for the mass transport. The decline

in CH₄ recovery was more pronounced with the mPVDF_{max} since this membrane presented a lower fouling resistance.

Regarding the membrane stability, the hydrophobic effect of the functionalisation layer was completely lost from the mPVDF_{max} after 50 h of operation with deionised water at a moderate-high liquid velocity. However, mPVDF_{max} showed a greater chemical resistance and stability than the nmPVDF when treating a real anaerobic effluent during >800 h, since lower water contact angles with the time and a water breakthrough were observed in the nmPVDF.

mPVDF_{max} suffered a higher fouling deposition due to a stronger foulant-membrane interaction than nmPVDF when treating an anaerobic effluent during a long-term operation (>800 h). However, the polysaccharides were completely removed from the mPVDF_{max} and a lower fouling related to biomass was inferred.

In general terms, proteins and polysaccharides were the major organic foulants and were mainly located at the surface of the membrane and of the fouling cake. On the other hand, inorganic fouling was composed mainly of salts of carbonate, calcium, and phosphate and was especially located in the centre bulk of the fouling cake, which indicates a stratification of the foulants.

A vacuum oxygen plasma treatment was used as an alternative to the alkali activation in order to evaluate a new methodology which avoid the generation of hazardous waste and could infer a higher effect in the hydrophobicity increase. The plasma activation in PVDF-Dp led to superhydrophobic membranes with a maximum water contact angle of ~157° at the optimal plasma condition (power and time of 15 W and 15 min, respectively) using APTES as silica precursor. The plasma treated membranes at the optimal conditions (PO₂-PVDF_{max}) presented a surface with a pillared-like structure, higher porosity, and roughness which contributed to increase the membrane hydrophobicity. In addition, the fluorine content increased after the

functionalisation, being higher than that of the alkali treated membranes (mPVDF_{max}).

PO₂-PVDF_{max} showed a higher stability under long-term operation than the alkali treated membrane mPVDF_{max}. In this sense, a water contact angle of ~130° was observed for the PO₂-PVDF_{max} membranes after 160 h of operation with deionised water at the moderate-high liquid velocity, which was higher than the water contact angle of the non-modified PVDF-Dp (119°). Nonetheless, the membrane surface of PO₂-PVDF_{max} membranes also experienced a plastic deformation, resulting in a reduced surface porosity.

Objective 2. Optimisation of the dissolved methane recovery with a polypropylene hollow fibre membrane contactor by means of the simultaneous application of vacuum and sweep gas.

The recovery of dissolved CH₄ from water by means of a microporous polypropylene hollow fibre membrane contactor, operating in combination mode, showed significantly greater removal efficiencies and lower mass transfer resistances than independent operational modes. Additionally, the combination mode mitigated the membrane wetting.

A maximum removal efficiency of ~90% and a CH₄ content higher than 35% in the reversed gas was obtained at low G/L ratios ≤0.20 and vacuum ≤200 mbar. Furthermore, a positive net energy production was always observed, allowing a self-sufficient process with a maximum net energy of 270 kJ m⁻³ of treated effluent at G/L of 0.30 and moderate vacuum of 200 mbar.

In conclusion, combination mode can enhance the performance of the membrane contactor to recover dissolved CH₄ from anaerobic effluents, reducing the carbon footprint of an anaerobic wastewater treatment plant by using this methane for electricity or heat production.

Objective 3. Integration of membrane crystallisation in the recovery of dissolved phosphorus in form of solid vivianite.

The P recovery from a liquid effluent by crystallisation of vivianite in a membrane-assisted reactive crystallisation showed a greater control in the nucleation process than conventional stirred tank reactors. Crystal nucleation was strongly influenced by the boundary layer inside the membrane module, in which nucleation rate increased as the liquid velocity decreased, also reducing the induction time. In addition, a porous membrane facilitated the micromixing of the reactants and lowered the energy barrier for nucleation, in which the induction time tended to decrease as the membrane hydrophobicity, roughness, pore size, and porosity increased. Therefore, the nucleation could be easily controlled by setting the appropriate hydraulic conditions and membrane properties.

The nucleation kinetic analysis showed that higher nucleation rates were associated to a lower vivianite supersaturation which was attributed to an ion-dependent collision crystallisation mechanism. Thus, the higher supersaturation rates promote greater mixing and a higher ion collision probability, reducing the activation energy requirement for nucleation even at low supersaturation levels. The higher supersaturation rates and micromixing led to the formation of vivianite nanoparticles of ~35 nm.

In conclusion, the membrane-assisted reactive crystallisation offers a potential feasible alternative to recover P from wastewaters, even though a deeper insight into the vivianite crystallisation and modelling of the nucleation kinetic in a membrane-assisted reactive crystallisation process is necessary.

5.2 FUTURE PROSPECT.

The dissolved CH₄ recovery from anaerobic effluents using gas-liquid membrane contactors has been demonstrated as a promising technology for the waste-to-energy conversion of residual waste. This thesis has provided a deep insight into the process optimisation from the point of view of operational and energy costs, developing membranes with a longer lifespan and testing the novel combination mode operation which maximised the net energy production. However, scale-up of this technology is still beyond the horizon due to some critical concerns that need substantial research:

- Fouling phenomena requires the development of fouling resistance surfaces to avoid the early membrane degradation and the separation efficiency decline. In this sense, functionalisation methodologies using modifying agents with both antifouling and antiwetting properties are proposed, especially those that lead to superhydrophobic and omniphobic membranes. Likewise, novel lithography techniques should be investigated since the generation of a pattern on the membrane surface could reduce the fouling deposition due to an additional local turbulence in the liquid flux on the surface.
- Functionalisation layer in modified membranes usually showed a relatively low stability in long-term operation under moderate-high liquid fluxes. Hence, new functionalisation methodologies that improve the fixation of the modifying agents are imperative to guarantee the effect of the functionalisation layer over long-term. Therefore, investigation of new protocols is proposed focused on the increase in the chemical grafting of the modifying agent.
- Cleaning strategies of the membrane surface are also proposed as an essential methodology to mitigate the fouling effects. Even membranes with high antifouling properties are prone to be fouled in long-term operation. Hence, cleaning protocols based on a flushing of the

membranes should be investigated in order to establish the suitable cleaning agents (water, alkalis, acids, organic solvents, disinfectants, etc.), their concentrations, and the frequency of each treatment. A suitable cleaning strategy must preserve the membrane performance as well as the membrane integrity.

- Membrane material and its properties define the efficiency of the process as well as its wetting and fouling resistance. Hence, the synthesis of new membrane materials with enhanced properties could avoid the application of a further functionalisation which will lower the costs associated with the membrane contactors. In this sense, the membrane properties could be tailored by means of the inclusion of additives during the membrane synthesis which will promote the pore formation, surface roughness, new functionalities, etc.

Regarding nutrients recovery, the dissolved P as phosphate from a liquid stream recovered by means of a membrane-assisted reactive crystallisation has been evaluated for first time at lab-scale. This process has been demonstrated as a useful approach to recover P and produce vivianite under a controllable environment. However, the implementation of this technology at industrial scale is still so far due to the scarcity of studies regarding membrane reactive crystallisation processes and vivianite synthesis. In order to widen the studies in the framework of nutrient recovery by membrane crystallisation, the following research lines could be implemented:

- Evaluation of the reactant dosing rate and concentration effects in the vivianite crystallisation since these parameters could affect the micromixing and ion collision probability.
- Determination of the crystallisation mechanisms for different hydrophilic and hydrophobic membranes. A deep insight into these mechanisms could provide useful information to avoid the consumption of the reactant in secondary reactions.

5. Conclusions and Future Prospect

- Modelling of the nucleation kinetic based on mixing effects and ion collision probability that enables the scaling up of the process.
- Recovery of dissolved P from a real wastewater to determine the feasibility of this process under real conditions.

6 REFERENCES.

- [1] IPCC, 2022: Annex I: Glossary [van Diemen, R., J.B.R. Matthews, V. Möller, J.S. Fuglestvedt, V. Masson-Delmotte, C. Méndez, A. Reisinger, S. Semenov (eds)]. In IPCC, 2022: *Climate Change 2022: Mitigation of Climate Change. Contribution of Working Group III to the Sixth Assessment Report of the Intergovernmental Panel on Climate Change* [P.R. Shukla, J. Skea, R. Slade, A. Al Khourdajie, R. van Diemen, D. McCollum, M. Pathak, S. Some, P. Vyas, R. Fradera, M. Belkacemi, A. Hasija, G. Lisboa, S. Luz, J. Malley, (eds.)]. Cambridge University Press, Cambridge, UK and New York, NY, USA. doi: 10.1017/9781009157926.020.
- [2] IPCC, 2023: Summary for Policymakers. In: *Climate Change 2023: Synthesis Report. A Report of the Intergovernmental Panel on Climate Change. Contribution of Working Groups I, II and III to the Sixth Assessment Report of the Intergovernmental Panel on Climate Change* [Core Writing Team, H. Lee and J. Romero (eds.)]. IPCC, Geneva, Switzerland, 36 pages. (in press).
- [3] IPCC, 2022: Annex II: Definitions, Units and Conventions [Al Khourdajie, A., R. van Diemen, W.F. Lamb, M. Pathak, A. Reisinger, S. de la Rue du Can, J. Skea, R. Slade, S. Some, L. Steg (eds)]. In IPCC, 2022: *Climate Change 2022: Mitigation of Climate Change. Contribution of Working Group III to the Sixth Assessment Report of the Intergovernmental Panel on Climate Change* [P.R. Shukla, J. Skea, R. Slade, A. Al Khourdajie, R. van Diemen, D. McCollum, M. Pathak, S. Some, P. Vyas, R. Fradera, M. Belkacemi, A. Hasija, G. Lisboa, S. Luz, J. Malley, (eds.)]. Cambridge University Press, Cambridge, UK and New York, NY, USA. doi: 10.1017/9781009157926.021.
- [4] Forster, P., V. Ramaswamy, P. Artaxo, T. Berntsen, R. Betts, D.W. Fahey, J. Haywood, J. Lean, D.C. Lowe, G. Myhre, J. Nganga, R. Prinn, G. Raga, M. Schulz and R. Van Dorland, 2007: Changes in Atmospheric Constituents and in Radiative Forcing. In: *Climate Change 2007: The Physical Science Basis. Contribution of Working Group I to the Fourth Assessment Report of the Intergovernmental Panel on Climate Change* [Solomon, S., D. Qin, M. Manning, Z. Chen, M. Marquis, K.B. Averyt, M. Tignor and H.L. Miller (eds.)]. Cambridge University Press, Cambridge, United Kingdom and New York, NY, USA.

- [5] Forster, P., T. Storelvmo, K. Armour, W. Collins, J.L. Dufresne, D. Frame, D.J. Lunt, T. Mauritsen, M.D. Palmer, M. Watanabe, M. Wild, H. Zhang, 2021, The Earth's Energy Budget, Climate Feedbacks, and Climate Sensitivity. In: *Climate Change 2021: The Physical Science Basis. Contribution of Working Group I to the Sixth Assessment Report of the Intergovernmental Panel on Climate Change* [Masson-Delmotte, V., P. Zhai, A. Pirani, S.L. Connors, C. Péan, S. Berger, N. Caud, Y. Chen, L. Goldfarb, M.I. Gomis, M. Huang, K. Leitzell, E. Lonnoy, J.B.R. Matthews, T.K. Maycock, T. Waterfield, O. Yelekçi, R. Yu, and B. Zhou (eds.)]. Cambridge University Press, Cambridge, United Kingdom and New York, NY, USA, pp. 923–1054, doi:10.1017/9781009157896.009.
- [6] European Environment Agency (EEA), Data viewer on greenhouse gas emissions and removals, sent by countries to UNFCCC and the EU Greenhouse Gas Monitoring Mechanism (EU Member States). Available online: <https://www.eea.europa.eu/data-and-maps/data/data-viewers/greenhouse-gases-viewer> (accessed on 7th July 2023).
- [7] R. Van Dingenen, J. Crippa, M., G. Anssens-Maenhout, D. Guizzardi, F. Dentener, Global trends of methane emissions and their impacts on ozone concentrations, *Off. Eur. Union. EUR29394EN* (2018) 1–90. <https://doi.org/10.2760/820175>.
- [8] A. Guisasola, D. de Haas, J. Keller, Z. Yuan, Methane formation in sewer systems, *Water Res.* 42 (2008) 1421–1430. <https://doi.org/10.1016/j.watres.2007.10.014>.
- [9] G. Tchobanoglous, F.L. Burton, H. David Stensel, *Wastewater engineering: treatment and reuse*, 4th ed., McGraw-hill, Boston, 2003.
- [10] IPCC, 2007: *Climate Change 2007: The Physical Science Basis. Contribution of Working Group I to the Fourth Assessment Report of the Intergovernmental Panel on Climate Change* [Solomon, S., D. Qin, M. Manning, Z. Chen, M. Marquis, K.B. Averyt, M. Tignor and,
- [11] United States Environmental Protection Agency (EPA), *Climate Change Indicators: Atmospheric Concentrations of Greenhouse Gases*. Available online: <https://www.epa.gov/climate-indicators/climate-change-indicators-atmospheric-concentrations-greenhouse-gases> (accessed on 7th July 2023).
- [12] European Commission, 2020: *Communication from the commission to the European parliament, the council, the European economic and social committee and the committee of the regions on an EU strategy to reduce*

- methane emissions (COM/2020/663). Available online: <https://www.eumonitor.eu/9353000/1/j9vvik7m1c3gyxp/vlcxt8splkzm> (accessed on 7th July 2023).
- [13] Encyclopaedia Britannica (2023), Methane. Available online: <https://www.britannica.com/science/methane> (accessed on 6th June 2023).
- [14] H. Ding, S. Tong, Z. Qi, F. Liu, S. Sun, L. Han, Syngas production from chemical-looping steam methane reforming: The effect of channel geometry on BaCoO₃/CeO₂ monolithic oxygen carriers, *Energy*. 263 (2023) 126000. <https://doi.org/10.1016/j.energy.2022.126000>.
- [15] A. Calbry-Muzyka, H. Madi, F. Rüsç-Pfund, M. Gandiglio, S. Biollaz, Biogas composition from agricultural sources and organic fraction of municipal solid waste, *Renew. Energy*. 181 (2022) 1000–1007. <https://doi.org/10.1016/j.renene.2021.09.100>.
- [16] European Biogas Association, Statistical report 2022. Tracking biogas and biomethane deployment across Europe, 2022.
- [17] Ministerio para la Transición Ecológica y el Reto Demográfico., Hoja de ruta del biogás, 2022. https://energia.gob.es/es-es/Novedades/Documents/00HR_Biogas_V6.pdf.
- [18] Instituto para Diversificación y Ahorro de Energía (IDAE), Biogás. Available online: <https://www.idae.es/tecnologias/energias-renovables/uso-termico/biogas> (accessed on 6th June 2023).
- [19] ONU, World Population Prospects 2019: Press Release. Available online: https://population.un.org/wpp/Publications/Files/WPP2019_PressRelease_EN.pdf (accessed on 11th June 2023).
- [20] FAO. 2018. The future of food and agriculture – Alternative pathways to 2050. Rome. 224 pp. Licence: CC BY-NC-SA 3.0 IGO.
- [21] OECD/FAO (2021), OECD-FAO Agricultural Outlook 2021-2030, OECD Publishing, Paris, <https://doi.org/10.1787/19428846-en..>
- [22] FAO. 2019. World fertilizer trends and outlook to 2022. Rome.
- [23] F. Rizzioli, D. Bertasini, D. Bolzonella, N. Frison, F. Battista, A critical review on the techno-economic feasibility of nutrients recovery from anaerobic digestate in the agricultural sector, *Sep. Purif. Technol.* 306 (2023) 122690. <https://doi.org/10.1016/j.seppur.2022.122690>.
- [24] B. Drog, W. Fuchs, T. Al Seadi, M. Madsen, B. Linke, Nutrient Recovery by Biogas Digestate Processing Bernhard, 2015.

- [25] C.M. Mehta, W.O. Khunjar, V. Nguyen, S. Tait, D.J. Batstone, Technologies to recover nutrients from waste streams: A critical review, *Crit. Rev. Environ. Sci. Technol.* 45 (2015) 385–427. <https://doi.org/10.1080/10643389.2013.866621>.
- [26] H. Ohtake, S. Tsuneda, eds., *Phosphorous: Recovery and recycling*, Springer Singapore, 2019. <https://doi.org/10.1007/978-981-10-8031-9>.
- [27] E. Walling, C. Vaneckhaute, Greenhouse gas emissions from inorganic and organic fertilizer production and use: A review of emission factors and their variability, *J. Environ. Manage.* 276 (2020). <https://doi.org/10.1016/j.jenvman.2020.111211>.
- [28] Fertilizers Europe, *Fertilisers Europe (2021). Forecast of Food, Farming and Fertilizer Use in the European Union 2021-2031*. Available online: <https://www.fertilizerseurope.com/wp-content/uploads/2021/12/Forecast-2021-31-Studio-final-web.pdf> (accessed on 7th July 2023).
- [29] Eurostat, *Statistics Explained (2022). Agri-environmental indicator - mineral fertiliser consumption*. Available online: https://ec.europa.eu/eurostat/statistics-explained/index.php?title=Agri-environmental_indicator_-_mineral_fertiliser_consumption#Analys (accessed on 7th July 2023).
- [30] Fertilizers Europe (2022). *Overview 2021/22*. Available online: <https://www.fertilizerseurope.com/AnnualOverview/images/FER-AR22%20web.pdf> (accessed on 11th June 2023).
- [31] M.P. Maniscalco, M. Volpe, A. Messineo, Hydrothermal carbonization as a valuable tool for energy and environmental applications: A review, *Energies*. 13 (2020). <https://doi.org/10.3390/en13164098>.
- [32] R.W. Scholz, A.H. Roy, F.S. Brand, D.T. Hellums, A.E. Ulrich, *Sustainable phosphorous management*, Springer Science and Business Media Deutschland GmbH, 2014. <https://doi.org/10.1007/978-94-007-7250-2>.
- [33] L. Egle, H. Rechberger, J. Krampe, M. Zessner, Phosphorus recovery from municipal wastewater: An integrated comparative technological, environmental and economic assessment of P recovery technologies, *Sci. Total Environ.* 571 (2016) 522–542. <https://doi.org/10.1016/j.scitotenv.2016.07.019>.
- [34] A. Jama-Rodzeńska, A. Białowiec, J.A. Koziel, J. Sowiński, Waste to phosphorus: A transdisciplinary solution to P recovery from wastewater based on the TRIZ approach, *J. Environ. Manage.* 287 (2021).

- <https://doi.org/10.1016/j.jenvman.2021.112235>.
- [35] Ordinance on the reorganisation of sewage sludge recycling, Federal Law Gazette of Germany, Part I, No. 65, Vol 27, September 2017. Available online:
https://www.bgbl.de/xaver/bgbl/start.xav?startbk=Bundesanzeiger_BGBl&jumpTo=bgbl117s3465.pdf#_bgbl_%2F%2F*%5B%40attr_id%3D%27bgbl117s3465.pdf%27%5D__1688743038207 (accessed on 7th July 2023).
- [36] S. Petzet, P. Cornel, Towards a complete recycling of phosphorus in wastewater treatment - options in Germany, *Water Sci. Technol.* 64 (2011) 29–35. <https://doi.org/10.2166/wst.2011.540>.
- [37] Environmental Protection Agency (EPA). (2012). Global Anthropogenic Non-CO₂ Greenhouse Gas Emissions: 1990 - 2030. Washington DC..
- [38] R. Sander, Compilation of Henry's law constants (version 4.0) for water as solvent, *Atmos. Chem. Phys.* 15 (2015) 4399–4981. <https://doi.org/10.5194/acp-15-4399-2015>.
- [39] B.C. Crone, J.L. Garland, G.A. Sorial, L.M. Vane, Significance of dissolved methane in effluents of anaerobically treated low strength wastewater and potential for recovery as an energy product: A review, *Water Res.* 104 (2016) 520–531. <https://doi.org/10.1016/j.watres.2016.08.019>.
- [40] J. Cookney, E. Cartmell, B. Jefferson, E.J. McAdam, Recovery of methane from anaerobic process effluent using poly-di-methyl-siloxane membrane contactors, *Water Sci. Technol.* 65 (2012) 604–610. <https://doi.org/10.2166/wst.2012.897>.
- [41] K.S. Singh, H. Harada, T. Viraraghavan, Low-strength wastewater treatment by a UASB reactor, *Bioresour. Technol.* 55 (1996) 187–194. [https://doi.org/10.1016/0960-8524\(96\)86817-9](https://doi.org/10.1016/0960-8524(96)86817-9).
- [42] W.M.K.R.T.W. Bandara, H. Satoh, M. Sasakawa, Y. Nakahara, M. Takahashi, S. Okabe, Removal of residual dissolved methane gas in an upflow anaerobic sludge blanket reactor treating low-strength wastewater at low temperature with degassing membrane, *Water Res.* 45 (2011) 3533–3540. <https://doi.org/10.1016/j.watres.2011.04.030>.
- [43] C.L. Souza, C.A.L. Chernicharo, S.F. Aquino, Quantification of dissolved methane in UASB reactors treating domestic wastewater under different operating conditions, *Water Sci. Technol.* 64 (2011) 2259–2264. <https://doi.org/10.2166/wst.2011.695>.

- [44] J. Cookney, A. Mcleod, V. Mathioudakis, P. Ncube, A. Soares, B. Jefferson, E.J. McAdam, Dissolved methane recovery from anaerobic effluents using hollow fibre membrane contactors, *J. Membr. Sci.* 502 (2016) 141–150. <https://doi.org/10.1016/j.memsci.2015.12.037>.
- [45] A.L. Smith, S.J. Skerlos, L. Raskin, Psychrophilic anaerobic membrane bioreactor treatment of domestic wastewater, *Water Res.* 47 (2013) 1655–1665. <https://doi.org/10.1016/j.watres.2012.12.028>.
- [46] J.B. Giménez, N. Martí, J. Ferrer, A. Seco, Methane recovery efficiency in a submerged anaerobic membrane bioreactor (SANMBR) treating sulphate-rich urban wastewater: Evaluation of methane losses with the effluent, *Bioresour. Technol.* 118 (2012) 67–72. <https://doi.org/10.1016/j.biortech.2012.05.019>.
- [47] V. Stazi, M.C. Tomei, Dissolved methane in anaerobic effluents: A review on sustainable strategies for optimization of energy recovery or internal process reuse, *J. Clean. Prod.* 317 (2021) 1–13. <https://doi.org/10.1016/j.jclepro.2021.128359>.
- [48] M.R.J. Daelman, E.M. van Voorthuizen, U.G.J.M. van Dongen, E.I.P. Volcke, M.C.M. van Loosdrecht, Methane emission during municipal wastewater treatment, *Water Res.* 46 (2012) 3657–3670. <https://doi.org/10.1016/j.watres.2012.04.024>.
- [49] X. Li, H.S. Lee, Z. Wang, J. Lee, State-of-the-art management technologies of dissolved methane in anaerobically-treated low-strength wastewaters: A review, *Water Res.* (2021). <https://doi.org/10.1016/j.watres.2021.117269>.
- [50] S. Heile, C.A.L. Chernicharo, E.M.F. Brandt, E.J. McAdam, Dissolved gas separation for engineered anaerobic wastewater systems, *Sep. Purif. Technol.* 189 (2017) 405–418. <https://doi.org/10.1016/j.seppur.2017.08.021>.
- [51] L. Kinidi, I. Ai, W. Tan, N. Binti, A. Wahab, K. Fikri, B. Tamrin, C.N. Hipolito, S.F. Salleh, Recent Development in Ammonia Stripping Process for Industrial Wastewater Treatment, *Int. J. Chem. Eng.* 2018 (2018) 14.
- [52] D. Fischer, Air stripping for drinking water, *Filtr. Sep.* 56 (2019) 28–30. [https://doi.org/10.1016/S0015-1882\(20\)30107-5](https://doi.org/10.1016/S0015-1882(20)30107-5).
- [53] R.. Glória, T.M. Motta, P.V.O. Silva, P. da Costa, E.M.F. Brandt, C.L. de Souza, C. de L. Chernicharo, Stripping and dissipation techniques for the removal of dissolved gases from anaerobic effluents., *Brazilian J. Chem. Eng.* 33 (2015) 713–721. <https://doi.org/10.1590/0104-6632.20160334s20150291>.

- [54] K. Hartley, P. Lant, Eliminating non-renewable CO₂ emissions from sewage treatment: An anaerobic migrating bed reactor pilot plant study, *Biotechnol. Bioeng.* 95 (2006) 384–398.
- [55] Y. Shen, J.L. Linville, M. Urgan-Demirtas, M.M. Mintz, S.W. Snyder, An overview of biogas production and utilization at full-scale wastewater treatment plants (WWTPs) in the United States: Challenges and opportunities towards energy-neutral WWTPs, *Renew. Sustain. Energy Rev.* 50 (2015) 346–362. <https://doi.org/10.1016/j.rser.2015.04.129>.
- [56] R.S. Hanson, T.E. Hanson, Methanotrophic bacteria, *Microbiol. Rev.* 60 (1996) 439–471. <https://doi.org/10.1128/membr.60.2.439-471.1996>.
- [57] M. Hatamoto, H. Yamamoto, T. Kindaichi, N. Ozaki, A. Ohashi, Biological oxidation of dissolved methane in effluents from anaerobic reactors using a down-flow hanging sponge reactor, *Water Res.* 44 (2010) 1409–1418.
- [58] W. Rongwong, K. Goh, T.H. Bae, Energy analysis and optimization of hollow fiber membrane contactors for recovery of dissolved methane from anaerobic membrane bioreactor effluent, *J. Membr. Sci.* 554 (2018) 184–194. <https://doi.org/10.1016/j.memsci.2018.03.002>.
- [59] P. Velasco, V. Jegatheesan, M. Othman, Recovery of Dissolved Methane From Anaerobic Membrane Bioreactor Using Degassing Membrane Contactors, *Front. Environ. Sci.* 6 (2018) 1–6. <https://doi.org/10.3389/fenvs.2018.00151>.
- [60] W. Rongwong, J. Lee, K. Goh, H.E. Karahan, T.H. Bae, Membrane-based technologies for post-treatment of anaerobic effluents, *Npj Clean Water.* 1 (2018) 1–21. <https://doi.org/10.1038/s41545-018-0021-y>.
- [61] E. Drioli, G. Di Profio, Curcio Efrem, *Membrane-Assisted Crystallization Technology*, World Scientific, London, 2015. https://doi.org/10.1142/9781783263325_0001.
- [62] M. Younas, M. Rezakazemi, *Membrane Contactor Technology*, Wiley-VCH Verlag GmbH, 2022. <https://doi.org/10.1002/9783527831036>.
- [63] M. Henares, M. Izquierdo, J.M. Peña-Roja, V. Martínez-Soria, Comparative study of degassing membrane modules for the removal of methane from Expanded Granular Sludge Bed anaerobic reactor effluent, *Sep. Purif. Technol.* 170 (2016) 22–29. <https://doi.org/10.1016/j.seppur.2016.06.024>.
- [64] P. Sanchis-Perucho, Á. Robles, F. Durán, J. Ferrer, A. Seco, PDMS membranes for feasible recovery of dissolved methane from AnMBR

- effluents, J. Membr. Sci. (2020) 118070. <https://doi.org/10.1016/J.MEMSCI.2020.118070>.
- [65] R.W. Baker, *Membrane Technology and Applications*, 3th ed., JohnWiley & Sons, Inc., Chichester, UK, 2012.
- [66] H. Verweij, *Inorganic membranes*, *Curr. Opin. Chem. Eng.* 1 (2012) 156–162. <https://doi.org/10.1016/j.coche.2012.03.006>.
- [67] M. Mulder, *Basic Principles of Membrane Technology*, 2nd ed., Kluwer Academic Publishers, 1996.
- [68] D. Rana, T. Matsuura, *Surface modifications for antifouling membranes*, *Chem. Rev.* 110 (2010) 2448–2471. <https://doi.org/10.1021/cr800208y>.
- [69] Y. Lee, K.H. Yun, D. Sethunga, T.H. Bae, *Membrane contactors for maximizing biomethane recovery in anaerobic wastewater treatments: Recent efforts and future prospect*, *Appl. Sci.* 11 (2021) 1–16. <https://doi.org/10.3390/app11041372>.
- [70] E. Centeno Mora, C. de L. Chernicharo, *Use of membrane contactors for removing and recovering dissolved methane from anaerobic reactors effluents: state-of-the-art, challenges, and perspectives*, *Rev. Environ. Sci. Biotechnol.* 19 (2020) 673–697. <https://doi.org/10.1007/s11157-020-09546-w>.
- [71] Y. Xu, K. Goh, R. Wang, T.H. Bae, *A review on polymer-based membranes for gas-liquid membrane contacting processes: Current challenges and future direction*, *Sep. Purif. Technol.* 229 (2019). <https://doi.org/10.1016/j.seppur.2019.115791>.
- [72] C. Liu, A.F. Faria, J. Jackson, Q. He, J. Ma, *Enhancing the anti-fouling and fouling removal properties of thin-film composite membranes through an intercalated functionalization method*, *Environ. Sci. Water Res. Technol.* 7 (2021) 1336–1347. <https://doi.org/10.1039/d1ew00188d>.
- [73] S. Zhao, Z. Liao, A. Fane, J. Li, C. Tang, C. Zheng, J. Lin, L. Kong, *Engineering antifouling reverse osmosis membranes: A review*, *Desalination.* 499 (2021) 1–31. <https://doi.org/10.1016/j.desal.2020.114857>.
- [74] C. Vallieres, E. Favre, *Vacuum versus sweeping gas operation for binary mixtures separation by dense membrane processes*, *J. Membr. Sci.* 244 (2004) 17–23. <https://doi.org/10.1016/j.memsci.2004.04.023>.
- [75] A.C.M. Franken, J.A.M. Nolten, M.H.V. Mulder, D. Bargeman, C.A. Smolders, *Wetting criteria for the applicability of membrane distillation*, *J. Membr. Sci.* 33 (1987) 315–328. [162](https://doi.org/10.1016/S0376-</p></div><div data-bbox=)

- 7388(00)80288-4.
- [76] V. Belessiotis, S. Kalogirou, E. Delyannis, Chapter four - Membrane Distillation, *Therm. Sol. Desalination*, Acad. Press. (2016). <https://doi.org/10.1016/B978-0-12-809656-7.00004-0>.
- [77] J.G. Lu, Y.F. Zheng, M.D. Cheng, Wetting mechanism in mass transfer process of hydrophobic membrane gas absorption, *J. Membr. Sci.* 308 (2008) 180–190. <https://doi.org/10.1016/j.memsci.2007.09.051>.
- [78] A.L. Ahmad, A.R. Sunarti, K.T. Lee, W.J.N. Fernando, CO₂ removal using membrane gas absorption, *Int. J. Greenh. Gas Control.* 4 (2010) 495–498. <https://doi.org/10.1016/j.ijggc.2009.12.003>.
- [79] W. Rongwong, R. Jiraratananon, S. Atchariyawut, Experimental study on membrane wetting in gas-liquid membrane contacting process for CO₂ absorption by single and mixed absorbents, *Sep. Purif. Technol.* 69 (2009) 118–125. <https://doi.org/10.1016/j.seppur.2009.07.009>.
- [80] J.A. Franco, D. deMontigny, S.E. Kentish, J.M. Perera, G.W. Stevens, Effect of amine degradation products on the membrane gas absorption process, *Chem. Eng. Sci.* 64 (2009) 4016–4023. <https://doi.org/10.1016/j.ces.2009.06.012>.
- [81] V.Y. Dindore, D.W.F. Brilman, P.H.M. Feron, G.F. Versteeg, CO₂ absorption at elevated pressures using a hollow fiber membrane contactor, *J. Membr. Sci.* 235 (2004) 99–109. <https://doi.org/10.1016/j.memsci.2003.12.029>.
- [82] T. Zhou, Y. Yao, R. Xiang, Y. Wu, Formation and characterization of polytetrafluoroethylene nanofiber membranes for vacuum membrane distillation, *J. Membr. Sci.* 453 (2014) 402–408. <https://doi.org/10.1016/j.memsci.2013.11.027>.
- [83] Z.Q. Dong, X. hua Ma, Z.L. Xu, W.T. You, F. bing Li, Superhydrophobic PVDF-PTFE electrospun nanofibrous membranes for desalination by vacuum membrane distillation, *Desalination.* 347 (2014) 175–183. <https://doi.org/10.1016/j.desal.2014.05.015>.
- [84] M. Henares, P. Ferrero, P. San-Valero, V. Martínez-Soria, M. Izquierdo, Performance of a polypropylene membrane contactor for the recovery of dissolved methane from anaerobic effluents: Mass transfer evaluation, long-term operation and cleaning strategies, *J. Membr. Sci.* 563 (2018) 926–937. <https://doi.org/10.1016/j.memsci.2018.06.045>.
- [85] G.S.M.D.P. Sethunga, H.E. Karahan, R. Wang, T.H. Bae, PDMS-coated

- porous PVDF hollow fiber membranes for efficient recovery of dissolved biomethane from anaerobic effluents, *J. Membr. Sci.* 584 (2019) 333–342. <https://doi.org/10.1016/j.memsci.2019.05.016>.
- [86] L. Zhang, R. Qu, Y. Sha, X. Wang, L. Yang, Membrane gas absorption for CO₂ capture from flue gas containing fine particles and gaseous contaminants, *Int. J. Greenh. Gas Control.* 33 (2015) 10–17. <https://doi.org/10.1016/j.ijggc.2014.11.017>.
- [87] F. Korminouri, M. Rahbari-Sisakht, T. Matsuura, A.F. Ismail, Surface modification of polysulfone hollow fiber membrane spun under different air-gap lengths for carbon dioxide absorption in membrane contactor system, *Chem. Eng. J.* 264 (2015) 453–461. <https://doi.org/10.1016/j.cej.2014.11.110>.
- [88] S. Atcharyawut, C. Feng, R. Wang, R. Jiraratananon, D.T. Liang, Effect of membrane structure on mass-transfer in the membrane gas-liquid contacting process using microporous PVDF hollow fibers, *J. Membr. Sci.* 285 (2006) 272–281. <https://doi.org/10.1016/j.memsci.2006.08.029>.
- [89] M.R. Dashtarzhandi, A.F. Ismail, T. Matsuura, Carbon dioxide stripping through water by porous PVDF/montmorillonite hollow fiber mixed matrix membranes in a membrane contactor, *RSC Adv.* 5 (2015) 21916–21924. <https://doi.org/10.1039/c5ra00998g>.
- [90] R.A. Al-Juboori, T. Yusaf, Biofouling in RO system: Mechanisms, monitoring and controlling, *Desalination.* 302 (2012) 1–23. <https://doi.org/10.1016/j.desal.2012.06.016>.
- [91] R. Wang, H.Y. Zhang, P.H.M. Feron, D.T. Liang, Influence of membrane wetting on CO₂ capture in microporous hollow fiber membrane contactors, *Sep. Purif. Technol.* 46 (2005) 33–40. <https://doi.org/10.1016/j.seppur.2005.04.007>.
- [92] Z. Yan, Z. Lu, X. Chen, Y. Jiang, Z. Huang, L. Liu, G. Fan, H. Chang, F. Qu, H. Liang, Membrane distillation treatment of landfill leachate: Characteristics and mechanism of membrane fouling, *Sep. Purif. Technol.* 289 (2022) 120787. <https://doi.org/10.1016/j.seppur.2022.120787>.
- [93] H. Lin, W. Peng, M. Zhang, J. Chen, H. Hong, Y. Zhang, A review on anaerobic membrane bioreactors: Applications, membrane fouling and future perspectives, *Desalination.* 314 (2013) 169–188. <https://doi.org/10.1016/j.desal.2013.01.019>.
- [94] F. Meng, B. Liao, S. Liang, F. Yang, H. Zhang, L. Song, Morphological visualization, componential characterization and microbiological

- identification of membrane fouling in membrane bioreactors (MBRs), *J. Membr. Sci.* 361 (2010) 1–14. <https://doi.org/10.1016/j.memsci.2010.06.006>.
- [95] F. Meng, S.R. Chae, A. Drews, M. Kraume, H.S. Shin, F. Yang, Recent advances in membrane bioreactors (MBRs): Membrane fouling and membrane material, *Water Res.* 43 (2009) 1489–1512. <https://doi.org/10.1016/j.watres.2008.12.044>.
- [96] M.R. Choudhury, N. Anwar, D. Jassby, M.S. Rahaman, Fouling and wetting in the membrane distillation driven wastewater reclamation process – A review, *Adv. Colloid Interface Sci.* 269 (2019) 370–399. <https://doi.org/10.1016/j.cis.2019.04.008>.
- [97] F.C.R. Costa, B.C. Ricci, B. Teodoro, K. Koch, J.E. Drewes, M.C.S. Amaral, Biofouling in membrane distillation applications - a review, *Desalination.* 516 (2021) 1–17. <https://doi.org/10.1016/j.desal.2021.115241>.
- [98] S.A. Parsons, J.A. Smith, Phosphorus removal and recovery from municipal wastewaters, *Elements.* 4 (2008) 109–112. <https://doi.org/10.2113/GSELEMENTS.4.2.109>.
- [99] P.I. Omwene, M. Koby, Treatment of domestic wastewater phosphate by electrocoagulation using Fe and Al electrodes: A comparative study, *Process Saf. Environ. Prot.* 116 (2018) 34–51. <https://doi.org/10.1016/j.psep.2018.01.005>.
- [100] USEPA: US Environmental Protection Agency, Advanced wastewater treatment to achieve low concentration of phosphorus. United States Environmental Protection Agency, Environ. Prot. Agency. (2007). https://yosemite.epa.gov/r10/water.nsf/Water+Quality+Standards/AWT-Phosphorus%0Ahttp://www.epa.gov/region10/pdf/tmdl/awt_report.pdf.
- [101] N. Martin, V. Ya, N. Leewiboonsilp, K.H. Choo, P. (Lek) Noophan, C.W. Li, Electrochemical crystallization for phosphate recovery from an electronic industry wastewater effluent using sacrificial iron anodes, *J. Clean. Prod.* 276 (2020) 124234. <https://doi.org/10.1016/j.jclepro.2020.124234>.
- [102] Y. Wu, J. Luo, Q. Zhang, M. Aleem, F. Fang, Z. Xue, J. Cao, Potentials and challenges of phosphorus recovery as vivianite from wastewater: A review, *Chemosphere.* 226 (2019) 246–258. <https://doi.org/10.1016/j.chemosphere.2019.03.138>.
- [103] Y. Hou, G.L. Velthof, J.P. Lesschen, I.G. Staritsky, O. Oenema, Nutrient Recovery and Emissions of Ammonia, Nitrous Oxide, and Methane from Animal Manure in Europe: Effects of Manure Treatment Technologies,

- Environ. Sci. Technol. 51 (2017) 375–383.
<https://doi.org/10.1021/acs.est.6b04524>.
- [104] E.M. Barampouti, S. Mai, D. Malamis, K. Moustakas, M. Loizidou, Exploring technological alternatives of nutrient recovery from digestate as a secondary resource, *Renew. Sustain. Energy Rev.* 134 (2020) 110379.
<https://doi.org/10.1016/j.rser.2020.110379>.
- [105] J. Zhang, Z. Chen, Y. Liu, W. Wei, B.J. Ni, Phosphorus recovery from wastewater and sewage sludge as vivianite, *J. Clean. Prod.* 370 (2022) 133439. <https://doi.org/10.1016/j.jclepro.2022.133439>.
- [106] J.L. Campos, D. Crutchik, Ó. Franchi, J.P. Pavissich, M. Belmonte, A. Pedrouso, A. Mosquera-Corral, Á. Val del Río, Nitrogen and Phosphorus Recovery From Anaerobically Pretreated Agro-Food Wastes: A Review, *Front. Sustain. Food Syst.* 2 (2019) 1–11.
<https://doi.org/10.3389/fsufs.2018.00091>.
- [107] P. Battistoni, R. Boccadoro, F. Fatone, P. Pavan, Auto-nucleation and crystal growth of struvite in a demonstrative fluidized bed reactor (FBR), *Environ. Technol.* 26 (2005) 975–982. <https://doi.org/10.1080/09593332608618486>.
- [108] R. Goedhart, S. Müller, M.C.M. van Loosdrecht, D. van Halem, Vivianite precipitation for iron recovery from anaerobic groundwater, *Water Res.* 217 (2022) 118345. <https://doi.org/10.1016/j.watres.2022.118345>.
- [109] J. Liu, X. Cheng, X. Qi, N. Li, J. Tian, B. Qiu, K. Xu, D. Qu, Recovery of phosphate from aqueous solutions via vivianite crystallization: Thermodynamics and influence of pH, *Chem. Eng. J.* 349 (2018) 37–46.
<https://doi.org/10.1016/j.cej.2018.05.064>.
- [110] E. Frossard, J.P. Bauer, F. Lothe, Evidence of vivianite in FeSO₄ - Flocculated sludges, *Water Res.* 31 (1997) 2449–2454.
[https://doi.org/10.1016/S0043-1354\(97\)00101-2](https://doi.org/10.1016/S0043-1354(97)00101-2).
- [111] T. Gienau, U. Brüb, M. Kraume, S. Rosenberger, Nutrient Recovery from Biogas Digestate by Optimised Membrane Treatment, *Waste and Biomass Valorization.* 9 (2018) 2337–2347. <https://doi.org/10.1007/s12649-018-0231-z>.
- [112] M. Zielińska, W. Mikucka, Membrane filtration for valorization of digestate from the anaerobitreatment of distillery stillage, *Desalin. Water Treat.* 215 (2021) 60–68. <https://doi.org/10.5004/dwt.2021.26772>.
- [113] C. Vaneekhaute, V. Lebuf, E. Michels, E. Belia, P.A. Vanrolleghem, F.M.G. Tack, E. Meers, Nutrient Recovery from Digestate: Systematic Technology

- Review and Product Classification, Waste and Biomass Valorization. 8 (2017) 21–40. <https://doi.org/10.1007/s12649-016-9642-x>.
- [114] F. Rizzioli, F. Battista, D. Bolzonella, N. Frison, Volatile Fatty Acid Recovery from Anaerobic Fermentate: Focusing on Adsorption and Desorption Performances, *Ind. Eng. Chem. Res.* 60 (2021) 13701–13709. <https://doi.org/10.1021/acs.iecr.1c03280>.
- [115] I. Uald-Lamkaddam, A. Dadrasnia, L. Llenas, S. Ponsá, J. Colón, E. Vega, M. Mora, Application of freeze concentration technologies to valorize nutrient-rich effluents generated from the anaerobic digestion of agro-industrial wastes, *Sustainability*. 13 (2021). <https://doi.org/10.3390/su132413769>.
- [116] A. Dadrasnia, I. de Bona Muñoz, E.H. Yáñez, I.U. Lamkaddam, M. Mora, S. Ponsá, M. Ahmed, L.L. Argelaguet, P.M. Williams, D.L. Oatley-Radcliffe, Sustainable nutrient recovery from animal manure: A review of current best practice technology and the potential for freeze concentration, *J. Clean. Prod.* 315 (2021). <https://doi.org/10.1016/j.jclepro.2021.128106>.
- [117] L. Shi, W.S. Simplicio, G. Wu, Z. Hu, H. Hu, X. Zhan, Nutrient Recovery from Digestate of Anaerobic Digestion of Livestock Manure: a Review, *Curr. Pollut. Reports.* 4 (2018) 74–83. <https://doi.org/10.1007/s40726-018-0082-z>.
- [118] R. Priambodo, Y.J. Shih, Y.H. Huang, Phosphorus recovery as ferrous phosphate (vivianite) from wastewater produced in manufacture of thin film transistor-liquid crystal displays (TFT-LCD) by a fluidized bed crystallizer (FBC), *RSC Adv.* 7 (2017) 40819–40828. <https://doi.org/10.1039/c7ra06308c>.
- [119] Y. Lu, H. Liu, W. Feng, Y. Xu, X. Chen, A new and efficient approach for phosphorus recovery from wastewater in the form of vivianite mediated by iron-reducing bacteria, *J. Water Process Eng.* 42 (2021) 102200. <https://doi.org/10.1016/j.jwpe.2021.102200>.
- [120] F. Wang, S. Zheng, H. Qiu, C. Cao, X. Tang, L. Hao, F. Liu, J. Li, Ferrihydrite reduction and vivianite biomineralization mediated by iron reducing bacterium *Shewanella oneidensis* MR-4, *Acta Microbiol. Sin.* 58 (2018) 573–583. <https://doi.org/10.13343/j.cnki.wsxb.20180029>.
- [121] S. Wang, J. An, Y. Wan, Q. Du, X. Wang, X. Cheng, N. Li, Phosphorus Competition in Bioinduced Vivianite Recovery from Wastewater, *Environ. Sci. Technol.* 52 (2018) 13863–13870. <https://doi.org/10.1021/acs.est.8b03022>.
- [122] X. Jiang, Y. Niu, S. Du, G. He, Membrane crystallization: Engineering the

- crystallization via microscale interfacial technology, *Chem. Eng. Res. Des.* 178 (2022) 454–465. <https://doi.org/10.1016/j.cherd.2021.12.042>.
- [123] E. Chabanon, D. Mangin, C. Charcosset, Membranes and crystallization processes: State of the art and prospects, *J. Membr. Sci.* 509 (2016) 57–67. <https://doi.org/10.1016/j.memsci.2016.02.051>.
- [124] G. Di Profio, E. Curcio, E. Drioli, Supersaturation control and heterogeneous nucleation in membrane crystallizers: Facts and perspectives, *Ind. Eng. Chem. Res.* 49 (2010) 11878–11889. <https://doi.org/10.1021/ie100418z>.
- [125] W.T. You, Z.L. Xu, Z.Q. Dong, M. Zhang, Vacuum membrane distillation–crystallization process of high ammonium salt solutions, *Desalin. Water Treat.* 55 (2015) 368–380. <https://doi.org/10.1080/19443994.2014.922499>.
- [126] J.C.W. Fern, S. Ohsaki, S. Watano, R. Pfeffer, Continuous synthesis of nano-drug particles by antisolvent crystallization using a porous hollow-fiber membrane module, *Int. J. Pharm.* 543 (2018) 139–150. <https://doi.org/10.1016/j.ijpharm.2018.03.025>.
- [127] D. Chen, B. Wang, K.K. Sirkar, Hydrodynamic modeling of porous hollow fiber anti-solvent crystallizer for continuous production of drug crystals, *J. Membr. Sci.* 556 (2018) 185–195. <https://doi.org/10.1016/j.memsci.2018.03.046>.
- [128] X. Zhou, X. Zhu, B. Wang, J. Li, Q. Liu, X. Gao, K.K. Sirkar, D. Chen, Continuous production of drug nanocrystals by porous hollow fiber-based anti-solvent crystallization, *J. Membr. Sci.* 564 (2018) 682–690. <https://doi.org/10.1016/j.memsci.2018.07.082>.
- [129] L. Tuo, X. Ruan, W. Xiao, X. Li, G. He, X. Jiang, A novel hollow fiber membrane-assisted antisolvent crystallization for enhanced mass transfer process control, *AIChE J.* 65 (2019) 734–744. <https://doi.org/10.1002/aic.16438>.
- [130] Z. Jia, Z. Liu, F. He, Synthesis of nanosized BaSO₄ and CaCO₃ particles with a membrane reactor: Effects of additives on particles, *J. Colloid Interface Sci.* 266 (2003) 322–327. [https://doi.org/10.1016/S0021-9797\(03\)00187-5](https://doi.org/10.1016/S0021-9797(03)00187-5).
- [131] Y. Yin, T. Li, K. Zuo, X. Liu, S. Lin, Y. Yao, T. Tong, Which Surface Is More Scaling Resistant? A Closer Look at Nucleation Theories for Heterogeneous Gypsum Nucleation in Aqueous Solutions, *Environ. Sci. Technol.* 56 (2022) 16315–16324. <https://doi.org/10.1021/acs.est.2c06560>.
- [132] A. Mersmann, Crystallization and precipitation, *Chem. Eng. Process.*

- Process Intensif. 38 (1999) 345–353. [https://doi.org/10.1016/S0255-2701\(99\)00025-2](https://doi.org/10.1016/S0255-2701(99)00025-2).
- [133] C. Charcosset, H. Fessi, Preparation of nanoparticles with a membrane contactor, *J. Membr. Sci.* 266 (2005) 115–120. <https://doi.org/10.1016/j.memsci.2005.05.016>.
- [134] R. Kieffer, D. Mangin, F. Puel, C. Charcosset, Precipitation of barium sulphate in a hollow fiber membrane contactor, Part I: Investigation of particulate fouling, *Chem. Eng. Sci.* 64 (2009) 1759–1767. <https://doi.org/10.1016/j.ces.2009.01.011>.
- [135] Z. Jia, Z. Liu, Synthesis of nanosized BaSO₄ particles with a membrane reactor: effects of operating parameters on particles, *J. Membr. Sci.* 209 (2002) 153–161. [https://doi.org/10.1016/S0376-7388\(02\)00326-5](https://doi.org/10.1016/S0376-7388(02)00326-5).
- [136] X. Dou, H. Huang, X. Wang, Q. Lin, J. Li, Y. Zhang, Y. Han, Collision dependent silver nucleation regulated by chemical diffusion and reaction, *Chem. Eng. Sci.* 262 (2022) 117965. <https://doi.org/10.1016/j.ces.2022.117965>.
- [137] X. Dou, H. Huang, Y. Han, The role of diffusion in the nucleation of calcium carbonate, *Chinese J. Chem. Eng.* 43 (2022) 275–281. <https://doi.org/10.1016/j.cjche.2021.03.039>.
- [138] R. Kieffer, D. Mangin, F. Puel, C. Charcosset, Precipitation of barium sulphate in a hollow fiber membrane contactor: Part II The influence of process parameters, *Chem. Eng. Sci.* 64 (2009) 1885–1891. <https://doi.org/10.1016/j.ces.2009.01.013>.
- [139] S. Bavarella, M. Hermassi, A. Brookes, A. Moore, P. Vale, G. Di Profio, E. Curcio, P. Hart, M. Pidou, E.J. McAdam, Is Chemically Reactive Membrane Crystallization Facilitated by Heterogeneous Primary Nucleation? Comparison with Conventional Gas-Liquid Crystallization for Ammonium Bicarbonate Precipitation in a CO₂-NH₃-H₂O System, *Cryst. Growth Des.* 20 (2020) 1552–1564. <https://doi.org/10.1021/acs.cgd.9b01276>.
- [140] C.A. Quist-Jensen, J.M. Sørensen, A. Svenstrup, L. Scarpa, T.S. Carlsen, H.C. Jensen, L. Wybrandt, M.L. Christensen, Membrane crystallization for phosphorus recovery and ammonia stripping from reject water from sludge dewatering process, *Desalination.* 440 (2018) 156–160. <https://doi.org/10.1016/j.desal.2017.11.034>.
- [141] R. Klaassen, P.H.M. Feron, A.E. Jansen, Membrane contactors in industrial applications, *Chem. Eng. Res. Des.* 83 (2005) 234–246.

- <https://doi.org/10.1205/cherd.04196>.
- [142] J. Kuhn, R. Lakerveld, H.J.M. Kramer, J. Grievink, P.J. Jansens, Characterization and dynamic optimization of membrane-assisted crystallization of adipic acid, *Ind. Eng. Chem. Res.* 48 (2009) 5360–5369. <https://doi.org/10.1021/ie802010z>.
- [143] A. Lautenschleger, E.Y. Kenig, A. Voigt, K. Sundmacher, Model-Based Analysis of a Gas/Vapor–Liquid Microchannel Membrane Contactor, *AIChE J.* 61 (2015) 2240–2256. <https://doi.org/10.1002/aic.14784>.
- [144] B. Akhavan, K. Jarvis, P. Majewski, Hydrophobic plasma polymer coated silica particles for petroleum hydrocarbon removal, *ACS Appl. Mater. Interfaces.* 5 (2013) 8563–8571. <https://doi.org/10.1021/am4020154>.
- [145] D.J. Miller, D.R. Dreyer, C.W. Bielawski, D.R. Paul, B.D. Freeman, Surface Modification of Water Purification Membranes, *Angew. Chemie - Int. Ed.* 56 (2017) 4662–4711. <https://doi.org/10.1002/anie.201601509>.
- [146] M. Asadollahi, D. Bastani, S.A. Musavi, Enhancement of surface properties and performance of reverse osmosis membranes after surface modification: A review, *Desalination.* 420 (2017) 330–383. <https://doi.org/10.1016/j.desal.2017.05.027>.
- [147] M. Farnam, H. bin Mukhtar, A. bin Mohd Shariff, A Review on Glassy and Rubbery Polymeric Membranes for Natural Gas Purification, *ChemBioEng Rev.* 8 (2021) 90–109. <https://doi.org/10.1002/cben.202100002>.
- [148] S. Nagandran, P.S. Goh, A.F. Ismail, T.W. Wong, W.R.Z.B.W. Dagang, The recent progress in modification of polymeric membranes using organic macromolecules for water treatment, *Symmetry (Basel).* 12 (2020). <https://doi.org/10.3390/sym12020239>.
- [149] S. Mosadegh-Sedghi, D. Rodrigue, J. Brisson, M.C. Iliuta, Wetting phenomenon in membrane contactors - Causes and prevention, *J. Membr. Sci.* 452 (2014) 332–353. <https://doi.org/10.1016/j.memsci.2013.09.055>.
- [150] S. Lee, J.S. Park, T.R. Lee, The wettability of fluoropolymer surfaces: Influence of surface dipoles, *Langmuir.* 24 (2008) 4817–4826. <https://doi.org/10.1021/la700902h>.
- [151] K. Nymeijer, T. Visser, R. Assen, M. Wessling, Super selective membranes in gas-liquid membrane contactors for olefin/paraffin separation, *J. Membr. Sci.* 232 (2004) 107–114. <https://doi.org/10.1016/j.memsci.2003.10.045>.
- [152] R.A. Amaral, A.C. Habert, C.P. Borges, Performance evaluation of composite

- and microporous gas-liquid membrane contactors for CO₂ removal from a gas mixture, *Chem. Eng. Process. Process Intensif.* 102 (2016) 202–209. <https://doi.org/10.1016/j.cep.2016.01.018>.
- [153] P.T. Nguyen, E. Lasseguette, Y. Medina-Gonzalez, J.C. Remigy, D. Roizard, E. Favre, A dense membrane contactor for intensified CO₂ gas/liquid absorption in post-combustion capture, *J. Membr. Sci.* 377 (2011) 261–272. <https://doi.org/10.1016/j.memsci.2011.05.003>.
- [154] M. Lejars, A. Margailan, C. Bressy, Fouling release coatings: A nontoxic alternative to biocidal antifouling coatings, *Chem. Rev.* 112 (2012) 4347–4390. <https://doi.org/10.1021/cr200350v>.
- [155] S. Chen, L. Li, C. Zhao, J. Zheng, Surface hydration: Principles and applications toward low-fouling/nonfouling biomaterials, *Polymer (Guildf)*. 51 (2010) 5283–5293. <https://doi.org/10.1016/j.polymer.2010.08.022>.
- [156] X. Zhao, Y. Su, Y. Li, R. Zhang, J. Zhao, Z. Jiang, Engineering amphiphilic membrane surfaces based on PEO and PDMS segments for improved antifouling performances, *J. Membr. Sci.* 450 (2014) 111–123. <https://doi.org/10.1016/j.memsci.2013.08.044>.
- [157] T. Hwang, M.R. Kotte, J.I. Han, Y.K. Oh, M.S. Diallo, Microalgae recovery by ultrafiltration using novel fouling-resistant PVDF membranes with in situ PEGylated polyethyleneimine particles, *Water Res.* 73 (2015) 181–192. <https://doi.org/10.1016/j.watres.2014.12.002>.
- [158] N. Shahkaramipour, T.N. Tran, S. Ramanan, H. Lin, Membranes with surface-enhanced antifouling properties for water purification, *Membranes (Basel)*. 7 (2017) 1–18. <https://doi.org/10.3390/membranes7010013>.
- [159] M. Gryta, Surface modification of polypropylene membrane by helium plasma treatment for membrane distillation, *J. Membr. Sci.* 628 (2021) 119265. <https://doi.org/10.1016/j.memsci.2021.119265>.
- [160] D.M. Correia, J. Nunes-Pereira, D. Alikin, A.L. Kholkin, S.A.C. Carabineiro, L. Rebouta, M.S. Rodrigues, F. Vaz, C.M. Costa, S. Lanceros-Méndez, Surface wettability modification of poly(vinylidene fluoride) and copolymer films and membranes by plasma treatment, *Polymer (Guildf)*. 169 (2019) 138–147. <https://doi.org/10.1016/j.polymer.2019.02.042>.
- [161] F. Liu, N.A. Hashim, Y. Liu, M.R.M. Abed, K. Li, Progress in the production and modification of PVDF membranes, *J. Membr. Sci.* 375 (2011) 1–27. <https://doi.org/10.1016/j.memsci.2011.03.014>.

- [162] R. Guan, H. Zou, D. Lu, C. Gong, Y. Liu, Polyethersulfone sulfonated by chlorosulfonic acid and its membrane characteristics, *Eur. Polym. J.* 41 (2005) 1554–1560. <https://doi.org/10.1016/j.eurpolymj.2005.01.018>.
- [163] B.C. Johnson, I. Yilgör, C. Tran, M. Iqbal, J.P. Wightman, D.R. Lloyd, J.E. McGrath, Synthesis and characterization of sulfonated poly(acrylene ether sulfones), *J. Polym. Sci. Polym. Chem. Ed.* 22 (1984) 721–737. <https://doi.org/10.1002/pol.1984.170220320>.
- [164] S. Belfer, R. Fainchtain, Y. Purinson, O. Kedem, Surface characterization by FTIR-ATR spectroscopy of polyethersulfone membranes-unmodified, modified and protein fouled, *J. Membr. Sci.* 172 (2000) 113–124. [https://doi.org/10.1016/S0376-7388\(00\)00316-1](https://doi.org/10.1016/S0376-7388(00)00316-1).
- [165] F.Q. Nie, Z.-K. Xu, X.-J. Huang, P. Ye, J. Wu, Acrylonitrile-based copolymer membranes containing reactive groups: Surface modification by the immobilization of biomacromolecules, *Langmuir.* 19 (2003) 9889–9895. <https://doi.org/10.1021/la035315h>.
- [166] G.J. Ross, J.F. Watts, M.P. Hill, P. Morrissey, Surface modification of poly(vinylidene fluoride) by alkaline treatment: 1. The degradation mechanism, *Polymer (Guildf).* 41 (2000) 1685–1696. [https://doi.org/10.1016/S0032-3861\(99\)00343-2](https://doi.org/10.1016/S0032-3861(99)00343-2).
- [167] S. Sairiam, C.H. Loh, R. Wang, R. Jiraratananon, Surface modification of PVDF hollow fiber membrane to enhance hydrophobicity using organosilanes, *J. Appl. Polym. Sci.* 130 (2013) 610–621. <https://doi.org/10.1002/app.39197>.
- [168] K. Fujimoto, Y. Takebayashi, H. Inoue, Y. Ikada, Ozone-induced graft polymerization onto polymer surface, *J. Polym. Sci. Part A Polym. Chem.* 31 (1993) 1035–1043. <https://doi.org/10.1002/pola.1993.080310426>.
- [169] J. Yamauchi, A. Yamaoka, K. Ikemoto, T. Matsui, Graft Copolymerization of Methyl Methacrylate onto Polyethylene Oxidized with Ozone, *J. Appl. Polym. Sci.* 43 (1991) 1197–1203. <https://doi.org/10.1002/app.1991.070430621>.
- [170] V. Arima, M. Bianco, A. Zacheo, A. Zizzari, E. Perrone, L. Marra, R. Rinaldi, Fluoropolymers coatings on polydimethylsiloxane for retarding swelling in toluene, *Thin Solid Films.* 520 (2012) 2293–2300. <https://doi.org/10.1016/j.tsf.2011.09.063>.
- [171] Y. Han, S. Song, Y. Lu, D. Zhu, A method to modify PVDF microfiltration membrane via ATRP with low-temperature plasma pretreatment, *Appl.*

- Surf. Sci. 379 (2016) 474–479. <https://doi.org/10.1016/j.apsusc.2016.04.114>.
- [172] J. Wang, X. Chen, R. Reis, Z. Chen, N. Milne, B. Winther-Jensen, L. Kong, L.F. Dumée, Plasma modification and synthesis of membrane materials—a mechanistic review, *Membranes (Basel)*. 8 (2018) 1–38. <https://doi.org/10.3390/membranes8030056>.
- [173] Plasma technology, Diener electronic GmbH + Co. KG, (2007) 1–83.
- [174] L.F. Dumée, H. Aglave, T. Chaffraix, B. Lin, K. Magniez, J. Schütz, Morphology-properties relationship of gas plasma treated hydrophobic mesoporous membranes and their improved performance for desalination by membrane distillation, *Appl. Surf. Sci.* 363 (2016) 273–285. <https://doi.org/10.1016/j.apsusc.2015.12.034>.
- [175] R. Jafari, S. Asadollahi, M. Farzaneh, Applications of plasma technology in development of superhydrophobic surfaces, *Plasma Chem. Plasma Process.* 33 (2013) 177–200.
- [176] C. Cardinaud, M.C. Peignon, P.Y. Tessier, Plasma etching: Principles, mechanisms, application to micro- and nano-technologies, *Appl. Surf. Sci.* 164 (2000) 72–83. [https://doi.org/10.1016/S0169-4332\(00\)00328-7](https://doi.org/10.1016/S0169-4332(00)00328-7).
- [177] L. Liu, F. Shen, X. Chen, J. Luo, Y. Su, H. Wu, Y. Wan, A novel plasma-induced surface hydrophobization strategy for membrane distillation: Etching, dipping and grafting, *J. Membr. Sci.* 499 (2016) 544–554. <https://doi.org/10.1016/j.memsci.2015.11.003>.
- [178] C. Yang, X.M. Li, J. Gilron, D. feng Kong, Y. Yin, Y. Oren, C. Linder, T. He, CF₄ plasma-modified superhydrophobic PVDF membranes for direct contact membrane distillation, *J. Membr. Sci.* 456 (2014) 155–161. <https://doi.org/10.1016/j.memsci.2014.01.013>.
- [179] S. Jeong, B. Shin, W. Jo, H.Y. Kim, M.W. Moon, S. Lee, Nanostructured PVDF membrane for MD application by an O₂ and CF₄ plasma treatment, *Desalination*. 399 (2016) 178–184. <https://doi.org/10.1016/j.desal.2016.09.001>.
- [180] Y.C. Woo, Y. Chen, L.D. Tijing, S. Phuntsho, T. He, J.S. Choi, S.H. Kim, H.K. Shon, CF₄ plasma-modified omniphobic electrospun nanofiber membrane for produced water brine treatment by membrane distillation, *J. Membr. Sci.* 529 (2017) 234–242. <https://doi.org/10.1016/j.memsci.2017.01.063>.
- [181] K.L. Tan, L.L. Woon, H.K. Wong, E.T. Tang, K.G. Neoh, Surface Modification of Plasma-Pretreated Poly(tetrafluoroethylene) Films by Graft

- Copolymerization, *Macromolecules*. 26 (1993) 2832–2836. <https://doi.org/10.1021/ma00063a030>.
- [182] J. Izdebska, S. Thomas, Chapter 8: Corona Treatment in Printing on Polymers: Fundamentals and Applications, Elsevier Inc., 2016. <https://doi.org/10.1016/B978-0-323-37468-2.00008-7>.
- [183] D.J. Dyer, Photoinitiated synthesis of grafted polymers, *Adv. Polym. Sci.* 197 (2006) 47–65. https://doi.org/10.1007/12_064.
- [184] T.H. Bae, T.M. Tak, Effect of TiO₂ nanoparticles on fouling mitigation of ultrafiltration membranes for activated sludge filtration, *J. Membr. Sci.* 249 (2005) 1–8. <https://doi.org/10.1016/j.memsci.2004.09.008>.
- [185] G. Decher, Fuzzy nanoassemblies: Toward layered polymeric multicomposites, *Science* (80-.). 277 (1997) 1232–1237. <https://doi.org/10.1126/science.277.5330.1232>.
- [186] Y. Li, L. Wang, X. Hu, P. Jin, X. Song, Surface modification to produce superhydrophobic hollow fiber membrane contactor to avoid membrane wetting for biogas purification under pressurized conditions, *Sep. Purif. Technol.* 194 (2018) 222–230. <https://doi.org/10.1016/j.seppur.2017.11.041>.
- [187] L. Zou, I. Vidalis, D. Steele, A. Michelmore, S.P. Low, J.Q.J.C. Verberk, Surface hydrophilic modification of RO membranes by plasma polymerization for low organic fouling, *J. Membr. Sci.* 369 (2011) 420–428. <https://doi.org/10.1016/j.memsci.2010.12.023>.
- [188] C. Yang, M. Tian, Y. Xie, X.M. Li, B. Zhao, T. He, J. Liu, Effective evaporation of CF₄ plasma modified PVDF membranes in direct contact membrane distillation, *J. Membr. Sci.* 482 (2015) 25–32. <https://doi.org/10.1016/j.memsci.2015.01.059>.
- [189] M. Tian, Y. Yin, C. Yang, B. Zhao, J. Song, J. Liu, X.M. Li, T. He, CF₄ plasma modified highly interconnective porous polysulfone membranes for direct contact membrane distillation (DCMD), *Desalination*. 369 (2015) 105–114. <https://doi.org/10.1016/j.desal.2015.05.002>.
- [190] B. Zhang, Principles, Methods, Formation Mechanisms, and Structures of Nanomaterials Prepared via Self-Assembly, 2018. <https://doi.org/10.1016/b978-0-12-410417-4.00005-8>.
- [191] Y. Lvov, G. Decher, M. Mohwald, Assembly, Structural Characterization, and Thermal Behavior of Layer-by-Layer Deposited Ultrathin Films of Poly(vinyl sulfate) and Poly(allylamine), *Langmuir*. 9 (1993) 481–486.

- <https://doi.org/10.1021/la00026a020>.
- [192] J.M. Dickson, R.F. Childs, B.E. McCarry, D.R. Gagnon, Development of a coating technique for the internal structure of polypropylene microfiltration membranes, *J. Membr. Sci.* 148 (1998) 25–36. [https://doi.org/10.1016/S0376-7388\(98\)00142-2](https://doi.org/10.1016/S0376-7388(98)00142-2).
- [193] G. Sun, T. Gao, X. Zhao, H. Zhang, Fabrication of micro/nano dual-scale structures by improved deep reactive ion etching, *J. Micromechanics Microengineering*. 20 (2010) 75028.
- [194] R. Di Mundo, M. Troia, F. Palumbo, M. Trotta, R. D'Agostino, Nanotexturing of transparent polymers with plasma etching: Tailoring topography for a low reflectivity, *Plasma Process. Polym.* 9 (2012) 947–954. <https://doi.org/10.1002/ppap.201200041>.
- [195] B. Chapman, *Glow Discharge Processes: Sputtering and plasma etching*, John Wiley & Sons, Ltd, Toronto, 1980.
- [196] M.E. Vlachopoulou, K. Tsougeni, P. Petrou, S. Kakabakos, A. Tserepi, E. Gogolides, High-Aspect-Ratio Plasma Induced Nanotexturing of Polymers (PDMS, PMMA, PEEK, ...) for protein adsorption applications, in: *Int. Conf. Electron, Ion Phot. Beam Technol. Nanofabrication*, Denver, 2007.
- [197] B. Bhushan, D. Hansford, K.K. Lee, Surface modification of silicon and polydimethylsiloxane surfaces with vapor-phase-deposited ultrathin fluorosilane films for biomedical nanodevices, *J. Vac. Sci. Technol. A Vacuum, Surfaces, Film.* 24 (2006) 1197–1202. <https://doi.org/10.1116/1.2167077>.
- [198] S.-H. Lin, K.-L. Tung, W.-J. Chen, H.-W. Chang, Absorption of carbon dioxide by mixed piperazine–alkanolamine absorbent in a plasma-modified polypropylene hollow fiber contactor, *J. Membr. Sci.* 333 (2009) 30–37.
- [199] M. Xie, W. Luo, S.R. Gray, Surface pattern by nanoimprint for membrane fouling mitigation: Design, performance and mechanisms, *Water Res.* 124 (2017) 238–243. <https://doi.org/10.1016/j.watres.2017.07.057>.
- [200] Y. Ding, S. Maruf, M. Aghajani, A.R. Greenberg, Surface patterning of polymeric membranes and its effect on antifouling characteristics, *Sep. Sci. Technol.* 52 (2017) 240–257. <https://doi.org/10.1080/01496395.2016.1201115>.
- [201] I. Topolniak, A.M. Elert, X. Knigge, G.C. Ciftci, J. Radnik, H. Sturm, High-Precision Micropatterning of Polydopamine by Multiphoton Lithography, *Adv. Mater.* 34 (2022) 1–10. <https://doi.org/10.1002/adma.202109509>.

- [202] J. Wei, G.S. Helm, N. Corner-Walker, X. Hou, Characterization of a non-fouling ultrafiltration membrane, *Desalination*. 192 (2006) 252–261. <https://doi.org/10.1016/j.desal.2005.06.049>.
- [203] F.F. Stengaard, Characteristic and performance of new types of ultrafiltration membranes with chemically modified surfaces, *Desalination*. 70 (1988) 207–224.
- [204] B. Zhao, W.J. Brittain, Polymer brushes: Surface-immobilized macromolecules, *Prog. Polym. Sci.* 25 (2000) 677–710. [https://doi.org/10.1016/S0079-6700\(00\)00012-5](https://doi.org/10.1016/S0079-6700(00)00012-5).
- [205] M. Ulbricht, Advanced functional polymer membranes, *Polymer (Guildf)*. 47 (2006) 2217–2262. <https://doi.org/10.1016/j.polymer.2006.01.084>.
- [206] A. Higuchi, N. Iwata, M. Tsubaki, T. Nakagawa, Surface-modified polysulfone hollow fibers, *J. Appl. Polym. Sci.* 36 (1988) 1753–1767. <https://doi.org/10.1002/app.1988.070360804>.
- [207] A. Higuchi, T. Nakagawa, Surface modified polysulfone hollow fibers. III. Fibers having a hydroxide group, *J. Appl. Polym. Sci.* 41 (1990) 1973–1979. <https://doi.org/10.1002/app.1990.070410904>.
- [208] A. Higuchi, N. Iwata, T. Nakagawa, Surface-modified polysulfone hollow fibers. II. Fibers having CH₂CH₂CH₂SO₃⁻ segments and immersed in HCl solution, *J. Appl. Polym. Sci.* 40 (1990) 709–717. <https://doi.org/10.1002/app.1990.070400508>.
- [209] H.T. Nguyen, H.M. Bui, Y.F. Wang, S.J. You, Non-fluoroalkyl functionalized hydrophobic surface modifications used in membrane distillation for cheaper and more environmentally friendly applications: A mini-review, *Sustain. Chem. Pharm.* 28 (2022) 1–20. <https://doi.org/10.1016/j.scp.2022.100714>.
- [210] W. Qing, X. Shi, W. Zhang, J. Wang, Y. Wu, P. Wang, C.Y. Tang, Solvent-thermal induced roughening: A novel and versatile method to prepare superhydrophobic membranes, *J. Membr. Sci.* 564 (2018) 465–472. <https://doi.org/10.1016/j.memsci.2018.07.035>.
- [211] S. Al-Gharabli, M.O. Mavukkandy, J. Kujawa, S.P. Nunes, H.A. Arafat, Activation of PVDF membranes through facile hydroxylation of the polymeric dope, *J. Mater. Res.* 32 (2017) 4219–4231. <https://doi.org/10.1557/jmr.2017.403>.
- [212] L. Upadhyaya, X. Qian, S. Ranil Wickramasinghe, Chemical modification of membrane surface — overview, *Curr. Opin. Chem. Eng.* 20 (2018) 13–18.

- <https://doi.org/10.1016/j.coche.2018.01.002>.
- [213] B. Zhu, W. Jiang, W. Wang, Y. Lin, T. Ruan, G. Jiang, Occurrence and Degradation Potential of Fluoroalkylsilane Substances as Precursors of Perfluoroalkyl Carboxylic Acids, *Environ. Sci. Technol.* 53 (2019) 4823–4831. <https://doi.org/10.1021/acs.est.9b00690>.
- [214] B. Bhushan, Y.C. Jung, K. Koch, Self-cleaning efficiency of artificial superhydrophobic surfaces, *Langmuir*. 25 (2009) 3240–3248.
- [215] K.R. Khedir, G.K. Kannarpady, C. Ryerson, A.S. Biris, An outlook on tunable superhydrophobic nanostructural surfaces and their possible impact on ice mitigation, *Prog. Org. Coatings*. 112 (2017) 304–318. <https://doi.org/10.1016/j.porgcoat.2017.05.019>.
- [216] M.A. Sarshar, C. Swarctz, S. Hunter, J. Simpson, C.-H. Choi, Effects of contact angle hysteresis on ice adhesion and growth on superhydrophobic surfaces under dynamic flow conditions, *Colloid Polym. Sci.* 291 (2013) 427–435.
- [217] P. Dimitrakellis, E. Gogolides, Hydrophobic and superhydrophobic surfaces fabricated using atmospheric pressure cold plasma technology: A review, *Adv. Colloid Interface Sci.* 254 (2018) 1–21. <https://doi.org/10.1016/j.cis.2018.03.009>.
- [218] M. Miwa, A. Nakajima, A. Fujishima, K. Hashimoto, T. Watanabe, Effects of the surface roughness on sliding angles of water droplets on superhydrophobic surfaces, *Langmuir*. 16 (2000) 5754–5760. <https://doi.org/10.1021/la991660o>.
- [219] W. Zhang, D. Wang, Z. Sun, J. Song, X. Deng, Robust superhydrophobicity: Mechanisms and strategies, *Chem. Soc. Rev.* 50 (2021) 4031–4061. <https://doi.org/10.1039/d0cs00751j>.
- [220] Q. Wen, Z. Guo, Recent advances in the fabrication of superhydrophobic surfaces, *Chem. Lett.* 45 (2016) 1134–1149. <https://doi.org/10.1246/cl.160621>.
- [221] M. Mulder, *Basic Principles of Membrane Technology*, 1st ed., Springer Netherlands, Netherlands, 1996.
- [222] A. McLeod, B. Jefferson, E.J. McAdam, Toward gas-phase controlled mass transfer in micro-porous membrane contactors for recovery and concentration of dissolved methane in the gas phase, *J. Membr. Sci.* 510 (2016) 466–471. <https://doi.org/10.1016/j.memsci.2016.03.030>.

- [223] R. Jiménez-Robles, C. Gabaldón, J.D. Badia, M. Izquierdo, V. Martínez-Soria, Recovery of dissolved methane through a flat sheet module with PDMS, PP, and PVDF membranes, *Sep. Purif. Technol.* 282 (2022) 1–11. <https://doi.org/10.1016/j.seppur.2021.120057>.
- [224] R. Jiménez-Robles, B.M. Moreno-Torrallbo, J.D. Badia, V. Martínez-Soria, M. Izquierdo, Flat PVDF membrane with enhanced hydrophobicity through alkali activation and organofluorosilanisation for dissolved methane recovery, *Membranes (Basel)*. 12 (2022) 1–19. <https://doi.org/10.3390/membranes12040426>.
- [225] V. Oldani, G. Sergi, C. Pirola, B. Sacchi, C.L. Bianchi, Sol-gel hybrid coatings containing silica and a perfluoropolyether derivative with high resistance and anti-fouling properties in liquid media, *J. Fluor. Chem.* 188 (2016) 43–49. <https://doi.org/10.1016/j.jfluchem.2016.06.005>.
- [226] P. Fabbri, M. Messori, M. Montecchi, F. Pilati, R. Taurino, C. Tonelli, M. Toselli, Surface properties of fluorinated hybrid coatings, *J. Appl. Polym. Sci.* 102 (2006) 1483–1488. <https://doi.org/10.1002/app.24350>.
- [227] S. Mikhaylin, L. Bazinet, Fouling on ion-exchange membranes: Classification, characterization and strategies of prevention and control, *Adv. Colloid Interface Sci.* 229 (2016) 34–56. <https://doi.org/10.1016/j.cis.2015.12.006>.
- [228] G. dong Kang, Y. ming Cao, Application and modification of poly(vinylidene fluoride) (PVDF) membranes - A review, *J. Membr. Sci.* 463 (2014) 145–165. <https://doi.org/10.1016/j.memsci.2014.03.055>.
- [229] X. Yang, R. Wang, L. Shi, A.G. Fane, M. Debowski, Performance improvement of PVDF hollow fiber-based membrane distillation process, *J. Membr. Sci.* 369 (2011) 437–447. <https://doi.org/10.1016/j.memsci.2010.12.020>.
- [230] X. Huang, J. Zhang, W. Wang, Y. Liu, Z. Zhang, L. Li, W. Fan, Effects of PVDF/SiO₂ hybrid ultrafiltration membranes by sol-gel method for the concentration of fennel oil in herbal water extract, *RSC Adv.* 5 (2015) 18258–18266. <https://doi.org/10.1039/c4ra15448g>.
- [231] S. Wongchitphimon, R. Wang, R. Jiraratananon, Surface modification of polyvinylidene fluoride-co-hexafluoropropylene (PVDF-HFP) hollow fiber membrane for membrane gas absorption, *J. Membr. Sci.* 381 (2011) 183–191. <https://doi.org/10.1016/j.memsci.2011.07.022>.
- [232] Y. Zhang, R. Wang, Fabrication of novel polyetherimide-fluorinated silica

- organic-inorganic composite hollow fiber membranes intended for membrane contactor application, *J. Membr. Sci.* 443 (2013) 170–180. <https://doi.org/10.1016/j.memsci.2013.04.062>.
- [233] Y. Zhang, R. Wang, Novel method for incorporating hydrophobic silica nanoparticles on polyetherimide hollow fiber membranes for CO₂ absorption in a gas-liquid membrane contactor, *J. Membr. Sci.* 452 (2014) 379–389. <https://doi.org/10.1016/j.memsci.2013.10.011>.
- [234] M. Bennett, B.J. Brisdon, R. England, R.W. Field, Performance of PDMS and organofunctionalised PDMS membranes for the pervaporative recovery of organics from aqueous streams, *J. Membr. Sci.* 137 (1997) 63–88. [https://doi.org/10.1016/S0376-7388\(97\)00183-X](https://doi.org/10.1016/S0376-7388(97)00183-X).
- [235] P. Sanchis-Perucho, Á. Robles, F. Durán, F. Rogalla, J. Ferrer, A. Seco, Widening the applicability of AnMBR for urban wastewater treatment through PDMS membranes for dissolved methane capture: Effect of temperature and hydrodynamics, *J. Environ. Manage.* 287 (2021) 1–11. <https://doi.org/10.1016/j.jenvman.2021.112344>.
- [236] J. Phattaranawik, T. Leiknes, W. Pronk, Mass transfer studies in flat-sheet membrane contactor with ozonation, *J. Membr. Sci.* 247 (2005) 153–167. <https://doi.org/10.1016/j.memsci.2004.08.020>.
- [237] Y.A. Çengel, M.A. Boles, M. Kanoğlu, *Thermodynamics: An Engineering Approach*, Ninth Edition, McGraw-hill, New York, 2019.
- [238] M. Dingemans, J. Dewulf, L. Braeckman, H. Van Langenhove, K. Friess, V. Hynek, M. Sipek, Mass transfer characteristics for VOC permeation through flat sheet porous and composite membranes: The impact of the different membrane layers on the overall membrane resistance, *J. Membr. Sci.* 322 (2008) 234–242. <https://doi.org/10.1016/j.memsci.2008.05.043>.
- [239] U. Beuscher, C. H. Gooding, The influence of the porous support layer of composite membranes on the separation of binary gas mixtures, *J. Membr. Sci.* 152 (1999) 99–116. [https://doi.org/10.1016/S0376-7388\(98\)00205-1](https://doi.org/10.1016/S0376-7388(98)00205-1).
- [240] J. R. Welty, C. E. Wicks, R. E. Wilson, G. L. Rorrer, *Fundamentals of Momentum, Heat, and Mass Transfer*, 5th ed., JohnWiley & Sons, Inc., Oregon, 2008.
- [241] E.N. Fuller, P.D. Schettler, J.C. Giddings, A new method for prediction of binary gas-phase diffusion coefficients, *Ind. Eng. Chem.* 58 (1966) 18–27. <https://doi.org/10.1021/ie50677a007>.

- [242] Z. Qi, E.L. Cussler, Microporous hollow fibers for gas absorption. II. Mass transfer across the membrane, *J. Membr. Sci.* 23 (1985) 321–332.
- [243] H. Kreulen, C.A. Smolders, W.P.M. Van Swaaij, Determination of mass transfer rates in wetted and non-wetted microporous membranes, *Chem. Eng. Sci.* 48 (1993) 2093–2102. [https://doi.org/10.1016/0009-2509\(93\)80084-4](https://doi.org/10.1016/0009-2509(93)80084-4).
- [244] E.L. Cussler, *Mass transfer in fluid systems*, Cambridge University Press, 1984.
- [245] S.A. Hashemifard, A.F. Ismail, T. Matsuura, M.R. Dashtarzhandi, Performance of silicon rubber coated polyetherimide hollow fibers for CO₂ removal via a membrane contactor, *RSC Adv.* 5 (2015) 48442–48455. <https://doi.org/10.1039/c5ra00085h>.
- [246] S.R. Wickramasinghe, M.J. Semmens, E.L. Cussler, Mass transfer in various hollow fiber geometries, *J. Membr. Sci.* 69 (1992) 235–250.
- [247] M.A. L ev eque, Les lois de la transmission de chaleur par convection, *Les Ann. Des Mines.* 13 (1928) 201–299.
- [248] M.-C. Yang, E.L. Cussler, Designing hollow-fiber contactors, *AIChE J.* 32 (1986) 1910–1915.
- [249] G. Zeng, H. Li, S. Huang, X. Wang, J. Chen, Determination of Metastable Zone Width and the Primary Nucleation Kinetics of Sodium Sulfate, *Theor. Found. Chem. Eng.* 49 (2015) 869–876. <https://doi.org/10.1134/S0040579515050309>.
- [250] K. Sangwal, A novel self-consistent Nývlt-like equation for metastable zone width determined by the polythermal method, *Cryst. Res. Technol.* 44 (2009) 231–247. <https://doi.org/10.1002/crat.200800501>.
- [251] R.S. Hebbar, A.M. Isloor, A.F. Ismail, Contact Angle Measurements, in: *Membr. Charact.*, Elsevier, 2017: pp. 219–255. <https://doi.org/10.1016/B978-0-444-63776-5.00012-7>.
- [252] M. Abbasgholipourghadim, M. Bin Mailah, I. Zaurah, A.F. Ismail, M. Rezaei Dashtarzhandi, M. Abbasgholipourghadim, Porosity and pore area determination of hollow fiber membrane incorporating digital image processing, in: C. Arapatsakos (Ed.), *Recent Adv. Mech. Mech. Eng.*, Kuala Lumpur, 2015: pp. 118–123.
- [253] W.T. Xu, Z.P. Zhao, M. Liu, K.C. Chen, Morphological and hydrophobic modifications of PVDF flat membrane with silane coupling agent grafting via

- plasma flow for VMD of ethanol-water mixture, *J. Membr. Sci.* 491 (2015) 110–120. <https://doi.org/10.1016/j.memsci.2015.05.024>.
- [254] L. Liu, L. Charlton, Y. Song, T. Li, X. Li, H. Yin, T. He, Scaling resistance by fluoro-treatments: The importance of wetting states, *J. Mater. Chem. A* 10 (2022) 3058–3068. <https://doi.org/10.1039/d1ta07695g>.
- [255] D.M. Correia, C. Ribeiro, V. Sencadas, G. Botelho, S.A.C. Carabineiro, J.L.G. Ribelles, S. Lanceros-Méndez, Influence of oxygen plasma treatment parameters on poly(vinylidene fluoride) electrospun fiber mats wettability, *Prog. Org. Coatings* 85 (2015) 151–158. <https://doi.org/10.1016/j.porgcoat.2015.03.019>.
- [256] R. Gregorio, M. Cestari, Effect of crystallization temperature on the crystalline phase content and morphology of poly(vinylidene fluoride), *J. Polym. Sci. Part B Polym. Phys.* 32 (1994) 859–870. <https://doi.org/10.1002/polb.1994.090320509>.
- [257] P. Martins, A.C. Lopes, S. Lanceros-Mendez, Electroactive phases of poly(vinylidene fluoride): Determination, processing and applications, *Prog. Polym. Sci.* 39 (2014) 683–706. <https://doi.org/10.1016/j.progpolymsci.2013.07.006>.
- [258] M. Herzberg, M. Elimelech, Biofouling of reverse osmosis membranes: Role of biofilm-enhanced osmotic pressure, *J. Membr. Sci.* 295 (2007) 11–20. <https://doi.org/10.1016/j.memsci.2007.02.024>.
- [259] M. Hu, T.C. Zhang, J. Stansbury, Y. Zhou, H. Chen, J. Neal, Contributions of Internal and External Fouling to Transmembrane Pressure in MBRs: Experiments and Modeling, *J. Environ. Eng.* 141 (2015) 04014097. [https://doi.org/10.1061/\(asce\)ee.1943-7870.0000925](https://doi.org/10.1061/(asce)ee.1943-7870.0000925).
- [260] E.W.R. Rodger B. Baird, Andrew D. Eaton, Standard methods for the examination of water and wastewater, 23rd ed., 2018.
- [261] R.E. Moosbrugger, M.C. Wentzel, G.A. Ekama, G.R. Marais, Simple titration procedures to determine H₂CO₃ alkalinity and short-chain fatty acids in aqueous solutions containing known concentration of ammonium, phosphate and sulphide weak acid/bases, Water Research Group, Department of Civil Engineering, University of Cape Town, 1992.
- [262] M. Dubois, K.A. Gilles, J.K. Hamilton, P.A. Rebers, F. Smith, Colorimetric Method for Determination of Sugars and Related Substances, *Anal. Chem.* 28 (1956) 350–356. <https://doi.org/10.1021/ac60111a017>.

- [263] Y.C. Juang, S.S. Adav, D.J. Lee, Influence of internal biofilm growth on residual permeability loss in aerobic granular membrane bioreactors, *Appl. Microbiol. Biotechnol.* 44 (2010) 1267–1273. <https://doi.org/10.1007/s00253-010-2527-1>.
- [264] A. Hafuka, R. Mashiko, R. Odashima, H. Yamamura, H. Satoh, Y. Watanabe, Digestion performance and contributions of organic and inorganic fouling in an anaerobic membrane bioreactor treating waste activated sludge, *Bioresour. Technol.* 272 (2019) 63–69. <https://doi.org/10.1016/j.biortech.2018.09.147>.
- [265] S. Wongchitphimon, R. Wang, R. Jiraratananon, L. Shi, C.H. Loh, Effect of polyethylene glycol (PEG) as an additive on the fabrication of polyvinylidene fluoride-co-hexafluoropropylene (PVDF-HFP) asymmetric microporous hollow fiber membranes, *J. Membr. Sci.* 369 (2011) 329–338. <https://doi.org/10.1016/j.memsci.2010.12.008>.
- [266] W. Rongwong, K. Goh, G.S.M.D.P. Sethunga, T.H. Bae, Fouling formation in membrane contactors for methane recovery from anaerobic effluents, *J. Membr. Sci.* 573 (2019) 534–543. <https://doi.org/10.1016/j.memsci.2018.12.038>.
- [267] A. Mansourizadeh, I. Rezaei, W.J. Lau, M.Q. Seah, A.F. Ismail, A review on recent progress in environmental applications of membrane contactor technology, *J. Environ. Chem. Eng.* 10 (2022) 1–21. <https://doi.org/10.1016/j.jece.2022.107631>.
- [268] L. Liu, Z. Xiao, Y. Liu, X. Li, H. Yin, A. Volkov, T. He, Understanding the fouling/scaling resistance of superhydrophobic/omniphobic membranes in membrane distillation, *Desalination.* 499 (2021) 1–18. <https://doi.org/10.1016/j.desal.2020.114864>.
- [269] L. Chen, Y. Wang, Z. Chen, Z. Cai, The fouling layer development on MD membrane for water treatments: An especial focus on the biofouling progress, *Chemosphere.* 264 (2021) 1–13. <https://doi.org/10.1016/j.chemosphere.2020.128458>.
- [270] A. Zarebska, Á.C. Amor, K. Ciurkot, H. Karring, O. Thygesen, T.P. Andersen, M.B. Hägg, K.V. Christensen, B. Norddahl, Fouling mitigation in membrane distillation processes during ammonia stripping from pig manure, *J. Membr. Sci.* 484 (2015) 119–132. <https://doi.org/10.1016/j.memsci.2015.03.010>.
- [271] R.A. Al-Juboori, T. Yusaf, V. Aravinthan, Investigating the efficiency of thermosonication for controlling biofouling in batch membrane systems,

- Desalination. 286 (2012) 349–357.
<https://doi.org/10.1016/j.desal.2011.11.049>.
- [272] J. Pan, F. Zhang, Z. Wang, S.P. Sun, Z. Cui, W. Jin, O. Bamaga, H. Abulkhair, M. Albeirutty, E. Drioli, Enhanced anti-wetting and anti-fouling properties of composite PFPE/PVDF membrane in vacuum membrane distillation, *Sep. Purif. Technol.* 282 (2022) 1–11.
<https://doi.org/10.1016/j.seppur.2021.120084>.
- [273] G.S.M.D.P. Sethunga, H.E. Karahan, R. Wang, T.H. Bae, Wetting- and fouling-resistant hollow fiber membranes for dissolved methane recovery from anaerobic wastewater treatment effluents, *J. Membr. Sci.* 617 (2021) 118621. <https://doi.org/10.1016/j.memsci.2020.118621>.
- [274] B. Abdu, S. Munirasu, P. Kallem, S.W. Hasan, F. Banat, Investigating the effect of various foulants on the performance of intrinsically superhydrophobic polyvinylidene fluoride membranes for direct contact membrane distillation, *Sep. Purif. Technol.* 252 (2020) 1–13.
<https://doi.org/10.1016/j.seppur.2020.117416>.
- [275] N.K. Saha, M. Balakrishnan, M. Ulbricht, Sugarcane juice ultrafiltration: FTIR and SEM analysis of polysaccharide fouling, *J. Membr. Sci.* 306 (2007) 287–297. <https://doi.org/10.1016/j.memsci.2007.09.006>.
- [276] G.S.M.D.P. Sethunga, J. Lee, R. Wang, T.H. Bae, Influence of membrane characteristics and operating parameters on transport properties of dissolved methane in a hollow fiber membrane contactor for biogas recovery from anaerobic effluents, *J. Membr. Sci.* 589 (2019) 117263.
<https://doi.org/10.1016/j.memsci.2019.117263>.
- [277] C.G. Jothi Prakash, R. Prasanth, Approaches to design a surface with tunable wettability: a review on surface properties, *J. Mater. Sci.* 56 (2021) 108–135. <https://doi.org/10.1007/s10853-020-05116-1>.
- [278] D. Ebert, B. Bhushan, Transparent, superhydrophobic, and wear-resistant surfaces using deep reactive ion etching on PDMS substrates, *J. Colloid Interface Sci.* 481 (2016) 82–90. <https://doi.org/10.1016/j.jcis.2016.07.035>.
- [279] S.H. Lin, K.L. Tung, H.W. Chang, K.R. Lee, Influence of fluorocarbon flat-membrane hydrophobicity on carbon dioxide recovery, *Chemosphere.* 75 (2009) 1410–1416. <https://doi.org/10.1016/j.chemosphere.2009.02.027>.
- [280] R.S. Juang, C. Huang, C.L. Hsieh, Surface modification of PVDF ultrafiltration membranes by remote argon/methane gas mixture plasma for fouling reduction, *J. Taiwan Inst. Chem. Eng.* 45 (2014) 2176–2186.

- <https://doi.org/10.1016/j.jtice.2014.06.025>.
- [281] M. Meyyappan, Plasma nanotechnology: Past, present and future, *J. Phys. D. Appl. Phys.* 44 (2011) 1–11. <https://doi.org/10.1088/0022-3727/44/17/174002>.
- [282] M.D. Duca, C.L. Plosceanu, T. Pop, Surface modifications of polyvinylidene fluoride (PVDF) under rf Ar plasma, *Polym. Degrad. Stab.* 61 (1998) 65–72. [https://doi.org/10.1016/S0141-3910\(97\)00130-4](https://doi.org/10.1016/S0141-3910(97)00130-4).
- [283] Y.W. Park, N. Inagaki, Surface modification of poly (vinylidene fluoride) film by remote Ar, H₂, and O₂ plasmas, *Polymer (Guildf)*. 44 (2003) 1569–1575.
- [284] W. Rongwong, S. Wongchitphimon, K. Goh, R. Wang, T.H. Bae, Transport properties of CO₂ and CH₄ in hollow fiber membrane contactor for the recovery of biogas from anaerobic membrane bioreactor effluent, *J. Membr. Sci.* 541 (2017) 62–72. <https://doi.org/10.1016/j.memsci.2017.06.090>.
- [285] S. Kartohardjono, A. Rabekka, Combination Vacuum and Sweep Gas Processes to Remove Dissolved Oxygen from Water through Hollow Fiber Membrane Contactors, *J. Mater. Sci. Eng. A* 1 (2011) 812–818.
- [286] I. Martić, A. Maslarević, S. Mladenović, U. Lukić, S. Budimir, Water deoxygenation using hollow fiber membrane module with nitrogen as inert gas, *Desalin. Water Treat.* 54 (2015) 1563–1567. <https://doi.org/10.1080/19443994.2014.888677>.
- [287] M. Henares, M. Izquierdo, P. Marzal, V. Martínez-Soria, Demethanization of aqueous anaerobic effluents using a polydimethylsiloxane membrane module: Mass transfer, fouling and energy analysis, *Sep. Purif. Technol.* 186 (2017) 10–19. <https://doi.org/10.1016/j.seppur.2017.05.035>.
- [288] G. Luo, W. Wang, I. Angelidaki, A new degassing membrane coupled upflow anaerobic sludge blanket (UASB) reactor to achieve in-situ biogas upgrading and recovery of dissolved CH₄ from the anaerobic effluent, *Appl. Energy*. 132 (2014) 536–542. <https://doi.org/10.1016/j.apenergy.2014.07.059>.
- [289] W. Rongwong, C. Fan, Z. Liang, Z. Rui, R.O. Idem, P. Tontiwachwuthikul, Investigation of the effects of operating parameters on the local mass transfer coefficient and membrane wetting in a membrane gas absorption process, *J. Membr. Sci.* 490 (2015) 236–246. <https://doi.org/10.1016/j.memsci.2015.04.071>.
- [290] M. Nanzyo, H. Onodera, E. Hasegawa, K. Ito, H. Kanno, Formation and Dissolution of Vivianite in Paddy Field Soil, *Soil Sci. Soc. Am. J.* 77 (2013)

- 1452–1459. <https://doi.org/10.2136/sssaj2012.0437n>.
- [291] R. Liu, D. Zhao, In situ immobilization of Cu(II) in soils using a new class of iron phosphate nanoparticles, *Chemosphere*. 68 (2007) 1867–1876. <https://doi.org/10.1016/j.chemosphere.2007.03.010>.
- [292] M. Rothe, A. Kleeberg, M. Hupfer, The occurrence, identification and environmental relevance of vivianite in waterlogged soils and aquatic sediments, *Earth-Science Rev.* 158 (2016) 51–64. <https://doi.org/10.1016/j.earscirev.2016.04.008>.
- [293] C.A. Quist-Jensen, A. Ali, S. Mondal, F. Macedonio, E. Drioli, A study of membrane distillation and crystallization for lithium recovery from high-concentrated aqueous solutions, *J. Membr. Sci.* 505 (2016) 167–173. <https://doi.org/10.1016/j.memsci.2016.01.033>.
- [294] C.A. Quist-Jensen, M.K. Jørgensen, M.L. Christensen, Treated seawater as a magnesium source for phosphorous recovery from wastewater—A feasibility and cost analysis, *Membranes (Basel)*. 6 (2016). <https://doi.org/10.3390/membranes6040054>.
- [295] A. Mersmann, M. Kind, Chemical engineering aspects of precipitation from solution, *Chem. Eng. Technol.* 11 (1988) 264–276. <https://doi.org/10.1002/ceat.270110136>.
- [296] D. Cai, Z. Chang, L. Gao, C. Chen, Y. Niu, P. Qin, Z. Wang, T. Tan, Acetone-butanol-ethanol (ABE) fermentation integrated with simplified gas stripping using sweet sorghum bagasse as immobilized carrier, *Chem. Eng. J.* 277 (2015) 176–185. <https://doi.org/10.1016/j.cej.2015.04.101>.

7 NOMENCLATURE.

$[i]_{ind}$	Molar concentration of component i at bulk induction time, M
$[i]^{m_{t_c}}$	Mean molar concentration of component i at time t_c of crystallisation test inside the membrane module, M
$[i]^{n_{t_c}}$	Molar concentration of component i at time t_c of crystallisation test in the retentate inlet ($n=a$), permeate inlet ($n=b$) and permeate outlet ($n=c$), and inside the membrane module ($n=m$) M
$[viv]^*$	Solubility of vivianite in water, M
$\sum v_i$	Especial atomic diffusion volume of $i = N_2$ and CH_4
A	Effective membrane area, m^2
A_e	Effective membrane external area of fibres, m^2
AE	Anaerobic reactor effluent
AFM	Atomic force microscope
A_G	Membrane interfacial area in contact with the gas phase, m^2
A_i	Effective membrane internal area of the fibres, m^2
A_L	Membrane interfacial area in contact with the liquid phase, m^2
A_{ml}	Logarithmic mean membrane area, m^2
AnMBR	Anaerobic Membrane Bioreactor
ANOVA	Analysis of variance
APTES	3-(triethoxysilyl)-propylamine
aPVDF-Ds	Altered PVDF-Ds membrane
ATR	Attenuated total reflectance
a_α	Absorbance of PVDF at the wavelengths of 766 cm^{-1}
a_β	Absorbance of PVDF at the wavelengths of 840 cm^{-1}
C^*_{L0}	Initial dissolved methane concentration in the liquid in equilibrium with the methane content in the outlet gas, mg L^{-1}
C^*_{L,t_d}	Dissolved methane concentration in the liquid in equilibrium with the methane content in the outlet gas at degasification time t_d , mg L^{-1}
C_G	Methane concentration in the gas, mg L^{-1}
$C_{G,eq}$	Methane concentration in the head-space gas in equilibrium with the liquid phase inside analysis vials, mg L^{-1}
C_{G1}	Methane concentration in the gas at the inlet of the membrane module, mg L^{-1}
C_{G2}	Methane concentration in the gas at the outlet of the membrane module, mg L^{-1}
C_L	Dissolved methane concentration in the liquid, mg L^{-1}
$C_{L,eq}$	Dissolved methane concentration in the liquid in equilibrium with the head-space gas inside the analysis vials, mg L^{-1}

C_{L0}	Initial dissolved methane concentration in the liquid feed tank, mg L ⁻¹
C_{L1}	Dissolved methane concentration in the liquid at the inlet of the membrane module, mg L ⁻¹
C*_{L1}	Dissolved methane concentration in the liquid in equilibrium with the methane content in the outlet gas, mg L ⁻¹
C_{L2}	Dissolved methane concentration in the liquid at the outlet of the membrane module, mg L ⁻¹
C*_{L2}	Dissolved methane concentration in the liquid in equilibrium with the methane content in the inlet gas, mg L ⁻¹
CLSM	Confocal laser scanning microscope
C_{L,td}	Dissolved methane concentration in the liquid feed tank at degasification time t _d , mg L ⁻¹
CNT	Classical nucleation theory
COD	Chemical oxygen demand, mg L ⁻¹
D-CH₄	Dissolved methane
D_{CH₄-i}	Binary diffusion coefficient of methane through specie i, m ² s ⁻¹
D_{G,CH₄}	Molecular diffusion coefficient of methane in the gas phase, m ² s ⁻¹
D_{G,eff}	Effective diffusion of methane through the membrane pores, m ² s ⁻¹
D_{G,Kn}	Knudsen diffusion coefficient of methane through the pores, m ² s ⁻¹
d_{hG}	Hydraulic diameter of the gas side of the membrane module, m
d_{hL}	Hydraulic diameter of the liquid side of the membrane module, m
d_i	Inner diameter of the membrane fibre, μm
D_{L,CH₄}	Molecular diffusion coefficient of methane in the liquid phase, m ² s ⁻¹
d_{lm}	Logarithmic mean membrane fibre diameter, m
d_o	Outer diameter of the membrane fibre, μm
DOE	Design of experiments
DSC	Differential scanning calorimetry
DW	De-ionised water
EDX	Energy dispersion X-ray
EGSB	Expanded Granular Sludge Bed
EPS	Extracellular polymeric substances
EU	European Union
FAS	Fluoroalkylsilane
FESEM	Field emission scanning electron microscope
FM	Flat-sheet membrane module
FM-MA	Methacrylate flat-sheet membrane module
FM-PLA	3-D printed polylactic acid flat-sheet membrane module
FM-SS	Stainless steel flat-sheet membrane module

FS	Functionalisation solution
FSi_x	Mixture of FAS and SiP with 'x' = T or A for TEOS and APTES, respectively
FSi_x ratio	FAS volume-to-FSi _x mixture volume ratio
FSi_x%_v	FSi _x volumetric percentage in the solvent, %
FTIR	Fourier transform infrared spectroscopy
G/L	Gas-to-liquid flow rate ratio
GHG	Greenhouse gas
GWP	Global warming potential
GWP100	Global warming potential over a 100 year horizon
H	Dimensionless Henry's constant
H^{ep}	Henry's Law constant, mol m ⁻³ Pa ⁻¹
HFC	Hydrofluorocarbon
HFMC	Hollow fibre membrane contactor
IAP	Ionic activity product
IPA	2-propanol
IPCC	Intergovernmental Panel on Climate Change
J_{CH₄}	Methane flux, g s ⁻¹ m ⁻²
J_{Fe}	Dosing rate of the Fe ²⁺ solution, mL min ⁻¹
k'	Nucleation constant, mg L ⁻¹ min ⁻¹
k^{FM_G}	Individual mass transfer coefficient of the gas phase in a flat-sheet membrane module, m s ⁻¹
k^{FM_L}	Individual mass transfer coefficient of the liquid phase in a flat-sheet membrane module, m s ⁻¹
K^{FM_{L,est}}	Estimated overall mass transfer coefficient based on the liquid phase in a flat-sheet membrane module, m s ⁻¹
K^{FM_{L,exp}}	Experimental overall mass transfer coefficient based on the liquid phase in a flat-sheet membrane module, m s ⁻¹
k^{HF_G}	Individual mass transfer coefficient of the gas phase in a hollow fibre membrane contactor, m s ⁻¹
k^{HF_L}	Individual mass transfer coefficient of the liquid phase in a hollow fibre membrane contactor, m s ⁻¹
K^{HF_{L,est}}	Estimated overall mass transfer coefficient based on the liquid phase in a hollow fibre membrane contactor, m s ⁻¹
K^{HF_{L,exp}}	Experimental overall mass transfer coefficient based on the liquid phase in a hollow fibre membrane contactor, m s ⁻¹
k_m	Individual mass transfer coefficient of the membrane, m s ⁻¹
k_{m,dense}	Individual mass transfer coefficient of a dense membrane, m s ⁻¹
k_{m,porous}	Individual mass transfer coefficient of a porous membrane, m s ⁻¹
K_{sp}	Solubility product constant of vivianite in water
l	Membrane length, m
l_{ef}	Effective membrane length, m

LEP	Liquid entry pressure, bar
m'	Apparent nucleation order
MAC	Membrane-assisted crystallisation
MARC	Membrane-assisted reactive crystallisation
M_{CH₄}	Methane molar mass, g mol ⁻¹
MFC	Microbial fuel cell
M_{N₂}	Nitrogen molar mass, g mol ⁻¹
mPVDF	Modified PVDF-Ds
mPVDF_{max}	Modified PVDF-Ds at the optimal modification conditions with alkali activation
M_T	Total liquid mass in the system, kg
M_{viv}	Vivianite molar mass, g mol ⁻¹
NaOH%wt	NaOH concentration in mass base, %
nmPVDF	Non-modified PVDF-Ds
OPEX	Operational expenditures
P	Pressure, Pa
PBS	Phosphate-buffered saline solution
PDMS	Polydimethylsiloxane
PEG	Polyethylene glycol
PET	Polyester
PFC	Perfluorocarbon
PFP	Poly(hexafluoropropylene)
PI	Propidium iodide
PI_m	Polyimide
PLA	Poly(lactic acid)
P_{m,CH₄}	Permeability of methane through the dense membrane, m ² Pa ⁻¹ s ⁻¹
PO₂-APTES	Modified PVDF-Dp at the optimal plasma conditions and APTES as silica precursor
PO₂-PVDF_{max}	Modified PVDF-Dp at the optimal plasma conditions
PO₂-TEOS	Modified PVDF-Dp at the optimal plasma conditions and TEOS as silica precursor
PP	Polypropylene
P_{p,eq}	Partial pressure of the methane in the headspace in equilibrium with the liquid phase, Pa
PS	Polysulfone
PTFE	Polytetrafluoroethylene
PU	Polyurethane
P_{vac}	Vacuum pressure, mbar
PVDF	Polyvinylidene fluoride
Q_L	Liquid flow rate, L h ⁻¹
Q_l	Liquid flow rate, m ³ s ⁻¹

Q_{N_2}	Nitrogen flow rate, $L h^{-1}$
R	Ideal gas constant, $m^3 Pa mol^{-1} K^{-1}$
r'	Nucleation rate of vivianite, $mg L^{-1} min^{-1}$
R^2	Level of confidence
$R-CH_4$	Recovered methane
RE	Removal efficiency, %
Re_G	Reynolds number of the gas phase
Re_L	Reynolds number of the liquid phase
Re_p	Reynolds number in the permeate side of the FM-MA
R^{FM_G}	Individual mass transfer resistance of the gas phase in a flat-sheet membrane module, $s m^{-1}$
R^{FM_L}	Individual mass transfer resistance of the liquid phase in a flat-sheet membrane module, $s m^{-1}$
$R^{FM_{ov}}$	Overall mass transfer resistance in a flat-sheet membrane module, $s m^{-1}$
$R^{HF_{G,est}}$	Estimated individual mass transfer resistance of the gas phase in the hollow fibre membrane contactor, $s m^{-3}$
$R^{HF_{L,est}}$	Estimated individual mass transfer resistance of the liquid phase in the hollow fibre membrane contactor, $s m^{-3}$
$R^{HF_{ov,est}}$	Estimated experimental mass transfer resistance in the hollow fibre membrane contactor, $s m^{-3}$
$R^{HF_{ov,exp}}$	Overall experimental mass transfer resistance in the hollow fibre membrane contactor, $s m^{-3}$
R_m	Individual mass transfer resistance of the membrane, $s m^{-1}$
$R_{m,est}$	Estimated individual mass transfer resistance of the membrane in the hollow fibre membrane contactor, $s m^{-3}$
r_p	Membrane pore size (equivalent to pore diameter), μm
$r_{p,max}$	Maximum membrane pore size (equivalent to maximum pore diameter), m
R_q	Root mean square roughness, nm
S	Supersaturation
$SAnMBR$	Submerged Anaerobic Membrane Bioreactor
Sc_G	Schmidt number of the gas phase
Sc_L	Schmidt number of the liquid phase
$SCSIE$	Servicio Central de Soporte a la Investigación Experimental de la Universitat de València
Sh_0	Limiting Sherwood number
Sh_∞	Limiting Sherwood number
Sh_G	Sherwood number of the gas phase
Sh_L	Sherwood number of the liquid phase
SI	Supersaturation index
SI^b	Supersaturation index of vivianite in the phosphate/permeate bulk solution
SI^m	Supersaturation index of vivianite inside the permeate side of the membrane module

SiP	Silica precursor
S^m_{ind}	Supersaturation of vivianite inside the membrane module at bulk induction time
SMP	Soluble microbial products
T	Temperature, K
t_c	Time of crystallisation test, min
t_c^{ind}	Bulk induction time, min
t_d	Time of degasification test, s
TEOS	Tetraethyl orthosilicate
TGA	Thermogravimetric analysis
TSS	Total suspended solids, mg L ⁻¹
UASB	Upflow Anaerobic Sludge Blanket
UNFCCC	United Nations Framework Convention on Climate Change
uPVDF-Ds	Unaltered PVDF-Ds membrane
UV	Ultraviolet
VFA	Volatile fatty acids
V_G	Gas volume, L
V_L	Liquid volume, L
v_L	Liquid velocity, m s ⁻¹
V_{m,CH₄}	Molar volume of methane, m ³ mol ⁻¹
V_{sol,t_c}	Liquid volume of the solution in the phosphate/permeate tank at time t _c , mL
VSS	Volatile suspended solids, mg L ⁻¹
WCA	Static water contact angle, °
x	Molar fraction of α phase of PVDF
XRD	X-ray diffraction
y	Molar fraction of β phase of PVDF
y_{CH₄}	Methane content in gas, %
y'_i	Mole fraction of specie i in gas evaluated on CH ₄ -free basis
α	Alpha value of the surface response analysis
β	Geometric pore coefficient
γ	Liquid surface tension, N m ⁻¹
δ	Membrane thickness, μm
ΔC_{lm}	Logarithmic mean concentration of methane, mg L ⁻¹
Δh_m	Melting enthalpy of sample, J g ⁻¹
Δh_α	Melting enthalpy of α phase of PVDF, J g ⁻¹
Δh_β	Melting enthalpy of β phase of PVDF, J g ⁻¹
ε	Membrane porosity, %
θ	Contact angle, °
K_α	Absorption coefficient of α phase of PVDF, cm ² mol ⁻¹
K_β	Absorption coefficient of β phase of PVDF, cm ² mol ⁻¹

μ_G	Gas viscosity, $\text{kg m}^{-1} \text{s}^{-1}$
ρ_{CH_4}	Methane density, mg L^{-1}
ρ_G	Gas density, mg L^{-1}
ρ_L	Liquid density, kg m^{-3}
τ	Membrane tortuosity
χ	Crystallinity, %

8 RESUMEN EXTENDIDO.

En esta sección se presenta un resumen de los principales resultados y conclusiones de la tesis doctoral, que se presenta como compendio de cinco artículos publicados y un artículo en proceso de revisión. El objetivo principal de la tesis doctoral es la evaluación de las dos tecnologías de membranas poliméricas en la valorización de efluentes líquidos residuales para la separación y recuperación de metano (CH_4) y fósforo (P) disueltos. Además, se han aplicado diferentes metodologías de funcionalización superficial de las membranas para aumentar la resistencia a la humectación de los poros y la vida útil de las membranas de polifluoruro de vinilideno (PVDF). Este objetivo principal se divide en tres objetivos parciales:

- 1) Evaluación del rendimiento de la membrana en la recuperación de metano disuelto de efluentes líquidos utilizando contactores de membrana plana (FM) gas-líquido. Se probaron diferentes materiales de membrana (porosos, densos y funcionalizados) y condiciones de operación con un agua sintética y un efluente anaerobio real en operaciones a corto y largo plazo.
- 2) Comparación del modo de operación a vacío, gas de arrastre o ambos simultáneamente (modo combinado), para optimizar el rendimiento de la recuperación de metano disuelto de efluentes líquidos con un contactor de membrana de fibra hueca (HFMC) de polipropileno (PP).
- 3) Integración de la cristalización asistida por membranas en la recuperación de fósforo disuelto en forma de vivianita. Se propuso un proceso de cristalización reactiva para tratar una solución rica en fosfato con una dosificación continua de una solución de hierro (II) para obtener cristales de vivianita utilizando un módulo de membrana plana.

Los principales resultados obtenidos se resumen a continuación divididos en seis subsecciones que corresponden a las seis contribuciones científicas de esta tesis doctoral recogidas en los apéndices.

8.1 RECUPERACIÓN DE METANO DISUELTO USANDO UN MÓDULO PLANO CON MEMBRANAS DE PDMS, PP Y PVDF.

Los contactores o módulos de membrana han demostrado ser una tecnología prometedora para evitar la pérdida de metano disuelto ($D-CH_4$) en aguas residuales tratadas anaeróbicamente [49,60,69,70] debido a sus características, como bajo consumo de energía, buena selectividad o fácil escalado y operación [296]. En comparación con los contactores de fibra hueca, los contactores de membrana plana pueden presentar varias ventajas relacionadas con su simplicidad y versatilidad. La membrana plana puede extraerse, analizarse y limpiarse fácilmente durante el funcionamiento y/o sustituirse, lo que permite un ahorro considerable de tiempo y costes. Esto permite que los contactores planos sean especialmente útiles cuando la resistencia a la humectación de los poros (“wetting”) y el ensuciamiento, o la estabilidad de la membrana en operación son el foco de la investigación, así como para facilitar la comparación del rendimiento de diferentes membranas.

El primer objetivo de este trabajo fue determinar la aplicabilidad y versatilidad (y también las limitaciones) del sistema de separación gas-líquido de membrana plana utilizando un módulo con un área efectiva de 17.3 cm^2 (FM-SS) para la recuperación de $D-CH_4$ en agua. Para ello, se determinó el efecto de las condiciones hidráulicas sobre la eficacia de eliminación de metano (RE) y se probaron diferentes tipos de membranas. Adicionalmente, se modeló la transferencia de materia de metano para el sistema en estudio y se evaluó la estabilidad a largo plazo de las membranas.

Con el fin de dilucidar el efecto de los parámetros de operación en la eficacia de cada membrana y la recuperación de $D-CH_4$, se realizaron pruebas de desgasificación con corrientes sintéticas de agua y membranas de polidimetilsiloxano (PDMS), polifluoruro de vinilideno (PVDF-Ds), y dos tipos de polipropileno (PP-1E y PP-2E). El FM-SS operó en modo gas de arrastre con

caudales de N_2 (Q_{N_2}) que oscilaban entre 0.05 y 15.00 L h⁻¹ (velocidad del gas de 0.0043 a 1.3 cm s⁻¹) y caudales de líquido (Q_L) que oscilaban entre 3.5 y 40.5 L h⁻¹ (velocidad del líquido de 2.8 a 32.5 cm s⁻¹). Se determinaron los perfiles de la RE y del contenido en metano (y_{CH_4}) en el gas recuperado en función del tiempo a las diferentes condiciones de operación. Además, se modeló el transporte de materia de metano en base al modelo de resistencias en serie, el cual fue validado en base a los resultados experimentales. Finalmente, también se determinó la estabilidad de la membrana con el tiempo de uso analizando el ángulo de contacto (hidrofobicidad) de la membrana y tomando imágenes de la superficie y sección transversal en busca de posible degradación mediante microscopía electrónica (FESEM).

Los efectos de los parámetros de operación en la RE y y_{CH_4} se estudiaron inicialmente con una membrana de PDMS. La RE aumentó con el tiempo de operación debido a la continua desgasificación del agua del tanque, alcanzando valores de hasta el 95% a las 22 h. Además, los resultados mostraron que la RE aumentó con Q_L , debido a la mayor velocidad de extracción de metano del sistema y a la mejora en la transferencia de materia. Así, se obtuvo una RE de 24% y 55% a las 5 h de operación a un Q_L de 3.5 y 40.5 L h⁻¹, respectivamente. Además, las velocidades más altas del líquido dentro del FM-SS condujeron a una mayor turbulencia que favoreció la transferencia de materia del metano, con coeficientes estimados de transferencia de materia en la fase líquida de $2.25 \cdot 10^{-5}$ y $5.85 \cdot 10^{-5}$ m s⁻¹ a 3.5 y 40.5 L h⁻¹, respectivamente. Por el contrario, la RE solo aumentó ligeramente cuando el Q_{N_2} se incrementó de 0.05 a 0.5 L h⁻¹ (RE de 40% y 45%, respectivamente, a las 5 h de operación), y después, la RE permaneció casi constante debido a la insignificante resistencia a la transferencia de materia estimada para la fase gaseosa, la cual solo representó menos de un 0.05% de la resistencia total.

En cuanto a la composición volumétrica del gas recuperado, el y_{CH_4} estuvo fuertemente influenciado por el Q_L y Q_{N_2} . Se obtuvo mayor y_{CH_4} a medida que aumentaba el Q_L , ya que se determinaron mayores flujos de metano. Así, se

obtuvo un máximo y_{CH_4} cercano al 5% para un flujo de metano de $118 \text{ g s}^{-1} \text{ m}^{-2}$ al mayor Q_L . Por el contrario, el y_{CH_4} disminuyó drásticamente al aumentar el Q_{N_2} por efecto de la dilución, con valores siempre inferiores al 0.4% para $Q_{\text{N}_2} \geq 4.0 \text{ L h}^{-1}$. Además, el flujo y y_{CH_4} disminuyó con el tiempo de operación hasta valores inferiores a $11 \text{ g s}^{-1} \text{ m}^{-2}$ y 0.5%, respectivamente, a las 22 h de operación. Esta observación fue coherente con la menor fuerza impulsora a medida que disminuía la concentración de D- CH_4 en el líquido.

Las dos membranas porosas de PP resultaron en una RE y y_{CH_4} similar al de la membrana densa de PDMS, atribuido a la despreciable resistencia a la transferencia de materia de la membrana. De hecho, la resistencia estimada de la membrana representó menos de un 0.5% de la resistencia total. A pesar de la capa densa del PDMS, la baja resistencia a la transferencia de materia se atribuyó al pequeño espesor de dicha capa ($2.5 \mu\text{m}$). Respecto a la membrana de PVDF-Ds, ésta mostró una menor RE atribuido a la humectación de los poros.

En cuanto a la estabilidad de las membranas, un Q_L moderado-alto de 21.0 L h^{-1} provocó una degradación relativamente rápida de las membranas, especialmente en las membranas de PP cuyo ángulo de contacto (WCA) disminuyó más de un 14% en solo 5 h de uso debido a una deformación de toda la membrana. La membrana de PDMS experimentó una ligera disminución del WCA de 101° a 94° tras 95 h de uso, aunque se detectaron fisuras y delaminación en la capa densa superior. Esta degradación provocó un flujo de agua a través de la membrana, lo que indica el final de su vida útil. En el caso de la membrana de PVDF-Ds, WCA aumentó hasta un valor estable de $\sim 115^\circ$ a las 90 h de uso, debido a la deformación inducida por el flujo de líquido sobre la membrana, reduciendo su porosidad. Por el contrario, las membranas de PDMS y PVDF-Ds mostraron una mayor estabilidad al Q_L más bajo de 3.5 L h^{-1} , ya que su WCA original se mantuvo casi sin cambios durante más de 175 h de uso, y no se observó deformación ni flujos de agua a su través. Por lo tanto, estas membranas podrían usarse para operaciones a largo plazo con bajas velocidades de líquido.

Finalmente, se determinaron los coeficientes experimentales de transferencia de materia y se compararon con los valores estimados en base a ecuaciones empíricas. De forma general, los coeficientes experimentales obtenidos fueron similares a los estimados con el modelo en ausencia de humectación de los poros, indicando que las ecuaciones empíricas utilizadas para el análisis de transferencia de materia parecían adecuadas para la predicción de la resistencia de transferencia de materia en el sistema. Los coeficientes de transferencia de materia globales experimentales oscilaron entre $1.66 \cdot 10^{-5}$ y $6.28 \cdot 10^{-5} \text{ m s}^{-1}$ y mostraron que la principal resistencia se encontraba en la fase líquida. Por lo tanto, el rendimiento en la recuperación de D-CH₄ mediante contactores planos depende principalmente de las condiciones hidráulicas del lado de alimentación de líquido.

En conclusión, se ha demostrado la aplicabilidad y versatilidad de un FM gas-líquido para la recuperación de D-CH₄ en el que la medida del WCA puede ser una metodología útil y de bajo coste para determinar la estabilidad de las membranas durante la operación. Además, se deben tener en cuenta los límites de cada membrana para establecer las condiciones de operación que maximicen la vida útil de la membrana y minimizar los costes de operación.

8.2 MEJORA DE LA HIDROFOBICIDAD DE UNA MEMBRANA PLANA DE PVDF MEDIANTE ACTIVACIÓN ALCALINA Y ORGANOFLUROSILANIZACIÓN PARA LA RECUPERACIÓN DE METANO DISUELTO.

Las dos principales desventajas en operaciones de separación con membranas son la humectación de los poros y ensuciamiento. En las membranas porosas, la presión del líquido sobre la superficie de la membrana puede provocar el llenado de los poros de la membrana [71,84]. Esta humectación de los poros puede provocar un aumento del ~20% de la resistencia a la transferencia de materia de la membrana con solo el 5% de los poros llenos [91]. Por otro lado, los agentes de ensuciamiento presentes en efluentes líquidos residuales pueden adherirse a la superficie de la membrana [90], lo que también provoca restricciones para la transferencia de materia y degradación de la membrana [68]. Estos inconvenientes se pueden evitar o mitigar mediante la adición de nuevas funcionalidades sobre la membrana [68,265]. En este sentido, los compuestos orgánicos fluorados y los siloxanos han sido desarrollados y evaluados como agentes modificadores, ya que se sabe que reducen la energía libre superficial y, en consecuencia, aumentan la hidrofobicidad y la resistencia a la humectación de los poros [71].

El objetivo de este trabajo fue evaluar el efecto de una modificación química superficial aplicada sobre una membrana de PVDF-Ds para la recuperación de D-CH₄ de corrientes acuosas. En primer lugar, se propuso un procedimiento de modificación basado en una activación alcalina seguida de una funcionalización. Después, se evaluaron la estabilidad y el rendimiento de la membrana en la recuperación de D-CH₄ de la membrana modificada y los resultados se compararon con la membrana no modificada. Estas membranas se probaron en un módulo plano de membrana con un área de 17.3 cm² (FM-SS) a varias condiciones de operación con agua desionizada y un efluente real de un reactor anaerobio.

Para aumentar la hidrofobicidad de la membrana, las membranas de PVDF-Ds ($WCA = 103 \pm 2^\circ$) se trataron mediante una activación alcalina húmeda con una solución de NaOH (concentración de NaOH, $NaOH\%_{wt}$, de 1 a 6%) seguida de una funcionalización con el fluoroalquilsilano (FAS) 1H,1H,2H,2H-perfluorooctiltrietoxisilano, utilizando tetraetilortosilicato (TEOS) como precursor de silicio ($SiPr$). La concentración y proporción FAS/ $SiPr$ ($FSiPr\%_v$, $FSiPr$, respectivamente) en la solución de funcionalización varió de 0.8 a 9.2% y de 0.17 a 0.94, respectivamente. La hidrofobicidad se maximizó mediante un diseño estadístico de experimentos para optimizar la concentración de cada reactivo. La superficie y la sección transversal de las membranas modificadas se caracterizaron por microscopía y espectroscopia (FESEM-EDX). Además, el rendimiento y la estabilidad de la membrana en la recuperación de $D-CH_4$ también se evaluaron mediante pruebas de desgasificación, estabilidad a largo plazo y ensuciamiento.

Las membranas modificadas de PVDF-Ds siempre presentaron valores de WCA superiores a la membrana no modificada (nmPVDF, $103.4 \pm 1.6^\circ$), lo que demostró que el procedimiento de funcionalización propuesto era adecuado para aumentar la hidrofobicidad de estas membranas. De acuerdo con el análisis del diseño de experimentos, las principales variables involucradas en el método de funcionalización que afectaron a la hidrofobicidad de la membrana fueron la concentración de NaOH para la activación de la membrana y la concentración y proporción de FAS/ $SiPr$. Como resultado, los factores individuales presentaron los mayores efectos sobre la respuesta, siendo los factores asociados a la etapa de funcionalización ($FSiPr$ y $FSiPr\%_v$) los más relevantes, ya que estos factores determinaron el número de enlaces O-Si en las cadenas de PVDF y el contenido total de flúor (F). Por lo tanto, el WCA resultante fue mayor a medida que aumentó el contenido de F. Finalmente, se obtuvo un WCA máximo de $143.2 \pm 2.5^\circ$ para las condiciones óptimas de modificación, que se establecieron en los valores de 5%, 7.2% y 0.55 para $NaOH\%_{wt}$, $FSiPr\%_v$ y $FSiPr$, respectivamente.

Se realizó una inspección de la superficie y sección transversal de la membrana nmPVDF y PVDF-Ds modificado que presentó el máximo WCA (mPVDF_{max}). El efecto de la modificación de la membrana resultó en una superficie heterogénea con zonas porosas y zonas con clústeres densos y menor porosidad superficial, dando lugar a una capa superior compacta con un espesor de entre 15 y 37 μm para la membrana mPVDF_{max}. Además, la membrana mPVDF_{max} mostró un contenido de F ligeramente mayor que el obtenido en la membrana nmPVDF (55% y 53%, respectivamente), lo que indica que el FAS se incorporó en la superficie. Esto provocó el aumento de la hidrofobicidad de la membrana, dando lugar a una mayor resistencia a la humectación de los poros.

La estabilidad de la membrana mPVDF_{max} se evaluó bajo un flujo de agua moderado-alto (Q_L de 21 L h⁻¹), resultando en una disminución continua del WCA hasta $105.4 \pm 2.5^\circ$ a las 47 h, y después se mantuvo constante en $\sim 100^\circ$, similar al WCA de la membrana nmPVDF ($103.4 \pm 1.6^\circ$). La disminución del WCA pudo deberse a la reducción del contenido de F detectada en el análisis mediante EDX de 55% a 53%. Esta pérdida de flúor se atribuyó al efecto de arrastre del líquido que eliminó parcialmente la capa de funcionalización. Esta hipótesis fue confirmada por la reducción del espesor de la membrana de 164 ± 1 a $148 \pm 12 \mu\text{m}$ a las 0 y 160 h, respectivamente.

En cuanto a los resultados con el efluente anaerobio a una velocidad de líquido más baja (Q_L de 3.5 L h⁻¹), el WCA tanto de la membrana nmPVDF como mPVDF_{max} disminuyó un 54% después de más de 800 h de uso. Este resultado indicó que la membrana estaba cubierta por una torta de ensuciamiento, enmascarando la naturaleza hidrófoba de la membrana. Además, se detectó un flujo de agua a través de la membrana nmPVDF a las 816 h, lo que indicó un grave deterioro mecánico o químico.

La membrana mPVDF_{max} dio lugar a una mayor RE que la membrana nmPVDF al mayor Q_L de 21 L h⁻¹, indicando una mayor transferencia de materia para el CH₄. Esto podría atribuirse al aumento en la resistencia a la humectación de los poros.

El efecto del ensuciamiento sobre la RE fue despreciable a un Q_L pequeño de 3.5 L h^{-1} a las 800 h. Por el contrario, la RE disminuyó un 13% y un 52% para las membranas nmPVDF y mPVDF_{max}, respectivamente, a $>650 \text{ h}$ a un Q_L más alto (21.0 L h^{-1}). Esto indicó que la membrana modificada presentó una menor resistencia al ensuciamiento.

En conclusión, el procedimiento de modificación mejoró significativamente la resistencia a la humectación de los poros y estabilidad de la membrana de PVDF-Ds en operaciones a largo plazo con efluentes anaerobios reales. En este sentido, se debe tener en cuenta la modificación de la superficie como una estrategia tanto para aumentar la eficacia de separación como la vida útil de la membrana, ya que da lugar a una mayor resistencia química y/o mecánica.

8.3 CARACTERIZACIÓN DEL ENSUCIAMIENTO EN CONTACTORES DE MEMBRANAS DE PVDF PARA LA RECUPERACIÓN DE METANO DISUELTO EN EFLUENTES ANAEROBIOS: EFECTO DE LA ORGANOFLUOROSILANIZACIÓN SUPERFICIAL.

El ensuciamiento de las membranas cuando tratan efluentes líquidos residuales da lugar a una resistencia adicional a la transferencia de materia y/o una reducción en la vida útil de la membrana [68,69,268]. El grado de ensuciamiento depende de varios factores relacionados con las características de la membrana, las condiciones hidráulicas y la naturaleza del agua tratada [68,90,92]. Para las membranas hidrofóbicas como las de PVDF, la causa principal del ensuciamiento es la fuerte interacción con la materia orgánica debido a la naturaleza hidrofóbica de la mayoría de los compuestos orgánicos [268] presentes en efluentes anaerobios. Además, los agentes de ensuciamiento podrían hidrofilar la superficie de la membrana, reduciendo la resistencia a la humectación de los poros y promoviendo la incrustación de sales y obstrucción de los poros [73,268,270]. Así, la determinación de los mecanismos de ensuciamiento en contactores de membrana se ha identificado recientemente como un punto crítico [267] que debe estudiarse con el fin de proponer estrategias para evitar o mitigar los efectos del ensuciamiento como la funcionalización o limpieza periódica de las membranas.

En este contexto, el objetivo principal de este trabajo fue la determinación de la composición del ensuciamiento y los posibles mecanismos en membranas planas de PVDF-Ds con diferentes grados de hidrofobicidad, utilizadas para la desgasificación del efluente de un reactor anaerobio. Para ello, se realizaron pruebas de ensuciamiento con un efluente anaerobio real en operación a largo plazo (>800 horas). Las pruebas se realizaron en un módulo plano de 17.3 cm² (FM-SS) usando la membrana comercial PVDF-Ds (WCA = 103.4 ± 1.6°) y la de PVDF-Ds modificada con hidrofobicidad mejorada mediante

organofluorosilanicación (mPVDF, WCA = $140.9 \pm 2.5^\circ$, funcionalizada a las condiciones óptimas determinadas en *Contribución II*). La torta de ensuciamiento se analizó en detalle mediante diferentes técnicas de microscopía y espectroscopia (FESEM-EDX y FTIR) con el fin de identificar los diferentes elementos y compuestos. También se utilizaron técnicas de tinción para la identificación y cuantificación de proteínas y polisacáridos y para el análisis del estado metabólico de las bacterias. Además, se realizó una extracción de la torta de ensuciamiento de la membrana con agua y una solución de NaOH para analizar la composición del ensuciamiento reversible e irreversible. Finalmente, también se analizó la influencia del ensuciamiento en la estabilidad de la membrana.

Tanto las membranas de PVDF-Ds como las de mPVDF experimentaron la formación de una torta de ensuciamiento sobre su superficie, aunque la membrana mPVDF sufrió un ensuciamiento más severo debido a su mayor hidrofobicidad. El ensuciamiento aumentó con el tiempo de operación debido a una deposición continua de materia presente en el efluente anaerobio y/o crecimiento de biomasa [259]. La torta de ensuciamiento resultante presentó una estructura densa, que redujo la porosidad de la superficie de la membrana y creó una resistencia adicional a la transferencia de masa para la difusión del metano.

El WCA disminuyó más de un 50% en ambas membranas al final de la prueba de ensuciamiento (>800 horas). Esta hidrofiliación superficial pudo verse especialmente favorecida por el depósito de proteínas anfífilas y polisacáridos [97,269,270,275] detectados en la torta de ensuciamiento. Por otro lado, la biomasa, los óxidos metálicos y los aluminosilicatos presentes en el ensuciamiento también pueden contribuir a la hidrofiliación [73,97]. Además, la pérdida de F de la superficie de la membrana debido a la degradación observada en las imágenes FESEM-EDX fue especialmente grave en la membrana PVDF-Ds, lo que contribuyó a la disminución del WCA.

Los principales agentes de ensuciamiento orgánicos fueron las proteínas y los polisacáridos, mientras que el ensuciamiento inorgánico estuvo compuesto principalmente por sales de calcio, fósforo y magnesio. Se determinaron diferencias claras entre la composición de la superficie y el interior de la torta de ensuciamiento, lo que denota una estratificación de la materia. Así, la deposición de proteínas y polisacáridos fue más dominante en la primera etapa del ensuciamiento debido a las grandes fuerzas de interacción hidrofóbica con la superficie de la membrana. Esta deposición inicial promovió la adherencia de compuestos inorgánicos y microorganismos [90,259], aunque la materia orgánica dominaba también las partes más externas de la torta.

Un mayor ensuciamiento irreversible se observó en la membrana mPVDF atribuible a su mayor hidrofobicidad. No obstante, no se encontraron cantidades significativas de polisacáridos en el ensuciamiento irreversible en la membrana mPVDF, lo que sugiere menores fuerzas de adhesión entre los polisacáridos y la superficie modificada y una potencial mejora en la eficiencia de los procesos de limpieza. Además, la capa de funcionalización condujo a una membrana con una mayor estabilidad en operación a largo plazo, ya que no se observó una degradación significativa, a diferencia de la membrana PVDF-Ds, la cual sufrió una degradación estructural severa dando lugar a fisuras en su superficie. La capa de funcionalización también dificultó el ensuciamiento relacionado con el crecimiento microbiano en la membrana mPVDF.

En conclusión, la funcionalización de membranas de PVDF con FAS se presenta como una estrategia interesante para mitigar los negativos efectos del inevitable ensuciamiento que experimentan las membranas al tratar un efluente anaerobio. Esto permitiría reducir los costes de operación relacionados con la limpieza periódica y reemplazo de la membrana.

8.4 ESTABILIDAD DE LA SUPERHIDROFOBICIDAD Y ESTRUCTURA DE MEMBRANAS DE PVDF TRATADAS POR PLASMA DE OXÍGENO A VACÍO Y ORGANOFLUOROSILANIZACIÓN.

La resistencia a la humectación de los poros de las membranas se puede aumentar mediante diferentes técnicas de modificación superficial [68,277]. En este sentido, se ha demostrado recientemente que las membranas superhidrofóbicas ($WCA \geq 150^\circ$) [278] mitigan significativamente la humectación de los poros y el ensuciamiento debido a la menor área de contacto entre la fase líquida y la membrana [188]. La modificación química de superficies implica la incorporación de agentes modificadores, la cual suele requerir de una etapa previa de activación de la superficie, como en membranas de PVDF, debido a su gran estabilidad química [228,229]. El tratamiento con plasma se considera un método versátil, escalable y económico para activar y texturizar superficies [170–172,279–281]. El plasma puede dar lugar a modificaciones químicas y/o físicas en la superficie de la membrana [174,282] debido a la interacción con las diferentes especies reactivas contenidas en el plasma [173,176,179,283]. Además, el uso de gases oxidantes crea un entorno más reactivo capaz de agregar grupos funcionales que contienen oxígeno a la superficie de la membrana. La estabilidad a largo plazo de la capa funcionalizada es un aspecto clave en la viabilidad del tratamiento, sin embargo, ha sido escasamente estudiado en membranas tratadas con plasma.

El objetivo de este trabajo fue evaluar el efecto del tratamiento con plasma de oxígeno a vacío en la modificación superficial de la membrana plana PVDF-Dp ($WCA = 119.4 \pm 1.7^\circ$), así como la evaluación de diferentes precursores de silicio para la posterior incorporación del FAS con el fin de producir membranas superhidrofóbicas. En primer lugar, se maximizó la hidrofobicidad de la membrana mediante la optimización de las condiciones del tratamiento por plasma. En segundo lugar, se evaluó la estabilidad de la membrana

modificada y se comparó con la membrana no modificada en términos de hidrofobicidad, propiedades térmicas, morfología y composición química.

Se realizó un diseño estadístico de experimentos variando la potencia del plasma de 3 a 17 W y el tiempo de aplicación de 3 a 17 min para dos precursores de silicio diferentes, TEOS y (3-aminopropil)triétoxosilano (APTES). Se utilizó un diseño central compuesto y un análisis de superficie de respuesta para optimizar las condiciones del plasma y maximizar el WCA de la membrana. Posteriormente, la membrana modificada que presentó el mayor WCA con TEOS y APTES (PO₂-TEOS y PO₂-APTES, respectivamente) fueron sometidas a pruebas de estabilidad en módulo plano con agua desionizada. Se realizaron análisis adicionales de estas membranas modificadas antes y después de la prueba de estabilidad con una corriente de agua para determinar las propiedades térmicas (TGA y DSC), la morfología (FESEM) y la composición química (EDX). Estos resultados se compararon con los obtenidos en la membrana original.

Después del tratamiento con plasma y la funcionalización de las membranas, se obtuvo un WCA superior al de la membrana original en todas las membranas modificadas, con un valor medio global de 153°. Esto demostró que el procedimiento de modificación con plasma propuesto en este trabajo fue adecuado para obtener membranas de PVDF superhidrofóbicas. El valor de WCA se vio principalmente influenciado por el tipo de precursor de silicio usado, TEOS o APTES. Los valores más altos de WCA se obtuvieron en las membranas tratadas con APTES, con un valor medio global de 155°, en comparación con las membranas modificadas con TEOS, con un valor medio global significativamente menor de 151°. La relación flúor-carbono (F/C) de la membrana original (0.92) aumentó a 0.99 y 0.95 al usar APTES y TEOS, respectivamente, para membranas tratadas a una potencia y tiempo de plasma de 15 W y 15 min, respectivamente. De ese modo, se confirmó la incorporación del FAS en la membrana de PVDF-Dp. Además, el mayor valor F/C de la

membrana tratada con APTES explica su mayor WCA en comparación con la membrana tratada con TEOS.

La potencia del plasma también afectó significativamente al WCA en las condiciones evaluadas. Los resultados sugirieron que un incremento de la potencia del plasma por encima de 3 W no generó sitios activos adicionales, lo que limitó la incorporación de SiP y FAS en la membrana. Sin embargo, el efecto de grabado (*etching* del término en inglés) se observó para una potencia superior a 10 W, lo que contribuyó al incremento del WCA. Finalmente, a partir del análisis de varianza y superficie de respuesta, las condiciones óptimas del plasma se fijaron a una potencia y tiempo de 15 W y 15 min, respectivamente, dando lugar a un WCA máximo de $\sim 157^\circ$. A mayores potencias y tiempos la membrana se volvió quebradiza.

Respecto a la estabilidad de las membranas PO₂-TEOS y PO₂-APTES usando una corriente de agua destilada, ambas experimentaron una disminución del WCA hasta $\sim 130^\circ$ a las 75 h y después se mantuvo casi constante y ligeramente más alta que el WCA de la membrana original hasta 160 h. Así, el efecto de la funcionalización se perdió parcialmente, probablemente debido al arrastre de las moléculas del agente de funcionalización. Sin embargo, los enlaces químicos e interacciones entre el SiP, el FAS y el PVDF activado con plasma parecían ser más fuertes o estables que en el caso de las membranas activadas con tratamiento alcalino, cuyo WCA disminuyó hasta valores similares a los de la membrana original en < 50 h (ver *Contribución II*). Además, la membrana PO₂-APTES siempre mostró un WCA ligeramente más alto que la membrana PO₂-TEOS, lo que se atribuyó principalmente al mayor F/C de la membrana PO₂-APTES (0.85) respecto de la membrana PO₂-TEOS (0.80) después de la prueba de estabilidad.

Los resultados de los análisis térmicos mostraron temperaturas de fusión y descomposición de $\sim 163^\circ\text{C}$ y $\sim 475^\circ\text{C}$ y una cristalinidad de 55 – 60% para todas las membranas, independientemente del tipo de tratamiento. Esto

indicó una gran estabilidad de las membranas de PVDF-Dp frente a las técnicas de modificación y operación a largo plazo.

Al aplicar una potencia y tiempo del plasma de 15 W y 15 min, respectivamente, la superficie de la membrana se convirtió en una estructura superficial en forma de pilares aumentando su porosidad superficial a un 15% tanto para la membrana PO₂-TEOS como para PO₂-APTES (porosidad superficial de la membrana original = 11%). Esto dio lugar a una superficie más rugosa que contribuyó a la superhidrofobicidad de la membrana. No obstante, después de las pruebas de estabilidad, todas las membranas experimentaron una reducción en la porosidad superficial a un valor de ~5%, debido a una deformación plástica.

En conclusión, las membranas funcionalizadas con activación por plasma de oxígeno presentaron un carácter superhidrofóbico y la mayor estabilidad a largo plazo de todas las membranas evaluadas en esta tesis. Esta técnica podría contribuir a la mejora de la eficacia de separación de membranas en aplicaciones gas-líquido o líquido-líquido gracias su mayor resistencia a la humectación de los poros y propiedades auto-limpiantes.

8.5 APLICACIÓN SIMULTÁNEA DE VACÍO Y GAS DE ARRASTRE EN UN CONTACTOR DE MEMBRANA DE FIBRA HUECA DE POLIPROPILENO PARA LA RECUPERACIÓN DE METANO DISUELTO EN AGUA.

La investigación en desgasificación de metano disuelto en efluentes líquidos anaerobios con HFMCs ha centrado el interés de la comunidad científica en los últimos años [39]. El HFMC puede operar en modo vacío o gas de arrastre en las operaciones de desgasificación para generar el gradiente de presión parcial del soluto como fuerza impulsora necesaria para la separación. Por un lado, cuando solo se aplica vacío se puede obtener una corriente de gas metano de alta pureza, mientras que el metano se diluye en el modo de gas de arrastre. Por otro lado, el modo vacío presenta el mayor consumo de energía, aunque el gas recuperado puede utilizarse directamente para la producción térmica y eléctrica [74]. Como alternativa para superar los inconvenientes de cada modo de operación, se pueden usar simultáneamente vacío y gas de arrastre. Sin embargo, solo unos pocos trabajos han estudiado este modo combinado [285,286], haciéndose necesario una investigación en profundidad de los posibles efectos sinérgicos y de las condiciones óptimas de operación.

El objetivo principal de este trabajo fue evaluar el rendimiento de un HFMC de polipropileno poroso que opera en modo combinado para la recuperación de metano. Para ello, se realizaron pruebas de desgasificación con una corriente de agua sintética que contenía D-CH₄ y se analizó la RE bajo diferentes condiciones de operación en estado estacionario. HFMC tenía un área efectiva interna de 0.18 m², la fase líquida circuló por el interior de las fibras y se utilizó N₂ como gas de arrastre. El Q_L varió de 5 a 28 L h⁻¹ (velocidad del líquido de 1.59 a 8.90 cm s⁻¹), la presión de vacío (P_{vac}) varió de 0 a 480 mbar y el Q_{N₂} varió de 0.5 a 1.5 L h⁻¹ (velocidad del gas de 0.04 a 0.13 cm s⁻¹). También se llevó a cabo un análisis de transferencia de materia y energía para estudiar

el efecto del modo combinado en el transporte de metano y la viabilidad de la producción de energía a partir del metano recuperado.

Al operar con el HFMC en modo combinado, la RE aumentó con la P_{vac} y el Q_{N_2} debido al aumento de la fuerza impulsora para el transporte de metano. La mayor RE (~90%) se obtuvo para el Q_L más pequeño (5.0 L h⁻¹), y valores de P_{vac} y Q_{N_2} superiores a 100 mbar y 0.5 L h⁻¹, respectivamente. Sin embargo, el aumento de la P_{vac} y Q_{N_2} por encima de 200 mbar y 1.0 L h⁻¹, respectivamente, no mejoró la eficacia del proceso de manera significativa. Esto demuestra que, desde un punto de vista práctico, una combinación de valores intermedios de P_{vac} y Q_{N_2} serían las condiciones operativas más adecuadas. Por ejemplo, a un Q_L de 5.0 L h⁻¹, la RE fue del 84% en modo combinado (P_{vac} de 100 mbar y Q_{N_2} de 0.5 L h⁻¹). Sin embargo, para obtener una RE similar (82%) en modo vacío sería necesario aplicar 500 mbar para un Q_L de 4.1 L h⁻¹ [84]. Estos resultados demuestran la mejora de la fuerza impulsora causada por el efecto aditivo de la combinación de vacío y gas de arrastre.

El y_{CH_4} del gas recuperado mostró una dependencia potencial con la relación de caudales gas-líquido ($G/L = Q_{N_2}/Q_L$) independientemente del vacío. El máximo y_{CH_4} obtenido fue del 45% para la mínima relación G/L ensayada (0.012), correspondiéndose con una RE de ~40%. Relaciones G/L inferiores a 0.030 serían necesarios para obtener un y_{CH_4} mínimo del 35%, correspondiéndose con REs entre 50% y 55%. En estas condiciones se podría utilizar directamente la corriente de gas recuperado para la generación de calor o electricidad.

A partir del análisis de transferencia de materia, el coeficiente de transferencia de materia total experimental osciló entre $1.65 \cdot 10^{-5}$ y $3.67 \cdot 10^{-5}$ m s⁻¹, que fue bastante similar a los estimados por el modelo propuesto. La resistencia a la transferencia de materia de la fase líquida representó más del 98% de la resistencia total, ya que la resistencia de la membrana y la fase gaseosa estuvieron siempre por debajo del 1%. Por lo tanto, la resistencia al transporte de materia para el metano se localizó principalmente en la fase

líquida. En este sentido, la eficiencia del proceso puede ser controlada principalmente por las condiciones hidráulicas del líquido de alimentación, es decir, la velocidad del líquido. En la operación en modo vacío se observó un impacto negativo y muy severo en la eficacia de eliminación atribuible a la humectación del poro [84], pero este fenómeno no se observó en modo combinado, dando lugar a una menor resistencia a la transferencia de materia. Por lo tanto, la presencia de gas de arrastre parecía implicar un efecto sinérgico en la superficie de la membrana, evitando sobrepasar la presión transmembrana crítica [63,85,289].

Se realizó un análisis energético, asumiendo que el principal consumo de energía estaba relacionado con las bombas (vacío y líquido) y que todo el metano recuperado se utilizó en la producción de energía. Así, se obtuvo una producción de energía neta positiva en todas las condiciones de operación. La energía neta máxima fue de 270 kJ m^{-3} , a un Q_{N_2} de 1.5 L h^{-1} , Q_L de 5.0 L h^{-1} y P_{vac} de 200 mbar. Sin embargo, en estas condiciones, el y_{CH_4} del gas recuperado es inferior al 35%, por lo que dicho gas convendría que se mezclara con la corriente principal de biogás del proceso anaerobio. En el caso del uso directo del gas recuperado en una microturbina (y_{CH_4} mínimo del 35%), la energía neta máxima real fue de 145 kJ m^{-3} para un Q_{N_2} y Q_L de 0.5 y 13.7 L h^{-1} , respectivamente, sin vacío.

En conclusión, el uso del modo combinado en contactores de membrana ha permitido maximizar la producción neta de energía a partir del metano recuperado y minimizar el consumo de gas de arrastre. Esto podría hacer posible la autosuficiencia y reducción de la huella de carbono de una planta de tratamiento anaerobio de aguas residuales.

8.6 CRISTALIZACIÓN REACTIVA ASISTIDA POR MEMBRANA PARA LA RECUPERACIÓN DE FÓSFORO DISUELTO EN EFLUENTES LÍQUIDOS EN FORMA DE VIVIANITA.

La configuración convencional de los cristalizadores de tanques agitados tienen el inconveniente del difícil control de la cristalización debido al bajo nivel de mezcla de los reactivos, lo que conduce a una mala regulación de la supersaturación, que es la fuerza impulsora del proceso de nucleación [123,124,138]. Por el contrario, los módulos de membrana pueden proporcionar un área interfacial fija y de gran tamaño que proporciona una regulación homogénea de la supersaturación, mientras que la formación de una capa límite bien definida cerca de la superficie de la membrana también crea una región de supersaturación elevada [123,139]. Además, la membrana puede proporcionar un alto nivel de micromezcla [126–129], lo que permite altos índices de supersaturación y tiempos de inducción bajos [122], ya que todos los poros de la superficie de la membrana podrían actuar como puntos de mezcla a nivel microscópico y molecular [122,126,130]. En consecuencia, el proceso de cristalización reactiva asistida por membrana (MARC) se ha posicionado en los últimos años como una tecnología potencialmente hábil para optimizar y controlar tanto la nucleación como el crecimiento de cristales [61,122,123]. Sin embargo, este proceso ha sido escasamente estudiado. En este sentido, la MARC podría facilitar la recuperación de fósforo (P) disuelto de aguas y efluentes residuales, evitando la pérdida este valioso nutriente.

En esta tesis se ha propuesto, por primera vez en la literatura, en lo que hasta la fecha conocemos, un proceso de MARC en discontinuo para la recuperación de fósforo en forma de vivianita mediante un módulo plano de membrana a escala de laboratorio. Este proceso se ha aplicado en el tratamiento de una solución rica en fosfatos como efluente sintético para la cristalización de vivianita mediante la dosificación de una solución de hierro (II) (Fe^{2+}) a través de la membrana. Los principales objetivos han sido: (i) investigar cómo se

pueden utilizar las condiciones de la capa límite para regular la cinética de supersaturación y nucleación mediante la aplicación de diferentes condiciones hidráulicas; (ii) estudiar los efectos de las propiedades de la membrana para determinar cómo podrían influir en la cinética de nucleación, y (iii) definir una hipótesis que permita relacionar las condiciones de la capa límite con la cinética de nucleación mediante la determinación directa del tiempo de inducción en la disolución y en la membrana.

Para la evaluación del proceso de MARC en la recuperación de fósforo se realizaron pruebas de cristalización en un módulo plano de 40 cm² (FM-MA) bajo diferentes condiciones hidráulicas, variando el Q_L de 8 a 30 L h⁻¹ (velocidades de líquido de 2.8 a 10.4 cm s⁻¹ y Reynolds [Re_p] de 105 a 395). Para dilucidar los efectos de las propiedades de la membrana en el proceso de cristalización, se evaluaron diferentes membranas de polifluoruro de vinilideno (PVDF-St, PVDF-Ds, PVDF-Ds activado y funcionalizado con activación alcalina, PVDF-Dp), polipropileno (PP-2E) y politetrafluoroetileno (PTFE-1 y PTFE-3). Los cristales sintetizados a partir de los ensayos de cristalización se analizaron posteriormente mediante técnicas de microscopía electrónica y espectroscopia para determinar su morfología, tamaño de cristal y composición química. Además, se estimó el nivel de supersaturación y se analizó la cinética del proceso de cristalización en base a los principios de la teoría clásica de la nucleación (CNT).

La aparición de turbidez en el efluente líquido evidenció el inicio de la nucleación, momento en la que se detectaron las primeras partículas sólidas en la disolución (tiempo de inducción en la disolución), a partir del cual la turbidez comenzó a aumentar. El tiempo de inducción aumentó a medida que se incrementó el Re_p de 105 a 395 (10.5 ± 0.7 y 26.0 ± 5.7 min, respectivamente). Después de la nucleación, la turbidez aumentó continuamente con el tiempo de ensayo, alcanzando valores mayores a medida que el Re_p disminuía, evidenciando mayores velocidades de nucleación.

Se estimaron valores del índice de supersaturación (SI) de 8.0 a 8.7 para tiempos de inducción de 10.5 a 26.0 min, respectivamente. Aunque la supersaturación es la principal fuerza impulsora de la nucleación, el SI fue independiente de las condiciones hidráulicas evaluadas, lo que se atribuyó a la baja solubilidad de la vivianita [295]. Sin embargo, se deben considerar dos aspectos: (i) a bajas velocidades de líquido, la capa límite en la interfase de la membrana puede dar lugar a una alta supersaturación local, lo que aumentaría la velocidad de nucleación en esa región [124], y (ii) el alto nivel de micromezcla favorecido por la membrana porosa [122,132] puede aumentar la frecuencia de colisión de los iones reactantes, lo que reduciría la energía de activación para la nucleación [136,137]. Por lo tanto, los tiempos de residencia mayores aumentarían la probabilidad de mezcla y colisión de iones dentro del módulo de membrana, acelerando la nucleación. Estos efectos podrían explicar las tendencias experimentales observadas.

Se estimaron velocidades de nucleación de 3.40 a 5.69 mg L⁻¹ min⁻¹ a medida que el tiempo de inducción disminuyó de 26.0 a 4.0 min. Este análisis cinético basado en el modelo empírico de la ley de potencia propuesto por Sangwal [250] mostró que las velocidades de nucleación mayores se asociaron con una supersaturación de vivianita menor. Sin embargo, la CNT postula que las velocidades de nucleación elevadas se corresponden con una elevada supersaturación. Por lo tanto, otros factores como los efectos de micromezcla, la probabilidad de colisión de iones, la difusión de iones y la supersaturación local parecen ejercer un efecto dominante en la velocidad de nucleación bajo las condiciones de operación evaluadas.

Las diferentes propiedades de las membranas también presentaron una influencia significativa en la reducción de la barrera energética de nucleación y/o en la modificación de las condiciones locales de mezcla, permitiendo reducir los tiempos de inducción. En términos generales, los tiempos de inducción estuvieron especialmente condicionados por el WCA y la porosidad de la membrana. Las membranas con el WCA y la porosidad superiores a 119° y 65%,

respectivamente, acortaron considerablemente el tiempo de inducción y resultaron en velocidades de nucleación mayores. Esta tendencia se atribuyó a una nucleación primaria heterogénea preferencial y un mayor nivel de mezcla.

Durante el proceso de cristalización se formaron nanopartículas esféricas de ~35 nm sin formar conglomerados. La formación de este tipo de partícula es propia de altas velocidades de nucleación, y también podría sugerir que la región de nucleación está limitada al interior del módulo de membrana impidiendo el crecimiento de los cristales. Estas partículas se correspondían a compuestos basados en vivianita amorfa y parcialmente oxidada, con una cantidad significativa de hidróxidos de hierro.

En conclusión, se ha demostrado que la integración de la tecnología de membranas junto con un adecuado patrón cinético puede facilitar la recuperación de fósforo de efluentes residuales proporcionando beneficios en cuanto a costes y rendimiento en procesos a gran escala.

8.7 CONCLUSIONES.

Esta tesis se ha centrado en la aplicabilidad de la tecnología de membranas en la recuperación de metano y fósforo disueltos en efluentes líquidos para su valorización. Además, se evaluaron métodos de funcionalización superficial de membranas para aumentar la resistencia a la humectación de los poros, el rendimiento y la vida útil de las membranas de PVDF. En términos generales, los contactores de membrana siempre proporcionaron altas eficacias de eliminación y un fácil control del proceso. Además, la funcionalización superficial de membranas con fluoroalquilsilanos aumentó la resistencia a la humectación de los poros y, especialmente, la vida útil de la membrana, lo que podría reducir considerablemente los costes operacionales a escala industrial.

Las conclusiones más significativas de todo el trabajo se resumen a continuación, divididas en tres apartados en relación a los tres objetivos parciales de esta tesis.

Objetivo 1. Evaluación del rendimiento de las membranas en la recuperación de metano disuelto de efluentes líquidos utilizando contactores de membrana plana gas-líquido.

Se ha demostrado la aplicabilidad y versatilidad de un contactor gas-líquido de membrana plana para la recuperación de metano disuelto de efluentes líquidos. La eficacia de eliminación estuvo influenciada principalmente por las condiciones hidráulicas ya que la resistencia de transferencia de masa de la membrana y la fase gaseosa fue despreciable. Sin embargo, las membranas de PVDF comerciales mostraron una menor eficacia de eliminación a velocidades de líquido moderadas-altas atribuidas a la humectación de los poros. Dicha humectación fue mitigada después de la funcionalización de la membrana con una activación alcalina, lo que llevó a un ligero aumento en la eficacia de eliminación.

Las mediciones del ángulo de contacto con agua fueron un indicador útil de la estabilidad de la membrana durante la operación. Así, las membranas comerciales de PDMS y PVDF presentaron una buena estabilidad (sin cambios significativos en su hidrofobicidad) después de 150 h a bajas velocidades de líquido (2.8 cm s^{-1}). Por el contrario, su hidrofobicidad se vio alterada con el tiempo a velocidades de líquido moderadas-altas (16.9 cm s^{-1}), en acuerdo con la deformación y degradación superficial observada, limitando su vida útil.

La modificación superficial de las membranas de PVDF-Ds con activación alcalina seguida de la funcionalización con un fluoroalquilsilano condujo a un máximo ángulo de contacto de $\sim 143^\circ$ en las condiciones óptimas, lo que representa un aumento del 39% respecto al valor inicial de la membrana no modificada (nmPVDF). Esta membrana modificada ($\text{mPVDF}_{\text{max}}$) presentó una superficie heterogénea con clústeres densos y un mayor contenido de flúor que la membrana nmPVDF, lo que condujo a una reducción de la porosidad de la superficie y un aumento de la hidrofobicidad.

La membrana $\text{mPVDF}_{\text{max}}$ mostró una eficacia de eliminación de metano ligeramente mayor en experimentos a corto plazo, lo que se atribuyó a la mayor resistencia a la humectación de los poros que la membrana nmPVDF. En operación a largo plazo con un efluente anaeróbico real, la eficacia de eliminación de ambos tipos de membrana se redujo con el tiempo debido a la formación de una torta de ensuciamiento y, en consecuencia, a la resistencia adicional para el transporte de materia. La disminución en la recuperación de metano fue más pronunciada en la membrana $\text{mPVDF}_{\text{max}}$ ya que ésta presentaba una menor resistencia al ensuciamiento.

En cuanto a la estabilidad de la membrana, el efecto hidrofóbico de la capa de funcionalización se perdió en la membrana $\text{mPVDF}_{\text{max}}$ después de 50 h de operación con agua desionizada a una velocidad de líquido moderada-alta. Sin embargo, esta membrana mostró una mayor resistencia química y estabilidad que la membrana nmPVDF al tratar un efluente anaerobio real

durante >800 h, ya que la membrana nmPVDF presentó menores ángulos de contacto con el tiempo y un flujo de agua a través de fisuras.

La membrana mPVDF_{max} sufrió una mayor cantidad de depósitos por ensuciamiento (*fouling* del término en inglés) atribuible a una interacción membrana-ensuciamiento más fuerte que en la membrana nmPVDF al tratar un efluente anaerobio durante una operación a largo plazo (>800 h). Sin embargo, los polisacáridos se eliminaron por completo de la membrana mPVDF_{max} y se observó un menor ensuciamiento relacionado con la biomasa.

En términos generales, las proteínas y los polisacáridos fueron los principales compuestos orgánicos de la torta de ensuciamiento y se localizaron principalmente en la superficie de la membrana y de la torta. Por otro lado, el ensuciamiento inorgánico estaba compuesto principalmente por sales de carbonato, calcio y fosfato y se localizaba especialmente en el centro de la torta de ensuciamiento, lo que indicaba una estratificación.

Se utilizó un tratamiento con plasma de oxígeno a vacío como alternativa a la activación alcalina para evaluar una nueva metodología que pueda inferir un mayor efecto en el aumento de la hidrofobicidad. La activación por plasma de las membranas PVDF-Dp condujo a membranas superhidrofóbicas con un máximo ángulo de contacto de $\sim 157^\circ$ en las condiciones óptimas del plasma (potencia y tiempo de 15 W y 15 min, respectivamente) utilizando APTES como precursor de sílice. Las membranas tratadas con plasma en las condiciones óptimas (PO₂-PVDF_{max}) presentaron una superficie estructurada en forma de pilares, mayor porosidad y rugosidad que contribuyó a aumentar la hidrofobicidad de la membrana. Además, el contenido de flúor aumentó tras la funcionalización, siendo superior al de las membranas tratadas con álcali (mPVDF_{max}).

PO₂-PVDF_{max} mostró una mayor estabilidad en operaciones a largo plazo que la membrana tratada con álcali mPVDF_{max}. En este sentido, se observó un ángulo de contacto de $\sim 130^\circ$ para las membranas de PO₂-PVDF_{max} después de 160 h de operación con agua desionizada a una velocidad de líquido

moderada-alta, que fue mayor que el ángulo de contacto de PVDF-Dp no modificado (119°). No obstante, la superficie de las membranas PO₂-PVDF_{max} también experimentó una deformación plástica, lo que resultó en una reducción de la porosidad de la superficie.

Objetivo 2. Optimización de la recuperación de metano disuelto con un contactor de membrana de fibra hueca de PP mediante la aplicación simultánea de vacío y gas de arrastre (modo combinado).

La recuperación de metano disuelto en agua por medio de un contactor de membrana de fibra hueca de polipropileno microporoso, que opera en modo combinado, mostró eficiencias de eliminación significativamente mayores y resistencias de transferencia de materia menores que los modos de operación independientes. Además, el modo combinado mitigó la humectación de los poros.

Se obtuvo una eficacia de eliminación máxima de ~90% y un contenido de metano superior al 35% en el gas recuperado a relaciones G/L bajas ≤ 0.20 y vacío 200 mbar. Además, siempre se observó una producción de energía neta positiva, lo que permitió un proceso autosuficiente con una energía neta máxima de 270 kJ m⁻³ de efluente tratado a G/L de 0.30 y vacío moderado de 200 mbar.

En conclusión, el modo combinado puede mejorar el rendimiento del contactor de membrana para recuperar el metano disuelto de los efluentes anaeróbicos, reduciendo la huella de carbono de una planta de tratamiento anaerobio de aguas residuales mediante el uso de este metano para la producción de electricidad o calor.

Objetivo 3. Integración de la cristalización por membrana en la recuperación de fósforo disuelto en forma de vivianita sólida

La recuperación de fósforo de un efluente líquido en forma de vivianita mediante cristalización reactiva asistida por membrana mostró un mayor control en el proceso de nucleación que los reactores convencionales de tanque agitado. La nucleación estuvo fuertemente influenciada por la capa límite dentro del módulo de la membrana, en la que la velocidad de nucleación aumentó a medida que disminuyó la velocidad del líquido, lo que también redujo el tiempo de inducción. Además, las membranas porosas facilitaron la micromezcla de los reactivos y redujo la barrera energética para la nucleación, en la que el tiempo de inducción tendía a disminuir a medida que aumentaba la hidrofobicidad, la rugosidad, el tamaño de poro y la porosidad de la membrana. Por lo tanto, la nucleación podría controlarse fácilmente estableciendo las condiciones hidráulicas y las propiedades de la membrana apropiadas.

El análisis cinético de nucleación mostró que las velocidades de nucleación mayores se asociaron con una sobresaturación de vivianita menor. Esta tendencia se atribuyó a un mecanismo de cristalización dependiente de la colisión de iones, en el que las velocidades de sobresaturación más altas promueven una mayor mezcla y una mayor probabilidad de colisión de iones, lo que reduce la energía de activación para la nucleación incluso a bajos niveles de sobresaturación. Las velocidades de sobresaturación más altas y la micromezcla condujeron a la formación de nanopartículas de vivianita de ~35 nm.

En conclusión, la cristalización reactiva asistida por membrana puede facilitar la perspectiva de recuperación de fósforo en forma de vivianita para obtener beneficios en términos de costes y rendimiento en procesos a gran escala, al mismo tiempo que se obtiene una calidad homogénea de las partículas precipitadas.

APPENDIX I: CONTRIBUTION I.

The contribution entitled “*Recovery of dissolved methane through a flat sheet module with PDMS, PP, and PVDF membranes*” is presented in this Appendix. This work corresponds with the main results and conclusions discussed in section 4.1. The details of the resulting paper are listed below:

Title	Recovery of dissolved methane through a flat sheet module with PDMS, PP, and PVDF membranes
Authors	Ramón Jiménez-Robles ^a , Carmen Gabaldón ^a , José David Badia ^b , Marta Izquierdo ^a , Vicente Martínez-Soria ^a
Affiliation	^a Research Group in Environmental Engineering (GI2AM), ^b Research Group in Materials Technology and Sustainability (MATS), both from Department of Chemical Engineering, School of Engineering, University of Valencia, Avda. Universitat s/n, 46100 Burjassot, Spain
Journal	Separation and Purification Technology
Year	2022
Volume	282, part B
Number	120057
DOI	10.1016/j.seppur.2021.120057
Cite	R. Jiménez-Robles, C. Gabaldón, J.D. Badia, M. Izquierdo, V. Martínez-Soria, Recovery of dissolved methane through a flat sheet module with PDMS, PP, and PVDF membranes, Sep. Purif. Technol. 282 (2022) 120057. https://doi.org/10.1016/j.seppur.2021.120057

The Journal Impact Factor (JIF) in the in the year of publication was 8.6, and the JIF rank was 12/140 in the category of Chemical Engineering (D1 first decile).



Recovery of dissolved methane through a flat sheet module with PDMS, PP, and PVDF membranes

R. Jiménez-Robles^a, C. Gabaldón^a, J.D. Badia^b, M. Izquierdo^a, V. Martínez-Soria^{a,*}

^a Research Group in Environmental Engineering (GIZAM), Department of Chemical Engineering, School of Engineering, University of Valencia, Avda. Universitat s/n, 46100 Burjassot, Spain

^b Research Group in Materials Technology and Sustainability (MATS), Department of Chemical Engineering, School of Engineering, University of Valencia, Avda. Universitat s/n, 46100 Burjassot, Spain

ARTICLE INFO

Keywords:

Methane recovery
Flat sheet membrane module
Polymeric membrane
Membrane stability
Mass transfer

ABSTRACT

A degassing contactor using a flat sheet membrane module (FM) was operated in sweep gas mode to study the performance of several commercial polymer membranes, both dense (polydimethylsiloxane, PDMS) and microporous (polypropylene, PP, and polyvinylidene fluoride, PVDF), for the recovery of dissolved methane from water. Non-steady state experiments were conducted at different liquid (Q_L , 3.5–40.5 L h⁻¹) and gas flow rates (Q_{N_2} , 0.05–15.00 L h⁻¹). In the case of PDMS, PP, and when PVDF was operated at moderate high Q_L (≥ 21 L h⁻¹), similar methane removal efficiencies (RE) were obtained. In the case of PVDF operated at relatively low Q_L (3.5 L h⁻¹), a lower RE was observed. A model for the mass transfer of methane has been selected that is adequate in predicting the experimental results. These results concluded that the mass transfer resistance was mainly located in the liquid phase. Microscopy and especially contact angle measurements were used to monitor the structural and surface stability on the membranes. The membranes were altered during the operation, especially for $Q_L \geq 21$ L h⁻¹, showing a decrease (PDMS and PP) or an increase (PVDF) in hydrophobicity and even cleavages (PDMS). The combination of the FM and contact angle technique has demonstrated to be very versatile and useful for monitoring the variation of the membrane properties during operation.

1. Introduction

The industrial implementation of a separation process based on membrane technology is becoming increasingly important [1,2], resulting in a greater research attention in recent years to the development of special membrane applications, such as pervaporation or gas–liquid contactors [3]. These membrane-based processes combine the advantages of providing very high contact area per unit volume and more flexibility in the operating conditions while avoiding some of the drawbacks of conventional technologies (flooding, loading, weeping, or foaming) [4]. In addition, the stated advantages are frequently complemented with high separation selectivity typical for the absorption process [3]. In this context, the potential use of membrane contactors in operations for the recovery of organic compounds from biological process effluents has been recently highlighted [5,6]. There has been a special focus on methane recovery from anaerobic effluents, with a considerable amount of comprehensive reviews recently published [7–10]. Membrane contactors have proven to be a promising technology

to avoid the loss of dissolved methane (D-CH₄) in anaerobically-treated low-strength wastewater, which could reach up to over one-third [11] of the produced methane, due to their attractive characteristics, such as low energy consumption, good selectivity, or ease of engineering [12]. Nevertheless, several aspects related to resistance to fouling and wetting, durability, or scalability must be solved before considering this technology to be at a sufficient level of maturity to become a commercially available tool for this application.

There are two main configurations of membrane contactors: hollow fibre and flat sheet [13]. Although many studies have focused on the hollow fibre membrane contactors, surely due to their compactness and cost-effectiveness, flat sheet membrane contactors can present several advantages related to their simplicity and versatility (easy to clean and replace), which make them attractive for their use in certain applications and in laboratory scale. Flat sheet membrane contactors can be especially useful where the fouling or membrane stability is the focus of the research or to facilitate the performance comparison of membrane materials with different characteristics since the influence of the fibre

* Corresponding author.

E-mail address: vmsoria@uv.es (V. Martínez-Soria).

<https://doi.org/10.1016/j.seppur.2021.120057>

Received 27 September 2021; Received in revised form 29 October 2021; Accepted 30 October 2021

Available online 5 November 2021

1383-5866/© 2021 Elsevier B.V. All rights reserved.

diameter and fibre packing density on mass transfer of hollow fibre configuration is avoided [13]. Flat sheet membrane studies have been frequently reported in some membrane processes, such as desalination or water treatment [14], but their use in methane recovery has not been reported. As previously stated, the influence of membrane properties like structural and surface stability or fouling and wetting resistance might be crucial for developing this particular application, and the use of flat sheet membranes could facilitate this task.

The most common surface feature of polymeric membranes is the hydrophilicity-hydrophobicity (wettability) since it has an important influence on their performance, like permeate flux, membrane rejection, or membrane fouling. The surface wettability of membranes can be determined by measuring the water contact angle, which depends on many factors such as surface energy or roughness [15]. Hydrophobic membranes are preferred for gas separation and purification applications since they favour the passage of gas and repel the entry of water through them [16]. In this regard, the use of hydrophobic membrane surface modifications to increase the wetting and fouling resistance [17,18] in the methane recovery application has been reported.

In this context, one of the aims of the present work was to determine the applicability and versatility (and also limitations) of a gas-liquid flat sheet membrane system based on our own design for the recovery of D-CH₄ from water. For this purpose, the effect of the range of operational conditions on the efficiency in methane recovery from water was determined, and membranes with different materials and properties (porosity, thickness, hydrophobicity, etc.) were tested. As a second aim, the durability and stability of membranes in this particular application were compared and characterized.

The experimental validation of this system will allow its use in further studies for the characterization of the fouling, cleaning strategies, stability, and durability of new or modified membranes for dissolved methane recovery, and it could also be used for other gas-liquid separations applications, such as pervaporation or membrane distillation.

2. Materials and methods

2.1. Experimental setup and procedure

A circular flat sheet membrane module (FM) made of stainless steel was designed for this work (Fig. 1a and b). The main characteristics and dimensions of the FM are shown in Table 1. A plastic spacer was coupled inside the FM to support the membrane to avoid deformation or breakage. The module was designed to be operated at similar liquid

Table 1

Characteristics of the flat sheet membrane module.

Property	Value
Effective diameter, cm	4.7 ^a
Liquid channel width, mm	1.0
Gas channel width, mm	8.0
Liquid side hydraulic diameter, cm	0.2
Gas side hydraulic diameter, cm	1.3
Effective contact area, cm ²	17.3

^a Delimited by the spacer

velocities to that usually applied in hollow fibre contactors [19], which favoured comparison purposes.

A lab scale system was assembled including the FM for degasification tests using a synthetic D-CH₄ water stream (Fig. 1c). Initially, the different elements of the system were fully filled with de-ionised water (<1 μS cm⁻¹), the gas bubbles were purged, and a leak checking was carried out. A synthetic water stream was used in this work to simulate an anaerobic reactor effluent preventing the potential interferences of soluble or suspended compounds presented in this type of effluents.

In the first step of a degasification test, the water was saturated in a packed-bed absorption column with 99.5 %v CH₄ (Carburos Metálicos, Spain) in a counter-current flux at atmospheric pressure in the outlet. The column was built of methacrylate with an inner diameter of 6.5 cm, an effective height of 50.0 cm, and filled with 1" pall rings (Refilltech, Germany). The CH₄ flow rate was fixed at 1000 mL min⁻¹ using a mass flow controller (Bronkhorst Hi-Tec, The Netherlands) with a manometric pressure in the bottom of the column < 0.1 bar [19]. During the saturation step, the on/off valve was kept opened and water was pumped from the bottom of the column to the liquid feed tank in order to fill it with saturated water. The liquid feed tank consisted of a 2 L glass bottle with a magnetic stirrer fixed at 500 rpm. The outlet water from the tank was pumped to the FM, keeping its gas ports closed. Finally, the water from the FM was discharged at the top of the column by means of the 3-way valve connecting the FM with the column. Thus, the water was continuously recirculated in every part of the system with a peristaltic pump (Watson-Marlow, USA.) operating in a closed loop (continuous line in Fig. 1c). The liquid flow rate ranged from 21 to 27 L h⁻¹ for the saturation step. The water saturation was conducted at room temperature (23 ± 1 °C). A stable behaviour was observed after 1 h of saturation, reaching a CH₄ concentration of 23.2 ± 3.4 mg L⁻¹, which is comparable to the CH₄ saturation in water, with a value of 23.8 mg L⁻¹ at 23 °C [20]. Similar CH₄ concentration values were reported by other authors for degasification tests with synthetic liquid streams [21,22].

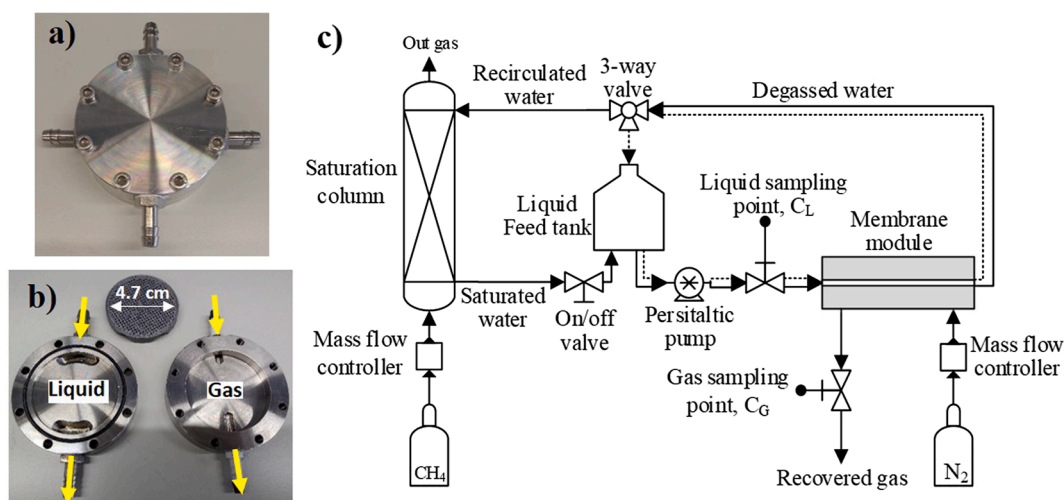


Fig. 1. a) External and b) internal view of the flat sheet membrane module. c) Scheme of the experimental system for dissolved methane recovery from water with a flat sheet membrane module.

Once the saturation with CH₄ was reached, the saturation column was disconnected from the rest of the system by closing the on/off valve and 3-way valve connecting the FM with the liquid tank (loop in dotted line, Fig. 1c). Then, water saturated with CH₄ was stored in the liquid feed tank. All experiments were carried out at the sweep gas mode using N₂ to generate a partial pressure gradient for CH₄ and to recover the D-CH₄ in the gas form. For the degasification test, the gas ports of the FM were opened and the N₂ mass flow controller was switched on. The tested N₂ flow rates (Q_{N2}) ranged from 0.05 to 15.00 L h⁻¹ supplied at atmospheric pressure (gas velocity ranging from 0.0043 to 1.3 cm s⁻¹). No significant pressure drop (<0.01 bar) was observed across the gas side of the FM. The liquid stream was pumped from the liquid feed tank to the FM and then continuously recirculated to the tank operating in a closed loop (dotted line in Fig. 1c). The liquid flow rates (Q_L) were fixed in values ranging from 3.5 to 40.5 L h⁻¹ (liquid velocity ranging from 2.8 to 32.5 cm s⁻¹). The tests were carried out at room temperature (23 ± 1 °C). The duration of the unsteady experiments was usually 5 h, although some tests were extended up to 22 h.

All the results shown in this work were obtained with liquid and sweep gas flowing in a cross flow configuration, as shown in Fig. 1a. Remarkably, the experiments carried out with counter-current flow showed no significant differences with respect to the cross flow configuration (see Supplementary Material S1), showing that the flow configuration was not crucial in these experiments.

Liquid and gas samples were periodically collected to analyse the evolution of the CH₄ concentration and to evaluate the performance of the system. Duplicates of liquid samples were collected at the outlet of the liquid feed tank. Gas samples were taken from the outlet gas port of the FM, which contained the recovered methane. A total of 3–6 samples were taken for liquid and gas.

The liquid samples were analysed by a modification of the head-space method previously described [19,23,24]. Shortly, 5 mL of the liquid samples were collected in sealed 16.0 mL vials prefilled with air. These vials were placed in an orbital shaker at 200 rpm and 25 °C for 30 min. After this, 0.5 mL of the head-space gas was injected into a gas chromatograph (Agilent GC 7820A, Spain) equipped with Agilent HP-PLOT/U and Agilent HP-MOLESIEVE columns and a thermal conductivity detector. The CH₄ concentration in the liquid sample was determined by applying Henry's Law:

$$C_{L,eq} = H^{cp} \cdot P^{p,eq} \cdot M_{CH_4} \quad (1)$$

where C_{L,eq} (mg L⁻¹ ≡ g m⁻³) is the CH₄ concentration in the liquid in equilibrium with the head-space gas, P^{p,eq} (Pa) is the partial pressure of CH₄ in the head-space in equilibrium with the liquid phase determined from the gas chromatography analysis, M_{CH₄} is the molar mass of CH₄ (16 g mol⁻¹), and H^{cp} is the Henry's Law constant (1.4·10⁻⁵ mol m⁻³ Pa⁻¹ at 25 °C [20]). The CH₄ concentration in the original liquid sample was determined as follows:

$$C_L = \frac{C_{G,eq} \cdot V_G + C_{L,eq} \cdot V_L}{V_L} \quad (2)$$

where C_L and C_{G,eq} (mg L⁻¹) are the CH₄ concentrations in the original sample and in the head-space of the analysis vials, respectively, and V_G and V_L (L) are the gas and liquid volumes inside the analysis vials, respectively.

The variation of the CH₄ removal efficiency (RE, %) was used to evaluate the performance of the CH₄ recovery process under unsteady state. RE is defined as:

$$RE = \frac{C_{L0} - C_{Lt}}{C_{L0}} \cdot 100 \quad (3)$$

where C_{L0} and C_{Lt} (mg L⁻¹) are the CH₄ concentrations in the liquid at initial time (t = 0) and at time on stream (t) from the liquid feed tank, respectively. In Eq. (3), a negligible variation of the liquid volume flow rate was assumed.

A sampling point located in the outlet gas port of the FM was used to

take 0.5 mL of recovered gas samples by means of a gas chromatography syringe, which were injected into the former gas chromatograph. The CH₄ content in the recovered gas (y_{CH₄}, %_v) was calculated by the following equation:

$$y_{CH_4} = \frac{C_G}{\rho_{CH_4}} \cdot 100 \quad (4)$$

where C_G (mg L⁻¹) is the CH₄ concentration in the recovered gas and ρ_{CH₄} (mg L⁻¹) is the CH₄ density.

2.2. Flat sheet membranes

Four commercial flat sheet membranes were tested: a dense polydimethylsiloxane (PDMS) supplied by Pervatech (The Netherlands), two types of microporous polypropylene (Accurel® PP-1E and PP-2EHF, 3M Liqui-Cel) supplied by Membrane GmbH (Germany), and a microporous polyvinylidene fluoride (PVDF) supplied by Dorsan Filtration (Spain). The PDMS membrane consisted of a support of porous polyester (PET) and polyimide (PI) and a superficial dense layer of PDMS. The PVDF membrane contained PET as the material substrate. Both polypropylene membranes (PP) had no support or substrate material. The properties of the membranes are listed in Table 2. As can be seen, all membranes presented a hydrophobic nature (water contact angle > 90°). Most of the experiments to study the influence of the operational conditions were carried out with PDMS. PP and PVDF were used for comparison purposes.

Circular membrane samples were prepared with a diameter of 6.5 cm. They were clamped into the FM by means of a rubber O-ring for leak-proof-seal so the membrane edge was fixed. The membranes were

Table 2
Properties of the flat sheet membranes.

	PDMS	PP-1E	PP-2EHF	PVDF
Structure Support	Dense PI/PET	Microporous Non supported	Microporous Non supported	Microporous PET
Water contact angle, °	100.9 ± 0.8 ^f	145.3 ± 1.4 ^f	140.2 ± 4.1 ^f	103.4 ± 1.6 ^f
Bubble point, bar	–	2.1	0.7	1.8
Pore radius, μm	PDMS: - PI: 7.2 ± 2.1 ^a PET: 0.2	0.21 ^d	0.57 ^d	0.20
Thickness, μm	PDMS: 2.5 ± 0.1 ^a PI: 63.9 ± 5 ^a PET: 108.6 ± 5 ^a (Overall: 175 ± 5)	100 ± 15	170 ± 15	159 ± 2 ^a
Porosity	PDMS: - PI: 0.72 ± 0.01 ^a PET: 0.32 ± 0.05 ^a	0.44 ± 0.04 ^e	0.44 ± 0.04 ^e	0.74 ± 0.11 ^g
Tortuosity	PDMS: - PI: 2.25 ± 0.04 ^e PET: 9.02 ± 2.19 ^e	5.61 ± 1.12 ^c	5.61 ± 1.12 ^c	2.27 ± 1.00 ^c
CH ₄ permeability, m ² Pa ⁻¹ s ⁻¹	PDMS: 7.13·10 ^{-15b}	–	–	–

^a Analysed by FESEM images.

^b Data from [25].

^c Calculated by porosity-tortuosity relationship [26,27].

^d Calculated from bubble point value [28].

^e Mean value from literature [19,21,29].

^f Measured with water contact angle technique.

^g Mean value from literature [26,30,31].

reused, and their water contact angle was measured after 2–5 experiments in order to check the membrane hydrophobicity.

2.3. Mass transfer evaluation

A mass transfer analysis of the transport of the CH₄ from the liquid phase to the gas phase was performed. From the mass balance and Fick's First Law, the experimental overall mass transfer coefficient ($K_{L,exp}$, m s⁻¹) based on the liquid phase was calculated with the following expression [32,33]:

$$K_{L,exp} = \frac{M_T}{A \cdot \rho \cdot t} \ln \left(\frac{C_{L0} - C_{L0}^*}{C_{Lt} - C_{Lt}^*} \right) \quad (5)$$

where M_T is the total liquid mass in the system (2.35 kg), A is the effective membrane area (0.00173 m²), ρ (kg m⁻³) is the liquid density, t (s) is the time on stream, and C_{L0}^* and C_{Lt}^* (mg L⁻¹) are the CH₄ concentrations in the liquid in equilibrium with the CH₄ content in the outlet gas (C_G , mg L⁻¹) at initial time ($t = 0$) and time t , respectively, calculated from Henry's Law ($C_L^* = C_G/H$, H being the dimensionless Henry's constant with a value of 29.55 at 25 °C [20]). Some assumptions were taken for using Eq. (5): (i) a constant membrane permeability coefficient and (ii) M_T was assumed constant due to the small quantity of CH₄ recovered (<52 mg) [32]. The derivation of Eq. (5) is shown in [Supplementary Material S2](#).

The overall mass transfer coefficient based on the liquid phase can be estimated using the resistance in series model for compounds transferring from the bulk liquid phase to the bulk gas phase ($K_{L,est}$, m s⁻¹) for a flat sheet membrane module [26]:

$$R_{ov} = \frac{1}{K_{L,est}} = \frac{1}{k_L} + \frac{1}{H \cdot k_m} + \frac{1}{H \cdot k_G} = R_L + R_m + R_G \quad (6)$$

where k_L , k_m , and k_G (m s⁻¹) are the individual mass transfer coefficients of the liquid phase, membrane, and gas phase, respectively, R_{ov} (s m⁻¹) is the overall mass transfer resistance, and R_L , R_m , and R_G (s m⁻¹) are the individual mass transfer resistances of the liquid phase, membrane, and gas phase, respectively. The liquid mass transfer coefficient has been estimated from the following empirical equation obtained for a FM with similar characteristics [26]:

$$Sh_L = \frac{k_L \cdot d_{hL}}{D_{M,L}} = 0.823 \cdot Re_L^{0.39} \cdot Sc_L^{1/3} \cdot \left(\frac{d_{hL}}{l} \right)^{0.075} \quad (7)$$

where Sh_L , Re_L , and Sc_L are the Sherwood, Reynolds, and Schmidt numbers of the liquid phase, respectively, d_{hL} (m) is the hydraulic diameter of the liquid side of the module, $D_{M,L}$ is the molecular diffusion coefficient of CH₄ in the liquid phase (1.76 · 10⁻⁹ m² s⁻¹ at 25 °C and 1 bar [34]), and l is the length of the module (m).

The gas mass transfer coefficient was also estimated with empirical equations obtained for similar flat sheet membrane modules [27,35]:

$$k_G = \frac{Sh_G \cdot D_{M,G}}{d_{hG}} \quad (8)$$

$$Sh_G = (Sh_0^4 + Sh_\infty^4)^{1/4} \quad (9)$$

$$Sh_0 = 2.52 \quad (10)$$

$$Sh_\infty = 0.808 \cdot Re_G^{0.405} \cdot Sc_G^{1/3} \quad (11)$$

where Sh_G , Re_G , and Sc_G are the Sherwood, Reynold, and Schmidt numbers of the gas phase, respectively, $D_{M,G}$ (m² s⁻¹) is the molecular diffusion coefficient of CH₄ in the gas phase, d_{hG} is the hydraulic diameter of the gas side (m), and Sh_0 and Sh_∞ are the limiting Sherwood numbers. In the gas side of the module, only N₂ as the sweep gas was applied; thus, molecular diffusion of CH₄ in the gas can be estimated as follows [36]:

$$D_{M,G} = \frac{0.01013 \cdot T^{1.75} \cdot \left(\frac{1}{M_{N_2}} + \frac{1}{M_{CH_4}} \right)^{1/2}}{P \cdot \left[(\sum v)_{N_2}^{1/3} + (\sum v)_{CH_4}^{1/3} \right]^2} \quad (12)$$

where T (K) is the temperature of the test, M (g mol⁻¹) is the molar mass, P (Pa) is the pressure in the gas phase, and $(\sum v)$ is the especial atomic diffusion volume (17.90 for N₂ and 24.42 for CH₄ [37]).

The membrane mass transfer coefficient can be estimated for both porous and dense membranes. For porous structures, it was estimated as follows [27]:

$$k_{m,porous} = \frac{D_{G,eff} \cdot \varepsilon}{\tau \cdot \delta} \quad (13)$$

where ε , τ , and δ (m) are the porosity, tortuosity, and thickness of the membrane or layer and $D_{G,eff}$ is the effective diffusion of the transferred species in the gas phase inside the pores, which was estimated as follows [38]:

$$\frac{1}{D_{G,eff}} = \frac{1}{D_{M,G}} + \frac{1}{D_{G,Kn}} \quad (14)$$

where $D_{G,Kn}$ (m² s⁻¹) is the Knudsen diffusion coefficient of CH₄ through the pores, which can be calculated by Eq. (15) [39]:

$$D_{G,Kn} = 97 \cdot r_p \cdot \left(\frac{T \cdot 1000}{M_{CH_4}} \right)^{1/2} \quad (15)$$

where r_p (m) is the pore radius. The pores were assumed to be completely filled with the sweep gas, N₂.

For the dense membrane, the following equation can be used to estimate the membrane mass transfer coefficient [40]:

$$k_{m,dense} = \frac{P_{m,CH_4} \cdot R \cdot T}{\delta \cdot v_m} \quad (16)$$

where P_{m,CH_4} is the permeability of CH₄ through the dense membrane (7.1256 · 10⁻¹⁵ m² Pa⁻¹ s⁻¹ at 25 °C for PDMS [25]), R is the ideal gas constant (8.314 m³ Pa mol⁻¹ K⁻¹), and v_m (m³ mol⁻¹) is the molar volume of CH₄.

The membranes can be composed of more than one layer of different materials, as the PDMS and PVFD tested in this study. The total membrane mass transfer coefficient can be estimated by means of the resistance in series model with Eq. (17) [27].

$$\frac{1}{k_m} = \sum_n \frac{1}{k_{m,layer\ n}} \quad (17)$$

2.4. Membrane surface and structural stability

In order to determine the operational lifetime of the membranes and potential surface and structural modifications, the membranes were repeatedly used in sequential degassing experiments for up to 200–300 h. The effect of the time on stream on the membrane hydrophobicity was studied, as reported by Oldani et al. [41]. Thus, the surface modification of the membrane hydrophobicity was monitored by periodical measurements of the water static contact angle (CA). CA measurements were performed with a water drop of 5.5 ± 0.1 μL using a syringe pump (KF Technology, USA) at 25 °C. The image capture was taken at 15 s with a digital microscope (Celestron Handheld Digital Microscope Pro, China) and white light (Philips HUE Lamp, The Netherlands). Examples of CA images with pristine membranes are shown in [Supplementary Material S3](#). ImageJ software was used for image processing using the *Contact Angle Plug-in* based on the ellipse approximation. A mean CA value was obtained from at least 6 measurements in different spots of the membranes. The CA values of the wet membranes were measured after removing the excess water and moisture evaporation at room temperature for approximately 1 h with forced aeration in the head.

The morphology of the membrane surface and cross-section was

analysed using a Field Emission Scanning Electron Microscope (FESEM) equipped with an Energy Dispersive X-ray Spectrometer (EDX) and applying an accelerating voltage of 20 kV (Hitachi S4800, Hitachi Ltd., Japan). For image acquisition, the sample surfaces were previously coated with a fine layer of Au/Pd by sputtering for 1 min.

3. Results and discussion

3.1. Effect of operational parameters on the performance of dissolved CH₄ degassing experiments

The efficiency of the CH₄ recovery process can be mainly followed through the CH₄ removal efficiency (RE). The effect of the operational parameters (Q_L and Q_{N_2}) on RE and CH₄ content (y_{CH_4}) in the recovered gas is discussed in this section. Most of the experiments to study the influence of liquid and N₂ flow rates on the RE and CH₄ content in the recovered gas were performed with PDMS since this material is one of the most widely used at both lab and industrial scale for degasification processes. Liquid flow rates (Q_L) of 3.5, 21.0, 27.0, and 40.5 L h⁻¹ and N₂ flow rates (Q_{N_2}) of 0.05, 0.50, 4.00, and 15.00 L h⁻¹ were used in these tests.

The profiles of RE with the degasification time are shown in Fig. 2a. Additionally, evolution of dissolved CH₄ concentration can be found in Supplementary Material S4. In these degassing tests, a constant N₂ flow rate of 0.5 L h⁻¹ was used at different liquid flow rates. The slope of the RE profiles and their values increased as Q_L increased. This result suggested that the liquid mass transfer resistance presented a critical role since increasing liquid flow velocity seemed to lead to an enhancement in performance. The RE reached values around 90% at 22 h on stream for $Q_L \geq 21.0$ L h⁻¹. A lower RE of 59% was observed for the lowest Q_L of 3.5 L h⁻¹ at 22 h. The increase in RE was higher in the first 5 h on stream, and then, the RE increase was less pronounced. For instance, a RE value of 55% was observed at 5 h on stream for the highest Q_L (40.5 L h⁻¹), and RE only increased 40% for the next 17 h (RE of 95% at 22 h). That trend was also reported by Dutta et al. [42] in a liquid–liquid extraction of CH₄ with a FM. This could be explained by taking into account that the driving force was lower as the CH₄ concentration in the water stream decreased. From these results, the duration of the experiments (at which the performance was considerably different) was established in 3–5 h as standard for comparison purposes.

The effect of the liquid flow rate on the removal efficiency can be seen in Fig. 3a at a constant N₂ flow rate of 0.5 L h⁻¹ at different times on stream. The RE continuously increased with Q_L from values between 16% and 24% to 39% and 55% for liquid flow rates of 3.5 and 40.5 L h⁻¹, respectively. This trend was observed at any time on stream, and it can

be explained by taking into account the non-steady state condition of the experimental system. Thus, the water inside the liquid feed tank was degassed at a higher rate as Q_L increased. In addition, it is well known that mass transfer can be improved at higher liquid velocities, increasing the flux of the transferred component [26,43,44]. On the contrary, other authors reported a lower RE with increasing Q_L with a FM or hollow fibre membrane contactors in steady state systems [23,35,45]. In those cases, the residence time governs the efficiency of the separation: as Q_L increases, a lower residence time of the liquid in contact with the membrane is obtained.

In contrast to the effect of Q_L , the RE stayed almost constant for Q_{N_2} higher than 0.05 L h⁻¹, as can be seen in Fig. 3b. A slight increase in the RE was observed for the lowest Q_{N_2} . For instance, the RE increased from 40% to 45% when the Q_{N_2} increased from 0.05 to 0.5 L h⁻¹, respectively, at 5 h on stream. For values of Q_{N_2} higher than 0.5 L h⁻¹, the RE stayed around 36%, 41%, and 46% at 3, 4, and 5 h on stream, respectively. In the case of PP-1E, similar results were obtained (see Supplementary Material S5) and no significant effect of Q_{N_2} on the RE was observed with this microporous membrane. All these results seem to indicate an almost negligible mass transfer resistance of the gas phase at the tested operational conditions with no dependence on the membrane structure (dense or porous). A similar trend was obtained by other authors applying Q_{N_2} between 0 and 900 L h⁻¹ in hollow fibre membrane contactors and the FM for pervaporation processes [22,35,46].

The CH₄ content in the recovered gas for tests at a constant N₂ flow rate of 0.5 L h⁻¹ and at different liquid flow rates is shown in Fig. 2b. Initially, the CH₄ content decreased quickly from values higher than 3.0% to around 1.4% in the first 5 h on stream for $Q_L \geq 21.0$ L h⁻¹. Then, the decrease rate of the CH₄ content was lower. Thus, the effect of the time on stream on the CH₄ content followed the same trend observed for the RE. A CH₄ content near 0% was observed at 22 h on stream in accordance with the high RE values and lower driving force discussed previously. This effect was not observed for a liquid flow rate of 3.5 L h⁻¹, where the CH₄ content decrease was very low during the whole experiment (a decrease from 0.8% to 0.5% at 1 and 22 h, respectively). A higher CH₄ content was observed as the liquid flow rate increased, and the differences were more noticeable between 1 and 2 h of operation. For instance, a CH₄ content of 0.8, 1.9, 2.2, and 2.6% was observed at 1 h on stream for Q_L of 3.5, 21.0, 27.0, and 40.5 L h⁻¹, respectively. From 5 h of operation, the CH₄ content was very low (<1.5%) and was similar for experiments at Q_L between 21.0 and 40.5 L h⁻¹. The obtained CH₄ fluxes (J_{CH_4} , g s⁻¹ m⁻²) followed the same trend that CH₄ content, decreasing as the driving force decreased with the time on stream from values of 118–36 g s⁻¹ m⁻² at 0 h to values lower than 11 g s⁻¹ m⁻² at 22 h with a constant Q_{N_2} of 0.5 L h⁻¹ (results shown in Supplementary

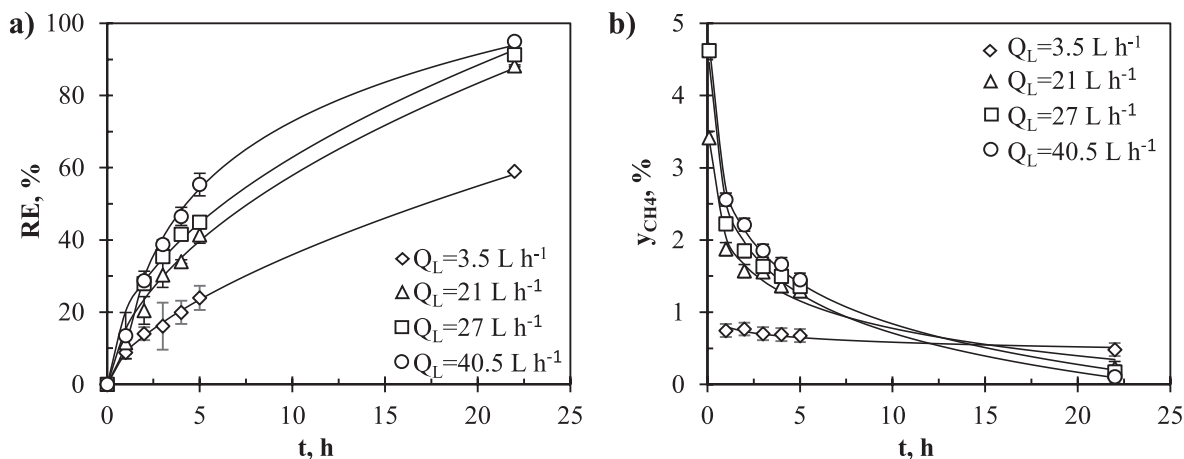


Fig. 2. a) CH₄ removal efficiency and b) CH₄ content in the recovered gas versus time on stream at different liquid flow rates and a constant N₂ flow rate of 0.5 L h⁻¹ with PDMS.

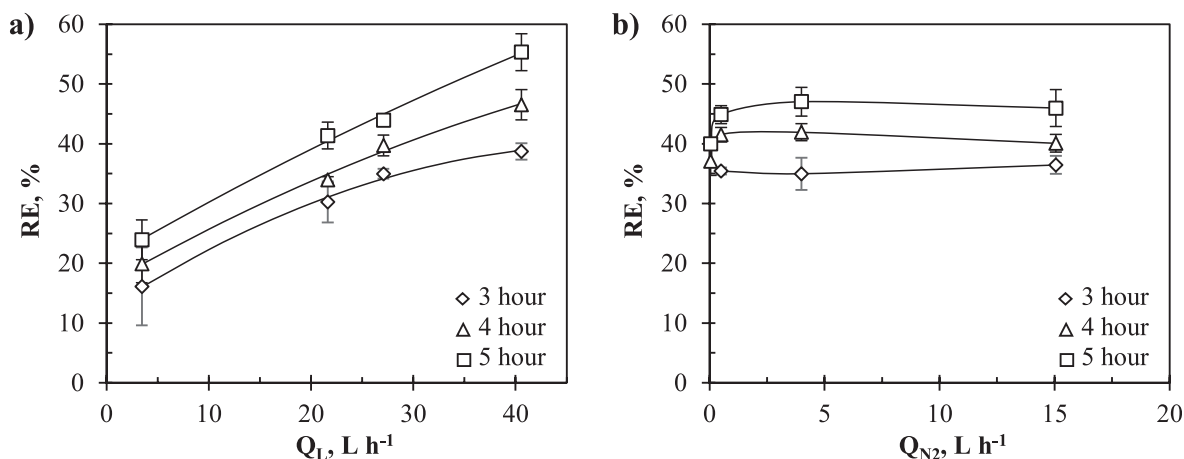


Fig. 3. Effect of a) liquid flow rate at a constant N₂ flow rate of 0.5 L h⁻¹ and b) N₂ flow rate at a constant liquid flow rate of 27 L h⁻¹ on the CH₄ removal efficiency at different times on stream with PDMS.

Material S4).

The CH₄ content in the recovered gas drastically decreased with increasing Q_{N2}, which was also observed in our previous work [19]. The CH₄ content was always under 0.4% and usually lower than the detection limit (<0.05%) at N₂ flow rates ≥ 4.0 L h⁻¹ (see [Supplementary Material S6](#)). In contrast, the CH₄ flux slightly increased from a Q_{N2} of 0.5 to 4.0 L h⁻¹ and stayed constant Q_{N2} ≥ 4.0 L h⁻¹, showing a maximum value of 128 g s⁻¹ m⁻² at 0 h and Q_{N2} of 4.0 L h⁻¹ (results shown in [Supplementary Material S4](#)). That increase was more pronounced at the beginning of the degasification test and negligible from a time on stream of 5 h. Thus, a low N₂ flow rate may be applied in order to maximize the CH₄ content in the recovered gas, remaining a high performance of the membrane module.

3.2. Effect of membrane materials on the performance of dissolved CH₄ degassing experiments

For comparison purposes, experiments with microporous PVDF and two types of PP membranes were also performed. The results obtained for PDMS and PP in the degassing tests carried out with a liquid and N₂ flow rate of 21.0 and 0.5 L h⁻¹, respectively, are compared in [Fig. 4a](#). Similar RE values for the three membranes operating in the FM with values between 42% and 46% at 5 h on stream were obtained. The CH₄ content in the recovered gas was also quite similar, decreasing from initial values between 2% and 3% to around 1% at 5 h on stream for PP

and PDMS (see [Supplementary Material S7](#)).

Higher REs and CH₄ content could be expected for microporous membranes due to a lower mass transfer resistance, as observed in hollow fibre contactors [17,29,45]. In contrast, the studies of Dingemans et al. [27] concluded that lower membrane mass transfer resistances can be obtained with dense membranes with a high gas permeability in experiments conducted in FMs. These authors used a flat sheet PDMS with an active layer between 2.0 and 2.5 μm similar to what was used in this work, whereas most mass transfer studies that are carried out with a PDMS hollow fibre contactor use a typical thickness between 110 and 2000 μm [23,43,44]. In this regard, Sethunga et al. [17] also reported greater performances with porous hollow fibre membranes possessing a dense thin film of PDMS than those with a thicker PDMS layer. Therefore, conclusions on the importance of membrane resistance could be affected by this fact, and a compromise between structural stability and performance must define the thickness of the membrane and their different layers.

Results obtained with PVDF can be seen in [Fig. 4b](#), along with PDMS, at a constant N₂ flow rate of 4.0 L h⁻¹ and different liquid flow rates. The RE of the PVDF increased with the total time of use of the membrane when a Q_L ≥ 21.0 L h⁻¹ was applied. Thus, a different RE was observed for what we called unaltered PVDF (uPVDF, operated always under a Q_L < 21 L h⁻¹ or with a time of use ≤ 5 h at Q_L ≥ 21.0 L h⁻¹) and for altered PVDF (aPVDF, operated at Q_L ≥ 21.0 L h⁻¹ for at least 5 h). Thus, the RE obtained with the aPVDF was higher than the uPVDF and similar to

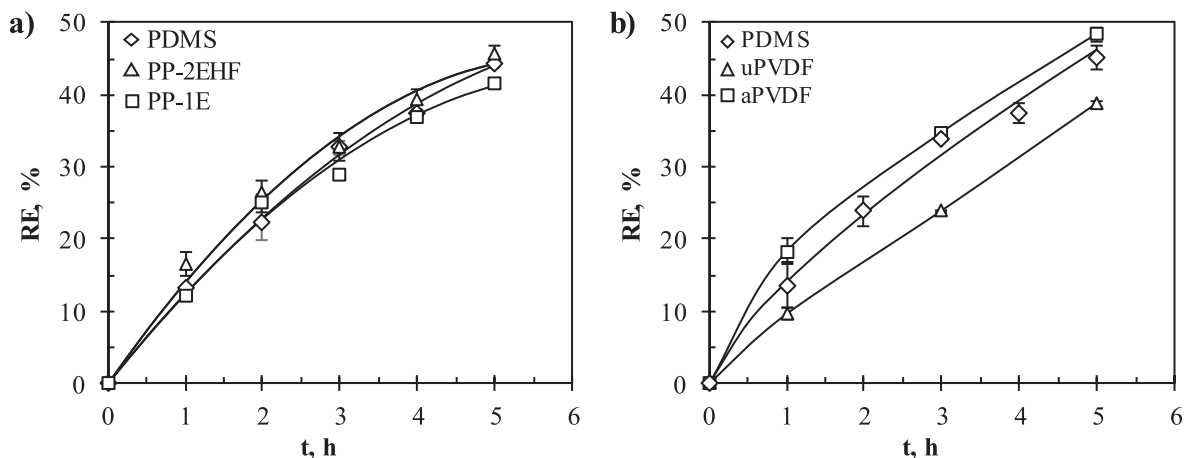


Fig. 4. CH₄ removal efficiency versus time on stream with different membrane materials at a constant liquid flow rate of 21 L h⁻¹ and a N₂ flow rate of a) 0.5 L h⁻¹ for PDMS, PP-1E, and PP-2EHF and b) 4.0 L h⁻¹ for PDMS, unaltered PVDF (uPVDF), and altered PVDF (aPVDF). aPVDF was operated for at least 5 h at Q_L of 21.0 L h⁻¹ before the experiment.

those obtained with PDMS, as can be seen in Fig. 4b. For example, REs of 39% and 48% were obtained with uPVDF and aPVDF, respectively, at Q_L of 21.0 L h^{-1} . The lowest REs were obtained for microporous uPVDF at all tested conditions, and results at a lower Q_L of 3.5 L h^{-1} are shown in Supplementary Material S8. The results suggested that the membrane mass transfer resistance of uPVDF cannot be neglected. As will be discussed in a later section, surface changes on uPVDF were observed after 5 h of time of use at $Q_L \geq 21.0 \text{ L h}^{-1}$, increasing their hydrophobicity and performance. No similar observations have been reported in the literature. The performance of the rest of the membranes (PDMS, PP-1E, and PP-2EHF) stayed constant for a total time of use up to 100–300 h if no breakages on the surface appear. Thus, a greater stability can be inferred.

3.3. Membrane surface and structural stability

The membrane inside the FM could be subjected to changes due to the stress caused by the liquid flow [47]. Hydrophobicity evaluation, measured as water contact angle (CA), has been frequently used to monitor the surface membrane stability and durability [41].

The CA variation versus time of use at Q_L of 21 L h^{-1} (liquid velocity of 16.8 cm s^{-1}) for different membranes is shown in Fig. 5a. The CA of PDMS was monitored until water breakthrough was detected at 95 h of total time of use. A slight decrease in CA from 101° to 94° at 0 and 95 h, respectively, was observed for PDMS. The inspection of the membrane surface with FESEM revealed the presence of cleavages on the top active layer, which was in contact with the liquid flow (see Supplementary Material S9). In addition, delamination of the membrane dense layer was observed, losing the adhesion force between the PDMS layer and support, showing that at least for this type of membrane and at the tested operational conditions ($Q_L = 21.0 \text{ L h}^{-1}$), this material suffered critical damage. From cross-section images, the delamination effect was appreciated as the top layer was not adhered to the support layer. More severe delamination and cracks were observed by other authors for flat sheet composite membranes with a top dense layer of polyamide in forward osmosis processes at liquid velocities around 26.0 cm s^{-1} [47]. Nevertheless, the RE for CH_4 recovery was not significantly affected for this loss of stability, up to cracks appeared on membrane.

In contrast, the CA stayed almost constant around 102° for PDMS at a Q_L of 3.5 L h^{-1} (liquid velocity of 2.8 cm s^{-1}) (Fig. 5b), and no signal degradation was detected. In conclusion, mechanical degradation is suggested as the main cause for the stability loss of the PDMS at liquid flow rates higher than 3.5 L h^{-1} .

The stability of the CA of the PP membranes was strongly altered in our experiments since a large decrease in their CA in the first 5 h of time of use was observed at an intermediate Q_L of 21 L h^{-1} . The CA of PP-1E

and PP-2EHF decreased from 145° to 105° and 140° to 122° , respectively (Fig. 5a). The loss of hydrophobicity could be also related to the high visual deformation observed on these membranes. Since no support was contained in the PP membranes, the mechanical resistance seemed to be lower than those with a support layer, such as PDMS or PVDF. Thus, it seems that the design of the fluid channels and spacer of the FM could play a critical role in this type of membrane in order to avoid high shear stress resulting in membrane deformation [48].

Regarding the stability of the PVDF (Fig. 5), an increase in the hydrophobicity of the aPVDF was obtained with the time of use at the highest Q_L (21.0 L h^{-1}). A gradual CA increase from 103° to 118° was observed during the first 70 h of use, and then, the CA stabilized to values around 115° from 90 h (Fig. 5a). FESEM images showed a less porous surface for that aPVDF with a higher CA (Fig. 6) with respect to the uPVDF, therefore substantial structural changes on the membrane surface occurred at Q_L of 21.0 L h^{-1} . That phenomenon may be attributed to a plastic deformation due to the stress induced by the liquid flow on the membrane. In contrast, the CA of uPVDF stayed almost constant with values around 103° at a lower Q_L of 3.5 L h^{-1} even though a higher surface heterogeneity was observed with values between 100° and 112° at 176 h (Fig. 5b).

As previously discussed, higher REs were obtained in degasification tests with aPVDF after its hydrophobicity was increased with respect to uPVDF (Fig. 4b). The hydrophobicity increase and surface porosity decrease favoured the CH_4 flux across the membrane, decreasing the mass transfer resistance. From these results, it can be concluded that the stability changes on the aPVDF structure improved the performance of the CH_4 recovery. On the contrary, Kim et al. [48] reported that deformation or structural changes on a flat sheet membrane of cellulose reduced the performance of an osmosis process.

Studies about the performance stability of the membranes during operation for flat sheet membranes are relatively scarce in the literature. In this regard, long-term tests have been reported to evaluate the wetting resistance of modified membranes using the CH_4 flux as the control parameter [30,49]. Other authors also reported membrane breakages in hollow fibre membrane contactors [50,51]. Taking into account this relatively scarce information, it seems that studies on the membrane stability changes are needed to enhance and deepen the knowledge of this effect on the membrane performance in order to establish the limiting operational condition and the useful lifetime of the membranes. For this purpose, the results suggest that CA measurements could be a useful methodological approach to determine the stability of membranes after their use.

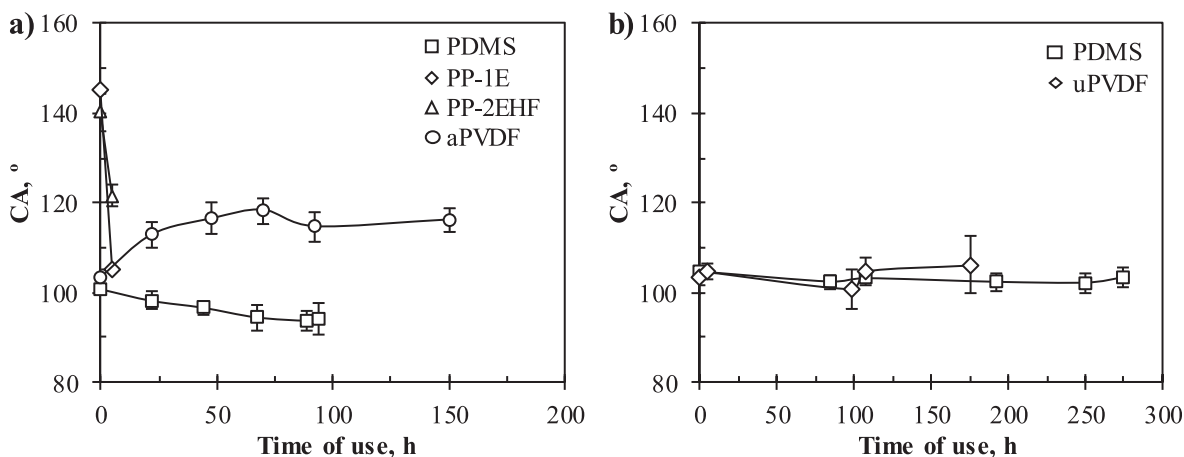


Fig. 5. Membrane water contact angle versus time of use for different membrane materials at a liquid flow rate of a) 21 L h^{-1} and b) 3.5 L h^{-1} . uPVDF: unaltered PVDF; aPVDF: altered PVDF.

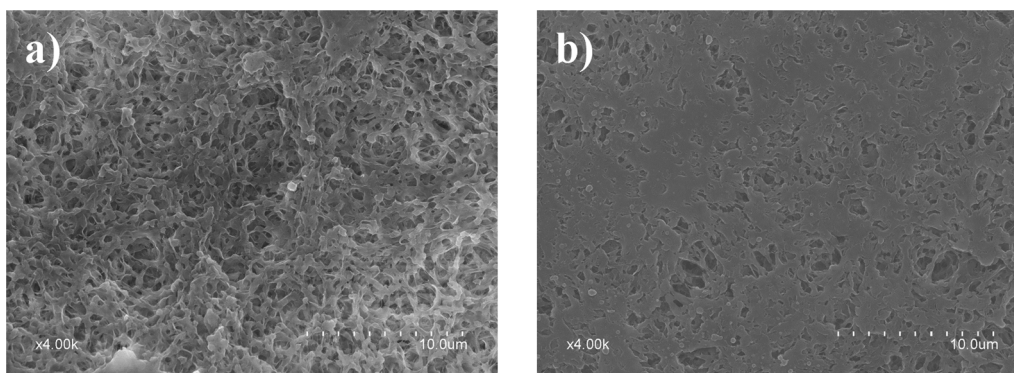


Fig. 6. Surface FESEM images of the a) pristine-unaltered PVDF and b) altered PVDF. Altered PVDF was operating for 150 h at a liquid flow rate (Q_L) of 21.0 L h⁻¹ before the image acquisition.

3.4. Mass transfer analysis

A study of the mass transfer process for CH₄ separation was carried out in order to evaluate the influence of the different operational conditions and membranes and validate the proposed empirical model. The experimental and estimated values of the overall and individual mass transfer coefficients are presented and evaluated in this section.

From the estimated values with Eq. (6) – Eq. (17), the lowest individual mass transfer coefficients were always obtained for the liquid phase ($k_{L,est}$), indicating that the main mass transfer resistance was located in the liquid phase. $k_{L,est}$ values ranging from $2.25 \cdot 10^{-5}$ to $5.87 \cdot 10^{-5}$ m s⁻¹ (see [Supplementary Material S10](#)) were obtained. The estimated mass transfer resistance (R_G) of the gas phase represented <0.05% of the overall mass transfer resistance (R_{ov}), with $k_{G,est}$ values between $369 \cdot 10^{-5}$ and $403 \cdot 10^{-5}$ m s⁻¹. Higher values were reported by Dingemans et al. [27] for the separation of volatile organic compounds (VOCs) from gas streams in a FM with an experimental coefficient ranging from $1500 \cdot 10^{-5}$ to $1900 \cdot 10^{-5}$ m s⁻¹ in the permeate side by applying higher Q_{N_2} between 12 and 60 L h⁻¹. Thus, the mass transfer resistance of the gas phase may be neglected for a FM under the tested operational condition. These results are in agreement with previous studies carried out with PDMS and PP hollow fibre contactors where the gas phase resistance was also considered negligible [45,52].

Regarding the estimated membrane mass transfer coefficient, the lowest $k_{m,est}$ was observed for the dense PDMS, with a value around $30 \cdot 10^{-5}$ m s⁻¹; so, the membrane mass transfer resistance (R_m) represented 0.5% of the R_{ov} . $k_{m,est}$ values of around $1549 \cdot 10^{-5}$, $911 \cdot 10^{-5}$, and $4247 \cdot 10^{-5}$ m s⁻¹ were obtained for PP-1E, PP-2EHF, and PVDF, respectively, with R_m representing <0.02% of the R_{ov} . As expected, the R_m was higher for PDMS due to its dense structure even though k_m had a negligible effect on the final value of $K_{L,est}$ and, therefore, on R_{ov} . In the case of the separation of VOCs from gas streams in a FM, experimental membrane mass transfer coefficient ($k_{m,exp}$) values of around $300 \cdot 10^{-5}$ m s⁻¹ were reported for composite porous PP/PVDF membranes [27] and around $450 \cdot 10^{-5}$ m s⁻¹ for composite porous membranes with a 2 μm dense layer of PDMS. It is noteworthy to highlight that the increase in membrane thickness leads to a decrease in the membrane mass transfer coefficient. Thus, a lower $k_{m,exp}$ value of around $1 \cdot 10^{-5}$ m s⁻¹ has been reported for PDMS hollow fibre contactors with a thickness of 110 μm for CH₄ degassing, representing up to 20% of the overall mass transfer coefficient [44]. Membrane mass transfer coefficients with values ranging from 10^{-1} to 10^{-4} m s⁻¹ have been, indeed, reported for membranes with similar characteristics [40]. According to the obtained results, it seems that the R_m could be neglected for microporous and dense membranes with a low thickness (≤ 2.5 μm) at least for liquid velocities no much higher than that used in this work.

From the negligible effect of the estimated membrane and gas phase mass transfer resistance, it seems reasonable that similar values of CH₄

removal efficiency would be obtained at similar liquid hydraulic conditions for different membranes. As seen in Fig. 4, the obtained REs were similar for PDMS, the two types of PP, and aPVDF with values around 45%.

The experimental overall mass transfer coefficient ($K_{L,exp}$) was calculated for all tested operational conditions with values ranging from $1.66 \cdot 10^{-5}$ to $6.28 \cdot 10^{-5}$ m s⁻¹. No previous references were found in the literature for D-CH₄ recovery by means of FMs, whilst hollow fibre membrane contactors have been widely studied for CH₄ recovery. Using hollow fibre contactors, $K_{L,exp}$ values between $0.16 \cdot 10^{-5}$ and $12.6 \cdot 10^{-5}$ m s⁻¹ have been reported for most typical membranes applied for CH₄ degassing as PDMS, PP, and PVDF at similar liquid velocities used in this work [10]. Slightly lower $K_{L,exp}$ values were observed for dense membranes than for porous membranes at similar liquid velocities in hollow fibre contactors, and consequently, lower REs were reported [53].

Due to the scarcity of studies about D-CH₄ recovery with flat sheet membranes, the mass transfer analysis of CH₄ degassing could only be compared with that of O₂ degassing [10]. A $K_{L,exp}$ value of $6.3 \cdot 10^{-5}$ m s⁻¹ was reported with a PP in FMs for dissolved O₂ removal from water [54]. Also, $K_{L,exp}$ values between $0.95 \cdot 10^{-5}$ to $1.55 \cdot 10^{-5}$ m s⁻¹ have been reported for O₂ absorption with PVDF [26], similar to those obtained in this work for D-CH₄ recovery. Regarding O₂ transport through hollow fibre contactors, $K_{L,exp}$ values between $0.3 \cdot 10^{-5}$ and $19 \cdot 10^{-5}$ m s⁻¹ have been reported for a PP hollow fibre contactor at liquid velocities lower than 0.02 cm s⁻¹ (liquid flow rates between 0.1 and 0.6 L h⁻¹) [54]. Other authors reported higher $K_{L,exp}$ for O₂ removal with values ranging from $1 \cdot 10^{-4}$ to $1 \cdot 10^{-3}$ m s⁻¹ with a PP hollow fibre contactor at higher liquid velocities between 38 and 80 cm s⁻¹ [55]. They associated the large $K_{L,exp}$ values to the low packing density of their hollow fibre contactors, getting better contact between the fibres and water and avoiding the channelling effect. In addition, $K_{L,exp}$ values between $3 \cdot 10^{-5}$ and $6 \cdot 10^{-5}$ m s⁻¹ have been reported for CO₂ absorption from a gas stream with a porous PP hollow fibre contactor at liquid velocities ranging from 10 to 50 cm s⁻¹ [56].

The experimental and estimated overall mass transfer coefficient clearly increased with liquid flow rate, as shown in Fig. 7. These results showed a strong influence of the R_L on R_{ov} , as previously discussed. Similar $K_{L,exp}$ and $K_{L,est}$ values were obtained when PDMS was used (Fig. 7a and b), so the model based on the empirical equations used for the mass transfer analysis seems suitable for the prediction of the mass transfer resistance. The obtained values for $K_{L,exp}$ were significantly lower than $K_{L,est}$ for uPVDF at all tested liquid flow rates (Fig. 7c) even though the estimated values showed a similar behaviour to PDMS since the main mass transfer resistance was in the liquid phase. These results seem to indicate that R_m was underestimated for uPVDF. In contrast, similar $K_{L,exp}$ and $K_{L,est}$ values were obtained for aPVDF with a time of use ≥ 5 h at Q_L of 21.0 L h⁻¹ (Fig. 7c). In this case, the obtained results agree with the negligible R_m estimated and with the REs obtained for the

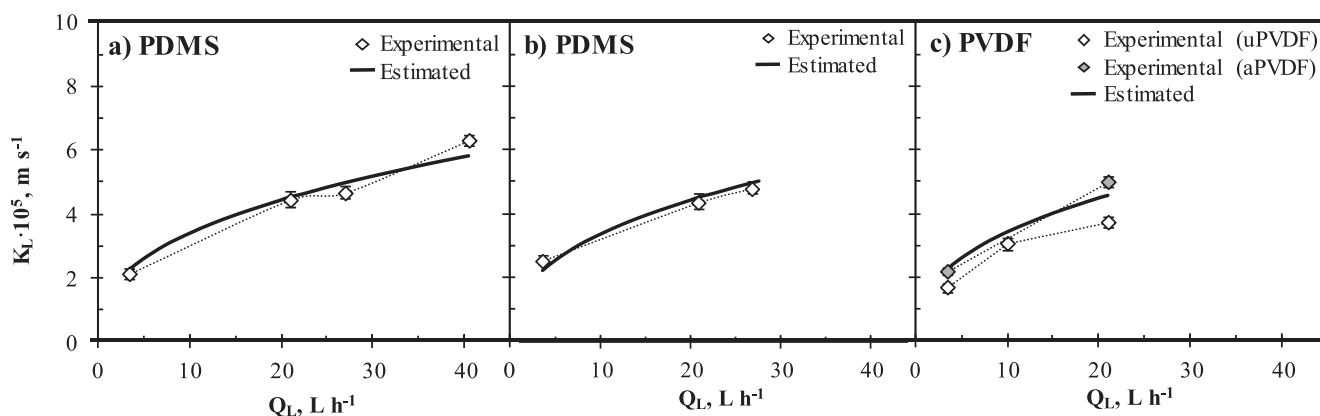


Fig. 7. Overall mass transfer coefficient versus liquid flow rate: a) for PDMS at a N_2 flow rate of 0.5 L h⁻¹ and b) 4.0 L h⁻¹ and c) for unaltered PVDF (uPVDF) and altered PVDF (aPVDF) at a N_2 flow rate of 4.0 L h⁻¹. aPVDF was operated for at least 5 h at 21.0 L h⁻¹ before the experiments.

aPVDF, similar to those obtained for PDMS and PP (Fig. 4). Thus, an additional mass transfer resistance on the uPVDF seemed to be initially present, which was permanently removed at a liquid flow rate of 21.0 L h⁻¹.

The wetting phenomenon (pores partially or totally fill with the liquid phase) has been reported as one of the major drawbacks for microporous membranes since the liquid inside the membrane pores creates an additional resistance [57]. The CH_4 mass transfer rate decreases since the stagnant water in the pores replaces the gas, so R_m may represent up to 50% of the R_{ov} and can be significant even at the low pore fraction occupied by the liquid [53,58]. In the case of the PVDF studied in this work, the reduction of the surface porosity of uPVDF from values $\sim 75\%$ to a dense-like surface for aPVDF (Fig. 6) and its hydrophobicity increase (Fig. 5) were in agreement with surfaces more resistant to wetting, removing the additional membrane mass transfer resistance.

As previously discussed, $K_{L,est}$ was not influenced by the N_2 flow rate. For PDMS, experimental $K_{L,exp}$ stayed almost constant at around $4.8 \cdot 10^{-5}$ m s⁻¹ (Fig. 8a) for all tested Q_{N_2} . For PP-1E, $K_{L,exp}$ was also underestimated, showing values slightly lower than those estimated for all tested operational conditions (Fig. 8b). $K_{L,exp}$ values around $4.1 \cdot 10^{-5}$ m s⁻¹ and $K_{L,est}$ of $4.5 \cdot 10^{-5}$ m s⁻¹ were obtained for PP-1E. In contrast, for PP-2EHF, similar values of $K_{L,exp}$ and $K_{L,est}$ were observed ($4.6 \cdot 10^{-5}$ and $4.5 \cdot 10^{-5}$ m s⁻¹, respectively) at the tested operational condition with liquid and N_2 flow rates of 21.0 and 0.5 L h⁻¹, respectively.

4. Future research and practical implications

The validation of a system based on a gas–liquid membrane contactor using a flat sheet membrane module has been shown in this work. Besides the degassing of methane from aqueous streams it could be also used in other applications such as stripping and gas absorption from air or flue gas (liquid–gas system), gas removal from aqueous solutions using *trans*-membrane chemical absorption (liquid–gas–liquid system) and removal of solubilized ions from water (liquid–liquid system) [59,60].

Due to its configuration and structure (small size of the flat module), this system can facilitate and enable future research focused both on the influence of different membrane properties, in particular those related to hydrophobicity, fouling resistance or cleaning strategies, and on the membrane characterization during its use, including fouling deposits or surface stability. In contrast to hollow fibre contactors, in flat sheet modules the membrane can easily be extracted, analysed and cleaned during operation and/or replaced, allowing considerable time and cost savings.

Hollow fibre contactors are frequently recommended for industrial applications, because usually they provide higher volumetric mass transfer coefficients and involve fewer capital costs than flat membrane contactors. Nevertheless, hollow fibre module cannot be easily repaired, which could lead to a non-negligible operational and maintenance cost and restrict its feasibility in certain applications where membrane can be damaged or loss its properties. In contrast, the replacement or cleaning of membrane can be easily carried out in flat sheet modules. In order to

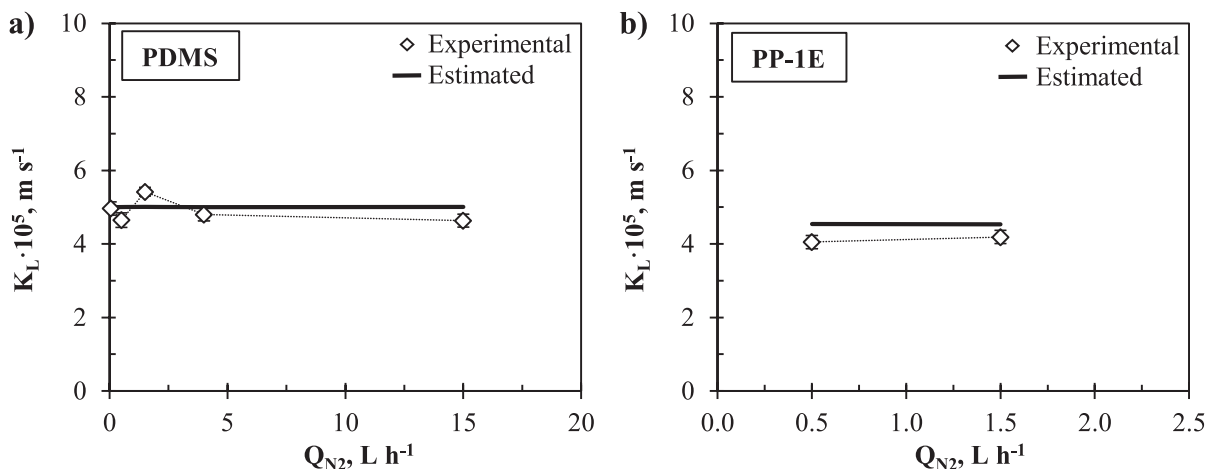


Fig. 8. Overall mass transfer coefficient versus N_2 flow rate for a) PDMS at a constant liquid flow rate of 27 L h⁻¹ and b) PP-1E at a constant liquid flow rate of 21 L h⁻¹.

compare the viability of both contactor configurations, suitable economic analyses might be tackled considering all these aspects.

5. Conclusions

The applicability and versatility of a gas–liquid flat sheet membrane module based on our design have been checked for the process of recovery of dissolved methane from water. PDMS, two types of PP, and PVDF membranes were tested and compared at different liquid flow rates (ranging from 3.5 to 40.5 L h⁻¹) and N₂ flow rates (ranging from 0.05 to 15.00 L h⁻¹). The methane removal efficiency increased with the liquid flow rate for all tested operational conditions and membranes. In contrast, the removal efficiency was not influenced by N₂ flow rates higher than 0.05 L h⁻¹. A maximum removal efficiency of 95% was observed at 22 h of time on stream with the highest liquid flow rate of 40.5 L h⁻¹ with PDMS.

Similar removal efficiencies were observed with dense PDMS and microporous PP membranes and when a microporous PVDF membrane was tested at a moderate-high liquid flow rate (21 L h⁻¹). On the contrary, the microporous PVDF membrane operated at the lowest liquid flow rate (3.5 L h⁻¹) showed lower removal efficiencies.

As expected, the mass transfer model for methane transport based on empirical equations agreed with most of the experimental results. This mass transfer analysis showed that the main transfer resistance was located in the liquid phase and that membrane and gas phase mass transfer were negligible.

The evaluation of the membrane stability showed that PDMS suffered a slight decrease in hydrophobicity at moderate liquid flow rates (21 L h⁻¹) even though the efficiency of the methane recovery was unaltered, and finally, cleavages appeared in the membrane at almost 100 h of time on stream. The hydrophobicity of PP membranes also strongly decreased with the time on stream, suggesting structural changes due to the membrane deformation. In the case of PVDF, a different behaviour was observed since an increase in the hydrophobicity of the membrane was observed when it was operated at a liquid flow rate of 21 L h⁻¹ for at least 5 h, which agreed with the improvement in performance. This behaviour could be related to the changes in superficial porosity when a moderate liquid flow rate was applied. These results also suggest that water contact angle measurements, as a hydrophobicity indicator, could be a useful parameter to infer the stability of membranes during their operations, especially in processes where the membrane resistance is negligible.

Funding

This research was supported by the Conselleria d'Innovació, Universitats, Ciència i Societat Digital – Generalitat Valenciana (project GV/2019/149); and the Ministerio de Ciencia, Innovación y Universidades – Agencia Estatal de Investigación, Spain (Project CTM2017-88042-R funded by MCIN/AEI/ <https://doi.org/10.13039/501100011033> and by “ERDF A way of making Europe”).

CRedit authorship contribution statement

R. Jiménez-Robles: Methodology, Validation, Formal analysis, Investigation, Writing – original draft, Writing – review & editing, Visualization. **C. Gabaldón:** Conceptualization, Validation, Project administration, Funding acquisition. **J.D. Badia:** Resources, Writing – review & editing. **M. Izquierdo:** Conceptualization, Methodology, Validation, Project administration, Writing – review & editing, Supervision, Funding acquisition. **V. Martínez-Soria:** Conceptualization, Methodology, Validation, Project administration, Writing – review & editing, Supervision.

Declaration of Competing Interest

The authors declare that they have no known competing financial interests or personal relationships that could have appeared to influence the work reported in this paper.

Acknowledgements

R. Jiménez acknowledges Ministerio de Ciencia, Innovación y Universidades, Spain, for financial support for his Ph.D. (Grant FPU19/02478 funded by MCIN/AEI/ 10.13039/501100011033 and by “ERDF A way of making Europe”). Especial thank to Norbert Selzer from the “Separation and Purification Sciences Division” of the company 3 M Deutschland Membrane GmbH for supplying PPs membranes.

Appendix A. Supplementary material

Supplementary data to this article can be found online at <https://doi.org/10.1016/j.seppur.2021.120057>.

References

- [1] S.P. Nunes, P.Z. Culfaz-Emecen, G.Z. Ramon, T. Visser, G.H. Koops, W. Jin, M. Ulbricht, Thinking the future of membranes: Perspectives for advanced and new membrane materials and manufacturing processes, *J. Membr. Sci.* 598 (2020), 117761, <https://doi.org/10.1016/j.memsci.2019.117761>.
- [2] M. Ulbricht, H. Susanto, Porous Flat Sheet, Hollow Fibre and Capsule Membranes by Phase Separation of Polymer Solutions, *Membr. React. Prep. Optim. Sel.* (2011) 511–529, <https://doi.org/10.1002/9780470977569.ch22>.
- [3] S.D. Bazhenov, A.V. Bilyukevich, A.V. Volkov, Gas-liquid hollow fiber membrane contactors for different applications 6 (4) (2018) 76, <https://doi.org/10.3390/fib6040076>.
- [4] S. Heile, C.A.L. Chernicharo, E.M.F. Brandt, E.J. McAdam, Dissolved gas separation for engineered anaerobic wastewater systems, *Sep. Purif. Technol.* 189 (2017) 405–418, <https://doi.org/10.1016/j.seppur.2017.08.021>.
- [5] W. Rongwong, K. Goh, Resource recovery from industrial wastewaters by hydrophobic membrane contactors: A review, *J. Environ. Chem. Eng.* 8 (2020) 1–14, <https://doi.org/10.1016/j.jece.2020.104242>.
- [6] K.L. Wasewar, Separation of Bio-Butanol, *UPI J. Eng. Technol.* 1 (2018) 25–30.
- [7] Y. Lee, K.H. Yun, D. Sethunga, T.H. Bae, Membrane contactors for maximizing biomethane recovery in anaerobic wastewater treatments: Recent efforts and future prospect, *Appl. Sci.* 11 (2021) 1–16, <https://doi.org/10.3390/app11041372>.
- [8] X. Li, H.S. Lee, Z. Wang, J. Lee, State-of-the-art management technologies of dissolved methane in anaerobically-treated low-strength wastewaters: A review, *Water Res.* (2021), <https://doi.org/10.1016/j.watres.2021.117269>.
- [9] W. Rongwong, J. Lee, K. Goh, H.E. Karahan, T.H. Bae, Membrane-based technologies for post-treatment of anaerobic effluents, *Npj Clean Water.* 1 (2018), <https://doi.org/10.1038/s41545-018-0021-y>.
- [10] E. Centeno Mora, C.L. Chernicharo, Use of membrane contactors for removing and recovering dissolved methane from anaerobic reactors effluents: state-of-the-art, challenges, and perspectives, *Rev. Environ. Sci. Biotechnol.* 19 (2020) 673–697, <https://doi.org/10.1007/s11157-020-09546-w>.
- [11] C.L. Souza, C.A.L. Chernicharo, S.F. Aquino, Quantification of dissolved methane in UASB reactors treating domestic wastewater under different operating conditions, *Water Sci. Technol.* 64 (2011) 2259–2264, <https://doi.org/10.2166/wst.2011.695>.
- [12] D. Cai, Z. Chang, L. Gao, C. Chen, Y. Niu, P. Qin, Z. Wang, T. Tan, Acetone-butanol-ethanol (ABE) fermentation integrated with simplified gas stripping using sweet sorghum bagasse as immobilized carrier, *Chem. Eng. J.* 277 (2015) 176–185, <https://doi.org/10.1016/j.cej.2015.04.101>.
- [13] B.L. Pangarkar, S.K. Deshmukh, V.S. Sapkal, R.S. Sapkal, Review of membrane distillation process for water purification, *Desalin. Water Treat.* 57 (7) (2016) 2959–2981, <https://doi.org/10.1080/19443994.2014.985728>.
- [14] S. Zare, A. Kargari, Membrane properties in membrane distillation, in: V.G. Gude (Ed.), *Emerging Technologies for Sustainable Desalination Handbook*, Elsevier Inc, 2018, pp. 107–156, <https://doi.org/10.1016/B978-0-12-815818-0.00004-7>.
- [15] Riya Sidhikku Kandath Valappil, Nayef Ghasem, Mohamed Al-Marzouqi, Current and future trends in polymer membrane-based gas separation technology: A comprehensive review, *J. Ind. Eng. Chem.* 98 (2021) 103–129, <https://doi.org/10.1016/j.jiec.2021.03.030>.
- [16] A. Marmor, Super-hydrophobicity fundamentals: Implications to biofouling prevention, *Biofouling.* 22 (2006) 107–115, <https://doi.org/10.1080/08927010600562328>.
- [17] G.S.M.D.P. Sethunga, H.E. Karahan, R. Wang, T.H. Bae, PDMS-coated porous PVDF hollow fiber membranes for efficient recovery of dissolved biomethane from anaerobic effluents, *J. Membr. Sci.* 584 (2019) 333–342, <https://doi.org/10.1016/j.memsci.2019.05.016>.
- [18] G.S.M.D.P. Sethunga, H.E. Karahan, R. Wang, T.H. Bae, Wetting- and fouling-resistant hollow fiber membranes for dissolved methane recovery from anaerobic

- wastewater treatment effluents, *J. Membr. Sci.* 617 (2021), 118621, <https://doi.org/10.1016/j.memsci.2020.118621>.
- [19] R. Jiménez-Robles, C. Gabaldón, V. Martínez-Soria, M. Izquierdo, Simultaneous application of vacuum and sweep gas in a polypropylene membrane contactor for the recovery of dissolved methane from water, *J. Membr. Sci.* 617 (2020) 1–10, <https://doi.org/10.1016/j.memsci.2020.118560>.
- [20] R. Sander, Compilation of Henry's law constants (version 4.0) for water as solvent, *Atmos. Chem. Phys.* 15 (8) (2015) 4399–4981, <https://doi.org/10.5194/acp-15-4399-2015>.
- [21] A. McLeod, B. Jefferson, E.J. McAdam, Toward gas-phase controlled mass transfer in micro-porous membrane contactors for recovery and concentration of dissolved methane in the gas phase, *J. Membr. Sci.* 510 (2016) 466–471, <https://doi.org/10.1016/j.memsci.2016.03.030>.
- [22] J. Cookney, A. McLeod, V. Mathioudakis, P. Ncube, A. Soares, B. Jefferson, E. J. McAdam, Dissolved methane recovery from anaerobic effluents using hollow fibre membrane contactors, *J. Membr. Sci.* 502 (2016) 141–150, <https://doi.org/10.1016/j.memsci.2015.12.037>.
- [23] J. Cookney, E. Cartmell, B. Jefferson, E.J. McAdam, Recovery of methane from anaerobic process effluent using poly-di-methyl-siloxane membrane contactors, *Water Sci. Technol.* 65 (2012) 604–610, <https://doi.org/10.2166/wst.2012.897>.
- [24] W.M.K.R.T.W. Bandara, Hisashi Satoh, Manabu Sasakawa, Yoshihito Nakahara, Masahiro Takahashi, Satoshi Okabe, Removal of residual dissolved methane gas in an upflow anaerobic sludge blanket reactor treating low-strength wastewater at low temperature with degassing membrane, *Water Res.* 45 (11) (2011) 3533–3540, <https://doi.org/10.1016/j.watres.2011.04.030>.
- [25] M. Mulder, *Basic Principles of Membrane Technology*, 1st ed., Springer, Netherlands, Netherlands, 1996.
- [26] J. Phattaranawik, T. Leiknes, W. Pronk, Mass transfer studies in flat-sheet membrane contactor with ozonation, *J. Membr. Sci.* 247 (1-2) (2005) 153–167, <https://doi.org/10.1016/j.memsci.2004.08.020>.
- [27] M. Dingemans, J. Dewulf, L. Braeckman, H. Van Langenhove, K. Friess, V. Hynek, M. Sipek, Mass transfer characteristics for VOC permeation through flat sheet porous and composite membranes: The impact of the different membrane layers on the overall membrane resistance, *J. Membr. Sci.* 322 (2008) 234–242, <https://doi.org/10.1016/j.memsci.2008.05.043>.
- [28] I.G. Wenten, K. Khoiruddin, A.N. Hakim, N.F. Himma, Chapter 11: The Bubble Gas Transport Method, in: *Membrane Characterization*, Elsevier B.V., 2017, pp. 199–218, <https://doi.org/10.1016/B978-0-444-63776-5.00011-5>.
- [29] G.S.M.D.P. Sethunga, J. Lee, R. Wang, T.H. Bae, Influences of operating parameters and membrane characteristics on the net energy production in dense, porous, and composite hollow fiber membrane contactors for dissolved biomethane recovery, *J. Membr. Sci.* 610 (2020), 118301, <https://doi.org/10.1016/j.memsci.2020.118301>.
- [30] G.S.M.D.P. Sethunga, W. Rongwong, R. Wang, T.H. Bae, Optimization of hydrophobic modification parameters of microporous polyvinylidene fluoride hollow-fiber membrane for biogas recovery from anaerobic membrane bioreactor effluent, *J. Membr. Sci.* 548 (2018) 510–518, <https://doi.org/10.1016/j.memsci.2017.11.059>.
- [31] B. Abdu, S. Munirasu, P. Kallem, S.W. Hasan, F. Banat, Investigating the effect of various foulants on the performance of intrinsically superhydrophobic polyvinylidene fluoride membranes for direct contact membrane distillation, *Sep. Purif. Technol.* 252 (2020) 1–13, <https://doi.org/10.1016/j.seppur.2020.117416>.
- [32] M. Bennett, B.J. Brisdon, R. England, R.W. Field, Performance of PDMS and organofunctionalised PDMS membranes for the pervaporative recovery of organics from aqueous streams, *J. Membr. Sci.* 137 (1-2) (1997) 63–88, [https://doi.org/10.1016/S0376-7388\(97\)00183-X](https://doi.org/10.1016/S0376-7388(97)00183-X).
- [33] P. Sanchis-Perucho, Á. Robles, F. Durán, F. Rogalla, J. Ferrer, A. Seco, Widening the applicability of AnMBR for urban wastewater treatment through PDMS membranes for dissolved methane capture: Effect of temperature and hydrodynamics, *J. Environ. Manage.* 287 (2021) 1–11, <https://doi.org/10.1016/j.jenvman.2021.112344>.
- [34] Y.A. Çengel, M.A. Boles, M. Kanoğlu, *Thermodynamics: An Engineering Approach*, Ninth Edition, McGraw-hill, New York, 2019.
- [35] U. Beuscher, C.H. Gooding, The influence of the porous support layer of composite membranes on the separation of binary gas mixtures, *J. Membr. Sci.* 152 (1999) 99–116, [https://doi.org/10.1016/S0376-7388\(98\)00205-1](https://doi.org/10.1016/S0376-7388(98)00205-1).
- [36] J.R. Welty, C.E. Wicks, R.E. Wilson, G.L. Rorrer, *Fundamentals of Momentum, Heat, and Mass Transfer*, 5th ed., John Wiley & Sons Inc, Oregon, 2008.
- [37] E.N. Fuller, P.D. Schettler, J.C. Giddings, A new method for prediction of binary gas-phase diffusion coefficients, *Ind. Eng. Chem.* 58 (5) (1966) 18–27, <https://doi.org/10.1021/ie50677a007>.
- [38] H. Kreulen, C.A. Smolders, G.F. Versteeg, W.P.M. Van Swaaij, Determination of mass transfer rates in wetted and non-wetted microporous membranes, *Chem. Eng. Sci.* 48 (1993) 2093–2102, [https://doi.org/10.1016/0009-2509\(93\)80084-4](https://doi.org/10.1016/0009-2509(93)80084-4).
- [39] E.L. Cussler, *Mass transfer in fluid systems*, Cambridge University Press, 1984.
- [40] P.T. Nguyen, E. Lasseugette, Y. Medina-Gonzalez, J.C. Remigy, D. Roizard, E. Favre, A dense membrane contactor for intensified CO₂ gas/liquid absorption in post-combustion capture, *J. Membr. Sci.* 377 (1-2) (2011) 261–272, <https://doi.org/10.1016/j.memsci.2011.05.003>.
- [41] V. Oldani, G. Sergi, C. Pirola, B. Sacchi, C.L. Bianchi, Sol-gel hybrid coatings containing silica and a perfluoropolyether derivative with high resistance and anti-fouling properties in liquid media, *J. Fluor. Chem.* 188 (2016) 43–49, <https://doi.org/10.1016/j.jfluchem.2016.06.005>.
- [42] A. Dutta, X. Li, J. Lee, Dissolved methane recovery from anaerobically treated wastewaters using solvent-based membrane contactor: An experimental and modelling study, *Sep. Purif. Technol.* 258 (2021) 118004, <https://doi.org/10.1016/j.seppur.2020.118004>.
- [43] P. Sanchis-Perucho, Á. Robles, F. Durán, J. Ferrer, A. Seco, PDMS membranes for feasible recovery of dissolved methane from AnMBR effluents, *J. Membr. Sci.* 604 (2020) 1–12, <https://doi.org/10.1016/j.memsci.2020.118070>.
- [44] M. Henares, M. Izquierdo, P. Marzal, V. Martínez-Soria, Demethanization of aqueous anaerobic effluents using a polydimethylsiloxane membrane module: Mass transfer, fouling and energy analysis, *Sep. Purif. Technol.* 186 (2017) 10–19, <https://doi.org/10.1016/j.seppur.2017.05.035>.
- [45] M. Henares, M. Izquierdo, J.M. Peña-Roja, V. Martínez-Soria, Comparative study of degassing membrane modules for the removal of methane from Expanded Granular Sludge Bed anaerobic reactor effluent, *Sep. Purif. Technol.* 170 (2016) 22–29, <https://doi.org/10.1016/j.seppur.2016.06.024>.
- [46] X. Tan, G. Capar, K. Li, Analysis of dissolved oxygen removal in hollow fibre membrane modules: Effect of water vapour, *J. Membr. Sci.* 251 (1–2) (2005) 111–119, <https://doi.org/10.1016/j.memsci.2004.11.005>.
- [47] L.A. Hoover, J.D. Schiffman, M. Elimelech, Nanofibers in thin-film composite membrane support layers: Enabling expanded application of forward and pressure retarded osmosis, *Desalination*. 308 (2013) 73–81, <https://doi.org/10.1016/j.desal.2012.07.019>.
- [48] Yu Chang Kim, Menachem Elimelech, Adverse impact of feed channel spacers on the performance of pressure retarded osmosis, *Environ. Sci. Technol.* 46 (8) (2012) 4673–4681, <https://doi.org/10.1021/es3002597>.
- [49] S. Wongchitphimon, W. Rongwong, C.Y. Chuah, R. Wang, T.H. Bae, Polymer-fluorinated silica composite hollow fiber membranes for the recovery of biogas dissolved in anaerobic effluent, *J. Membr. Sci.* 540 (2017) 146–154, <https://doi.org/10.1016/j.memsci.2017.06.050>.
- [50] A.J. Gijsbertsen-Abrahamse, E.R. Cornelissen, J.A.M.H. Hofman, Fiber failure frequency and causes of hollow fiber integrity loss, *Desalination*. 194 (1-3) (2006) 251–258, <https://doi.org/10.1016/j.desal.2005.11.010>.
- [51] Amy E. Childress, Pierre Le-Clech, Joanne L. Daugherty, Caifeng Chen, Greg L. Leslie, Mechanical analysis of hollow fiber membrane integrity in water reuse applications, *Desalination*. 180 (1-3) (2005) 5–14, <https://doi.org/10.1016/j.desal.2004.12.026>.
- [52] G.S.M.D.P. Sethunga, J. Lee, R. Wang, T.H. Bae, Influence of membrane characteristics and operating parameters on transport properties of dissolved methane in a hollow fiber membrane contactor for biogas recovery from anaerobic effluents, *J. Membr. Sci.* 589 (2019), 117263, <https://doi.org/10.1016/j.memsci.2019.117263>.
- [53] M. Henares, P. Ferrero, P. San-Valero, V. Martínez-Soria, M. Izquierdo, Performance of a polypropylene membrane contactor for the recovery of dissolved methane from anaerobic effluents: Mass transfer evaluation, long-term operation and cleaning strategies, *J. Membr. Sci.* 563 (2018) 926–937, <https://doi.org/10.1016/j.memsci.2018.06.045>.
- [54] S.R. Wickramasinghe, Michael J. Semmens, E.L. Cussler, Mass transfer in various hollow fiber geometries, *J. Membr. Sci.* 69 (3) (1992) 235–250, [https://doi.org/10.1016/0376-7388\(92\)80042-I](https://doi.org/10.1016/0376-7388(92)80042-I).
- [55] S. Kartohardjono, A. Rabekka, *Combination Vacuum and Sweep Gas Processes to Remove Dissolved Oxygen from Water through Hollow Fiber Membrane Contactors*, *J. Mater. Sci. Eng. A* 1 (2011) 812–818.
- [56] R. Wang, H.Y. Zhang, P.H.M. Feron, D.T. Liang, Influence of membrane wetting on CO₂ capture in microporous hollow fiber membrane contactors, *Sep. Purif. Technol.* 46 (1-2) (2005) 33–40, <https://doi.org/10.1016/j.seppur.2005.04.007>.
- [57] P. Velasco, V. Jegatheesan, K. Thangavadeivel, M. Othman, Y. Zhang, A focused review on membrane contactors for the recovery of dissolved methane from anaerobic membrane bioreactor (AnMBR) effluents, *Chemosphere*. 278 (2021) 1–20, <https://doi.org/10.1016/j.chemosphere.2021.130448>.
- [58] Y. Xu, K. Goh, R. Wang, T.H. Bae, A review on polymer-based membranes for gas-liquid membrane contacting processes: Current challenges and future direction, *Sep. Purif. Technol.* 229 (2019) 1–19, <https://doi.org/10.1016/j.seppur.2019.115791>.
- [59] S. Alex, F. Biasotto, P.R. Rout, P. Bhunia, Membrane contactors: an overview of their applications, *ResearchGate* (2017). <https://cutt.ly/6RSy66p>.
- [60] R. Klaassen, P.H.M. Feron, A.E. Jansen, Membrane contactors in industrial applications, *Chem. Eng. Res. Des.* 83 (3) (2005) 234–246, <https://doi.org/10.1205/cherd.04196>.

Supplementary Material for

Recovery of dissolved methane through a flat sheet module with PDMS, PP and PVDF membranes

R. Jiménez-Robles^a, C. Gabaldón^a, J.D. Badia^b, M. Izquierdo^a, V. Martínez-Soria^{a*}

^aResearch Group in Environmental Engineering (GI²AM), ^bResearch Group in Material Technology and Sustainability (MATS), Department of Chemical Engineering, School of Engineering, University of Valencia, Avda. Universitat s/n, 46100 Burjassot, Spain.

*e-mail: Vicente.Mtnez-Soria@uv.es. Phone: +34 963 54 31 69.

S1. Effect of liquid-gas flow configuration on performance

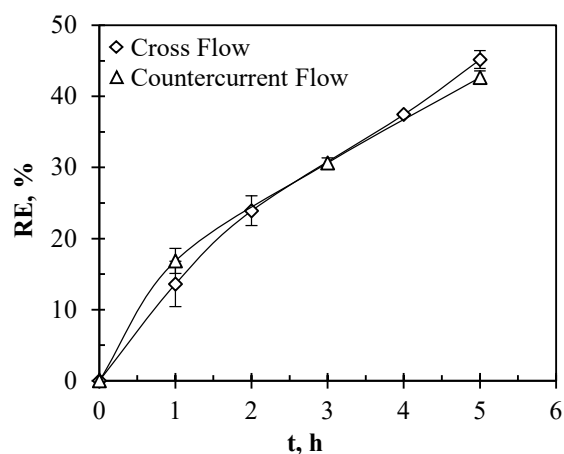


Fig. S 1. Dissolved methane removal efficiency (RE, %) versus time on stream in degassing tests for different liquid-gas flow configurations with PDMS at liquid and sweep gas flow rate of 21.0 L h^{-1} and 4.0 L h^{-1} , respectively.

S2. Derivation of the equation for the experimental overall mass transfer coefficient

Experimental overall mass transfer coefficient ($K_{L,exp}$, $m\ s^{-1}$) can be calculated from the Fick's First Law [1,2]:

$$J_{CH_4} = K_{L,exp} \cdot \Delta C_L \quad (\text{Eq. S1})$$

where J_{CH_4} ($kg\ m^{-2}\ s^{-1}$) is the CH_4 flux through the membrane and ΔC_L represents the driving force for CH_4 transport calculated based on the liquid phase.

In our system, a mass balance for methane in the liquid phase can be defined as follow:

$$J_{CH_4} = -\frac{1}{A} \frac{dM_{CH_4}}{dt} \quad (\text{Eq. S2})$$

$$-\frac{dM_{CH_4}}{dt} = \frac{M_T}{\rho_b} \frac{d\Delta C_L}{dt} + \frac{\Delta C_L}{\rho_b} \frac{dM_T}{dt} \quad (\text{Eq. S3})$$

where M_{CH_4} (kg) is the CH_4 mass, M_T (kg) is the total mass of the treated water, A (m^2) is the effective membrane area, t (s) is the time on stream of the degasification test and ρ_b ($kg\ m^{-3}$) is the density of the liquid stream. M_T was assumed constant due to the small quantity of dissolved CH_4 recovered ($< 52\ mg$) respect to the total mass of water in the system (2.35 kg). In addition, ρ_b may be assumed equal to water density (ρ_w , $1000\ kg\ m^{-3}$) due to the low dissolved CH_4 concentration. Thus, Eq. S1, Eq. S2 and Eq. S3 can be combined resulting in the following differential equation:

$$-\frac{M_T}{\rho_w} \frac{d\Delta C_L}{dt} = A \cdot K_{L,exp} \cdot \Delta C_L \quad (\text{Eq. S4})$$

The driving force based on liquid phase can be defined as $\Delta C_L = C_L - C_L^*$, where C_L and C_L^* ($mg\ L^{-1} \equiv g\ m^{-3}$) are the CH_4 concentration in the liquid feed and in the liquid in equilibrium with the CH_4 content in the outlet gas, respectively. Assuming a constant membrane permeability for methane ($K_{L,exp} \approx \text{constant}$), the integration of the differential equation Eq. S4 results as follow:

$$-\int_{\Delta C_0}^{\Delta C_t} \frac{d\Delta C_L}{\Delta C_L} = \frac{K_{L,\text{exp}} \cdot A \cdot \rho_w}{M_T} \int_0^t dt \quad (\text{Eq. S5})$$

$$K_{L,\text{exp}} = \frac{M_T}{A \cdot \rho_w \cdot t} \cdot \ln \left(\frac{C_{L0} - C_{L0}^*}{C_{Lt} - C_{Lt}^*} \right) \quad (\text{Eq. S6})$$

Although, in most of the experiments, where $C_L \gg C_L^*$, this equation could be simplified to:

$$K_{L,\text{exp}} = \frac{M_T}{A \cdot \rho_w \cdot t} \cdot \ln \left(\frac{C_{L0}}{C_{Lt}} \right) \quad (\text{Eq. S7})$$

S3. Contact angle images

Static water contact angle measurements were carried out for pristine PDMS, PP-1E, PP-2EHF and PVDF in order to determine their hydrophobicity and monitor their superficial and structural stability.

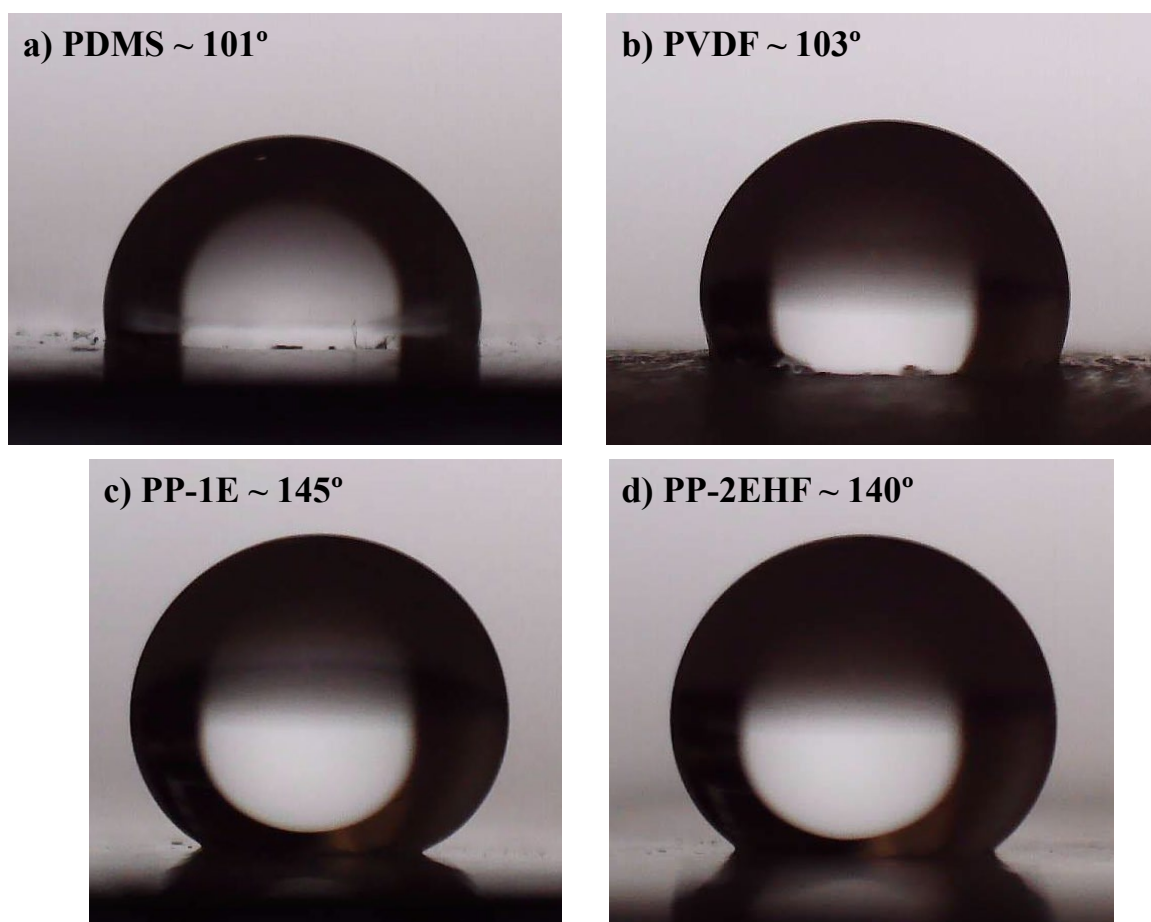


Fig. S 2. Water droplets for static contact angle measurements for pristine a) PDMS, b) PVDF, c) PP-1E and d) PP-2EHF.

S4. Effect of the time on stream and nitrogen flow rate on the methane flux and dissolved methane concentration

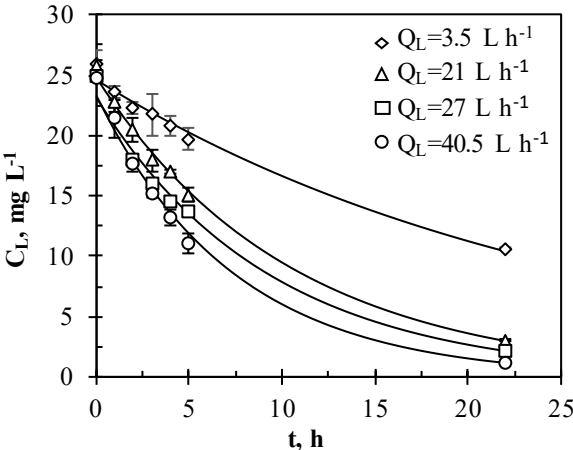


Fig. S 3. Dissolved methane concentration (C_L) in the liquid stream versus time on stream at different liquid flow rates (Q_L) at a constant nitrogen flow rate (Q_{N2}) of 0.5 L h^{-1} in degassing tests carried out with PDMS.

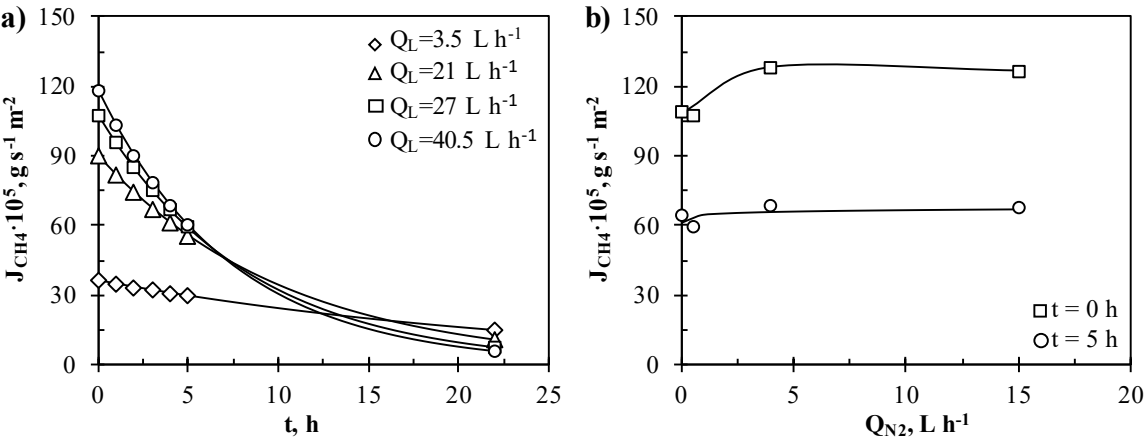


Fig. S 4. Methane flux versus a) time on stream at different liquid flow rates (Q_L) and at constant nitrogen flow rate (Q_{N2}) of 0.5 L h^{-1} and b) Q_{N2} at different time on stream and at constant Q_L of 27 L h^{-1} in degassing tests carried out with PDMS.

S5. Effect of sweep gas flow rate on removal efficiency for microporous PP-1E

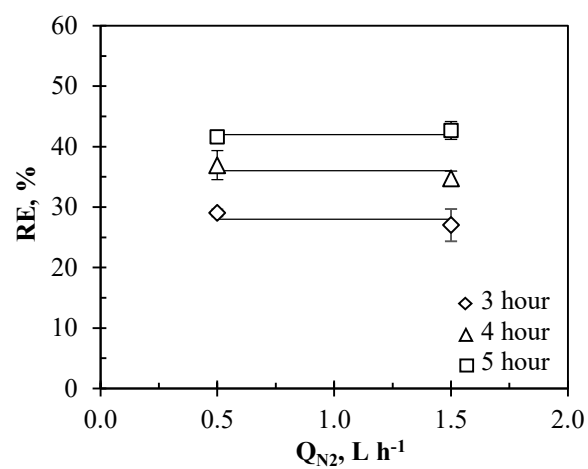


Fig. S 5. Dissolved methane removal efficiency (RE, %) versus sweep gas flow rate (Q_{N_2} , L h⁻¹) at different time on stream and at a constant liquid flow rate (Q_L) of 21 L h⁻¹ in degassing tests carried out with PP-1E.

S6. Effect of sweep gas flow rate on methane content for PDMS

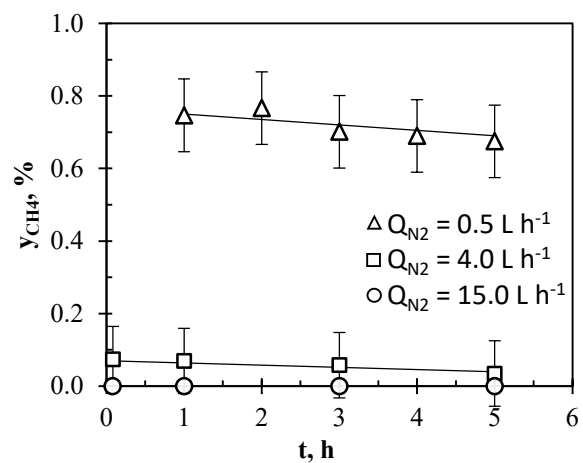


Fig. S 6. Methane content (y_{CH_4} , %) versus time on stream of degassing tests at different sweep gas flow rates (Q_{N_2} , $L h^{-1}$) with PDMS at a constant liquid flow rate (Q_L) of 3.5 L h^{-1} .

S7. Effect of membrane material on methane content

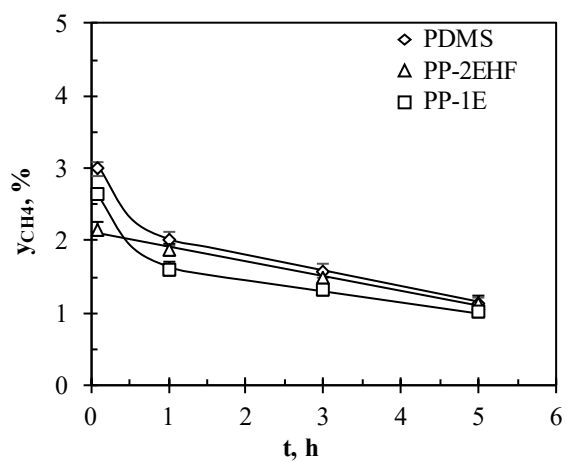


Fig. S 7. Methane content (y_{CH_4} , %) in the recovered gas versus time on stream of degassing tests with different membranes at a liquid (Q_L , $L h^{-1}$) and sweep gas flow rate (Q_{N_2} , $L h^{-1}$) of 21.0 and 3.5 $L h^{-1}$, respectively.

S8. Effect of membrane structural changes on methane removal efficiency

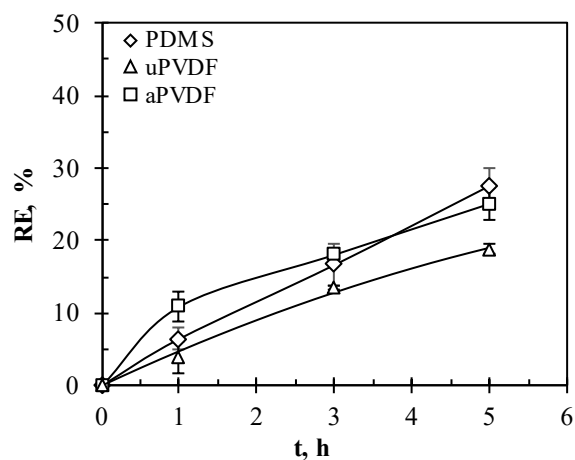


Fig. S 8. Dissolved methane removal efficiency (RE, %) versus time on stream in degassing tests for PDMS, unaltered PVDF (uPVDF) and altered PVDF (aPVDF) at liquid (Q_L) and sweep gas (Q_{N_2}) flow rates of 3.5 L h^{-1} and 4.0 L h^{-1} , respectively. aPVDF was operated during at least 5 hours at Q_L of 21.0 L h^{-1} before the experiment.

S9. Microscopy analysis on PDMS and PVDF

Morphology of the membrane surface and membrane cross-section were analysed using a Field Emission Scanning Electron Microscopy (FESEM) equipped with an Energy Dispersive X-ray Spectroscopy (EDX) and applying a voltage of 20 kV (Hitachi S4800, Hitachi Ltd., Japan). For image acquisition, the sample surfaces were coated with a fine layer of Au/Pd by sputtering for 1 minute.

FESEM-EDX analysis was carried out on pristine PDMS and on altered PDMS after 95 hours of time of use with a liquid flow rate (Q_L) of 21.0 L h⁻¹ (Fig. S and Fig. S). Cleavages and delamination were observed on the altered PDMS.

Also, FESEM-EDX analysis was carried out on pristine PVDF and on altered PVDF (aPVDF) after 150 hours of time of use with a liquid flow rate (Q_L) of 21.0 L h⁻¹ (Fig. S and Fig. S). A less porous surface was observed on the aPVDF attributed to a permanent deformation. Changes inside the membrane can be also observed.

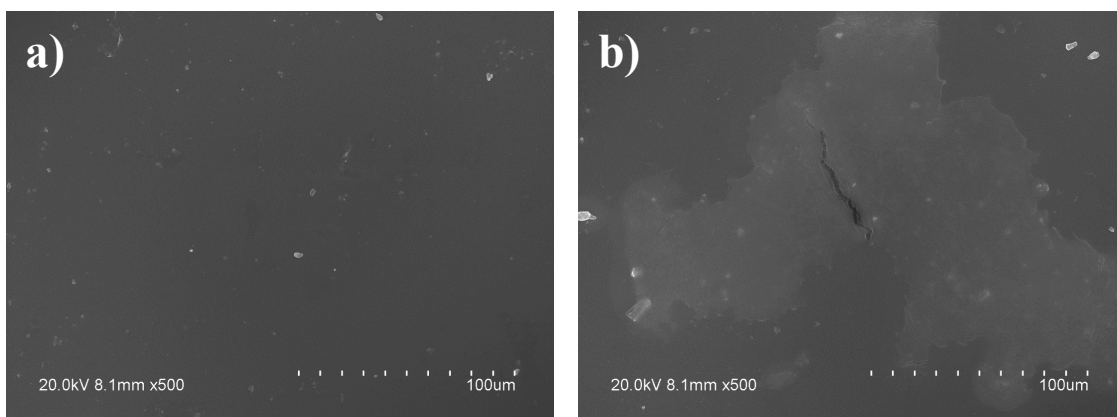


Fig. S 9. Superficial FESEM images of the a) pristine-unaltered and b) altered PDMS membrane. Altered PDMS was operated 95 hours at a liquid flow rate (Q_L) of 21.0 L h⁻¹ before the image acquisition.

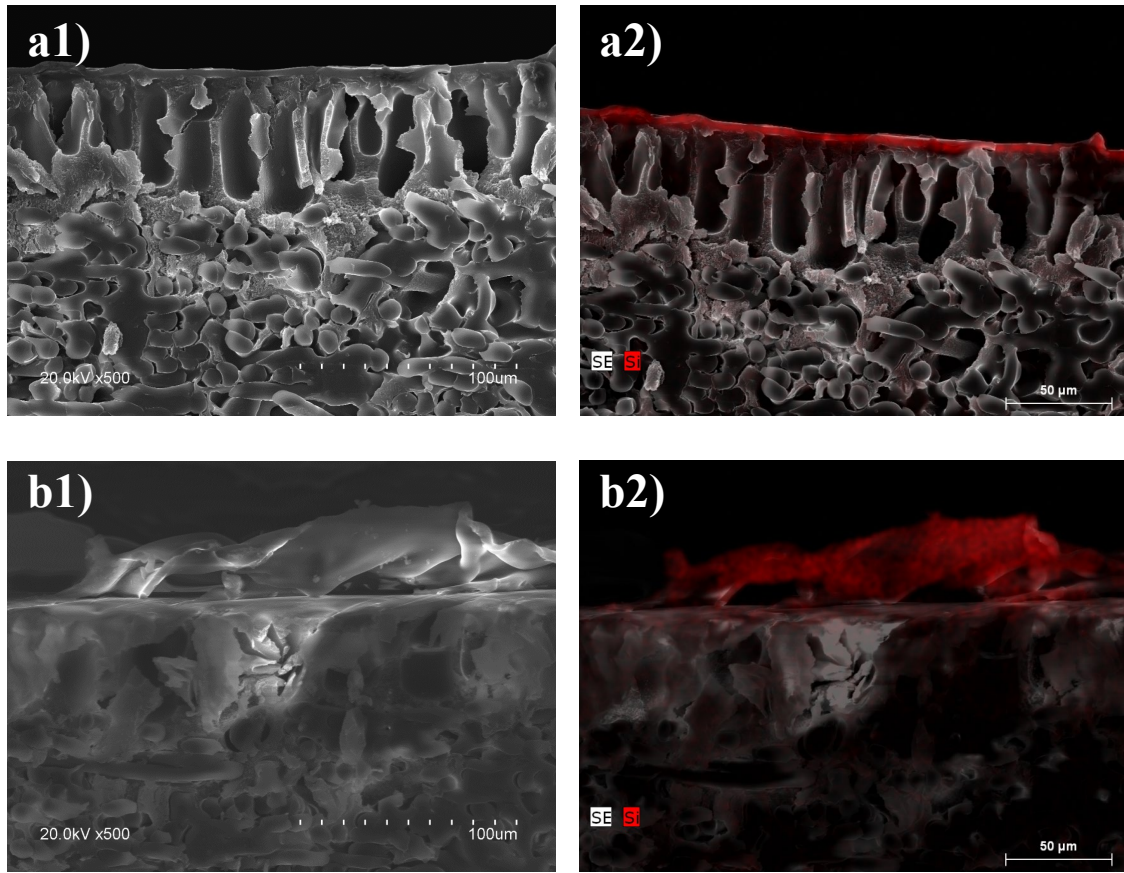


Fig. S 10. Cross section FESEM images and EDX analysis of the pristine-unaltered PDMS, a1) and a2), and altered PDMS, b1) and b2). Altered PDMS was operated 95 hours at a liquid flow rate (Q_L) of 21.0 L h^{-1} before the image acquisition.

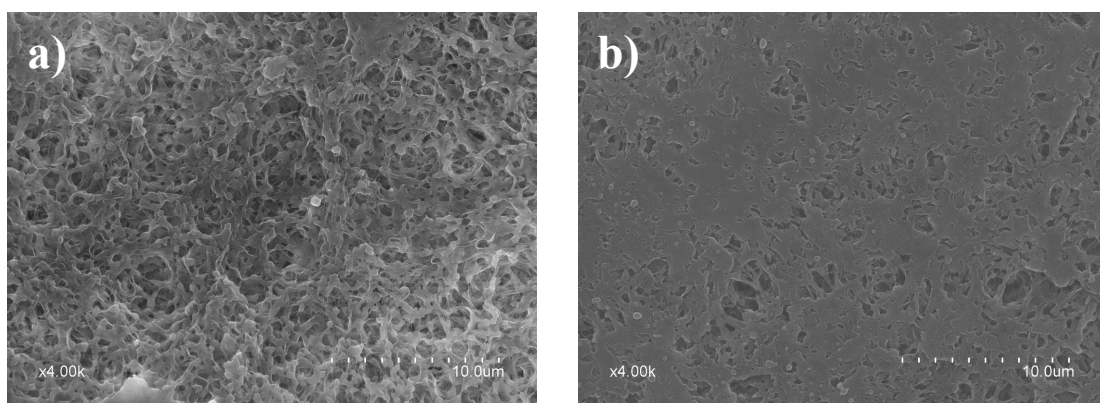


Fig. S 11. Superficial FESEM images of the a) pristine-unaltered and b) altered PVDF. Altered PVDF was operated 150 hours at a liquid flow rate (Q_L) of 21.0 L h^{-1} before the image acquisition.

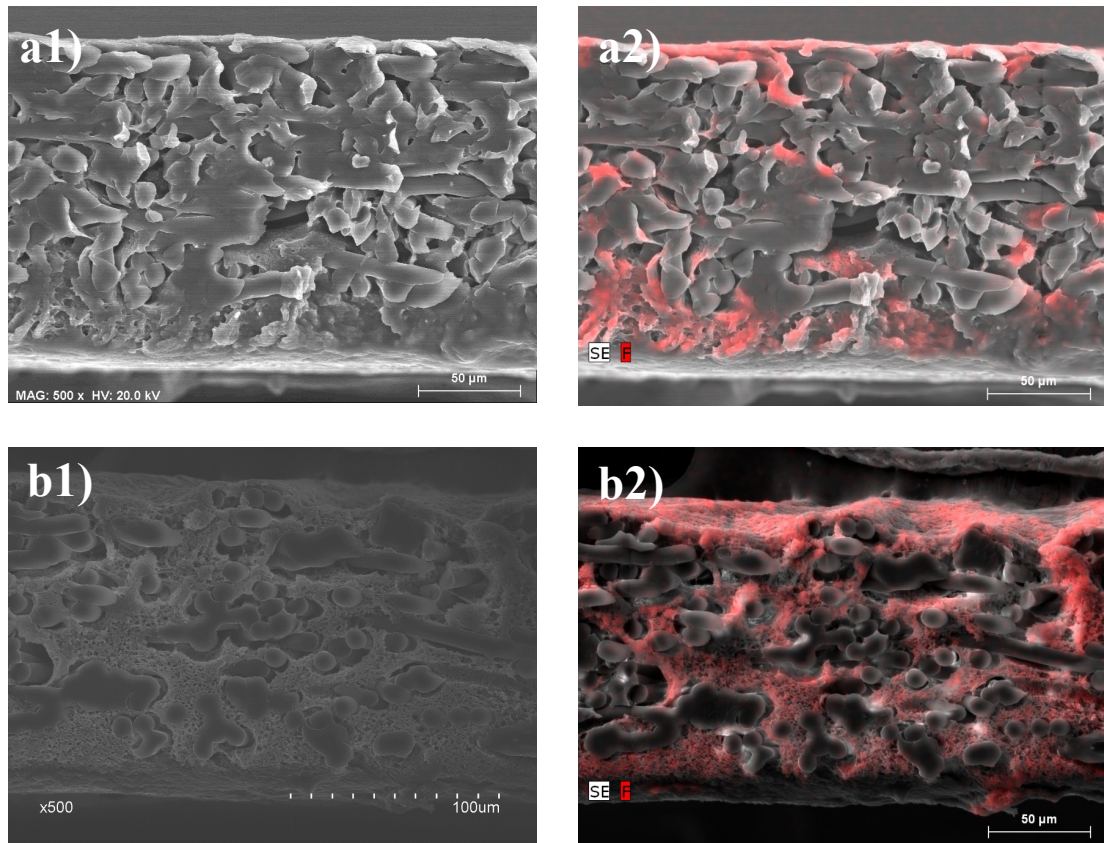


Fig. S 12. Cross section FESEM images and EDX analysis of the pristine-unaltered PVDF, a1) and a2), and altered PVDF, b1) and b2). Altered PVDF was operated 150 hours at a liquid flow rate (Q_L) of 21.0 L h⁻¹ before the image acquisition.

S10. Mass transfer coefficients

Table S1. Mass transfer coefficients at different liquid (Q_L) and sweep gas flow rates (Q_{N_2}) for dense PDMS and microporous PP-1E, PP-2EHF and unaltered PVDF (uPVDF) and altered PVDF (aPVDF). Estimated ($K_{L,est}$) and experimental ($K_{L,exp}$) overall mass transfer coefficients and estimated individual mass transfer coefficients of liquid, membrane and gas phase (k_L , k_m and k_G , respectively) are presented. aPVDF was operated during at least 5 hours at Q_L of 21.0 $L h^{-1}$ before the experiment.

Membrane	Q_L , $L h^{-1}$	Q_{N_2} , $L h^{-1}$	$k_{G,est} \cdot 10^5$ $m s^{-1}$	$k_{m,est} \cdot 10^5$ $m s^{-1}$	$k_{L,est} \cdot 10^5$ $m s^{-1}$	$K_{L,est} \cdot 10^5$ $m s^{-1}$	$K_{L,exp} \cdot 10^5$ $m s^{-1}$
PDMS	27.0	0.05	369.29	29.85	5.03	5.00	4.97 ± 0.18
	3.5	0.50	371.89	29.85	2.25	2.24	2.12 ± 0.18
	21.0	0.50	371.89	29.85	4.54	4.53	4.43 ± 0.24
	27.0	0.50	371.89	29.85	5.03	5.00	4.65 ± 0.20
	40.5	0.50	371.89	29.85	5.87	5.82	6.28 ± 0.18
	27.0	1.50	373.52	29.85	5.03	5.00	5.42 ± 0.12
	27.0	4.00	376.50	29.85	5.03	5.00	4.80 ± 0.18
	27.0	15.00	402.78	29.85	5.03	5.00	4.63 ± 0.18
	3.5	4.00	376.50	29.85	2.25	2.24	2.53 ± 0.14
	21.0	4.00	376.50	29.85	4.54	4.53	4.36 ± 0.24
PP-2EHF	21.0	0.50	371.89	911.45	4.54	4.53	4.59 ± 0.18
PP-1E	21.0	0.50	371.89	1549.46	4.54	4.53	4.05 ± 0.18
	21.0	1.50	373.52	1549.46	4.54	4.53	4.19 ± 0.18
uPVDF	3.5	4.00	376.50	4247.33	2.25	2.24	1.66 ± 0.14
	10.0	4.00	376.50	4247.33	3.41	3.41	3.02 ± 0.18
	21.0	4.00	376.50	4247.33	4.54	4.53	3.70 ± 0.18
aPVDF	3.5	4.00	376.50	4247.33	2.25	2.24	2.18 ± 0.10
	21.0	4.00	376.50	4247.33	4.54	4.53	4.97 ± 0.18

References

- [1] M. Bennett, B.J. Brisdon, R. England, R.W. Field, Performance of PDMS and organofunctionalised PDMS membranes for the pervaporative recovery of organics from aqueous streams, *J. Memb. Sci.* 137 (1997) 63–88. [https://doi.org/10.1016/S0376-7388\(97\)00183-X](https://doi.org/10.1016/S0376-7388(97)00183-X).

- [2] P. Sanchis-Perucho, Á. Robles, F. Durán, F. Rogalla, J. Ferrer, A. Seco, Widening the applicability of AnMBR for urban wastewater treatment through PDMS membranes for dissolved methane capture: Effect of temperature and hydrodynamics, *J. Environ. Manage.* 287 (2021) 1–11. <https://doi.org/10.1016/j.jenvman.2021.112344>.

APPENDIX II: CONTRIBUTION II.

The contribution entitled “*Flat PVDF membrane with enhanced hydrophobicity through alkali activation and organofluorosilanisation for dissolved methane recovery*” is presented in this Appendix. This work corresponds with the main results and conclusions discussed in section 4.2. The details of the resulting paper are listed below:

Title	Flat PVDF membrane with enhanced hydrophobicity through alkali activation and organofluorosilanisation for dissolved methane recovery
Authors	Ramón Jiménez-Robles ^a , Beatriz María Moreno-Torrallbo ^b , José David Badia ^b , Vicente Martínez-Soria ^a , Marta Izquierdo ^a
Affiliation	^a Research Group in Environmental Engineering (GI2AM), ^b Research Group in Materials Technology and Sustainability (MATS), both from Department of Chemical Engineering, School of Engineering, University of Valencia, Avda. Universitat s/n, 46100 Burjassot, Spain
Journal	Membranes
Year	2022
Volume	12
Issue	4
Number	426
DOI	10.3390/ membranes12040426
Cite	R. Jiménez-Robles, B.M. Moreno-Torrallbo, J.D. Badia, V. Martínez-Soria, M. Izquierdo, Flat PVDF membrane with enhanced hydrophobicity through alkali activation and organofluorosilanisation for dissolved methane recovery, Membranes. 12 (2022) 426. https://doi.org/10.3390/membranes12040426

The Journal Impact Factor (JIF) in the in the year of publication was 4.2, and the JIF rank was 47/140 in the category of Chemical Engineering (Q2 second quartile) and 25/86 in the category of Polymer Science (Q2 quartile).

Article

Flat PVDF Membrane with Enhanced Hydrophobicity through Alkali Activation and Organofluorosilanisation for Dissolved Methane Recovery

Ramón Jiménez-Robles ¹, Beatriz María Moreno-Torralbo ², Jose David Badia ², Vicente Martínez-Soria ¹ and Marta Izquierdo ^{1,*}

¹ Research Group in Environmental Engineering (GI2AM), Department of Chemical Engineering, School of Engineering, University of Valencia, Avda. Universitat s/n, 46100 Burjassot, Spain; ramon.jimenez@uv.es (R.J.-R.); vmsoria@uv.es (V.M.-S.)

² Research Group in Materials Technology and Sustainability (MATS), Department of Chemical Engineering, School of Engineering, University of Valencia, Avda. Universitat s/n, 46100 Burjassot, Spain; bmmortor@itq.upv.es (B.M.M.-T.); jose.badia@uv.es (J.D.B.)

* Correspondence: marta.izquierdo-sanchis@uv.es; Tel.: +34-963-543-737; Fax: +34-963-544-898

Abstract: A three-step surface modification consisting of activation with NaOH, functionalisation with a silica precursor and organofluorosilane mixture (FSi_T), and curing was applied to a poly(vinylidene fluoride) (PVDF) membrane for the recovery of dissolved methane (D-CH₄) from aqueous streams. Based on the results of a statistical experimental design, the main variables affecting the water contact angle (WCA) were the NaOH concentration and the FSi_T ratio and concentration used. The maximum WCA of the modified PVDF (mPVDF_{max}) was >140° at a NaOH concentration of 5%, an FSi_T ratio of 0.55 and an FSi_T concentration of 7.2%. The presence of clusters and a lower surface porosity of mPVDF was detected by FESEM analysis. In long-term stability tests with deionised water at 21 L h⁻¹, the WCA of the mPVDF decreased rapidly to around 105°, similar to that of pristine nmPVDF. In contrast, the WCA of the mPVDF was always higher than that of nmPVDF in long-term operation with an anaerobic effluent at 3.5 L h⁻¹ and showed greater mechanical stability, since water breakthrough was detected only with the nmPVDF membrane. D-CH₄ degassing tests showed that the increase in hydrophobicity induced by the modification procedure increased the D-CH₄ removal efficiency but seemed to promote fouling.

Keywords: anaerobic digestion; hydrophobicity; membrane stability; methane recovery; organofluorosilane; PVDF; surface modification



Citation: Jiménez-Robles, R.; Moreno-Torralbo, B.M.; Badia, J.D.; Martínez-Soria, V.; Izquierdo, M. Flat PVDF Membrane with Enhanced Hydrophobicity through Alkali Activation and Organofluorosilanisation for Dissolved Methane Recovery. *Membranes* **2022**, *12*, 426. <https://doi.org/10.3390/membranes12040426>

Academic Editor: Isabel Coelho

Received: 24 February 2022

Accepted: 11 April 2022

Published: 15 April 2022

Publisher's Note: MDPI stays neutral with regard to jurisdictional claims in published maps and institutional affiliations.



Copyright: © 2022 by the authors. Licensee MDPI, Basel, Switzerland. This article is an open access article distributed under the terms and conditions of the Creative Commons Attribution (CC BY) license (<https://creativecommons.org/licenses/by/4.0/>).

1. Introduction

Methane (CH₄) produced as biogas in anaerobic digesters is partially dissolved in the digestate, so the anaerobic reactor effluents can present high amounts of dissolved CH₄ (D-CH₄), the discharge of which causes fugitive emissions of this important greenhouse gas and biofuel. The use of membrane contactors as desorption devices for the recovery of D-CH₄ from anaerobic reactor effluents has attracted the strong interest of researchers in recent years [1–5]. As well as CH₄ degassing from aqueous streams, membrane contactors can also be used in other stripping and gas absorption processes such as CO₂ capture from flue gas or biogas streams or gas removal from aqueous solutions using transmembrane chemical absorption [6,7]. The most common industrial configuration is the hollow-fibre membrane contactor (HFMC), characterised by a high specific surface area, compactness, ease of scaling, and cost-effectiveness. Nevertheless, HFMC is easy to damage and susceptible to pore blocking owing to the stress from the liquid flux and/or the fouling phenomenon [6,8,9], and it cannot be easily repaired or refreshed which can dramatically increase the maintenance and operation costs. Although many studies have

focused on HFMCs, flat-sheet membrane modules (FMs) present several advantages related to their simplicity, versatility, and ease of cleaning and replacement, which make them attractive for use in some applications and also in investigations at a laboratory scale [8]. FMs can be especially useful where fouling or membrane stability are the focus of the research, or to facilitate the performance comparison of membrane materials with different characteristics [8,10]. The most typically used polymers for commercial membrane contactors include polydimethylsiloxane (PDMS), polysulfone (PSF), polyacrylonitrile (PAN), polypropylene (PP), polytetrafluoroethylene (PTFE), and poly(vinylidene fluoride) (PVDF). PVDF membranes have been intensively studied in recent years [11] due to their high performance and thermal, mechanical, and chemical resistance [5,12]. In addition, they present a lower raw material cost and ease of synthesis, casting, and extrusion to form different membrane configurations [12] as well as having a good thermodynamic affinity with various fluoropolymers [13].

Despite the numerous advantages of polymeric membrane contactors relative to traditional separation units, two major shortcomings are apparent when operating with membranes: wetting and fouling phenomena. In microporous membranes, the liquid pressure over the membrane surface can induce the partial or total filling of the membrane pores with the liquid phase when a critical transmembrane pressure is surpassed [5,14]. This membrane wetting increases the mass transfer resistance and, consequently, reduces the separation efficiency. Only 5% of membrane pores occupied by the liquid phase can induce an increase of around 20% in the overall mass transfer resistance [15]. The wetting resistance is influenced by membrane properties such as the pore size and distribution, roughness and, especially, the hydrophobicity of the membrane material [5,16,17]. In operation with anaerobic reactor effluents, the fouling agents contained in the stream can adhere to the membrane surface [18]. This fouling cake adds restrictions for mass transfer and can also physically and chemically deteriorate the membrane [9]. The tendency of the membrane to be fouled depends mainly on issues such as membrane hydrophobicity and roughness, the concentration of the foulants and ionic strength of the solution, and membrane module configuration, among other factors [9,18,19].

In order to overcome these shortcomings, polymer membranes can be enhanced at the synthesis step by controlling different operational conditions or by using additives to add new functionalities or change the membrane morphology [9,20]. The surface modification of existing membranes has gained a great deal of attention in recent years due to the versatility offered by the different techniques [9,12]. Surface modification techniques can be divided into physical and chemical treatments. Chemical treatments commonly involve grafting modifying agents onto the membrane by means of covalent bonding, thus achieving a stronger adhesion force. Consequently, the modifiers are less susceptible to removal from the membrane by liquid flux. Recently, surface chemical modification has focused on increasing the hydrophobicity of the membrane surface to avoid the wetting phenomenon [10,21,22]. Thus, fluorinated organic compounds and siloxanes have been developed and evaluated as modifying agents, since they are well-known to reduce surface free energy and, consequently, to increase hydrophobicity [5]. Indeed, the superhydrophobic degree (water contact angle, WCA > 150°) has been reported after surface modification with organosilanes [23]. In the case of PVDF, PTFE, or PDMS, with poor reactivity, a step prior to grafting the modifiers is needed to activate the membranes [5,12]. Different techniques, such as hydroxylation by NaOH or plasma treatment, have been evaluated, in which the membrane is subjected to an alkaline or oxygen-radical environment, respectively, in order to form active sites on the membrane (e.g., hydroxide or peroxide groups) to react further with the functionalisation agents that confer enhanced surface performance [17,24,25].

The long-term stability of the membrane during operation plays a critical role in the design of the surface modification [26]. The stress and dragging effect of a continuous liquid flux over the modified membranes in long-term operations can remove the coating in the case of physical modification or alter the surface morphology, producing a change in the

surface properties such as the hydrophobicity [8,19,27] and reducing the membrane lifetime. Reports into the evaluation of the structural and chemical stability of modified membranes after long-term operations for D-CH₄ recovery are very scarce but would provide useful preview information about the economic viability of applying membrane modification procedures at the industrial scale. The absorption of CO₂ using membrane contactors has been more widely investigated, and higher CO₂ fluxes and stability in long-term tests have been reported with modified membranes compared to non-modified membranes under different modification procedures [25,28–31].

In this context, the general aim of this work was to evaluate the effect of a chemical surface modification applied over a commercial PVDF membrane for the recovery of D-CH₄ from aqueous streams. Firstly, a statistical experimental design of a three-step modification procedure (activation, functionalisation, and curing) was proposed to optimise the surface hydrophobicity of the membrane, measured by the WCA. Then, the stability and the membrane performance in D-CH₄ recovery by modified PVDF membranes were evaluated and benchmarked with non-modified PVDF. These membranes were tested in an FM module under several operational conditions with deionised water (DW) and real anaerobic reactor effluent (AE).

2. Materials and Methods

2.1. Membrane Surface Modification Procedure

Flat-sheet PVDF membranes were supplied by Dorsan Filtration (Spain). The membrane was composed of hydrophobic PVDF supported on a polyester (PET) non-woven support, resulting in a microporous structure. The main characteristics of the membrane are reported in Table 1.

Table 1. Characteristics of the flat-sheet PVDF membrane.

Property	Value
Structure	Microporous
Support	Polyester (PET)
Thickness, μm	$159 \pm 2^{\text{a}}$
Pore diameter, μm	0.2^{b}
Porosity, %	$62 \pm 3^{\text{c}}$
Liquid entry pressure, bar	1.8^{b}
Static water contact angle, $^{\circ}$	$103.4 \pm 1.6^{\text{a}}$

^a Measured. ^b Provided by the manufacturer (Dorsan Filtration, Spain). ^c Determined by gravimetric analysis [32].

The surface modification of the PVDF was carried out in a three-step procedure: (1) activation, (2) functionalisation, and (3) curing.

In the activation step, the PVDF was hydroxylated with 2.5 mL of sodium hydroxide (NaOH) solution per cm² of membrane in an orbital shaker at 150 rpm. According to preliminary experiments (Supplementary Material S1), the temperature and time of the activation step were fixed at 50 °C and 1 h, respectively, and the NaOH concentration (NaOH%_{w/w}) ranged from 1 to 6%, as suitable for the purposes of activation. Afterwards, the activated membranes were immediately rinsed with milliQ water to stop the reaction and the excess of water on the sample surface was gently removed. In the hydroxylation reaction, the OH[−] ions replaced the F atoms from the PVDF chains, which promoted a decrease in its hydrophobicity, mainly by a defluorination mechanism [24]. The detailed reactions proposed for the modification of PVDF are shown in the Supplementary Material S2.

In the functionalisation step, the organofluorosilane 1H,1H,2H,2H-perfluorooctyltriethoxysilane (Dyn; Dynasylan[®] F8261, Evonik GmbH, Hanau-Wolfgang, Germany) and tetraethyl orthosilicate (TEOS; $\geq 99\%$, Sigma-Aldrich, Saint Louis, MI, USA) were used as modifying agent and silica precursor, respectively, to carry out the grafting of additional fluoride chains onto the PVDF. A mixture of 2-propanol (IPA; HPLC grade, VWR Chemicals, Radnor, PA, USA) and milliQ water in a molar ratio of 57:1 was used as solvent

(labelled as IPA/H₂O). For the preparation of the functionalisation solution (FS), an initial mixture of the organofluorosilane and silica precursor was prepared and then the IPA/H₂O solvent was added dropwise [27]. The presence of water in the FS was needed in order to hydrolyse the silica precursor, as reported by several authors [27,31,33,34]. Once the solvent was fully added, in order to promote the hydrolysis of the TEOS [27,34], the pH of the FS was adjusted with concentrated HCl (37 wt %, reagent grade, VWR Chemicals, Radnor, PA, USA) to a value of 2–3. Finally, the FS remained under magnetic stirring at 200 rpm at room temperature for 24 h in order to achieve the complete hydrolysis of the TEOS. The mixture of Dyn and TEOS in the FS was labelled 'FSi_T', where 'F' denotes the fluorine modifying agent Dyn and 'Si_T' the silica precursor TEOS. The volumetric ratio of the modifying agent in the FSi_T mixture (FSi_T ratio = Dyn volume/FSi_T mixture volume) ranged from 0.17 to 0.94, and the FSi_T volumetric percentage in the solvent (FSi_T%_v) ranged from 0.8 to 9.2%. The ranges of both parameters were set from the preliminary experiments shown in Supplementary Material S1. In the functionalisation step, the membrane samples were immersed in 2 mL of the FS per cm² of the membrane for 1 h at 100 rpm and room temperature and then rinsed with IPA. The reactions involved in the functionalisation are detailed in Supplementary Material S2.

Finally, for the curing step, the membrane was kept in an oven at 60 °C overnight on a Petri dish. Functionalisation and curing times were also established based on the preliminary experiments. The modified PVDF was labelled 'mPVDF' and the non-modified PVDF as 'nmPVDF'. A scheme of the membrane modification procedure is shown in Figure 1.

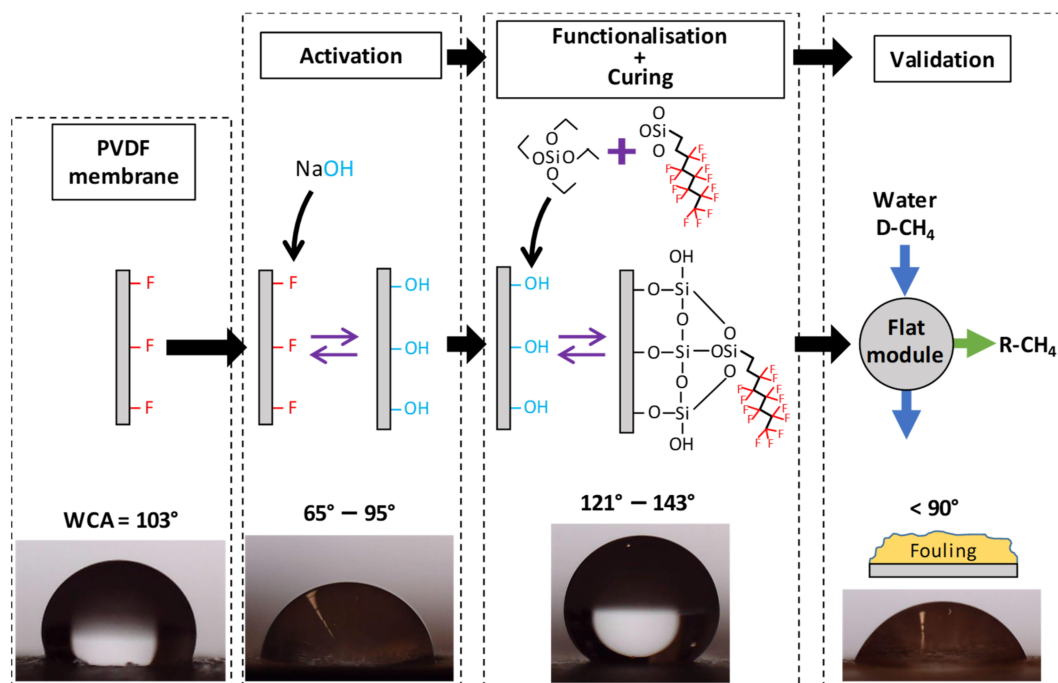


Figure 1. Scheme of the modification procedure of poly(vinylidene fluoride) (PVDF) membranes and the validation step. Water contact angle (WCA): static water contact angle; D-CH₄: methane dissolved in liquid streams; R-CH₄: methane recovered in gaseous form.

2.2. Design of Experiments and Statistical Analysis

The effect of the modification procedure on the hydrophobicity of PVDF was initially evaluated on 2 × 2-cm membrane specimens. The main variables involved in the modification procedure were analysed by means of a statistical experimental design in order to maximise the static WCA of the membrane surface. After preliminary experiments in which the activation time (1 h) and temperature (50 °C), and functionalisation and curing times (1 h and >12 h, respectively) were fixed, the main variables affecting the final

hydrophobicity of the PVDF were attributed to FSi_T ratio, FSi_T%_v, and NaOH%_{wt}. These variables (factors) were evaluated at the values (levels) shown in Table 2. A 3³ complete factorial design with the central point and corner levels was carried out in order to identify the significant effects of the factors and their interactions on the response variable, i.e., the WCA. Then, statistical analysis based on multiple linear regression and a response surface was carried out for the determination of the optimum values of the factors leading to the maximum response. This analysis included the additional axial points specified in Table 2. The different runs of the set of experiments were carried out randomly in duplicate to avoid systematic errors. The statistical software Minitab[®] (Minitab, LLC., State College, PA, USA) was used for the design of the experiments and the statistical analysis.

Table 2. Factors and levels used in the design of the experiments and statistical analysis of the modification procedure.

Independent Variables (Factors)		Levels				
		Axis (−)	Corner (−)	Central Point	Corner (+)	Axis (+)
A	FSi _T ratio	0.17	0.29	0.55	0.79	0.94
B	FSi _T % _v , %	0.8	2.4	4.6	7.2	9.2
C	NaOH% _{wt} , %	1.0	2.0	3.5	5.0	6.0

2.3. Evaluation of the Modified Membrane Performance

The performance of recovery of D-CH₄ from liquid streams and the long-term stability of both nmPVDF and mPVDF were evaluated in degassing tests and long-term tests, respectively. Experiments were carried out using DW (<1 μS cm^{−1}) and an effluent stream from an anaerobic digester for comparison purposes. The anaerobic effluent (AE) was collected from the anaerobic reactor of the urban Quart-Benager II wastewater treatment plant (Valencia, Spain) and filtered with a 10–20 μm filter before use in the tests. The pH, conductivity, alkalinity, chemical oxygen demand, and total and volatile suspended solids of the filtered AE were 7.84, 8.61 mS cm^{−1}, 2102 mg CaCO₃ L^{−1}, 414 mg O₂ L^{−1}, 75.75 mg L^{−1}, and 67.50 mg L^{−1}, respectively. A circular FM made of stainless steel with an effective contact area of 17.3 cm² was used for both performance and long-term stability tests.

2.3.1. Dissolved Methane Recovery from Water Streams

The laboratory-scale system with the FM used for the non-steady-state degassing tests was extensively described in our previous work [8] and is depicted in Figure 2. For the degassing test, a 2 L glass bottle acting as the liquid feed tank was filled initially with the liquid (DW or AE). In the first step, the liquid was saturated with 99.5%_v CH₄ (Carburos Metálicos, Barcelona, Spain) in a packed-bed absorption column in counter-current flux. The liquid stream flowed in a closed loop through the system using a peristaltic pump (Watson-Marlow Fluid Technology Solutions, Falmouth, UK), keeping the gas ports of the module closed (dashed line, Figure 2). This liquid stream reached a concentration of 20.7 ± 1.1 mg CH₄ L^{−1}. In the second step, the saturated liquid was pumped from the liquid feed tank to the FM and then recirculated continuously to the tank operating in a closed loop in order to recover the D-CH₄ (continuous line, Figure 2). The total duration of these non-steady-state experiments was 5 h, and the liquid flow rates (Q_L) were fixed at 3.5 and 21.0 L h^{−1} (liquid velocity ranging from 2.8 to 16.9 cm s^{−1}) based on our previous work [8]. All experiments were carried out in the sweep-gas mode, using a N₂ flow rate (Q_{N2}) of 4 L h^{−1} (gas velocity of 0.3 cm s^{−1}). The liquid and sweep gas flowed in a cross-flow configuration inside the FM and the experiments were conducted at room temperature (24 ± 1 °C). Removal of D-CH₄ was evaluated from liquid samples of 5 mL collected at different times during the degassing test to determine the change in D-CH₄ concentration

measured by gas chromatography. Duplicates of liquid samples were collected at the outlet of the liquid feed tank. The results reported in this paper are the removal efficiency (RE, %) and the CH_4 flux (J_{CH_4}) obtained after 5 h of experimentation. As an example, the profiles of the D- CH_4 concentration, RE, and J_{CH_4} obtained at a Q_L of 21 L h^{-1} are shown in Supplementary Material S3.

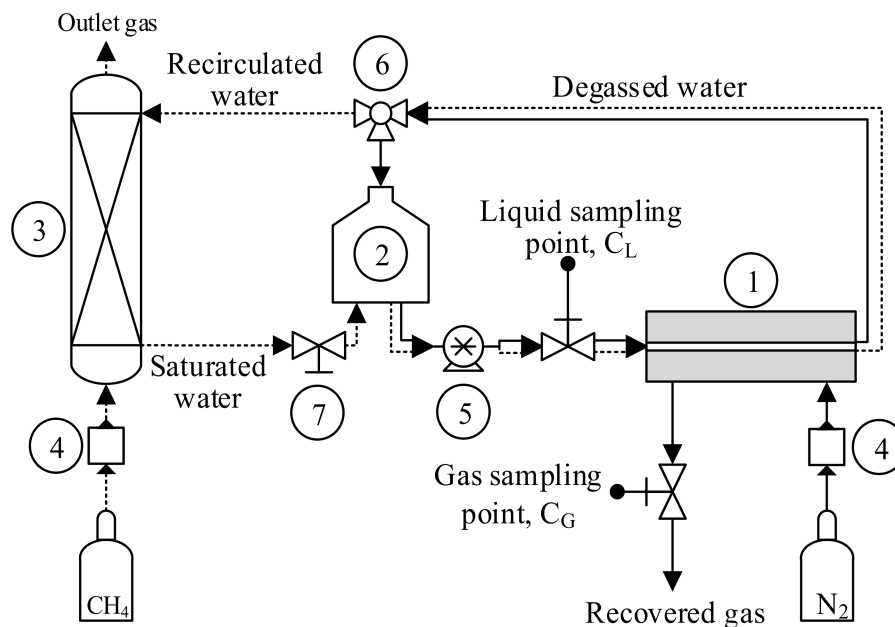


Figure 2. Scheme of the experimental system for dissolved methane degassing tests from aqueous streams with a flat-sheet membrane module. (1) membrane module, (2) liquid feed tank, (3) saturation column, (4) mass flow controller, (5) peristaltic pump, (6) 3-way valve, and (7) on/off valve.

2.3.2. Long-Term Surface Stability Tests

Experiments using DW and AE were carried out to evaluate the behaviour of the PVDF membranes during long-term operation using the former laboratory-scale system and FM. The long-term tests were carried out to evaluate the stability of the hydrophobicity of the membrane surface under a continuous liquid flux with different types of aqueous stream. Initially, the liquid feed tank was filled with DW or AE, the saturation column disconnected, and the gas ports of the FM closed for this type of test. Then, a constant water flux was applied through the liquid side of the FM in the closed loop defined by the continuous line in Figure 2. Based on our previous study [8], the long-term tests with DW were operated at the highest value of Q_L of 21 L h^{-1} until a constant WCA was reached. The long-term tests with AE were carried out at the lowest Q_L tested, 3.5 L h^{-1} , in order to promote the potential fouling deposition on the membrane for up to around 830 h. In the experiments with AE, the anaerobic water inside the system was replaced up to three times. The membrane was extracted periodically to measure its WCA in order to monitor the surface hydrophobicity with time of use, as reported in the literature [8,27,33]. Similarly, for the membranes treating the AE, the membrane performance for D- CH_4 degasification was evaluated at different times of use using AE saturated with CH_4 as the liquid stream.

2.4. Analytical Methods

The surface hydrophobicity of the membranes was evaluated by means of the WCA as mentioned above. WCA measurements were conducted by the sessile drop technique [35] of depositing a water drop of $5.5 \pm 0.1 \mu\text{L}$ onto the membrane surface using a syringe pump (KF Technology s.r.l., Rome, Italy) at room temperature ($\sim 25 \text{ }^\circ\text{C}$). An image of the water drop profile was captured at 15 s with a digital microscope (Handheld Digital Microscope Pro, Celestron LLC., Torrance, CA, USA) under white light (Philips HUE Lamp, Koninklijke Philips NV, Amsterdam, The Netherlands). ImageJ software was used for

image processing using the *Contact Angle Plug-in* based on the ellipse approximation. The WCA was evaluated at different positions on the membrane and a mean value obtained from at least four measurements. The WCA values of the wet membranes from the long-term stability tests were measured after removing excess water and evaporation of moisture at room temperature for approximately 1 h with forced aeration.

The morphology of the membrane surface and cross-section, as well as its chemical composition, were analysed by field emission scanning electron microscopy (FESEM) equipped with energy dispersive X-ray spectrometer (EDX) with an accelerating voltage of 20 kV (Hitachi S4800, Hitachi Ltd., Tokyo, Japan). For image acquisition, the samples were placed on a metal holder and then coated with a fine layer of Au/Pd by sputtering in vacuum for 1 min. FESEM was also applied to measure the membrane thickness and the surface porosity by means of the abovementioned ImageJ software [36].

The liquid samples collected from the degassing tests were analysed by the adapted head-space method described elsewhere [37–40]. Briefly, 5 mL liquid samples were collected in sealed 16 mL vials prefilled with air. These vials were allowed to reach equilibrium between phases in an orbital shaker at 200 rpm and 25 °C for 30 min. After this, 0.5 mL of head-space gas was injected into a gas chromatograph (GC 7820 A, Agilent Technologies Spain S.L., Madrid, Spain) equipped with Agilent HP-PLOT/U and Agilent HP-MOLESIEVE columns and a thermal conductivity detector to measure the CH₄ concentration in the gas phase. The CH₄ concentration in the liquid phase was calculated by applying Henry's Law, and then both the gas and liquid phase concentrations were used to calculate the concentration in the liquid sample (C_L, mg L⁻¹).

The RE of D-CH₄ (%) and CH₄ flux (J_{CH₄}, g s⁻¹ m⁻²) through the membrane were used to evaluate the performance of the D-CH₄ recovery process in the degassing tests, defined as follows:

$$RE = \frac{C_{L0} - C_{Lt}}{C_{L0}} \times 100 \quad (1)$$

$$J_{CH_4} = \frac{V_T \times 10}{A} \times \frac{dC_L}{dt} \quad (2)$$

where C_{L0} and C_{Lt} (mg L⁻¹) are the CH₄ concentrations in the liquid at the beginning and at time on stream (t) of the degassing test from the liquid feed tank, respectively; V_T is the total liquid volume in the system (2.35 L); and A (cm²) is the effective membrane area. The variation in liquid volume flow rate was assumed to be negligible for the application of Equation (1).

3. Results and Discussion

3.1. Maximisation of Membrane Hydrophobicity

A statistical experimental design evaluating the main parameters that affect the membrane surface hydrophobicity was conducted to maximise the response variable, i.e., the WCA, of the modified membranes. After the preliminary experiments (Supplementary Material S1), the variables FSi_T ratio, FSi_T%_v, and NaOH%_{wt} were found to be the main factors to be optimised. Initially, a 3³ complete factorial design was carried out in order to determine the effects of the different factors, including individual effects and those of the 2-way and 3-way interactions on the response. The effects of the factors and their interactions can be observed in the Pareto diagram of the factorial design shown in Figure 3. The critical standardised effect (2.05) was calculated from the Student's T distribution (t_{α/2,ν}) with a significance level (α) of 0.05 and 27 degrees of freedom (ν), associated with the error of the factorial design. As observed in the Pareto diagram, the standardised effect of the different factors and their interactions were higher than the critical value, except for the interaction between FSi_T ratio and FSi_T%_v. Thus, the interaction of these two factors did not seem to affect the WCA of the mPVDF and their effects could be ignored.

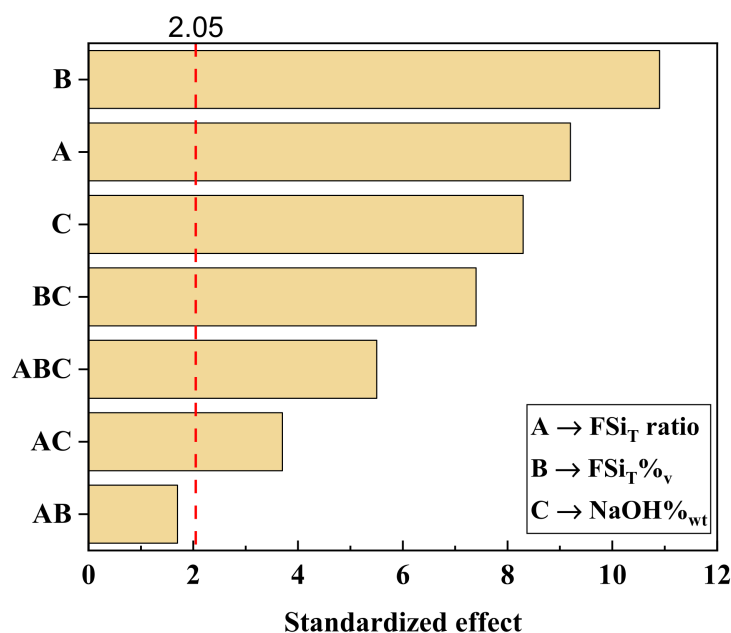


Figure 3. Pareto diagram of the standardised effects of the factors analysed in the 3^3 complete factorial design. The dashed red line represents the critical standardised effect for a significance level of 0.05.

The individual factors presented the highest effects on the response, the most important being those involved in the functionalisation step (FSi_T ratio and FSi_T%_v). This result can be understood, since the FSi_T ratio and FSi_T%_v determined the number of O–Si bonds on the PVDF chains and the total F content at the end of the functionalisation process, these resulting in higher WCA values as the F content on the surface increased. Additionally, the increase in O–Si bonds grafted onto the PVDF chains allowed reaction with higher numbers of Dyn molecules, increasing the total F content of the surface of the modified membrane. The NaOH%_{wt} also showed a high effect on the response, since this factor determined the number of active sites (OH[−]) on the PVDF chains where the silanol groups from TEOS were grafted, leading to O–Si bonds [23,25]. Consequently, the higher the NaOH%_{wt} applied, the higher the number of F atoms from the PVDF chains that were substituted by OH[−] groups, allowing a higher number of O–Si bonds and Dyn molecules to be grafted. This was in accordance with the significant standardised effect of the interaction of FSi_T ratio and FSi_T%_v with NaOH%_{wt} (ABC) observed in the Pareto diagram.

The effects of the individual factors on the response are depicted in the main-effects plot shown in Figure 4. A WCA higher than that of the nmPVDF ($103.4 \pm 1.6^\circ$) was obtained for all the modified membranes used, with an overall mean value of 131° , showing that the functionalisation procedure proposed in this work was suitable to increase the PVDF membrane hydrophobicity. The WCA clearly increased with the FSi_T%_v and NaOH%_{wt}, in accordance with the previous discussion, although NaOH%_{wt} should not be higher than 5% in order to avoid membrane degradation. In contrast, a maximum WCA was found with the variation of the FSi_T ratio, as reported by other authors [23,31]. In that case, the WCA increased initially with the FSi_T ratio until a maximum value was reached at a FSi_T ratio of around 0.55. An increase in FSi_T ratio caused a higher number of Dyn molecules to be grafted onto the PVDF chains. In contrast, a higher FSi_T led to a decrease in WCA, which could be explained by taking into account that the amount of TEOS decreased as Dyn increased, and therefore fewer O–Si bonds were formed for the subsequent grafting of Dyn molecules. Thus, a value of around 0.55 seemed to provide an appropriate number of O–Si bonds to graft the available Dyn onto the FS and avoid a large excess of unreacted Dyn.

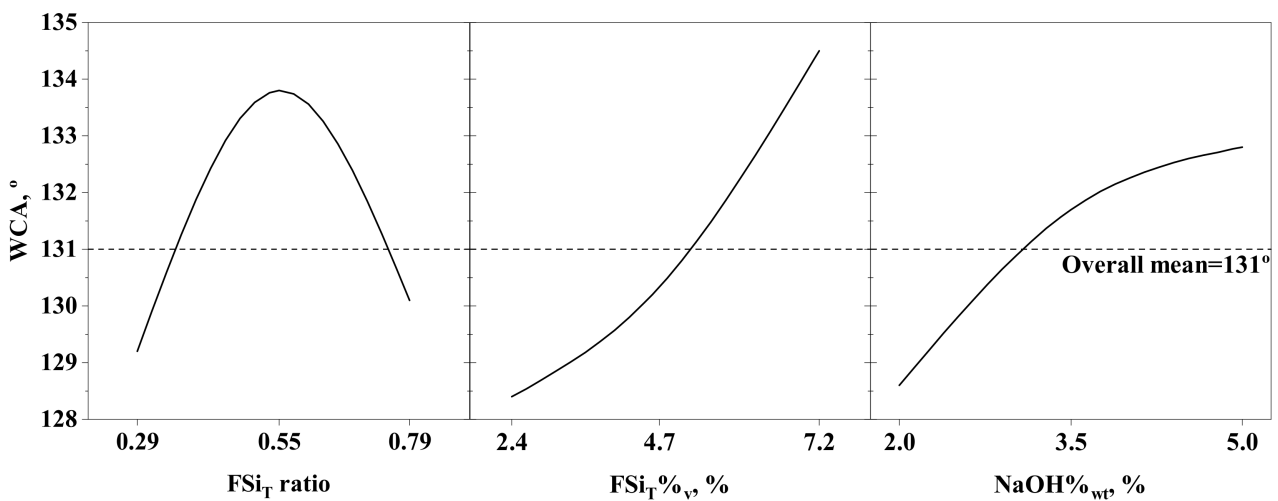


Figure 4. Main-effects plot of the factors analysed in the 3^3 complete factorial design.

After determining the main effects of the factors and their interactions with the 3^3 factorial design, a new set of experiments was conducted at the axis levels of the three factors. A statistical analysis based on response surface methodology was carried out on all the data obtained at the central point, corner, and axis levels. All these data were fitted by means of a multiple linear regression model including the linear (A, B, C), square (AA, BB, CC), 2-way interaction (AB, AC, BC), and 3-way interaction (ABC) terms. The 2-way interaction between FSi_T ratio and $FSi_T\%_v$ was also included in the model. Since large effects were observed for the individual factors (A, B, and C, Figure 3), their square terms could also present high significance in the model and were therefore included. The resulting model is represented in the form of a response surface and contour plot at a $NaOH\%_{wt}$ of 5% in Figure 5.

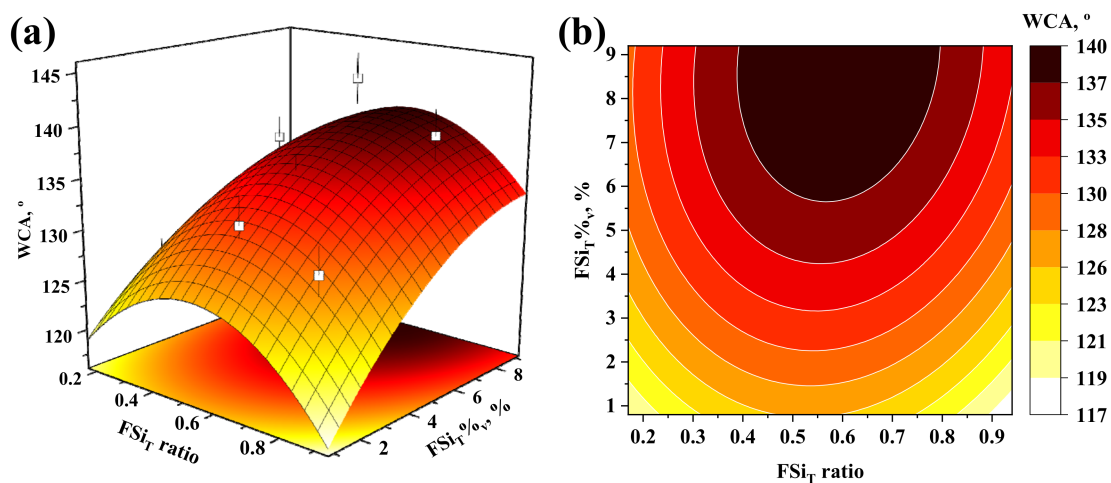


Figure 5. (a) Response surface and (b) contour plot obtained by linear regression from the overall data of the design of the experiments with a $NaOH$ concentration of 5%. Experimental values are depicted as open symbols in the response surface plot and the error bars denote the standard deviation.

Based on the model explained above, the WCA initially increased with $FSi_T\%_v$ up to a value around 6% and then remained nearly constant for a fixed FSi_T ratio. For example, the model predicted a WCA of $137\text{--}140^\circ$ for $FSi_T\%_v$ ranging from 6 to 9.2% at a constant FSi_T ratio of 0.55 with a level of confidence of 95%. Regarding the effect of the FSi_T ratio on the WCA, the predicted trend showed a maximum value of WCA at intermediate values of FSi_T ratio, as reported in the literature [23,31]. Thus, the maximum WCA values were achieved

for a FSi_T ratio of around 0.55 at any $\text{FSi}_T\%_v$ value. This trend was in accordance with the previous analysis of effects and the experimental results shown in Figure 5a (open symbols). Thus, the maximum experimental WCA obtained was $143.2 \pm 2.5^\circ$, while the model predicted a WCA of $138.8 \pm 2.2^\circ$ at an FSi_T ratio of 0.55, $\text{FSi}_T\%_v$ of 7.2%, and $\text{NaOH}\%_{wt}$ of 5%. Likewise, the maximum WCA value predicted by the model was $140.5 \pm 6.6^\circ$ at an FSi_T ratio of 0.59, $\text{FSi}_T\%_v$ of 9.2%, and $\text{NaOH}\%_{wt}$ of 6%. These results led to the conclusion that increases in FSi_T ratio, $\text{FSi}_T\%_v$, and $\text{NaOH}\%_{wt}$ over 0.55, 7.2%, and 5%, respectively, would not significantly increase the WCA and that they could be set as the optimal experimental conditions to achieve the highest hydrophobicity. The PVDF sample modified under the optimal conditions is termed hereafter as 'mPVDF_{max}'.

For the sake of benchmarking the results, the maximum WCA obtained in this work ($143.2 \pm 2.5^\circ$) represented a 39% increase from the initial value of the nmPVDF ($103.4 \pm 1.6^\circ$) and was higher than most values found in the literature for comparable surface modification approaches. The maximum WCA was obtained at a low $\text{NaOH}\%_{wt}$ (5%) with IPA as solvent, unlike the other hazardous solvents such as toluene, hexane and tetrahydrofuran reported in the literature. Similar results of WCA increase have been reported by other authors. Sairiam et al. [25] reported a maximum WCA of 119.5° (from an initial value of 68.9°) with the same modifying agent as used in this work, using hexane as solvent. They applied longer treatments, and no WCA increase for the modified membranes was reported with $\text{NaOH}\%_{wt}$ higher than 10%. Wongchitphimon et al. [31] found a maximum WCA of 127.8° for modified PVDF (from an initial value of 95.5°) at a $\text{NaOH}\%_{wt}$, activation time, and temperature of 10%, 1 h, and 60°C , respectively, and functionalised with the commercial organofluorosilane Fluorolink[®] S10 (FS10) at a FSi_T concentration of 5% and a ratio of FS10 to TEOS of 3:2 using toluene as solvent. In addition, they suggested destruction of the membrane integrity, since they reported a final WCA decrease and an increase in pore size at activation times higher than 1 h and a $\text{NaOH}\%_{wt}$ of 10%. Moreover, Sethunga et al. [21] obtained a modified PVDF with a maximum WCA of 111.7° (from an initial value of 84.5°) with a somewhat lower $\text{NaOH}\%_{wt}$ (pH = 10) and activation and functionalisation times of 0.5 and 1.5 h using Fluorolink[®] S10 and toluene as modifying agent and solvent, respectively. They also reported a final WCA decrease with an increase in $\text{NaOH}\%_{wt}$ and activation time, suggesting a conversion of the hydroxide groups to carbonyl groups that hindered the attachment of TEOS [21]. The maximum value was reported by Zheng et al. [23], with a maximum WCA of 157° (from an initial value of 89°) under more severe activation conditions with a $\text{NaOH}\%_{wt}$ of 30% and an activation time of 3 h and using organosilanes free of fluorine groups at a concentration of around 25% in the FS and toluene as solvent.

3.2. Structure and Chemical Composition of the Modified PVDF

An inspection of the surface and cross-section of nmPVDF and mPVDF_{max} was carried out by means of a FESEM analysis. The nmPVDF presented a homogenous surface with a high surface porosity of around 55% (Figure 6a). The effect of membrane modification resulted in a heterogeneous surface with porous zones and zones with dense and smooth clusters (Figure 6b) and less surface porosity of around 27%. Similar observations have been reported by other authors [23,25]. This can be attributed mainly to a coating-like effect of the polymerisation/condensation of the FSi_T components (TEOS and Dyn) on the surface leading to a higher hydrophobicity. Thus, these observations led to the conclusion that the homogeneous distribution and availability of the OH^- groups on the PVDF chains are critical factors for the grafting and condensation of the FSi_T in order to promote a homogeneous surface, since the OH^- groups act as active sites [21].

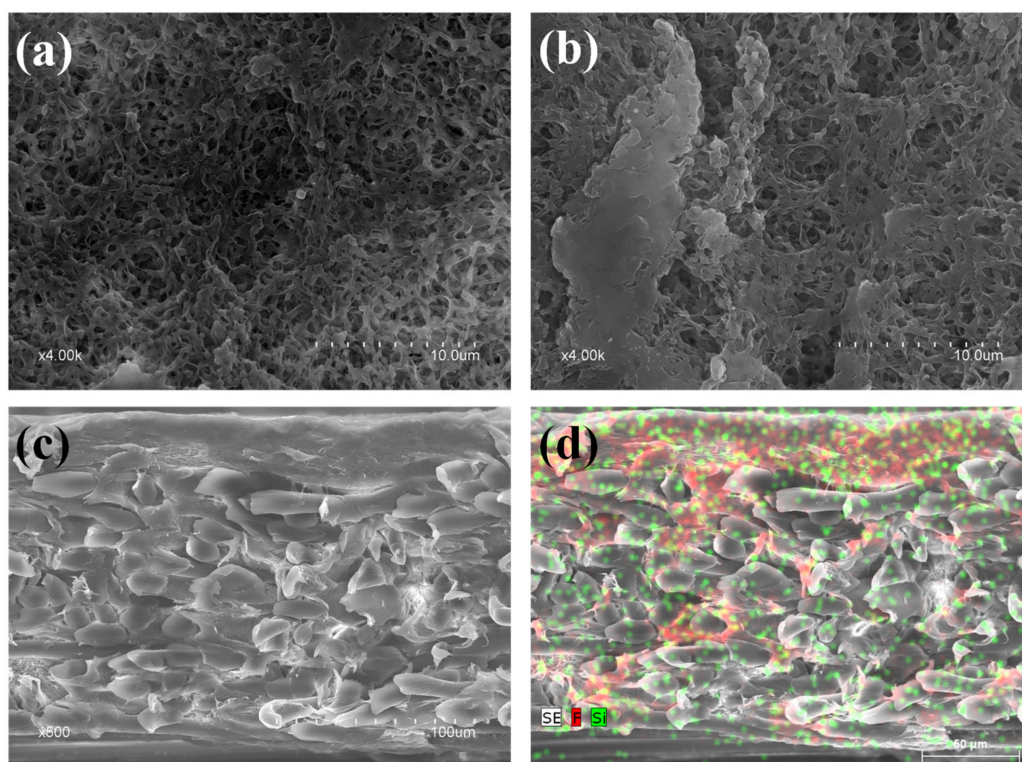


Figure 6. FESEM images of (a) non-modified PVDF (nmPVDF) surface, (b) modified PVDF (mPVDF_{max}) surface, (c) modified PVDF (mPVDF_{max}) cross-section, and (d) EDX mapping of modified PVDF (mPVDF_{max}) cross-section (red dots for F and green dots for Si).

The grafting of the FSi_T onto the membrane surface was also verified by measuring the fluorine and silicon content of both nmPVDF and mPVDF_{max} by EDX spectroscopy. The mPVDF_{max} showed a slightly higher F content than that obtained for the nmPVDF (55% and 53%, respectively) indicating that the Dyn had been grafted on the surface. Additionally, the mPVDF_{max} presented a Si content of 0.5% due to the grafting and condensation of the silanols from TEOS over the surface as well as the grafting of Dyn.

From the cross-section inspection, the overall thickness of the mPVDF_{max} was slightly greater than that of the nmPVDF, with values of $164 \pm 1 \mu\text{m}$ and $159 \pm 2 \mu\text{m}$, respectively. A dense and thick top layer was observed for the mPVDF_{max} with a thickness between 15 and $37 \mu\text{m}$ (Figure 6c), composed of the residual PVDF chains and especially of the grafted Dyn, since EDX analysis showed a high F content distributed homogeneously throughout this layer (red dots in Figure 6d). An FESEM image of the nmPVDF cross-section is shown in Supplementary Material S4 as an example, and a detailed analysis can be found in our previous work [8]. The Dyn seemed to be grafted both at the surface level and inside the membrane pores, reaching the interface between the PVDF and the PET membrane support and increasing the thickness of that top layer. The presence of this top layer was probably responsible for the increase in hydrophobicity and likely to improve the wetting resistance of the membrane. The EDX analysis also showed the presence of Si (green dots in Figure 6d) from the silica precursor TEOS, located mainly in the top layer, but Si was also found in all the sections but at a lower concentration, as also reported in the literature [41]. Therefore, the condensation of silanols occurred mainly at the surface level [24]. The Si content detected inside the membrane could be attributed to a deposition of the residual FSi_T after solvent evaporation in the curing step, since no reactions between silanols and the PET support were expected [21].

Degradation of the mPVDF activated at NaOH%_{wt} levels above 6% was confirmed by FESEM-EDX analyses (Supplementary Material S1 and S4). Circular holes were observed on the membrane surface showing a chemical degradation of the active layer, since no F was

detected inside the holes. This degradation was accompanied with a visual colour change of orange stains to the membrane surface. The high concentration of NaOH degraded the membrane by the loss of PVDF chains affecting the membrane integrity [21,31]. The increase in NaOH%_wt or activation time increased the extent of defluorination, leading to a severe alteration to the surface chemical structure. For instance, this reaction under severe conditions could convert the PVDF to polyacetylene chains followed by detaching from the surface [24]. Other authors observed a similar colour change in PVDF treated with an alkaline solution, and they established that the F content was lower as the colour became darker [42,43]. A decrease in the mechanical properties of the PVDF after NaOH treatment has been reported, especially for NaOH%_wt ≥ 10%, leading to a severe reduction in the degree of crystallinity of the PVDF structure [43]. The PET support could also be degraded, since PET is hydrolysed under severe alkali concentrations and temperature, so the membrane support can play a critical role in the selection of the activation technique and conditions.

3.3. Performance of the PVDF Membranes in Stability in Long-Term Operation Tests

The stability of PVDF in long-term operation was evaluated by monitoring its WCA as a useful indicator of changes or alterations occurring on the membrane surface [8,27,33]. The results of the variation in WCA during use of the nmPVDF and mPVDF_{max} are shown in Figures 7a,b for tests with DW and AE, respectively.

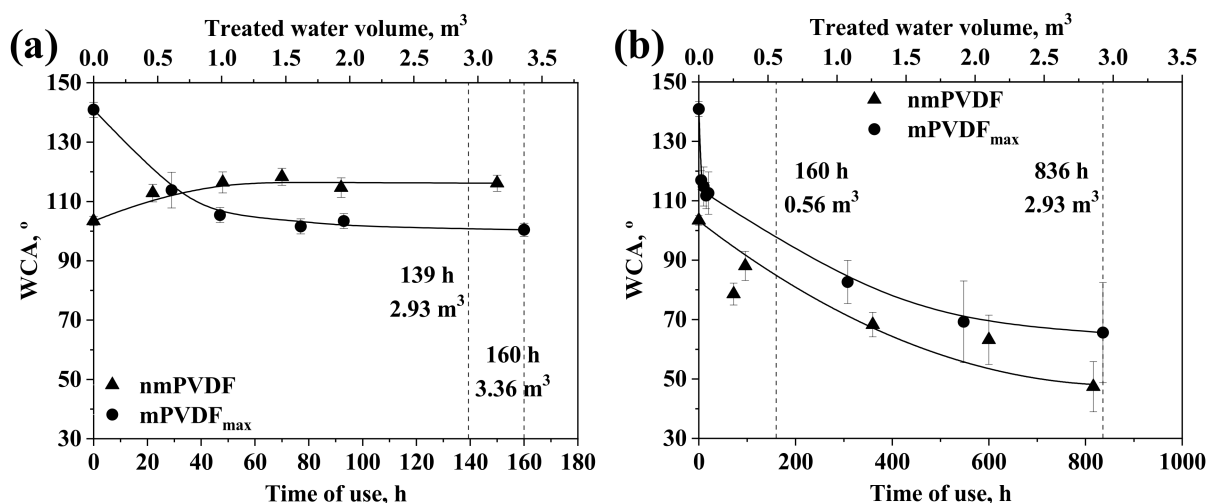


Figure 7. Water contact angle versus time of use (bottom axis) and volume of treated water (top axis) for non-modified PVDF (nmPVDF) and PVDF modified under optimal conditions (mPVDF_{max}) with (a) deionised water at a liquid flow rate of 21 L h⁻¹ and (b) anaerobic reactor effluent at a liquid flow rate of 3.5 L h⁻¹. Data on nmPVDF with deionised water from [8]. The error bars denote the standard deviation.

The WCA of the mPVDF_{max} decreased continuously from 140.9 ± 2.5° at 0 h to 100.5 ± 2.2° at 160 h in the test with DW (Figure 7a). The WCA decrease was more pronounced in the first 47 h, reaching a value of 105.4 ± 2.5° and then staying almost constant; the final WCA of mPVDF_{max} was similar to the initial value of the nmPVDF (100.5 ± 2.2° and 103.4 ± 1.6°, respectively). The WCA decrease could be due to the reduction of F content detected in the EDX analysis from 55% to 53%, similar to the pristine nmPVDF. This F loss could be attributed to the stress and dragging effect of the liquid flux removing the polymeric chains and/or clusters weakly linked to the surface. Nevertheless, Si content increased up to values of 2% suggesting that the most external layer was composed of the Dyn molecules and the silica precursor was strongly linked to the membrane surface. The WCA after the activation step was of 88.5 ± 5.4°, lower than that of the mPVDF_{max} at 160 h (100.5 ± 2.2°), indicating that siloxane chains and Dyn

molecules remained on the surface at the end of the long-term experiment with a moderate liquid flow rate of 21 L h^{-1} . Future research would be needed to improve the fixation of macromolecules onto the membrane.

At the end of the long-term test with DW, a permanent plastic deformation at surface level was observed for the mPVDF_{max} from the FESEM images (Supplementary Material S4) in which the surface porosity declined at values lower than 10%. Similar observations were found for the nmPVDF resulting in a dense-like surface [8]. Moreover, the functional top layer formed onto the membrane appeared to have been substantially reduced and the membrane thickness decreased to a value of $148 \pm 12 \mu\text{m}$, indicating that part of this surface layer was removed.

Some authors have monitored membrane stability and wetting resistance in long-term operations by means of the gas flux change instead of WCA. Using tap water, Sethunga et al. [21] reported a stable CH_4 flux of around $36 \times 10^{-5} \text{ g m}^{-2} \text{ s}^{-1}$ over 240 h at a liquid flow rate of 0.6 L h^{-1} using a modified PVDF, and Wongchitphimon et al. [44] also reported a stable CH_4 flux of around $66.7 \times 10^{-5} \text{ g m}^{-2} \text{ s}^{-1}$ over 300 h at a liquid flow rate of 5.2 L h^{-1} using polyimide membranes functionalised with organofluorosilanes.

Regarding the results with AE at a liquid flow rate of 3.5 L h^{-1} (Figure 7b), the WCA of the nmPVDF decreased continuously from $103.4 \pm 1.6^\circ$ at the beginning to $47.4 \pm 8.4^\circ$ after 816 h, showing a reduction of 54% from the initial value. A gradual darkening of the membrane was apparent during the tests with AE (Supplementary Material S5), indicating that the entire surface was covered by a fouling cake, which could explain the WCA decrease due to the hydrophilisation promoted by some fouling agents [45]. The WCA trend was similar for both the nmPVDF and mPVDF_{max}, but the final WCA of the mPVDF_{max} was higher, with a value of $65.6 \pm 16.9^\circ$ after 836 h, representing a reduction of 53% from the initial value ($140.9 \pm 2.5^\circ$) in spite of the mPVDF_{max} surface being darker at the end of the test. In addition, the presence of a fouling cake on the membrane could be confirmed by two additional observations: (1) the WCA initially decreased faster with AE than with DW despite the lower liquid flow rate in both the nmPVDF and mPVDF_{max} membranes (dashed line at 160 h in Figure 7) and (2) the final WCA obtained with AE was lower than with DW at the same volume of treated water and with lower flow rate (dashed line at 2.93 m^3 of treated water in Figure 7). Regarding observation number (1), the relatively sudden WCA decline of the mPVDF_{max} in the first 50 h could be attributed to a fast attachment of organic/biological matter in AE with more affinity with hydrophobic surfaces [46]. All these results indicated that the membrane surface was covered by the deposition of fouling agents, obscuring the hydrophobic nature of the membrane surface; the hydrophobic level of the surface was dominated by the nature and amount of fouling agents present.

A water breakthrough was detected on the nmPVDF at 816 h, indicating mechanical or chemical deterioration of the membrane surface. Interestingly, a longer useful lifetime was achieved for the mPVDF_{max} since no water breakthrough was observed. Thus, the modification procedure seemed to improve the stability of the PVDF in long-term operations with real AEs. In this regard, the surface modification should be taken into account as a strategy to increase the useful lifetime of the membrane since a greater chemical or mechanical resistance could be induced. In order to compare the viability of using both non-modified and modified membranes, a suitable economic analysis should also consider the additional cost of the modification procedure and its effect on the membrane performance and useful lifetime.

3.4. Performance of the PVDF Membranes for the Recovery of Dissolved Methane from Water

The performance of the mPVDF_{max} in degassing tests for D- CH_4 recovery was evaluated for both DW and AE and compared with the performance of the nmPVDF.

Results obtained with DW are presented in Table 3, in which the D- CH_4 RE and the methane flux (J_{CH_4}) at different liquid flow rates (Q_L) for both materials are compared. An RE of 42% and 21% were obtained for mPVDF_{max} at a Q_L of 21.0 and 3.5 L h^{-1} ,

respectively. A slight improvement in membrane performance was achieved after the membrane modification process, especially when a Q_L higher than 3.5 L h^{-1} was applied. Thus, the RE at a Q_L of 21.0 L h^{-1} was slightly higher than that seen with the nmPVDF (39%). No significant differences were observed in the RE at the lowest Q_L of 3.5 L h^{-1} for both membranes, this being attributed mainly to the limiting mass transfer resistance in the liquid phase, especially at low liquid flow rates and velocities [8,37,47].

Table 3. Effect of the time of use on the dissolved CH_4 removal efficiency (RE) and CH_4 flux (J_{CH_4}) in degassing tests (at 5 h of time on stream) with non-modified PVDF (nmPVDF) and modified PVDF (mPVDF_{max}) at different liquid flow rates (Q_L) of distilled water and anaerobic reactor effluent.

Membrane	$Q_L, \text{ L h}^{-1}$	Time of Use, h	RE, %	$J_{\text{CH}_4} \times 10^5, \text{ g s}^{-1} \text{ m}^{-2}$
(a) With deionised water				
nmPVDF	3.5	0	19 ± 1^a	27 ^a
	21.0	0	39 ± 1^a	46 ^a
mPVDF _{max}	3.5	0	21 ± 2	29
	21.0	0	42 ± 1	52
(b) With anaerobic effluent				
nmPVDF	3.5	0	19 ± 1	27
	3.5	720	19 ± 2	26
	21.0	0	39 ± 1	46
	21.0	744	34 ± 2	39
mPVDF _{max}	3.5	0	22 ± 3	29
	3.5	528	19 ± 1	24
	21.0	0	42 ± 1	52
	21.0	672	20 ± 1	26

^a Previous work [8].

The CH_4 flux was also calculated for the degassing tests, and the results are shown in Table 3. The maximum CH_4 flux was observed for the mPVDF_{max} at the highest Q_L of 21 L h^{-1} with a value of $52 \times 10^{-5} \text{ g s}^{-1} \text{ m}^{-2}$ since this test showed the maximum RE value. The CH_4 fluxes obtained in this work under unsteady-state conditions were similar to those reported by other authors operating under steady-state conditions. Wongchitphimon et al. [44] obtained CH_4 fluxes of 42×10^{-5} to $80 \times 10^{-5} \text{ g s}^{-1} \text{ m}^{-2}$ for polyimide membranes modified with organofluorosilanes at liquid flow rates ranging from 2.6 to 5.8 L h^{-1} . Sethunga et al. [21] reported CH_4 fluxes of 17×10^{-5} to $39 \times 10^{-5} \text{ g s}^{-1} \text{ m}^{-2}$ for PVDF modified with organofluorosilanes with Q_L ranging from 0.2 to 0.5 L h^{-1} . Another work of Sethunga et al. [48] used polydimethylsiloxanes as modifying agents, and CH_4 fluxes between 16×10^{-5} and $48 \times 10^{-5} \text{ g s}^{-1} \text{ m}^{-2}$ were reported with Q_L ranging from 0.05 to 3.0 L h^{-1} . All these abovementioned works conducted degassing tests under steady-state conditions with tap water and initial D- CH_4 concentrations between 12 and 15 mg L^{-1} .

The mPVDF_{max} showed a greater mass transport of CH_4 than did the nmPVDF under the same liquid and gas hydraulic conditions and at the highest Q_L (21.0 L h^{-1}), since the obtained RE and CH_4 flux were higher with the mPVDF_{max}. Thus, these results indicated that the mass transfer resistance of the mPVDF_{max} membrane was lower than that of nmPVDF, which could be due to the prevention of membrane wetting associated with the increase in WCA obtained after the modification of the membrane. The lower surface porosity and slightly higher thickness in the mPVDF_{max} seemed not to significantly affect to the overall mass transfer resistance, being that the hydrophobicity increase was the predominant factor in the decrease of the mass transfer resistance. The higher hydrophobicity

observed on the surface of the mPVDF_{max} involved an increase in the liquid entry pressure; therefore, the membrane pores were less susceptible to being wetted or filled with the liquid phase. It is well-known that membrane wetting leads to an increase in membrane mass transfer resistance for CH₄ transport from the liquid phase to the gas phase, since CH₄ presents a higher diffusion coefficient in air than in water [15,49]. Similarly, an increase in degree of wetting with liquid flow rate has been reported, showing a huge influence on membrane resistance, especially for porous membranes [14]. In addition, the reduction in surface porosity observed after modification can also increase wetting resistance, as previously explained.

Likewise, a RE value of 41% was obtained at a Q_L of 21.0 L h⁻¹ with mPVDF_{max} after 20 h, when its WCA was reduced to 122°. This RE was similar to the initial value of 42% obtained for the mPVDF_{max} with a WCA of ~140°. Thus, it can be concluded that the modification procedure improved the stability of the PVDF in terms of membrane performance, in contrast to those structural and performance changes previously observed for the nmPVDF [8].

Both the nmPVDF and mPVDF_{max} used in the long-term stability tests (Section 3.3) with AE were evaluated in degassing tests at different times of use in order to determine the effect on D-CH₄ recovery of an actual stream and level of hydrophobicity. The AE previously saturated with CH₄ was used as the liquid stream. The results in terms of RE and J_{CH₄} at different times of use and at liquid flow rates of 3.5 and 21.0 L h⁻¹ for the nmPVDF and mPVDF_{max} are shown in Table 3. Similar performances were obtained at a Q_L of 3.5 L h⁻¹ for the pristine membranes (time of use of 0 h), with nmPVDF at 720 h and mPVDF_{max} at 528 h, with values of RE and J_{CH₄} of around 20% and 26 × 10⁻⁵ g s⁻¹ m⁻², respectively. Thus, the potential effect on membrane performance of the foulants contained in the liquid stream could be considered negligible for both membranes at low liquid flow rates, at least, for a time of use less than 800 h. In contrast, lower RE values were obtained at the higher Q_L of 21.0 L h⁻¹ for the used nmPVDF and mPVDF_{max} membranes at 744 and 672 h, respectively. For example, REs of 39% and 34% were obtained for the pristine and used nmPVDF, respectively (decline in J_{CH₄} of 17%). This RE decline was more severe for the mPVDF_{max} in that it decreased from 42% to 20% for the pristine and used membrane, respectively, at a liquid flow rate of 21.0 L h⁻¹ (decline in J_{CH₄} of 51%). In this case, the deposition of foulants onto the membrane involved an additional and non-negligible mass transfer resistance, since the liquid resistance decreased at higher liquid flow rates. Similar declines in CH₄ flux, and even a severe reduction of up to 90% after only 40 h, have been reported by other authors using modified membranes to treat AEs [10,48,50], while a stable flux was maintained when using tap water [21,44]. The results allowed the conclusion that the modification of PVDF promoted a higher additional mass transfer resistance due to the deposition of foulants contained in the AE hindering D-CH₄ recovery, even though greater stability and resistance were achieved, since no water breakthrough was observed during the long-term test. The apparent higher fouling deposition on the mPVDF could be due to the increase in membrane hydrophobicity which favoured the deposition of hydrophobic foulants, and/or the change in the surface charge which could promote an increase of the electrostatic attraction between foulants and the modified membrane [46,51]. Further investigations should be focused on the mechanisms and characterisation of fouling in order to propose strategies for its control and prevention.

4. Conclusions

The hydrophobicity of a PVDF membrane surface has been maximised by chemical grafting in a three-step procedure (activation, functionalisation, and curing) in order to increase the membrane performance in the recovery of dissolved methane from aqueous streams. The main variables in the modification procedure that significantly affected the water contact angle were found to be the NaOH concentration in the activation step and the modifying agent/precursor (FSi_T) ratio and concentration in the functionalisation step. The contact angle of the modified PVDF increased continuously with NaOH and

FSi_T concentration, although the concentration of NaOH was limited by the degradation observed on the membrane surface at concentrations of >5%. In addition, no significant increase in contact angle was observed at an FSi_T concentration of >7.2%. In contrast, a maximum contact angle was observed for an FSi_T ratio of 0.55. Thus, these values were established as the optimal conditions in order to maximise the hydrophobicity of the membrane surface, achieving a contact angle of >140°. This value represented an increase of >36% with respect to the initial contact angle of the non-modified PVDF (103°).

Regarding the stability of the membrane under long-term operation, the modified PVDF experienced a continuous decrease in contact angle to similar values as the pristine non-modified PVDF in a distilled water stream. In contrast, the contact angle of the modified PVDF was always higher when real anaerobic reactor effluent was used as the liquid stream. However, the final contact angle was quite low, at values of around 70° and 50° for the modified and non-modified PVDF, respectively, after ~800 h. In addition, the non-modified PVDF was strongly degraded at ~800 h since a water breakthrough occurred. Those outcomes allowed the conclusion that the modified PVDF presented greater chemical resistance and stability under operational conditions.

With regard to methane recovery, at the highest liquid flow rate tested (21 L h⁻¹), the modified PVDF showed a slightly higher performance than the non-modified PVDF. However, when real AE was used, the performance of the modified PVDF membrane decreased faster, suggesting that modification could favour fouling. In contrast, at the lowest liquid flow rate (3.5 L h⁻¹) no significant differences were observed between the modified and non-modified membranes, which could be explained by taking into account the high and limiting mass transfer resistance of the liquid phase under this operational condition, and so the effect of the additional resistances of the membrane could be ignored.

Supplementary Materials: The following supporting information can be downloaded at: <https://www.mdpi.com/article/10.3390/membranes12040426/s1>: Figure S1. (a) Effect of the NaOH concentration (NaOH%_w) (activation time of 1 h at 60 °C) and (b) the activation time (5% NaOH at 50 °C) on the water contact angle (WCA) after activation step. Table S1. Effect of the composition of the functionalisation solution on the water contact angle (WCA) after the curing step of the modified PVDF (activation: 5% NaOH, 1 h, 50 °C; functionalisation: 1 h, room temperature; curing: overnight, 60 °C), Figure S2. Effect of the functionalisation time on the water contact angle (WCA) after the curing step (activation: 5% NaOH, 50 °C, 1 h; functionalisation: FSi_T%_v = 3.6%, FSi_T ratio = 0.41; curing: overnight, 60 °C), Figure S3. Effect of the curing time on water contact angle (WCA) after the curing step (activation: 5% NaOH, 50 °C, 1 h; functionalisation: FSi_T%_v = 3.6%, FSi_T ratio = 0.41, 1 h; curing: 60 °C), Figure S4. Hydroxylation reaction of the poly(vinylidene fluoride) (PVDF) with sodium hydroxide in the activation step, Figure S5. Hydrolysis reaction of the tetraethyl orthosilicate (TEOS), Figure S6. Condensation reaction of the silanols on the hydroxylated PVDF in the functionalisation step, Figure S7. Condensation reaction of the 1H,1H,2H,2H-perfluorooctyltriethoxysilane (Dynasylan F8261®) onto the membrane surface in the functionalisation step, Figure S8. Examples of the profiles of (a) dissolved methane concentration (C₁) and removal efficiency (RE) and (b) CH₄ flux (J_{CH₄}) versus time on stream for degassing tests with the modified PVDF with the highest hydrophobicity (mPVDF_{max}) at a liquid and N₂ flow rate of 21 L h⁻¹ and 4 L h⁻¹, respectively, Figure S9. Cross section FESEM image of the non-modified PVDF, Figure S10. (a) FESEM image of a modified PVDF surface focused on a degraded zone (membrane activated with a 50%_w NaOH solution). (b) Fluor distribution on the membrane surface around a degraded zone, Figure S11. FESEM images of the (a) surface and (b) cross section of the modified PVDF (mPVDF_{max}) surface after 160 h of use with de-ionized water at a liquid flow rate of 21 L h⁻¹, Figure S12. Images of the non-modified and modified PVDF membrane surface (nmPVDF and mPVDF_{max}, respectively) during the long-term tests with an anaerobic reactor effluent at a liquid flow rate of 3.5 L h⁻¹. References [23–25,27,29–31,33,34,42,43] are cited in supplementary materials.

Author Contributions: Conceptualization, M.I., J.D.B. and V.M.-S.; methodology, R.J.-R., B.M.M.-T., J.D.B., V.M.-S. and M.I.; validation, R.J.-R., B.M.M.-T., J.D.B. and M.I.; formal analysis, R.J.-R.; investigation, R.J.-R. and B.M.M.-T.; resources, J.D.B.; data curation, R.J.-R. and B.M.M.-T.; writing—original draft preparation, R.J.-R.; writing—review and editing, R.J.-R., J.D.B., V.M.-S. and M.I.; visualization,

R.J.-R.; supervision, M.I., J.D.B. and V.M.-S.; project administration, M.I., J.D.B. and V.M.-S.; funding acquisition, M.I. and V.M.-S. All authors have read and agreed to the published version of the manuscript.

Funding: This research was funded by the Conselleria d’Innovació, Universitats, Ciència i Societat Digital—Generalitat Valenciana (project GV/2019/149). The PhD grant of R. Jiménez-Robles was funded by the Ministerio de Universidades, Spain (Beca de Formación de Profesorado Universitario FPU19/02478).

Institutional Review Board Statement: Not applicable.

Informed Consent Statement: Not applicable.

Data Availability Statement: The data presented in this study are available on request from the corresponding author.

Conflicts of Interest: The authors declare no conflict of interest.

References

1. Crone, B.C.; Garland, J.L.; Sorial, G.A.; Vane, L.M. Significance of dissolved methane in effluents of anaerobically treated low strength wastewater and potential for recovery as an energy product: A review. *Water Res.* **2016**, *104*, 520–531. [[CrossRef](#)] [[PubMed](#)]
2. Heile, S.; Chernicharo, C.; Brandt, E.; McAdam, E. Dissolved gas separation for engineered anaerobic wastewater systems. *Sep. Purif. Technol.* **2017**, *189*, 405–418. [[CrossRef](#)]
3. Mora, E.C.; Chernicharo, C.D.L. Use of membrane contactors for removing and recovering dissolved methane from anaerobic reactors effluents: State-of-the-art, challenges, and perspectives. *Rev. Environ. Sci. Bio/Technol.* **2020**, *19*, 673–697. [[CrossRef](#)]
4. Rongwong, W.; Lee, J.; Goh, K.; Karahan, H.E.; Bae, T.-H. Membrane-based technologies for post-treatment of anaerobic effluents. *npj Clean Water* **2018**, *1*, 21. [[CrossRef](#)]
5. Xu, Y.; Goh, K.; Wang, R.; Bae, T.-H. A review on polymer-based membranes for gas-liquid membrane contacting processes: Current challenges and future direction. *Sep. Purif. Technol.* **2019**, *229*, 115791. [[CrossRef](#)]
6. Zhang, N.; Pan, Z.; Zhang, Z.; Zhang, W.; Zhang, L.; Moreno, F.M.B.; Lichtfouse, E. CO₂ capture from coalbed methane using membranes: A review. *Environ. Chem. Lett.* **2019**, *18*, 79–96. [[CrossRef](#)]
7. Klaassen, R.; Feron, P.; Jansen, A. Membrane Contactors in Industrial Applications. *Chem. Eng. Res. Des.* **2005**, *83*, 234–246. [[CrossRef](#)]
8. Jiménez-Robles, R.; Gabaldón, C.; Badia, J.; Izquierdo, M.; Martínez-Soria, V. Recovery of dissolved methane through a flat sheet module with PDMS, PP, and PVDF membranes. *Sep. Purif. Technol.* **2021**, *282 Pt B*, 120057. [[CrossRef](#)]
9. Rana, D.; Matsuura, T. Surface Modifications for Antifouling Membranes. *Chem. Rev.* **2010**, *110*, 2448–2471. [[CrossRef](#)]
10. Sethunga, G.; Karahan, H.E.; Wang, R.; Bae, T.-H. Wetting- and fouling-resistant hollow fiber membranes for dissolved methane recovery from anaerobic wastewater treatment effluents. *J. Membr. Sci.* **2020**, *617*, 118621. [[CrossRef](#)]
11. Liu, F.; Hashim, N.A.; Liu, Y.; Moghareh Abed, M.R.; Li, K. Progress in the production and modification of PVDF membranes. *J. Membr. Sci.* **2011**, *375*, 1–27. [[CrossRef](#)]
12. Kang, G.; Cao, Y. Application and modification of poly(vinylidene fluoride) (PVDF) membranes—A review. *J. Membr. Sci.* **2014**, *463*, 145–165. [[CrossRef](#)]
13. Al-Gharabli, S.; Mavukkandy, M.O.; Kujawa, J.; Nunes, S.; Arafat, H.A. Activation of PVDF membranes through facile hydroxylation of the polymeric dope. *J. Mater. Res.* **2017**, *32*, 4219–4231. [[CrossRef](#)]
14. Henares, M.; Ferrero, P.; San-Valero, P.; Martínez-Soria, V.; Izquierdo, M. Performance of a polypropylene membrane contactor for the recovery of dissolved methane from anaerobic effluents: Mass transfer evaluation, long-term operation and cleaning strategies. *J. Membr. Sci.* **2018**, *563*, 926–937. [[CrossRef](#)]
15. Wang, R.; Zhang, H.; Feron, P.; Liang, D. Influence of membrane wetting on CO₂ capture in microporous hollow fiber membrane contactors. *Sep. Purif. Technol.* **2005**, *46*, 33–40. [[CrossRef](#)]
16. Velasco, P.; Jegatheesan, V.; Thangavadeivel, K.; Othman, M.; Zhang, Y. A focused review on membrane contactors for the recovery of dissolved methane from anaerobic membrane bioreactor (AnMBR) effluents. *Chemosphere* **2021**, *278*, 130448. [[CrossRef](#)]
17. Miller, D.J.; Dreyer, D.R.; Bielawski, C.W.; Paul, D.R.; Freeman, B.D. Surface Modification of Water Purification Membranes. *Angew. Chem. Int. Ed.* **2017**, *56*, 4662–4711. [[CrossRef](#)]
18. Al-Juboori, R.; Yusaf, T. Biofouling in RO system: Mechanisms, monitoring and controlling. *Desalination* **2012**, *302*, 1–23. [[CrossRef](#)]
19. Zhao, S.; Liao, Z.; Fane, A.; Li, J.; Tang, C.; Zheng, C.; Lin, J.; Kong, L. Engineering antifouling reverse osmosis membranes: A review. *Desalination* **2020**, *499*, 114857. [[CrossRef](#)]
20. Wongchitphimon, S.; Wang, R.; Jiratananon, R.; Shi, L.; Loh, C.H. Effect of polyethylene glycol (PEG) as an additive on the fabrication of polyvinylidene fluoride-co-hexafluoropropylene (PVDF-HFP) asymmetric microporous hollow fiber membranes. *J. Membr. Sci.* **2011**, *369*, 329–338. [[CrossRef](#)]

21. Sethunga, G.; Rongwong, W.; Wang, R.; Bae, T.-H. Optimization of hydrophobic modification parameters of microporous polyvinylidene fluoride hollow-fiber membrane for biogas recovery from anaerobic membrane bioreactor effluent. *J. Membr. Sci.* **2018**, *548*, 510–518. [[CrossRef](#)]
22. Hashemifard, S.A.; Ismail, A.F.; Matsuura, T.; DashtArzhandi, M.R. Performance of silicon rubber coated polyetherimide hollow fibers for CO₂ removal via a membrane contactor. *RSC Adv.* **2015**, *5*, 48442–48455. [[CrossRef](#)]
23. Zheng, Z.; Gu, Z.; Huo, R.; Luo, Z. Superhydrophobic poly(vinylidene fluoride) film fabricated by alkali treatment enhancing chemical bath deposition. *Appl. Surf. Sci.* **2009**, *256*, 2061–2065. [[CrossRef](#)]
24. Ross, G.; Watts, J.; Hill, M.; Morrissey, P. Surface modification of poly(vinylidene fluoride) by alkaline treatment 1. The degradation mechanism. *Polymer* **2000**, *41*, 1685–1696. [[CrossRef](#)]
25. Sairiam, S.; Loh, C.H.; Wang, R.; Jiratananon, R. Surface modification of PVDF hollow fiber membrane to enhance hydrophobicity using organosilanes. *J. Appl. Polym. Sci.* **2013**, *130*, 610–621. [[CrossRef](#)]
26. Badia, J.; Gil-Castell, O.; Ribes-Greus, A. Long-term properties and end-of-life of polymers from renewable resources. *Polym. Degrad. Stab.* **2017**, *137*, 35–57. [[CrossRef](#)]
27. Oldani, V.; Sergi, G.; Pirola, C.; Sacchi, B.; Bianchi, C. Sol-gel hybrid coatings containing silica and a perfluoropolyether derivative with high resistance and anti-fouling properties in liquid media. *J. Fluor. Chem.* **2016**, *188*, 43–49. [[CrossRef](#)]
28. Zhang, Y.; Wang, R.; Yi, S.; Setiawan, L.; Hu, X.; Fane, A.G. Novel chemical surface modification to enhance hydrophobicity of polyamide-imide (PAI) hollow fiber membranes. *J. Membr. Sci.* **2011**, *380*, 241–250. [[CrossRef](#)]
29. Zhang, Y.; Wang, R. Novel method for incorporating hydrophobic silica nanoparticles on polyetherimide hollow fiber membranes for CO₂ absorption in a gas–liquid membrane contactor. *J. Membr. Sci.* **2013**, *452*, 379–389. [[CrossRef](#)]
30. Zhang, Y.; Wang, R. Fabrication of novel polyetherimide-fluorinated silica organic-inorganic composite hollow fiber membranes intended for membrane contactor application. *J. Membr. Sci.* **2013**, *443*, 170–180. [[CrossRef](#)]
31. Wongchitphimon, S.; Wang, R.; Jiratananon, R. Surface properties of fluorinated hybrid coatings(PVDF–HFP) hollow fiber membrane for membrane gas absorption. *J. Membr. Sci.* **2011**, *381*, 183–191. [[CrossRef](#)]
32. Liu, L.; Shen, F.; Chen, X.; Luo, J.; Su, Y.; Wu, H.; Wan, Y. A novel plasma-induced surface hydrophobization strategy for membrane distillation: Etching, dipping and grafting. *J. Membr. Sci.* **2015**, *499*, 544–554. [[CrossRef](#)]
33. Fabbri, P.; Messori, M.; Montecchi, M.; Pilati, F.; Taurino, R.; Tonelli, C.; Toselli, M. Surface properties of fluorinated hybrid coatings. *J. Appl. Polym. Sci.* **2006**, *102*, 1483–1488. [[CrossRef](#)]
34. Huang, X.; Zhang, J.; Wang, W.; Liu, Y.; Zhang, Z.; Li, L.; Fan, W. Effects of PVDF/SiO₂ hybrid ultrafiltration membranes by sol–gel method for the concentration of fennel oil in herbal water extract. *RSC Adv.* **2015**, *5*, 18258–18266. [[CrossRef](#)]
35. Hebbar, R.S.; Isloor, A.M.; Ismail, A.F. Contact Angle Measurements. In *Membrane Characterization*, 1st ed.; Hilal, N., Ismail, A., Matsuura, T., Oatley-Radcliffe, D., Eds.; Elsevier: Amsterdam, The Netherlands, 2017; pp. 219–255. [[CrossRef](#)]
36. Abbasgholipourghadim, M.; Mailah, M.; Darus, I.Z.M.; Ismail, A.F.; Dashtarzhandi, M.R.; Abbasgholipourghadim, M.; Khademi, S. Porosity and Pore Area Determination of Hollow Fiber Membrane Incorporating Digital Image Processing. In *Recent Advances in Mechanics and Mechanical Engineering, Proceedings of the 6th International Conference on Fluid Mechanics and Heat & Mass Transfer (FLUIDSHEAT '15), Proceedings of the 1st International Conference on Mechanical and Transportation Engineering (ICMTE '15), Kuala Lumpur, Malaysia, 23–25 April 2015*; WSEAS Press: Athens, Greece, 2015; pp. 118–123.
37. Jiménez-Robles, R.; Gabaldón, C.; Martínez-Soria, V.; Izquierdo, M. Simultaneous application of vacuum and sweep gas in a polypropylene membrane contactor for the recovery of dissolved methane from water. *J. Membr. Sci.* **2020**, *617*, 118560. [[CrossRef](#)]
38. Cookney, J.; Cartmell, E.; Jefferson, B.; McAdam, E.J. Recovery of methane from anaerobic process effluent using poly-di-methylsiloxane membrane contactors. *Water Sci. Technol.* **2012**, *65*, 604–610. [[CrossRef](#)]
39. Bandara, W.M.; Satoh, H.; Sasakawa, M.; Nakahara, Y.; Takahashi, M.; Okabe, S. Removal of residual dissolved methane gas in an upflow anaerobic sludge blanket reactor treating low-strength wastewater at low temperature with degassing membrane. *Water Res.* **2011**, *45*, 3533–3540. [[CrossRef](#)]
40. Henares, M.; Izquierdo, M.; Marzal, P.; Martínez-Soria, V. Demethanization of aqueous anaerobic effluents using a polydimethylsiloxane membrane module: Mass transfer, fouling and energy analysis. *Sep. Purif. Technol.* **2017**, *186*, 10–19. [[CrossRef](#)]
41. Sethunga, G.; Lee, J.; Wang, R.; Bae, T.-H. Influences of operating parameters and membrane characteristics on the net energy production in dense, porous, and composite hollow fiber membrane contactors for dissolved biomethane recovery. *J. Membr. Sci.* **2020**, *610*, 118301. [[CrossRef](#)]
42. Ross, G.; Watts, J.; Hill, M.; Morrissey, P. Surface modification of poly(vinylidene fluoride) by alkaline treatment Part 2. Process modification by the use of phase transfer catalysts. *Polymer* **2001**, *42*, 403–413. [[CrossRef](#)]
43. Hashim, N.A.; Liu, Y.; Li, K. Stability of PVDF hollow fibre membranes in sodium hydroxide aqueous solution. *Chem. Eng. Sci.* **2011**, *66*, 1565–1575. [[CrossRef](#)]
44. Wongchitphimon, S.; Rongwong, W.; Chuah, C.Y.; Wang, R.; Bae, T.-H. Polymer-fluorinated silica composite hollow fiber membranes for the recovery of biogas dissolved in anaerobic effluent. *J. Membr. Sci.* **2017**, *540*, 146–154. [[CrossRef](#)]
45. Zarebska, A.; Amor, C.; Ciurkot, K.; Karring, H.; Thygesen, O.; Andersen, T.; Hägg, M.-B.; Christensen, K.; Norddahl, B. Fouling mitigation in membrane distillation processes during ammonia stripping from pig manure. *J. Membr. Sci.* **2015**, *484*, 119–132. [[CrossRef](#)]
46. Costa, F.C.; Ricci, B.C.; Teodoro, B.; Koch, K.; Drewes, J.E.; Amaral, M.C. Biofouling in membrane distillation applications—A review. *Desalination* **2021**, *516*, 115241. [[CrossRef](#)]

47. Henares, M.; Izquierdo, M.; Peña-Roja, J.; Martínez-Soria, V. Comparative study of degassing membrane modules for the removal of methane from Expanded Granular Sludge Bed anaerobic reactor effluent. *Sep. Purif. Technol.* **2016**, *170*, 22–29. [[CrossRef](#)]
48. Sethunga, G.; Karahan, H.E.; Wang, R.; Bae, T.-H. PDMS-coated porous PVDF hollow fiber membranes for efficient recovery of dissolved biomethane from anaerobic effluents. *J. Membr. Sci.* **2019**, *584*, 333–342. [[CrossRef](#)]
49. Sethunga, G.; Lee, J.; Wang, R.; Bae, T.-H. Influence of membrane characteristics and operating parameters on transport properties of dissolved methane in a hollow fiber membrane contactor for biogas recovery from anaerobic effluents. *J. Membr. Sci.* **2019**, *589*, 117263. [[CrossRef](#)]
50. Rongwong, W.; Goh, K.; Sethunga, G.; Bae, T.-H. Fouling formation in membrane contactors for methane recovery from anaerobic effluents. *J. Membr. Sci.* **2018**, *573*, 534–543. [[CrossRef](#)]
51. Guo, J.; Farid, M.U.; Lee, E.-J.; Yan, D.Y.-S.; Jeong, S.; An, A.K. Fouling behavior of negatively charged PVDF membrane in membrane distillation for removal of antibiotics from wastewater. *J. Membr. Sci.* **2018**, *551*, 12–19. [[CrossRef](#)]

Supplementary Material for

Flat PVDF membrane with enhanced hydrophobicity through alkali activation and organofluorosilanisation for dissolved methane recovery

R. Jiménez-Robles^a, B.M. Moreno-Torralbo^b, J.D. Badia^b, V. Martínez-Soria^a, M. Izquierdo^{a*}

^aResearch Group in Environmental Engineering (GI²AM) and ^bResearch Group in Materials Technology and Sustainability (MATS), both from Department of Chemical Engineering, School of Engineering, University of Valencia, Avda. Universitat s/n, 46100 Burjassot, Spain.

*Corresponding author's e-mail: marta.izquierdo-sanchis@uv.es. Phone: +34 963543737. Fax: +34 963544898

S1. Preliminary experiments: effect on surface hydrophobicity of activation, functionalisation and curing time, and solutions composition.

Several preliminary experiments were carried out in order to establish the suitable range of the different parameters involved in the surface modification process that affected the membrane hydrophobicity. The suitable values determined for those parameters were used for the design of experiments to maximize the static water contact angle (WCA) of the modified PVDF.

The NaOH concentration (NaOH%_{wt}) applied in the activation step and the activation time were evaluated, with NaOH weight concentrations ranging from 0.04% to 50% (Figure S 1a). The WCA of the membrane after activation decreased continuously with the increase of NaOH%_{wt} due to a higher extent of the defluorination process of the PVDF as reported by [1,2] with a less hydrophobic surface. The degradation on the membrane surface was observed since a colour change was detected on the membranes activated at NaOH%_{wt} higher than 6% appearing orange stains in a heterogeneous way. FESEM images confirmed this degradation in the form of holes for NaOH%_{wt} \geq 10% mainly due to the severe degradation of the PVDF chains and the PET support of the membrane in a concentrated alkali solution [3] (Supplementary Material S4). Thus, NaOH%_{wt} was kept in values lower than or equal to 6%.

Regarding the activation time (Figure S 1b), no significant changes were observed in the WCA after 1 h, and important degradation on the membrane surface with FESEM images was observed at 2 hours of activation. Thus, an activation time of 1 h was established for all the following experiments. This result was in accordance with that reported by Ross et al. [4], who determined that the most of the defluorination/hydroxylation reaction occurred within the first hour with a F content decrease from a 45.0% to a 25.5%, and stayed in values of 24.4 and 23.6% at 2 and 4 h, respectively. Zheng et al. [1] also reported a clear decrease of the WCA of the PVDF treated at a higher NaOH%_{wt} of 30% with an activation time of 1 h.

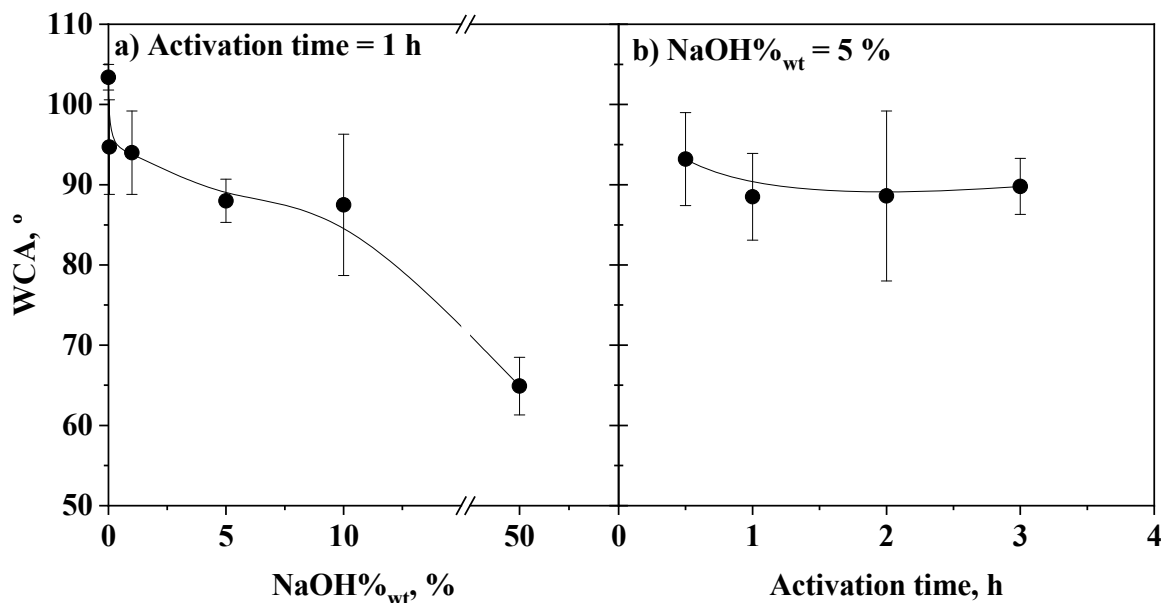


Figure S 1. a) Effect of the NaOH concentration (NaOH%_{wt}) (activation time of 1 h at 60°C) and b) the activation time (5% NaOH at 50°C) on the water contact angle (WCA) after activation step.

An initial mixture of Dynasylan F8261® (Dyn) and TEOS for the preparation of the functionalisation solution is labelled as FSi_T, where “F” denotes the fluorine modifying agent Dynasylan F8261® and “Si_T” the silica precursor TEOS. Different parameters involved in the functionalisation step were also evaluated (Table S 1). Regarding the volumetric ratio between the Dyn and TEOS in the functionalisation solution (FSi_T ratio = Dyn volume / FSi_T mixture volume), the WCA showed similar values (~130°) from a FSi_T ratio of 0.41 to 0.74 (Table S 1, exp. b – d), with a FSi_T percentage in the functionalisation solution (FSi_T%_v) of 3.6%. Also, the WCA did not increase when FSi_T%_v was increased from 3.6% to 15.1% (Table S 1, exp. d - e). In addition, other authors reported a WCA decrease for an organosilanes concentration higher than 20% due to the self-condensation of the silanols groups [1]. Thus, the optimum values of FSi_T ratio and FSi_T%_v that maximize the WCA of the modified PVDF were expected to be found in those ranges.

Table S 1. Effect of the composition of the functionalisation solution on the water contact angle (WCA) after the curing step of the modified PVDF (activation: 5% NaOH, 1 h, 50 °C; functionalisation: 1 h, room temperature; curing: overnight, 60°C).

Exp.	FSi _T ratio	FSi _T % _v %	IPA/H ₂ O ratio mol:mol	WCA °
a	0.17	3.6	57:1	120.4 ± 5.1
b	0.41	3.6	57:1	131.6 ± 4.0
c	0.52	3.6	57:1	129.8 ± 3.8
d	0.74	3.6	57:1	134.0 ± 4.7
e	0.74	15.1	57:1	129.6 ± 4.4

FSi_T ratio: volumetric ratio between the modifying agent and the silica precursor (Dyn volume / FSi_T mixture volume).

FSi_T%_v: volumetric percentage of the FSi_T mixture in the functionalization solution.

IPA: 2-propanol.

Regarding the functionalisation time, Sairiam et al. [2] reported a WCA increase from 69° to around 85° from 0 to 6 h using hexane as solvent for the functionalisation solution and the same fluorine modifying agent (1H,1H,2H,2H-perfluorooctyltriethoxysilane). In contrast, in our experiments with a mixture of IPA/H₂O as solvent, the WCA remained constant after 1 h (Figure S 2), so a functionalisation time of 1 h was established for the experiments.

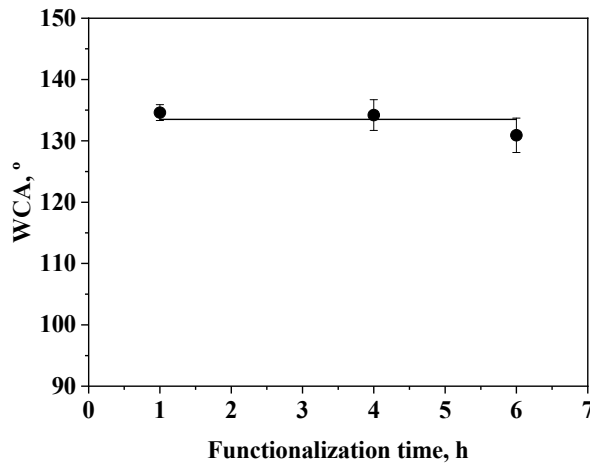


Figure S 2. Effect of the functionalisation time on the water contact angle (WCA) after the curing step (activation: 5% NaOH, 50°C, 1 h; functionalisation: FSi_T%_v = 3.6%, FSi_T ratio = 0.41; curing: overnight, 60°C).

The duration of the curing step was also evaluated. The WCA initially increased with the curing time and it remained constant from 7 h (Figure S 3). Thus, a curing time of at least 7 h was applied for the modification procedure of the PVDF.

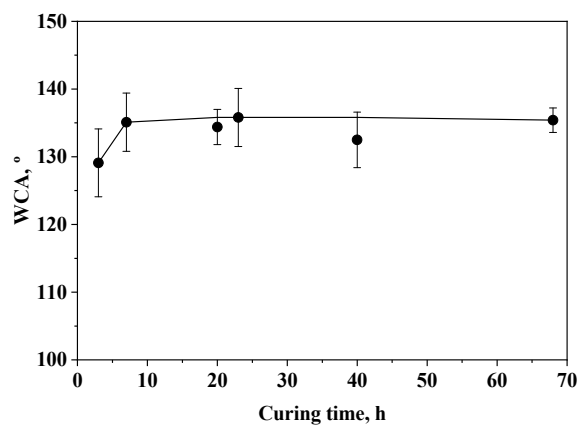


Figure S 3. Effect of the curing time on water contact angle (WCA) after the curing step (activation: 5% NaOH, 50°C, 1 h; functionalisation: $FSi_T\%_v = 3.6\%$, FSi_T ratio = 0.41, 1 h; curing: 60°C).

S2. Chemical reactions in the activation, functionalisation and curing steps

The surface chemical modification of poly(vinylidene fluoride) (PVDF) consisted in a three-step procedure: 1) activation, 2) functionalisation and 3) curing. In the activation step, PVDF was immersed in a NaOH solution in order to substitute the F atoms from the fluorine chains by OH⁻ [3–5]. This reaction is called hydroxylation and is shown in Figure S 4. Secondary reactions could occur involving the formation of carbonyl (C=O) when severe conditions of the activation step, i.e. high temperature, time and NaOH concentration, are used or when a not homogeneous NaOH attack is produced [4]. C-O-F groups can also be formed since the total defluorination does not occur [4].

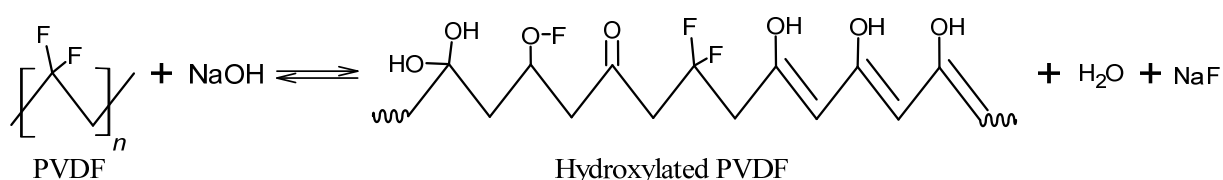


Figure S 4. Hydroxylation reaction of the poly(vinylidene fluoride) (PVDF) with sodium hydroxide in the activation step.

For the functionalisation step, the ethoxy groups of the tetraethyl orthosilicate (TEOS) were hydrolysed to silanols during the preparation of the functionalisation solution [6–9] (Figure S 5). The silanol molecules coordinate with the hydroxyl group on the activated PVDF grafting the silica precursor [2,7]. In addition, silanols are chemically reactive and they can condensate forming oxane bonds between Si atoms [2,10,11]. Thus, the proposed chemical reaction and structure is shown in Figure S 6.

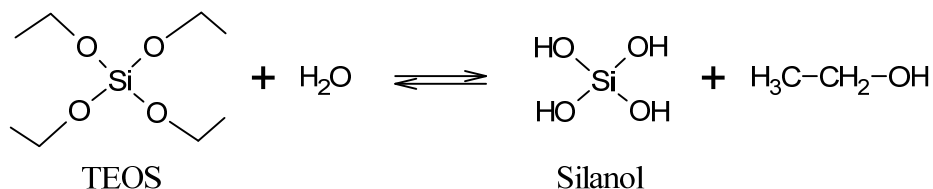


Figure S 5. Hydrolysis reaction of the tetraethyl orthosilicate (TEOS)

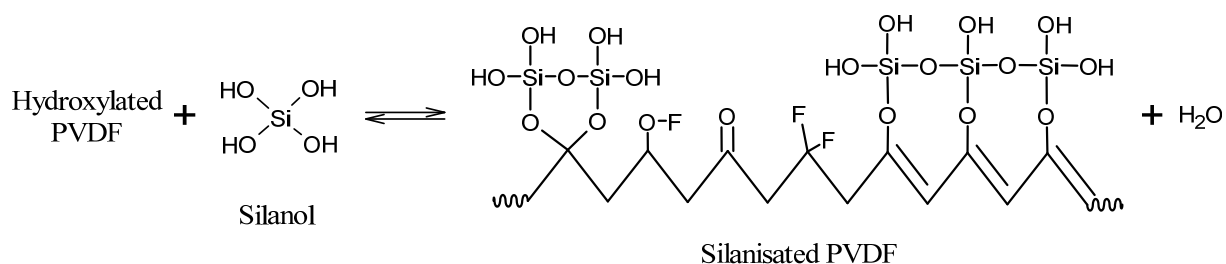


Figure S 6. Condensation reaction of the silanols on the hydroxylated PVDF in the functionalisation step.

Finally, the organofluorosilane 1H,1H,2H,2H-perfluorooctyltriethoxysilane (Dynasylan F8261®) as modifying agent is grafted on the membrane by coordinating with the silanols groups [7], as proposed in Figure S 7. The secondary reaction involved in the activation step, the residual fluorine and the non-homogeneous condensation of the silanols can lead to a heterogeneous surface.

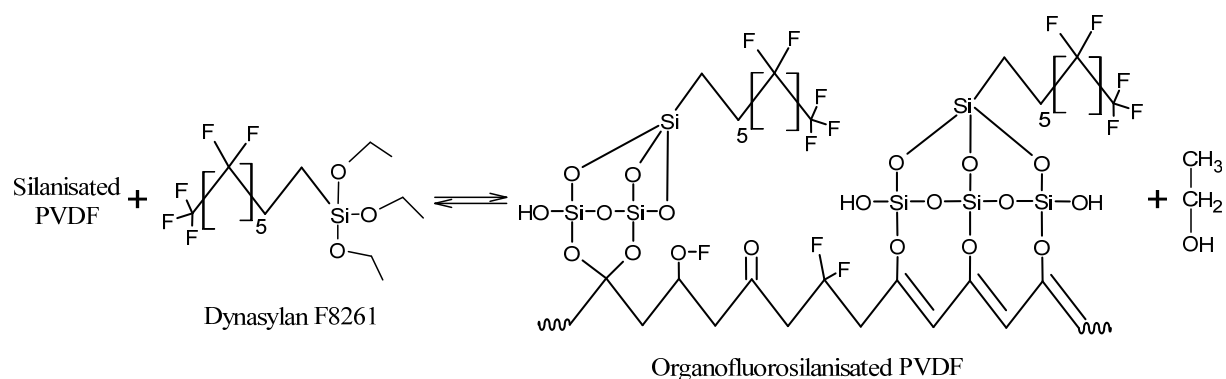


Figure S 7. Condensation reaction of the 1H,1H,2H,2H-perfluorooctyltriethoxysilane (Dynasylan F8261®) onto the membrane surface in the functionalisation step.

S3. Dissolved methane concentration, removal efficiency and methane flux profiles

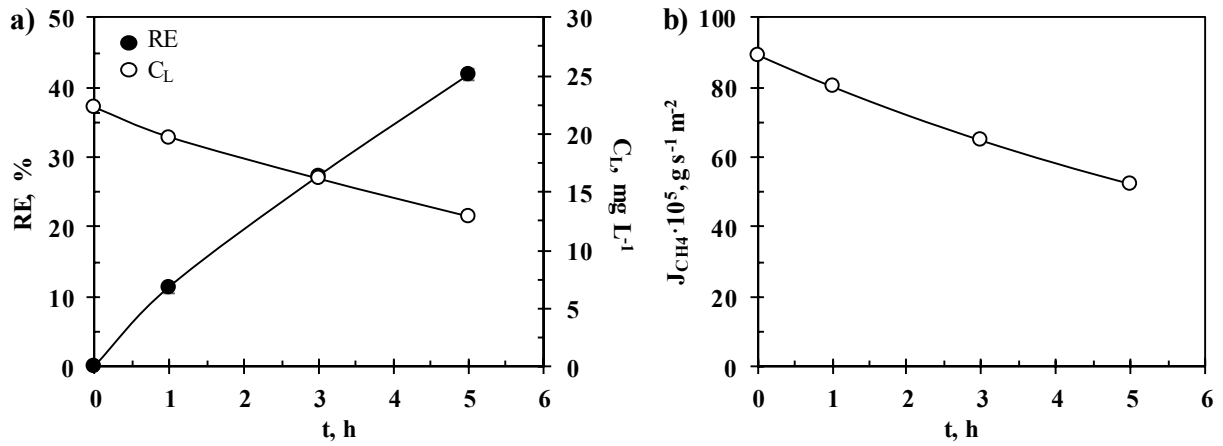


Figure S 8. Examples of the profiles of a) dissolved methane concentration (C_L) and removal efficiency (RE) and b) CH_4 flux (J_{CH_4}) versus time on stream for degassing tests with the modified PVDF with the highest hydrophobicity ($mPVDF_{max}$) at a liquid and N_2 flow rate of 21 L h⁻¹ and 4 L h⁻¹, respectively.

S4. Microscopy and elemental analysis on PVDF membranes

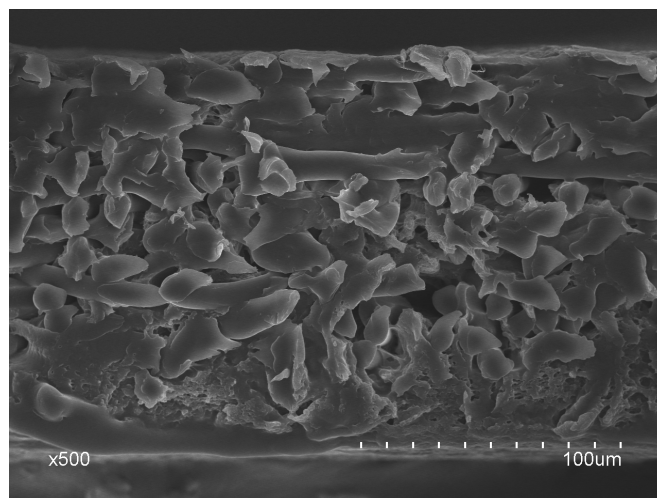


Figure S 9. Cross section FESEM image of the non-modified PVDF.

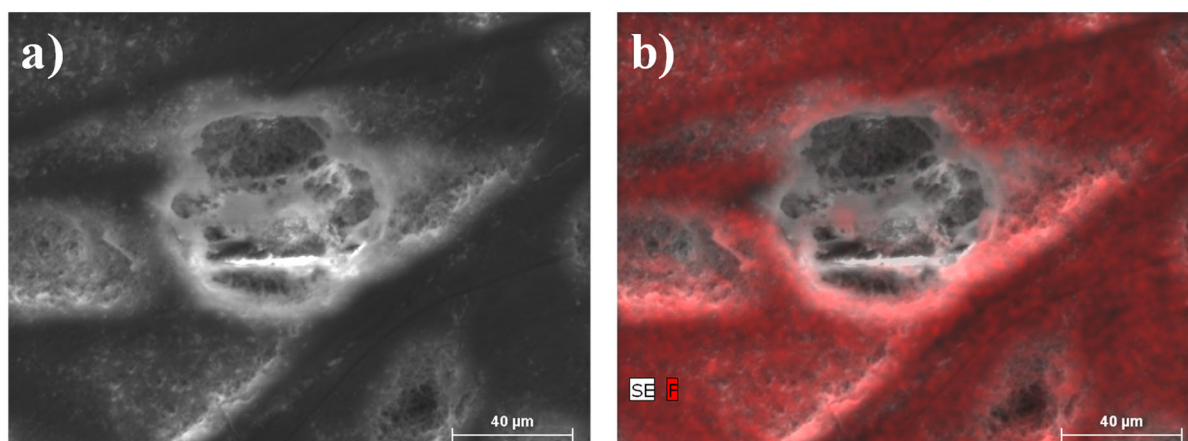


Figure S 10. a) FESEM image of a modified PVDF surface focused on a degraded zone (membrane activated with a 50%_{w/w} NaOH solution). b) Fluor distribution on the membrane surface around a degraded zone.

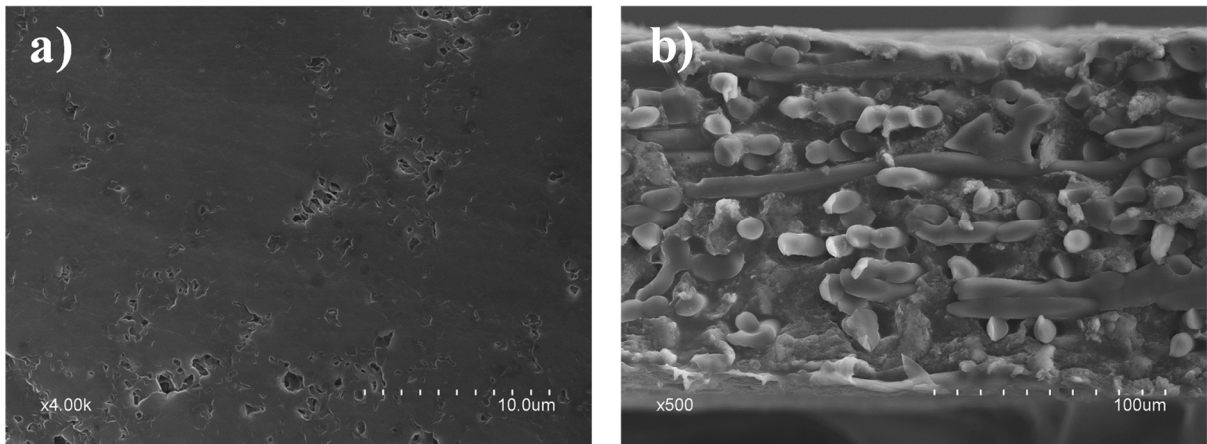


Figure S 11. FESEM images of the a) surface and b) cross section of the modified PVDF (mPVDF_{max}) surface after 160 h of use with de-ionized water at a liquid flow rate of 21 L h⁻¹.

S5. Images of the membrane surfaces during the long-term tests with an anaerobic reactor effluent

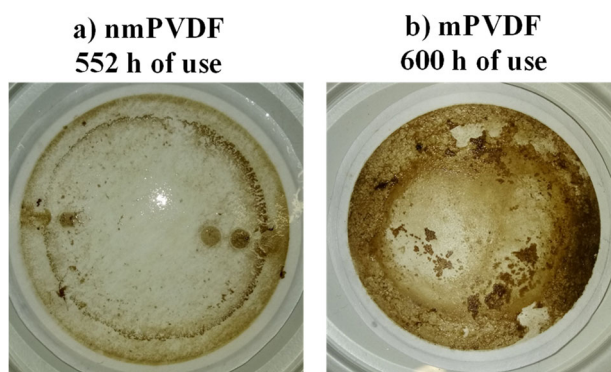


Figure S 12. Images of the non-modified and modified PVDF membrane surface (nmPVDF and mPVDF_{max}, respectively) during the long-term tests with an anaerobic reactor effluent at a liquid flow rate of 3.5 L h⁻¹.

References

- [1] Z. Zheng, Z. Gu, R. Huo, Z. Luo, Superhydrophobic poly(vinylidene fluoride) film fabricated by alkali treatment enhancing chemical bath deposition, *Appl. Surf. Sci.* 256 (2010) 2061–2065. <https://doi.org/10.1016/j.apsusc.2009.09.048>.
- [2] S. Sairiam, C.H. Loh, R. Wang, R. Jiratananon, Surface modification of PVDF hollow fiber membrane to enhance hydrophobicity using organosilanes, *J. Appl. Polym. Sci.* 130 (2013) 610–621. <https://doi.org/10.1002/app.39197>.
- [3] N. Awanis Hashim, Y. Liu, K. Li, Stability of PVDF hollow fibre membranes in sodium hydroxide aqueous solution, *Chem. Eng. Sci.* 66 (2011) 1565–1575. <https://doi.org/10.1016/j.ces.2010.12.019>.
- [4] G.J. Ross, J.F. Watts, M.P. Hill, P. Morrissey, Surface modification of poly(vinylidene fluoride) by alkaline treatment: 1. The degradation mechanism, *Polymer (Guildf)*. 41 (2000) 1685–1696. [https://doi.org/10.1016/S0032-3861\(99\)00343-2](https://doi.org/10.1016/S0032-3861(99)00343-2).
- [5] G.J. Ross, J.F. Watts, M.P. Hill, P. Morrissey, Surface modification of poly(vinylidene fluoride) by alkaline treatment Part 2. Process modification by the use of phase transfer catalysts, *Polymer (Guildf)*. 42 (2001) 403–413. [https://doi.org/10.1016/S0032-3861\(00\)00328-1](https://doi.org/10.1016/S0032-3861(00)00328-1).
- [6] P. Fabbri, M. Messori, M. Montecchi, F. Pilati, R. Taurino, C. Tonelli, M. Toselli, Surface properties of fluorinated hybrid coatings, *J. Appl. Polym. Sci.* 102 (2006) 1483–1488. <https://doi.org/10.1002/app.24350>.
- [7] S. Wongchitphimon, R. Wang, R. Jiratananon, Surface modification of polyvinylidene fluoride-co-hexafluoropropylene (PVDF-HFP) hollow fiber membrane for membrane

- gas absorption, *J. Membr. Sci.* 381 (2011) 183–191.
<https://doi.org/10.1016/j.memsci.2011.07.022>.
- [8] V. Oldani, G. Sergi, C. Pirola, B. Sacchi, C.L. Bianchi, Sol-gel hybrid coatings containing silica and a perfluoropolyether derivative with high resistance and anti-fouling properties in liquid media, *J. Fluor. Chem.* 188 (2016) 43–49.
<https://doi.org/10.1016/j.jfluchem.2016.06.005>.
- [9] X. Huang, J. Zhang, W. Wang, Y. Liu, Z. Zhang, L. Li, W. Fan, Effects of PVDF/SiO₂ hybrid ultrafiltration membranes by sol-gel method for the concentration of fennel oil in herbal water extract, *RSC Adv.* 5 (2015) 18258–18266.
<https://doi.org/10.1039/c4ra15448g>.
- [10] Y. Zhang, R. Wang, Fabrication of novel polyetherimide-fluorinated silica organic-inorganic composite hollow fiber membranes intended for membrane contactor application, *J. Membr. Sci.* 443 (2013) 170–180.
<https://doi.org/10.1016/j.memsci.2013.04.062>.
- [11] Y. Zhang, R. Wang, Novel method for incorporating hydrophobic silica nanoparticles on polyetherimide hollow fiber membranes for CO₂ absorption in a gas-liquid membrane contactor, *J. Membr. Sci.* 452 (2014) 379–389.
<https://doi.org/10.1016/j.memsci.2013.10.011>.

APPENDIX III: CONTRIBUTION III.

The contribution entitled “*Fouling characterisation in PVDF membrane contactors for dissolved methane recovery from anaerobic effluents: effect of surface organofluorosilanisation*” is presented in this Appendix. This work corresponds with the main results and conclusions discussed in section 4.3. The details of the resulting paper are listed below:

Title	Fouling characterisation in PVDF membrane contactors for dissolved methane recovery from anaerobic effluents: effect of surface organofluorosilanisation
Authors	Ramón Jiménez-Robles, Vicente Martínez-Soria, Marta Izquierdo
Affiliation	Research Group in Environmental Engineering (GI2AM), Department of Chemical Engineering, School of Engineering, University of Valencia, Avda. Universitat s/n, 46100 Burjassot, Spain
Journal	Environmental Science and Pollution Research
Year	2022
Volume	30
Issue	March 2023
Pages	29164–29179
DOI	10.1007/s11356-022-24019-z
Cite	R. Jiménez-Robles, V. Martínez-Soria, M. Izquierdo, Fouling characterisation in PVDF membrane contactors for dissolved methane recovery from anaerobic effluents: effect of surface organofluorosilanisation, <i>Environmental Science and Pollution Research</i> . 30 (2023) 29164–29179. https://doi.org/10.1007/s11356-022-24019-z

The Journal Impact Factor (JIF) in the in the year of publication was 5.8, and the JIF rank was 67/274 in the category of Environmental Sciences (Q1 first quartile).



Fouling characterisation in PVDF membrane contactors for dissolved methane recovery from anaerobic effluents: effect of surface organofluorosilanisation

Ramón Jiménez-Robles¹ · Vicente Martínez-Soria¹ · Marta Izquierdo¹

Received: 15 August 2022 / Accepted: 1 November 2022 / Published online: 21 November 2022
© The Author(s) 2022

Abstract

Characterisation of the fouling attached to PVDF membranes treating an anaerobic effluent for dissolved CH₄ recovery was carried out. A commercial flat-sheet PVDF membrane and a PVDF functionalised by grafting of organofluorosilanes (mPVDF) that increased its hydrophobicity were subjected to a continuous flux of an anaerobic reactor effluent in long-term operation tests (> 800 h). The fouling cakes were studied by the membrane autopsy after these tests, combining a staining technique, FTIR, and FESEM-EDX, and the fouling extraction with water and NaOH solutions. Both organic and inorganic fouling were observed, and the main foulants were proteins, polysaccharides, and different calcium and phosphate salts. Also, a significant amount of live cells was detected on the fouling cake (especially on the non-modified PVDF). Although the fouling cake composition was quite heterogeneous, a stratification was observed, with the inorganic fouling mainly in the bulk centre of the cake and the organic fouling mainly located in the lower and upper surfaces of the cake. The mPVDF suffered a more severe fouling, likely owing to a stronger hydrophobic-hydrophobic interaction with the foulants. Irreversible fouling remained on both membranes after the extraction, although a higher irreversible fouling was detected in the mPVDF; however, a complete polysaccharide removal was observed. Regarding the operation performance, PVDF showed a lower stability and suffered a severe degradation, resulting in a lower thickness and perforations. Finally, the decrease in the methane recovery performance of both membranes was associated with the fouling depositions.

Keywords Fluoroalkylsilane · Hydrophobic membrane · Membrane fouling · Membrane stability · PVDF flat-sheet · Surface functionalisation

Introduction

Membrane contactor processes have shown great feasibility in different applications due to their high energy efficiency and small footprint (Jiménez-Robles et al. 2020; Lee et al. 2021; Liu et al. 2021b; Sohaib et al. 2022). Such applications include CO₂ capture from biogas and flue gases, nutrient recovery from wastewaters, biobutanol recovery from fermentation broths, and CH₄ degassing (Klaassen et al.

2005; Centeno-Mora et al. 2020; Davey et al. 2020; Zhang et al. 2020; Zhu et al. 2020). In an anaerobic digestion, more than 40% of the produced CH₄ could be lost as dissolved CH₄ (D-CH₄) in the anaerobic effluent (AE) (Crone et al. 2016; Li et al. 2021; Stazi and Tomei 2021), leading to environmental and security issues (Lee et al. 2021; Stazi and Tomei 2021). In the last few years, membrane contactors for D-CH₄ recovery from AE have been successfully implemented at the bench scale and at the prototype scale with a D-CH₄ removal efficiency of up to 99% (Bandara et al. 2011; Cookney et al. 2016; Henares et al. 2016; Velasco et al. 2018; Rongwong et al. 2019; Sanchis-Perucho et al. 2020). The main challenge related to the implementation of this technology is the prevention of both fouling and wetting of the membranes in order to extend the membrane lifetime and maintain the performance. Such shortcomings could drastically increase the operational and maintenance costs (Wang et al. 2005; Rana and Matsuura 2010; Al-Juboori

Responsible Editor: Guilherme L. Dotto

✉ Marta Izquierdo
marta.izquierdo-sanchis@uv.es

¹ Research Group in Environmental Engineering (GI2AM), Department of Chemical Engineering, School of Engineering, University of Valencia, Avda. Universitat S/N, 46100 Burjassot, Spain

and Yusaf 2012; Al-Juboori et al. 2012; Rongwong et al. 2015; Yan et al. 2022). In this regard, the elucidation of fouling mechanisms in the membrane contactor has recently been identified as a critical issue that needs to be overcome for the application of this technology at the industrial level (Mansourizadeh et al. 2022).

The fouling phenomenon consists of the deposition or adsorption of unwanted compounds onto the membrane surface as well as in the membrane pores (Hu et al. 2014; Abdu et al. 2020; Lee et al. 2021). The different foulants can be classified (Chen et al. 2021; Costa et al. 2021; Liu et al. 2021b) into (i) inorganic matter and (ii) organic matter, which in biological processes are mainly related to growing microorganisms and the extracellular polymeric substances (EPSs) and soluble microbial products (SMPs) secreted by them, i.e. biofouling. The fouling layer on the membrane surface can induce an additional mass transfer resistance and/or a reduction in the useful lifetime of the membrane (Rana and Matsuura 2010; Lee et al. 2021; Liu et al. 2021b). The fouling grade relies on several factors related to membrane characteristics, hydrodynamic conditions, the nature of the treated water, the nature of the foulants, and the interaction forces between the membrane and the foulants (Rana and Matsuura 2010; Al-Juboori and Yusaf 2012; Yan et al. 2022). For hydrophobic membranes such as polyvinylidene fluoride (PVDF), polydimethylsiloxane (PDMS), and polypropylene (PP) used to treat different wastewaters and residual effluents, a strong interaction with organic matter is the main cause of fouling due to the hydrophobic nature of most organic compounds (Liu et al. 2021b). Therefore, proteins and polysaccharides are the major foulants (Rongwong et al. 2019; Chen et al. 2021). Furthermore, these organic foulants could hydrophilise the membrane surface, reducing the wetting resistance and promoting scaling and pore clogging (Zarebska et al. 2015; Liu et al. 2021b; Zhao et al. 2021).

The fouling may be reversible or irreversible depending on the type of interactions between the foulants and the membrane (Costa et al. 2021). In particular, microbial biofouling has been related to physically irreversible membrane fouling (Herzberg and Elimelech 2007; Chen et al. 2021). Different strategies have been proposed in order to prevent or minimise the negative effect of the fouling on the membrane performance, such as membrane cleaning procedures and disinfection of the feed (Al-Juboori and Yusaf 2012; Al-Juboori et al. 2012; Costa et al. 2021). Periodic cleaning with water could prevent or hinder the fouling development and irreversible attachment during long periods of operation (Henares et al. 2017). However, chemical cleaning with alkalis or acid solutions is usually needed to remove foulants strongly adhered to the membrane even though irreversible fouling is commonly reported after the cleaning procedures (Henares et al. 2017; Liu et al. 2021b). The amount of this irreversible fouling and the potential degradation of

the membrane due to the attack of the foulants and chemical cleaners limit the useful lifetime of the membrane (Al-Juboori et al. 2012; Liu et al. 2021b; Pan et al. 2022).

To overcome the limitations related to fouling and wetting, new membrane synthesis and modification techniques have emerged with the goal of developing membranes with higher fouling and wetting resistance surfaces (Rana and Matsuura 2010). Thus, the fouling resistance can be improved by adding different additives in the synthesis step or by an ulterior modification of the membrane surface. In general terms, it is well accepted that the hydrophilisation of the membrane surface provides a higher fouling resistance for water treatment, avoiding the hydrophobic-hydrophobic interaction with organic foulants (Rana and Matsuura 2010; Lee et al. 2021). Thus, Sethunga et al. (2021) developed a membrane surface modification of PVDF, reducing its water contact angle (WCA) from 98.5 to as low as 14.0° and obtaining a surface with a higher fouling resistance for D-CH₄ recovery from an AE. However, divergent results can be found in the literature because superhydrophobic membranes (WCA > 150°) that provide high fouling resistance in membrane distillation have more recently been reported (Liu et al. 2021b). In this regard, Abdu et al. (2020) synthesised a superhydrophobic PVDF (WCA of 164°) with a lower propensity to fouling compared with a conventional PVDF membrane with a lower hydrophobicity (WCA of 77°) when treating synthetic wastewater and actual seawater in membrane distillation at 60 °C.

In our recently published work (Jiménez-Robles et al. 2022b), we studied the performance of a modified PVDF membrane with enhanced hydrophobicity for D-CH₄ recovery from an AE, and an improved performance and useful lifetime was inferred when comparing to the non-modified PVDF. Research works tackling the fouling effect on hydrophobic membranes treating AE for D-CH₄ recovery are still very scarce. The works of Sanchis-Perucho et al. (2021) and Bandara et al. (2011, 2012) reported an insignificant fouling in a short-term period (90 min) with a PDMS membrane and in long-term experiments (> 30 days) with a polyethylene membrane, respectively. The negligible fouling reported in these works could be attributed to the dense structure of the membranes because a porous and rough membrane seems to be more susceptible to fouling deposition (Xu et al. 2019; Liu et al. 2021a; Zhao et al. 2021). Nevertheless, Henares et al. (2017, 2018) observed a similar decrease in the D-CH₄ removal efficiency with microporous PP and dense PDMS membranes for a long-term period of > 200 h. Such divergent results could be explained by taking into account other operational factors such as the different hydrodynamic conditions of the fluid, since a higher turbulence hinders the fouling deposition onto the surfaces (Mikhaylin and Bazinet 2016). Furthermore, the fouling mechanisms in membrane contactor processes have been scarcely studied (Mansourizadeh

et al. 2022). Rongwong et al. (2019) and Sethunga et al. (2021) characterised the fouling cake on modified PVDF membranes and reported that the compact fouling cakes were composed mainly of organic matter, with protein-like substances being the dominant foulants.

In this context, the main aim and contribution of this work was the determination of the fouling composition and potential mechanisms on PVDF membrane contactors with different hydrophobicity grades for the degassing of an anaerobic reactor effluent. For this purpose, fouling tests under a long-term operation were conducted with a flat-sheet membrane module using a commercial PVDF and an organofluorosilanised PVDF with enhanced hydrophobicity. Then, the fouling cake was analysed in detail by means of different microscopy and spectroscopy techniques (FESEM-EDX and FTIR) in order to identify the different elements and compounds. Staining techniques were also used for the identification and quantification of proteins and polysaccharides and for the sensing of the metabolic status of the bacteria. In addition, a fouling extraction from the membrane was carried out with water and a NaOH solution in order to analyse the composition of the reversible and irreversible fouling. Finally, the influence of the fouling on the membrane performance and stability in D-CH₄ recovery was also elucidated.

Materials and methods

Membrane material and functionalisation

The flat-sheet PVDF membrane was supplied by Dorsan Filtration S.L. (Spain). The membrane was composed of hydrophobic PVDF supported on a polyester (PET) non-woven support, resulting in a microporous structure with an overall porosity of $62 \pm 3\%$, gravimetrically measured with 1-octanol (99%, Acros Organics, Germany) (Liu et al. 2016). The membrane pore size and liquid entry pressure were 0.2 μm and 1.8 bar, respectively, according to the supplier. The thickness and static WCA were measured, resulting in values of $159 \pm 2 \mu\text{m}$ and $103.4 \pm 1.6^\circ$, respectively.

The surface modification of the PVDF was carried out in a three-step procedure consisting of (1) activation with a NaOH solution, (2) functionalisation by means of a mixture containing 1H,1H,2H,2H-perfluorooctyltriethoxysilane (Dynasylan® F8261, Evonik GmbH, Germany) as the modifying agent and tetraethyl orthosilicate (TEOS, $\geq 99\%$, Sigma-Aldrich, USA) as the silica precursor, and (3) curing. A detailed description of the modification procedure can be found in our previous work (Jiménez-Robles et al. 2022b), and the modification conditions in each step were established and based on the optimal conditions that maximised the surface WCA, which were the following: activation

with a 5% NaOH solution and functionalised with a concentration and ratio of Dynasylan/TEOS of 7.2% and 0.55, respectively. The modified PVDF (mPVDF) presented a thickness of $164 \pm 1 \mu\text{m}$ and a WCA of $140.9 \pm 2.5^\circ$. The overall porosity of the mPVDF was $59 \pm 2\%$, similar to that of the non-modified PVDF.

Experimental setup and operation procedure

Fouling tests using an AE as the liquid stream were conducted with both membranes for comparison purposes. The AE was collected from the anaerobic reactor of the urban wastewater treatment plant Quart-Benager II (Valencia, Spain), filtered with a 10–20 μm filter, and stored in the fridge ($< 4^\circ\text{C}$) before use in the tests. The characteristics of the filtered AE are provided in the Supplementary Material S1.

The fouling tests were carried out under long-term operation (> 800 h) using the laboratory-scale system depicted in Supplementary Material S2. Initially, a membrane sample was placed inside a circular flat-sheet module (FM) made of stainless steel with an effective contact area of 17.3 cm^2 and a 2-L liquid feed tank was filled with AE. Then, a constant liquid flow rate (Q_L) of 3.5 L h^{-1} was pumped in a closed loop through the liquid side of the FM using a peristaltic pump (Watson-Marlow Fluid Technology Solutions, UK) for up to around 830 h. Q_L was set based on our previous work (Jiménez-Robles et al. 2022a) and to promote the fouling deposition on the membrane because high fluxes increase the turbulence and favour the fouling mitigation (Mikhaylin and Bazinet 2016). At the end of the fouling tests, the membranes were extracted from the FM and subjected to different analysis techniques and methodologies (FESEM-EDX, FTIR, staining, and fouling extraction). In addition, water samples were taken at different times of operation to measure the concentration of proteins and polysaccharides and the chemical oxygen demand (COD).

Methods for visualising and identifying the fouling on the membrane surface

FESEM-EDX

An inspection of the membrane surface and cross-section, as well as of the fouling cake deposited onto the membrane, was conducted by a field emission scanning electron microscope (FESEM) equipped with an energy dispersive X-ray (EDX) spectrometer with an accelerating voltage of 20 kV (Hitachi S4800, Hitachi Ltd., Japan). For the image acquisition, the membrane coupons were softly dehydrated in an ethanol series in a sequence of 50, 80, 100, and 100% for 3 min each and then air-dried overnight. Afterwards, the coupons were placed on an aluminium holder and then

coated with a fine layer of Au/Pd by sputtering in a vacuum for 1 min. The FESEM-EDX technique was used to analyse the surface and cross-section morphology, thickness, and chemical composition of the membrane and the fouling cake.

FTIR

The surface chemical composition of the fouling cake was also studied by means of Fourier transform-infrared spectroscopy (FTIR) in the attenuated total reflectance mode (Cary 630 FTIR Spectrometer, Agilent Technologies, Inc., USA). The infrared spectra were recorded in the range of 4000–650 cm^{-1} and a resolution of 4 cm^{-1} and processed with the Agilent MicroLab FTIR software. For the infrared spectra acquisition, the membrane coupons were previously dehydrated with ethanol, as previously detailed.

Staining of proteins and polysaccharides

The identification and quantification of protein and polysaccharides attached to the membrane surface and fouling cake were carried out by means of staining and imaging with a confocal laser scanning microscope (CLSM) (Olympus FV1000, Olympus Corporation, Japan) equipped with a 10 \times magnification objective. The SYPRO Orange Dye and the Concanavalin A conjugates to Alexa Fluor 633 (Molecular Probes, Inc., USA) were applied to stain proteins and polysaccharides, respectively.

The protein staining solution was prepared by diluting the SYPRO Orange Dye with 7.5%_v acetic acid (acetic acid 100%, VWR Chemicals, USA) until a volume ratio of 1:5000 was achieved. The polysaccharide staining solution was prepared at a concentration of 100 μg of Concanavalin A mL^{-1} using a phosphate-buffered saline solution (PBS) as the solvent.

For the staining technique, a 1 cm \times 1 cm membrane coupon was first immersed in 1 mL of the protein staining solution and placed in a rotary shaker in the dark for 1 h at 75 rpm and room temperature. Then, the membrane was rinsed in 7.5%_v acetic acid to remove the excess staining solution (< 1 min) and then immersed in a PBS solution to remove the residual acetic acid (< 1 min). Afterwards, the membrane coupon was immersed in 1 mL of the polysaccharide staining solution and shaken for 1 h at 75 rpm at room temperature in the dark. Then, the membrane was rinsed in the PBS solution (< 1 min). Finally, the stained membrane coupon was air-dried with force aeration for ~2 h and stored in the dark at 4 °C.

The stained samples were observed with the CLSM, and at least two different series of images were taken at different depths with an imaged surface size of 1300 $\mu\text{m} \times 1300 \mu\text{m}$. Each series of the CLSM images was processed with the *Imaris* software to reconstruct a 3D image (Herzberg and

Elimelech 2007; Hu et al. 2014). In order to quantify the volume of the stained proteins and polysaccharides on the membrane, a 3D model was generated from the CLSM images also using the *Imaris* software (Hu et al. 2014). Thus, the specific volume of the foulant (proteins or polysaccharides) is defined as the total volume per unit of membrane area ($\mu\text{m}^3 \mu\text{m}^{-2}$) (Hu et al. 2014).

Water contact angle

The membrane surface hydrophobicity was evaluated by the static WCA. WCA measurements were carried out by the sessile drop technique (Hebbar et al. 2017). A water droplet of $5.5 \pm 0.1 \mu\text{L}$ was deposited onto the membrane surface using a syringe pump (KF Technology s.r.l., Italy) at room temperature (~25 °C). An image of the water drop profile was taken at 15 s with a digital microscope (Handheld Digital Microscope Pro, Celestron LLC, USA) under white light (Philips HUE Lamp, Koninklijke Philips NV, The Netherlands). ImageJ software was used for image processing using the *Contact Angle Plug-in* based on the ellipse approximation. The WCA was evaluated at different spots on the membrane, and a mean value was obtained from at least 10 measurements. Wet membranes were dried prior to the WCA measurements by removing the excess water and moisture with forced aeration at room temperature for approximately 2 h.

Methods for the extraction and analysis of the membrane foulants in solution

Fouling extraction procedure

The fouling agents were also analysed after the detachment of the fouling cake from a membrane coupon of 8.7 cm^2 using a sonication bath (Bransonic® 1510E-MT, Branson Ultrasonic Corporation, USA) with different solutions: a soft cleaning with 20-mL MilliQ water for 60 min and an alkaline cleaning with 20 mL of 0.01 M NaOH solution for 60 min. Then, the membrane was dried in an oven at 45 °C overnight. Both water and NaOH extraction solutions were analysed to measure the concentration of proteins, polysaccharides, phosphates, alkalinity, COD, total suspended solids (TSS), volatile suspended solids (VSS), and the metabolic status of the bacteria.

Liquid sample analysis techniques

The characterisation of the filtered AE and the water and NaOH extraction solutions was conducted. The determination of TSS and VSS was carried out according to standard methods (Baird et al. 2018). Alkalinity was determined by means of the 5 pH point titration procedure (Moosbrugger

et al. 1992) (848 Titrino Plus, Metrohm, Switzerland). The polysaccharide content was analysed by the phenol–sulfuric acid method proposed by Dubois et al. (1956) with glucose as the standard (Juang et al. 2010; Hafuka et al. 2019). The protein content was determined according to the modified Lowry methods by Onishi and Bar (Total protein kit, micro Lowry, Onishi & Bar modification, Sigma-Aldrich, USA) using bovine serum albumin as the standard. The COD and phosphate content were determined using colorimetric analysis kits (COD Cell Test 0–150 mg L⁻¹ and PO₄³⁻ Cell Test 1.5–76.7 mg L⁻¹, respectively, Merck Chemicals, Germany).

Analysis of the bacteria viability

The metabolic status of the bacteria contained in the AE and in the fouling extraction solutions was evaluated to investigate the influence of the biofouling on the fouling cake development. The quantification of the live and dead cells was conducted by means of a flow cytometry using the LIVE/DEAD BacLight™ Bacterial Viability Kit L7012 (Molecular Probes Inc., USA) for the bacteria staining in the liquid samples. The viability kit is composed of the SYTO 9 and propidium iodide (PI) dyes to stain the live and dead cells, respectively. A staining solution was firstly prepared with a volume ratio of 1:1 (SYTO 9:PI) according to the specifications. Three µL of the staining solution was added to 1 mL of the liquid sample. The sample was vigorously shaken and incubated in the dark for 15 min at 200 rpm. Afterwards, the stained samples were filtered with a 50 µm filter and analysed in a flow cytometer (FACSVerse 3L 8C, Becton, Dickinson and Company, USA) equipped with a 488-nm laser and using BD Trucount™ Tubes (Becton, Dickinson and Company, USA) for the quantification of live and dead cells. Data acquisition and treatment were carried out with the FACS-Suite software.

Results

Characterisation of the fouling deposited on the membrane surface

The evolution of the fouling formation on the membranes can be observed in the pictures taken from the PVDF and mPVDF membrane surfaces (Supplementary Material S3). The development of the fouling cake was clearly observed during the fouling tests. At the end of these tests, zones with a different fouling grade at the visual level on the membrane sample were selected for analysis.

Staining of proteins and polysaccharides

The distribution of the proteins and polysaccharides on the membranes was observed in the samples of PVDF and mPVDF at the end of the fouling tests. As an example, Fig. 1 shows a stained sample of the non-modified membrane (PVDF) before and after the fouling extraction in which the protein and polysaccharide distribution in 2-D (Fig. 1a and b), the 3-D image reconstruction (Fig. 1c), and the 3-D model (Fig. 1d) can be observed.

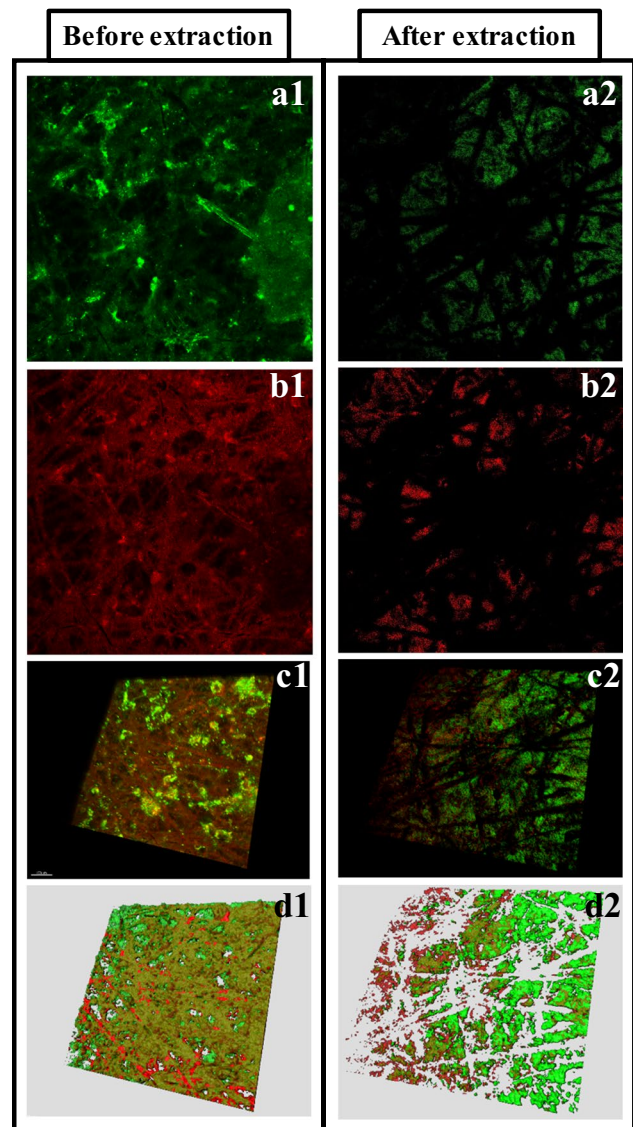


Fig. 1 CLSM images of the staining of (a) proteins and (b) polysaccharides deposited on the non-modified PVDF membrane surface after the fouling test (before fouling extraction, 1) and after the extraction (2). (c) Reconstruction in 3D and (d) 3D model of the protein and polysaccharide distribution. Proteins are in green and polysaccharides are in red. Imaged surface size of 1300 µm × 1300 µm

Table 1 Specific volume ranges of proteins and polysaccharides ($\mu\text{m}^3 \mu\text{m}^{-2}$) on the non-modified (PVDF) and modified PVDF (mPVDF) membranes measured in different surface locations after the fouling test (time of operation > 800 h) with the anaerobic reactor effluent (before extraction) and after the fouling extraction. Imaged surface size of $1300 \mu\text{m} \times 1300 \mu\text{m}$

	Before extraction		After extraction	
	PVDF	mPVDF	PVDF	mPVDF
Proteins	27–37	21–29	10–12	12–15
Polysaccharides	15–17	18–19	9–21	n.d

n.d: not detected

The CLSM images show the widespread presence of proteins and polysaccharides all over the fouling cake for both membranes before the extraction. After the fouling extraction, proteins and polysaccharides were also identified on the non-modified membrane (PVDF) (Fig. 1a2 and b2), but only proteins were found on the mPVDF membrane (images not shown). In both membranes, the distribution of proteins and polysaccharides on the surface was quite uneven with locations with a high concentration of them and others locations with hardly any of them (Fig. 1c1 and c2 for the non-modified PVDF).

The specific volumes of proteins and polysaccharides on the membrane surfaces before and after the fouling extraction obtained from the 3-D models are shown in Table 1 (examples of the models in Fig. 1d). These outcomes showed that the content of both foulants varied from different analysed surface locations (size of $1300 \mu\text{m} \times 1300 \mu\text{m}$) of the same membrane according to the heterogeneous distribution mentioned above. It is important to note that the polysaccharide content, unlike the protein content, was quite uniform along the surfaces in both membranes before the extraction. In this regard, surface locations of the membrane sample with a macroscopic darker brown colour presented a higher and lower protein content on the PVDF and mPVDF membranes, respectively, compared with those lighter brown zones before the extraction. After the fouling extraction, the protein content was always reduced and the complete removal of polysaccharides was observed in the mPVDF membrane. These outcomes could indicate a higher protein deposition rate on the membrane surface during the first steps of the fouling formation with a further coverage by other foulants, especially on the mPVDF membrane with a higher hydrophobicity.

Fourier transform infrared spectroscopy (FTIR)

The representative infrared spectra of the pristine PVDF and mPVDF membranes are shown and compared with the spectra after the fouling tests and after the fouling extraction in Fig. 2. The assignment of each band attributable to the

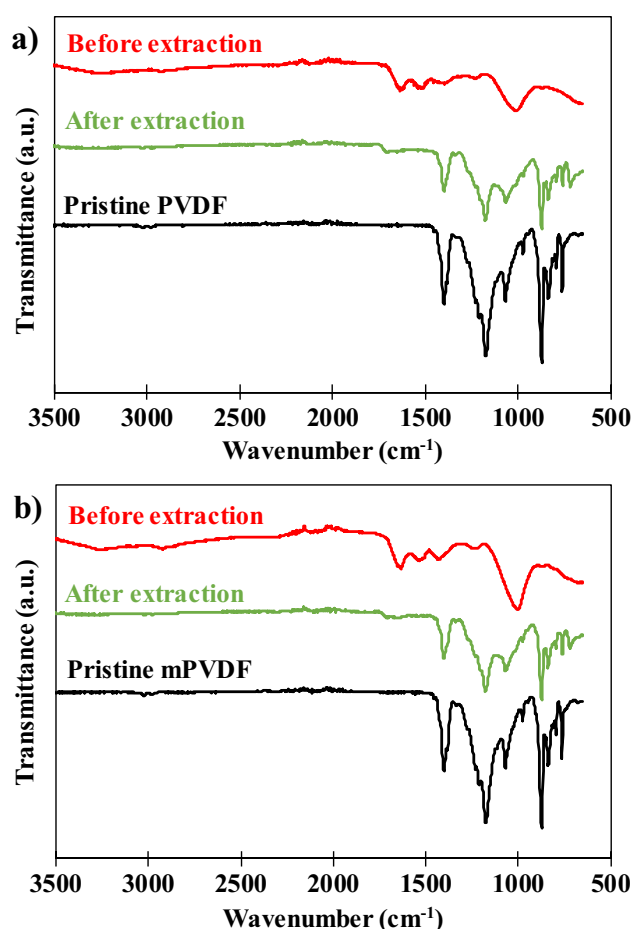


Fig. 2 Fourier transform infrared spectra of the pristine, before fouling extraction (fouled), and after the fouling extraction surfaces of (a) PVDF and (b) modified PVDF (mPVDF) used in the fouling tests (operation time > 800 h). Transmittance is expressed in arbitrary units (a.u.)

foulants is shown in Table 2, and the representative bands of the spectra for the PVDF base material are shown in Supplementary Material S4. The spectra of both pristine PVDF and mPVDF membranes are very similar because the membrane modification occurred at mostly the surface level and FTIR-ATR analysis is not very surface sensitive (Rana and Matsuura 2010).

The spectra of the fouled membranes were significantly different with respect to the pristine state for both membranes, which can be attributed to the presence of a significant fouling cake on the membrane surface. In fact, most of the identified peaks in the fouled membranes can be related to organic compounds and/or microorganisms (biofouling) (Xue et al. 2016) according to the complex organic nature of the AE feed used in these experiments. Bands of functional groups attributed to proteins and polysaccharides were found at wavenumbers of 3250 , 1700 – 1500 , and 1200 – 800 cm^{-1} . The peak at 2922 cm^{-1} was attributed to fatty acids involved

Table 2 Major FTIR absorption bands obtained in the analysis of both fouled PVDF and modified PVDF (mPVDF) membranes after the fouling tests (before the fouling extraction)

Wavenumber, cm ⁻¹	Band	Group	Reference
3250	Amide I (N–H stretching)	Proteins	(Dean 1998; Davis and Mauer 2010; Sairiam et al. 2013; Mohamed et al. 2017)
2922	C–H asymmetric stretching	Fatty acids	(Dean 1998; Davis and Mauer 2010; Mohamed et al. 2017)
1636	Amide I (C=O and C=N stretching)	Proteins	(D'Abzac et al. 2010; Mikhaylin and Bazinet 2016; Chen et al. 2018)
1533	Amide II (C–N stretching and N–H deformation)	Proteins	(Saha et al. 2007; D'Abzac et al. 2010; Zarebska et al. 2015)
1429	COO ⁻ symmetrical stretching and phenolic C–O bond	Carboxylates and humic substances	(Zarebska et al. 2015; Chen et al. 2018; Yan et al. 2022)
1230	Phosphate ester asymmetric stretching (P=O)	Phospholipids and nucleic acids	(Davis and Mauer 2010; Xue et al. 2016)
1172	O–H stretching	Polysaccharides	(D'Abzac et al. 2010)
1010	C–O–C and C–O stretching	Polysaccharides	(Saha et al. 2007; Davis and Mauer 2010)
1000–800	Bands associated with polysaccharides and polysaccharide-like substances		(Gómez-Ordóñez and Rupérez 2011; Chen et al. 2018; Yan et al. 2022)

in the metabolic activity of the bacteria, and the peak at 1429 cm⁻¹ was attributed to the potential carboxylates generated in the anaerobic treatment, such as acetate, propionate, lactate, butyrate, and valerate (Cabrera-Rodríguez et al. 2017), and to humic substances. The presence of microorganisms such as bacteria was identified by the band at 1230 cm⁻¹ that represents phospholipids and nucleic acids.

Similar infrared spectra of both membranes were obtained even though higher band intensities were usually observed for the mPVDF membrane, suggesting a higher foulant deposition as visually identified (Supplementary Material S3). It could be noted that the intensity of the band at 1230 cm⁻¹ was quite similar, which could denote a lower proportion of microorganisms in the fouling cake of the mPVDF membrane.

After the fouling extraction, the obtained infrared spectra were similar to those of the pristine state for both membranes (Fig. 2). Bands owing to the PVDF base material presented lower intensities in both spectra after the fouling extraction, and a new peak appeared at ~ 700 cm⁻¹, which could be related to EPSs (Chen et al. 2018). These outcomes indicated that an irreversible fouling covered the membrane surface composed of protein- and/or polysaccharide-like compounds, in accordance with the light brown colour observed on the membrane after the extraction (Supplementary Material S3). Comparing both membranes, mPVDF presented zones with a higher irreversible fouling grade at the visual level because a darker brown colour was observed, and the infrared spectra in these zones showed the characteristic band for proteins at ~ 1600 cm⁻¹. This could indicate that antifouling properties dropped upon making the surface more hydrophobic. Additionally, a new band appeared at

1707 cm⁻¹ after the extraction, which could be attributed mainly to the carbonyl group (C=O) from the PET support of the membranes, suggesting a surface degradation, especially in the PVDF membrane.

Microscopy and X-ray spectroscopy (FESEM-EDX)

The morphology of the surface and cross section of the PVDF and mPVDF membranes was analysed by FESEM, and the chemical composition was also determined by EDX. The surface morphology of the pristine membranes and the membranes after the fouling tests and the fouling extraction is shown in Fig. 3. The membranes were clearly covered by a dense-like fouling cake, leading to a severe reduction in the surface porosity (Fig. 3a and b). Some cracks on the fouling cake can be visualised due to the drying process (Fig. 3b1). The presence of spheres and needle-like biomass particles was quite noticeable on the PVDF membrane (Fig. 3b1) and could be associated with *Bacillus* and *Streptococcus*, respectively. On the contrary, a higher content of larger crystals was observed on the mPVDF membrane than on the PVDF membrane (Fig. 3b2).

After the fouling extraction, perforations were observed all over the PVDF membrane surface (Fig. 3c1), indicating a severe degradation of the top layer, i.e. the PVDF material, because the PET non-woven support was clearly identified through these perforations. The rest of the surface suffered a decrease in the surface porosity owing mainly to the irreversible fouling mentioned above (Fig. 3a1 and c1). The mPVDF membrane also experienced a similar decrease in surface porosity (Fig. 3a2 and c2) even though the severe

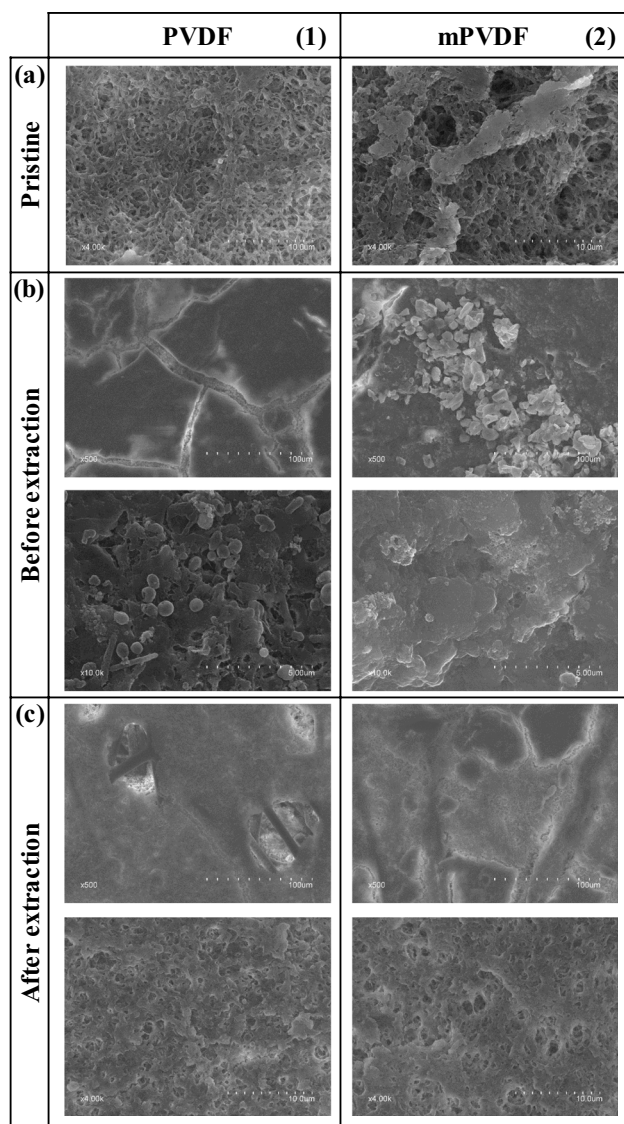


Fig. 3 FESEM images of the surface of the (1) PVDF and (2) modified PVDF (mPVDF) captured from the (a) pristine membranes, (b) fouled membranes before the fouling extraction (operation time > 800 h), and (c) after the extraction

degradation and perforations on the top layer were not detected as in the PVDF membrane (Fig. 3c).

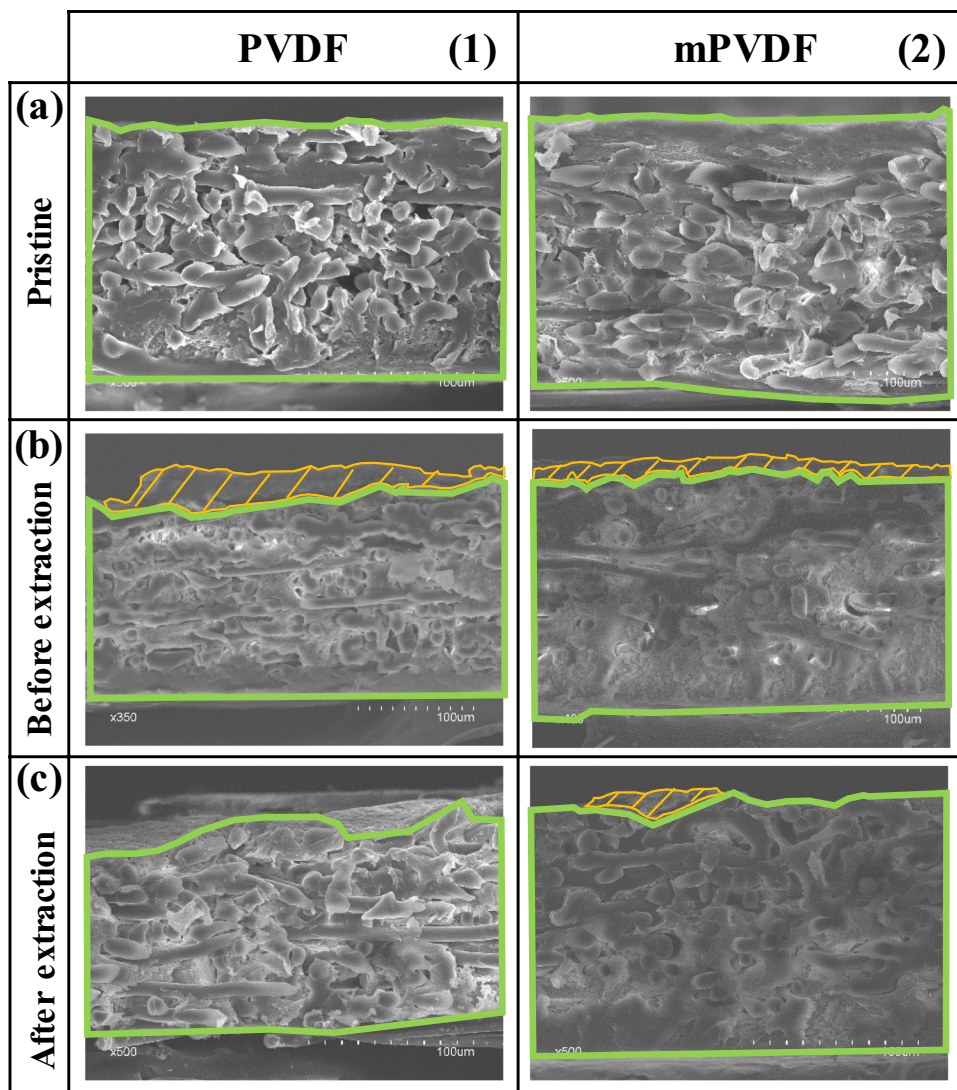
The FESEM images of the cross section are shown in Fig. 4. The bulk of the fouling cake observed on the membranes was dense-like, and the measured overall membrane thickness was somewhat uneven, especially on the PVDF membrane, as reported by other authors (Juang et al. 2010). Compared to the pristine PVDF ($159 \pm 2 \mu\text{m}$), the non-uniform deposition of foulants resulted in thicker sections with values up to $195 \mu\text{m}$ due to the fouling cake (Fig. 4b1) and thinner sections with values as low as $134 \mu\text{m}$. These low thickness values suggested the degradation of the membrane during the long-term operation. The reduction

in the membrane thickness was confirmed from the FESEM images of PVDF after the fouling extraction because a quite irregular surface was observed with an overall thickness of $142 \pm 16 \mu\text{m}$ (Fig. 4c1). It should be noted that in Fig. 4c1, the membrane surface can be seen as background above the upper cross-section boundary due to the membrane degradation. In the case of mPVDF (Fig. 4b2), the fouling cake appeared more uniformly distributed with a maximum overall membrane thickness of up to $187 \mu\text{m}$. After the fouling extraction (Fig. 4c2), a thickness of $161 \pm 2 \mu\text{m}$ was measured, similar to the pristine mPVDF ($164 \pm 1 \mu\text{m}$).

The surface chemical composition of the pristine membranes and the membranes after the fouling tests and the fouling extraction are shown in Table 3. The surface F content drastically decreased in both membranes after the fouling tests, which is attributed to the formation of a fouling cake that masks the top membrane surface, as observed by other authors (Yan et al. 2022). Comparing the fouled membranes, a lower F content on mPVDF with respect to the PVDF was observed, which indicates a higher coverage grade with fouling on the mPVDF. The O content increased to values of around 26% and 37% in PVDF and mPVDF, respectively, and an N content of around 5% was observed, which could be related to the presence of biomass, protein, and protein-like substances (Al-Juboori and Yusaf 2012; Rongwong et al. 2019). In addition, the predominant content of O and C denoted mainly an organic fouling and high O to C ratios (O/C) suggested the presence of EPSs in both membranes (Khan et al. 2010; Zarebska et al. 2015). This high content of O and C could also indicate a scaling of carbonate and hydroxide salts. Ca, P, and Mg represented the other major elements found on the surface, and a higher content of these elements was observed on the mPVDF. The Ca was found all over the surface likely in the form of carbonates, and also particles composed mainly of P and Mg were detected, which could be related to crystals of struvite ($(\text{NH}_4)\text{MgPO}_4$) or struvite analogues (P-Mg) (Choo and Lee 1996). In addition, other minor elements and particles of aluminosilicates and others composed of Cu–Zn–Na were detected on the surface. FESEM-EDX images with the distribution of the different elements and composition of particles on the membrane surfaces can be found in Supplementary Material S5.

After the fouling extraction, a surface F content lower than that of the pristine membranes was recorded from both membranes. This decrease in the F content could be attributed to the presence of the irreversible fouling and/or to a loss of F atoms due to the membrane degradation by the foulants or to the dragging effect by the liquid flux stress (Jiménez-Robles et al. 2022b). The membrane surface degradation in the PVDF was also identified from the absence of F inside the perforations that appeared after the fouling removal mentioned above (distribution of F atoms shown in

Fig. 4 FESEM images of the cross section of the (1) PVDF and (2) modified PVDF (mPVDF) captured from the (a) pristine membranes, (b) fouled membranes before the fouling extraction (operation time > 800 h), and (c) after the extraction. The boundaries of the membrane and fouling cake are highlighted in green and orange, respectively



Supplementary Material S6). The F content detected on the surface was lower for the mPVDF, likely owing to a higher amount of irreversible foulants that masked the membrane surface. Ca, P, Mg, and N remained as the main elements of the irreversible fouling even though N was not found on PVDF. Moreover, the ratio O/C remained higher than that in the pristine membranes, which could indicate the presence of EPS. Other minor inorganic elements were not completely removed after the extraction, which could suggest the need for an additional acid-cleaning step.

The cross section of the fouling cakes deposited on both membranes was also analysed, and the results are shown in Table 3. FESEM-EDX images of the distribution of F, Ca, and P are shown in Supplementary Material S7 for both membranes. The fouling cake cross section was composed mainly of Ca, P, and C. Comparing the results from the surface and cross section, a significantly higher inorganic fouling was detected in the centre bulk of the cake, denoting a

stratification of foulants across this cake. The low N content with values $\leq 1\%$ and the higher amount of Ca in the cross section of both membranes could indicate a Ca scaling that was furthered covered by a microbial and organic layer, as reported by other authors (Chen et al. 2021). Other minor elements presented a higher content with respect to the surface, such as Fe, Cu, and Zn, promoting an inorganic type of fouling.

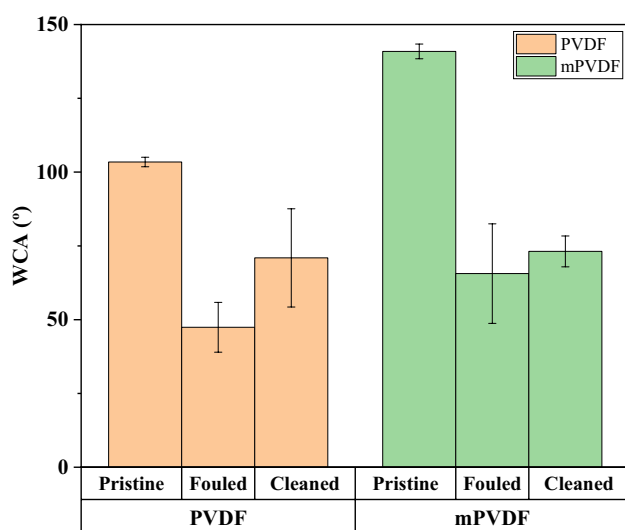
Water contact angle analysis

The surface hydrophobicity was evaluated by measuring the static WCA of both membranes after the fouling tests and after the fouling extraction, and the results are presented in Fig. 5. A lower WCA was observed after the fouling tests, with a decrease of more than 50% from the initial value for both membranes, and the WCA measurements showed a large deviation, owing mainly to the heterogeneous

Table 3 EDX analysis of the membrane surface and the fouling cake cross section from the fouled PVDF and modified PVDF (mPVDF) after the fouling test (> 800 h) and after the fouling extraction. Valuesexpressed in %_w. The errors denote the standard deviation of at least 3 measurements in different spots

Element	PVDF				mPVDF			
	Membrane surface			Fouling cake cross section	Membrane surface			Fouling cake cross section
	Pristine	Before extraction	After extraction	Before extraction	Pristine	Before extraction	After extraction	Before extraction
F	52.67 ± 5.90	17.24 ± 6.40	51.06 ± 0.41	0.00 ± 0.00	54.94 ± 6.50	6.45 ± 1.76	46.39 ± 4.31	1.36 ± 1.94
C	43.32 ± 5.00	39.23 ± 1.84	39.67 ± 1.11	6.57 ± 6.89	41.16 ± 5.40	29.91 ± 1.24	34.86 ± 1.24	21.63 ± 9.55
O	3.61 ± 0.60	26.37 ± 3.17	6.92 ± 0.50	4.16 ± 6.02	3.45 ± 0.70	36.52 ± 1.85	11.63 ± 2.71	8.67 ± 2.45
N	-	5.97 ± 0.92	0.00 ± 0.00	0.00 ± 0.00	-	4.90 ± 0.06	0.74 ± 0.23	0.56 ± 0.57
Ca	-	5.79 ± 0.35	0.84 ± 0.25	67.20 ± 12.55	-	9.66 ± 3.32	3.03 ± 1.35	43.92 ± 9.81
P	-	3.15 ± 0.26	0.45 ± 0.14	10.46 ± 2.24	-	6.21 ± 0.37	1.58 ± 0.69	15.78 ± 2.68
Mg	-	0.78 ± 0.26	0.22 ± 0.03	0.00 ± 0.00	-	2.54 ± 1.27	0.21 ± 0.04	0.21 ± 0.12
Si	-	0.12 ± 0.02	0.08 ± 0.02	0.73 ± 1.26	0.46 ± 0.10	0.21 ± 0.05	0.29 ± 0.02	0.01 ± 0.01
Na	-	0.31 ± 0.04	0.46 ± 0.02	0.00 ± 0.00	-	0.95 ± 0.34	0.34 ± 0.09	0.00 ± 0.00
K	-	0.04 ± 0.04	0.01 ± 0.01	0.26 ± 0.31	-	0.22 ± 0.09	0.01 ± 0.01	0.07 ± 0.04
Fe	-	0.28 ± 0.03	0.07 ± 0.02	4.18 ± 1.74	-	0.41 ± 0.07	0.10 ± 0.05	1.61 ± 0.46
Cu	-	0.18 ± 0.03	0.12 ± 0.02	1.74 ± 0.85	-	0.27 ± 0.05	0.22 ± 0.09	0.79 ± 0.23
Zn	-	0.00 ± 0.00	0.00 ± 0.00	3.49 ± 1.06	-	0.47 ± 0.15	0.47 ± 0.21	2.62 ± 0.62
Al	-	0.15 ± 0.06	0.05 ± 0.01	0.00 ± 0.00	-	0.12 ± 0.03	0.04 ± 0.02	1.40 ± 0.64
S	-	0.39 ± 0.06	0.06 ± 0.02	0.65 ± 0.11	-	0.46 ± 0.03	0.10 ± 0.05	1.35 ± 0.47
Cl	-	0.00 ± 0.00	0.00 ± 0.00	0.54 ± 0.93	-	0.70 ± 0.40	0.00 ± 0.00	0.00 ± 0.00

formation of the fouling cake. This decrease in the WCA can be attributed to the hydrophilisation promoted by some fouling agents (Zarebska et al. 2015), masking the membrane surface properties (Khan et al. 2010; Zhao et al. 2021). After the fouling extraction, the WCA increased to $70.9 \pm 16.6^\circ$

**Fig. 5** Variation in the static water contact angle of the pristine, fouled (before the fouling extraction), and cleaned (after the fouling extraction) PVDF and modified PVDF membranes (mPVDF)

and $73.1 \pm 5.2^\circ$ for the PVDF and mPVDF, respectively, representing 69% and 55% of their initial WCA. Thus, an incomplete extraction of the foulants or membrane degradation can be inferred, as the initial hydrophobicity grade was not restored. It is noteworthy to highlight that the increase in the WCA after the fouling extraction of the mPVDF was almost negligible, which suggests the presence of a high irreversible fouling grade and/or a stronger foulant-membrane interaction.

Fouling analysis in the extraction solution

The solutions obtained from the extraction of the fouling cake with MilliQ water and a 0.01 M NaOH solution were analysed, and the results are shown in Table 4. The presence of both organic and inorganic matter as well as microorganisms was detected. The soluble COD and the presence of proteins, polysaccharides, and VSS were indicators of organic fouling, and the presence of microorganisms was confirmed by the significant amount of live and dead cells detected in all the extraction solutions. Most of the foulants were detached in the first sonication with water, though the second extraction with NaOH also contributed to the membrane cleaning, especially removing organic foulants. The extracted inorganic fouling was mainly recovered with water, as indicated by the higher alkalinity and PO_4^{3-} concentration

Table 4 Characterisation of the foulants in the extraction solutions (MilliQ water and 0.01 M NaOH solution) from the PVDF and modified PVDF membrane (mPVDF). Results are expressed per unit of membrane area

	PVDF			mPVDF		
	Water	NaOH	Total	Water	NaOH	Total
COD*, $\mu\text{g O}_2 \text{ cm}^{-2}$	109.8	0.0	109.8	98.3	28.9	127.2
Alkalinity*, $\mu\text{g CaCO}_3 \text{ cm}^{-2}$	147.1	36.8	183.9	144.9	38.6	183.5
Proteins*, $\mu\text{g cm}^{-2}$	45.3	13.4	58.7	48.7	6.7	55.4
Polysaccharides*, $\mu\text{g cm}^{-2}$	31.1	5.3	36.4	38.2	7.1	45.2
PO_4^{3-*} , $\mu\text{g cm}^{-2}$	164.7	2.9	167.6	101.2	0.0	101.2
TSS, $\mu\text{g cm}^{-2}$	0.18	0.00	0.18	0.72	0.05	0.77
VSS, $\mu\text{g cm}^{-2}$	0.18	0.00	0.18	0.53	0.05	0.58
Number of live cells*, $\text{cells cm}^{-2} 10^{-5}$	38	4	41	10	6	16
Number of dead cells*, $\text{cells cm}^{-2} 10^{-5}$	22	1	23	8	1	9

*Measured after sample filtration (0.7 μm)

in the water extraction solutions (around 180 $\mu\text{g CaCO}_3 \text{ cm}^{-2}$ and 100–170 $\mu\text{g PO}_4^{3-} \text{ cm}^{-2}$), which indicated the presence of carbonate, bicarbonate, and phosphate salts. A significantly higher content of phosphates was extracted from the fouling cake of PVDF with respect to the mPVDF, and also a higher content of live and dead cells was detected, which could indicate the presence of a greater biomass. The extracted TSS from the PVDF membrane was associated with the organic matter (where TSS = VSS), so the total extracted inorganic foulants from the PVDF were mainly dissolved. In the case of mPVDF, 25% of the TSS extracted corresponded with the inorganic solids.

Discussion

Characterisation of the fouling deposited on the membranes

Both PVDF and mPVDF membranes were susceptible to fouling when treating an AE for D-CH₄ recovery. Visually, the fouling content increased with the time of operation owing to a continuous deposition of foulants from the anaerobic water and/or biofilm growth, as also reported by other authors (Hu et al. 2014). The decrease in the WCA at the end of the fouling test was in agreement with the fouling cake development in which WCA decreased as the fouling increased. This surface hydrophilisation can be especially favoured by the deposition of amphiphilic proteins and polysaccharides with hydrophilic moieties such as O–H, N–H, and COO, which are susceptible to the formation of hydrogen bonds with water molecules (Saha et al. 2007; Zarebska et al. 2015; Chen et al. 2021; Costa et al. 2021). Also, the biofilms, metal oxides, and aluminosilicates contribute to the hydrophilisation, inducing wetting (Costa et al. 2021; Zhao et al. 2021). In addition, the potential loss of F atoms from the membrane surface owing to the degradation observed in the FESEM images was especially severe on the PVDF, contributing to the decrease in the WCA.

Both organic and inorganic fouling were found on the membrane, and proteins and polysaccharides were the major organic foulants. The presence of proteins in the fouling cake was in accordance with the decrease observed in the protein content in the analysed anaerobic water samples from the fouling tests collected at different times of operation. The decrease in the protein content was more pronounced in the anaerobic water used for the PVDF, with a decrease of 12% in the first 3 days, whilst a decrease of less than 8% was observed in the test with the mPVDF. This result was in accordance with the higher protein content detected on PVDF at the end of the fouling test. By contrast, the variation in the polysaccharide content in the anaerobic water was not significant. Also, a slight decrease (5–10%) in the COD of the anaerobic water used in the fouling tests with the time of operation was observed in both membranes, which also suggested a deposition of organic matter on the membranes. Henares et al. (2017, 2018) also analysed the anaerobic water stream at the inlet and outlet of different hollow fibre membrane contactors and reported a decrease in the VSS, proteins, and turbidity at the outlet of the contactor attributed to the fouling deposition. Also, other authors have qualitatively identified the aromatic proteins and SMP substances as the main organic matter in the fouling extraction solution when treating AEs (Rongwong et al. 2019; Sethunga et al. 2021).

The fouling could be aggravated by the microbial biofouling because the large number of live cells detected in the extraction solution could also promote the generation of EPSs and other SMPs. Thus, the higher protein content observed on the fouling cake surface of the PVDF could also be attributed to the presence of a higher number of live cells. The grafting of fluoroalkyl chains on the PVDF could be responsible for the lower number of live and dead cells determined in the mPVDF because the microbes present a much weaker interaction with this chemical structure, which reduces the biofouling (Zhu et al. 2020).

The inorganic fouling was composed mainly of Ca, P, and Mg. Other authors have also reported those elements as the major inorganic foulants from different wastewaters in membrane distillation (Yan et al. 2022). Other minor elements

found, such as Na, Cu, Zn, Fe, Al, Si, and S, could involve different types of scaling, as observed by other authors (Zarebska et al. 2015; Chen et al. 2021). In addition to the inorganic particles detected in the fouling cake, other salts could be deposited, such as metal hydroxides and oxides (Mikhaylin and Bazinet 2016; Zhao et al. 2021). The differences between the surface and centre bulk composition of the fouling cake denote a clear stratification of foulants across the cake with predominantly inorganic fouling in the bulk centre and organic fouling mainly located on the surfaces of the cake. Therefore, the fouling cake showed a complex and non-uniform matrix of several inorganic and organic/biological foulants that could hinder the cleaning procedures needed to maintain the membrane performance and avoid early membrane deterioration.

The surface morphology of the dense-like fouling cake was similar to those reported by other authors on distillation membranes (Chen et al. 2021; Pan et al. 2022; Yan et al. 2022) and on reverse osmosis membranes (Herzberg and Elimelech 2007; Zhao et al. 2021) treating different types of wastewaters. In these works, organic matter deposition and adsorption of EPS secreted by microorganisms have been reported as well as a decrease in the membrane surface porosity.

Regarding the fouling removal from the membrane surfaces, MilliQ water was firstly used in order to simulate a soft and desirable cleaning and to avoid any interaction and deterioration of the membrane owing to the cleaning agent attacks (Henares et al. 2017, 2018). A second alkaline sonication was applied because a residual fouling cake with a brown colour was observed on the membrane surface that was mainly attributed to organic and biofilm fouling. This second sonication with a NaOH solution was conducted because an alkali solution is usually proposed to remove organic fouling such as polysaccharides, proteins, peptides, fatty acids, humate, and surfactants (Mikhaylin and Bazinet 2016; Henares et al. 2018; Hafuka et al. 2019; Costa et al. 2021). Finally, the irreversible fouling observed on the membranes was mainly attributed to a strong hydrophobic-hydrophobic interaction of the proteins and polysaccharides with the membrane (Hu et al. 2014), especially with the mPVDF with a higher hydrophobicity. Additionally, the outcomes from the EDX analysis suggest the need for an additional cleaning step to enhance the removal of inorganic compounds so that a cleaning with weak organic acid solutions could be proposed (Mikhaylin and Bazinet 2016; Henares et al. 2017, 2018).

Especially in the case of PVDF, the irreversible fouling could also be favoured by the penetration of the foulants in the pores (Juang et al. 2010; Hu et al. 2014) because the membranes with a lower WCA and wetting resistance are more susceptible to pore blocking (Abdu et al. 2020). Simultaneously, fouling could also aggravate the wetting phenomenon (Zarebska et al. 2015; Chen et al. 2021) due to

hydrophilic moieties of some other additional foulants such as fatty acids or surfactants (Li et al. 2021). Also, the organic compounds in the treated anaerobic water may reduce the surface tension of the liquid, leading to an increase in the membrane wetting (Henares et al. 2018). Therefore, cleaning strategies should be evaluated in future studies with a special focus on the prevention of irreversible fouling and improvement in the membrane lifetime.

The prior organofluorosilanisation conducted over the PVDF led to a membrane with a greater stability under long-term operation because no significant degradation and a higher WCA were observed on mPVDF after the fouling tests in spite of the higher fouling compared to PVDF. By contrast, the PVDF membrane even experienced a water breakthrough at ~800 h, resulting in a shorter useful lifetime. That suggests that the functionalisation layer protected the surface against the potential damage from foulants and/or cleaning agents. Nevertheless, the greater hydrophobicity of the mPVDF seemed to promote the fouling development and hamper the detachment of the foulants, attributed mainly to the stronger hydrophobic-hydrophobic interaction between hydrophobic moieties of the proteins and polysaccharides and the membrane surface (Rongwong et al. 2019). That was corroborated by several findings after the fouling extraction: (i) the darker colour of the irreversible fouling cake on the mPVDF suggesting a higher amount of foulants, (ii) higher content of the foulants analysed by the EDX than for the PVDF, (iii) a higher organic matter content in the fouling extraction solution from mPVDF, and (iv) a negligible restoration of the WCA. Nevertheless and according to the staining analysis, the absence of polysaccharides in the irreversible fouling cake on the mPVDF suggests lower adhesion forces between polysaccharides and the modified surface and/or an improvement in the cleaning/removal efficiency of this type of foulant from organofluorosilanised PVDF. Thereby, polysaccharide fouling was totally reversible when using the mPVDF.

In general terms, the deposition tendency of the foulants and, therefore, the fouling cake development on both PVDF and mPVDF seemed similar because similar results were obtained. Thus, these outcomes persuaded to conclude that protein and polysaccharide deposition was more dominant in the first stage of the fouling formation according to the large hydrophobic interaction forces with the membrane surface. Then, this deposition led to a conditioning layer and promoted the adherence of other foulants, including inorganic compounds and microorganisms, as reported by other authors (Al-Juboori and Yusaf 2012; Hu et al. 2014). Therefore, this initial deposition could explain the high amount of inorganic elements such as Ca and P located in the bulk of the fouling cake even though the organic matter dominates the most external parts of the layer, as indicated by the EDX analysis.

Effect of the fouling on the membrane performance for dissolved methane recovery

In order to elucidate the effect of the fouling cake on the membrane performance, degassing tests for D-CH₄ recovery with the pristine and fouled PVDF and mPVDF membranes at different times of operation and liquid flow rates during the fouling tests using the same AE feed were studied in our previous work (Jiménez-Robles et al. 2022b). The removal efficiency (RE), which is defined as the percentage of recovered D-CH₄ from the liquid feed respect to the initial D-CH₄, was significantly affected by the presence of a fouling cake at the highest liquid flow rate tested of 21 L h⁻¹ (Fig. 6). The mPVDF with a higher fouling experienced a 50% decrease in the RE after 672 h of operation, whilst the RE only decreased 15% with the PVDF after 744 h. On the other hand, at the lowest liquid flow rate of 3.5 L h⁻¹ the RE kept almost constant even after the fouling cake formation, mainly attributed to the limiting mass transfer resistance located in the liquid phase (Li et al. 2021; Sanchis-Perucho et al. 2021; Velasco et al. 2021; Jiménez-Robles et al. 2022a). The RE decline observed during the long-term operation indicated an additional mass transfer resistance provided by the fouling cake (Henares et al. 2017). The wetting phenomenon induced by some foulants should also be taken into account in the increase of the overall mass transfer resistance, as mentioned above.

From the outcomes presented, a proper cleaning strategy of membranes is required to preserve the membrane performance. For the cleaning protocols, it is essential to

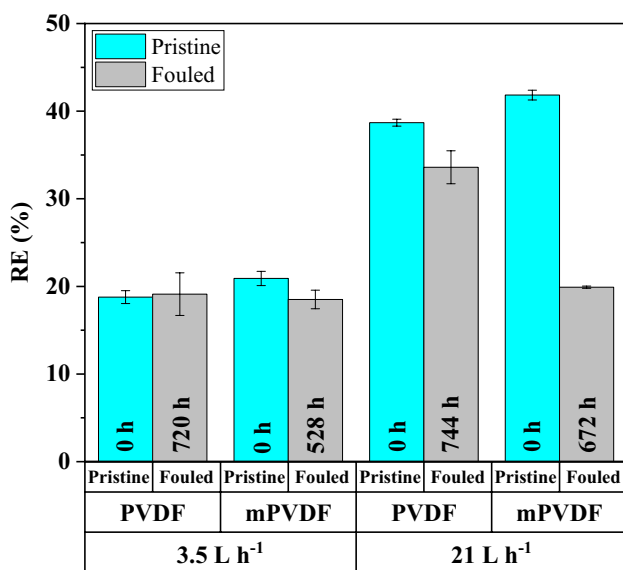


Fig. 6 Effect of the fouling time on the dissolved CH₄ removal efficiency (RE) in degassing tests with the PVDF and modified PVDF (mPVDF) at different liquid flow rates. Data from Jiménez-Robles et al. (2022b)

consider the nature and concentration of foulants in the feed when choosing the cleaning agents in order to optimise the frequency and chemical concentration (Costa et al. 2021). Therefore, membrane structural damages and exacerbated maintenance costs could be avoided. Taking into account the fouling cake development on hydrophobic PVDF membrane contactors treating AE elucidated in this work, the following preventive cleaning protocol could be tested in future studies: daily flushing with a diluted alkaline cleaning solution for 5–10 min followed by flushing with pure water for 5–10 min and a weekly flushing with ≤ 1% citric acid (Henares et al. 2018) and biocide solutions (Mikhaylin and Bazinet 2016) for 5–10 min. All cleaning solutions should be applied with a flow rate representing the 90–95% capacity of the membrane contactor in order to increase the turbulence. However, further studies are required to evaluate and optimise a suitable cleaning protocol for each membrane and operational condition.

Conclusions

A commercial PVDF membrane and an organofluorinated PVDF membrane with enhanced hydrophobicity experienced a fouling cake formation on their surfaces when treating an anaerobic reactor effluent for dissolved methane recovery during a long-term operation (> 800 h). Organic and inorganic fouling were identified in a somewhat heterogeneous fouling cake. Proteins and polysaccharides were the major organic foulants and were mainly located at the surface of the membrane and of the fouling cake. Inorganic fouling was composed mainly of salts of carbonate, calcium, and phosphate and was especially located in the centre bulk of the fouling cake, which indicates a stratification of the foulants.

The modified PVDF suffered a higher fouling deposition due to a stronger foulant-membrane interaction. However, the polysaccharides were completely removed from the mPVDF, a lower fouling related to biomass was inferred, and a higher membrane stability was demonstrated. Therefore, the functionalised surface layer protected the membrane from the potential foulants and/or damaging attack of the cleaning agents.

In conclusion, hydrophobic organic matter was initially attached to the hydrophobic membrane surface with a subsequent adhesion of microorganisms and especially a high deposition of other inorganic foulants. A preventive cleaning protocol should be established to avoid the loss of membrane performance during a long-term operation.

Regarding the membrane performance, the decline in methane recovery during the long-term operation was also related to the fouling cake formation, and consequently, to the additional resistance for the mass transport. Thus, the

decline in methane recovery was more pronounced with the mPVDF, presenting a lower fouling resistance.

Supplementary Information The online version contains supplementary material available at <https://doi.org/10.1007/s11356-022-24019-z>.

Acknowledgements The authors thank Global Omium for supplying the anaerobic effluent. Also the authors gratefully acknowledge the technical assistance in the fouling characterisation of the personnel at the Servicio Central de Soporte a la Investigación Experimental (SCSIE) of the University of Valencia and of Rosa Ballester Murat.

Author contribution R. Jiménez-Robles: methodology, validation, formal analysis, investigation, writing—original draft, writing—review and editing, and visualisation. V. Martínez-Soria: conceptualisation, methodology, validation, writing—review and editing, and supervision. M. Izquierdo: conceptualisation, methodology, validation, writing—review and editing, supervision, and funding acquisition.

Funding Open Access funding provided thanks to the CRUE-CSIC agreement with Springer Nature. This research was funded by the Conselleria d'Innovació, Universitats, Ciència i Societat Digital – Generalitat Valenciana (project GV/2019/149). PhD grant of R. Jiménez-Robles was funded by Ministerio de Universidades, Spain (Beca de Formación de Profesorado Universitario FPU19/02478).

Data availability The authors declare that the relevant data supporting the findings of this study are available within the article and its supplementary information files.

Declarations

Ethical approval Not applicable.

Consent to participate Not applicable.

Consent for publication Not applicable.

Competing interests The authors declare no competing interests.

Open Access This article is licensed under a Creative Commons Attribution 4.0 International License, which permits use, sharing, adaptation, distribution and reproduction in any medium or format, as long as you give appropriate credit to the original author(s) and the source, provide a link to the Creative Commons licence, and indicate if changes were made. The images or other third party material in this article are included in the article's Creative Commons licence, unless indicated otherwise in a credit line to the material. If material is not included in the article's Creative Commons licence and your intended use is not permitted by statutory regulation or exceeds the permitted use, you will need to obtain permission directly from the copyright holder. To view a copy of this licence, visit <http://creativecommons.org/licenses/by/4.0/>.

References

- Abdu B, Munirasu S, Kalleem P et al (2020) Investigating the effect of various foulants on the performance of intrinsically superhydrophobic polyvinylidene fluoride membranes for direct contact membrane distillation. *Sep Purif Technol* 252:1–13. <https://doi.org/10.1016/j.seppur.2020.117416>
- Al-Juboori RA, Yusaf T (2012) Biofouling in RO system: mechanisms, monitoring and controlling. *Desalination* 302:1–23. <https://doi.org/10.1016/j.desal.2012.06.016>
- Al-Juboori RA, Yusaf T, Aravinthan V (2012) Investigating the efficiency of thermosonication for controlling biofouling in batch membrane systems. *Desalination* 286:349–357. <https://doi.org/10.1016/j.desal.2011.11.049>
- Baird RB, Andrew D, Eaton EWR (2018) Standard methods for the examination of water and wastewater, 23rd edition. APHA, AWWA and WEF ed.
- Bandara WMKRTW, Kindaichi T, Satoh H et al (2012) Anaerobic treatment of municipal wastewater at ambient temperature: analysis of archaeal community structure and recovery of dissolved methane. *Water Res* 46:5756–5764. <https://doi.org/10.1016/j.watres.2012.07.061>
- Bandara WMKRTW, Satoh H, Sasakawa M et al (2011) Removal of residual dissolved methane gas in an upflow anaerobic sludge blanket reactor treating low-strength wastewater at low temperature with degassing membrane. *Water Res* 45:3533–3540. <https://doi.org/10.1016/j.watres.2011.04.030>
- Cabrera-Rodríguez CI, Moreno-González M, de Weerd FA et al (2017) Esters production via carboxylates from anaerobic paper mill wastewater treatment. *Bioresour Technol* 237:186–192. <https://doi.org/10.1016/j.biortech.2017.02.030>
- Centeno-Mora E, Fonseca PR, Andreão WL et al (2020) Mitigation of diffuse CH₄ and H₂S emissions from the liquid phase of UASB-based sewage treatment plants: challenges, techniques, and perspectives. *Environ Sci Pollut Res* 27:35979–35992. <https://doi.org/10.1007/s11356-020-08644-0>
- Chen L, Wang Y, Chen Z, Cai Z (2021) The fouling layer development on MD membrane for water treatments: An especial focus on the biofouling progress. *Chemosphere* 264:1–13. <https://doi.org/10.1016/j.chemosphere.2020.128458>
- Chen W, Qian C, Zhou KG, Yu HQ (2018) Molecular spectroscopic characterization of membrane fouling: a critical review. *Chem* 4:1492–1509. <https://doi.org/10.1016/j.chempr.2018.03.011>
- Choo KH, Lee CH (1996) Membrane fouling mechanisms in the membrane-coupled anaerobic bioreactor. *Water Res* 30:1771–1780. [https://doi.org/10.1016/0043-1354\(96\)00053-X](https://doi.org/10.1016/0043-1354(96)00053-X)
- Cookney J, McLeod A, Mathioudakis V et al (2016) Dissolved methane recovery from anaerobic effluents using hollow fibre membrane contactors. *J Membr Sci* 502:141–150. <https://doi.org/10.1016/j.memsci.2015.12.037>
- Costa FCR, Ricci BC, Teodoro B et al (2021) Biofouling in membrane distillation applications - a review. *Desalination* 516:1–17. <https://doi.org/10.1016/j.desal.2021.115241>
- Crone BC, Garland JL, Sorial GA, Vane LM (2016) Significance of dissolved methane in effluents of anaerobically treated low strength wastewater and potential for recovery as an energy product: a review. *Water Res* 104:520–531. <https://doi.org/10.1016/j.watres.2016.08.019>
- D'Abzac P, Bordas F, Van Hullebusch E et al (2010) Extraction of extracellular polymeric substances (EPS) from anaerobic granular sludges: comparison of chemical and physical extraction protocols. *Appl Microbiol Biotechnol* 85:1589–1599. <https://doi.org/10.1007/s00253-009-2288-x>
- Davey CJ, Hermassi M, Allard E et al (2020) Integrating crystallisation into transmembrane chemical absorption: process intensification for ammonia separation from anaerobic digestate. *J Membr Sci* 611:1–11. <https://doi.org/10.1016/j.memsci.2020.118236>
- Davis R, Mauer LJ (2010) Fourier transform infrared (FT-IR) spectroscopy: a rapid tool for detection and analysis of foodborne pathogenic bacteria. In: Mendez-Vilas A (ed.) *Current research, technology and education topics in Applied Microbiology and Microbial Biotechnology*, Formatex Research Center, pp 1582–1594
- Dean JA (1998) Spectroscopy. In: Dean JA (ed) *Lange's handbook of chemistry*, 15th edn. McGraw-hill Inc., US, section 7.1

- Dubois M, Gilles KA, Hamilton JK et al (1956) Colorimetric method for determination of sugars and related substances. *Anal Chem* 28:350–356. <https://doi.org/10.1021/ac60111a017>
- Gómez-Ordóñez E, Rupérez P (2011) FTIR-ATR spectroscopy as a tool for polysaccharide identification in edible brown and red seaweeds. *Food Hydrocoll* 25:1514–1520. <https://doi.org/10.1016/j.foodhyd.2011.02.009>
- Hafuka A, Mashiko R, Odashima R et al (2019) Digestion performance and contributions of organic and inorganic fouling in an anaerobic membrane bioreactor treating waste activated sludge. *Bioresour Technol* 272:63–69. <https://doi.org/10.1016/j.biortech.2018.09.147>
- Hebbbar RS, Isloor AM, Ismail AF (2017) Contact angle measurements. In: Hilal N, Ismail AF, Matsuura T, Oatley-Radcliffe D (eds.) *Membrane characterization*. Elsevier B.V, Amsterdam (The Netherlands), pp 219–255. <https://doi.org/10.1016/B978-0-444-63776-5.00012-7>
- Henares M, Ferrero P, San-Valero P et al (2018) Performance of a polypropylene membrane contactor for the recovery of dissolved methane from anaerobic effluents: mass transfer evaluation, long-term operation and cleaning strategies. *J Membr Sci* 563:926–937. <https://doi.org/10.1016/j.memsci.2018.06.045>
- Henares M, Izquierdo M, Marzal P, Martínez-Soria V (2017) Demethanization of aqueous anaerobic effluents using a polydimethylsiloxane membrane module: mass transfer, fouling and energy analysis. *Sep Purif Technol* 186:10–19. <https://doi.org/10.1016/j.seppur.2017.05.035>
- Henares M, Izquierdo M, Peña-Roja JM, Martínez-Soria V (2016) Comparative study of degassing membrane modules for the removal of methane from Expanded Granular Sludge Bed anaerobic reactor effluent. *Sep Purif Technol* 170:22–29. <https://doi.org/10.1016/j.seppur.2016.06.024>
- Herzberg M, Elimelech M (2007) Biofouling of reverse osmosis membranes: role of biofilm-enhanced osmotic pressure. *J Membr Sci* 295:11–20. <https://doi.org/10.1016/j.memsci.2007.02.024>
- Hu M, Zhang TC, Stansbury J et al (2014) Contributions of internal and external fouling to transmembrane pressure in MBRs: experiments and modeling. *J Environ Eng* 04014097:1–9. [https://doi.org/10.1061/\(asce\)jee.1943-7870.0000925](https://doi.org/10.1061/(asce)jee.1943-7870.0000925)
- Jiménez-Robles R, Gabaldón C, Badia JD et al (2022a) Recovery of dissolved methane through a flat sheet module with PDMS, PP, and PVDF membranes. *Sep Purif Technol* 282:1–11. <https://doi.org/10.1016/j.seppur.2021.120057>
- Jiménez-Robles R, Gabaldón C, Martínez-Soria V, Izquierdo M (2020) Simultaneous application of vacuum and sweep gas in a polypropylene membrane contactor for the recovery of dissolved methane from water. *J Membr Sci* 617:1–10. <https://doi.org/10.1016/j.memsci.2020.118560>
- Jiménez-Robles R, Moreno-Torralbo BM, Badia JD et al (2022b) Flat PVDF membrane with enhanced hydrophobicity through alkali activation and organofluorosilanisation for dissolved methane recovery. *Membranes (basel)* 12:1–19. <https://doi.org/10.3390/membranes12040426>
- Juang YC, Adav SS, Lee DJ (2010) Influence of internal biofilm growth on residual permeability loss in aerobic granular membrane bioreactors. *Appl Microbiol Biotechnol* 44:1267–1273. <https://doi.org/10.1007/s00253-010-2527-1>
- Khan MMT, Stewart PS, Moll DJ et al (2010) Assessing biofouling on polyamide reverse osmosis (RO) membrane surfaces in a laboratory system. *J Membr Sci* 349:429–437. <https://doi.org/10.1016/j.memsci.2009.12.006>
- Klaassen R, Feron PHM, Jansen AE (2005) Membrane contactors in industrial applications. *Chem Eng Res Des* 83:234–246. <https://doi.org/10.1205/cherd.04196>
- Lee Y, Yun KH, Sethunga D, Bae TH (2021) Membrane contactors for maximizing biomethane recovery in anaerobic wastewater treatments: recent efforts and future prospect. *Appl Sci* 11:1–16. <https://doi.org/10.3390/app11041372>
- Li X, Lee HS, Wang Z, Lee J (2021) State-of-the-art management technologies of dissolved methane in anaerobically-treated low-strength wastewaters: a review. *Water Res.* <https://doi.org/10.1016/j.watres.2021.117269>
- Liu C, Faria AF, Jackson J et al (2021a) Enhancing the anti-fouling and fouling removal properties of thin-film composite membranes through an intercalated functionalization method. *Environ Sci Water Res Technol* 7:1336–1347. <https://doi.org/10.1039/d1ew00188d>
- Liu L, Shen F, Chen X et al (2016) A novel plasma-induced surface hydrophobization strategy for membrane distillation: etching, dipping and grafting. *J Membr Sci* 499:544–554. <https://doi.org/10.1016/j.memsci.2015.11.003>
- Liu L, Xiao Z, Liu Y et al (2021b) Understanding the fouling/scaling resistance of superhydrophobic/omniphobic membranes in membrane distillation. *Desalination* 499:1–18. <https://doi.org/10.1016/j.desal.2020.114864>
- Mansourizadeh A, Rezaei I, Lau WJ et al (2022) A review on recent progress in environmental applications of membrane contactor technology. *J Environ Chem Eng* 10:1–21. <https://doi.org/10.1016/j.jece.2022.107631>
- Mikhaylin S, Bazinet L (2016) Fouling on ion-exchange membranes: classification, characterization and strategies of prevention and control. *Adv Colloid Interface Sci* 229:34–56. <https://doi.org/10.1016/j.cis.2015.12.006>
- Mohamed MA, Jaafar J, Ismail AF, et al (2017) Fourier Transform Infrared (FTIR) Spectroscopy. In: Hilal N, Ismail AF, Matsuura T, Oatley-Radcliffe D (eds.) *Membrane characterization*. Elsevier B.V, Amsterdam (The Netherlands), pp 3–29. <https://doi.org/10.1016/B978-0-444-63776-5.00001-2>
- Moosbrugger RE, Wentzel MC, Ekama GA, Marais GR (1992) Simple titration procedures to determine H2CO3 alkalinity and short-chain fatty acids in aqueous solutions containing known concentration of ammonium, phosphate and sulphide weak acid/bases. Department of Civil Engineering, University of Cape Town, Water Research Group
- Pan J, Zhang F, Wang Z et al (2022) Enhanced anti-wetting and anti-fouling properties of composite PFPE/PVDF membrane in vacuum membrane distillation. *Sep Purif Technol* 282:1–11. <https://doi.org/10.1016/j.seppur.2021.120084>
- Rana D, Matsuura T (2010) Surface modifications for antifouling membranes. *Chem Rev* 110:2448–2471. <https://doi.org/10.1021/cr800208y>
- Rongwong W, Fan C, Liang Z et al (2015) Investigation of the effects of operating parameters on the local mass transfer coefficient and membrane wetting in a membrane gas absorption process. *J Membr Sci* 490:236–246. <https://doi.org/10.1016/j.memsci.2015.04.071>
- Rongwong W, Goh K, Sethunga GSMDP, Bae TH (2019) Fouling formation in membrane contactors for methane recovery from anaerobic effluents. *J Membr Sci* 573:534–543. <https://doi.org/10.1016/j.memsci.2018.12.038>
- Saha NK, Balakrishnan M, Ulbricht M (2007) Sugarcane juice ultrafiltration: FTIR and SEM analysis of polysaccharide fouling. *J Membr Sci* 306:287–297. <https://doi.org/10.1016/j.memsci.2007.09.006>
- Sairiam S, Loh CH, Wang R, Jiraratananon R (2013) Surface modification of PVDF hollow fiber membrane to enhance hydrophobicity using organosilanes. *J Appl Polym Sci* 130:610–621. <https://doi.org/10.1002/app.39197>
- Sanchis-Perucho P, Robles Á, Durán F et al (2020) PDMS membranes for feasible recovery of dissolved methane from AnMBR effluents. *J Membr Sci* 604:1–12. <https://doi.org/10.1016/j.memsci.2020.118070>
- Sanchis-Perucho P, Robles Á, Durán F et al (2021) Widening the applicability of AnMBR for urban wastewater treatment through

- PDMS membranes for dissolved methane capture: effect of temperature and hydrodynamics. *J Environ Manage* 287:1–11. <https://doi.org/10.1016/j.jenvman.2021.112344>
- Sethunga GSMDP, Karahan HE, Wang R, Bae TH (2021) Wetting- and fouling-resistant hollow fiber membranes for dissolved methane recovery from anaerobic wastewater treatment effluents. *J Membr Sci* 617:118621. <https://doi.org/10.1016/j.memsci.2020.118621>
- Sohaib Q, Kalakech C, Charmette C et al (2022) Hollow-fiber membrane contactor for biogas recovery from real anaerobic membrane bioreactor permeate. *Membranes (basel)* 12:1–24. <https://doi.org/10.3390/membranes12020112>
- Stazi V, Tomei MC (2021) Dissolved methane in anaerobic effluents: a review on sustainable strategies for optimization of energy recovery or internal process reuse. *J Clean Prod* 317:1–13. <https://doi.org/10.1016/j.jclepro.2021.128359>
- Velasco P, Jegatheesan V, Othman M (2018) Recovery of dissolved methane from anaerobic membrane bioreactor using degassing membrane contactors. *Front Environ Sci* 6:1–6. <https://doi.org/10.3389/fenvs.2018.00151>
- Velasco P, Jegatheesan V, Thangavadeivel K et al (2021) A focused review on membrane contactors for the recovery of dissolved methane from anaerobic membrane bioreactor (AnMBR) effluents. *Chemosphere* 278:1–20. <https://doi.org/10.1016/j.chemosphere.2021.130448>
- Wang R, Zhang HY, Feron PHM, Liang DT (2005) Influence of membrane wetting on CO₂ capture in microporous hollow fiber membrane contactors. *Sep Purif Technol* 46:33–40. <https://doi.org/10.1016/j.seppur.2005.04.007>
- Xu Y, Goh K, Wang R, Bae TH (2019) A review on polymer-based membranes for gas-liquid membrane contacting processes: current challenges and future direction. *Sep Purif Technol* 229:1–19. <https://doi.org/10.1016/j.seppur.2019.115791>
- Xue W, Yamamoto K, Tobino T (2016) Membrane fouling and long-term performance of seawater-driven forward osmosis for enrichment of nutrients in treated municipal wastewater. *J Membr Sci* 499:555–562. <https://doi.org/10.1016/j.memsci.2015.11.009>
- Yan Z, Lu Z, Chen X et al (2022) Membrane distillation treatment of landfill leachate: characteristics and mechanism of membrane fouling. *Sep Purif Technol* 289:120787. <https://doi.org/10.1016/j.seppur.2022.120787>
- Zarebska A, Amor AC, Ciurkot K et al (2015) Fouling mitigation in membrane distillation processes during ammonia stripping from pig manure. *J Membr Sci* 484:119–132. <https://doi.org/10.1016/j.memsci.2015.03.010>
- Zhang N, Pan Z, Zhang Z et al (2020) CO₂ capture from coalbed methane using membranes: a review. *Environ Chem Lett* 18:79–96. <https://doi.org/10.1007/s10311-019-00919-4>
- Zhao S, Liao Z, Fane A et al (2021) Engineering antifouling reverse osmosis membranes: a review. *Desalination* 499:1–31. <https://doi.org/10.1016/j.desal.2020.114857>
- Zhu H, Li X, Pan Y et al (2020) Fluorinated PDMS membrane with anti-biofouling property for in-situ biobutanol recovery from fermentation-pervaporation coupled process. *J Membr Sci* 609:118225. <https://doi.org/10.1016/j.memsci.2020.118225>

Publisher's note Springer Nature remains neutral with regard to jurisdictional claims in published maps and institutional affiliations.

Supplementary Material for

Fouling characterization in PVDF membrane contactors for dissolved methane recovery from anaerobic effluents: Effect of surface organofluorosilanisation.

R. Jiménez-Robles, V. Martínez-Soria, M. Izquierdo*

Research Group in Environmental Engineering (GI²AM), Department of Chemical Engineering, School of Engineering, University of Valencia, Avda. Universitat s/n, 46100 Burjassot, Spain.

*e-mail: marta.izquierdo-sanchis@uv.es. Phone: +34 354 37 37. Fax: +34 963 54 48 98.

S1. Characteristics of the anaerobic reactor effluent

Table S 1. Characteristics of the filtered anaerobic reactor effluent. TSS and VSS: total and volatile suspended solids, respectively; COD: chemical oxygen demand, VFA: volatile fatty acids.

Parameter	Value
pH	7.84
Conductivity, mS cm ⁻¹	8.61
Turbidity, NTU	6.7
Alkalinity, mg CaCO ₃ L ⁻¹	2102
TSS, mg L ⁻¹	75.75
VSS, mg L ⁻¹	67.50
COD, mg O ₂ L ⁻¹	414
VFA, mg CH ₃ COOH L ⁻¹	<5.0 ^a
Proteins, mg L ⁻¹	125.06
Polysaccharides, mg L ⁻¹	79.19
NH ₄ ⁺ , mg L ⁻¹	1500
NO ₃ ⁻ , mg L ⁻¹	2500
NO ₂ ⁻ , mg L ⁻¹	400
PO ₄ ³⁻ , mg L ⁻¹	74
SO ₄ ²⁻ , mg L ⁻¹	<200 ^a
Ca ⁺ , mg L ⁻¹	50
Fe ²⁺ , mg L ⁻¹	0
Live cells, L ⁻¹	3.15·10 ¹⁰
Dead cells, L ⁻¹	0.40·10 ¹⁰

^aBelow detection limit

The turbidity was measured with a turbidimeter (Merck Turbiquant 1500IR, Germany), volatile fatty acids (VFA) were determined using potentiometer titration (848 Titrino Plus, Metrohm, Switzerland) and a pH and conductivity meter was used (pH/Cond 340i WTW, Germany). The concentration of sulphates (SO₄²⁻), ammonium (NH₄⁺), nitrates (NO₃⁻), nitrites (NO₂⁻), calcium (Ca⁺) and iron (Fe²⁺) were determined by means of test strips supplier by Merck-Quant.

S2. Experimental system for the fouling tests

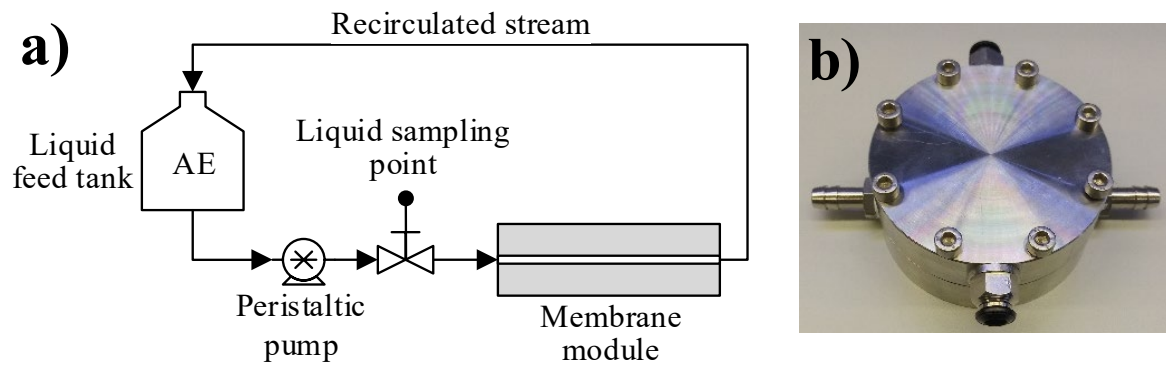


Figure S 1. a) Scheme of the experimental system for the fouling tests with a flat-sheet membrane module using an anaerobic reactor effluent (AE) and b) image of the homemade flat-sheet module used in the tests.

S3. Images of the evolution of the fouling on the membrane during the fouling tests

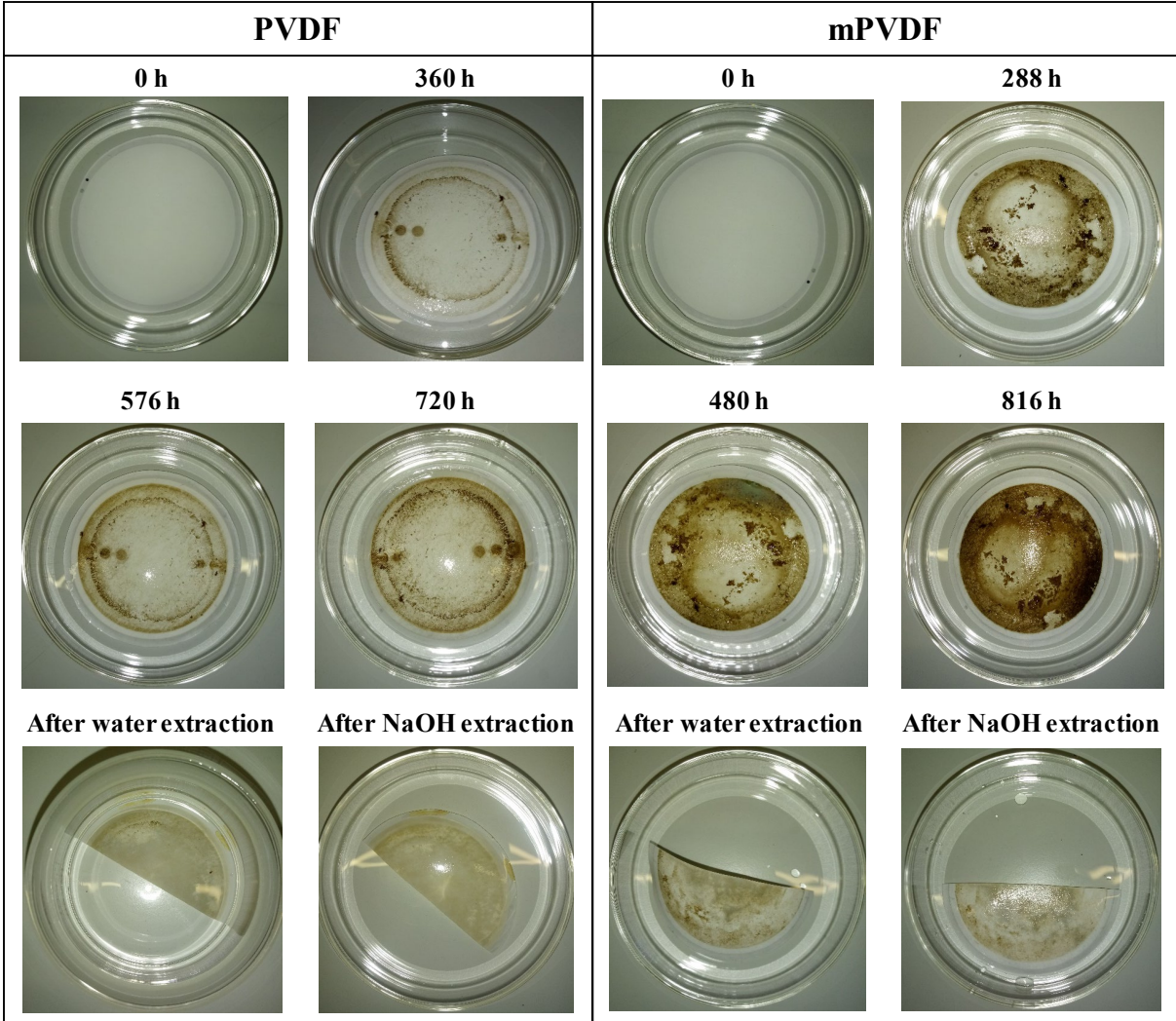


Figure S 2. Pictures of the PVDF and modified PVDF (mPVDF) membranes at different operation times of the fouling test with an anaerobic reactor effluent, and after the fouling extraction with a sonication bath in milliQ water and 0.01 M NaOH solution.

S4. Absorption bands of the infrared spectra of the pristine PVDF membrane

Table S 2. Major FTIR absorption bands obtained in the analysis of the pristine PVDF membrane.

Wavenumber, cm⁻¹	Band	Group	Reference
762	PVDF α -crystal shape	PVDF	[1,2]
839	PVDF β -crystal shape	PVDF	[1,2]
872	C-F stretching vibration	PVDF	[1,3,4]
975	PVDF α -crystal shape	PVDF	[1,2]
1070 – 1401	Fluorocarbon frequencies	PVDF	[4–8]
3024	C-H (alkenes stretching)	PVDF	[3]

S5. Energy Dispersive X-Ray analysis and distribution of different elements on the surface of the PVDF and modified PVDF membranes after the fouling tests

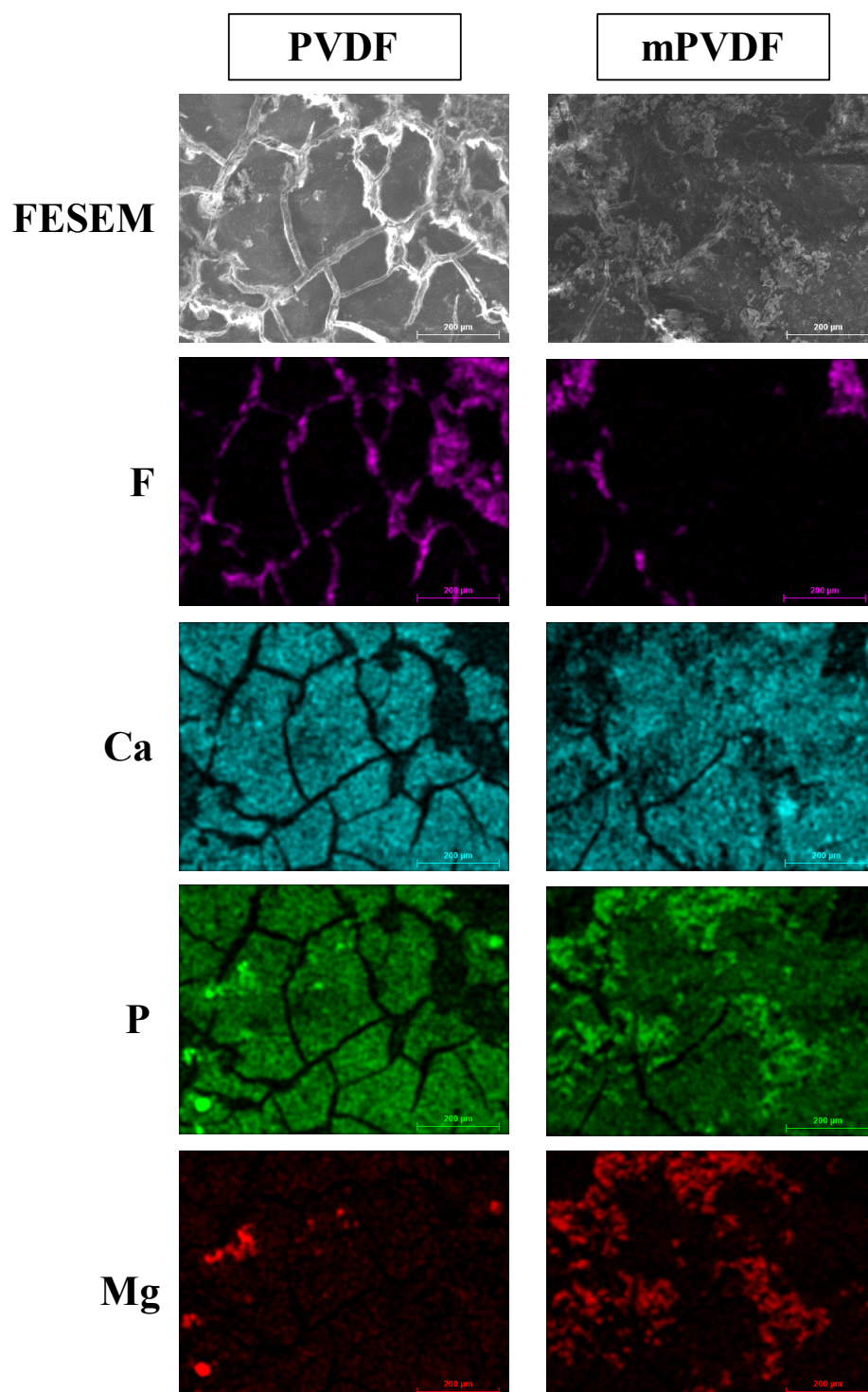


Figure S 3. Distribution of the major elements detected on the surface of the PVDF and modified PVDF (mPVDF) membranes after the fouling tests (operation time > 800 h).

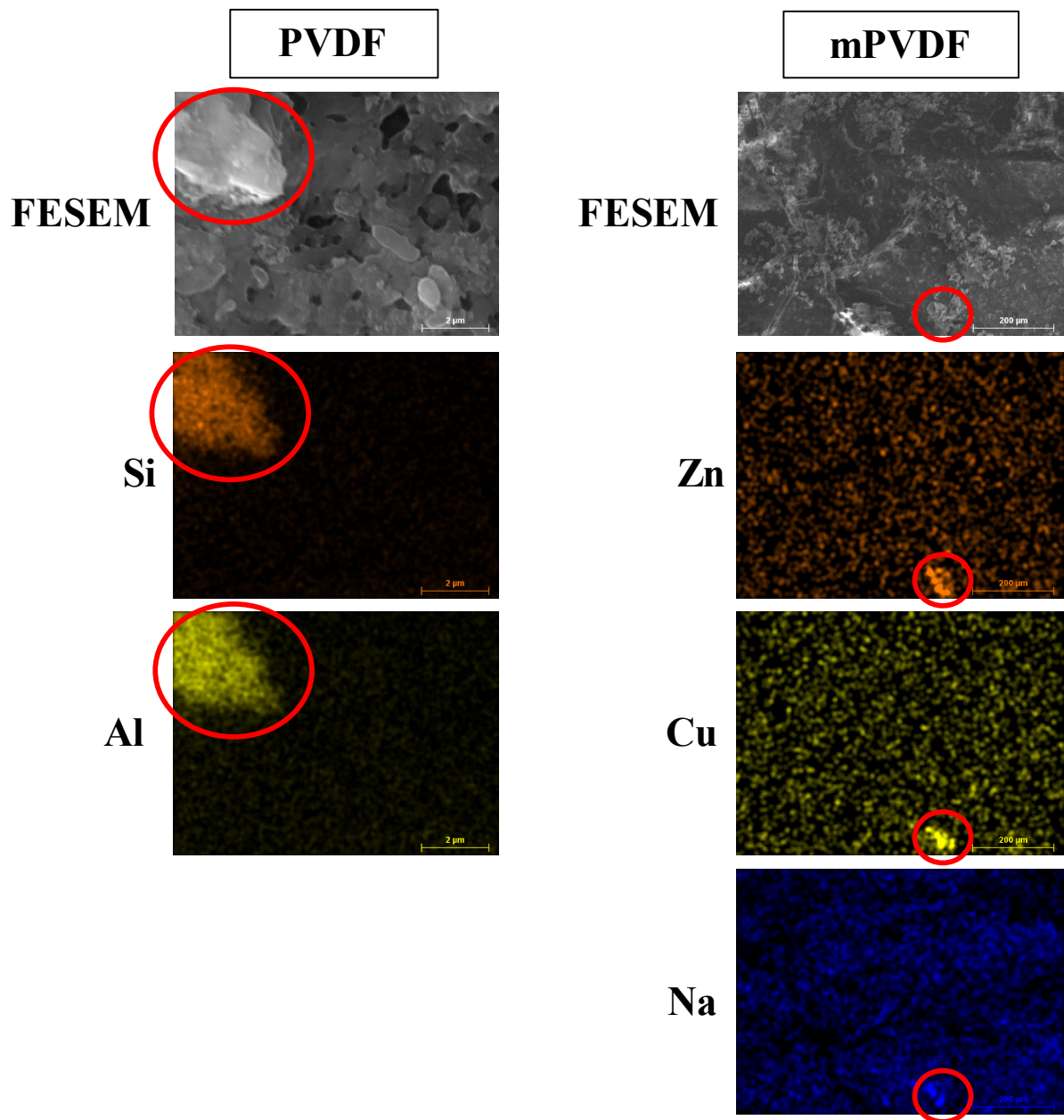


Figure S 4. Distribution of minor inorganic foulants in solid particles detected on the surface of the PVDF and modified PVDF (mPVDF) membranes after the fouling tests (operation time > 800 h). Target particles rounded in red colour.

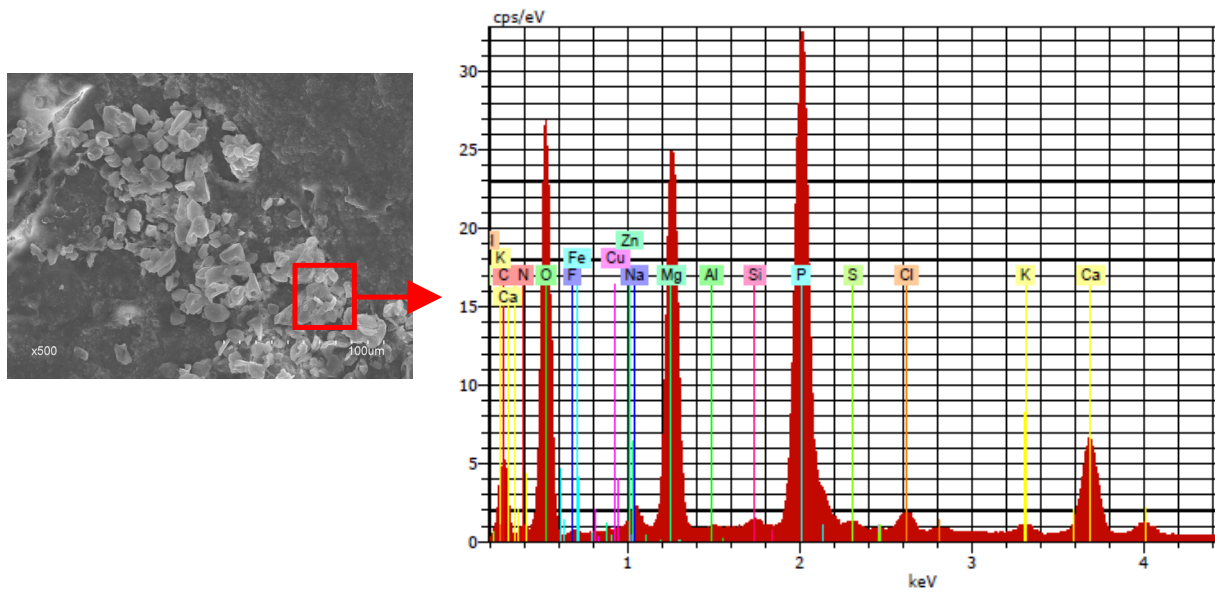


Figure S 5. Spectra of the EDX analysis over a cluster of particles deposited on the fouling cake of the modified PVDF (operation time > 800 h).

S6. Energy Dispersive X-Ray analysis and distribution of fluorine on the surface of the PVDF and modified PVDF after the fouling extraction

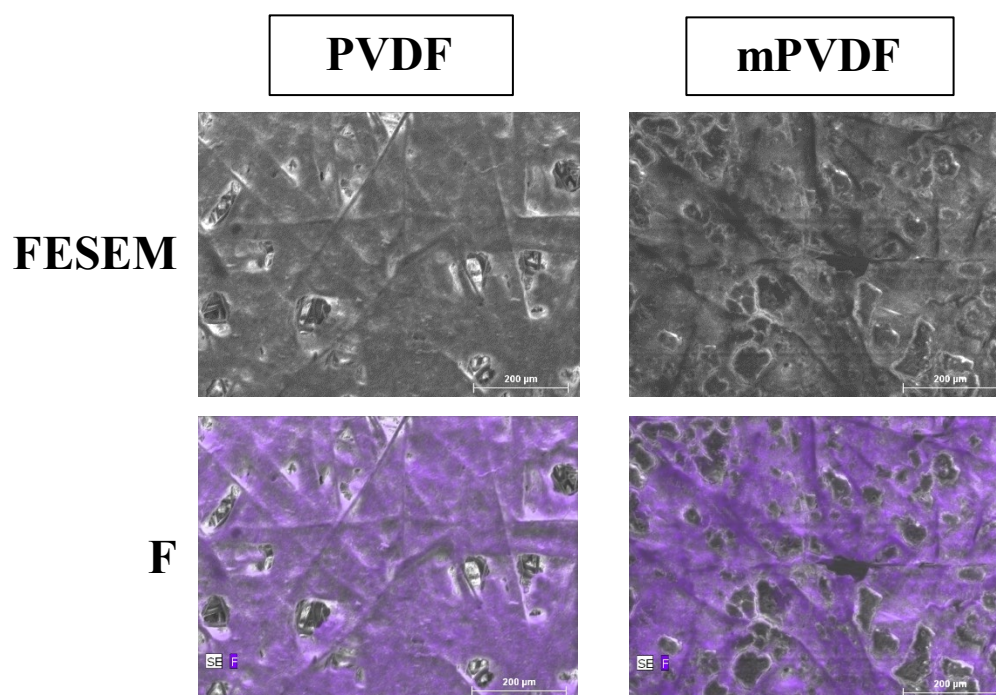


Figure S 6. Distribution of the fluorine on the surface of the PVDF and modified PVDF (mPVDF) membranes after the fouling extraction. FESEM images of the pristine membrane surfaces are presented in Figure 3 of the main manuscript.

S7. Energy Dispersive X-Ray analysis and distribution of different elements on the cross section of the PVDF and modified PVDF after the fouling tests

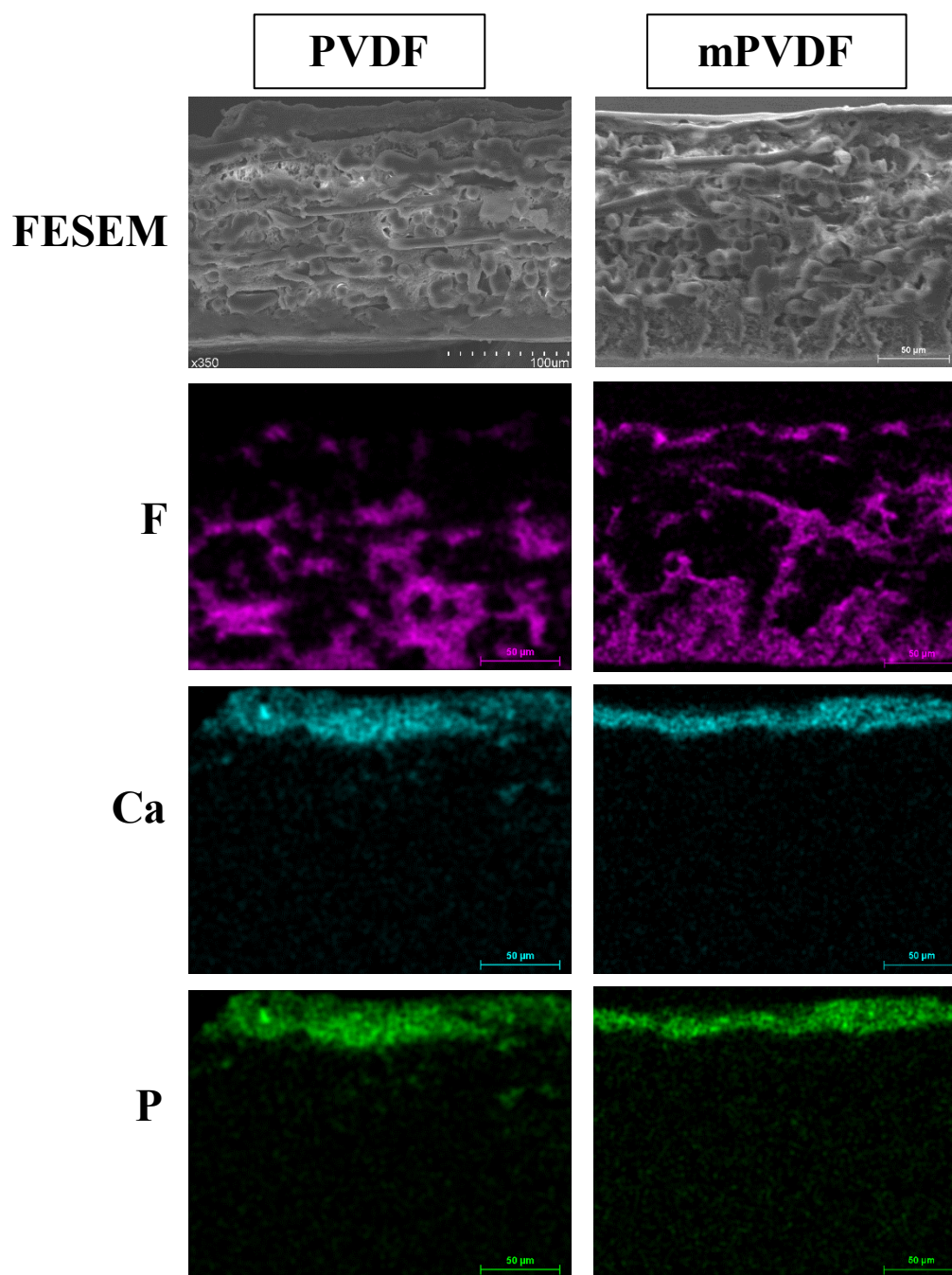


Figure S 7. Distribution of different elements along the cross section of the PVDF and modified PVDF (mPVDF) membranes after the fouling tests (> 800 h). FESEM images of the pristine membrane cross section are presented in Figure 4 of the main manuscript.

References

- [1] H. Dong, K. Xiao, X. Tang, Z. Zhang, J. Dai, R. Long, W. Liao, Preparation and characterization of polyurethane (PU)/polyvinylidene fluoride (PVDF) blending membrane, *Desalin. Water Treat.* 57 (2016) 3405–3413. <https://doi.org/10.1080/19443994.2014.988659>.
- [2] S. Al-Gharabli, M.O. Mavukkandy, J. Kujawa, S.P. Nunes, H.A. Arafat, Activation of PVDF membranes through facile hydroxylation of the polymeric dope, *J. Mater. Res.* 32 (2017) 4219–4231. <https://doi.org/10.1557/jmr.2017.403>.
- [3] M.A. Mohamed, J. Jaafar, A.F. Ismail, M.H.D. Othman, M.A. Rahman, Membrane Characterization. Chapter 1: Fourier Transform Infrared (FTIR) Spectroscopy, Elsevier B.V., 2017. <https://doi.org/10.1016/B978-0-444-63776-5.00001-2>.
- [4] Z. Yan, Z. Lu, X. Chen, Y. Jiang, Z. Huang, L. Liu, G. Fan, H. Chang, F. Qu, H. Liang, Membrane distillation treatment of landfill leachate: Characteristics and mechanism of membrane fouling, *Sep. Purif. Technol.* 289 (2022) 120787. <https://doi.org/10.1016/j.seppur.2022.120787>.
- [5] G.J. Ross, J.F. Watts, M.P. Hill, P. Morrissey, Surface modification of poly(vinylidene fluoride) by alkaline treatment: 1. The degradation mechanism, *Polymer (Guildf)*. 41 (2000) 1685–1696. [https://doi.org/10.1016/S0032-3861\(99\)00343-2](https://doi.org/10.1016/S0032-3861(99)00343-2).
- [6] H. Zhu, X. Li, Y. Pan, G. Liu, H. Wu, M. Jiang, W. Jin, Fluorinated PDMS membrane with anti-biofouling property for in-situ biobutanol recovery from fermentation-pervaporation coupled process, *J. Membr. Sci.* 609 (2020) 118225. <https://doi.org/10.1016/j.memsci.2020.118225>.

- [7] X. Huang, J. Zhang, W. Wang, Y. Liu, Z. Zhang, L. Li, W. Fan, Effects of PVDF/SiO₂ hybrid ultrafiltration membranes by sol-gel method for the concentration of fennel oil in herbal water extract, *RSC Adv.* 5 (2015) 18258–18266. <https://doi.org/10.1039/c4ra15448g>.
- [8] N. Awanis Hashim, Y. Liu, K. Li, Stability of PVDF hollow fibre membranes in sodium hydroxide aqueous solution, *Chem. Eng. Sci.* 66 (2011) 1565–1575. <https://doi.org/10.1016/j.ces.2010.12.019>.

APPENDIX IV: CONTRIBUTION IV.





The contribution entitled “*Stability of superhydrophobicity and structure of PVDF membranes treated by vacuum oxygen plasma and organofluorosilanisation*” is presented in this Appendix. This work corresponds with the main results and conclusions discussed in section 4.4. The details of the resulting paper are listed below:

Title	Stability of superhydrophobicity and structure of PVDF membranes treated by vacuum oxygen plasma and organofluorosilanisation
Authors	Ramón Jiménez-Robles ^a , Marta Izquierdo ^a , Vicente Martínez-Soria ^a , Laura Martí ^b , Alicia Monleón ^{b, c} , José David Badia ^a
Affiliation	^a Research Group in Materials Technology and Sustainability (MATS), Department of Chemical Engineering, School of Engineering, University of Valencia, Avda. Universitat s/n, 46100 Burjassot, Spain ^b Decarbonisation Department, Plastic Technology Institute (AIMPLAS), C/Gustave Eiffel 4, 46980 Paterna, Spain ^c Department of Organic Chemistry, School of Chemistry, University of Valencia, Dr Moliner 50, 46100 Burjassot, Spain
Journal	Membranes
Year	2023
Volume	13
Issue	3
Number	314
DOI	10.3390/membranes13030314
Cite	R. Jiménez-Robles, M. Izquierdo, V. Martínez-Soria, L. Martí, A. Monleón, J.D. Badia, Stability of superhydrophobicity and structure of PVDF membranes treated by vacuum oxygen plasma and organofluorosilanisation, Membranes. 13 (2023) 314. https://doi.org/10.3390/membranes13030314

The Journal Impact Factor (JIF) in 2022 (last available data) was 4.2, and the JIF rank was 47/140 in the category of Chemical Engineering (Q2 second quartile) and 25/86 in the category of Polymer Science (Q2 quartile).

Article

Stability of Superhydrophobicity and Structure of PVDF Membranes Treated by Vacuum Oxygen Plasma and Organofluorosilanisation

Ramón Jiménez-Robles ¹, Marta Izquierdo ^{1,*}, Vicente Martínez-Soria ¹, Laura Martí ², Alicia Monleón ^{2,3} and José David Badia ^{1,*}

- ¹ Research Group in Materials Technology and Sustainability (MATS), Department of Chemical Engineering, School of Engineering, University of Valencia, Avda. Universitat s/n, 46100 Burjassot, Spain
- ² Decarbonisation Department, Plastic Technology Institute (AIMPLAS), C/Gustave Eiffel 4, 46980 Paterna, Spain
- ³ Department of Organic Chemistry, School of Chemistry, University of Valencia, Dr Moliner 50, 46100 Burjassot, Spain
- * Correspondence: marta.izquierdo-sanchis@uv.es (M.I.); jose.badia@uv.es (J.D.B.); Tel.: +34-96-35-43737 (M.I.); +34-96-35-44319 (J.D.B.)

Abstract: Superhydrophobic poly(vinylidene fluoride) (PVDF) membranes were obtained by a surface treatment consisting of oxygen plasma activation followed by functionalisation with a mixture of silica precursor (SiP) (tetraethyl-orthosilicate [TEOS] or 3-(triethoxysilyl)-propylamine [APTES]) and a fluoroalkylsilane (1H,1H,2H,2H-perfluorooctyltriethoxysilane), and were benchmarked with coated membranes without plasma activation. The modifications acted mainly on the surface, and the bulk properties remained stable. From a statistical design of experiments on surface hydrophobicity, the type of SiP was the most relevant factor, achieving the highest water contact angles (WCA) with the use of APTES, with a maximum WCA higher than 155° for membranes activated at a plasma power discharge of 15 W during 15 min, without membrane degradation. Morphological changes were observed on the membrane surfaces treated under these plasma conditions, showing a pillar-like structure with higher surface porosity. In long-term stability tests under moderate water flux conditions, the WCA of coated membranes which were not activated by oxygen plasma decreased to approximately 120° after the first 24 h (similar to the pristine membrane), whilst the WCA of plasma-treated membranes was maintained around 130° after 160 h. Thus, plasma pre-treatment led to membranes with a superhydrophobic performance and kept a higher hydrophobicity after long-term operations.

Keywords: functionalisation; membrane stability; polymeric membrane; polyvinylidene fluoride; oxygen plasma; superhydrophobicity



Citation: Jiménez-Robles, R.; Izquierdo, M.; Martínez-Soria, V.; Martí, L.; Monleón, A.; Badia, J.D. Stability of Superhydrophobicity and Structure of PVDF Membranes Treated by Vacuum Oxygen Plasma and Organofluorosilanisation.

Membranes **2023**, *13*, 314. <https://doi.org/10.3390/membranes13030314>

Academic Editor: Tan Yong Zen

Received: 31 January 2023

Revised: 25 February 2023

Accepted: 6 March 2023

Published: 9 March 2023



Copyright: © 2023 by the authors. Licensee MDPI, Basel, Switzerland. This article is an open access article distributed under the terms and conditions of the Creative Commons Attribution (CC BY) license (<https://creativecommons.org/licenses/by/4.0/>).

1. Introduction

The interest in membrane technology is continuously increasing due to the high efficiency in separation processes, compactness of the membrane modules and lower energy consumption compared with conventional separation units that present problems related to flooding, foaming and emulsions [1,2]. In this regard, recent efforts have especially focused on the development of membrane distillation for the water desalination of seawater, brackish water and brines [3–5], gas separation for carbon dioxide (CO₂) removal from flue gases and biogas [6,7], and pervaporation systems for the biobutanol and dissolved methane (CH₄) recovery from biological effluents and wastewaters [8,9]. However, membranes tend to suffer from wetting and fouling, especially in those applications that involve highly contaminated or quite complex liquid feeds, such as industrial brines or anaerobic effluents [10–13]. Wetting and fouling phenomena lead to an additional mass transfer

resistance located inside and on the surface of the membrane, respectively, reducing the separation efficiency and involving additional cleaning processes [14]. Therefore, the useful lifetime of the membrane can decline considerably, and the operational cost would rise [15–17]. Up to now, these issues are not completely resolved, hindering the large-scale application of membrane technology in areas such as the desalination of seawater or methane recovery from anaerobic effluents [18,19].

Different techniques for tailoring polymeric membrane characteristics have been successfully implemented to improve the wetting resistance of the membranes [20,21]. In this regard, superhydrophobic membranes with a water contact angle (WCA) higher than or equal to 150° [22] have been reported to significantly mitigate the wetting, which was attributed to the low contact area between the liquid phase and the membrane [23,24]. Additionally, superhydrophobicity has been related to the improvement in the self-cleaning properties of the membrane surface [12,19]. Thus, membrane surface functionalisation has been applied to increase its hydrophobicity at the surface level, whilst the bulk properties remain unchanged [25] by means of the addition of new hydrophobic functional groups, such as siloxanes and fluoroalkyls [26,27].

Surface modification techniques can be classified into two main categories: physical and chemical treatments [27]. Physical treatments involve a physical interaction between the modifying agents and the membrane, and the initial composition of the membrane remains unchanged. Among physical treatments, surface coatings have been widely studied to confer hydrophobicity to surfaces [28,29] and, more recently, different lithography and nanotexturing techniques have been reported to increase the fouling resistance and self-cleaning behaviour [30–33]. However, physical treatments such as surface coating could be unstable over long-term operations [34]. In contrast, chemical treatments involve the grafting of the modifying agents on the membrane surface by means of chemical bonding, such as covalent, ionic and hydrogen bonds, thus achieving a stronger adhesion force [35]. An activation step prior to the grafting of the modifying agents is frequently needed in membranes that present a high inertness and chemical stability, such as polyvinylidene fluoride (PVDF) [3,27]. This activation is usually based on the addition of oxygen-containing functional groups such as hydroxyls (-O-H), peroxides (-O-O-) and carbonyls (-C=O) that act as active sites for the subsequent grafting [36–38]. This activation has been successfully carried out by an alkali treatment with sodium hydroxide (NaOH) or lithium hydroxide (LiOH), plasma treatment and high-energy radiation, among other processes [3,39,40].

Plasma treatment is considered an environmentally friendly, versatile, reproducible, easily scalable and inexpensive method for activating and texturing polymer surfaces [16,41–45]. This technique consists of a high-energy discharge that ionises the gas near the electrodes and produces a complex gas mixture of excited ions and electrons, atoms and molecule fragments and free radicals [39,46,47]. The gas plasma is also a source of radiation that can break chemical bonds of the material [48]. The effect of the plasma discharge in the treated membrane relies on the type and conditions of the supplied gas, pressure, the power of the discharge, the duration of the treatment and the configuration of the chamber and electrodes [44,49–51]. Thus, a chemical and/or physical modification can be induced on the membrane surface depending on the plasma conditions [47,49] since the ion bombardment and interaction with the different reactive species contained in the plasma can produce sputtering of the membrane material (etching), substitution reactions, atom abstraction, removal of volatile substances and/or scission of polymer chains [4,46,52,53]. Additionally, the use of oxidative gases, such as oxygen (O₂), CO₂ and water (H₂O), for plasma treatment creates a more reactive environment capable of adding oxygen-containing functional groups onto the membrane surface.

Plasma treatment has been reported as a useful approach for tailoring the chemical composition and/or surface morphology of different polymeric membranes and surfaces, such as polydimethylsiloxane (PDMS) [41,54,55], polypropylene (PP) [36,56], polytetrafluoroethylene (PTFE) [49], polyethylene (PE) [57], polycarbonate (PC) [33,58], polyacrylonitrile (PAN) [35,59] and polyethersulfone (PES) [35]. In contrast, PVDF has been extensively

studied and commercialised as a membrane material, owing to its outstanding features such as high mechanical, chemical and thermal resistance, inertness, ease of processing and relatively low cost of the raw materials [25,27,60,61]. Hence, PVDF has been treated to improve the hydrophobicity for membrane distillation and CO₂ absorption [24,39,62] or to induce hydrophilicity for filtration processes and enhance the fouling resistance [42,61,63]. The effects of membrane modifications with plasma treatments have mostly been evaluated based on the membrane properties at microscopic (morphology, chemical composition) and macroscopic (hydrophobicity) levels after the modification procedure, and the performance of the modified membranes is often benchmarked against the pristine membrane.

Only a few studies have evaluated the effects of long-term operation on the chemical properties, morphology and stability of hydrophobicity of the modified membranes [36]. For example, the work by Jiménez-Robles et al. [64] showed that the modification of PVDF membranes with alkali activation and functionalisation with fluoroalkylsilanes (FAS) kept a higher surface hydrophobicity and avoided the water breakthrough that non-modified PVDF suffered after approximately 800 h treating an anaerobic effluent for the dissolved CH₄ recovery. Therefore, it is an area of interest requiring further studies into the effects of the combination of plasma activation and surface grafting on the long-term stability of membrane properties.

In this context, the aim of this work was to evaluate the effect of the oxygen plasma treatment on the surface modification of a commercial PVDF membrane. An evaluation of different silica precursors for further grafting of a FAS in order to produce superhydrophobic membranes was also carried out. First, a statistical experimental design was conducted considering the power and time of the plasma treatment and the type of silica precursors to maximise the surface hydrophobicity of the membrane by measuring the static water contact angle. Second, membrane stability tests over long-term operation were conducted in a flat-sheet membrane module with a constant flux of deionised water. The stability of the membranes was evaluated and benchmarked against the pristine PVDF in terms of hydrophobicity, thermal properties, morphology and chemical composition.

2. Materials and Methods

2.1. Membrane Surface Functionalisation Procedure

Flat-sheet PVDF membranes (Durapore, Merck KGaA, Darmstadt, Germany) were used for the application and evaluation of different modification procedures. The membrane was composed only of hydrophobic PVDF without any support, resulting in a microporous structure. The main characteristics of the membrane are reported in Table 1.

Table 1. Characteristics of the flat-sheet PVDF membrane.

Property	Value
Structure	Microporous
Thickness, μm	125 ^a
Pore diameter, μm	0.22 ^a
Bubble point, bar	≥ 1.24 ^a
Porosity, %	75 ^a
Static water contact angle, $^\circ$	119.4 ± 1.7 ^b

^a Provided by the Merck KGaA. ^b Measured as explained in Section 2.4.

The surface modification of PVDF was conducted with a procedure consisting of an initial activation with an oxygen plasma treatment followed by an organofluorosilanisation-based functionalisation. The activation of the membrane surface was conducted and evaluated with a vacuum plasma system (Femto, Diener electronic GmbH & Co., Ebhausen, Germany) equipped with a generator frequency of 40 kHz and a stainless-steel vacuum chamber of 100 mm diameter and 278 mm length. Initially, each membrane sample was placed in the middle of the chamber with the target surface upward, and O₂ was flowed at 1.5 standard cubic centimetre per minute during the plasma treatment, maintaining a

constant absolute pressure of 0.4 mbar inside the chamber. The power and time of the plasma treatment ranged from 3 to 17 W and 3 to 17 min, respectively, according to the design of experiments explained in Section 2.2.

In the functionalisation step, FAS 1H,1H,2H,2H-perfluorooctyltriethoxysilane (Dynasylan[®] F8261, Evonik GmbH, Essen, Germany) was used as the modifying agent, and two different silica precursors (SiP), tetraethyl orthosilicate (TEOS, $\geq 99\%$, Sigma-Aldrich, USA) and 3-(triethoxysilyl)-propylamine (APTES, Sigma-Aldrich, Saint Louis, MI, USA), were evaluated. A detailed description of the functionalisation is found in earlier work [64], where the modification conditions were established based on the optimal conditions which maximised the surface WCA, using a functionalisation solution which had a FAS/SiP volumetric ratio of 0.5, a FAS/SiP concentration of 7.5%_v in a mixture of 2-propanol (IPA; HPLC grade, VWR Chemicals, Radnor, PA, USA) and water with a molar ratio of 57:1. After the plasma treatment, the activated membrane was immersed in the functionalisation solution for 1 h at room temperature in an orbital shaker. Afterwards, the membrane was rinsed with 2-propanol to stop the gel reaction and cured in the oven at 60 °C overnight.

For comparison purposes, coated membranes were evaluated. Through the dip-coating technique, membranes were immersed in the functionalisation solution and cured in an oven at 60 °C overnight without oxygen plasma treatment. Therefore, no chemical bonding between membranes and FAS or SiP was anticipated due to the high inertness of PVDF. The coated PVDF membranes treated with TEOS or APTES as SiP are identified as Coat-TEOS and Coat-APTES, respectively.

2.2. Design of Experiments and Statistical Analysis

The effect of the modification procedure with an oxygen plasma treatment on the hydrophobicity of PVDF membranes was initially evaluated on 2 cm × 2 cm membrane specimens by measuring their WCA after the functionalisation. The main variables involved in the modification procedure with the oxygen plasma treatment were analysed by means of a statistical experimental design to maximise the hydrophobicity of the PVDF membrane surface. The power and time of the plasma treatment and the SiP were the main variables (factors) that affected the membrane hydrophobicity. Table 2 shows the factor values (levels) used in the design of the experiments and statistical analysis of the functionalisation procedure. A central composite design for the analysis of variance (ANOVA) and surface response was conducted with an alpha (α) value of 1.41 and a level of confidence of 95% to identify the significant effects of the factors and their interactions on the response variable, i.e., the WCA. Then, a statistical analysis based on a multiple linear regression was conducted to determine the optimum values of the factors leading to the maximum response. The different experimental runs were conducted randomly in duplicate to avoid systematic errors. The statistical software Minitab[®] (Lead Technologies, Inc., Charlotte, NC, USA) was used to aid in the design of experiments and the statistical analysis.

Table 2. Factors and levels used in the design of the experiments and statistical analysis (with $\alpha = 1.41$) of the functionalisation procedure.

Independent Variables (Factors)		Levels				
		$-\alpha$	-1	0	$+1$	$+\alpha$
A	Power (W)	3	5	10	15	17
B	Time (min)	3	5	10	15	17
C	Silica precursor (SiP) *	TEOS—APTES				

* Categorical factor.

2.3. Evaluation of Membrane Stability

2.3.1. Long-Term Stability Tests

The tests in long-term operation with pristine, coated and plasma-activated and functionalised flat-sheet membranes were carried out to evaluate the stability of the morphological and chemical structures and hydrophobicity of the membrane under a continuous liquid flux of deionised water in the lab-scale system depicted in Supplementary Material (S1). Initially, the membrane was coupled inside a 3D-printed flat-sheet module (FM) with an effective area of 25 cm², and a 2-L liquid feed tank was filled with deionised water. A constant water flux was applied through the liquid side of the FM, in a closed loop, by using a peristaltic pump (Watson-Marlow Fluid Technology Solutions, Cornwall, UK). For comparison purposes and based on previous studies [64,65], the long-term tests were operated at the liquid flow rate of 21 L h⁻¹ for a period of 160 h or until a constant WCA was achieved. The membrane was extracted periodically to measure its WCA in order to monitor the surface hydrophobicity as a function of time of use [28,65,66]. The morphology, thickness, chemical composition, surface porosity and thermal stability of the tested membranes were evaluated after the long-term operation.

2.3.2. Thermal Analysis

Thermal analysis of the pristine, coated and plasma-activated and functionalised membranes were conducted to evaluate their thermal characteristics and crystalline nature of the PVDF structure. To determine the thermal stability of the membranes under different environments, thermogravimetric analysis (TGA) measurements were conducted in nitrogen and air atmospheres with a TGA Q5000 IR analyser (TA Instruments, New Castle, DE, USA) using high-temperature platinum pans. A 10 mg sample was placed in the holder, and the heating rate and gas flow rate were set at 10 °C min⁻¹ and 50 mL min⁻¹, respectively. The specimens were heated from room temperature to 800 °C. Moreover, differential scanning calorimetry (DSC) was conducted with samples of 5 mg under a flowing nitrogen atmosphere (50 mL min⁻¹) at a heating rate of 10 °C min⁻¹ from room temperature to 200 °C. The DSC measurements were performed with a DSC 214 Polyma (NETZSCH-Gerätebau GmbH, Selb, Germany) using aluminium pans.

The degree of crystallinity, χ (%), of the membranes was determined by using Equation (1) [38]:

$$\chi = \frac{\Delta h_m}{x\Delta h_\alpha + y\Delta h_\beta} \times 100 \quad (1)$$

where Δh_m (J g⁻¹) is the experimental melting enthalpy of the sample, Δh_α (93.07 J g⁻¹) and Δh_β (103.40 J g⁻¹) are the melting enthalpies of a 100% crystalline PVDF in the α and β phases [67], and x and y are the molar fractions of the α and β phases in the sample, respectively, which were assumed to be the predominant phases ($x + y = 1$). The fraction of the β phase in a sample containing both phases can be estimated using Equation (2) [68]:

$$y = \frac{A_\beta}{\left(\frac{K_\beta}{K_\alpha}\right)A_\alpha + A_\beta} \times 100 \quad (2)$$

where A_α and A_β represent the absorbance at the wavelengths of 766 cm⁻¹ and 840 cm⁻¹, respectively, from the infrared spectra, and K_α (6.1×10^4 cm² mol⁻¹) and K_β (7.7×10^4 cm² mol⁻¹) are the absorption coefficients of the α and β phases [69]. The measured absorbance at the wavelengths of 766 cm⁻¹ and 840 cm⁻¹ were 0.167 and 0.187, respectively, for all the tested membranes. Measurements were taken using a Fourier transform-infrared (FTIR) spectrometer in the attenuated total reflectance (ATR) mode (Cary 630 FTIR Spectrometer, Agilent Technologies, Inc., Santa Clara, CA, USA). The fraction values of the α and β phases were 0.53 and 0.47, respectively.

2.4. Contact Angle Measurements

The membrane surface hydrophobicity was evaluated by means of the measurement of the static WCA following the sessile drop technique [70] by depositing a water droplet of $5.5 \pm 0.1 \mu\text{L}$ onto the membrane surface using a syringe pump (KF Technology s.r.l., Italy) at room temperature. An image of the water droplet was taken at 15 s with a digital microscope (Handheld Digital Microscope Pro, Celestron LLC, Torrance, CA, USA) under white light (Philips HUE Lamp, Koninklijke Philips NV, Amsterdam, the Netherlands). The ImageJ software (National Institutes of Health, Bethesda, MD, USA) was used for image processing of the droplet profile using the contact angle plug-in based on the ellipse approximation. The WCA was evaluated at different surface locations on the membrane, and a mean value was obtained from at least four measurements using the standard deviation as a measure of the associated error. For monitoring the WCA of the membranes during the stability tests, the membranes were extracted from the FM and dried prior to the WCA measurements, removing the excess water and moisture with forced aeration at room temperature for approximately 2 h.

2.5. Membrane Morphology and Chemical Composition

An inspection of the membrane surface and cross-section was conducted by a field emission scanning electron microscope (FESEM) with an accelerating voltage of 10 kV (Hitachi S4800, Hitachi Ltd., Tokyo, Japan). The FESEM was equipped with an energy dispersive x-ray (EDX) spectrometer, which was used for the atomic content determination of different elements. For image acquisition, the membrane coupons were previously dried in an oven at 45°C overnight. Afterwards, the coupons were placed on a metal holder and then coated with a fine layer of Au/Pd by sputtering in vacuum for 45 s. The surface and cross-section morphology, thickness and chemical composition were analysed. The surface porosity of the membranes was measured from the surface FESEM images by using ImageJ software [19,60,71]. The average membrane thickness and surface porosity were measured in at least six separate locations on the membrane, and the chemical composition was determined at a minimum of three locations on the surface using the standard deviation as a measure of the associated error.

3. Results and Discussion

3.1. Effect of the Oxygen Plasma Activation and Organofluorosilanisation on Membrane Hydrophobicity

A statistical experimental design evaluating the main parameters that affect the membrane surface hydrophobicity was conducted to maximise the response variable, i.e., the WCA of the plasma-activated and functionalised membranes. It is relevant to remark that after the previous plasma activation, with no further functionalisation, the droplets deposited onto the membranes were quickly absorbed, resulting in superhydrophilic surfaces with a WCA lower than 10° , as reported by other authors [38]. This hydrophilic behaviour was mainly attributed to the generation of oxygen functional groups (hydroxyls, peroxides and carbonyls) [38]. After the preliminary experiments, and based on the literature [50], the power and time of the plasma treatment and the type of SiP were found to be the main factors to be optimised. The effects of these factors and their interactions can be observed in the Pareto diagram of the design shown in Figure 1. The critical standardised effect (2.015) was calculated from the Student's T distribution ($t_{\alpha/2,\nu}$) with a significance level (α) of 0.05 and 16 degrees of freedom (ν), associated with the error of the design of the experiments. As observed in the Pareto diagram, the SiP presented the highest standardised effect (8.830), indicating that the WCA was mainly influenced using TEOS or APTES. Likewise, the power of the plasma treatment significantly affected the WCA in the tested conditions with a standardised effect value of 3.723. However, the plasma time showed a standardised effect of 2.045, which was similar to the critical value (2.015), indicating a low effect on the response, at least with the evaluated operational conditions. The interaction between the factors did not appear to affect the WCA of the modified membranes since lower values of

the standardised effects were obtained respective to the critical value. Hence, the effects of the interactions in the WCA of the treated membranes could be neglected, thereby easing future scale-up technology.

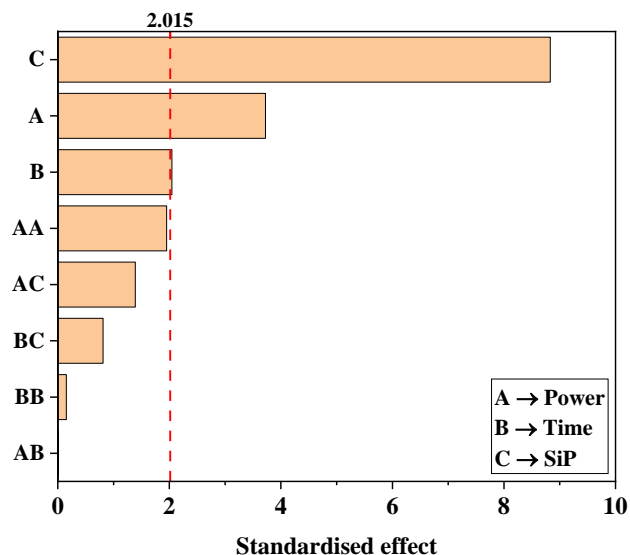


Figure 1. Pareto diagram of the standardised effects of the factors analysed in the central composite design (power and time of the oxygen plasma and silica precursor [SiP]). The dashed red line represents the critical standardised effect for a level of confidence of 95%.

The effects of the individual factors on the response are depicted in the main effects plot shown in Figure 2. A WCA higher than that of the pristine PVDF ($119.4 \pm 1.7^\circ$) was obtained for all the tested plasma-treated membranes, with an overall mean value of 153.3° , showing that the modification procedure with the oxygen plasma activation proposed in this work was suitable to obtain superhydrophobic PVDF membranes. As observed by other authors [19,72], droplets placed on the membranes for the WCA measurements easily rolled off the surface in most of plasma-treated membranes, which is an essential condition for superhydrophobic and self-cleaning surfaces.

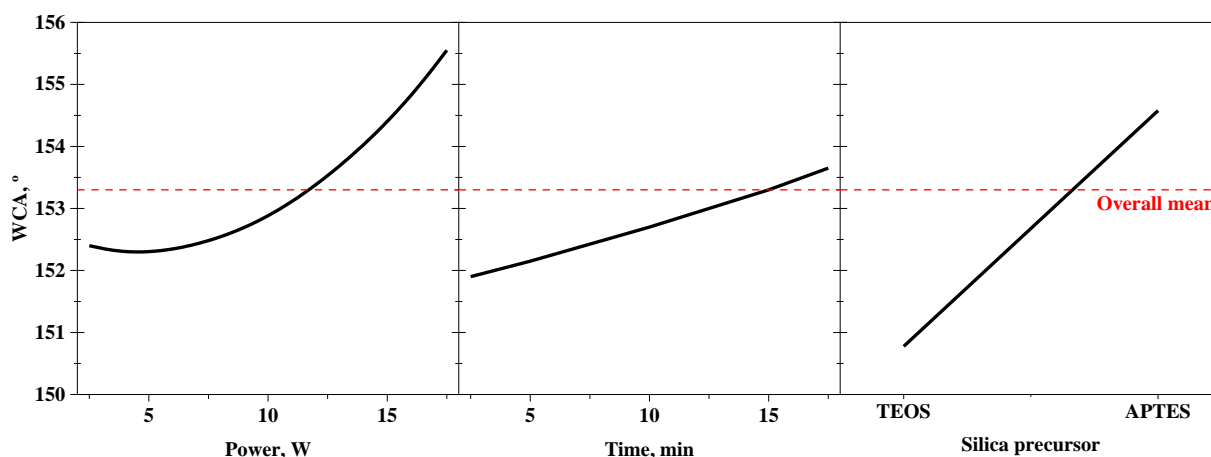


Figure 2. Main effects plot of the individual factors analysed in the central composite design (power and time of the oxygen plasma and silica precursor).

As can be observed in the main effects plot (Figure 2), the WCA of the PVDF membranes achieved values of around 152.5° with the lowest plasma power (3 W) and maintained similar values for power less than or equal to 10 W. This could indicate that the membrane was saturated with oxygen active sites at only 3 W of power, limiting the

grafting of the SiP and FAS. During plasma treatment, C-H and C-F bonds from PVDF chains are broken by the effect of the ion bombardment and radicals and electron interactions [44,51,53,67], generating volatile substances such as carbon monoxide (CO), CO₂ or hydrogen fluoride (HF) [4,47,48] that are removed from the membrane, inducing active sites on the surface. The high reactivity of some removed substances inside the plasma chamber could lead to reabsorption on those active sites on the membrane [16]. Thus, the rate of atom removal and reabsorption on the membrane seemed to be in equilibrium under the low plasma power values of 3 to 10 W at the time points evaluated. However, the WCA of the modified membranes continuously increased with plasma power values higher than or equal to 10 W, indicating a greater performance of the plasma treatment at high power. This improvement was mainly attributed to the etching effect on the membrane surface, inducing an increase in the roughness. This phenomenon will be discussed in further sections.

The time of plasma treatment presented the lowest effect in the WCA since a slight increase in the WCA (less than 2°) was observed when increasing the plasma time from 3 to 17 min. Kim et al. [73] reported that the changes in the WCA of PVDF membranes after the oxygen plasma treatment at 10 W occurred in the first 60 s of the discharge, after which the WCA remained constant. It is worth mentioning that PVDF samples treated at a plasma power and time higher than 17 W and 17 min, respectively, became brittle and easily destroyed during their manipulation in the membrane modification and/or analysis. Hence, modified membranes could neither be evaluated nor obtained at higher plasma power and time, limiting the working upper limit of these factors for the treatment of PVDF with oxygen plasma. This is in agreement with previously reported results, which have shown an increase in membrane rigidity after the plasma treatment [74].

Regarding the main effect of the categorical factor (Figure 2), the type of SiP presented the highest effect, as previously indicated by the Pareto diagram. The highest WCA values of the plasma-treated membranes were obtained with APTES, with an overall mean value of 155°, compared to those membranes modified with TEOS, with a significantly lower overall mean value of 151°. The use of TEOS as SiP led to the seeding of siloxane chains (-Si-O-Si-O-) onto the membrane surface in the active sites generated during the plasma treatment. The reactions involved in the grafting process with TEOS are detailed elsewhere [64]. In contrast, the use of APTES can lead to the formation of siloxane chains with additional alkyl chains [39] that are naturally hydrophobic [40,50] and come from the aminopropyl group present in the APTES molecule. Moreover, the presence of an amine group can involve additional grafting reactions in the oxygen-rich active sites on the plasma-treated surfaces. Such reactions include amide formation and even breakage or scission of the PVDF backbones [22,26,36,75]. Hence, the incorporation of an additional reactive group, such as the primary amine of the APTES, can lead to the formation of a more complex and uneven structure on the membrane surface, compared to the more symmetric siloxane structure originated from TEOS. Likewise, subsequent grafting of the FAS could have taken place in a heterogeneous way when APTES was used, which positively increased the WCA.

An ANOVA and surface response analysis based on a linear multiple regression were conducted to create a model that fit the experimental results and to determine the values of the factors that maximised the WCA of the plasma-treated membranes. The response surface for each categorical factor value (TEOS and APTES) is shown in Figure 3. From the ANOVA of the model, the F-values of the quadratic and two-way interaction terms were low (less than 2), indicating that they could be neglected compared to the lineal terms with a higher F-value of 32, which agreed with the previous main effects analysis. In addition, the ANOVA showed no evidence of lack-of-fit (*p*-value of 0.58), indicating that the model can adequately predict the WCA of the modified membranes under the operational conditions tested, as observed when comparing the response surface with the experimental data (open symbols in Figure 3). The maximum WCA values predicted by the model were $155.2 \pm 2.7^\circ$ and $157.3 \pm 2.1^\circ$ with TEOS and APTES, respectively, at the highest plasma power and time of 17 W and 17 min, respectively. However, these maximum WCAs did not show

significant differences compared with those WCAs predicted at a lower plasma power and time of 15 W and 15 min, respectively, and the experimental WCAs obtained at these conditions were $155.5 \pm 1.5^\circ$ and $157.0 \pm 0.9^\circ$ for TEOS and APTES, respectively. Thus, the conditions for the plasma treatment were established at 15 W and 15 min in order to achieve high superhydrophobic membranes for their further characterisation. The oxygen plasma-activated and functionalised PVDF membranes at these conditions and TEOS or APTES as SiP are labelled as PO₂-TEOS and PO₂-APTES, respectively. The infrared spectra of these membranes and the pristine PVDF are shown in Supplementary Material (S2), even though no significant differences were observed due to the penetration depth of the FTIR-ATR analysis [21].

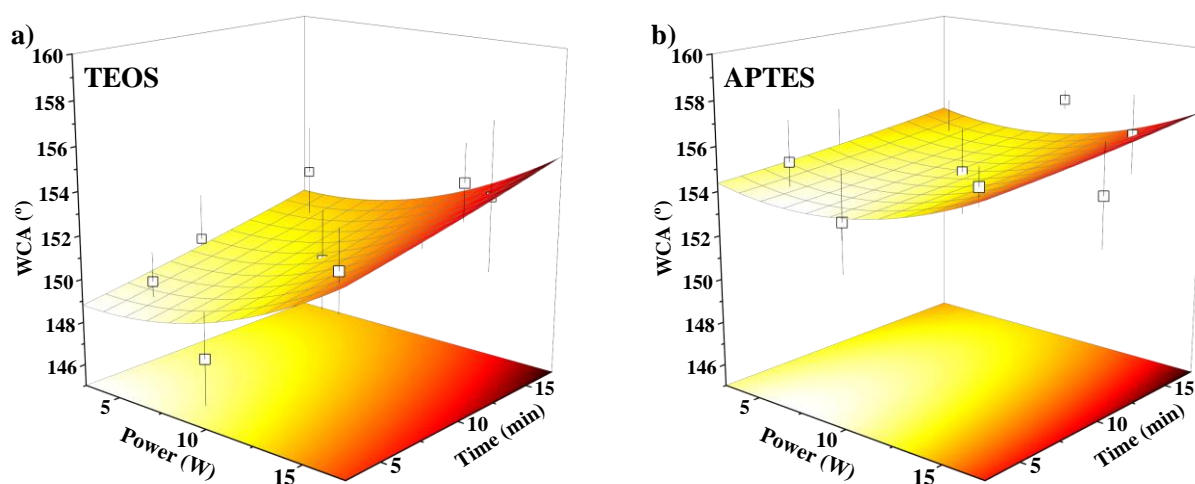


Figure 3. Response surface obtained from the central composite design for (a) TEOS and (b) APTES as silica precursors compared to experimental data (open square—□).

Only a few works evaluating a membrane modification procedure with plasma activation followed by grafting of FASs can be found in the literature. In a similar approach to this work, Liu et al. [19] activated a PVDF membrane with oxygen plasma at 50 W for 1 min, followed by grafting of the FAS 1H,1H,2H,2H-perfluorodecyltriethoxysilane, achieving a WCA of $162.0 \pm 2.3^\circ$ in membrane surfaces with a pillar surface structure. The higher WCA reported in that work could be ascribed to the higher fluorine chain length of the modifying agent used [39] and the high initial WCA of the pristine membrane ($155.3 \pm 1.7^\circ$) [19]. Sairiam et al. [39] also evaluated the previous FAS for the modification of PVDF membranes with a helium plasma activation at 80 W for 180 s, and they reported an increase in the WCA from $68.9 \pm 0.9^\circ$ to $145.6 \pm 3.1^\circ$.

3.2. Membrane Stability Tests in Long-Term Operation

Long-term performance is a design requirement of high relevance for polymer-based dispositives [76], but research works evaluating the effect of long-term operation on the stability of modified membranes are still very scarce and mainly focused on the stability in the separation performance [39].

In this section, the effect of long-term operation on the stability of different membrane properties was evaluated. First, the results regarding the stability of the membrane bulk properties after long-term operation are shown, followed by the stability evaluation of the surface properties during the operation. For comparison purposes, the outcomes obtained with the different treated membranes were benchmarked with the pristine PVDF membrane (p-PVDF).

3.2.1. Stability of the Bulk Properties after Operation

Thermal analysis is a quality tool to characterise the performance of polymers at the design stage and after operation [77]. The results from thermogravimetric analysis under

different atmospheres are shown in Figure 4 in the form of derivative thermogravimetric (DTG) curves for the pristine, coated and plasma-treated PVDF membranes before and after the long-term stability tests. Under an oxidative environment, all the membranes before the stability test showed a similar trend until the complete decomposition of the samples was observed in the range of 450 to 600 °C (Figure 4a). Under an inert environment (Figure 4c), the decomposition profile was similar to the outcomes under an oxidative atmosphere, showing main decomposition peaks at temperatures around 475 °C. However, a char was observed at the end of the TGA analysis for all the PVDF membranes representing 20 to 30% of the initial weight of the sample, similar to the pristine PVDF analysed by other authors [59]. These outcomes indicate that the chemical structure of the pristine PVDF was not affected by plasma activation and functionalisation.

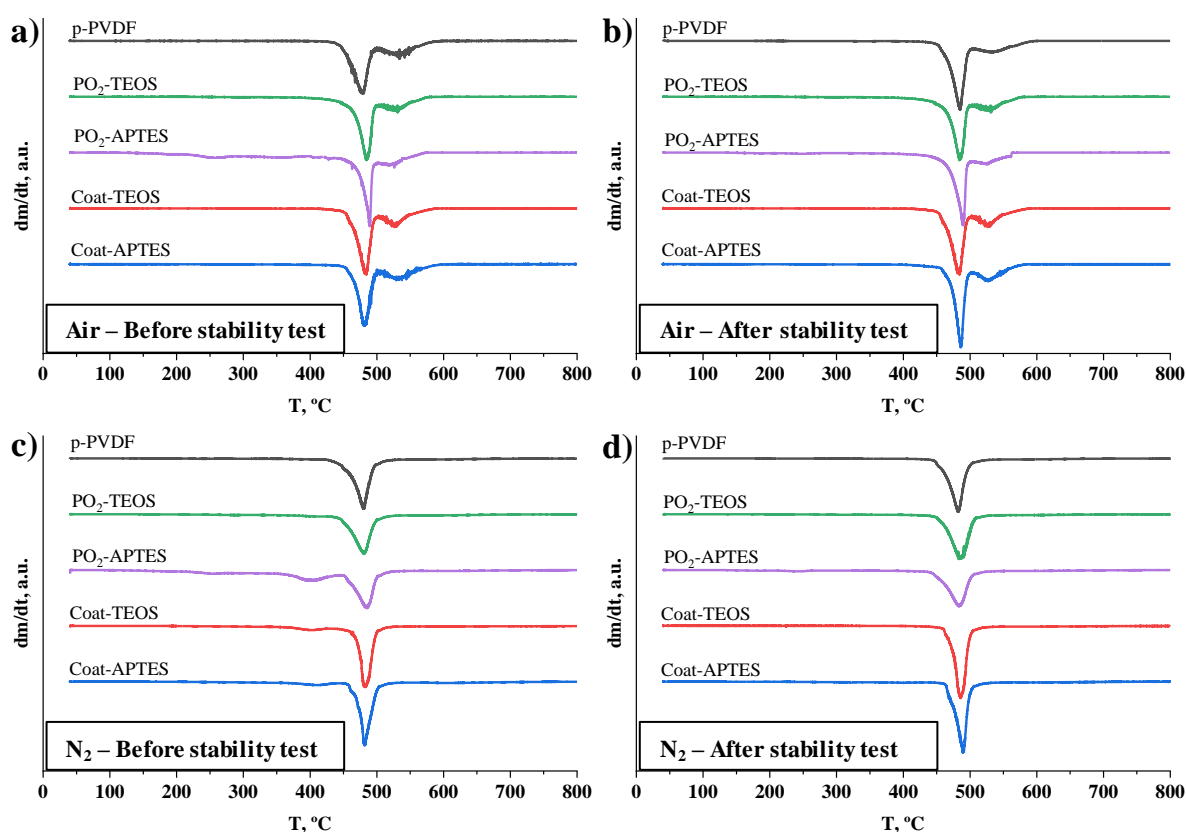


Figure 4. Thermogravimetric analyses under an oxidative atmosphere with air (a,b) and an inert atmosphere with nitrogen (c,d) of the pristine PVDF (p-PVDF) membrane, coated membranes with FAS/TEOS and FAS/APTES (Coat-TEOS and Coat-APTES, respectively) and modified membranes with oxygen plasma activation at 15 W for a period of 15 min and functionalised with FAS/TEOS and FAS/APTES (PO₂-TEOS and PO₂-APTES) before (a,c) and after (b,d) long-term stability tests. The derivative thermogravimetric curves (dm/dt) as the derivative of the mass (%) with respect to the time (min) as a function of temperature (°C) and expressed in arbitrary units (a.u.).

The DTG thermograms of the membranes after long-term operation (Figure 4b,d) showed the same trends that the non-used membranes had with no significant variation in the decomposition temperatures, indicating that long-term operation did not affect the thermal behaviour and stability of the bulk membrane.

DSC measurements were conducted to detect potential modifications in the amorphous/crystalline configuration and thermal performance of the membranes after the modification procedures and operation. The DSC thermograms of the pristine, coated and modified PVDF membranes under a nitrogen atmosphere are shown in Figure 5. The melting temperature and enthalpy, together with the crystallinity degree before and after

the long-term stability tests, are shown in Table 3. Similar values were observed for all membranes, regardless of the membrane treatment and operation, which highlights the stability of the bulk PVDF toward surface modification technologies, as stated by other authors [35,39,43,48]. The characteristic melting temperature was approximately between 160 and 180 °C, with an endothermic peak at around 163 °C. These outcomes are consistent with the literature [38,67].

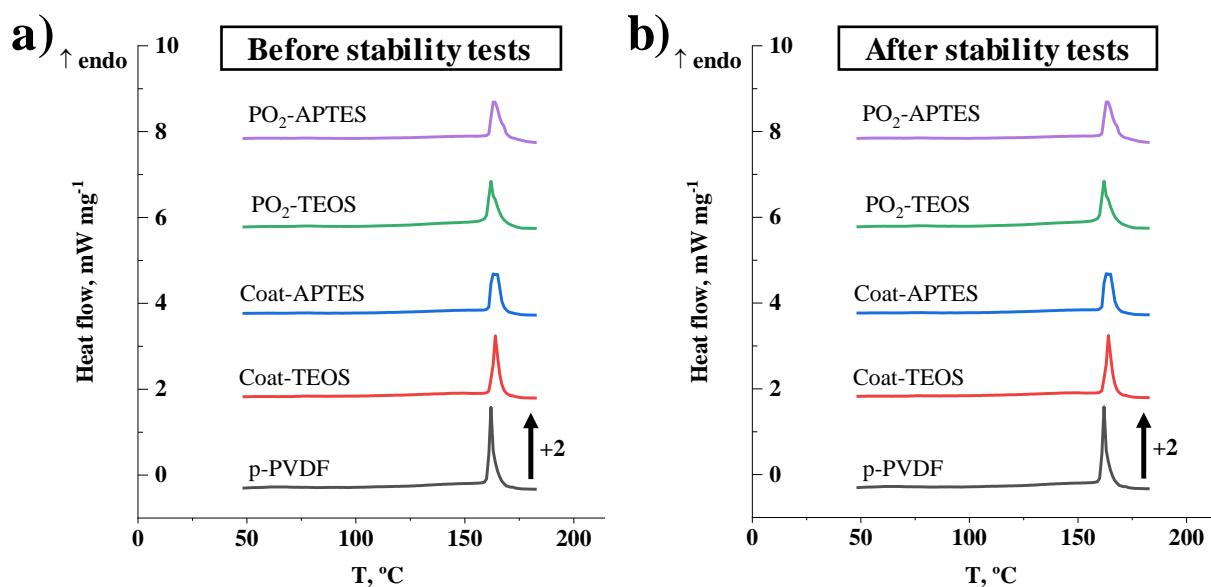


Figure 5. Differential scanning calorimetry of the pristine PVDF membrane (p-PVDF), coated membranes with FAS/TEOS and FAS/APTES (Coat-TEOS and Coat-APTES, respectively) and modified membranes with oxygen plasma activation at 15 W for a period of 15 min and functionalised with FAS/TEOS and FAS/APTES (PO₂-TEOS and PO₂-APTES, respectively) (a) before and (b) after the stability tests.

Table 3. Effect of different modification methods before and after the stability tests on the melting temperature (T_m), enthalpy (Δh_m) and the degree of crystallinity (χ) in the pristine PVDF membrane (p-PVDF), coated membranes with FAS/TEOS and FAS/APTES (Coat-TEOS and Coat-APTES, respectively) and modified membranes with oxygen plasma activation at 15 W for a period of 15 min and functionalised with FAS/TEOS and FAS/APTES (PO₂-TEOS and PO₂-APTES, respectively).

	Before Stability Test			After Stability Test		
	T_m , °C	Δh_m , J g ⁻¹	χ , %	T_m , °C	Δh_m , J g ⁻¹	χ , %
p-PVDF	162.3	59.3	60.6	162.0	62.2	63.5
Coat-TEOS	164.0	53.0	54.1	164.0	54.9	56.1
Coat-APTES	164.3	55.0	56.2	162.6	54.7	55.9
PO ₂ -TEOS	162.3	54.2	55.4	161.8	58.1	59.3
PO ₂ -APTES	162.9	57.0	58.2	163.4	58.9	60.2

The melting enthalpies of the samples were between 53 and 59 J g⁻¹, and maximum crystallinity with a value of 61% was observed for the pristine PVDF. The treated membranes showed slightly lower crystallinity degrees with values between 54 and 58%. Other authors have also reported similar crystallinity degrees of around 54% for PVDF membranes treated with argon and oxygen plasma at 100 W for a period ranging from 200 to 600 s [38].

Similar findings and trends were observed on the membranes after the stability tests (Figure 5b and Table 3). In general terms, neither membrane treatment nor long-term operation induced any significant modification of the thermal behaviour of the membranes.

The works of Correia et al. [38,67] also reported no significant effect of argon and oxygen plasmas on the crystallinity of PVDF membranes.

3.2.2. Stability of the Surface Hydrophobicity in Operation

The stability of PVDF membranes during long-term operation was evaluated by monitoring its WCA as a useful indicator of changes or alterations occurring on the membrane surface [28,64–66]. The results of the variation in WCA with the time of use of the coated PVDF membranes (Coat-TEOS and Coat-APTES) and plasma-treated PVDF membranes at the optimal conditions (PO₂-TEOS and PO₂-APTES) are shown in Figure 6a,b, respectively. The initial WCA of Coat-TEOS and Coat-APTES were $144.8 \pm 3.2^\circ$ and $149.8 \pm 2.7^\circ$, respectively. These values were lower than their respective plasma-treated membranes (PO₂-TEOS and PO₂-APTES), suggesting a lower presence of FAS and SiP on the membrane surface due to the absence of a previous activation. Kaur et al. [25] studied the grafting of methacrylic acid on non-treated and plasma-treated PVDF membranes, and they reported that grafting was facilitated by the formation of radicals and peroxide groups in argon plasma-treated membranes.

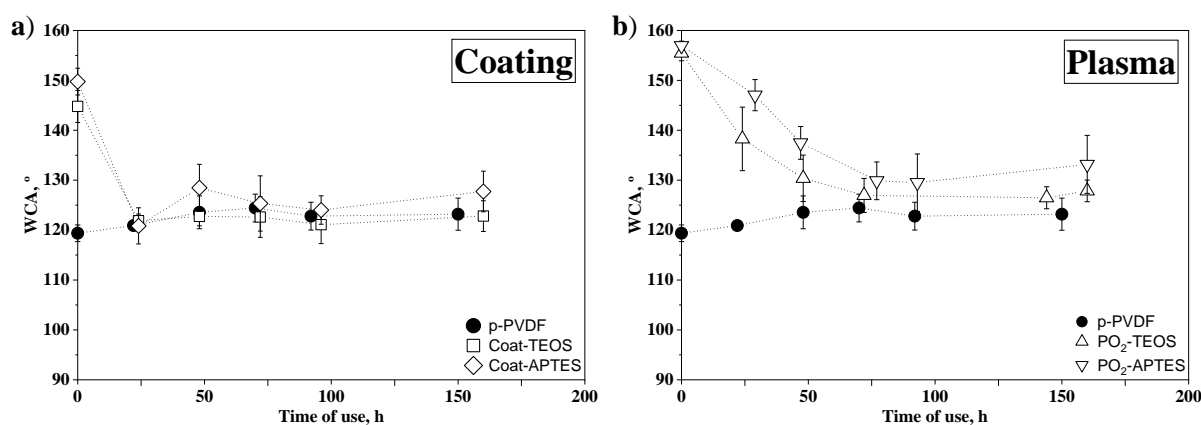


Figure 6. (a) Water contact angle versus time of use for pristine PVDF membrane (p-PVDF) and coated membranes with FAS/TEOS and FAS/APTES (Coat-TEOS and Coat-APTES, respectively) and (b) p-PVDF and modified membranes with oxygen plasma activation at 15 W for a period of 15 min and functionalised with FAS/TEOS and FAS/APTES (PO₂-TEOS and PO₂-APTES, respectively).

As can be seen in Figure 6a, the WCA of both coated membranes decreased pronouncedly during the first 24 h, reaching similar values to those of the p-PVDF. Then, the WCA of the coated membranes remained constant after 24 h, as did the p-PVDF. Hence, it can be concluded that the effect of the coating with FAS/TEOS and FAS/APTES solutions was completely lost from the surface-coated membranes before 24 h. This fact suggests that only a physical deposition of FAS and SiP was involved without further chemical reactions, creating an unstable surface layer that would be removed by dragging effects under a constant liquid flux over the membrane [34,64].

In contrast, although the WCA of the plasma-treated membranes PO₂-TEOS and PO₂-APTES decreased from the initial values of $155.5 \pm 1.5^\circ$ and $157.0 \pm 0.9^\circ$ to $127.0 \pm 3.4^\circ$ and $129.9 \pm 3.8^\circ$ at approximately 75 h, respectively, the WCA values stayed almost constant and slightly higher than those of the p-PVDF after 75 h (Figure 6b). These results suggested that the effect of the functionalisation was partially lost, likely due to removal of grafted molecules by the dragging effect, as reported in a previous work with modified membranes activated with an alkali solution [64]. However, WCA of the plasma-treated membranes after the stability tests was slightly higher than that of p-PVDF, suggesting a remnant of FAS and/or SiP on the surface. Hence, stronger chemical bonding and interactions could be inferred between the SiP, FAS and activated PVDF than those shown by the coated membranes. Comparing the effect of the SiP on the membrane stability, both

PO₂-APTES and PO₂-TEOS membranes experienced a similar decrease rate with the time of use. However, PO₂-APTES always showed slightly higher WCAs, mainly attributed to the additional hydrophobic aminopropyl segments from the APTES grafted on the membrane, as previously discussed.

Research works evaluating the effect of long-term operation on the stability of modified membranes are still very scarce, with most of them focusing on the stability of the separation performance. For example, our previous study [64] evaluated a functionalisation protocol using an alkali-based activation and showed that the WCA of the modified PVDF decreased to values lower than the pristine membrane in the first 50 h of operation at a liquid flow rate of 27 L h⁻¹. In this regard, the plasma pretreatment seemed to provide a more stable hydrophobic surface. Moreover, Sairiam et al. [38] performed long-term tests for CO₂ absorption with helium plasma-treated and functionalised PVDF membranes, and they reported a stable gas flux during the 15 days, unlike the unmodified membrane and the membrane activated with an alkali solution. Liang et al. [60] evaluated the stability of PVDF membranes modified with Ar plasma activation and grafting with methacrylic acid by immersing the membranes in solutions with different pH for only 15 min, and they reported a similar WCA before and after the stability tests. Moreover, Gryta [36] reported that PP membranes treated with helium (He) plasma for enhancing hydrophilicity showed a greater and more stable performance than non-treated membranes during 300 h of treating actual seawater for water purification, in which a higher water flux and lower permeate conductivity have been reported.

3.3. Structure and Chemical Composition of the Modified Membranes

Microscopy using FESEM and EDX analyses was conducted in order to determine the morphology of the surface, cross-section and chemical composition of the pristine, coated and plasma-treated membranes, both before and after the stability tests. The FESEM images of the surface and cross-section of the different analysed membranes before the stability tests are shown in Figure 7. The surface morphology of the Coat-TEOS and Coat-APTES membranes (Figure 7b1,c1) was similar to that of the p-PVDF (Figure 7a1), and a surface coating layer covering the membrane surface was not observed. In addition, the measured surface porosities of the pristine and coated membranes were similar, with values around 10% (Table 4).

The surface morphology of the plasma-treated membranes (Figure 7d1,e1) was similar to that of the pristine PVDF when a low plasma power and time of 5 W and 5 min were applied, respectively, independently of using TEOS or APTES as SiP. In contrast, at a higher plasma power and time of 15 W and 15 min, respectively, the surface became a pillar-like structure, resulting in a rougher and more open surface structure with larger pore sizes (Figure 7d1,e1), and the surface porosity increased to approximately 15% (Table 4) for both PO₂-TEOS and PO₂-APTES. This increase in the surface roughness also contributed to the increase of the WCAs, leading to superhydrophobic membranes in which the droplets easily rolled off, suggesting a Cassie state, which is desirable for wetting and fouling resistant surfaces [33,55]. This severe change at the surface was explained by the etching effect of plasma treatment, especially at a plasma time higher than or equal to 15 min [46].

Table 4. Surface porosity (%) of the pristine PVDF (p-PVDF), coated PVDF membranes with FAS/TEOS (Coat-TEOS) and FAS/APTES (Coat-APTES) and modified membranes with oxygen plasma activation at 15 W for a period of 15 min and functionalised with FAS/TEOS (PO₂-TEOS) and FAS/APTES (PO₂-APTES) before and after its use in the long-term stability tests.

Membrane	Before Stability Test	After Stability Test
p-PVDF	11 ± 3%	5 ± 1%
Coat-TEOS	8 ± 1%	4 ± 2%
Coat-APTES	10 ± 2%	3 ± 3%
PO ₂ -TEOS	15 ± 4%	6 ± 3%
PO ₂ -APTES	15 ± 3%	7 ± 1%

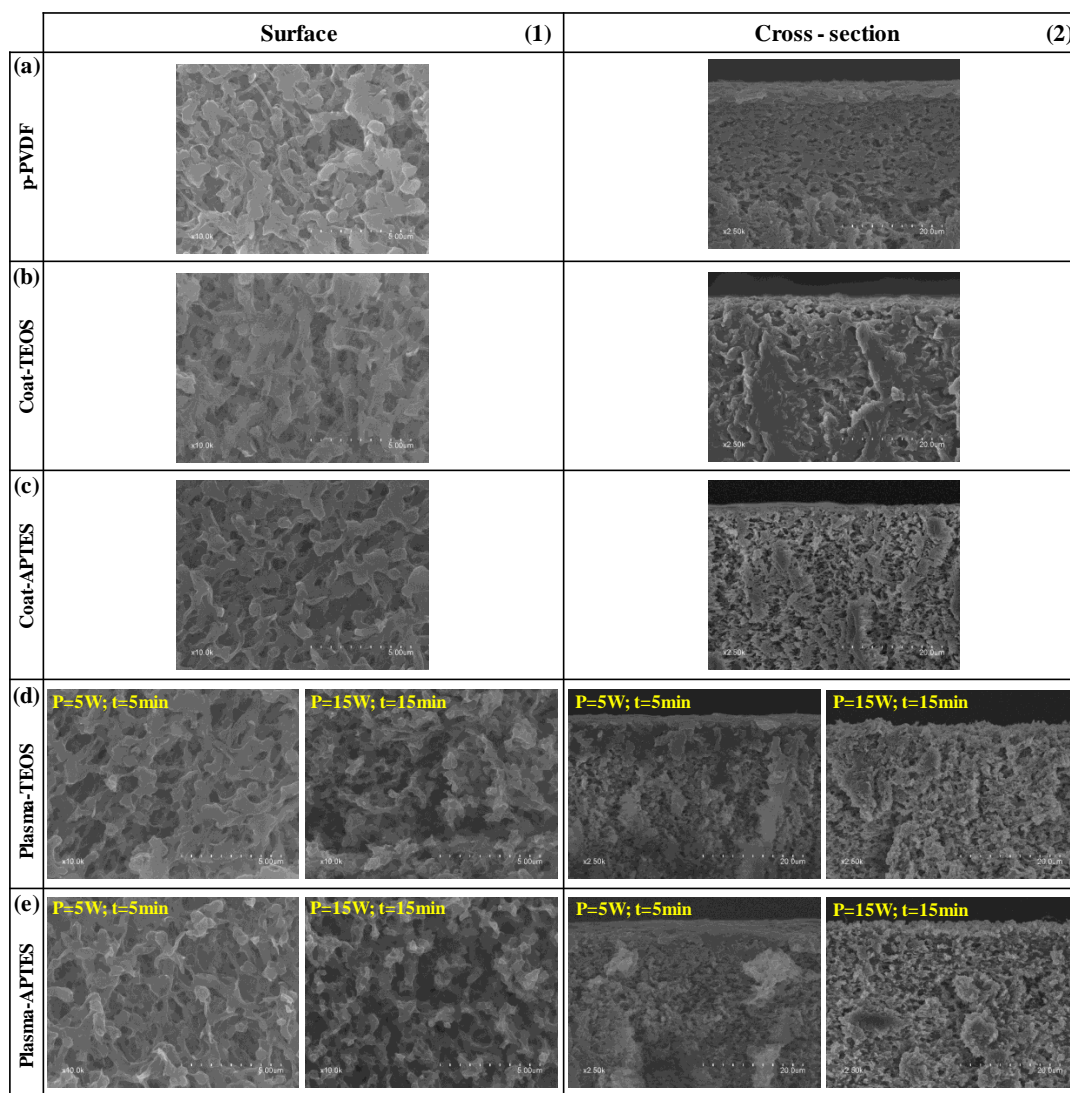


Figure 7. FESEM images of the (1) surface and (2) cross-section of the (a) pristine PVDF (p-PVDF), coated membranes by (b) FAS/TEOS (Coat-TEOS) and (c) FAS/APTES (Coat-APTES) and modified membranes with oxygen plasma activation at different plasma conditions and functionalised with (d) FAS/TEOS (Plasma-TEOS) and (e) FAS/APTES (Plasma-APTES).

Different authors have reported similar observations regarding surface morphology changes after plasma treatment. Lin et al. [43] reported an increase of the pores on the surface caused by etching during a plasma treatment with methane at a power higher than 50 W and time less than 5 min, and they suggested that the formation and breakage rates of C-F bonds were equal for plasma time periods higher than 5 min. Liang et al. [61] also reported an increase of the surface pore size and porosity of PVDF membranes after argon plasma treatment at 18 W and time less than or equal to 120 s, attributed to the etching effect. Yang et al. [62] obtained a more open structure on PVDF membranes after plasma treatment with carbon tetrafluoride at 150 W and 15 min. Xu et al. [60] observed an increase in the surface porosity from 13 to 34% after an argon plasma treatment at 30 W and 120 s, and this value declined to 12% after the grafting of an organosilane similar to the FAS used in this work. Jeong et al. [4] observed that the PVDF surface became a pillar-like structure after an oxygen and carbon tetrafluoride plasma treatment at 62 W for plasma time periods higher than 30 min.

The FESEM images of the membrane cross-section before the stability tests were taken and shown in Figure 7. They focused on the target surface at high magnification. In

Supplementary Material (S3), images were taken at lower magnification to show the entire membrane. The cross-section of the upper layer of p-PVDF (Figure 7a2) changed after the coating treatment (Figure 7b2,c2), showing a more porous structure. Only in the case of the plasma-treated membranes under soft conditions of 5 W and 5 min (Figure 7d2,e2), a dense-like cross-section was observed at the upper surface ($\leq 7 \mu\text{m}$), likely owing to the grafting of SiP and FAS, especially when TEOS was used, as observed in our previous study [64]. In contrast, the upper layers of the plasma-treated membranes at 15 W and 15 min showed a highly porous structure and rougher surface (Figure 7d2,e2), in which a surface profile with ridges and valleys was observed, as reported by other authors [38]. Regarding the thickness of the PVDF membranes, it remained unchanged in values ranging from 120 to 130 μm after the coating treatment and plasma activation and functionalisation (Supplementary Material (S3)), as reported by other authors [24].

After the stability tests, all the membranes experienced a reduction in surface porosity to a value of approximately 5% (Table 4), which was attributed to plastic deformation observed at the surface level (Figure 8), which also contributed to the WCA decrease during the stability test. However, no significant changes were observed on the cross-section with membrane thickness values of approximately 120 μm (Figure 8). This indicated a high membrane bulk stability and mechanical resistance under the tested operational conditions.

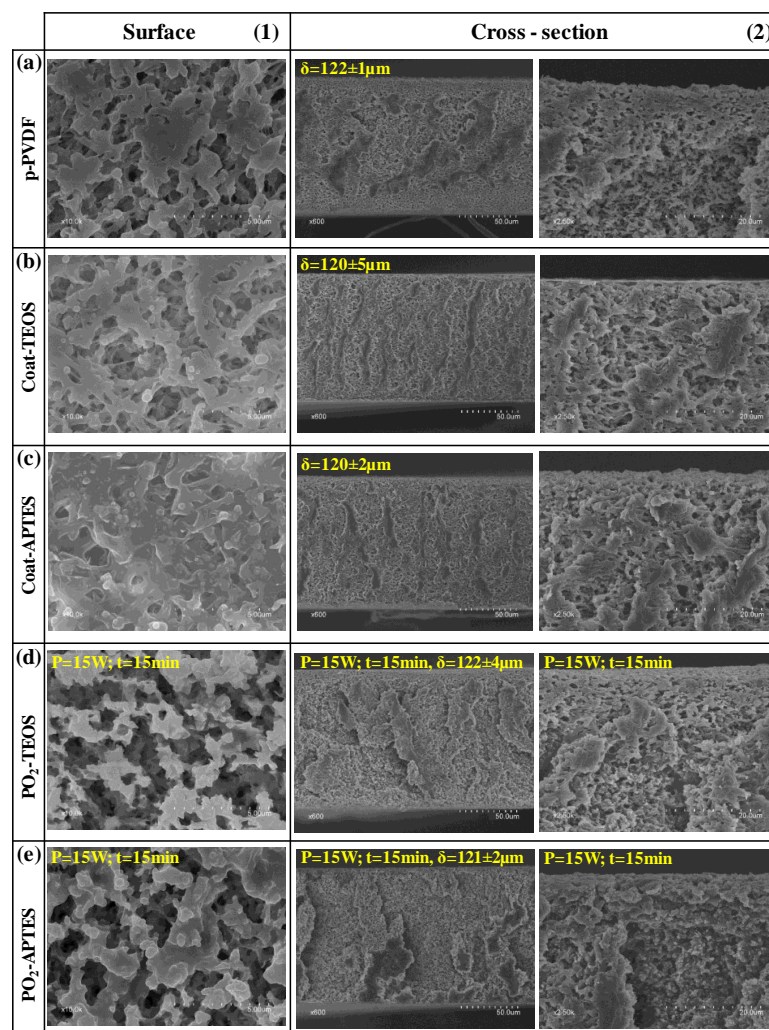


Figure 8. FESEM images of the (1) surface and (2) cross-section of the (a) pristine PVDF (p-PVDF), coated membranes by (b) FAS-TEOS (Coat-TEOS) and (c) FAS-APTES (Coat-APTES) and modified membranes with oxygen plasma activation at 15W and 15 min and functionalised with (d) FAS/TEOS (PO₂-TEOS) and (e) FAS/APTES (PO₂-APTES) after the long-term stability test.

The surface chemical composition of the pristine, coated and plasma-treated membranes was determined by the EDX, and the atomic ratios of F, O, Si and N with respect to C (%_{atomic}/_{atomic}) are shown in Table 5. The F/C ratio of p-PVDF was 0.92, quite far from the theoretically value of 1.00 for pure PVDF, indicating a raw PVDF membrane with the presence of other organic carbon compounds.

Table 5. Fluorine-, Oxygen-, Silicon- and Nitrogen-to-Carbon atomic ratio of the pristine PVDF membrane (p-PVDF), coated membranes with FAS/TEOS (Coat-TEOS) and FAS/APTES (Coat-APTES) and modified membranes with oxygen plasma activation at 15 W and 15 min and functionalised with FAS/TEOS (PO₂-TEOS) and FAS/APTES (PO₂-APTES) before and after its use in the long-term stability tests. Standard deviation \leq 0.05.

Membrane	Before Stability Test				After Stability Test			
	F/C	O/C	Si/C	N/C	F/C	O/C	Si/C	N/C
p-PVDF	0.92	-	-	-	0.90	-	-	-
Coat-TEOS	0.95	0.02	<0.01	-	0.94	0.02	<0.01	-
Coat-APTES	0.95	0.03	<0.01	0.03	0.91	0.04	0.01	<0.01
PO ₂ -TEOS	0.95	0.04	0.01	-	0.80	0.03	<0.01	-
PO ₂ -APTES	0.99	0.05	0.01	0.04	0.85	0.09	0.02	0.04

After the coating of PVDF, in both Coat-TEOS and Coat-APTES membranes, the F/C ratio slightly increased to 0.95 due to the deposition of FAS. The presence of O, Si and N indicated the deposition of SiPs. A similar deposition grade of FAS and SiP could be inferred independently of the SiP applied since similar atomic ratios were obtained. The highest F/C ratio of 0.99 was obtained for the PO₂-APTES membrane, indicating a higher grafting grade of FAS with respect to the coated membranes and PO₂-TEOS. This can help explain the greater hydrophobicity of the membranes treated with oxygen plasma and APTES. Both PO₂-TEOS and PO₂-APTES membranes presented slightly higher O/C, Si/C and N/C ratios than Coat-TEOS and Coat-APTES, respectively, indicating a higher presence of SiP molecules because of the generation of active sites on the membrane during the plasma treatment. The higher O/C ratios in the plasma-treated membranes with respect to the coated membranes could also be attributed to the increase in the oxygen content during the plasma treatment [48,53,67].

After the stability tests, the F/C ratio decline was more noticeable in the plasma-treated and functionalised membranes (Table 5), indicating a loss of fluorine in accordance with the decrease of the WCA with the time of use. The F/C ratio decreased from 0.95 to 0.80 and 0.99 to 0.85 in the PO₂-TEOS and PO₂-APTES membranes, respectively. These outcomes showed a similar decrease of around 15% in the F/C ratio, suggesting that a similar amount of FAS moieties was removed. In addition, the O/C, Si/C and N/C ratios stayed the same or slightly higher after the stability test, which could indicate that the condensation and grafting of SiP led to a stronger interaction/chemical bonding with the membrane than those involved with FAS, hindering the dragging of SiP by the liquid flux. Furthermore, the higher amount of fluorine and SiP on the PO₂-APTES after the stability tests could explain its higher WCA with respect to the PO₂-TEOS at the end of the test. The F/C ratio of the coated membranes decreased slightly after the stability test and kept at similar values to that of the pristine membrane, indicating a loss of the coating layer and showing similar WCAs. In addition, the F/C ratio of the plasma-treated membranes was lower than those of the pristine and coated membranes despite their higher WCAs after the stability tests. This result suggests that the higher surface roughness and pore size had a predominant effect on the WCA.

From the previous results, new modification protocols should be evaluated in future studies in this direction, with special focus on the stability of grafting compounds on the modified membranes, preventing the removal or dragging of the modifying agents under moderate liquid fluxes at long-term operations. This prolonged useful lifetime of the

functionalisation layer would lead to a reduction in the operational costs during large-scale applications.

4. Conclusions

Superhydrophobic PVDF membranes were prepared by means of surface treatment based on an initial oxygen plasma activation followed by functionalisation with a fluoroalkylsilane and silica precursors. The outcomes of the statistical design of the experiments showed that the type of silica precursor had the highest effect on the water contact angle of the modified membrane. Particularly, the use of APTES as silica precursors always led to membranes with higher water contact angles than those obtained by using TEOS, which was ascribed to the asymmetric structure of APTES. Other factors, such as the power and, especially, the time of the plasma discharge, showed less significant effects on the water contact angle. From those results, optimal values for the oxygen plasma treatment were established at a power of 15 W and a time of 15 min, obtaining contact angles higher than 155° and avoiding membrane degradation. In fact, the modifications acted primarily on the surface, and the bulk properties remained stable and maintained the thermal features of PVDF membranes after the treatments. Moreover, at those plasma conditions, the membrane surface showed a pillar-like morphology, with higher porosity and roughness, which favoured the hydrophobicity.

During long-term operation tests under a continuous liquid flux, the contact angle decreased with the time of use, which was attributed mainly to the removal of fluoroalkylsilane molecules from the surface since a lower fluorine content was observed after the long-term tests, and also to the reduction of the surface porosity due to a surface plastic deformation. However, the functionalisation layer of the oxygen plasma-activated membranes showed high stability, in comparison with the coated membranes without any activation step. After 160 h of operation, the plasma-treated membranes showed a water contact angle of approximately 130°, which was still higher than that of the non-modified membranes (119°). Further research should focus on the improvement of the anchoring of the modifying agents onto the PVDF substrate and the feasibility and scalability of the functionalisation methodologies for their implementation at an industrial scale.

Supplementary Materials: The following supporting information can be downloaded at: <https://www.mdpi.com/article/10.3390/membranes13030314/s1>, S1: Experimental system for the long-term stability tests; S2: Infrared spectra of the pristine PVDF and modified membranes with oxygen plasma activation and functionalization; S3: FESEM images at low magnification of the cross section of the pristine, coated and plasma treated PVDF membranes before the stability tests.

Author Contributions: R.J.-R.: methodology, validation, formal analysis, investigation, writing—original draft, writing—review and editing, visualisation. M.I.: conceptualisation, methodology, validation, writing—review and editing, supervision, funding acquisition. V.M.-S.: conceptualisation, methodology, validation, writing—review and editing, supervision. L.M.: conceptualisation, validation, funding acquisition. A.M.: conceptualisation, writing—review and editing, validation. J.D.B.: conceptualisation, methodology, validation, writing—review and editing, supervision, funding acquisition. All authors have read and agreed to the published version of the manuscript.

Funding: This research was supported by project IMMDEA/2020/015 funded by the Institut Valencià de Competitivitat Empresarial-Generalitat Valenciana and project TED2021-131276A-I00 funded by MCIN/AEI/10.13039/501100011033 and by European Union NextGenerationEU/PRTR. PhD grant of R. Jiménez-Robles was funded by Ministerio de Universidades, Spain (Beca de Formación de Profesorado Universitario FPU19/02478).

Institutional Review Board Statement: Not applicable.

Informed Consent Statement: Not applicable.

Data Availability Statement: Not applicable.

Acknowledgments: The authors thank Pablo Contreras-García for his technical support in the preliminary experiments of the membrane modification and constant attitude towards learning.

Conflicts of Interest: The authors declare that they have no known competing financial interests or personal relationships that could have appeared to influence the work reported in this paper.

References

1. Stazi, V.; Tomei, M.C. Dissolved methane in anaerobic effluents: A review on sustainable strategies for optimization of energy recovery or internal process reuse. *J. Clean. Prod.* **2021**, *317*, 128359. [[CrossRef](#)]
2. Lee, Y.; Yun, K.H.; Sethunga, D.; Bae, T.H. Membrane contactors for maximizing biomethane recovery in anaerobic wastewater treatments: Recent efforts and future prospect. *Appl. Sci.* **2021**, *11*, 1372. [[CrossRef](#)]
3. Yang, X.; Wang, R.; Shi, L.; Fane, A.G.; Debowski, M. Performance improvement of PVDF hollow fiber-based membrane distillation process. *J. Memb. Sci.* **2011**, *369*, 437–447. [[CrossRef](#)]
4. Jeong, S.; Shin, B.; Jo, W.; Kim, H.Y.; Moon, M.W.; Lee, S. Nanostructured PVDF membrane for MD application by an O₂ and CF₄ plasma treatment. *Desalination* **2016**, *399*, 178–184. [[CrossRef](#)]
5. Woo, Y.C.; Chen, Y.; Tijging, L.D.; Phuntsho, S.; He, T.; Choi, J.S.; Kim, S.H.; Shon, H.K. CF₄ plasma-modified omniphobic electrospun nanofiber membrane for produced water brine treatment by membrane distillation. *J. Memb. Sci.* **2017**, *529*, 234–242. [[CrossRef](#)]
6. Klaassen, R.; Feron, P.H.M.; Jansen, A.E. Membrane contactors in industrial applications. *Chem. Eng. Res. Des.* **2005**, *83*, 234–246. [[CrossRef](#)]
7. Zhang, N.; Pan, Z.; Zhang, Z.; Zhang, W.; Zhang, L.; Baena-Moreno, F.M.; Lichtfouse, E. CO₂ capture from coalbed methane using membranes: A review. *Environ. Chem. Lett.* **2020**, *18*, 79–96. [[CrossRef](#)]
8. Zhu, H.; Li, X.; Pan, Y.; Liu, G.; Wu, H.; Jiang, M.; Jin, W. Fluorinated PDMS membrane with anti-biofouling property for in-situ biobutanol recovery from fermentation-pervaporation coupled process. *J. Memb. Sci.* **2020**, *609*, 118225. [[CrossRef](#)]
9. Henares, M.; Izquierdo, M.; Penya-Roja, J.M.; Martínez-Soria, V. Comparative study of degassing membrane modules for the removal of methane from Expanded Granular Sludge Bed anaerobic reactor effluent. *Sep. Purif. Technol.* **2016**, *170*, 22–29. [[CrossRef](#)]
10. Jiménez-Robles, R.; Martínez-Soria, V.; Izquierdo, M. Fouling characterization in PVDF membrane contactors for dissolved methane recovery from anaerobic effluents: Effect of surface organofluorosilanisation. *Environ. Sci. Pollut. Res.* **2022**. [[CrossRef](#)]
11. Pan, J.; Zhang, F.; Wang, Z.; Sun, S.P.; Cui, Z.; Jin, W.; Bamaga, O.; Abulhair, H.; Albeirutty, M.; Drioli, E. Enhanced anti-wetting and anti-fouling properties of composite PFPE/PVDF membrane in vacuum membrane distillation. *Sep. Purif. Technol.* **2022**, *282*, 1–11. [[CrossRef](#)]
12. Liu, L.; Xiao, Z.; Liu, Y.; Li, X.; Yin, H.; Volkov, A.; He, T. Understanding the fouling/scaling resistance of superhydrophobic/omniphobic membranes in membrane distillation. *Desalination* **2021**, *499*, 114864. [[CrossRef](#)]
13. Sethunga, G.S.M.D.P.; Karahan, H.E.; Wang, R.; Bae, T.H. Wetting- and fouling-resistant hollow fiber membranes for dissolved methane recovery from anaerobic wastewater treatment effluents. *J. Memb. Sci.* **2021**, *617*, 118621. [[CrossRef](#)]
14. Henares, M.; Ferrero, P.; San-Valero, P.; Martínez-Soria, V.; Izquierdo, M. Performance of a polypropylene membrane contactor for the recovery of dissolved methane from anaerobic effluents: Mass transfer evaluation, long-term operation and cleaning strategies. *J. Memb. Sci.* **2018**, *563*, 926–937. [[CrossRef](#)]
15. Al-Juboori, R.A.; Yusaf, T. Biofouling in RO system: Mechanisms, monitoring and controlling. *Desalination* **2012**, *302*, 1–23. [[CrossRef](#)]
16. Wang, J.; Chen, X.; Reis, R.; Chen, Z.; Milne, N.; Winther-Jensen, B.; Kong, L.; Dumée, L.F. Plasma modification and synthesis of membrane materials—A mechanistic review. *Membranes* **2018**, *8*, 56. [[CrossRef](#)]
17. Zhao, X.; Xuan, H.; Qin, A.; Liu, D.; He, C. Improved antifouling property of PVDF ultrafiltration membrane with plasma treated PVDF powder. *RSC Adv.* **2015**, *5*, 64526–64533. [[CrossRef](#)]
18. Sethunga, G.S.M.D.P.; Lee, J.; Wang, R.; Bae, T.H. Influence of membrane characteristics and operating parameters on transport properties of dissolved methane in a hollow fiber membrane contactor for biogas recovery from anaerobic effluents. *J. Memb. Sci.* **2019**, *589*, 117263. [[CrossRef](#)]
19. Liu, L.; Charlton, L.; Song, Y.; Li, T.; Li, X.; Yin, H.; He, T. Scaling resistance by fluoro-treatments: The importance of wetting states. *J. Mater. Chem. A* **2022**, *10*, 3058–3068. [[CrossRef](#)]
20. Jothi Prakash, C.G.; Prasanth, R. Approaches to design a surface with tunable wettability: A review on surface properties. *J. Mater. Sci.* **2021**, *56*, 108–135. [[CrossRef](#)]
21. Rana, D.; Matsuura, T. Surface modifications for antifouling membranes. *Chem. Rev.* **2010**, *110*, 2448–2471. [[CrossRef](#)] [[PubMed](#)]
22. Ebert, D.; Bhushan, B. Transparent, superhydrophobic, and wear-resistant surfaces using deep reactive ion etching on PDMS substrates. *J. Colloid Interface Sci.* **2016**, *481*, 82–90. [[CrossRef](#)] [[PubMed](#)]
23. Li, Z.; Wu, Z.; Cen, X.; Liu, Y.; Zhang, Y.; Liu, D.; Chen, Z. Efficient Production of 1,3-Propanediol from Diverse Carbohydrates via a Non-natural Pathway Using 3-Hydroxypropionic Acid as an Intermediate. *ACS Synth. Biol.* **2021**, *10*, 478–486. [[CrossRef](#)]
24. Yang, C.; Tian, M.; Xie, Y.; Li, X.M.; Zhao, B.; He, T.; Liu, J. Effective evaporation of CF₄ plasma modified PVDF membranes in direct contact membrane distillation. *J. Memb. Sci.* **2015**, *482*, 25–32. [[CrossRef](#)]
25. Kaur, S.; Ma, Z.; Gopal, R.; Singh, G.; Ramakrishna, S.; Matsuura, T. Plasma-induced graft copolymerization of poly(methacrylic acid) on electrospun poly(vinylidene fluoride) nanofiber membrane. *Langmuir* **2007**, *23*, 13085–13092. [[CrossRef](#)]

26. Nguyen, H.T.; Bui, H.M.; Wang, Y.F.; You, S.J. Non-fluoroalkyl functionalized hydrophobic surface modifications used in membrane distillation for cheaper and more environmentally friendly applications: A mini-review. *Sustain. Chem. Pharm.* **2022**, *28*, 100714. [[CrossRef](#)]
27. Kang, G.d.; Cao, Y.M. Application and modification of poly(vinylidene fluoride) (PVDF) membranes—A review. *J. Memb. Sci.* **2014**, *463*, 145–165. [[CrossRef](#)]
28. Oldani, V.; Sergi, G.; Pirola, C.; Sacchi, B.; Bianchi, C.L. Sol-gel hybrid coatings containing silica and a perfluoropolyether derivative with high resistance and anti-fouling properties in liquid media. *J. Fluor. Chem.* **2016**, *188*, 43–49. [[CrossRef](#)]
29. Taurino, R.; Fabbri, E.; Messori, M.; Pilati, F.; Pospiech, D.; Synytska, A. Facile preparation of superhydrophobic coatings by sol-gel processes. *J. Colloid Interface Sci.* **2008**, *325*, 149–156. [[CrossRef](#)]
30. Xie, M.; Luo, W.; Gray, S.R. Surface pattern by nanoimprint for membrane fouling mitigation: Design, performance and mechanisms. *Water Res.* **2017**, *124*, 238–243. [[CrossRef](#)] [[PubMed](#)]
31. Won, Y.-J.; Lee, J.; Choi, D.-C.; Chae, H.R.; Kim, I.; Lee, C.-H.; Kim, I.-C. Preparation and application of patterned membranes for wastewater treatment. *Environ. Sci. Pollut. Res.* **2012**, *46*, 11021–11027. [[CrossRef](#)] [[PubMed](#)]
32. Kim, I.; Choi, D.C.; Lee, J.; Chae, H.R.; Hee Jang, J.; Lee, C.H.; Park, P.K.; Won, Y.J. Preparation and application of patterned hollow-fiber membranes to membrane bioreactor for wastewater treatment. *J. Memb. Sci.* **2015**, *490*, 190–196. [[CrossRef](#)]
33. Palumbo, F.; Di Mundo, R.; Cappelluti, D.; Dagostino, R. SuperHydrophobic and SuperHydrophilic polycarbonate by tailoring chemistry and nano-texture with plasma processing. *Plasma Process. Polym.* **2011**, *8*, 118–126. [[CrossRef](#)]
34. Zhao, S.; Liao, Z.; Fane, A.; Li, J.; Tang, C.; Zheng, C.; Lin, J.; Kong, L. Engineering antifouling reverse osmosis membranes: A review. *Desalination* **2021**, *499*, 114857. [[CrossRef](#)]
35. Liu, L.; Shen, F.; Chen, X.; Luo, J.; Su, Y.; Wu, H.; Wan, Y. A novel plasma-induced surface hydrophobization strategy for membrane distillation: Etching, dipping and grafting. *J. Memb. Sci.* **2016**, *499*, 544–554. [[CrossRef](#)]
36. Gryta, M. Surface modification of polypropylene membrane by helium plasma treatment for membrane distillation. *J. Memb. Sci.* **2021**, *628*, 119265. [[CrossRef](#)]
37. Miller, D.J.; Dreyer, D.R.; Bielawski, C.W.; Paul, D.R.; Freeman, B.D. Surface Modification of Water Purification Membranes. *Angew. Chemie—Int. Ed.* **2017**, *56*, 4662–4711. [[CrossRef](#)]
38. Correia, D.M.; Nunes-Pereira, J.; Alikin, D.; Kholkin, A.L.; Carabineiro, S.A.C.; Rebouta, L.; Rodrigues, M.S.; Vaz, F.; Costa, C.M.; Lanceros-Méndez, S. Surface wettability modification of poly(vinylidene fluoride) and copolymer films and membranes by plasma treatment. *Polymer* **2019**, *169*, 138–147. [[CrossRef](#)]
39. Sairiam, S.; Loh, C.H.; Wang, R.; Jiraratananon, R. Surface modification of PVDF hollow fiber membrane to enhance hydrophobicity using organosilanes. *J. Appl. Polym. Sci.* **2013**, *130*, 610–621. [[CrossRef](#)]
40. Cortese, G.; Martina, F.; Vasapollo, G.; Cingolani, R.; Gigli, G.; Ciccarella, G. Modification of micro-channel filling flow by poly(dimethylsiloxane) surface functionalization with fluorine-Substituted aminonaphthols. *J. Fluor. Chem.* **2010**, *131*, 357–363. [[CrossRef](#)]
41. Arima, V.; Bianco, M.; Zacheo, A.; Zizzari, A.; Perrone, E.; Marra, L.; Rinaldi, R. Fluoropolymers coatings on polydimethylsiloxane for retarding swelling in toluene. *Thin Solid Films* **2012**, *520*, 2293–2300. [[CrossRef](#)]
42. Han, Y.; Song, S.; Lu, Y.; Zhu, D. A method to modify PVDF microfiltration membrane via ATRP with low-temperature plasma pretreatment. *Appl. Surf. Sci.* **2016**, *379*, 474–479. [[CrossRef](#)]
43. Lin, S.H.; Tung, K.L.; Chang, H.W.; Lee, K.R. Influence of fluorocarbon flat-membrane hydrophobicity on carbon dioxide recovery. *Chemosphere* **2009**, *75*, 1410–1416. [[CrossRef](#)]
44. Juang, R.S.; Huang, C.; Hsieh, C.L. Surface modification of PVDF ultrafiltration membranes by remote argon/methane gas mixture plasma for fouling reduction. *J. Taiwan Inst. Chem. Eng.* **2014**, *45*, 2176–2186. [[CrossRef](#)]
45. Meyyappan, M. Plasma nanotechnology: Past, present and future. *J. Phys. D. Appl. Phys.* **2011**, *44*, 174002. [[CrossRef](#)]
46. *Plasma Technology*, 4th ed.; Diener Electronic GmbH + Co. KG: Ebhausen, Germany, 2011; Available online: http://lampx.tugraz.at/~hadley/semi/ch9/instruments/Diener/Plasmatechnik_eng.pdf (accessed on 5 March 2023).
47. Duca, M.D.; Plosceanu, C.L.; Pop, T. Surface modifications of polyvinylidene fluoride (PVDF) under rf Ar plasma. *Polym. Degrad. Stab.* **1998**, *61*, 65–72. [[CrossRef](#)]
48. Vesel, A.; Zaplotnik, R.; Primc, G.; Mozetič, M.; Katan, T.; Kargl, R.; Mohan, T.; Kleinschek, K.S. Non-equilibrium plasma methods for tailoring surface properties of polyvinylidene fluoride: Review and challenges. *Polymers* **2021**, *13*, 4243. [[CrossRef](#)]
49. Dumée, L.F.; Algave, H.; Chaffraix, T.; Lin, B.; Magniez, K.; Schütz, J. Morphology-properties relationship of gas plasma treated hydrophobic meso-porous membranes and their improved performance for desalination by membrane distillation. *Appl. Surf. Sci.* **2016**, *363*, 273–285. [[CrossRef](#)]
50. Jafari, R.; Asadollahi, S.; Farzaneh, M. Applications of plasma technology in development of superhydrophobic surfaces. *Plasma Chem. Plasma Process.* **2013**, *33*, 177–200. [[CrossRef](#)]
51. Huang, C.; Lin, P.J.; Tsai, C.Y.; Juang, R.S. Electrospun microfibrillar membranes with atmospheric-pressure plasma surface modification for the application in dye-sensitized solar cells. *Plasma Process. Polym.* **2013**, *10*, 938–947. [[CrossRef](#)]
52. Cardinaud, C.; Peignon, M.C.; Tessier, P.Y. Plasma etching: Principles, mechanisms, application to micro- and nano-technologies. *Appl. Surf. Sci.* **2000**, *164*, 72–83. [[CrossRef](#)]
53. Park, Y.W.; Inagaki, N. Surface modification of poly(vinylidene fluoride) film by remote Ar, H₂, and O₂ plasmas. *Polymer* **2003**, *44*, 1569–1575. [[CrossRef](#)]

54. Vlachopoulou, M.E.; Tsougeni, K.; Petrou, P.; Kakabakos, S.; Tserapi, A.; Gogolides, E. High-Aspect-Ratio Plasma Induced Nanotexturing of Polymers (PDMS, PMMA, PEEK,...) for protein adsorption applications. In Proceedings of the International Conference on Electron, Ion and Photon Beam Technology and Nanofabrication, Denver, CO, USA, 29 May–1 June 2007.
55. Bhushan, B.; Hansford, D.; Lee, K.K. Surface modification of silicon and polydimethylsiloxane surfaces with vapor-phase-deposited ultrathin fluorosilane films for biomedical nanodevices. *J. Vac. Sci. Technol. A Vacuum Surfaces Film.* **2006**, *24*, 1197–1202. [[CrossRef](#)]
56. Lin, S.-H.; Tung, K.-L.; Chen, W.-J.; Chang, H.-W. Absorption of carbon dioxide by mixed piperazine–alkanolamine absorbent in a plasma-modified polypropylene hollow fiber contactor. *J. Memb. Sci.* **2009**, *333*, 30–37. [[CrossRef](#)]
57. Akamatsu, K.; Furue, T.; Han, F.; Nakao, S.I. Plasma graft polymerization to develop low-fouling membranes grafted with poly(2-methoxyethylacrylate). *Sep. Purif. Technol.* **2013**, *102*, 157–162. [[CrossRef](#)]
58. Di Mundo, R.; Troia, M.; Palumbo, F.; Trotta, M.; D’Agostino, R. Nano-texturing of transparent polymers with plasma etching: Tailoring topography for a low reflectivity. *Plasma Process. Polym.* **2012**, *9*, 947–954. [[CrossRef](#)]
59. Yalcinkaya, F.; Yalcinkaya, B.; Pazourek, A.; Mullerova, J.; Stuchlik, M.; Maryska, J. Surface Modification of Electrospun PVDF/PAN Nanofibrous Layers by Low Vacuum Plasma Treatment. *Int. J. Polym. Sci.* **2016**, *2016*, 4671658. [[CrossRef](#)]
60. Xu, W.T.; Zhao, Z.P.; Liu, M.; Chen, K.C. Morphological and hydrophobic modifications of PVDF flat membrane with silane coupling agent grafting via plasma flow for VMD of ethanol-water mixture. *J. Memb. Sci.* **2015**, *491*, 110–120. [[CrossRef](#)]
61. Liang, S.; Kang, Y.; Tiraferri, A.; Giannelis, E.P.; Huang, X.; Elimelech, M. Highly hydrophilic poly(vinylidene fluoride) (PVDF) ultrafiltration membranes via postfabrication grafting of surface-tailored silica nanoparticles. *ACS Appl. Mater. Interfaces* **2013**, *5*, 6694–6703. [[CrossRef](#)] [[PubMed](#)]
62. Yang, C.; Li, X.M.; Gilron, J.; Kong, D.F.; Yin, Y.; Oren, Y.; Linder, C.; He, T. CF₄ plasma-modified superhydrophobic PVDF membranes for direct contact membrane distillation. *J. Memb. Sci.* **2014**, *456*, 155–161. [[CrossRef](#)]
63. Liu, F.; Hashim, N.A.; Liu, Y.; Abed, M.R.M.; Li, K. Progress in the production and modification of PVDF membranes. *J. Memb. Sci.* **2011**, *375*, 1–27. [[CrossRef](#)]
64. Jiménez-Robles, R.; Moreno-Torrallbo, B.M.; Badia, J.D.; Martínez-Soria, V.; Izquierdo, M. Flat PVDF membrane with enhanced hydrophobicity through alkali activation and organofluorosilanisation for dissolved methane recovery. *Membranes* **2022**, *12*, 426. [[CrossRef](#)] [[PubMed](#)]
65. Jiménez-Robles, R.; Gabaldón, C.; Badia, J.D.; Izquierdo, M.; Martínez-Soria, V. Recovery of dissolved methane through a flat sheet module with PDMS, PP, and PVDF membranes. *Sep. Purif. Technol.* **2022**, *282*, 120057. [[CrossRef](#)]
66. Fabbri, P.; Messori, M.; Montecchi, M.; Pilati, F.; Taurino, R.; Tonelli, C.; Toselli, M. Surface properties of fluorinated hybrid coatings. *J. Appl. Polym. Sci.* **2006**, *102*, 1483–1488. [[CrossRef](#)]
67. Correia, D.M.; Ribeiro, C.; Sencadas, V.; Botelho, G.; Carabineiro, S.A.C.; Ribelles, J.L.G.; Lanceros-Méndez, S. Influence of oxygen plasma treatment parameters on poly(vinylidene fluoride) electrospun fiber mats wettability. *Prog. Org. Coatings* **2015**, *85*, 151–158. [[CrossRef](#)]
68. Gregorio, R.; Cestari, M. Effect of crystallization temperature on the crystalline phase content and morphology of poly(vinylidene fluoride). *J. Polym. Sci. Part B Polym. Phys.* **1994**, *32*, 859–870. [[CrossRef](#)]
69. Martins, P.; Lopes, A.C.; Lanceros-Méndez, S. Electroactive phases of poly(vinylidene fluoride): Determination, processing and applications. *Prog. Polym. Sci.* **2014**, *39*, 683–706. [[CrossRef](#)]
70. Hebbbar, R.S.; Isloor, A.M.; Ismail, A.F. Contact Angle Measurements. In *Membrane Characterization*; Elsevier: Amsterdam, The Netherlands, 2017; pp. 219–255. ISBN 9780444637918.
71. Abbasgholipourghadim, M.; Mailah, M.B.; Zaurah, I.; Ismail, A.F.; Rezaei Dashtarzhandi, M.; Abbasgholipourghadim, M. Porosity and pore area determination of hollow fiber membrane incorporating digital image processing. In Proceedings of the Recent Advances in Mechanics and Mechanical Engineering, Kuala Lumpur, Malaysia, 23–25 April 2015; pp. 118–123.
72. Tserapi, A.D.; Vlachopoulou, M.E.; Gogolides, E. Nanotexturing of poly (dimethylsiloxane) in plasmas for creating robust super-hydrophobic surfaces. *Nanotechnology* **2006**, *17*, 3977. [[CrossRef](#)]
73. Kim, E.S.; Kim, Y.J.; Yu, Q.; Deng, B. Preparation and characterization of polyamide thin-film composite (TFC) membranes on plasma-modified poly(vinylidene fluoride) (PVDF). *J. Memb. Sci.* **2009**, *344*, 71–81. [[CrossRef](#)]
74. Hanh Le, T.M.; Singto, S.; Sajomsang, W.; Mongkolnavin, R.; Nuisin, R.; Painmanakul, P.; Sairiam, S. Hydrophobic PVDF hollow fiber membrane modified with pulse inductively coupling plasma activation and chloroalkylsilanes for efficient dye wastewater treatment by ozonation membrane contactor. *J. Memb. Sci.* **2021**, *635*, 119443. [[CrossRef](#)]
75. Zhang, Y.; Wang, R. Novel method for incorporating hydrophobic silica nanoparticles on polyetherimide hollow fiber membranes for CO₂ absorption in a gas-liquid membrane contactor. *J. Memb. Sci.* **2014**, *452*, 379–389. [[CrossRef](#)]
76. Badia, J.D.; Gil-Castell, O.; Ribes-Greus, A. Long-term properties and end-of-life of polymers from renewable resources. *Polym. Degrad. Stab.* **2017**, *137*, 35–57. [[CrossRef](#)]
77. Badía, J.D.; Vilaplana, F.; Karlsson, S.; Ribes-Greus, A. Thermal analysis as a quality tool for assessing the influence of thermo-mechanical degradation on recycled poly(ethylene terephthalate). *Polym. Test.* **2009**, *28*, 169–175. [[CrossRef](#)]

Disclaimer/Publisher’s Note: The statements, opinions and data contained in all publications are solely those of the individual author(s) and contributor(s) and not of MDPI and/or the editor(s). MDPI and/or the editor(s) disclaim responsibility for any injury to people or property resulting from any ideas, methods, instructions or products referred to in the content.

Supplementary Material for

Stability of superhydrophobicity and structure of PVDF membranes treated by vacuum-oxygen plasma and organofluorosilanisation

R. Jiménez-Robles^a, M. Izquierdo^a, V. Martínez-Soria^a, L. Martí^b, A. Monleón^{b,c}, J.D. Badia^{a*}

^a Research Group in Materials Technology and Sustainability (MATS), Department of Chemical Engineering, School of Engineering, University of Valencia, Avda. Universitat s/n, 46100 Burjassot, Spain.

^b Decarbonisation Department, Plastic Technology Institute (AIMPLAS), C/Gustave Eiffel 4, 46980 Paterna, Spain.

^c Department of Organic Chemistry, School of Chemistry, University of Valencia, Dr Moliner 50, 46100 Burjassot, Spain.

*e-mail: jose.badia@uv.es. Phone: +34 96 35 44319.

S1. Experimental system for the long-term stability tests

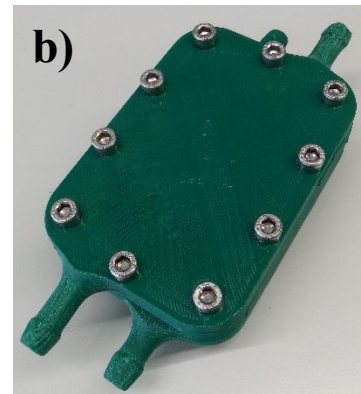
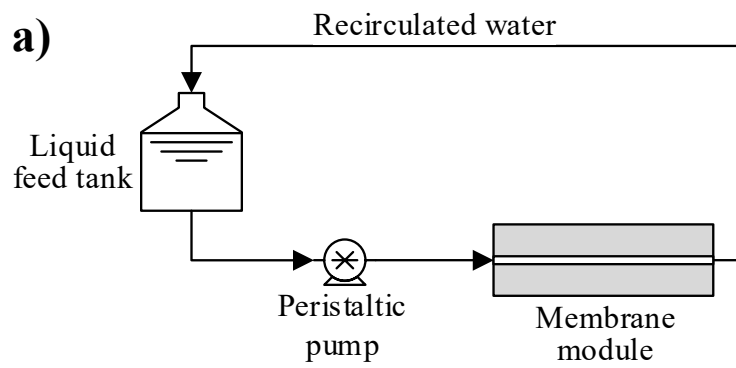


Figure S 1. a) Scheme of the experimental system for the long-term stability tests with a flat-sheet membrane module using distillate water and b) image of the 3-D printed flat-sheet module used in the tests.

S2. Infrared spectra of the pristine PVDF and modified membranes with oxygen plasma activation and functionalisation

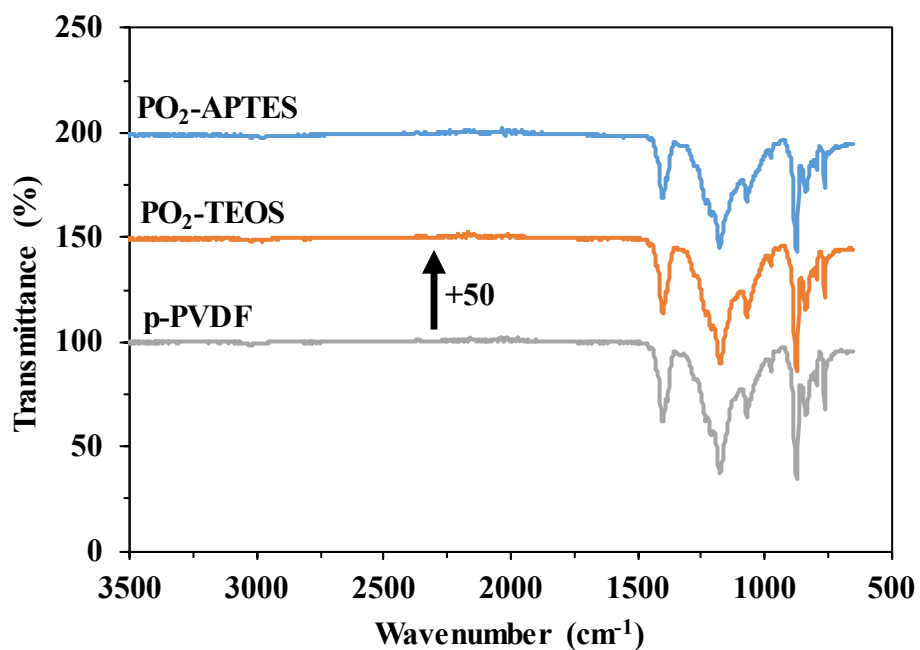


Figure S 2. Infrared spectra of the pristine PVDF (p-PVDF) and modified membranes with O₂ plasma activation at 15 W during 15 min and functionalised with FAS/TEOS (PO₂-TEOS) and FAS/APTES (PO₂-APTES) obtained from the Fourier transform-infrared (FTIR) spectrometer in the attenuated total reflectance (ATR) mode.

S3. FESEM images at low magnification of the cross section of the pristine, coated and plasma treated PVDF membranes before the stability tests

FESEM images of the whole cross section of the pristine, coated and plasma treated PVDF membranes before the long-term stability test are shown in Figure S 3 at a magnification of 500 – 600. FESEM images at a higher magnification of 2500 and focused on the surface are shown in the main paper (Figure 7).

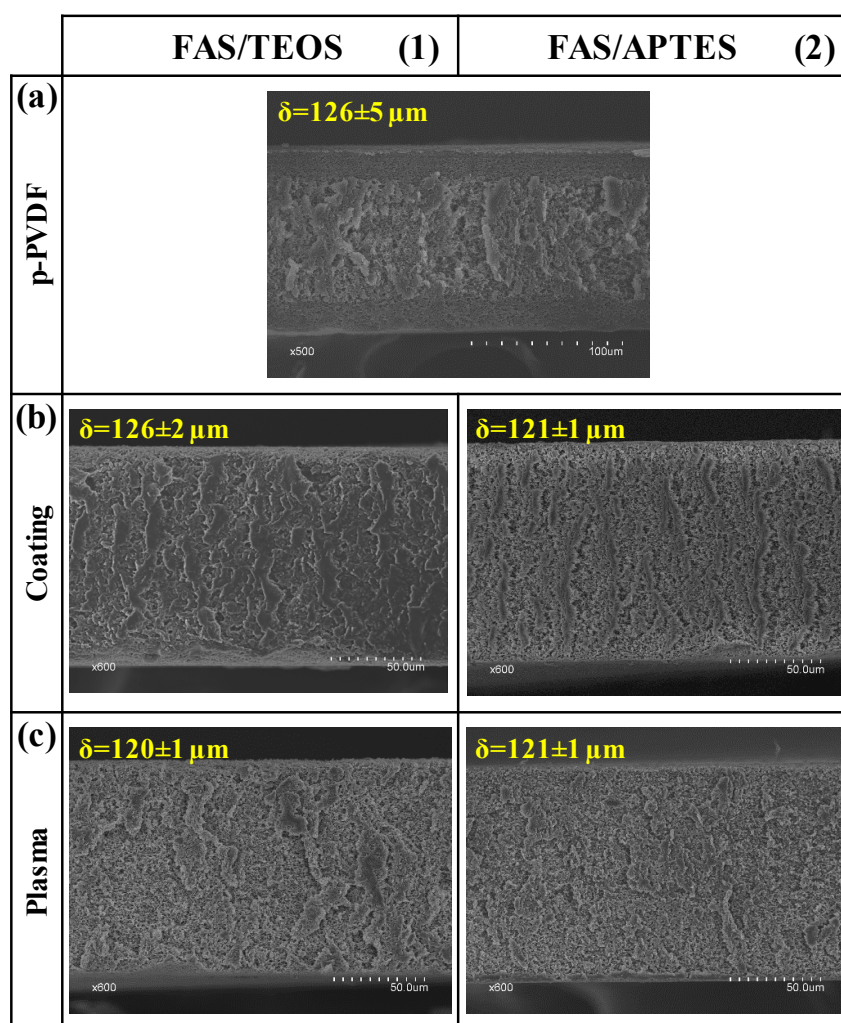


Figure S 3. FESEM images of the cross section of the (a) pristine PVDF (p-PVDF), (b) coated PVDF membranes with (1) FAS/TEOS and (2) FAS/APTES and (c) modified membranes with O_2 plasma activation at 15 W during 15 min and functionalised with FAS/TEOS and FAS/APTES.

APPENDIX V: CONTRIBUTION V.

The contribution entitled “*Simultaneous application of vacuum and sweep gas in a polypropylene membrane contactor for the recovery of dissolved methane from water*” is presented in this Appendix. This work corresponds with the main results and conclusions discussed in section 4.5. The details of the resulting paper are listed below:

Title	Simultaneous application of vacuum and sweep gas in a polypropylene membrane contactor for the recovery of dissolved methane from water
Authors	Ramón Jiménez-Robles, Carmen Gabaldón, Vicente Martínez-Soria, Marta Izquierdo
Affiliation	Research Group in Environmental Engineering (GI2AM), Department of Chemical Engineering, School of Engineering, University of Valencia, Avda. Universitat s/n, 46100 Burjassot, Spain.
Journal	Journal of Membrane Science
Volume	617
Issue	January 2021
Number	118560
DOI	10.1016/j.memsci.2020.118560
Cite	R. Jiménez-Robles, C. Gabaldón, V. Martínez-Soria, M. Izquierdo, Simultaneous application of vacuum and sweep gas in a polypropylene membrane contactor for the recovery of dissolved methane from water, <i>J Memb Sci.</i> 617 (2021) 118560. https://doi.org/10.1016/j.memsci.2020.118560

The Journal Impact Factor (JIF) in the in the year of publication was 10.53, and the JIF rank was 11/143 in the category of Chemical Engineering (Q1 quartile) and 4/90 in the category of Polymer Science (D1 first decile).



Simultaneous application of vacuum and sweep gas in a polypropylene membrane contactor for the recovery of dissolved methane from water

R. Jiménez-Robles, C. Gabaldón, V. Martínez-Soria, M. Izquierdo*

Research Group G²AM, Department of Chemical Engineering, University of Valencia, Avda. Universitat s/n, 46100, Burjassot, Spain

ARTICLE INFO

Keywords:

Combination mode operation
Methane degassing
Mass transfer
Energy analysis
Greenhouse gas emission

ABSTRACT

Vacuum and nitrogen as sweep gas were used simultaneously (combination mode) to generate the driving force in a microporous polypropylene membrane contactor for the recovery of dissolved methane from water. Experiments were carried out under different liquid flow-rates (5.0–28.0 L h⁻¹), N₂ flow-rates (0.5–1.5 L h⁻¹) and vacuum pressures (0–480 mbar). The maximum removal efficiency of methane was >90% at moderate values of gas-to-liquid ratios (G/L) and vacuum of 0.2 and ≤ 200 mbar, respectively. Removal efficiencies obtained in combination mode were usually higher than when using vacuum or sweep gas, separately. To achieve a methane content >35% in the recovered gas, G/L values lower than 0.03 are necessary, with removal efficiency up to 55%. Even at these soft conditions, gas phase mass transfer resistance was demonstrated as being negligible, so the limiting resistance was in the liquid phase. G/L ratios increased until values of 0.3, with a vacuum of 200 mbar, maximised the energy output (>250 kJ m⁻³ of treated water), in the case of recovered methane mixed with biogas produced in an anaerobic reactor. The results show that combination mode could be used to improve the performance of methane degassing in membrane contactors.

1. Introduction

Methane emissions have an important effect on the global atmospheric greenhouse gas (GHG) concentration, not least because its global-warming potential (GWP) is 28 times higher than carbon dioxide (100 years horizon) [1]. Additionally, in the presence of nitrogen oxides tropospheric methane oxidation leads to the formation of health-damaging tropospheric ozone. In this regard, methane concentrations have notably increased over the last decade, which can be mainly related to anthropogenic sources, about 50% greater than natural sources [2]. Indeed, methane emissions represent 10–15% of global GHG emissions [3] whose origins can be found in agriculture and livestock (49%), manufacture of fossil fuel (33%), solid urban waste (11%) and wastewater treatment (7%) in 2019 [4], with an average annual emission of 0.3 Gt [1].

In recent years, anaerobic wastewater treatment plants have received special attention due to the simultaneous production of biogas as the most attractive second-generation biofuel. Biogas can supply 13.5 MJ COD⁻¹ removed (1.5 kWh with 40% efficiency) [5], achieving a self-sufficient process [6], and a negative carbon footprint for an expanded granular sludge bed (EGSB) reactor has also been reported

[7]. Anaerobic treatment offers multiple advantages over aerobic processes: lower requirements of volume and nutrients, lower energy requirements (lack of aeration) and lower sludge production. On the contrary, the anaerobic effluent has high amounts of dissolved methane (D-CH₄), so once the effluent is discharged, fugitive emissions of methane take place, contributing to the most important source of GHG emissions in wastewater treatment plants [8]. These methane emissions involve the loss of a potential energy source, environmental problems and an explosive atmosphere if methane concentration is above the lower flammable limit (5%) in a confined space [9]. In this regard, the water discharged with a relatively low D-CH₄ concentration of 1.4 mg L⁻¹ can result in a CH₄ content in air of 5% at 15 °C and atmospheric pressure (estimated from Henry's Law [10]), when spontaneous degasification occurs in a confined space, such as closed vessels or sewers.

Estimates of D-CH₄ losses through anaerobic effluent can represent between 11% and 88% of the total methane produced in the anaerobic reactor for low strength wastes [6]. Some benefits of methane removal from the anaerobic effluent have been reported, for example better sedimentation of the anaerobic particles by means of dissolution of methane microbubbles [11] and higher COD removal efficiency by reducing the dissolved H₂ content in the liquid phase [12]. Recovered

* Corresponding author.

E-mail address: marta.izquierdo-sanchis@uv.es (M. Izquierdo).

<https://doi.org/10.1016/j.memsci.2020.118560>

Received 5 June 2020; Received in revised form 29 July 2020; Accepted 31 July 2020

Available online 11 August 2020

0376-7388/© 2020 Elsevier B.V. All rights reserved.

methane from the anaerobic effluents can also be a potential energy source, which could be directly stored with the biogas collected from the bioreactor.

Hollow fibre membrane contactors (HFMC) have emerged as a promising alternative for degasification of liquid streams where the transport of the gas molecules takes place through the membrane wall without contact or dispersion of one phase into the other. These HFMC are able to achieve high removal efficiencies of dissolved gases, with very compact units since they show high volumetric mass transfer coefficients. The HFMC avoids the flooding, foaming and emulsion problems commonly observed in direct contact units, such as packing columns and spray aerators [13–15], resulting in an easier and economically advantageous process. Membranes have been implemented extensively in recent years, due to the huge variety of available membrane contactors and their versatility for any application [16–20]. In this regard, the methane degassing in anaerobic liquid effluents with HFMC has received increasing research attention [6] and studies showing the viability of this technology operating in vacuum [7,11] or sweep gas mode [19,21,22] have recently been reported.

HFMC can operate in vacuum or sweep gas mode, in order to generate a partial pressure gradient of the solute as the driving force. On the one hand, when only vacuum is applied, high purity gas methane can be obtained whilst methane is diluted at sweep gas mode. On the other hand, vacuum mode shows the greatest energy consumption, even though the recovered gas methane can be directly used for thermal and electricity production without previous concentration [23]. As an alternative to overcome the drawbacks of each operation mode, vacuum and sweep gas can be used simultaneously.

In spite of the considerable amount of references to industrial applications of water degassing via combination vacuum and sweep gas processing with HFMC [24–26], mainly removing dissolved oxygen, only a few studies have reported results for this combination mode [27, 28]. In this regard, the work of Kartohardjono et al. [27] focused only on a mass transfer analysis, while the study of Martić et al. [28] was interested in the influence of the purity of nitrogen (as sweep gas) in the de-oxygenating of water, showing the effectiveness of HFMC in the operation (with removal efficiencies of approximately 99%), and estimating that the cost of the combination process with HFMC was significant lower (~50%) than conventional degassing processes. Taking into account this scarce information, it seems that studies on the combination mode are needed to enhance and deepen the knowledge of this technology, which could be especially suitable in cases of methane degassing applications.

Since there is no available data in the literature about membrane operation in combination mode for the degassing of methane from water, the main aim of this work was to evaluate the performance of a microporous polypropylene HFMC operating by means of both vacuum and sweep gas simultaneously for methane recovery. This represents the extension of our previous studies [29,30], where both modes were studied independently with the same HFMC. For this purpose, the methane removal performance from a synthetic water stream containing D-CH₄ under different operational and hydraulic conditions was analysed, by varying the liquid flow-rate, vacuum pressure and sweep gas flow-rate in short-term experiments. Also, the effect of the combination mode on the mass transfer and feasibility for energy production from the recovered methane stream has been determined.

2. Materials and methods

2.1. Experimental setup and procedure

A synthetic D-CH₄ water stream was used to carry out demethanization tests in this work. This stream was obtained from a packed-bed absorption column by using de-ionised water (<1 μS cm⁻¹) and 99.5%_v CH₄ (Carbueros Metálicos, Spain) flowing in counter-current. The column was built in methacrylate with an inner diameter of 6.5 cm, an

effective height of 50.0 cm and filled with polypropylene Pall Rings of 1" (Refilltech, Germany). The CH₄ flow-rate was fixed at 1000 mL min⁻¹ using a mass flow controller (Bronkhorst Hi-Tec, The Netherlands). With the absorption column system, the mean concentration of CH₄ in the liquid effluent was 21.65 ± 0.62 mg L⁻¹, similar to values reported by other authors [21,22,31,32]. This value represents the 95% saturation of CH₄ in water (22.81 mg L⁻¹ at 25 °C [10]). CH₄ oversaturation in the water did not take place, in contrast to what is observed in real anaerobic effluents, where oversaturation was frequently reported [6]. The total volume of the system was 1.5 L of water and the total operation time of each experiment was 1 h, until a steady-state condition was reached.

Synthetic D-CH₄ water column effluent was introduced to the HFMC. Fig. 1 shows the flowchart of the experimental system used to carry out the degassing tests and evaluate the membrane performance. Experiments were carried out at room temperature (23 °C ± 3 °C). Synthetic water was used in this study in order to prevent the potential interference of suspended or soluble compounds in the performance of the system. Long-term performance of the same PP membrane contactor treating the anaerobic effluent of an EGSB reactor was reported in a previous work [30].

In our experimental setup, water operated in a closed loop. Thus, water was recirculated in the system by using a peristaltic pump (Watson-Marlow, EE.UU.), with liquid flow-rates (Q_L, L h⁻¹) ranging from 5.0 to 28.0 L h⁻¹.

In a typical test, the system was run without the operation of the HFMC (gas ports were closed) in an initial pre-start period, to ensure that the effluent from the column reached a stable value near saturation. After this, membrane gas ports were opened and the N₂ mass flow controller and the vacuum system were simultaneously switched on. The desired N₂ flow-rate and vacuum pressure stabilized in less than 1 min and the degassing process started. As an example, in Fig. 2 a typical pattern of the liquid and gas outlet methane concentrations in HFMC is shown. As can be seen, stable behaviour was observed after 20–30 min of HFMC operation. The results presented in this work were those obtained when this steady state performance was reached.

In HFMC, duplicate liquid samples were collected at the inlet and outlet ports and gas samples were taken from the outlet gas port, which contained the recovered methane (R-CH₄). All samples were collected without the samples being exposed to the atmosphere.

The liquid samples were analysed by using the head-space method described previously [7,11,29]. Briefly, 50 mL of liquid samples were collected and injected in sealed vials of 125 mL, prefilled with air. These vials were kept in an orbital shaker at 150 rpm and 25 °C for 1.5 h (to ensure gas-liquid equilibrium). After this, 0.5 mL of the head-space gas was injected into a gas chromatograph (Agilent GC 7820A, Spain) equipped with Agilent HP-PLOT/U and Agilent HP-MOLESIEVE and a thermal conductivity detector. In order to determine the methane concentration in the liquid sample, it was necessary to apply Henry's Law:

$$H^{\text{cp}} = \frac{C_{\text{L,eq}}}{P^{\text{p,eq}} \cdot M_{\text{CH}_4}} \quad (1)$$

where $C_{\text{L,eq}}$ (mg L⁻¹ ≡ g m⁻³) is the methane concentration in the liquid in equilibrium with the head-space gas, $P^{\text{p,eq}}$ (Pa) is the partial pressure of the CH₄ in the head-space in equilibrium with the liquid phase, M_{CH_4} is the molecular weight of the CH₄ (16 g mol⁻¹) and H^{cp} is the Henry's Law constant, expressed in mol m⁻³ Pa⁻¹. The value of H^{cp} is 1.4 · 10⁻⁵ mol m⁻³ Pa⁻¹ at 25 °C [10]. So, the methane concentration in the original liquid sample was determined from:

$$C_{\text{L}} = \frac{C_{\text{G,eq}} \cdot V_{\text{G}} + C_{\text{L,eq}} \cdot V_{\text{L}}}{V_{\text{L}}} \quad (2)$$

where C_{L} and $C_{\text{G,eq}}$ (mg L⁻¹) is the methane concentration in the original sample and in the head-space of the analysis vials, respectively, and V_{G} and V_{L} (L) is the gas and liquid volume inside the analysis vials,

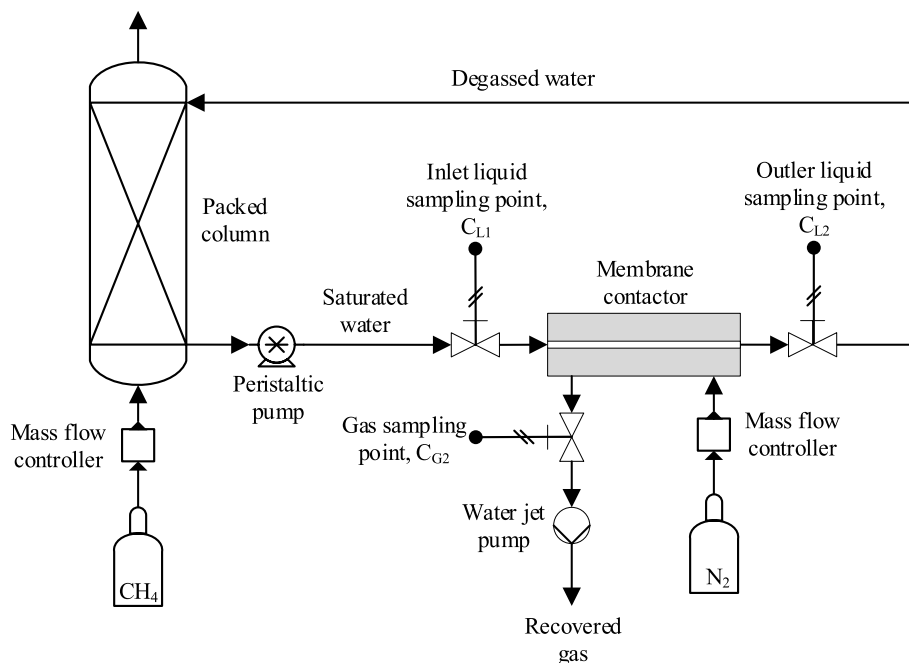


Fig. 1. Flowchart of the degassing system, including the packed column for the saturation, sweep gas and vacuum generation equipment, sampling points and the hollow fibre membrane contactor.

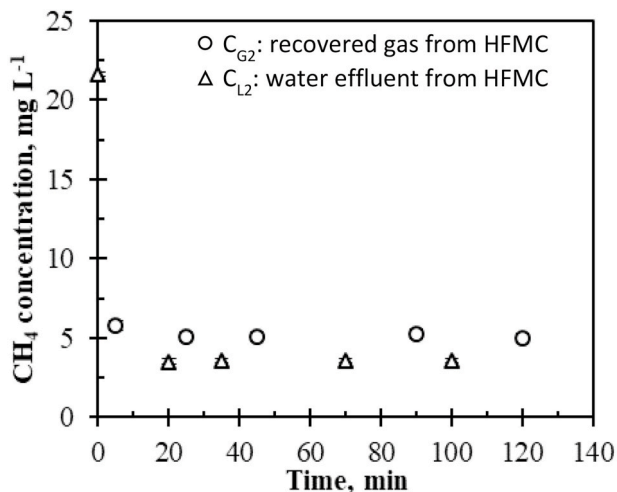


Fig. 2. Pattern of the concentration of methane at the liquid (C_{L2}) and gas (C_{G2}) outlet of the hollow fibre membrane contactor (HFMC) in a typical test. Operational conditions: sweep gas mode, $Q_{N_2} = 26.0 \text{ L h}^{-1}$ and $Q_L = 13.7 \text{ L h}^{-1}$.

respectively.

The performance of the CH_4 recovery process was evaluated through the removal efficiency of methane (RE, %) which is defined as:

$$RE = \frac{C_{L1} - C_{L2}}{C_{L1}} \cdot 100 \quad (3)$$

where C_{L1} and C_{L2} (mg L^{-1}) is the methane concentration in the inlet and outlet liquid from the HFMC, respectively. In Eq. (3) a negligible variation of the liquid volume flow-rate was assumed.

A sampling point was used to take 0.5 mL of HFMC outlet gas samples, by means of a gas chromatography syringe, which were injected into the former gas chromatograph. Moisture content of the recovered gas was measured using a hygrometer model HygroPalm-HP21, (Rotronic Instruments, Switzerland). The moisture of the recovered gas was close to saturation point in the whole range of sweep-gas flow

rate tested ($0.5\text{--}1.5 \text{ L h}^{-1}$), with a value of relative humidity $>90\%$, which correspond to a H_2O content close to 3% at standard conditions.

To verify the absence of membrane fouling or malfunction, a control test was carried out weekly. A mean deviation of 0.83% was obtained, confirming that the HFMC maintained its performance during this study.

2.2. Degassing membrane contactor

A commercial polypropylene (PP) hollow fibre membrane contactor (1×5.5 MiniModule, Liqui-Cel, Membrane GmbH, Germany) with a microporous and hydrophobic structure was selected to develop this study. The main features of the membrane are summarised in Table 1. This HFMC was considered to be representative of the membranes in real industrial applications and it has been used in previous studies [29,30].

The HFMC was operated in lumen side mode, where experiments were carried out with the liquid flowing in the lumen side and vacuum or sweep gas applied in the shell side, and in counter-current flow. Liquid flow-rate (Q_L) was varied between 5.0 and 28.0 L h^{-1} , with a pressure drop ranging from 40 to 60 mbar. N_2 (99.9%, Carbusos Metálicos, Spain) was used as sweep gas, with a flow-rate (Q_{N_2}) ranging from 0.5 to 1.5 L h^{-1} adjusted by means of a mass flow controller

Table 1
Characteristics of the PP membrane contactor (provided by the manufacturer).

Property	Value
Structure	Microporous
Shell tube inner diameter, m	0.025
Module length, m	0.176
Number of fibres	2300
Effective length (L), m	0.1132
Inner diameter (d_i), μm	220
Outer diameter (d_o), μm	300
Effective internal area (A_i), m^2	0.180
Effective external area (A_e), m^2	0.245
Pore diameter, μm	0.04
Porosity	0.4
Tortuosity	1.4
Packing fraction	0.33
Maximum liquid flow-rate (Q_L), L h^{-1}	30
Maximum sweep gas flow-rate (Q_{N_2}), L h^{-1}	800

(Bronkhorst Hi-Tec, The Netherlands). Under these operational conditions, the gas-to-liquid ratio (G/L) varied from 0.012 to 0.302. Vacuum was generated by using a water jet pump (VWR, Spain). The applied vacuum pressure (P_{vac}) ranged from 0 to 480 mbar (manometric pressure was from 0 to -480 mbar) and it was measured with a digital manometer (Kimo MP112, Kimo Instruments, France) at the inlet and outlet of the membrane contactor to ensure stable vacuum along the module.

2.3. Mass transfer evaluation

The mass transfer of the separation process was evaluated in the liquid-membrane-gas system. For this purpose, the overall experimental mass transfer coefficient ($K_{L,exp}$, $m\ s^{-1}$) was calculated from the following differential mass balance applied to the liquid phase [33]:

$$Q_l \cdot \frac{dC}{dA} = -K_L \cdot (\Delta C_{lm}) \quad (4)$$

The integration resulting from Eq. (4) is as follows [34]:

$$K_{L,exp} = \frac{Q_l}{A_L} \frac{C_{L2} - C_{L1}}{\Delta C_{lm}} \quad (5)$$

ΔC_{lm} is defined as [34]:

$$\Delta C_{lm} = \frac{(C_{L2}^* - C_{L2}) - (C_{L1}^* - C_{L1})}{\ln\left(\frac{C_{L2}^* - C_{L2}}{C_{L1}^* - C_{L1}}\right)} \quad (6)$$

where A_L (m^2) is the interfacial area in contact with the liquid phase, Q_l ($m^3\ s^{-1}$) is the liquid flow-rate and C_{L1}^* and C_{L2}^* ($mg\ L^{-1}$) are the methane concentration in the liquid in equilibrium with the methane content in the outlet gas (C_{G2} , $mg\ L^{-1}$) and inlet gas ($C_{G1} = 0\ mg\ L^{-1}$), respectively, calculated from Henry's Law ($C_L^* = C_G/H$, H being the dimensionless Henry's constant; a value of 29.55 at 25 °C [10]). With the liquid flowing in lumen side mode, A_L is the membrane's internal area (A_i). The mass transfer can also be evaluated through the overall experimental mass transfer resistance ($R_{ov,exp}$, $s\ m^{-3}$):

$$R_{ov,exp} = \frac{1}{K_{L,exp} \cdot A_L} \quad (7)$$

The overall resistance for a hydrophobic, microporous membrane with gas filled pores consists of three resistances in series: the liquid phase boundary layer ($R_{L,est}$), the membrane ($R_{m,est}$), and the gaseous phase boundary layer ($R_{G,est}$). The estimated overall mass transfer resistance ($R_{ov,est}$) can be obtained by adding the partial resistances in series. Thus, in a cylindrical geometry like in the HFMC, the overall resistance can be described by means of the equation:

$$R_{ov,est} = R_{L,est} + R_{m,est} + R_{G,est} = \frac{1}{k_L \cdot A_L} + \frac{1}{H \cdot k_m \cdot A_{ml}} + \frac{1}{H \cdot k_G \cdot A_G} = \frac{1}{K_{L,est} \cdot A_L} \quad (8)$$

where k_G , k_m and k_L ($m\ s^{-1}$) stand for the individual mass transfer coefficients in the gas, membrane and liquid, respectively, $K_{L,est}$ ($m\ s^{-1}$) is the estimated overall mass transfer coefficient, A_G and A_L (m^2) are the membrane surfaces in contact with gas and liquid, respectively, and A_{ml} (m^2) is the logarithmic mean membrane surface.

The k_L value can be estimated from the Lévêque equation [35] with the liquid flowing in the lumen side:

$$k_L = 1.62 \cdot \frac{D_{L,CH_4}}{d_i} \cdot \left(\frac{d_i^2 \cdot v_L}{D_{L,CH_4} \cdot L}\right)^{1/3} \quad (9)$$

where v_L ($m\ s^{-1}$) is the liquid velocity and D_{L,CH_4} ($m^2\ s^{-1}$) is the diffusion coefficient of methane in water ($1.76 \cdot 10^{-9}\ m^2\ s^{-1}$ at 25 °C and 1 bar [36]). Eq. (9) is adequate for the Graetz Number (Gz) > 4.

For the gas phase, k_G is estimated for a stripping process with a shell

side and parallel flow of the gas [37]:

$$k_G = 1.25 \cdot \left(\frac{\mu_G}{D_{G,CH_4} \cdot \rho_G}\right)^{0.33} \cdot \left(Re_G \frac{d_e}{L}\right)^{0.93} \quad (10)$$

where D_{G,CH_4} ($m^2\ s^{-1}$) is the diffusion coefficient of methane through the gas (nitrogen and water vapour mixture), ρ_G ($kg\ m^{-3}$) is the gas density, μ_G ($kg\ m^{-1}\ s^{-1}$) is the gas viscosity, Re_G is the Reynold number in the gas phase and d_e (m) is the equivalent diameter.

The value of k_m can be estimated by mean of the equation based on the diffusion of the solutes through the pores without convection [38]:

$$k_m = \frac{D_{G,eff} \cdot \epsilon}{\tau \cdot l} \quad (11)$$

where ϵ , τ and l (m) is the porosity, tortuosity and thickness of the membrane, respectively, and $D_{G,eff}$ ($m^2\ s^{-1}$) is the effective diffusion of the transferred species in the gas phase inside the pores and can be estimated as follows [39]:

$$\frac{1}{D_{G,eff}} = \frac{1}{D_{G,CH_4}} + \frac{1}{D_{G,Kn}} \quad (12)$$

where $D_{G,Kn}$ ($m^2\ s^{-1}$) is the Knudsen diffusion coefficient of CH_4 through the pores.

D_{G,CH_4} was calculated by Eq. (13)–(15) [40,41]:

$$D_{G,CH_4} = \frac{1}{\sum_i \frac{y_i}{D_{CH_4-i}}} \quad (13)$$

$$y_i = \frac{y_i}{1 - y_{CH_4}} \quad (14)$$

$$D_{CH_4-i} = \frac{0.01013 \cdot T^{1.75} \cdot \left(\frac{1}{M_i} + \frac{1}{M_{CH_4}}\right)^{1/2}}{P \cdot \left[\left(\sum v_i\right)^{1/3} + \left(\sum v_{CH_4}\right)^{1/3}\right]^2} \quad (15)$$

where i correspond to N_2 or H_2O molecules, y_i is the mole fraction of specie i evaluated on CH_4 -free basis, D_{CH_4-i} is the binary diffusion coefficient of CH_4 through specie i , T (K) is the temperature, M is the molecular weight, P (Pa) is the pressure in the gas phase and $(\sum v)$ is the special atomic diffusion volume (17.90 for N_2 , 12.70 for H_2O and 24.42 for CH_4).

$D_{G,Kn}$ was calculated by Eq. (16) [42]:

$$D_{G,Kn} = 97 \cdot r_p \cdot \left(\frac{T}{M_{CH_4}}\right)^{1/2} \quad (16)$$

where r_p (m) is the pore radius.

Finally, $K_{L,est}$ can be calculated as follows [33]:

$$\frac{1}{K_{L,est}} = \frac{1}{k_L} + \frac{d_i}{H \cdot k_m \cdot d_{lm}} + \frac{d_i}{H \cdot k_G \cdot d_o} \quad (17)$$

where d_{lm} (m) is the logarithmic mean fibre diameter.

3. Results and discussion

3.1. Influence of operational parameters: vacuum pressure and flow-rates of liquid and sweep gas

Experiments with liquid flow-rates (Q_l) of 5.0, 13.7, 21.0 and 28.0 $L\ h^{-1}$ and with nitrogen sweep gas flow-rates (Q_{N_2}) of 0.5, 1.0 and 1.5 $L\ h^{-1}$ were performed at sweep gas mode ($P_{vac} = 0$) and combination mode with vacuum pressures of 100, 200, 400 and 480 mbar. The influence of these parameters on the dissolved methane removal efficiency (RE) and on the content of methane in the recovered gas (C- CH_4) is discussed in this section.

As expected, the removal efficiency decreased with the increase in Q_L in combination mode for all the N_2 flow-rates and vacuum pressures. As an example, the results obtained with a N_2 flow-rate of 0.5 L h^{-1} are shown in Fig. 3a. This trend can be explained by taking into account the lower residence time for CH_4 inside the fibres [7,11], even though the mass transfer is improved at higher liquid velocities. Operating with a N_2 flow-rate of 0.5 L h^{-1} , the RE decreased from values of around 85–89% (for the lowest Q_L of 5.0 L h^{-1}) up to values in the range of 39–51% (for the highest Q_L of 28.0 L h^{-1}).

The C- CH_4 in the recovered gas was higher with increasing Q_L , for all the Q_{N_2} tested, and the increase of C- CH_4 was more pronounced at low Q_L . For instance, Fig. 3b shows data for a Q_{N_2} of 0.5 L h^{-1} and C- CH_4 values increased from 17 to 21% (for Q_L of 5.0 L h^{-1}) to values of 30–38% (for Q_L of 13.7 L h^{-1}). For liquid flow-rates higher than 13.7 L h^{-1} , C- CH_4 was always greater than 35% for all of the P_{vac} tested.

Experiments with the highest N_2 flow-rates tested (1.0 and 1.5 L h^{-1}) showed the same trends as for a N_2 flow-rate of 0.5 L h^{-1} , although with higher values of RE and lower values of C- CH_4 , as discussed below.

In spite of RE decreasing with the Q_L , the estimated total mass flow of recovered methane (R- CH_4) was higher, in agreement with the increase in the C- CH_4 . For example, at P_{vac} of 200 mbar and Q_{N_2} of 0.5 L h^{-1} , the estimated mass flow of R- CH_4 ranged from 78 to 201 $\text{mg CH}_4 \text{ h}^{-1}$ for Q_L of 5.0 and 28.0 L h^{-1} , respectively (Fig. S1 as supplementary material).

The effect of P_{vac} on RE is shown at different Q_L and a constant N_2 flow-rate of 0.5 L h^{-1} in Fig. 3c. The results show that RE continuously increased with P_{vac} as a consequence of greater driving forces. For example, RE varied from 39% to 51% at P_{vac} of 0 and 480 mbar, respectively, for Q_L of 28.0 L h^{-1} . Other authors reported the same trend [7,19,43,44]. The highest increment of RE was generally observed from 0 to 200 mbar of vacuum and, in contrast, results obtained at 400 and 480 mbar were quite similar. These results show that in combination mode, greater REs can be obtained than in sweep gas mode (P_{vac} of 0 mbar). At the lowest liquid flow-rate tested (5.0 L h^{-1}), RE increase with the vacuum was the lowest (from 85% to 89% when the vacuum varied

from 0 to 480 mbar), so no substantial enhancement under combination mode operation was observed. Increase in RE was more significant when the tested liquid flow-rate increased.

For Q_{N_2} higher than 0.5 L h^{-1} (Fig. S2 as supplementary material), the effect of P_{vac} on RE was negligible. For example, at a Q_{N_2} of 1.0 L h^{-1} , RE was kept constant at values around 90%, 67% and 56% at Q_L of 5.0, 13.7 and 21.0 L h^{-1} , respectively, for any value of P_{vac} . For a Q_{N_2} of 1.5 L h^{-1} , the same trend with P_{vac} was observed.

In Fig. 3d, the general trend of the experimental C- CH_4 in the recovered gas showed a slightly decreased with the vacuum pressure at Q_{N_2} of 0.5 L h^{-1} . This fact can mainly be attributed to the increase of water vapour in the gas phase when the vacuum rises. Typically, membranes used in this kind of application, both microporous and dense membranes, are permeable for water vapour and create a vapour flux through the membrane in the same way as CH_4 [44]. Also, other dissolved compounds, such as O_2 and CO_2 , are degassed from the liquid stream and, consequently, involve the dilution of CH_4 in the recovered gas. The results suggest that the composition and hydrophobic character of the membrane play a critical role in bringing down the permeability of water vapour [45–47].

Regarding the effect of sweep gas flow-rate, the RE increased with the Q_{N_2} for all the liquid flow-rates and vacuum conditions. Results obtained at 200 mbar and for different Q_L are presented in Fig. 4a. The increase in RE was more significant at low Q_{N_2} . So, at P_{vac} of 200 mbar, the RE clearly increased when Q_{N_2} rose from 0.5 to 1.0 L h^{-1} but RE remained almost constant when Q_{N_2} rose from 1.0 to 1.5 L h^{-1} for any liquid flow-rate.

C- CH_4 in the recovered gas clearly decreases with Q_{N_2} (Fig. 4b), showing a remarkable dilution effect of the sweep gas. This behaviour was expected, considering the slight effect of sweep gas flow-rate on the RE, especially for Q_{N_2} higher than 1.0 L h^{-1} . Calculated dilution factors, when doubling the Q_{N_2} , were equal to or lower than 1.5. As can be seen in Fig. 4b, to obtain C- CH_4 values higher than 35%, Q_{N_2} lower than or equal to 0.5 L h^{-1} and Q_L higher than 13.7 L h^{-1} were needed, which

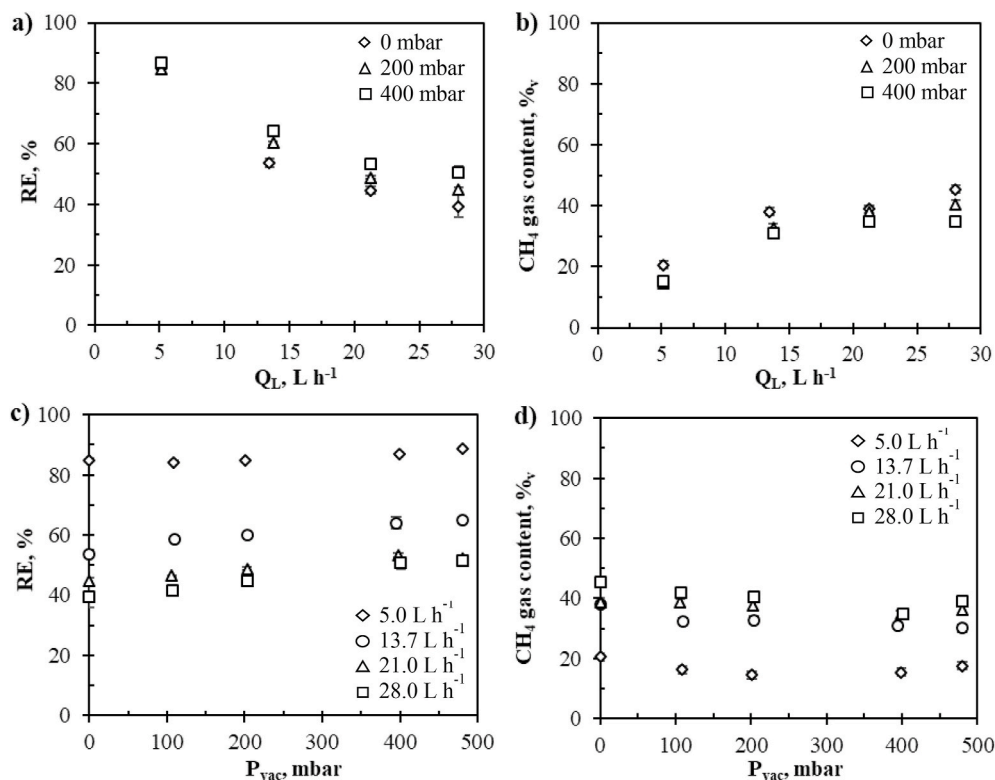


Fig. 3. Effect of liquid flow-rate and vacuum pressure on CH_4 removal efficiency (RE), a) and c), and on the content of CH_4 in the recovered gas, b) and d), at constant sweep gas flow-rate, $Q_{N_2} = 0.5 \text{ L h}^{-1}$.

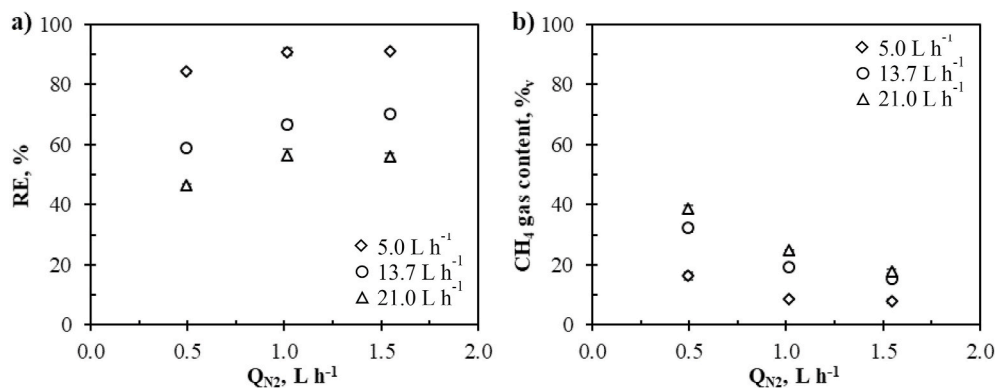


Fig. 4. a) Dissolved CH₄ removal efficiency (RE) and b) content of CH₄ in the recovered gas from the membrane contactor versus sweep gas flow-rate for the combination mode operation at constant vacuum pressure, $P_{vac} = 200$ mbar.

corresponds to RE ranging from 39% to 53% (Fig. 3a). For higher Q_{N_2} values (1.0 and 1.5 L h⁻¹), C-CH₄ in the recovered gas remained below 35% for all of the liquid flow-rates and vacuum pressures. Despite the low C-CH₄ in the recovered gas at high Q_{N_2} , this gas stream could be mixed with the main biogas stream from an anaerobic process, maintaining high levels of C-CH₄.

Comparison of these results with those obtained in our previous work [30], carried out with exactly the same HFMC under similar operational conditions in vacuum mode operation, is shown in Table 2. Similar RE values can be obtained with a combination of low vacuum and sweep gas flow-rate, rather than using only a high vacuum at any Q_L values. For example, at Q_L of 5.0 L h⁻¹, RE was 84% in combination mode (with P_{vac} of 100 mbar and Q_{N_2} of 0.5 L h⁻¹) whilst a P_{vac} of 500 mbar was necessary to obtain a similar RE (82%) when only using vacuum at Q_L of 4.1 L h⁻¹. For low vacuum values (100–140 mbar), the application of a simultaneous low Q_{N_2} of 0.5 L h⁻¹ increased RE from 69% to 84% and from 32% to 42%, for low and high Q_L , respectively. These results demonstrate the potential enhancement of the driving force caused by the additive effect of the combination of vacuum and sweep gas.

The highest REs obtained in this work (~90%) were achieved for the minimum Q_L (5.0 L h⁻¹), and values of P_{vac} and Q_{N_2} higher than 100 mbar and 0.5 L h⁻¹, respectively. However, the increase of these parameter values from P_{vac} 200 mbar or Q_{N_2} 1.0 L h⁻¹ did not improve the efficiency of the process, significantly. This shows that, from a practical point of view, a combination of intermediate values of P_{vac} and Q_{N_2} would be the most suitable operational conditions.

Similar RE values (~90%) have been previously reported for sweep gas or vacuum operations with porous and dense membrane contactors [7,19,21,22]. As an example, Cookney et al. [22] obtained maximum RE values of 93% and 99% for a PDMS (dense) and PP (microporous) HFMC, respectively, operating in sweep gas mode with v_L of 0.04 cm s⁻¹ (Q_L calculated as 0.2 and 0.4 L h⁻¹, respectively) and v_G of 33.00 and 19.00 cm s⁻¹ (Q_{N_2} calculated as 330.0 and 610.0 L h⁻¹, respectively). In general, the highest RE values have been reported in sweep gas operations and these values of RE can only be obtained with high vacuum values (800–950 mbar) [11,14,30,43]. For instance, Bandara et al. [11] obtained a maximum RE of 86% in vacuum mode with P_{vac} of 800 mbar

Table 2

Comparison of methane removal efficiency obtained in vacuum (Henares et al. [30]) and combination mode (this work).

Q_L , L h ⁻¹	Q_{N_2} , L h ⁻¹	P_{vac} , mbar	RE, %	Reference
4.1	–	500	82	[30]
27.2	–	500	45	[30]
4.1	–	140	69	[30]
27.2	–	140	32	[30]
5.0	0.5	100	84	This work
28.0	0.5	100	42	This work

and Q_L of 0.1 L h⁻¹ (v_L of 0.02 cm s⁻¹) and a composite, dense membrane.

3.2. Gas-to-liquid ratio analysis

Gas-to-liquid ratio (G/L) is defined as follows (with flow-rates measured at atmospheric pressure):

$$G/L = \frac{Q_{N_2}}{Q_L} \quad (18)$$

Increasing G/L involves a higher driving force and, consequently, major RE are obtained (Fig. 5a). At the lowest Q_{N_2} value of 0.5 L h⁻¹ (open symbols) a significant increase in RE was observed when P_{vac} was increased for the same G/L ratio. For example, at a G/L ratio of 0.037, RE values of 60% and 65% were obtained for P_{vac} of 200 and 400 mbar, respectively. In contrast, for a higher Q_{N_2} of 1.0 L h⁻¹ (filled grey symbols) and G/L of 0.048, the results showed similar REs independent of P_{vac} for all Q_L tested. Thus, the application of vacuum improved removal performance when using 0.5 L h⁻¹ at all G/L ratios but, at higher Q_{N_2} , the application of vacuum did not significantly increase RE, in agreement with previous findings.

In the case of C-CH₄ (Fig. 5b), a notable effect of G/L was observed, especially at low G/L (<0.050). The maximum C-CH₄ obtained was 45% for the minimum G/L tested (0.012) and without vacuum in the gas line. Generally, no notable effect of P_{vac} in the final C-CH₄ was observed for any G/L tested. The decrease of the C-CH₄ with G/L followed a power regression equation, indicating the high sensitivity of the C-CH₄ in the recovered gas at low values of G/L, especially between 0.010 and 0.050.

According to the results, the maximum G/L which allows us to obtain C-CH₄ values higher than 35%, in order to efficiently produce electricity from the recovered gas, was 0.030 with REs between 50% and 55%. From a theoretical point of view and taking into account Henry's Law, for a G/L of 0.030, a maximum RE value of ~90% could be obtained [21]. As in our case, reported experimental RE values are often far from this maximum theoretical value [21,22,48].

A compromise between the final C-CH₄ and RE achieved should be required for a proper optimisation of the process, from an energetic point of view. In this regard, the use of several membranes coupled in series has been proposed as an alternative to achieve higher overall REs for the lowest G/L [22,28,49]. For example, Martić et al. [28] used three HFMC, coupled in series in combination mode for O₂ removal at a G/L of 0.3 and P_{vac} of 200 mbar; an overall RE value of ~99% was reported.

3.3. Mass transfer analysis

The obtained results seem to point to the fact that the mass transfer resistance of the gas phase was usually negligible, since the dependence of RE on P_{vac} and on sweep gas flow-rate was relatively low, especially at

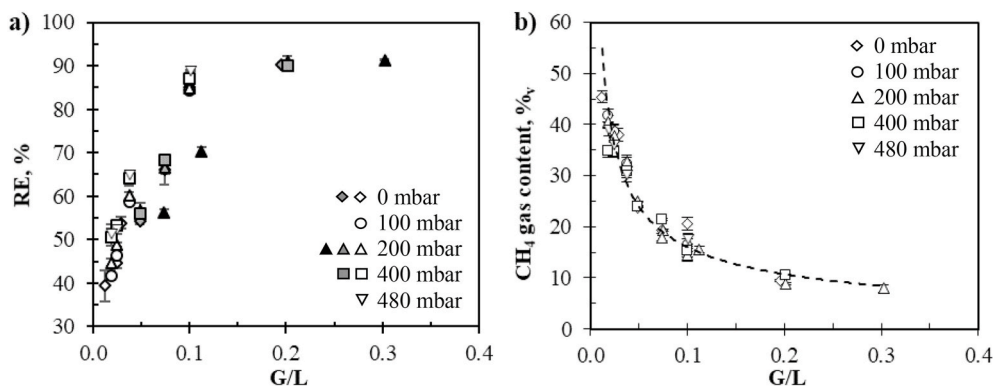


Fig. 5. a) Dissolved CH₄ removal efficiency (RE) with $Q_{N_2} = 0.5 \text{ L h}^{-1}$ (open symbols), $Q_{N_2} = 1.0 \text{ L h}^{-1}$ (filled grey symbols) and $Q_{N_2} = 1.5 \text{ L h}^{-1}$ (filled black symbols) and b) content of CH₄ in the recovered gas from the membrane contactor versus gas-to-liquid ratio (G/L) for the combination mode operation at different vacuum pressures.

the highest vacuum and flow-rate (Fig. 4a). This suggests that, under these conditions, the limiting mass transfer resistance is mainly located in the liquid phase.

This fact is in agreement with the theoretical estimation of the three individual mass transfer resistances, obtained from Eq. (9)–(17). In this regard, $R_{L,est}$ values range from $1.7 \cdot 10^5 \text{ s m}^{-3}$ to $2.9 \cdot 10^5 \text{ s m}^{-3}$ for the studied conditions, which represents at least 98.74% of the overall estimated resistance ($R_{ov,est}$). R_m and R_G were always below 0.01% and 1.0%, respectively, which is similar to those obtained by Rongwong et al. [19] for a porous polyimide membrane. Membrane mass transfer resistance has been also estimated using the Wilson plot method (Supplementary material S3) with similar results. Therefore, the estimated values of $R_{m,est}$ and $R_{G,est}$ are negligible compared with $R_{L,est}$ and, consequently, it can be assumed that $R_{ov,est} \approx R_{L,est}$. These results are in agreement with most previous studies of methane degassing [7,14,19,22,44–46], where the theoretical resistance to mass transfer was mainly located in the liquid phase.

Estimated ($R_{ov,est}$) and experimental ($R_{ov,exp}$) overall mass transfer resistance results are compared and shown in Fig. 6a. At the lowest Q_{N_2} studied, $R_{ov,exp}$ ranged from $3.37 \cdot 10^5 \text{ s m}^{-3}$, for Q_L of 5.0 L h^{-1} and P_{vac} of 200 mbar, to $1.18 \cdot 10^5 \text{ s m}^{-3}$, for Q_L of 28.0 L h^{-1} and P_{vac} of 0 mbar, with a significant influence of the liquid flow-rate and an almost negligible impact of the vacuum pressure. No noticeable difference in the mass transfer resistance was observed between the combination and sweep gas modes (P_{vac} of 0 mbar). Similar values and trends were obtained for the higher Q_{N_2} studied (Fig. 6b). It is important to point out that most of the experimental values were slightly higher than the estimated values (Fig. 6a), especially at low liquid flow-rates for the lowest Q_{N_2} studied (Fig. 6b). These results seem to indicate that gas

phase resistance could be underestimated for the lowest Q_{N_2} studied.

Comparing the results from this work in combination mode with those previously obtained operating in vacuum mode [30], lower $R_{ov,exp}$ was usually obtained in combination mode than in vacuum mode, mainly due to the absence of wetting (membrane pores totally or partially filled with liquid phase). Wetting phenomenon involves an additional resistance located in the membrane phase with an increase of the pressure into the lumen side being in agreement with the rise of the liquid flow-rate. In combination mode, the wetting phenomenon was not observed, at least not in the range of the values tested, in contrast to when vacuum mode was operated under similar conditions [30]. It seems that the presence of sweep gas involves an additional effect on the membrane surface, avoiding the overcoming of the critical transmembrane pressure [29,45,50].

In Table 3, our $K_{L,exp}$ can be compared with that reported in previous studies carried out with different microporous HFMC, operated in sweep gas mode and on the lumen side. No significant differences were observed for $K_{L,exp}$ between the different experiments for polypropylene HFMCs and similar liquid velocities. No significant effects of the gas velocity were observed on $K_{L,exp}$, which is in agreement with the negligible resistance of the gas phase. The greater reported values of $K_{L,exp}$ for the polyamide HFMC (66% of porosity), rather than for the PP HFMC (around 40% of porosity), seem to indicate an important role of the membrane properties, especially its porosity. In this case, greater $K_{L,exp}$ values were observed with a higher porosity.

From the scarcity of papers found in the literature, regarding combination mode, Kartohardjono's work can be highlighted. For removal of O₂, Kartohardjono et al. [27] obtained $K_{L,exp}$ values ranging from $10 \cdot 10^{-5} \text{ m s}^{-1}$ to $35 \cdot 10^{-5} \text{ m s}^{-1}$ at liquid velocities varying between 35

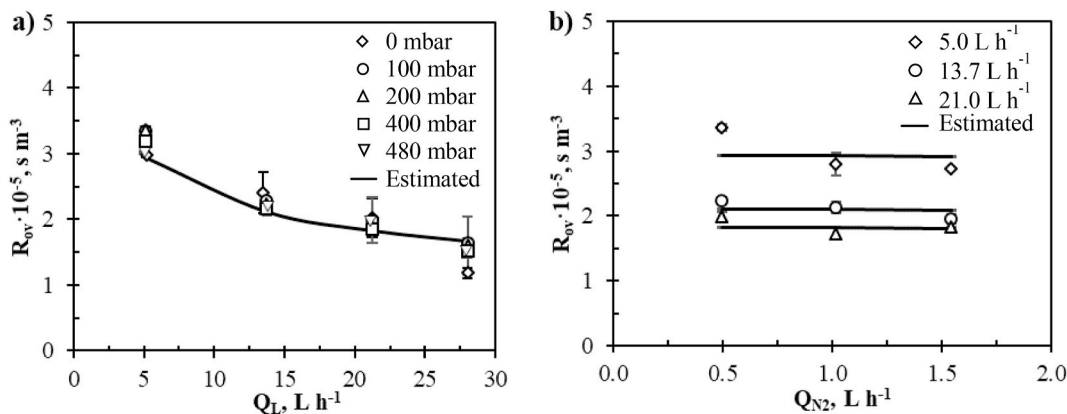


Fig. 6. Comparison of the experimental (open symbols) and estimated (black line) overall mass transfer resistance (R_{ov}) versus a) liquid flow-rate at $Q_{N_2} = 0.5 \text{ L h}^{-1}$ and different vacuum pressures and b) sweep gas flow-rate at $P_{vac} = 200 \text{ mbar}$ and different liquid flow-rates.

Table 3

Summary of overall mass transfer coefficients from different authors for methane recovery from liquid effluents operating in sweep gas mode and lumen side with microporous degassing membranes. Combination mode with P_{vac} ranging from 0 to 480 mbar in this work.

Effluent	Membrane	v_L , cm s ⁻¹ (Q_L , L h ⁻¹)	v_G , cm s ⁻¹ (Q_{N2} , L h ⁻¹)	$K_L \cdot 10^5$, m s ⁻¹	Reference
Saturated water	PP	1.59–8.90 (5.0–28.0)	0.04–0.13 (0.5–1.5)	1.65–3.67	This work
EGBS	PP	1.27–8.58 (4.1–27.0)	2.20–67.69 (26–800)	1.94–3.74	[30]
Saturated water	PP	1.20–4.50 (12.2–45.6)	18.61 (600)	1.56–2.14	[22]
Saturated water	PP	11.84 (120)	1.86–18.61 (60–600)	1.20–1.54	[21]
Saturated water	Polyamide	9.19–31.52 (0.7–2.4)	1.28 (1.2)	4.84–7.83	[19]

and 80 cm s⁻¹ and with a PP membrane operating in combination mode and liquid flowing through the shell side.

3.4. Energy analysis

In order to determine the feasibility of the operation in terms of its energy requirements, an energy analysis was carried out, assuming that the main energy consumption was related to the pumps (vacuum and liquid) and the efficiency of the combustion of methane should be decreased by around 20% due to the dilution effect of the sweep gas.

The energy consumption of the vacuum pump (W_{vp} , J/s) was estimated for the adiabatic compression process (a common, polytropic compression [6]) by using the following equation [9]:

$$W_{vp} = \frac{F_{G,tot} \cdot R \cdot T_G \cdot \gamma}{(1 - \gamma) \cdot \eta_{vp}} \left(\frac{P_{G,out} \frac{\gamma-1}{\gamma}}{P_{G,in}} - 1 \right) \quad (19)$$

where $F_{G,tot}$ (mol s⁻¹) is the molar flow-rate of the recovered gas, R (J mol⁻¹ K⁻¹) is the gas constant with a value of 8.314, T_G (K) is the gas temperature, $P_{G,in}$ and $P_{G,out}$ (Pa) are the pressure in the suction and discharge ports of the vacuum pump, respectively, and γ and η_{vp} are the estimated adiabatic coefficient and vacuum pump efficiency, respectively [48].

The energy consumption of the liquid pump (W_{lp} , J/s) used to drive the liquid and overcome the pressure drop (ΔP_L , Pa) along the HFMC can be estimated as follows [9]:

$$W_{lp} = \frac{Q_L \cdot \Delta P_L}{\eta_{lp}} \quad (20)$$

where Q_L (m³ s⁻¹) is the flow-rate of the liquid pump and η_{lp} is the pump efficiency, assumed to be equal at 65%. The pressure drop estimation is based on the Hagen-Poiseuille equation [48]:

$$\Delta P_L = \frac{8 \cdot \mu_w \cdot v_L \cdot L}{d_i^2} \quad (21)$$

where μ_w (kg m⁻¹ s⁻¹) is the viscosity of water.

The normalized energy consumption (sum of vacuum and liquid pumps) is expressed per gram of recovered CH₄ and m³ of the treated water, taking into account the quantity of methane recovered in each experiment and the liquid flow-rate. Results are shown in Fig. 7. For the lowest liquid flow-rate ($Q_L = 5.0$ L h⁻¹), the normalized energy consumption was highly dependent on the vacuum pressure, since the energy consumed in the vacuum device was the major contribution, which accounted for around 50% and 90% of the total energy consumption for P_{vac} of 100 and 480 mbar, respectively. For higher values of Q_L , energy consumption resulted in values around $1.90 \cdot 10^3$ kJ g⁻¹ CH₄ m⁻³ (mean values of $1.89 \pm 0.66 \cdot 10^3$, $1.90 \pm 0.19 \cdot 10^3$ and $1.94 \pm 0.01 \cdot 10^3$ kJ g⁻¹ CH₄ m⁻³, for Q_L of 13.7, 21.0 y 28.0 L h⁻¹, respectively), and for all the Q_{N2} tested. For the lowest Q_L (5.0 L h⁻¹), the increase in the sweep gas flow-rate resulted in an increase in the normalized energy consumption, attributed again to the low consumption of the liquid pump in comparison with the vacuum device.

For energy production, a combustion heat for CH₄ of 38 MJ m⁻³ (at 25 °C and 1 atm) was assumed [51]. Electrical efficiencies of around 35% are usually reported for biogas in microturbines but, taking into account the fact that the concentration of methane was lower than in reactor biogas (mainly due to the dilution of sweep gas), a decrease of around 20% has been applied in the efficiency of the combustion process.

Finally, the net recovered energy (Net E, kJ m⁻³) was obtained from the difference between the energy produced in a microturbine and total energy consumption by the pumps. Net E is expressed for 1 m³ of the liquid treated.

The energy analysis showed a positive net recovered energy under all operating conditions (Fig. 8a). The maximum Net E recovered was 270 kJ m⁻³, which resulted in a net recovered energy of CH₄ of $6.31 \cdot 10^3$ kJ g⁻¹ CH₄ m⁻³, for Q_{N2} of 1.5 L h⁻¹ and Q_L of 5.0 L h⁻¹ with P_{vac} of 200 mbar (Fig. 8b). In these conditions ($Q_{N2} > 0.5$ L h⁻¹ and $Q_L < 13.7$ L h⁻¹), C-CH₄ values are lower than 35%, thus the recovered gas should be mixed with a main biogas stream from the anaerobic process in order to recover the maximum energy from the R-CH₄ for electricity production. In the case of the direct use of the recovered gas in a microturbine (35% C-CH₄), the actual maximum Net E was 145 kJ m⁻³ ($2.37 \cdot 10^3$ kJ g⁻¹ CH₄ m⁻³) when Q_{N2} and Q_L were 0.5 L h⁻¹ and 13.7 L

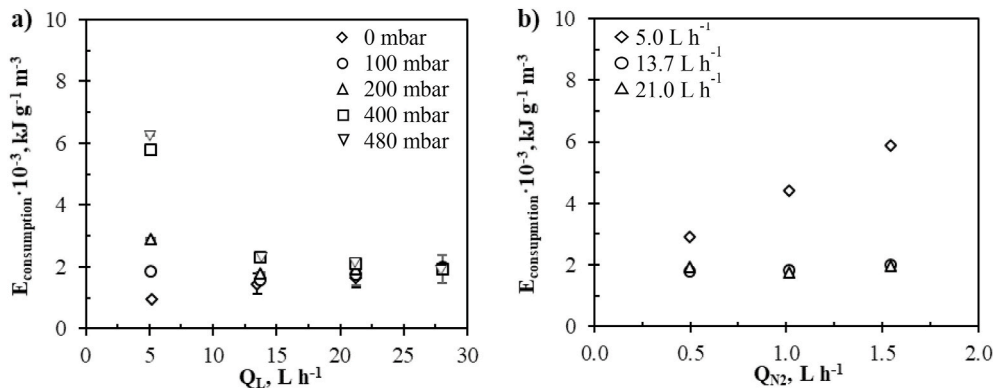


Fig. 7. Energy consumption per gram of CH₄ and m³ of treated effluent versus a) liquid flow-rate (at constant sweep gas flow-rate, $Q_{N2} = 0.5$ L h⁻¹, and different vacuum pressure) and b) sweep gas flow-rate (at constant vacuum pressure, $P_{vac} = 200$ mbar, and different liquid flow-rates).

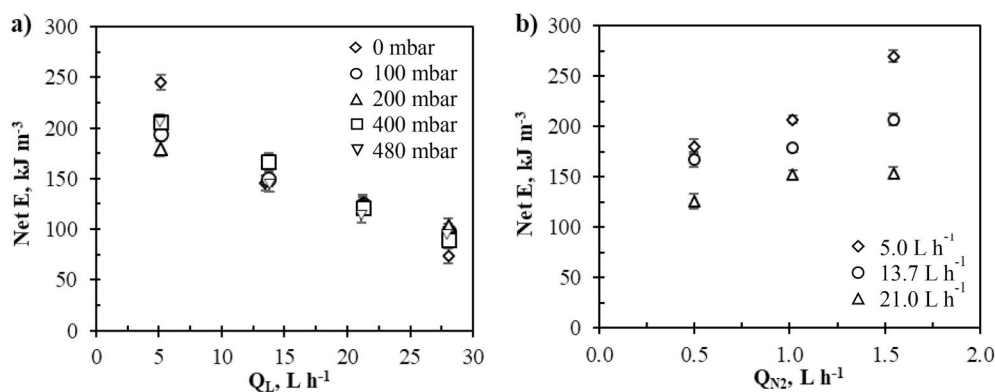


Fig. 8. Net energy obtained from the combustion of methane recovered in the membrane contactor for the treatment of 1 m³ of effluent (Net E) versus a) liquid flow-rate (at constant sweep gas flow-rate, $Q_{N_2} = 0.5 \text{ L h}^{-1}$, and different vacuum pressure) and b) sweep gas flow-rate (at constant vacuum pressure, $P_{vac} = 200 \text{ mbar}$, and different liquid flow-rates).

h⁻¹, respectively, without vacuum. When Q_L was 21.0 and 28.0 L h⁻¹ the maximum Net E was obtained at P_{vac} of 200 mbar with values of 126 and 103 kJ m⁻³ ($1.49 \cdot 10^3$ and $0.98 \cdot 10^3 \text{ kJ g}^{-1} \text{CH}_4 \text{ m}^{-3}$), respectively. The reduction of Net E with the Q_L (Fig. 8a) was a consequence of the lower REs associated with higher liquid velocities (Fig. 3a). The applied vacuum for the extraction of CH₄ did not show a significant effect on Net E. Net E results were in concordance with theoretical estimations, which predicted a maximum Net E of 178 kJ m⁻³ at P_{vac} of 100 mbar and Q_{N_2} of 6.6 L h⁻¹ [48] and a carbon neutral process [14,21].

The Levelized Cost of Energy (LCOE) of an anaerobic digestion of wastewater sludge with dissolved methane recovery was calculated according to the cost metric methodology used by the International Renewable Energy Agency [52]. For LCOE calculations, standardized assumptions values for bioenergy production technologies in OECD countries were used [52]. A scheme of the process and its specific values can be found as Supplementary material (S4). LCOE resulted in a value of 79 € MWh⁻¹ similar to those obtained for bioenergy plants in Europe with values ranging from 50 to 100 € MWh⁻¹ [52]. Implementation of the membrane contactor system for dissolved CH₄ recovery does not significantly increase the LCOE value.

4. Conclusions

The removal and recovery of dissolved methane from water by means of a microporous polypropylene hollow fibre membrane contactor, operating in combination mode (vacuum and nitrogen as sweep gas, simultaneously), showed significantly greater removal efficiencies of methane and lower mass transfer resistances than independent operational modes in practically all operational conditions. The maximum removal efficiency observed was higher than 90% in soft operational conditions (low nitrogen flow-rate and vacuum) and a G/L ratio from 0.20.

An increase of methane content in the recovered gas was observed with a rise in liquid flow-rate. On the contrary, the methane content was not significantly affected by the vacuum pressure which could be due to the presence of other desorbed gases. A gas composition higher than 35% of methane was achieved at the lowest G/L ratios (<0.03) and moderate vacuum (<200 mbar).

The mass transfer analysis showed that wetting phenomenon did not take place in combination mode in the operational conditions tested. The main mass transfer resistance was located in the liquid phase with negligible resistances of the gas phase and microporous membrane.

The energy balance showed that the energy production from recovered methane was greater than the energy consumption by the degasification process in all experiments, allowing a self-sufficient process. The influence of vacuum pressure on the net produced energy was negligible due to the rise of removal efficiency of methane and energy

consumption of the vacuum pump, simultaneously. The maximum net energy obtained was 270 kJ m⁻³ of treated effluent at G/L of 0.30 and moderate vacuum of 200 mbar.

Combination mode can enhance the performance of the membrane contactor to recover dissolved methane from anaerobic effluent, reducing the carbon footprint of an anaerobic wastewater treatment plant by using this methane for electricity or heat production.

CRedit authorship contribution statement

R. Jiménez-Robles: Methodology, Validation, Formal analysis, Investigation, Writing - original draft, Writing - review & editing, Visualization. **C. Gabaldón:** Conceptualization, Validation, Project administration, Funding acquisition. **V. Martínez-Soria:** Conceptualization, Methodology, Validation, Writing - review & editing, Supervision. **M. Izquierdo:** Conceptualization, Methodology, Validation, Writing - review & editing, Supervision, Funding acquisition.

Declaration of competing interest

The authors declare that they have no known competing financial interests or personal relationships that could have appeared to influence the work reported in this paper.

Acknowledgements

This work was supported by the Conselleria d'Innovació, Universitats, Ciència i Societat Digital – Generalitat Valenciana (project GV/2019/149). Financial support was also obtained from the FEDER/Ministerio de Ciencia e Innovación – Agencia Estatal de Investigación/Project CTM2017-88042-R (Spain).

Appendix A. Supplementary data

Supplementary data to this article can be found online at <https://doi.org/10.1016/j.memsci.2020.118560>.

References

- [1] F.J. Dentener, D.R. Easterling, R.A. Uk, R.A. Uk, O. Cooper, F. Canada, J.K. Uk, E. K. Uk, S.K. Germany, C.M. Uk, C. Morice, IPCC climate change 2013: the physical science basis. Chapter 2: observations: atmosphere and surface, clim. Chang. 2013 phys. Sci. Basis work. Gr. I contrib. To fifth assess, Rep. Intergov. Panel Clim. Chang. 9781107057 (2013) 159–254, <https://doi.org/10.1017/CBO9781107415324.008>.
- [2] R. Van Dingenen, J. Crippa, M.G. Anssens-Maenhout, D. Guizzardi, F. Dentener, Global trends of methane emissions and their impacts on ozone concentrations, Off. Eur. Union. (2018) 1–90, <https://doi.org/10.2760/820175>. EUR29394EN.
- [3] Greenhouse Gas Emissions by Country and Sector (Infographic), European Parliament News, 2018 (accessed June 3, 2020), <https://www.europarl.europa.eu>

- /news/en/headlines/society/20180301STO98928/greenhouse-gas-emissions-by-country-and-sector-infographic.
- [4] Global Methane Emissions and Mitigation Opportunities, Global Methane Initiative, 2019. https://www.globalmethane.org/documents/GMI_Mitigation-Factsheet_Spanish.pdf. (Accessed 3 June 2020).
- [5] J.B. van Lier, F.P. van der Zee, C.T.M.J. Frijters, M.E. Ersahin, Celebrating 40 years anaerobic sludge bed reactors for industrial wastewater treatment, *Rev. Environ. Sci. Biotechnol.* 14 (2015) 681–702, <https://doi.org/10.1007/s11157-015-9375-5>.
- [6] B.C. Crone, J.L. Garland, G.A. Sorial, L.M. Vane, Significance of dissolved methane in effluents of anaerobically treated low strength wastewater and potential for recovery as an energy product: a review, *Water Res.* 104 (2016) 520–531, <https://doi.org/10.1016/j.watres.2016.08.019>.
- [7] J. Cookney, E. Cartmell, B. Jefferson, E.J. McAdam, Recovery of methane from anaerobic process effluent using poly-di-methyl-siloxane membrane contactors, *Water Sci. Technol.* 65 (2012) 604–610, <https://doi.org/10.2166/wst.2012.897>.
- [8] M.R.J. Daelman, E.M. van Voorhuizen, U.G.J.M. van Dongen, E.I.P. Volcke, M.C. M. van Loosdrecht, Methane emission during municipal wastewater treatment, *Water Res.* 46 (2012) 3657–3670, <https://doi.org/10.1016/j.watres.2012.04.024>.
- [9] D.W. Green, Perry's Chemical Engineers' Handbook, eighth ed., McGraw-hill, New York, 2008 <https://doi.org/10.1036/0071422943>.
- [10] R. Sander, Compilation of Henry's law constants (version 4.0) for water as solvent, *Atmos. Chem. Phys.* 15 (2015) 4399–4981, <https://doi.org/10.5194/acp-15-4399-2015>.
- [11] W.M. Bandara, H. Satoh, M. Sasakawa, Y. Nakahara, M. Takahashi, S. Okabe, Removal of residual dissolved methane gas in an upflow anaerobic sludge blanket reactor treating low-strength wastewater at low temperature with degassing membrane, *Water Res.* 45 (2011) 3533–3540, <https://doi.org/10.1016/j.watres.2011.04.030>.
- [12] W.M. Bandara, M. Ikeda, H. Satoh, M. Sasakawa, Y. Nakahara, M. Takahashi, S. Okabe, Introduction of a degassing membrane technology into anaerobic wastewater treatment, *Water Environ. Res.* 85 (2013) 387–390, <https://doi.org/10.2175/106143013x13596524516707>.
- [13] S. Heile, C.A.L. Chernicharo, E.M.F. Brandt, E.J. McAdam, Dissolved gas separation for engineered anaerobic wastewater systems, *Sep. Purif. Technol.* 189 (2017) 405–418, <https://doi.org/10.1016/j.seppur.2017.08.021>.
- [14] M. Henares, M. Izquierdo, P. Marzal, V. Martínez-Soria, Demethanization of aqueous anaerobic effluents using a polydimethylsiloxane membrane module: mass transfer, fouling and energy analysis, *Sep. Purif. Technol.* 186 (2017) 10–19, <https://doi.org/10.1016/j.seppur.2017.05.035>.
- [15] W. Rongwong, K. Goh, G.S.M.D.P. Sethunga, T.H. Bae, Fouling formation in membrane contactors for methane recovery from anaerobic effluents, *J. Memb. Sci.* 573 (2019) 534–543, <https://doi.org/10.1016/j.memsci.2018.12.038>.
- [16] R. Klaassen, P.H.M. Feron, A.E. Jansen, Membrane contactors in industrial applications, *Chem. Eng. Res. Des.* 83 (2005) 234–246, <https://doi.org/10.1205/cherd.04196>.
- [17] A. Gabelman, S. Hwang, Hollow fiber membrane contactors, *J. Memb. Sci.* 159 (1999) 61–106.
- [18] M. Stanojević, B. Lazarević, D. Radić, Review of membrane contactors designs and applications of different modules in industry, *FME Trans* 31 (2003) 91–98.
- [19] W. Rongwong, S. Wongchitphimon, K. Goh, R. Wang, T.H. Bae, Transport properties of CO₂ and CH₄ in hollow fiber membrane contactor for the recovery of biogas from anaerobic membrane bioreactor effluent, *J. Memb. Sci.* 541 (2017) 62–72, <https://doi.org/10.1016/j.memsci.2017.06.090>.
- [20] B. Miller, J. Munoz, F. Wiesler, M.I. Separations, Boiler feed water degasification using membrane contactors — new methods for optimized performance, in: *Int. Water Conf.*, 2005, pp. 3–7.
- [21] A. McLeod, B. Jefferson, E.J. McAdam, Toward gas-phase controlled mass transfer in micro-porous membrane contactors for recovery and concentration of dissolved methane in the gas phase, *J. Memb. Sci.* 510 (2016) 466–471, <https://doi.org/10.1016/j.memsci.2016.03.030>.
- [22] J. Cookney, A. McLeod, V. Mathioudakis, P. Ncube, A. Soares, B. Jefferson, E. J. McAdam, Dissolved methane recovery from anaerobic effluents using hollow fiber membrane contactors, *J. Memb. Sci.* 502 (2016) 141–150, <https://doi.org/10.1016/j.memsci.2015.12.037>.
- [23] C. Vallières, E. Favre, Vacuum versus sweeping gas operation for binary mixtures separation by dense membrane processes, *J. Memb. Sci.* 244 (2004) 17–23, <https://doi.org/10.1016/j.memsci.2004.04.023>.
- [24] R. Singh, Hybrid Membrane Systems for Water Purification: Technology, Systems Design and Operations, Elsevier Science & Technology Books, 2006.
- [25] Membrana-GmbH, Contactors improve production yields, *Membr. Technol.* (2006) 1–5, [https://doi.org/10.1016/S0958-2118\(06\)70674-7](https://doi.org/10.1016/S0958-2118(06)70674-7).
- [26] J. Mann, J. Houtz, Membrana aids ASR deoxygenation trial and ships contactors to South Korea, *Membr. Technol.* (2009) 4–5, [https://doi.org/10.1016/s0958-2118\(09\)70044-8](https://doi.org/10.1016/s0958-2118(09)70044-8).
- [27] S. Kartohardjono, A. Rabekka, Combination vacuum and sweep gas processes to remove dissolved oxygen from water through hollow fiber membrane contactors, *J. Mater. Sci. Eng. A* 1 (2011) 812–818.
- [28] I. Martić, A. Maslarević, S. Mladenović, U. Lukić, S. Budimir, Water deoxygenation using hollow fiber membrane module with nitrogen as inert gas, *Desalin. Water Treat.* 54 (2015) 1563–1567, <https://doi.org/10.1080/19443994.2014.888677>.
- [29] M. Henares, M. Izquierdo, J.M. Peña-Roja, V. Martínez-Soria, Comparative study of degassing membrane modules for the removal of methane from Expanded Granular Sludge Bed anaerobic reactor effluent, *Sep. Purif. Technol.* 170 (2016) 22–29, <https://doi.org/10.1016/j.seppur.2016.06.024>.
- [30] M. Henares, P. Ferrero, P. San-Valero, V. Martínez-Soria, M. Izquierdo, Performance of a polypropylene membrane contactor for the recovery of dissolved methane from anaerobic effluents: mass transfer evaluation, long-term operation and cleaning strategies, *J. Memb. Sci.* 563 (2018) 926–937, <https://doi.org/10.1016/j.memsci.2018.06.045>.
- [31] S. Wongchitphimon, W. Rongwong, C.Y. Chuah, R. Wang, T.H. Bae, Polymer-fluorinated silica composite hollow fiber membranes for the recovery of biogas dissolved in anaerobic effluent, *J. Memb. Sci.* 540 (2017) 146–154, <https://doi.org/10.1016/j.memsci.2017.06.050>.
- [32] Y. Lester, D. Avisar, I. Gozlan, H. Mamane, Removal of pharmaceuticals using combination of UV/H₂O₂/O₃ advanced oxidation process, *Water Sci. Technol.* 64 (2011) 2230–2238, <https://doi.org/10.2166/wst.2020.250>.
- [33] S.A. Hashemifard, A.F. Ismail, T. Matsuura, M.R. Dashtarzhadi, Performance of silicon rubber coated polyetherimide hollow fibers for CO₂ removal via a membrane contactor, *RSC Adv.* 5 (2015) 48442–48455, <https://doi.org/10.1039/c5ra00085h>.
- [34] S.R. Wickramasinghe, M.J. Semmens, E.L. Cussler, Mass transfer in various hollow fiber geometries, *J. Memb. Sci.* 69 (1992) 235–250.
- [35] M.A. Lévêque, Les lois de la transmission de chaleur par convection, *Les Ann. Des Mines.* 13 (1928) 201–299.
- [36] Y.A. Çengel, M.A. Boles, M. Kanoglu, Thermodynamics: an Engineering Approach, ninth ed., McGraw-hill, New York, 2019.
- [37] M.-C. Yang, E.L. Cussler, Designing hollow-fiber contactors, *AIChE J.* 32 (1986) 1910–1915.
- [38] Z. Qi, E.L. Cussler, Microporous hollow fibers for gas absorption. II. Mass transfer across the membrane, *J. Memb. Sci.* 23 (1985) 321–332.
- [39] H. Kreulen, C.A. Smolders, W.P. Swaaij, Determination of mass transfer rates in wetted and non-wetted microporous membranes, *Chem. Eng. Sci.* 48 (1993).
- [40] E.N. Fuller, P.D. Schettler, J.C. Giddings, A new method for prediction of binary gas-phase diffusion coefficients, *Ind. Eng. Chem.* 58 (1966) 18–27, <https://doi.org/10.1021/ie50677a007>.
- [41] J.R. Welty, C.E. Wicks, R.E. Wilson, G.L. Rorrer, Fundamentals of Momentum, Heat, and Mass Transfer, fifth ed., John Wiley & Sons, Inc., Oregon, 2008.
- [42] E.L. Cussler, Mass Transfer in Fluid Systems, Cambridge University Press, 1984.
- [43] G. Luo, W. Wang, I. Angelidaki, A new degassing membrane coupled upflow anaerobic sludge blanket (UASB) reactor to achieve in-situ biogas upgrading and recovery of dissolved CH₄ from the anaerobic effluent, *Appl. Energy* 132 (2014) 536–542, <https://doi.org/10.1016/j.apenergy.2014.07.059>.
- [44] X. Cao, H.S. Lee, X. Feng, Extraction of dissolved methane from aqueous solutions by membranes: modelling and parametric studies, *J. Memb. Sci.* 596 (2020) 117594, <https://doi.org/10.1016/j.memsci.2019.117594>.
- [45] G.S.M.D.P. Sethunga, H.E. Karahan, R. Wang, T.H. Bae, PDMS-coated porous PVDF hollow fiber membranes for efficient recovery of dissolved biomethane from anaerobic effluents, *J. Memb. Sci.* 584 (2019) 333–342, <https://doi.org/10.1016/j.memsci.2019.05.016>.
- [46] G.S.M.D.P. Sethunga, J. Lee, R. Wang, T.H. Bae, Influence of membrane characteristics and operating parameters on transport properties of dissolved methane in a hollow fiber membrane contactor for biogas recovery from anaerobic effluents, *J. Memb. Sci.* 589 (2019), 117263, <https://doi.org/10.1016/j.memsci.2019.117263>.
- [47] G.S.M.D.P. Sethunga, W. Rongwong, R. Wang, T.H. Bae, Optimization of hydrophobic modification parameters of microporous polyvinylidene fluoride hollow-fiber membrane for biogas recovery from anaerobic membrane bioreactor effluent, *J. Memb. Sci.* 548 (2018) 510–518, <https://doi.org/10.1016/j.memsci.2017.11.059>.
- [48] W. Rongwong, K. Goh, T.H. Bae, Energy analysis and optimization of hollow fiber membrane contactors for recovery of dissolve methane from anaerobic membrane bioreactor effluent, *J. Memb. Sci.* 554 (2018) 184–194, <https://doi.org/10.1016/j.memsci.2018.03.002>.
- [49] F. Wiesler, Membrane contactors: an introduction to the technology, *Ultrapure Water* 130427 (1996) 27–31.
- [50] W. Rongwong, C. Fan, Z. Liang, Z. Rui, R.O. Idem, P. Tontiwachwuthikul, Investigation of the effects of operating parameters on the local mass transfer coefficient and membrane wetting in a membrane gas absorption process, *J. Memb. Sci.* 490 (2015) 236–246, <https://doi.org/10.1016/j.memsci.2015.04.071>.
- [51] D.R. Lide, CRC Handbook of Chemistry and Physics, CRC Press. Taylor Fr. Boca Rat. FL, 2005, p. 2660, [https://doi.org/10.1016/0165-9936\(91\)85111-4](https://doi.org/10.1016/0165-9936(91)85111-4). Internet Version 2005.
- [52] Irena, Renewable Power Generation Costs in 2018, International Renewable Energy Agency, Abu Dhabi, 2019.

Supplementary Material for

Simultaneous application of vacuum and sweep gas in a polypropylene membrane contactor for the recovery of dissolved methane from water

R. Jiménez-Robles, C. Gabaldón, V. Martínez-Soria, M. Izquierdo*

Research Group GI²AM, Department of Chemical Engineering, University of Valencia, Avda. Universitat s/n, 46100 Burjassot, Spain.

*e-mail: marta.izquierdo-sanchis@uv.es. Phone: +34 354 37 37. Fax: +34 963 54 48 98.

S1. Estimated mass flow of recovered methane (R-CH₄)

Influence of liquid flow-rate (Q_L , L h⁻¹) on the estimated mass flow of recovered methane (mg CH₄ h⁻¹) at sweep gas flow-rate (Q_{N_2} , L h⁻¹) of 0.5 L h⁻¹. Calculations were made based on liquid mass balance.

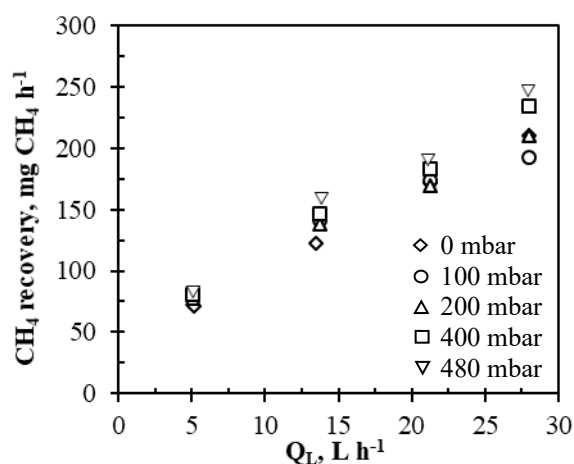


Fig. S1. Estimated mass flow of recovered methane (R-CH₄) versus liquid flow-rate for the combination mode operation with $Q_{N_2} = 0.5$ L h⁻¹.

S2. Effect of vacuum pressure

Influence of vacuum pressure (P_{vac} , mbar) on methane removal efficiency (RE, %) and content of methane in the recovered gas from the membrane contactor at sweep gas flow-rate (Q_{N_2} , $L h^{-1}$) higher than $0.5 L h^{-1}$.

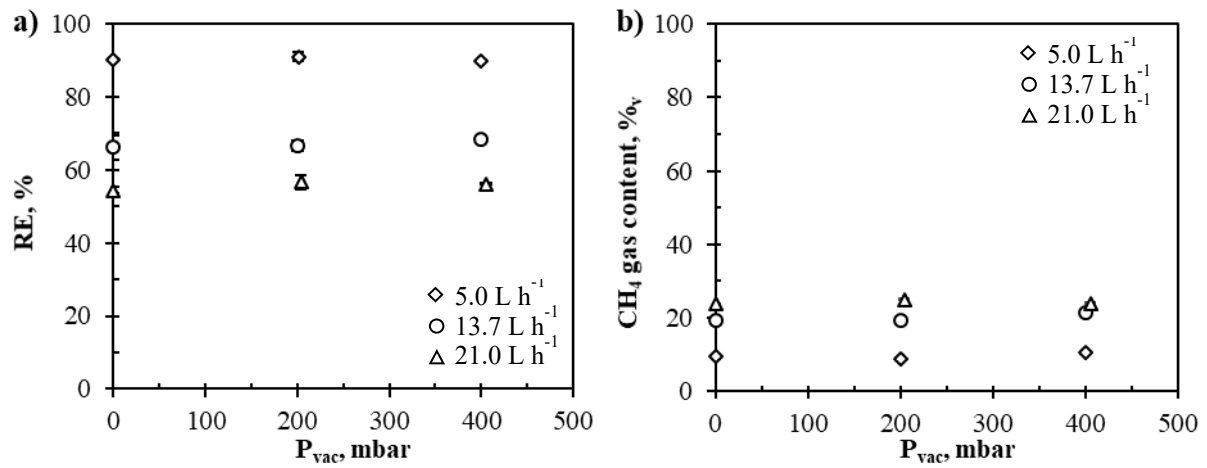


Fig. S2. a) Dissolved CH_4 removal efficiency (RE, %) and b) content of CH_4 in the recovered gas from the membrane contactor versus vacuum pressure for the combination mode operation with $Q_{N_2} = 1.0 L h^{-1}$.

S3. Wilson's Plot Analysis

A Wilson's Plot analysis was carried out in order to estimate the mass transfer coefficient (k_m , m s^{-1}) of the PP membrane (Fig. S3). Assuming a negligible gas phase resistance, the results listed in Table S1 indicate a negligible mass transfer resistance of the membrane ($R_m \ll R_L$).

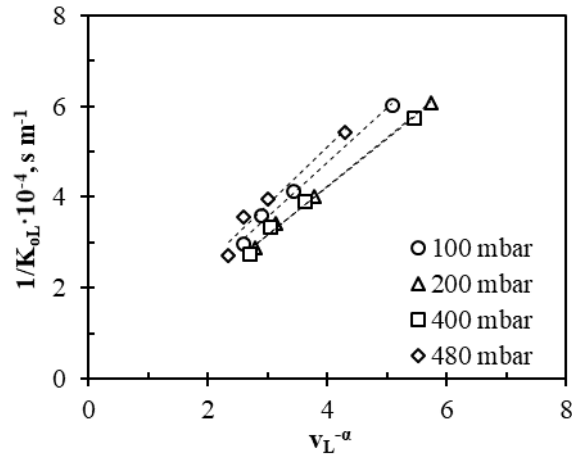


Fig. S3. Wilson's Plot Analysis from the mass transfer data obtained for the combination mode operation with $Q_{N_2} = 0.5 \text{ L h}^{-1}$ as a function of the liquid velocity and the parameter α .

Table S1. Details of the Wilson's Plot Analysis and the obtained mass transfer coefficients and resistances of the PP membrane at different vacuum pressures for the combination mode operation with $Q_{N_2} = 0.5 \text{ L h}^{-1}$ and liquid flow-rates between 5.0 and 28.0 L h^{-1} .

$P_{\text{vac}}, \text{ mbar}$	α	R^2	$k_m \cdot 10^2, \text{ m s}^{-1}$	$R_m, \text{ s m}^{-3}$
100	0.39	0.993	2.62	5.46
200	0.42	0.998	3.21	4.94
400	0.41	0.993	2.88	4.98
480	0.35	0.961	2.42	4.47

S4. Levelized Cost of Energy Analysis (LCOE)

The Levelized Cost of Energy (LCOE) of an energy plant based on an anaerobic digestion of wastewater sludge with dissolved methane recovery was calculated. A scheme of the process and detailed values are shown in Fig. S4.

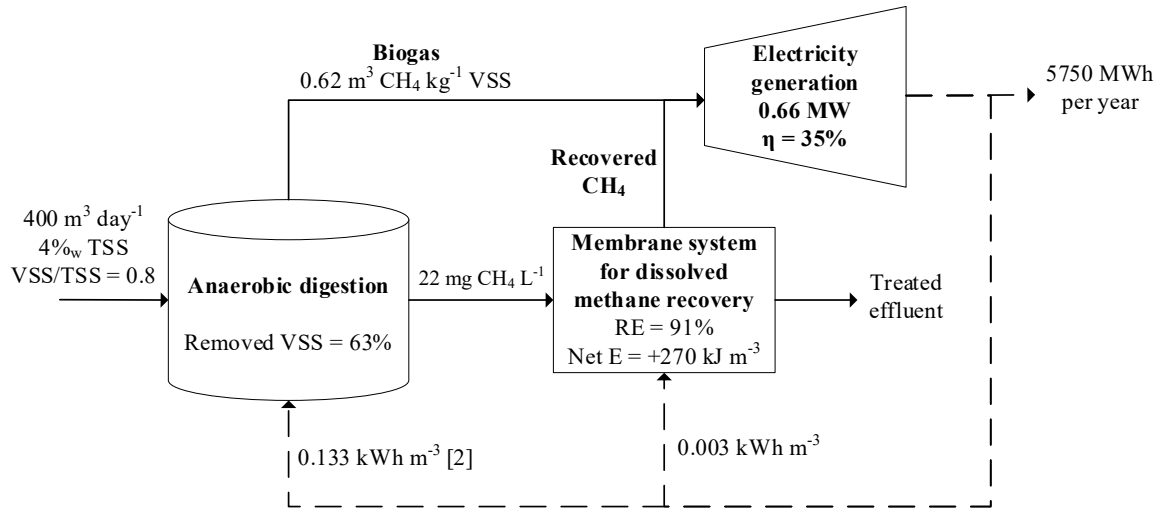


Fig. S4. Scheme of an energy plant integrated in an anaerobic digester of wastewater sludge (from an urban wastewater treatment plant) with a dissolved methane recovery system by membrane contactors, and values used for Levelized Cost of Energy (LCOE) calculation. (TSS and VSS: total and volatile suspended solid respectively, RE: dissolved methane removal efficiency, Net E: net energy recovered from methane, η : microturbine efficiency for electricity conversion)

LCOE value was calculated according to the cost metric methodology used by the International Renewable Energy Agency [1], using the following equation:

$$\text{LCOE} = \frac{\sum_{t=1}^n \frac{I_t + M_t + F_t}{(1+r)^t}}{\sum_{t=1}^n \frac{E_t}{(1+r)^t}} \quad (\text{S1})$$

where I_t is investment cost in the year t , M_t is the operation and maintenance costs in the year t , F_t is the fuel cost in the year t , E_t is the electricity generation in the year t , r is the discount rate and n is the economic life of the plant.

For LCOE calculations, standardized assumptions values for bioenergy production technologies in OECD countries were used [1] with a capacity factor of 85% and an economic life of the plant of 20 years. LCOE value of the studied process resulted in 79 € MWh⁻¹.

References

- [1] IRENA (2019), Renewable Power Generation Costs in 2018, International Renewable Energy Agency, Abu Dhabi.
- [2] B.C. Crone, J.L. Garland, G.A. Sorial, L.M. Vane, Significance of dissolved methane in effluents of anaerobically treated low strength wastewater and potential for recovery as an energy product: A review, *Water Res.* 104 (2016) 520–531. <https://doi.org/10.1016/j.watres.2016.08.019>.

APPENDIX VI: CONTRIBUTION VI.

The contribution entitled “*Membrane-assisted reactive crystallisation for the recovery of dissolved phosphorous in vivianite form from liquid effluents*” is presented in this Appendix. This work corresponds with the main results and conclusions discussed in section 4.6. The details of the pre-print resulting from the paper under peer review are listed below:

Title	Membrane-assisted reactive crystallisation for the recovery of dissolved phosphorous in vivianite form from liquid effluents
Authors	Ramón Jiménez-Robles ^a , Marta Izquierdo ^a , Vicente Martínez-Soria ^a , Lo-I Chen ^b , Le Corre Pidou ^b , Ewan McAdam ^b
Affiliation	^a Research Group in Materials Technology and Sustainability (MATS), Department of Chemical Engineering, School of Engineering, University of Valencia, Avda. Universitat s/n, 46100 Burjassot, Spain ^b School of Water, Energy and Environment, Cranfield University, Bedfordshire, MK43 0AL, UK
Journal	Separation and Purification Technology
DOI	10.2139/ssrn.4481071
Cite	R. Jiménez-Robles, M. Izquierdo, V. Martínez-Soria, Lo-I Chen, K. Le Corre Pidou, E.J. McAdam, Membrane-assisted reactive crystallisation for the recovery of dissolved phosphorous in vivianite form from liquid effluents. Under review in Sep. Purif. Technol. Pre-print available at http://dx.doi.org/10.2139/ssrn.4481071

The Journal Impact Factor (JIF) in 2022 (last available data) was 8.6, and the JIF rank was 12/140 in the category of Chemical Engineering (D1 first decile).

1 **Membrane-assisted reactive crystallisation for the recovery of dissolved phosphorous in**
2 **vivianite form from liquid effluents**

3 R. Jiménez-Robles^a, V. Martínez-Soria^a, M. Izquierdo^a, Lo-I Chen^b, K. Le Corre Pidou^b, E.J.
4 McAdam^{b,*}

5 ^aResearch Group in Materials Technology and Sustainability (MATS), Department of Chemical Engineering,
6 School of Engineering, University of Valencia, Avda. Universitat s/n, 46100 Burjassot, Spain.

7 ^bSchool of Water, Energy and Environment, Cranfield University, Bedfordshire, MK43 0AL, UK

8 *Corresponding author. e-mail: e.mcadam@cranfield.ac.uk

9

10 **Keywords**

11 Membrane-assisted crystallisation; nanoparticles; nucleation kinetic; phosphorous recovery;
12 polymeric membrane; vivianite

13

14 **1. Introduction**

15 Phosphorous (P) is an essential element for life on Earth [1–3], being involved in the metabolic
16 activity of plants and microorganisms among other biological and geological processes [2–6].

17 Consequently, P is also an important component of the most used fertilizers, whereas P
18 compounds such as phosphoric acid and its derivates are valuable chemicals for the electronic
19 industry and immobilization of heavy metals, among others applications [3,5,6,7]. However,
20 the available P in nature, which is mainly obtained from the mining of phosphate rock (apatites)
21 [2,7], is depleting at an accelerated rate due to the rising global demand, accordingly with
22 population growth and improved living standards [2,8,9]. Thus, natural P sources are expected
23 to be used up by the end of this century [2,6,7,10]. Therefore, the search and exploitation of
24 new and renewable P sources are important to ensure the feasible supply of this element [6,11].

25 Urban wastewaters are a potential source of P which could be recovered in form of salts by
26 means of crystallisation reactions [2]. The most common technique for P recovery in
27 wastewater treatment plants is the crystallisation by the addition of Mg salts, leading to the
28 formation of struvite ((NH₄)MgPO₄·6H₂O) [11,12]. The large quantity of chemicals and the

29 relative low efficiency of the process, coupled with the high capital cost of installation, hinder
30 the application and feasibility at large-scale [1,2,10]. However, stricter environmental
31 regulations are lowering the admissible limit of P content in treatment plant effluents, and P
32 recovery from wastewater has become a mandatory operation in some countries [2,9,13].
33 Therefore, an emergent need exists for the development of new processes that enable lower cost
34 and higher efficiency P recovery.

35 Vivianite ($\text{Fe}_3(\text{PO}_4)_2 \cdot 8\text{H}_2\text{O}$) is a phosphate mineral that is naturally present in iron (Fe) and P
36 rich environments under reducing conditions [14] such as in freshwater and marine sediments,
37 and waterlogged and organic soils [2–5,14]. Different crystalline and amorphous phases are
38 associated with vivianite-based compounds (vivianite, metavivianite, santabarbaraite...) [1–5].
39 Vivianite is considered a valuable chemical for its use as a slow-release fertilizer, for the
40 production of lithium-ion batteries and in the electronics industry [2,6,14]. Vivianite presents
41 an extremely low solubility in water [9,14], thereby, it could be easily obtained by precipitation
42 of phosphates contained in a liquid matrix after the addition of a Fe^{2+} salt [1,15]. Frossard et al.
43 [15] evidenced the presence of vivianite in wastewater sludge flocculated with FeSO_4 .
44 Compared with struvite, the synthesis of vivianite through precipitation could reduce operating
45 costs of P recovery mainly due to an easier operation and lower consumption of chemicals
46 [1,2,9]. The lower solubility limit of vivianite also implies that higher removal efficiencies can
47 be achieved and may be viable for a broader range of feed water concentrations. Priambodo et
48 al. [6] added a Fe^{2+} salt to a real wastewater from the electronic industry for the crystallisation
49 of P in vivianite form in a fluidised bed crystalliser, reporting a P removal of 95% at the optimal
50 operational condition. However, few studies on vivianite synthesis have been published [2,6,9],
51 requiring greater depth in understanding of nucleation and crystal growth processes.

52 Supersaturation is the driving force for nucleation and crystal growth. Sparingly soluble salts
53 such as vivianite require significant supersaturation to develop before induction. Mixing is also
54 important as the increased likelihood for molecular collision can reduce the activation energy
55 requirement for nucleation [16,17]. However, the regulation of supersaturation in existing
56 crystallisers is extremely challenging due to the poorly defined hydrodynamic conditions,
57 leading to inconsistent mixing of reactants [18–20]. This can result in overdosing of reactant
58 and inconsistent crystal product quality which can be important for downstream applications.
59 Membrane contactors offer fixed interfacial area to foster the homogeneous regulation of
60 supersaturation, while the formation of a well-defined laminar boundary layer also creates a
61 region of elevated supersaturation which is thought to enable the independent control of
62 nucleation from crystal growth [19,21]. Consequently, membrane contactors offer greater
63 control over nucleation, and their high interfacial area creates a more scalable and lower cost
64 alternative to conventional equipment for separation and reactions processes [10,22–24]. The
65 application of membrane-assisted crystallisation (MAC) has primarily focused on evaporative
66 crystallisation of high soluble aqueous salts, and antisolvent crystallisation for the production
67 of high value but poorly soluble active pharmaceutical ingredients [20,25,26]. Membrane-
68 assisted reactive crystallisation (MARC) is physically analogous to antisolvent crystallisation,
69 as the membrane regulates the inclusion of liquid reactant into the reaction zone through an
70 overpressure within the pores. However, the mechanism of crystallisation is distinct since the
71 reactant is used to raise supersaturation rather than to reduce the solubility limit [22]. While the
72 concept has been proposed, MARC has been rarely studied. In principle, the membrane can
73 provide a high level of micromixing [26–29], allowing high supersaturation indices and low
74 induction times [30], since all the surface pores of the membrane could act as mixing points at
75 a microscopic and molecular level [26,30,31]. The membrane has also been proposed to
76 promote heterogeneous nucleation [19,22,32], by reducing the free energy barrier through

77 advancing solute-membrane interactions [20,30]. Thus, the quality of the final crystals could
78 be adjusted by the selection of the appropriate membrane properties and hydraulic conditions
79 [22,33–35].

80 This study therefore examines how membrane crystallisation can be used to modify the
81 nucleation kinetics for reactive sparingly soluble systems, to provide a controlled engineered
82 environment for P recovery through vivianite crystallisation. The microporous membrane in
83 MARC was used to facilitate dosing of an Fe^{2+} solution into a phosphate-rich solution, with the
84 ambition to: (i) investigate how boundary layer conditions can be used to modify
85 supersaturation leading to the advancement in regulation of nucleation kinetics by applying
86 different hydrodynamic conditions inside the membrane module; (ii) study the effects of
87 membrane properties to determine how they might regulate nucleation kinetics through their
88 role in reducing critical surface free energy requirement for nucleation, and micromixing, and;
89 (iii) develop a framework that can describe how nucleation kinetics can be modified by MARC
90 by means of direct determination of induction time in the bulk solution and at the membrane.
91 The direct determination of induction time is rarely reported, and is the basis for establishing
92 new knowledge in vivianite crystallisation and for the development of membrane-assisted
93 crystallisation as a platform technology for reactive systems.

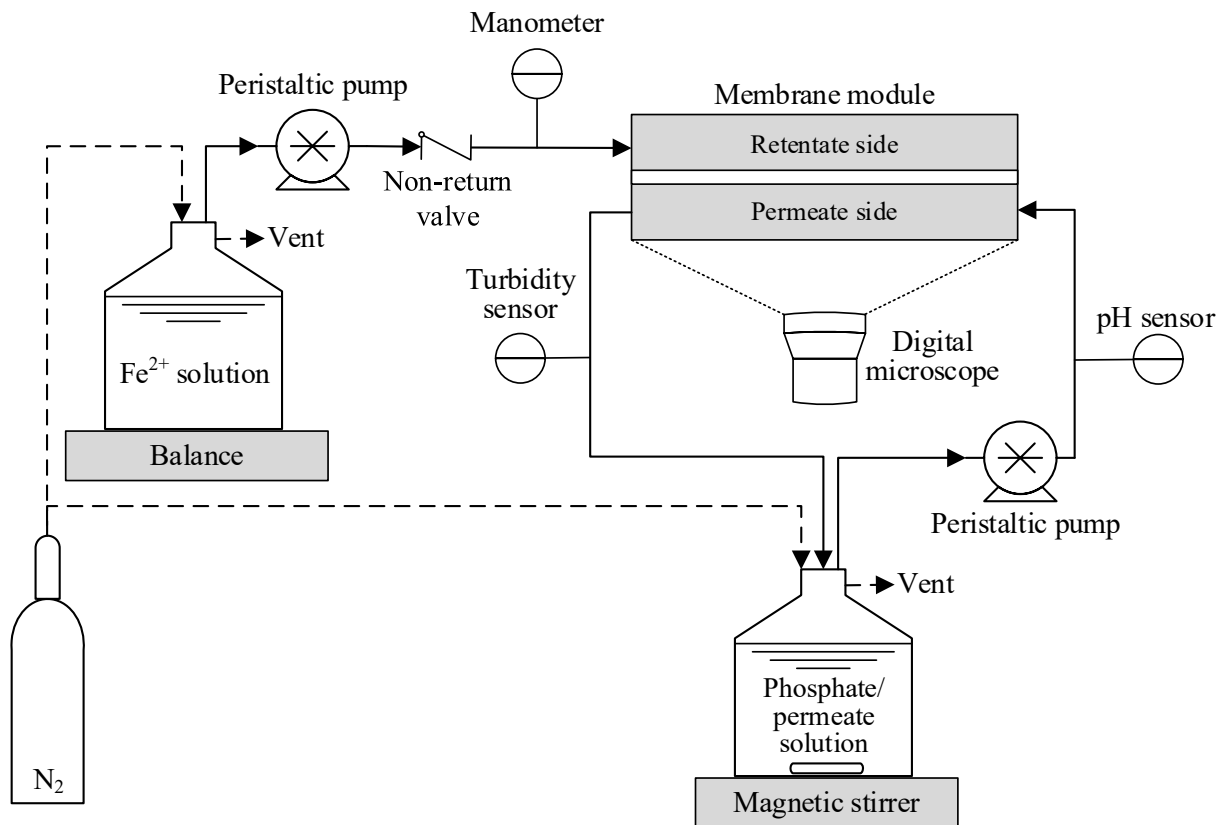
94

95 **2. Materials and methods**

96 **2.1. Experimental setup and vivianite crystallisation tests**

97 The crystallisation tests for the P recovery in vivianite form by means of a MARC were
98 conducted in the laboratory-scale system shown in Figure 1. First, a phosphate stock solution
99 at a concentration of 1.1 mM was prepared with sodium phosphate dibasic heptahydrate
100 ($\text{Na}_2\text{HPO}_4 \cdot 7\text{H}_2\text{O}$, $\geq 99\%$, Acros Organics, Geel, Belgium), and a ferrous stock solution (Fe^{2+})
101 at a concentration of 1.6 mM was prepared with iron (II) chloride tetrahydrate ($\text{FeCl}_2 \cdot 4\text{H}_2\text{O}$, \geq

102 99%, Sigma-Aldrich, Saint Louis, MI, USA). MilliQ water was used as the solvent for both
103 solutions, and flushed with N₂ prior to use in order to remove the residual dissolved oxygen and
104 avoid the oxidation of the ferrous ion [9,14].

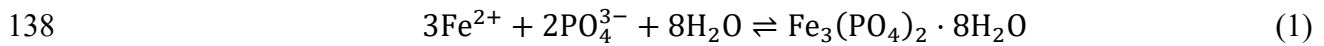


105
106 *Figure 1. Flowchart of the membrane-assisted reactive crystallisation for the phosphorous*
107 *recovery in vivianite form. Continuous line denotes liquid stream, and dashed line denotes gas*
108 *stream.*

109 A 500 mL glass bottle was initially filled with 250 mL of the phosphate stock solution, and it
110 was placed on a magnetic stirrer (Super-nuova multi-place, Thermo Scientific, MA, USA) at
111 300 rpm with a 2 cm magnetic bar for the continuous agitation of the solution. Also, another
112 500 mL glass bottle was initially filled with 250 mL of the Fe^{2+} stock solution and placed on a
113 precision balance (PCB, Kern & Sohn GmbH, Balinge, Germany) in order to carry out a mass

114 balance. The headspace of both bottles was kept under a continuous N₂ flow to avoid the
115 inclusion of oxygen into the solutions during the crystallisation tests.

116 A flat-sheet membrane was coupled inside a flat-sheet membrane module (FM) build in
117 methacrylate with an effective contact area of 40 cm² (a picture of the FM can be found in
118 supplementary material S1), and the permeate and retentate side of the FM were connected to
119 the phosphate and Fe²⁺ solutions, respectively. Initially, the phosphate solution was recirculated
120 through the permeate side at a liquid flow rate (Q_L) ranging from 8 to 30 L h⁻¹ using a peristaltic
121 pump (323, Watson-Marlow, Cornwall, UK), which resulted in liquid velocities between 2.8
122 and 10.4 cm s⁻¹ what it meant Reynold numbers (*Re*) from 105 to 395 inside the FM. The liquid
123 velocity inside the FM was set based on a previous work [36]. Also, the Fe²⁺ solution was driven
124 to the retentate side of the FM at a flow rate of 4.66 ± 0.12 mL min⁻¹ with a peristaltic pump
125 (Easy-Load Masterflex L/S, Cole Parmer, Illinois, USA), keeping the outlet port of the retentate
126 side closed. The pressure increased in the retentate side of the FM as consequence of the
127 continuous Fe²⁺ solution pumping, and the pressure was monitored with a digital manometer
128 (RS-8890G, RS Group, London, UK). The beginning of the crystallisation tests (*t* = 0) was set
129 at the time in which the pressure of the retentate side reached the liquid entry pressure (LEP)
130 of the membrane (Table 1), thereby, the dosing of Fe²⁺ into the permeate side started. The
131 crystallisation test was stopped after the dosing of 250 mL of Fe²⁺ solution, resulting in an iron-
132 to-phosphorous atomic ratio (Fe:P) of 1.5 in the phosphate/permeate solution. This Fe:P ratio
133 satisfied the stoichiometry of the overall chemical reaction between Fe²⁺ and PO₄³⁻ for the
134 vivianite formation (Eq. 1), and it has been reported as the optimal value for the vivianite
135 formation [1]. Crystallisation tests were conducted at room temperature without additional
136 control (21.3 ± 1.3 °C), since the temperature has a negligible effect on the solubility product
137 of vivianite in this range of values [9,14].



139 Vivianite crystallisation was monitored based on the turbidity of the phosphate/permeate
140 solution by means of a twin-axial turbidity probe (InPro 8200/Epoxy/120, Mettler Toledo,
141 Leicester, UK) mounted at the outlet of the permeate side of the FM, which provides sensitive
142 detection for the onset of nucleation. The turbidity profiles were used for the determination of
143 bulk induction time and nucleation kinetics. In addition, the pH of the phosphate/permeate
144 solution was monitored with a pH probe (Easy Ferm PlusPHI Arc 325, Hamilton Company,
145 GR, Switzerland) and maintained at pH 7, at which vivianite formation is believed to dominate
146 the Fe-P reactions [2,9]. The pH was adjusted [9] with the addition of 1M sodium hydroxide
147 (NaOH pellets, Fisher Chemicals, Loughborough, UK) and 1 M hydrochloric acid (HCl, 37%,
148 Fisher Scientific, Loughborough, UK) solutions. The total added volume of pH adjusting
149 solutions during a test was always lower than 0.5 mL, thus this extra volume was neglected for
150 further calculations. In order to analyse the scaling/deposition of solid particles onto the
151 membrane, the membrane surface facing the permeate side was recorded throughout the
152 crystallisation test using a digital microscope (Kopa, Ostec, Guangzhou, China). Frames were
153 taken at different times of the tests from the recordings and processed with the ImageJ software
154 (National Institutes of Health, USA) for the determination of membrane induction time and
155 extent of the scaling/deposition [32]. Each crystallisation test was conducted in duplicate at the
156 different experimental conditions tested in this work.

157 Immediately after the end of the test, a 5 mL sample of the phosphate/permeate solution was
158 filtered in a vacuum filtration system using mixed cellulose esters filters with a pore size of
159 0.025 μm (MF-Millipore®, Merck KGaA, Darmstadt, Germany) for the collection and ulterior
160 analysis of the crystals. After the filtration, the filters were dried under a N_2 flow of 0.1 L min^{-1}
161 ¹ overnight, and finally, they were stored in zip bags inside a desiccator.

162 The supersaturation index (SI) of the produced vivianite was estimated using the Visual
163 MINTEQ 3.1 software (Swedish University of Agricultural Sciences, Sweden) based on the
164 ratio of the ionic activity product (IAP) to the vivianite solubility product constant in water (K_{sp}
165 $= 1.82 \cdot 10^{-41}$ at 25°C [9]) as $SI = \log(IAP / K_{sp})$. Thus, SI was estimated in the bulk of the
166 phosphate/permeate solution (SI_b) at the different PO_4^{3-} and Fe^{2+} concentrations with the test
167 time, which were calculated from a mass balance conducted in the overall system (mass balance
168 shown in supplementary material S2). Also, the SI inside the FM (SI_m) was estimated using
169 mean PO_4^{3-} and Fe^{2+} concentrations values between the inlet and outlet of the permeate side
170 based on a mass balance, relying on the time and Q_L (mass balance shown in supplementary
171 material S3). This mass balance is intended only to illustrate the overall concentration gradient,
172 since a complete description of mass transport within the boundary layer requires significant
173 numerical analysis and validation to describe the relative role of local mixing.

174

175 **2.2. Membrane materials and surface modification**

176 A total of six microporous flat-sheet membranes were tested in this work: hydrophilic supported
177 polyvinylidene fluoride (PVDF-St) (Trisep UB70, Microdyn-Nadir, Hessen, Germany),
178 hydrophobic supported polyvinylidene fluoride (PVDF-Ds) (Dorsan Filtration S.L., Barcelona,
179 Spain), hydrophobic unsupported polyvinylidene fluoride (PVDF-Dp) (Durapore, Merck
180 KGaA, Darmstadt, Germany), two hydrophobic polytetrafluoroethylene with pore size of 1 and
181 3 μm (PTFE-1 and PTFE-3, respectively) (PF-1F and PF-3W, respectively, Cobetter Filtration
182 Equipment Co., Ltd., Hangzhou, China) and polypropylene (PP) (Accurel® PP-2EHF, 3M
183 Liqui-Cel, MN, USA). The main properties of the membranes are shown in Table 1.

184 *Table 1. Main properties of the flat-sheet membranes used in this work: water contact angle*
 185 *(WCA), mean pore size (r_p), porosity (ϵ), root mean square roughness (R_q), and liquid entry*
 186 *pressure (LEP).*

Membrane	WCA^b, °	r_p^a, μm	ϵ^b, %	R_q^b, nm	LEP^b, bar
PVDF-St	36 ± 3	0.03	63 ± 2	163 ± 14	0.13 ± 0.04
Act_PVDF-Ds	87 ± 3	0.20	60 ± 5	573 ± 77	2.39 ± 0.58
PVDF-Ds	103 ± 2	0.20	62 ± 3	387 ± 63	2.79 ± 0.28
PVDF-Dp	119 ± 2	0.22	69 ± 1	548 ± 72	2.27 ± 0.02
Fun_PVDF-Ds	144 ± 2	0.20	59 ± 2	577 ± 89	2.98 ± 0.27
PTFE-1	148 ± 2	1.00	90 ± 5	202 ± 43	0.58 ± 0.13
PTFE-3	148 ± 2	3.00	91 ± 5	467 ± 91	0.57 ± 0.02
PP	154 ± 3	0.24	79 ± 5	269 ± 57	2.67 ± 0.10

187 ^a Provided by the manufacturer

188 ^b Measured in this work

189

190 A modification technique of the PVDF-Ds membranes based on an initial alkali activation step
 191 followed by a functionalisation step was conducted in order to modify its hydrophobicity. This
 192 modification protocol was based on our previous works [37,38]. Thus, NaOH was used for the
 193 activation step, and 1H,1H,2H,2H-perfluorooctyltriethoxysilane (Dynasylan[®] F8261, Evonik
 194 GmbH, Essen, Germany) and 3-(triethoxysilyl)-propylamine (APTES, Sigma-Aldrich, Saint
 195 Louis, MI, USA) were used as the modifying agent and the silica precursor, respectively, for
 196 the functionalisation step. The activated and functionalised PVDF-Ds were denoted as
 197 Act_PVDF-Ds and Fun_PVDF-Ds, respectively, and their properties are shown in Table 1.

198

199 **2.3. Analysis methods**

200 The membrane surface hydrophobicity was evaluated by means of the measurement of the static
 201 water contact angle (WCA, °) with a goniometer (OCA25, DataPhysics, Filderstadt, Germany),
 202 following the sessile drop technique [39] in which a water droplet of 5 μL was placed onto the
 203 membrane surface at room temperature. An image of the water droplet was taken at 3 s and the

204 WCA was determined with the SCA20 software (DataPhysics, Filderstadt, Germany). The
205 WCA was evaluated at different surface locations on the membrane and a mean value was
206 obtained from at least five measurements, using the standard deviation as a measure of the
207 associated error.

208 The overall porosity (ϵ , %) of the membranes was gravimetrically measured with 1-octanol
209 (99%, Acros Organics, Geel, Belgium), and the procedure can be found elsewhere [40,41].
210 Briefly, 2x2 cm samples were weighed and immersed in vials with 10 mL of 1-octanol. The
211 vials were kept in an orbital shaker for 2 hours at room temperature. Finally, the membranes
212 samples were surface dried with absorbent paper and weighed. At least five samples of each
213 membrane were analysed.

214 The liquid entry pressure (LEP, bar) of the membranes was evaluated using the same
215 experimental setup detailed previously for the crystallisation tests. A membrane sample was
216 placed inside the FM, the outlet port of the retentate side was kept closed, and the ports of the
217 permeate side were opened to the atmosphere. Deionised water was pumped inside the retentate
218 side at a flow rate of $\sim 5 \text{ mL min}^{-1}$ in order to increase the pressure slowly and gradually, and
219 the membrane surface of the permeate side was continuously monitored with the digital
220 microscope. The pressure at which the first drop appeared on the membrane surface was
221 established as the LEP. At least five measurements were conducted for each membrane.

222 Membrane roughness was determined by atomic force microscopy (AFM) in tapping mode
223 (Digital Instruments, Dimension 3100 SPM with Nanoscope V controller, Veeco Instruments,
224 Inc., NY, USA), using AFM probes with a force constant and length of 42 N/m and 125 μm ,
225 respectively (PPP-NCHR, NanosensorsTM, Neuchatel, Switzerland). Images of the membrane
226 topography were taken with a size scan of 25x25 μm , and Gwyddion data analysis software
227 (Department of Nanometrology, Czech Metrology Institute, Brno, Czech Republic) was used

228 for image processing and determination of the root mean square roughness (R_q , nm). A mean
229 value of R_q was determined in at least three different locations of the surface.

230 Crystal size and shape was analysed by field emission scanning electron microscopy (FESEM)
231 at an accelerating voltage of 10 kV (Tescan Vega 4, Tescan Orsay Holding, a.s., Kohoutovice,
232 Czech Republic). The microscope was equipped with an energy dispersive x-ray (EDX)
233 spectrometer, which was used for the atomic content determination of different elements. For
234 image acquisition, the filter samples with the collected crystals were previously placed on a
235 metal holder and then coated with a fine layer of Au. The mean crystal size was obtained by
236 measuring the diameter of at least 300 particles from three FESEM images with the
237 abovementioned ImageJ software.

238 X-ray diffraction (XRD) analysis was carried out for the identification of crystalline phases in
239 the solid particles formed in the crystallisation tests. The diffractograms were obtained with an
240 XRD system (AXS D8 ADVANCE A25, Bruker, MA, USA) and the patterns were processed
241 with QualX2.0 software (Software IC, Institute of Crystallography – CNR, Bari, Italy).

242

243 **2.4. Crystallisation kinetic analysis**

244 Nucleation kinetics were characterised for vivianite, assuming that only primary nucleation was
245 of relevance due to the low solubility of vivianite [42]. The nucleation rate of vivianite
246 expressed in mass basis (r , $\text{mg L}^{-1} \text{min}^{-1}$) was assumed to be the supersaturation rate at the bulk
247 induction time [43]:

$$248 \quad r = \frac{C_{\text{viv}}^{\text{ind}}}{t^{\text{ind}}} M_{\text{viv}} \quad (2)$$

249 where $C_{\text{viv}}^{\text{ind}}$ (M) is the mean concentration of vivianite inside the FM at bulk induction time
250 (t^{ind} , min), and M_{viv} is the molar mass of vivianite ($501610 \text{ mg mol}^{-1}$). For the estimation of

251 $C_{\text{viv}}^{\text{ind}}$, a complete reaction between Fe^{2+} and PO_4^{3-} towards vivianite, and no secondary
252 reactions were assumed (mass balance shown in supplementary material S3).

253 The empirical power-law relationship between the nucleation rate and supersaturation (S)
254 developed by Sangwal (2009) [44] was used to determine whether the primary nucleation
255 kinetic inside the FM was in accordance with the classical nucleation theory (CNT) principles
256 [44]:

$$257 \quad r = k(\ln S_m^{\text{ind}})^m \quad (3)$$

258 where m is the so-called the apparent nucleation order, k is the nucleation constant related with
259 the number of stable nuclei forming per unit volume per unit time, and S_m^{ind} is the
260 supersaturation of the vivianite inside the FM at bulk induction time calculated as follows:

$$261 \quad S_m^{\text{ind}} = \frac{C_{\text{viv}}^{\text{ind}}}{C_{\text{viv}}^*} \quad (4)$$

262 where C_{viv}^* is the solubility of the vivianite calculated from the K_{sp} ($C_{\text{viv}}^* = 3.47 \cdot 10^{-9}$ M from
263 a $K_{\text{sp}} = 1.82 \cdot 10^{-41}$ at 25°C [9]). The linearization of Sangwal's power-law yields:

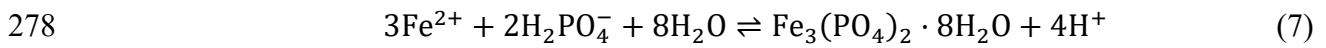
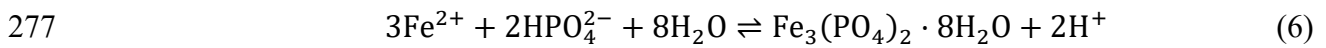
$$264 \quad \ln(r) = \ln(k) + m \cdot \ln(\ln(S_m^{\text{ind}})) \quad (5)$$

265 **3. Results and discussion**

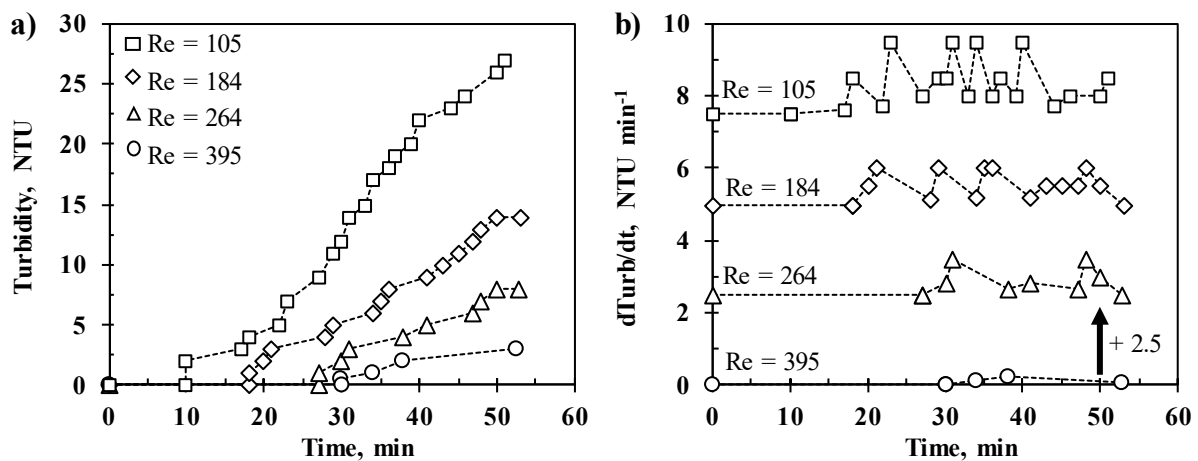
266 **3.1. Effect of hydrodynamic conditions in the vivianite crystallisation**

267 Crystallisation tests were conducted with the PVDF-St membrane at different Re to evaluate
268 the role of the boundary layer in modifying the nucleation rate of vivianite. The turbidity of the
269 phosphate/permeate solution always kept in 0 until the bulk induction time was reached, and
270 then the turbidity started to increase with the operation time (Figure 2a), indicating a continuous

271 crystallisation in the bulk of the phosphate/permeate solution. According to the simulations
272 carried out with Visual MINTEQ for the system used in this work, the Fe and P were initially
273 in the form of Fe^{2+} , HPO_4^{2-} and H_2PO_4^- . Moreover, the speciation of the Fe and P were in
274 accordance with those reported by other authors [9,14]. Thus, the chemical reactions involved
275 in the current system for a pH of 7 were presumed to lead mainly to the formation of vivianite
276 (Eq. 6 and 7) [9,14].



279 Turbidity evidenced the onset of nucleation (bulk induction time). The time at which turbidity
280 commenced was delayed when Re was increased from 105 to 395 (Figure 2a). Following
281 nucleation, the turbidity continued to increase, reaching a maximum value of 27 ± 4 NTU at Re
282 105. In comparison, a lower final turbidity of 4 ± 1 NTU was obtained in the test conducted at
283 the highest Re of 395. This indicates that nucleation rate could be increased through modifying
284 process hydrodynamics. We suggest this is due to the reduction in Fe^{2+} reactant concentration
285 within the boundary layer as the liquid velocity increased, which will encourage back transport
286 into the bulk solution.



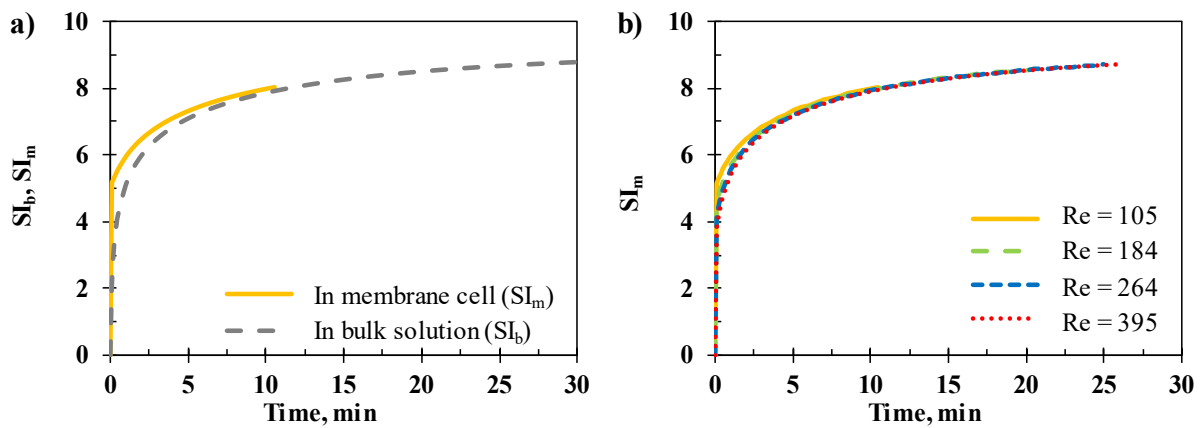
287

288 *Figure 2. a) Representative turbidity profiles and b) their derivatives of the turbidity with*
 289 *respect to the time (dTurb/dt) of the phosphate/permeate solution with the time of the*
 290 *crystallisation test with PVDF-St membrane at different Reynold numbers inside the membrane*
 291 *module (Re).*

292 The turbidity profiles presented a stepped tendency from the bulk induction time until the end
 293 of the crystallisation test (Figure 2a). In order to elucidate this tendency, a differential analysis
 294 of the turbidity profiles was conducted, in which the derivative of the turbidity with respect to
 295 time (dTurb/dt) were calculated by regressive differences, and this derivative represented the
 296 nucleation rate (Figure 2b). The obtained dTurb/dt curves evidenced the stepped tendency of
 297 the profiles, showing a periodical increase in the nucleation rate in form of peaks followed by
 298 a decline. These peaks may indicate exceedance of the primary nucleation threshold, where
 299 sufficient supersaturation has been achieved to overcome the energy barrier to create formation
 300 of a new crystal phase. The frequency and height of the peaks were greater as *Re* decreased,
 301 indicating higher overall nucleation rates and a greater frequency of new nucleation events.

302 At the outset of dosing, the SI increased rapidly due to the injection of new reactant (Figure 3).
 303 Within this initial phase, the estimated SI of vivianite was slightly higher in the membrane
 304 module compared to the bulk solution, but became comparable following the progressive

305 addition of injection volume which gradually diluted P in the system (Figure 3a). A similar
306 observation was made when modifying Re , where the concentration within the membrane was
307 slightly elevated at the lowest Re but tends toward an equivalent value independent of Re
308 following the continued addition of reactant (Figure 3b). The negligible influence of Re in
309 estimated SI may be attributed to the low solubility of vivianite, since sparingly soluble
310 substances reach high supersaturation levels very quickly [42]. However, two aspects should
311 be considered: (i) the SI values were estimated based on mean concentration mass balances,
312 and so do not take into consideration the relative ratio of the shear component to the diffusivity
313 for mass transfer occurring within the boundary layer, which will be modified by Re and could
314 lead to relatively higher local supersaturation, which would increase the nucleation rate [20];
315 and (ii) the high level of micromixing provided by the porous membrane [30,33] may enhance
316 the mass transfer of the reactants at molecular level and add turbulence in the boundary layer
317 [45]. These phenomena could increase the collision frequency of the reactive ions, lowering the
318 activation energy for nucleation [16,17]. Thus, longer residence times at low Re would increase
319 the probability for mixing and ion collision inside the membrane module, accelerating the
320 nucleation especially for sparingly soluble salts due to their low ion densities. The higher local
321 supersaturation and ion collision probability at lower Re was in agreement with the
322 experimental results (Figure 2). Thus, the integration of the membrane technology in a
323 crystallisation process was demonstrated to allow the control of the nucleation by setting the
324 hydrodynamic conditions.

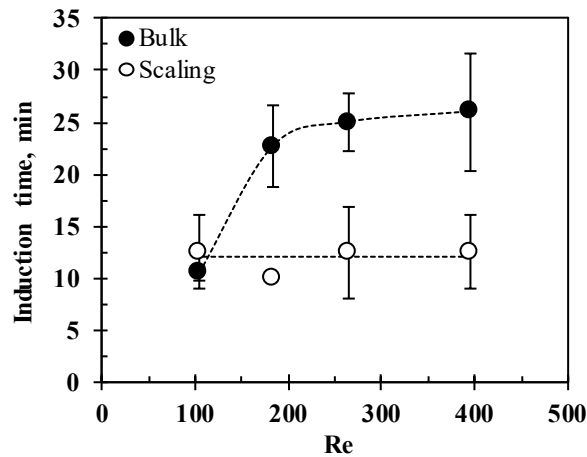


325

326 *Figure 3. a) Supersaturation index (SI) estimated inside the bulk phosphate/permeate solution*
 327 *(SI_b) and inside the membrane module (SI_m) with the time of crystallisation test at a Reynold*
 328 *(Re) of 105. b) SI_m with the time of crystallisation test at different Re. SI_m was estimated until*
 329 *the bulk induction time at each Re.*

330 The induction time is defined as the time difference between the solution achieving a saturated
 331 state ($SI = 0$, or $C/C^* = 1$) and the time in which the solid particles were detected for first time
 332 in the phosphate/permeate solution (bulk induction time) and in the membrane surface (scaling
 333 induction time). The induction time therefore represents the time in which the crystallising
 334 system is in a metastable state, and according to CNT is inversely proportional to the nucleation
 335 rate [43,44,46]. The bulk induction time increased markedly from 10.5 ± 0.7 min ($SI_m \approx 7.9$) to
 336 22.7 ± 4.0 min ($SI_m \approx 8.6$) at a Re of 105 and 184, respectively, for the crystallisation tests
 337 carried out with the PVDF-St membrane (Figure 4), whereas an apparent plateau was achieved
 338 in induction for $Re \geq 184$ with values of around 25 min ($SI_m \approx 8.7$). Shorter induction times
 339 corresponded to higher turbidity increase within the phosphate/permeate solution (Figure 2a).
 340 Therefore, higher nucleation rates were inferred for lower SI which did not agree with the CNT.
 341 Hence, these results suggested that the local supersaturation, mixing effect and/or the
 342 probability of ion collision could be especially favoured at the lowest Re , rising the nucleation
 343 rate.

344



345

346 *Figure 4. Bulk and scaling induction time versus Reynold number (Re) in the permeate side of*
347 *the membrane module for crystallisation tests with PVDF-St. Error bars denotes the standard*
348 *deviations.*

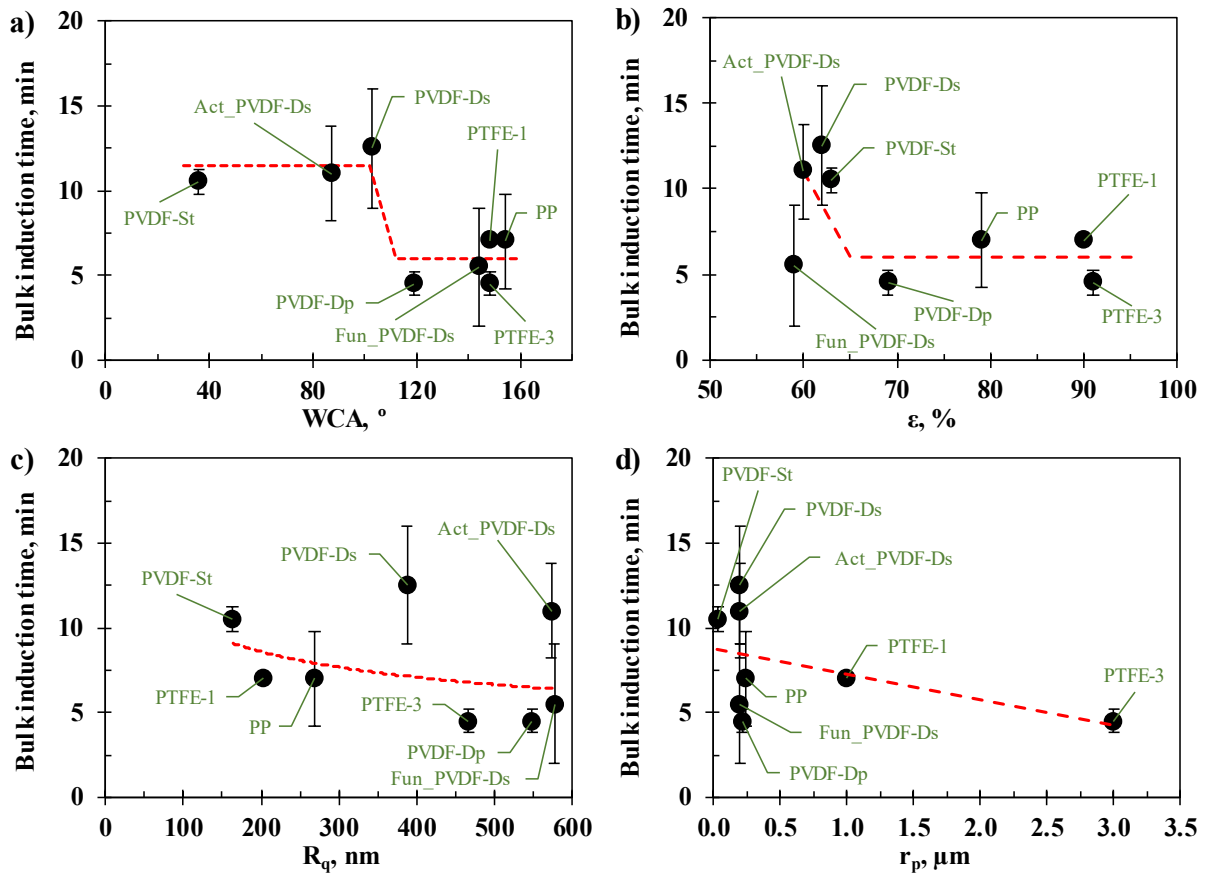
349 To elucidate the potential mechanisms for vivianite crystallisation, scaling induction time was
350 also determined for the crystallisation tests using PVDF-St membrane at different *Re* (Figure
351 4). An example of image processing for scaling analysis can be found in supplementary material
352 S4. The scaling induction time was always in mean values around 12 min, independently of the
353 *Re*, which may indicate that scaling was more closely controlled by dose rate, dose
354 concentration and/or membrane properties, as these were fixed for each condition. Scaling
355 seemingly occurred before bulk nucleation, suggesting that scaling is likely to be dominated by
356 deposition rather than through adhesive growth and can therefore be controlled through
357 hydrodynamics and system orientation (i.e. vertical alignment to avoid sedimentation).

358

359 **3.2. Effect of the membrane material and properties**

360 Membrane materials of different properties were evaluated to determine their role in lowering
361 the free energy requirement of nucleation, and/or their role in modifying local mixing

362 conditions to shorten induction time. In this work, the supersaturation rate was fixed in the
363 crystallisation tests, unlike previous research that have looked at these properties such as in
364 membrane distillation or osmotic crystallisation, in which the flux (and hence supersaturation
365 rate) was modified as a function of the membrane properties, making it difficult to provide an
366 independent assessment of the relative role of material properties. In order to elucidate the
367 individual effect of each membrane property, Re was fixed to 105, and the induction time was
368 plotted against the WCA, R_q , r_p and ε (Figure 5). The bulk induction time was in values of
369 around 12 min for a WCA ranging from 36° to 103° , and then the induction time suddenly
370 declined to values around 6 min for a WCA from 119° to 154° (Figure 5a). This result suggested
371 that the WCA range from 103° to 119° marked a transition zone in which the kinetic and
372 thermodynamic behaviour of the vivianite nucleation changed, leading to higher nucleation
373 rates when membranes with a WCA higher than 119° were used. A similar behaviour was
374 observed with the membrane porosity, in which values between 60 and 65% led to induction
375 times ≈ 10 min, whilst higher ε values ($> 65\%$) lowered the induction times to values of around
376 6 min (Figure 5b).



377

378 *Figure 5. Bulk induction time in the crystallisation tests versus membrane a) water contact*
 379 *angle (WCA), b) porosity (ϵ), c) root mean square roughness (R_q), and d) pore size (r_p), at a*
 380 *Reynold of 105. Membrane nomenclature as in Table 1.*

381 In general terms, the bulk induction time tended to decrease with membrane roughness and pore
 382 size (Figure 5c and d). However, the PVDF-Ds and Act_PVDF-Ds membranes with a R_q of
 383 387 and 573 nm, respectively, were out of the tendency, showing an induction time of ~ 12 min
 384 (Figure 5c) likely due to the lower WCA ($\leq 103^\circ$). Regarding the pore size, this tendency was
 385 not observed in membranes with a r_p of $\sim 0.2 \mu\text{m}$ which led to induction times between 4.5 and
 386 12.5 min (Figure 5d), likely due to the conflation of different properties. These results suggest
 387 that membrane roughness and pore size present a smaller effect on encouraging nucleation than
 388 other properties such as WCA and porosity. While this analysis indicates that nucleation
 389 kinetics can be modified using membrane properties, this may be occurred due to symbiotic

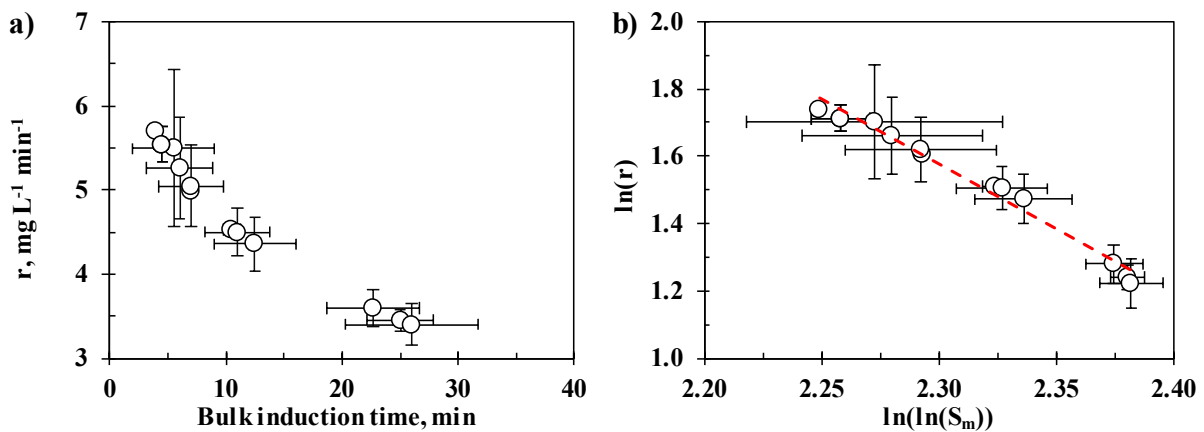
390 effects. For example, although micromixing may be enhanced by single properties such as
391 porosity, multiple converging factors (e.g. WCA, R_q and r_p) will likely define local fluid
392 velocities and mixing patterns, that can serve to lower the activation energy requirement for
393 nucleation.

394 The influence of membrane properties in conditioning induction time can also be ascribed to
395 the critical surface free energy requirement for nucleation. The presence of a solid substrate
396 (membrane) decreases the interfacial free energy, which also leads to a reduction of the
397 nucleation energy barrier [47]. Therefore, the membrane surface can promote the heterogeneous
398 nucleation, allowing the crystallisation onset at lower supersaturation ratios than in the
399 homogeneous case [19,22]. However, there is a lack of models in the literature which consider
400 the different membrane properties in modifying the nucleation energy barrier. While instructive
401 for membrane design, the most common model which relates membrane hydrophobicity and
402 porosity to the preferential heterogeneous nucleation [21,48–50] cannot provide a unified
403 perspective on the probability for heterogeneous nucleation on porous surfaces (model shown
404 and discussed in supplementary material S5). This may be due to competing factors in material
405 design, that can similarly modify Gibbs free energy requirement for nucleation through
406 competing mechanisms (e.g. solute entrapment) [19]. There is also recognition that despite the
407 high interfacial energy requirement of sparingly soluble salts setting a high surface free energy
408 requirement for nucleation, the supersaturation (volumetric free energy) requirement to create
409 the critical nucleus is sufficiently high for primary nucleation to proceed via a homogeneous
410 mechanism that is therefore less dependent on membrane properties [42].

411

412 3.3. Crystallisation kinetic inside the membrane module

413 The power-law model proposed by Sangwal [44] was used to relate how membrane parameters
414 and flow conditions inform nucleation kinetics based on CNT, where the supersaturation rate
415 is an analogy to the primary nucleation rate (r) at induction. Higher primary nucleation rates
416 were identified at shorter induction times, in which r increased from 3.40 to 5.69 $\text{mg L}^{-1} \text{min}^{-1}$
417 as the bulk induction time decreased from 26.0 to 4.0 min (Figure 6a). This is in accordance
418 with CNT, where the longer induction times corresponded with the lower turbidity data that
419 was experimentally observed (Figure 2a). Higher nucleation rates are ordinarily facilitated
420 within a region of elevated supersaturation (wider metastable zone width). However, in this
421 study, higher nucleation rates were associated to a lower vivianite supersaturation at induction
422 (Figure 6b). This can be explained by an ion-dependent collision mechanism in which the
423 higher supersaturation rates promote greater mixing and a higher ion collision probability to
424 reduce the activation energy requirement for nucleation.



425

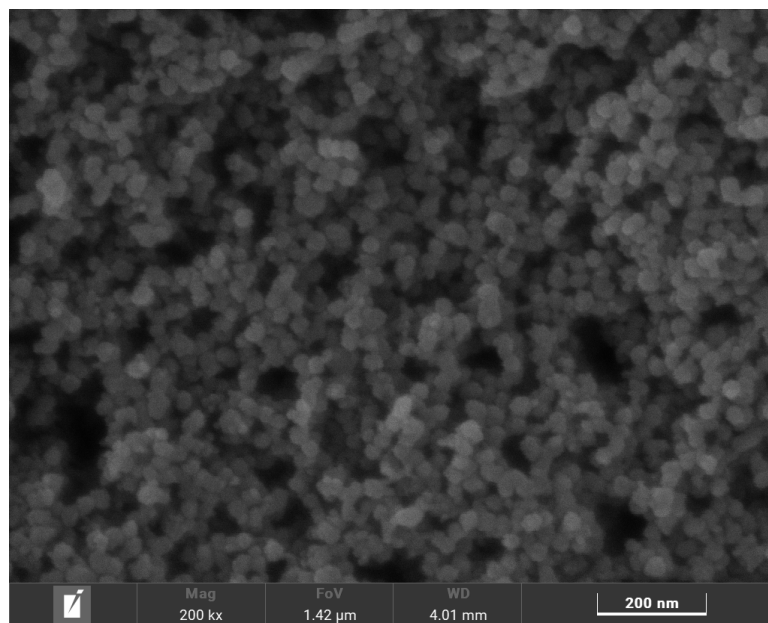
426 *Figure 6. a) Nucleation rate (r) versus bulk induction time, and b) Sangwal's power law*
427 *relationship between nucleation rate and supersaturation level inside the membrane module*
428 *(S_m) at the bulk induction time. All the crystallisation tests under the different operational*
429 *conditions and membranes has been included in the graphs.*

430 A fairly linear tendency was observed (R^2 , 0.98) between the supersaturation achieved and
431 supersaturation rate that was set either by a modification of Re (105-395) or discrete changes
432 to membrane properties at a fixed Re 105 (Eq. 5) (Figure 6b). The kinetic parameters of the
433 model m and k showed values of -3.848 and 33691 $\text{mg L}^{-1} \text{min}^{-1}$, respectively, for this system.
434 The low value of the apparent nucleation order m indicates a low energy barrier for formation
435 of stable nuclei [44] which could result from the high micromixing in the boundary layer,
436 complemented by the *relatively* high supersaturation achieved for vivianite induction. The
437 nucleation kinetics therefore conform more closely to a diffusion-dependent rather than a
438 supersaturation-dependent nucleation mechanism, which has been previously recognised for
439 sparingly soluble reactive salts [16,17]. The correlated kinetic response of nucleation to system
440 modifications by membrane properties and hydrodynamics emphasise the extent to which the
441 reaction zone within MARC may offer control over nucleation, and could be further regulated
442 through adjustments in dosing rate and dose concentration to broaden the range of
443 supersaturation trajectories that could be delivered.

444 **3.4. Characterisation of the vivianite particles**

445 The solid particles formed during the crystallisation tests were collected from the
446 phosphate/permeate solution and analysed by microscopy and spectroscopy to determine their
447 morphology, particle size and composition. Nanoparticles were always observed with a
448 spherical and a smooth shape and no conglomerates were observed in any of the crystallisation
449 tests (Figure 7). The presence of nanoparticles and their glassy-like form (showing no faces) is
450 ascribed to very fast nucleation rates within regions of high *relative* supersaturation [51]. The
451 particle size distribution was very narrow with mean particle sizes ranging from 29 to 44 nm
452 and standard deviations lower than 10 nm (Table 2). Hence, the vivianite crystallisation
453 mechanism in the bulk solution was independent of the membrane properties and hydraulic

454 conditions tested. In sparingly soluble systems, high nucleation rates quickly consume the
455 available ions within solution, resulting in a high number of small crystals, and since the ions
456 are diffuse and the supersaturation is consumed by the production of new nuclei, crystal growth
457 is limited. The consistency in particle size may be due to the confined length of the reaction
458 zone in the membrane where the supersaturation is consumed particularly quickly, and the Fe^{2+}
459 dosing was consistently applied. Increasing Fe^{2+} dose would assure non-limiting reaction
460 conditions within the boundary layer, while a longer reaction zone (longer membrane) can
461 supply a greater degree of supersaturation with an extended residence time to encourage growth
462 of newly formed nuclei. Importantly, this study also demonstrates how membrane
463 crystallisation can be applied for the consistent formation of nanocrystals with a tight crystal
464 size distribution which is important for a range of critical applications, such as the production
465 of long acting injectable medicines, through stricter control over nucleation [19,30,35].



467 *Figure 7. FESEM images of the solid particles collected from the phosphate/permeate solution*
468 *at the end of the crystallisation tests at a Reynolds of 105.*

469 Table 2. Mean particle size of the solid particles collected at the end of the crystallisation tests
 470 with different membranes and at different Reynolds (Re). The error denotes the standard
 471 deviation of the mean particle size distribution.

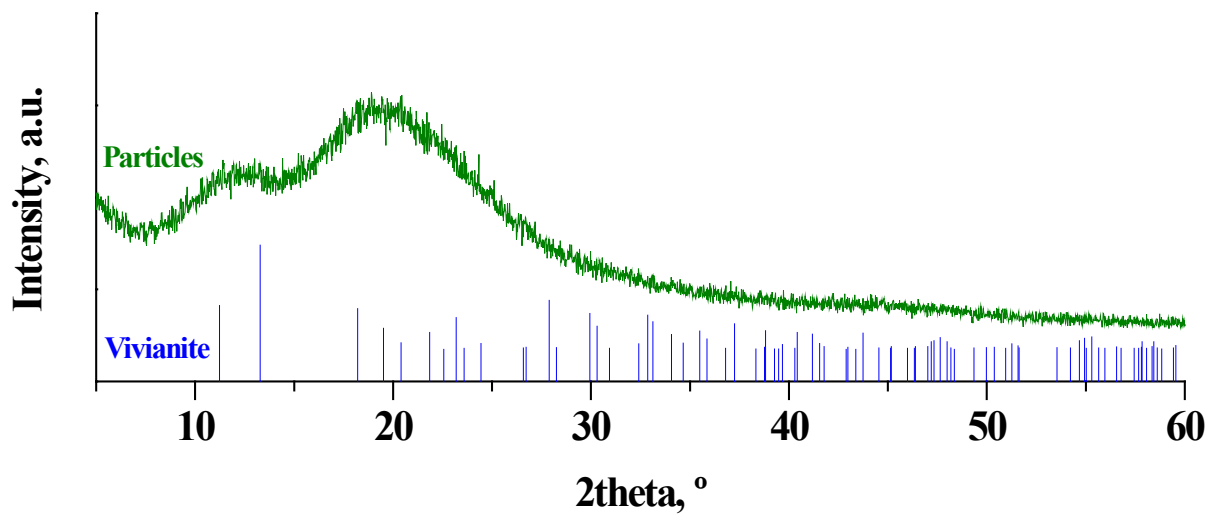
<i>With different membranes at $Re = 105$</i>	
Membrane	Mean particle size, nm
PVDF-St	43 ± 9
Act_PVDF-Ds	34 ± 8
PVDF-Ds	35 ± 8
PVDF-Dp	30 ± 7
Fun_PVDF-Ds	36 ± 10
PTFE-1 μm	29 ± 8
PTFE-3 μm	29 ± 8
PP-2E	29 ± 7

<i>With PVDF-St at different Re</i>	
Re	Mean particle size, nm
105	43 ± 9
184	39 ± 9
264	44 ± 10
395	31 ± 7

472

473 The composition of the collected particles was analysed by EDX, and Fe:P atomic ratio values
 474 ranging from 1.9 to 3.3 were obtained, with no appreciable tendencies between the different
 475 operational conditions. The Fe:P atomic ratio for pure vivianite is 1.5, which was the set
 476 condition for performing the crystallisation tests. The obtained higher ratios indicated a higher
 477 presence of Fe compounds different from vivianite, likely attributed to OH^- -bound in form of
 478 iron hydroxides [1,2,9,14]. The XRD pattern of the collected particles did not show crystalline
 479 peaks (Figure 8), which suggested the presence of oxidised and poorly crystalline forms of
 480 vivianite, such as santabarbaraite ($\text{Fe}_3^{3+}(\text{PO}_4)_2(\text{OH})_3 \cdot 5\text{H}_2\text{O}$), lipscombite
 481 ($\text{Fe}^{2+}\text{Fe}_2^{3+}(\text{PO}_4)_2(\text{OH})_2$), and strengite ($\text{FePO}_4 \cdot 2\text{H}_2\text{O}$) [5,52]. While further work is required, we
 482 suggest the crystallinity may be further modified through local adjustments of reactants and
 483 reaction rate. The colour of the collected particles in this work was of yellowish-brown hue
 484 (supplementary material S6) which could be related to the presence of iron hydroxides and

485 santabarbarite [6,52]. For the conditions examined, we therefore suggest that the MARC led
486 to formation of amorphous vivianite-based particles and iron hydroxides. While the effective
487 removal of phosphorous through this crystallisation pathway is compelling, further research on
488 vivianite recovery is warranted to avoid the consumption of Fe^{2+} reactant in secondary
489 reactions, particularly if it is the purity and crystallinity of the recovered vivianite that is critical
490 to its downstream application.



491
492 *Figure 8. XRD diffractogram of the collected solid particles from the crystallisation tests and*
493 *reference peaks of pure vivianite from [4]. Intensity expressed in arbitrary units (a.u.).*

494

495 **4. Conclusions**

496 The membrane-assisted reactive crystallisation has been demonstrated as a useful approach for
497 controlling and modifying nucleation processes, unlike conventional stirred tank crystallisers
498 where the poor mixing levels lead to overdosing of reactant and heterogeneous crystal product
499 quality. Thus, a membrane crystallisation process has been introduced to enable the vivianite
500 crystallisation for phosphorous recovery from a liquid effluent by the dosing of an iron (II)

501 solution. The nucleation process was continuously monitored based on the turbidity of the
502 solution which allowed the direct determination of induction time as well as provided useful
503 information regarding nucleation rate. Lower induction times were obtained at lower liquid
504 velocities, leading to higher nucleation rates. Thus, crystal nucleation was strongly influenced
505 by the boundary layer in the interphase membrane-liquid, therefore, the nucleation could be
506 controlled by the hydrodynamic conditions inside the membrane module. In addition, the
507 integration of a porous membrane in the vivianite crystallisation process facilitated the
508 micromixing of the reactants and lowered the energy barrier for nucleation. Therefore, the
509 nucleation could also be controlled by selecting the appropriate membrane properties, in which
510 the induction time tended to decrease as the membrane hydrophobicity, roughness, pore size,
511 and porosity increased.

512 Finally, the nucleation kinetic was modelled using the Sangwal's power law based on the
513 classical nucleation theory. This kinetic analysis showed that higher nucleation rates were
514 associated to a lower vivianite supersaturation which was attributed to an ion-dependent
515 collision mechanism in that the higher supersaturation rates promote greater mixing and a
516 higher ion collision probability, reducing the activation energy requirement for nucleation even
517 at low supersaturation degrees. Hence, the nucleation rate was related to the boundary layer and
518 mixing conditions, which allows a strict control of the nucleation as a function of the operational
519 condition set.

520 This work represents the first integration of membrane technology in phosphorous recovery
521 from liquid effluents in form of vivianite which has been demonstrated to be a practical
522 approach for controlling vivianite crystallisation. Thus, a membrane-assisted reactive
523 crystallisation can ease the prospect of phosphorous recovery in vivianite to realise benefits to

524 cost and yield at large-scale processes, while also taking advantage of downstream value due
525 to a homogeneous quality of crystals.

526 **Funding**

527 This research was funded by European Research Council Starting Grant “*Sustainable Chemical*
528 *Alternatives for Reuse in the Circular Economy* (SCARCE, ERC StG #714080). PhD grant of
529 R. Jiménez-Robles was funded by Ministerio de Universidades, Spain (Beca de Formación de
530 Profesorado Universitario FPU19/02478). The research stay of R. Jiménez-Robles at Cranfield
531 University was funded by Ministerio de Educación y Formación Profesional, Spain (Ayudas
532 Complementarias para Estancias Breves y Traslados Temporales EST22/00167).

533 **Acknowledgements**

534 **Author contributions**

535 R. Jiménez-Robles: Methodology, Validation, Formal analysis, Investigation, Resources, Data
536 curation, Writing - original draft, Writing - review & editing, Visualization. V. Martínez-Soria:
537 Writing - review & editing, Supervision. M. Izquierdo: Writing - review & editing, Supervision.
538 Lo-I Chen: Methodology, Resources. K. Le Corre Pidou: Writing - review & editing. E.J.
539 McAdam: Conceptualization, Methodology, Validation, Writing - review & editing,
540 Supervision, Project administration, Funding acquisition.

541 **Conflicts of interest**

542 The authors declare that they have no known competing financial interests or personal
543 relationships that could have appeared to influence the work reported in this paper.

544 **References**

- 545 [1] J. Zhang, Z. Chen, Y. Liu, W. Wei, B.J. Ni, Phosphorus recovery from wastewater and
546 sewage sludge as vivianite, *J. Clean. Prod.* 370 (2022) 133439.
547 <https://doi.org/10.1016/j.jclepro.2022.133439>.
- 548 [2] Y. Wu, J. Luo, Q. Zhang, M. Aleem, F. Fang, Z. Xue, J. Cao, Potentials and challenges
549 of phosphorus recovery as vivianite from wastewater: A review, *Chemosphere*. 226
550 (2019) 246–258. <https://doi.org/10.1016/j.chemosphere.2019.03.138>.
- 551 [3] M. Nanzyo, H. Onodera, E. Hasegawa, K. Ito, H. Kanno, Formation and Dissolution of
552 Vivianite in Paddy Field Soil, *Soil Sci. Soc. Am. J.* 77 (2013) 1452–1459.
553 <https://doi.org/10.2136/sssaj2012.0437n>.
- 554 [4] M. Rothe, T. Frederichs, M. Eder, A. Kleeberg, M. Hupfer, Evidence for vivianite
555 formation and its contribution to long-term phosphorus retention in a recent lake
556 sediment: A novel analytical approach, *Biogeosciences*. 11 (2014) 5169–5180.
557 <https://doi.org/10.5194/bg-11-5169-2014>.
- 558 [5] M. Rothe, A. Kleeberg, M. Hupfer, The occurrence, identification and environmental
559 relevance of vivianite in waterlogged soils and aquatic sediments, *Earth-Science Rev.*
560 158 (2016) 51–64. <https://doi.org/10.1016/j.earscirev.2016.04.008>.
- 561 [6] R. Priambodo, Y.J. Shih, Y.H. Huang, Phosphorus recovery as ferrous phosphate
562 (vivianite) from wastewater produced in manufacture of thin film transistor-liquid crystal
563 displays (TFT-LCD) by a fluidized bed crystallizer (FBC), *RSC Adv.* 7 (2017) 40819–
564 40828. <https://doi.org/10.1039/c7ra06308c>.
- 565 [7] G. Simoni, B.S. Kirkebaek, C.A. Quist-Jensen, M.L. Christensen, A. Ali, A comparison

- 566 of vacuum and direct contact membrane distillation for phosphorus and ammonia
567 recovery from wastewater, *J. Water Process Eng.* 44 (2021) 102350.
568 <https://doi.org/10.1016/j.jwpe.2021.102350>.
- 569 [8] C.A. Quist-Jensen, A. Ali, S. Mondal, F. Macedonio, E. Drioli, A study of membrane
570 distillation and crystallization for lithium recovery from high-concentrated aqueous
571 solutions, *J. Membr. Sci.* 505 (2016) 167–173.
572 <https://doi.org/10.1016/j.memsci.2016.01.033>.
- 573 [9] J. Liu, X. Cheng, X. Qi, N. Li, J. Tian, B. Qiu, K. Xu, D. Qu, Recovery of phosphate
574 from aqueous solutions via vivianite crystallization: Thermodynamics and influence of
575 pH, *Chem. Eng. J.* 349 (2018) 37–46. <https://doi.org/10.1016/j.cej.2018.05.064>.
- 576 [10] C.A. Quist-Jensen, J.M. Sørensen, A. Svenstrup, L. Scarpa, T.S. Carlsen, H.C. Jensen,
577 L. Wybrandt, M.L. Christensen, Membrane crystallization for phosphorus recovery and
578 ammonia stripping from reject water from sludge dewatering process, *Desalination.* 440
579 (2018) 156–160. <https://doi.org/10.1016/j.desal.2017.11.034>.
- 580 [11] C.A. Quist-Jensen, M.K. Jørgensen, M.L. Christensen, Treated seawater as a magnesium
581 source for phosphorous recovery from wastewater—A feasibility and cost analysis,
582 *Membranes (Basel).* 6 (2016). <https://doi.org/10.3390/membranes6040054>.
- 583 [12] F. Rizzioli, D. Bertasini, D. Bolzonella, N. Frison, F. Battista, A critical review on the
584 techno-economic feasibility of nutrients recovery from anaerobic digestate in the
585 agricultural sector, *Sep. Purif. Technol.* 306 (2023) 122690.
586 <https://doi.org/10.1016/j.seppur.2022.122690>.
- 587 [13] Ordinance on the reorganisation of sewage sludge recycling, Federal Law Gazette of
588 Germany, Part I, No. 65, Vol 27, September 2017. Available online:

- 589 [https://www.bgbl.de/xaver/bgbl/start.xav?startbk=Bundesanzeiger_BGBI&jumpTo=bg](https://www.bgbl.de/xaver/bgbl/start.xav?startbk=Bundesanzeiger_BGBI&jumpTo=bgbl117s3465.pdf#__bgbl__%2F%2F)
590 [bl117s3465.pdf#__bgbl__%2F%2F](https://www.bgbl.de/xaver/bgbl/start.xav?startbk=Bundesanzeiger_BGBI&jumpTo=bgbl117s3465.pdf#__bgbl__%2F%2F), (n.d.).
- 591 [14] R. Goedhart, S. Müller, M.C.M. van Loosdrecht, D. van Halem, Vivianite precipitation
592 for iron recovery from anaerobic groundwater, *Water Res.* 217 (2022) 118345.
593 <https://doi.org/10.1016/j.watres.2022.118345>.
- 594 [15] E. Frossard, J.P. Bauer, F. Lothe, Evidence of vivianite in FeSO₄ - Flocculated sludges,
595 *Water Res.* 31 (1997) 2449–2454. [https://doi.org/10.1016/S0043-1354\(97\)00101-2](https://doi.org/10.1016/S0043-1354(97)00101-2).
- 596 [16] X. Dou, H. Huang, X. Wang, Q. Lin, J. Li, Y. Zhang, Y. Han, Collision dependent silver
597 nucleation regulated by chemical diffusion and reaction, *Chem. Eng. Sci.* 262 (2022)
598 117965. <https://doi.org/10.1016/j.ces.2022.117965>.
- 599 [17] X. Dou, H. Huang, Y. Han, The role of diffusion in the nucleation of calcium carbonate,
600 *Chinese J. Chem. Eng.* 43 (2022) 275–281. <https://doi.org/10.1016/j.cjche.2021.03.039>.
- 601 [18] R. Kieffer, D. Mangin, F. Puel, C. Charcosset, Precipitation of barium sulphate in a
602 hollow fiber membrane contactor: Part II The influence of process parameters, *Chem.*
603 *Eng. Sci.* 64 (2009) 1885–1891. <https://doi.org/10.1016/j.ces.2009.01.013>.
- 604 [19] E. Chabanon, D. Mangin, C. Charcosset, Membranes and crystallization processes: State
605 of the art and prospects, *J. Membr. Sci.* 509 (2016) 57–67.
606 <https://doi.org/10.1016/j.memsci.2016.02.051>.
- 607 [20] G. Di Profio, E. Curcio, E. Drioli, Supersaturation control and heterogeneous nucleation
608 in membrane crystallizers: Facts and perspectives, *Ind. Eng. Chem. Res.* 49 (2010)
609 11878–11889. <https://doi.org/10.1021/ie100418z>.
- 610 [21] S. Bavarella, M. Hermassi, A. Brookes, A. Moore, P. Vale, G. Di Profio, E. Curcio, P.

- 611 Hart, M. Pidou, E.J. McAdam, Is Chemically Reactive Membrane Crystallization
612 Facilitated by Heterogeneous Primary Nucleation? Comparison with Conventional Gas-
613 Liquid Crystallization for Ammonium Bicarbonate Precipitation in a CO₂-NH₃-H₂O
614 System, *Cryst. Growth Des.* 20 (2020) 1552–1564.
615 <https://doi.org/10.1021/acs.cgd.9b01276>.
- 616 [22] E. Drioli, G. Di Profio, Curcio Efrem, *Membrane-Assisted Crystallization Technology*,
617 World Scientific, London, 2015. https://doi.org/10.1142/9781783263325_0001.
- 618 [23] R. Klaassen, P.H.M. Feron, A.E. Jansen, Membrane contactors in industrial applications,
619 *Chem. Eng. Res. Des.* 83 (2005) 234–246. <https://doi.org/10.1205/cherd.04196>.
- 620 [24] J. Kuhn, R. Lakerveld, H.J.M. Kramer, J. Grievink, P.J. Jansens, Characterization and
621 dynamic optimization of membrane-assisted crystallization of adipic acid, *Ind. Eng.*
622 *Chem. Res.* 48 (2009) 5360–5369. <https://doi.org/10.1021/ie802010z>.
- 623 [25] W.T. You, Z.L. Xu, Z.Q. Dong, M. Zhang, Vacuum membrane distillation–
624 crystallization process of high ammonium salt solutions, *Desalin. Water Treat.* 55 (2015)
625 368–380. <https://doi.org/10.1080/19443994.2014.922499>.
- 626 [26] J.C.W. Fern, S. Ohsaki, S. Watano, R. Pfeffer, Continuous synthesis of nano-drug
627 particles by antisolvent crystallization using a porous hollow-fiber membrane module,
628 *Int. J. Pharm.* 543 (2018) 139–150. <https://doi.org/10.1016/j.ijpharm.2018.03.025>.
- 629 [27] D. Chen, B. Wang, K.K. Sirkar, Hydrodynamic modeling of porous hollow fiber anti-
630 solvent crystallizer for continuous production of drug crystals, *J. Membr. Sci.* 556 (2018)
631 185–195. <https://doi.org/10.1016/j.memsci.2018.03.046>.
- 632 [28] X. Zhou, X. Zhu, B. Wang, J. Li, Q. Liu, X. Gao, K.K. Sirkar, D. Chen, Continuous

- 633 production of drug nanocrystals by porous hollow fiber-based anti-solvent
634 crystallization, *J. Membr. Sci.* 564 (2018) 682–690.
635 <https://doi.org/10.1016/j.memsci.2018.07.082>.
- 636 [29] L. Tuo, X. Ruan, W. Xiao, X. Li, G. He, X. Jiang, A novel hollow fiber membrane-
637 assisted antisolvent crystallization for enhanced mass transfer process control, *AIChE J.*
638 65 (2019) 734–744. <https://doi.org/10.1002/aic.16438>.
- 639 [30] X. Jiang, Y. Niu, S. Du, G. He, Membrane crystallization: Engineering the crystallization
640 via microscale interfacial technology, *Chem. Eng. Res. Des.* 178 (2022) 454–465.
641 <https://doi.org/10.1016/j.cherd.2021.12.042>.
- 642 [31] Z. Jia, Z. Liu, F. He, Synthesis of nanosized BaSO₄ and CaCO₃ particles with a
643 membrane reactor: Effects of additives on particles, *J. Colloid Interface Sci.* 266 (2003)
644 322–327. [https://doi.org/10.1016/S0021-9797\(03\)00187-5](https://doi.org/10.1016/S0021-9797(03)00187-5).
- 645 [32] Y. Yin, T. Li, K. Zuo, X. Liu, S. Lin, Y. Yao, T. Tong, Which Surface Is More Scaling
646 Resistant? A Closer Look at Nucleation Theories for Heterogeneous Gypsum Nucleation
647 in Aqueous Solutions, *Environ. Sci. Technol.* 56 (2022) 16315–16324.
648 <https://doi.org/10.1021/acs.est.2c06560>.
- 649 [33] A. Mersmann, Crystallization and precipitation, *Chem. Eng. Process. Process Intensif.*
650 38 (1999) 345–353. [https://doi.org/10.1016/S0255-2701\(99\)00025-2](https://doi.org/10.1016/S0255-2701(99)00025-2).
- 651 [34] C. Charcosset, H. Fessi, Preparation of nanoparticles with a membrane contactor, *J.*
652 *Membr. Sci.* 266 (2005) 115–120. <https://doi.org/10.1016/j.memsci.2005.05.016>.
- 653 [35] R. Kieffer, D. Mangin, F. Puel, C. Charcosset, Precipitation of barium sulphate in a
654 hollow fiber membrane contactor, Part I: Investigation of particulate fouling, *Chem. Eng.*

- 655 Sci. 64 (2009) 1759–1767. <https://doi.org/10.1016/j.ces.2009.01.011>.
- 656 [36] R. Jiménez-Robles, C. Gabaldón, J.D. Badia, M. Izquierdo, V. Martínez-Soria, Recovery
657 of dissolved methane through a flat sheet module with PDMS, PP, and PVDF
658 membranes, Sep. Purif. Technol. 282 (2022) 1–11.
659 <https://doi.org/10.1016/j.seppur.2021.120057>.
- 660 [37] R. Jiménez-Robles, B.M. Moreno-Torralbo, J.D. Badia, V. Martínez-Soria, M.
661 Izquierdo, Flat PVDF membrane with enhanced hydrophobicity through alkali activation
662 and organofluorosilanisation for dissolved methane recovery, Membranes (Basel). 12
663 (2022) 1–19. <https://doi.org/10.3390/membranes12040426>.
- 664 [38] R. Jiménez-Robles, M. Izquierdo, V. Martínez-Soria, L. Martí, A. Monleón, J.D. Badia,
665 Stability of Superhydrophobicity and Structure of PVDF Membranes Treated by
666 Vacuum Oxygen Plasma and Organofluorosilanisation, Membranes (Basel). 13 (2023).
667 <https://doi.org/10.3390/membranes13030314>.
- 668 [39] R.S. Hebbar, A.M. Isloor, A.F. Ismail, Contact Angle Measurements, in: Membr.
669 Charact., Elsevier, 2017: pp. 219–255. [https://doi.org/10.1016/B978-0-444-63776-](https://doi.org/10.1016/B978-0-444-63776-5.00012-7)
670 [5.00012-7](https://doi.org/10.1016/B978-0-444-63776-5.00012-7).
- 671 [40] L. Liu, F. Shen, X. Chen, J. Luo, Y. Su, H. Wu, Y. Wan, A novel plasma-induced surface
672 hydrophobization strategy for membrane distillation: Etching, dipping and grafting, J.
673 Membr. Sci. 499 (2016) 544–554. <https://doi.org/10.1016/j.memsci.2015.11.003>.
- 674 [41] R. Jiménez-Robles, V. Martínez-Soria, M. Izquierdo, Fouling characterisation in PVDF
675 membrane contactors for dissolved methane recovery from anaerobic effluents: effect of
676 surface organofluorosilanisation, Environ. Sci. Pollut. Res. 30 (2023) 29164–29179.
677 <https://doi.org/10.1007/s11356-022-24019-z>.

- 678 [42] A. Mersmann, M. Kind, Chemical engineering aspects of precipitation from solution,
679 Chem. Eng. Technol. 11 (1988) 264–276. <https://doi.org/10.1002/ceat.270110136>.
- 680 [43] G. Zeng, H. Li, S. Huang, X. Wang, J. Chen, Determination of Metastable Zone Width
681 and the Primary Nucleation Kinetics of Sodium Sulfate, Theor. Found. Chem. Eng. 49
682 (2015) 869–876. <https://doi.org/10.1134/S0040579515050309>.
- 683 [44] K. Sangwal, A novel self-consistent Nývlt-like equation for metastable zone width
684 determined by the polythermal method, Cryst. Res. Technol. 44 (2009) 231–247.
685 <https://doi.org/10.1002/crat.200800501>.
- 686 [45] Z. Jia, Z. Liu, Synthesis of nanosized BaSO₄ particles with a membrane reactor: effects
687 of operating parameters on particles, J. Membr. Sci. 209 (2002) 153–161.
688 [https://doi.org/10.1016/S0376-7388\(02\)00326-5](https://doi.org/10.1016/S0376-7388(02)00326-5).
- 689 [46] K.J. Kim, A. Mersmann, Estimation of metastable zone width in different nucleation
690 processes, Chem. Eng. Sci. 56 (2001) 2315–2324. [https://doi.org/10.1016/S0009-
691 2509\(00\)00450-4](https://doi.org/10.1016/S0009-2509(00)00450-4).
- 692 [47] T. Horseman, Y. Yin, K.S. Christie, Z. Wang, T. Tong, S. Lin, Wetting, Scaling, and
693 Fouling in Membrane Distillation: State-of-the-Art Insights on Fundamental
694 Mechanisms and Mitigation Strategies, ACS ES&T Eng. 1 (2021) 117–140.
695 <https://doi.org/10.1021/acsestengg.0c00025>.
- 696 [48] E. Curcio, E. Fontananova, G. Di Profio, E. Drioli, Influence of the structural properties
697 of poly(vinylidene fluoride) membranes on the heterogeneous nucleation rate of protein
698 crystals, J. Phys. Chem. B. 110 (2006) 12438–12445. <https://doi.org/10.1021/jp061531y>.
- 699 [49] A. McLeod, P. Buzatu, O. Autin, B. Jefferson, E. McAdam, Controlling shell-side crystal

700 nucleation in a gas-liquid membrane contactor for simultaneous ammonium bicarbonate
701 recovery and biogas upgrading, *J. Membr. Sci.* 473 (2015) 146–156.
702 <https://doi.org/10.1016/j.memsci.2014.07.063>.

703 [50] C.J. Davey, M. Hermassi, E. Allard, M. Amine, N. Sweet, T.S. Gaité, A. McLeod, E.J.
704 McAdam, Integrating crystallisation into transmembrane chemical absorption: Process
705 intensification for ammonia separation from anaerobic digestate, *J. Membr. Sci.* 611
706 (2020) 118236. <https://doi.org/10.1016/j.memsci.2020.118236>.

707 [51] A. Myerson, D. Erdemir, A. Lee, *Handbook of industrial crystallisation*, Third Ed.,
708 Cambridge University Press, 2019. <https://doi.org/10.1017/9781139026949>.

709 [52] M. Shen, Z. Lu, Y. Xu, X. He, Vivianite and Its Oxidation Products in Mammoth Ivory
710 and Their Implications to the Burial Process, *ACS Omega.* 6 (2021) 22284–22291.
711 <https://doi.org/10.1021/acsomega.1c02964>.

712

Supplementary Material for

Membrane-assisted reactive crystallisation for the recovery of dissolved phosphorous in vivianite form from liquid effluents

R. Jiménez-Robles^a, V. Martínez-Soria^a, M. Izquierdo^a, Lo-I Chen^b, K. Le Corre Pidou^b, E.J. McAdam^{b,*}

^aResearch Group in Materials Technology and Sustainability (MATS), Department of Chemical Engineering, School of Engineering, University of Valencia, Avda. Universitat s/n, 46100 Burjassot, Spain.

^bSchool of Water, Energy and Environment, Cranfield University, Bedfordshire, MK43 0AL, UK

*Corresponding author. e-mail: e.mcadam@cranfield.ac.uk

S1. Flat-sheet membrane module

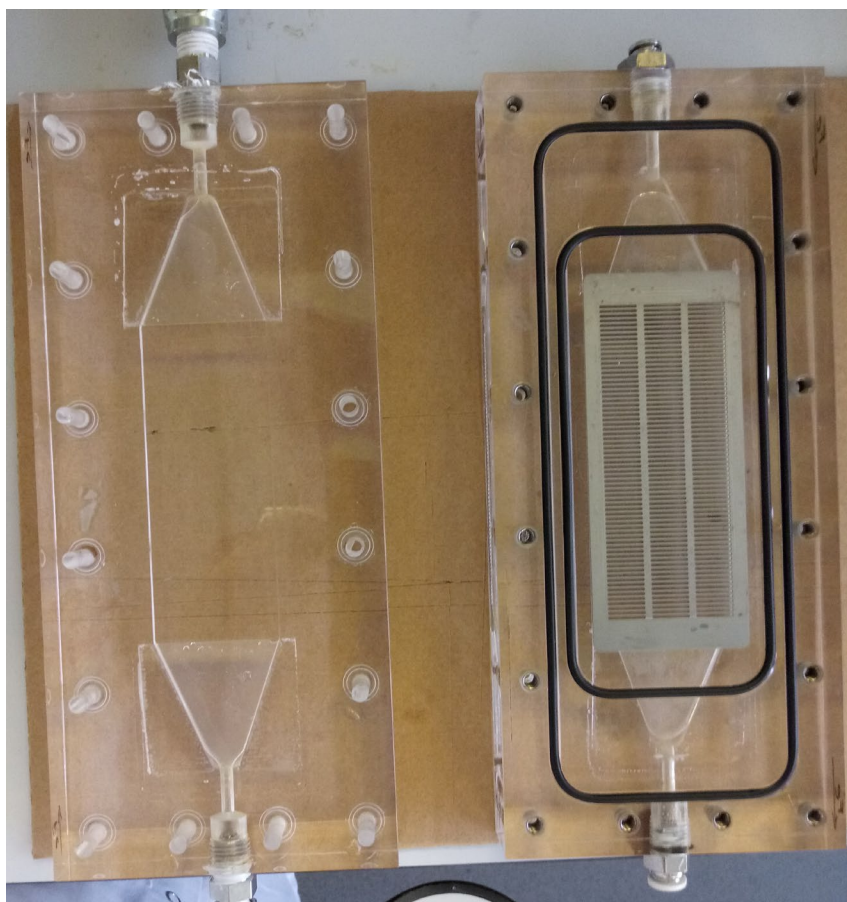


Figure S 1. Methacrylate flat-sheet membrane module used in the crystallisation tests.

S2. Overall mass balance of the components in the system

The estimation of the mean concentrations of the different components (phosphate, iron, sodium and chloride) present in the system with the time were calculated based on a mass balance applied in the overall system (Figure S 2). There was only one inlet in the system which corresponded with the dosed stream of the Fe^{2+} solution.

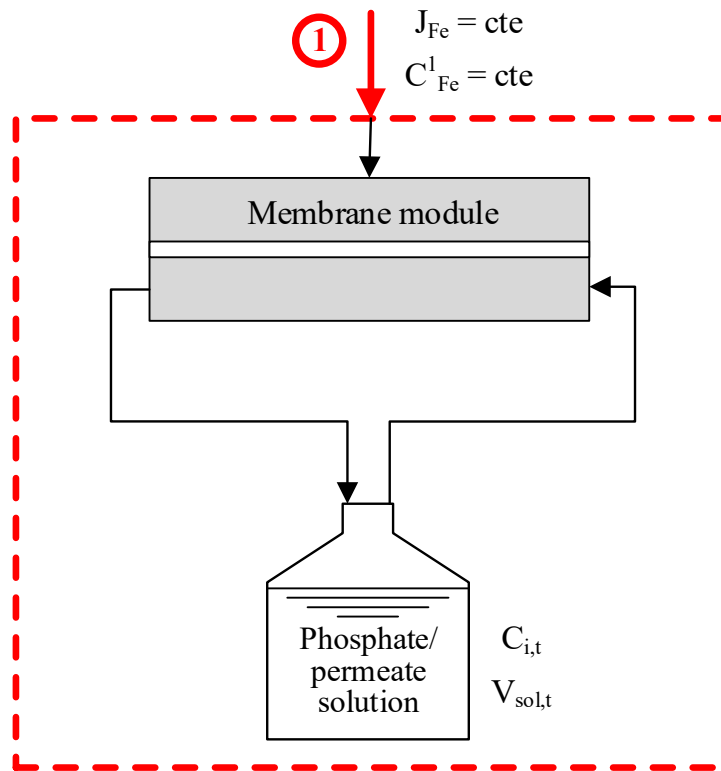


Figure S 2. Scheme of the mass balance applied in the overall system. Red dashed line denotes the limits for the mass balance. J_{Fe} : dosing rate of Fe^{2+} solution (mL min^{-1}); $C_{i,t}$: concentration of component i (M) at a time t minutes; $V_{\text{sol},t}$: liquid volume of the solution in the tank (mL) at a time t minutes; and superscript 1 denotes the inlet of the Fe^{2+} solution.

The mean concentrations of each component in the system was calculated as follows:

$$V_{\text{sol},t} = V_{\text{sol},0} + t \cdot J_{\text{Fe}} \quad (\text{S } 1)$$

$$C_{\text{PO}_4,t} = C_{\text{PO}_4,0} \cdot \frac{V_{\text{sol},0}}{V_{\text{sol},t}} \quad (\text{S } 2)$$

$$C_{\text{Fe},t} = \frac{C_{\text{Fe}}^1 \cdot t \cdot J_{\text{Fe}}}{V_{\text{sol},t}} \quad (\text{S } 3)$$

$$C_{\text{Na},t} = C_{\text{PO}_4,t} \quad (\text{S } 4)$$

$$C_{\text{Cl},t} = 2 \cdot C_{\text{Fe},t} \quad (\text{S } 5)$$

where $V_{\text{sol},0}$ and $V_{\text{sol},t}$ (mL) are the total volume of the solution inside the phosphate/permeate tank at the beginning of the tests ($t = 0$) and at a time t (min), J_{Fe} (mL min^{-1}) is the dosing rate of the Fe^{2+} solution, and $C_{i,0}$ and $C_{i,t}$ (M) are the mean concentrations of the component i in the system at the beginning of the tests ($t = 0$) and at a time t , with i being phosphate, iron, sodium and chloride. According with the results of the chemical speciation calculations from Visual MINTEQ software, the phosphate components inside the phosphate/permeate solution were mainly present in the form of HPO_4^{2-} , H_2PO_4^- , FeHPO_4 (aq), and $\text{FeH}_2\text{PO}_4^+$ (being HPO_4^{2-} , H_2PO_4^- the major species), the iron components in the form of Fe^{2+} , and FeHPO_4 (aq) (being Fe^{2+} the major specie), the sodium components in the form of Na^+ , and chloride components in form of Cl^- .

S3. Mass balance of the components inside the membrane module

The estimation of the mean concentrations of the different components (phosphate, iron, sodium and chloride) inside the permeate side of the flat sheet membrane module were calculated based on a mass balance applied in the membrane module (Figure S 3). There were two inlets in the considered system: the constant dosing of the Fe^{2+} solution, and the inlet of the phosphate/permeate solution into the membrane module, and one exit from the system which returned to the phosphate/permeate tank.

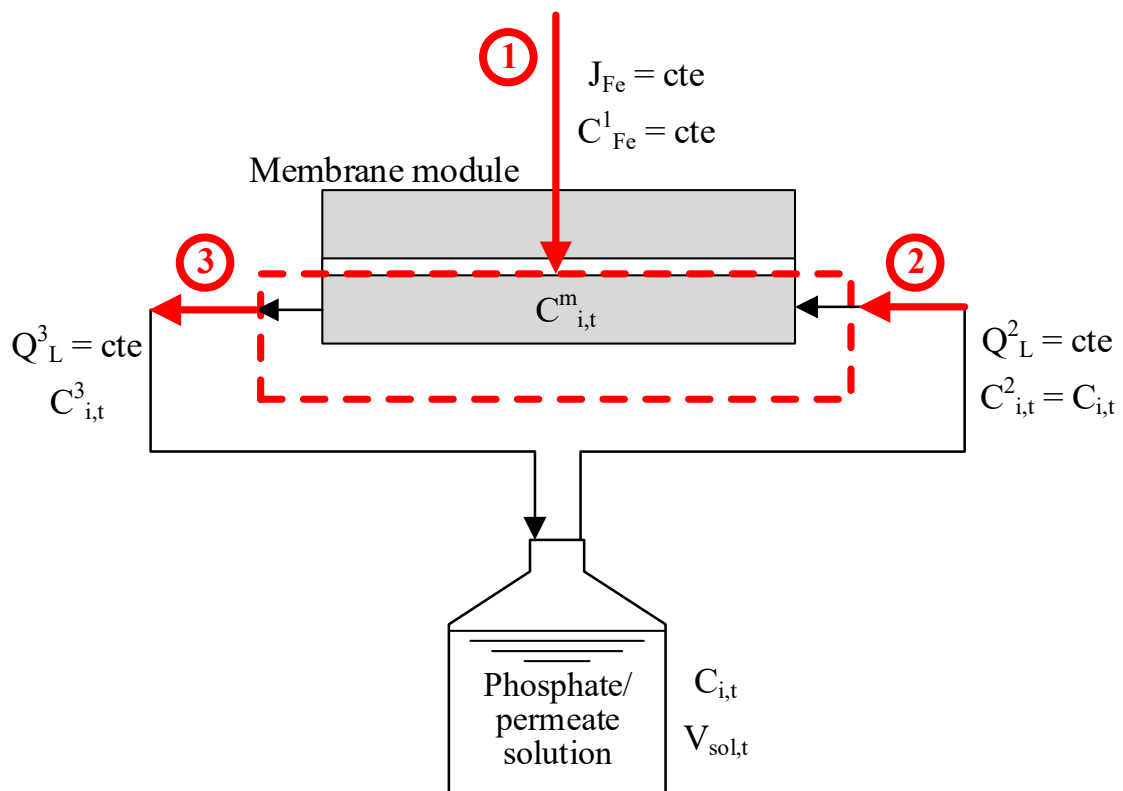


Figure S 3. Scheme of the mass balance applied in the permeate side of the membrane module. Red dashed line denotes the limits for the mass balance. J_{Fe} : dosing rate of Fe^{2+} solution (mL min^{-1}); $C_{i,t}$: concentration of component i (M) at a time t minutes; Q_L : liquid flow rate ($L h^{-1}$); $V_{\text{sol},t}$: liquid volume of the solution in the tank (mL) at a time t minutes; and superscript 1, 2, 3, and m denote the inlets 1 and 2, outlet 3 and the inside of the membrane module where the mass balance was applied.

The volume of the solution and concentration of each component i inside the phosphate/permeate tank at a time t ($V_{sol,t}$ and $C_{i,t}$, respectively) were determined using equations S1 – S5. The mean concentrations of the different components inside the membrane module ($C_{mi,t}$, M) were calculated as follows:

$$Q_L^3 = Q_L^2 + \frac{J_{Fe} \cdot 60}{1000} \quad (\text{S } 6)$$

$$C_{PO4,t}^3 = \frac{C_{PO4,t}^2 \cdot Q_L^2}{Q_L^3} \quad (\text{S } 7)$$

$$C_{Fe,t}^3 = \frac{C_{Fe,t}^2 \cdot Q_L^2 + \frac{J_{Fe} \cdot 60}{1000} \cdot C_{Fe}^1}{Q_L^3} \quad (\text{S } 8)$$

$$C_{Na,t}^3 = C_{PO4,t}^3 \quad (\text{S } 9)$$

$$C_{Cl,t}^3 = 2 \cdot C_{Fe,t}^3 \quad (\text{S } 10)$$

$$C_{i,t}^m = \frac{C_{i,t}^2 + C_{i,t}^3}{2} \quad (\text{S } 11)$$

where Q_L ($L h^{-1}$) is the liquid flow rate, and the superscripts 1, 2, 3, and m denote the point corresponding to the inlet of the Fe^{2+} solution dosing, the inlet of the permeate side, the outlet of the permeate side and the inside of the membrane module.

In addition, the mean concentration of vivianite inside the membrane module with the time of operation t ($C_{viv,t}^m$, M) was estimated assuming a complete reaction between Fe^{2+} and PO_4^{3-} towards vivianite and no secondary reactions:

$$C_{viv,t}^m = \frac{C_{Fe,t}^m}{3} \quad (\text{S } 12)$$

S4. Evolution of the scaling on membrane during crystallisation tests

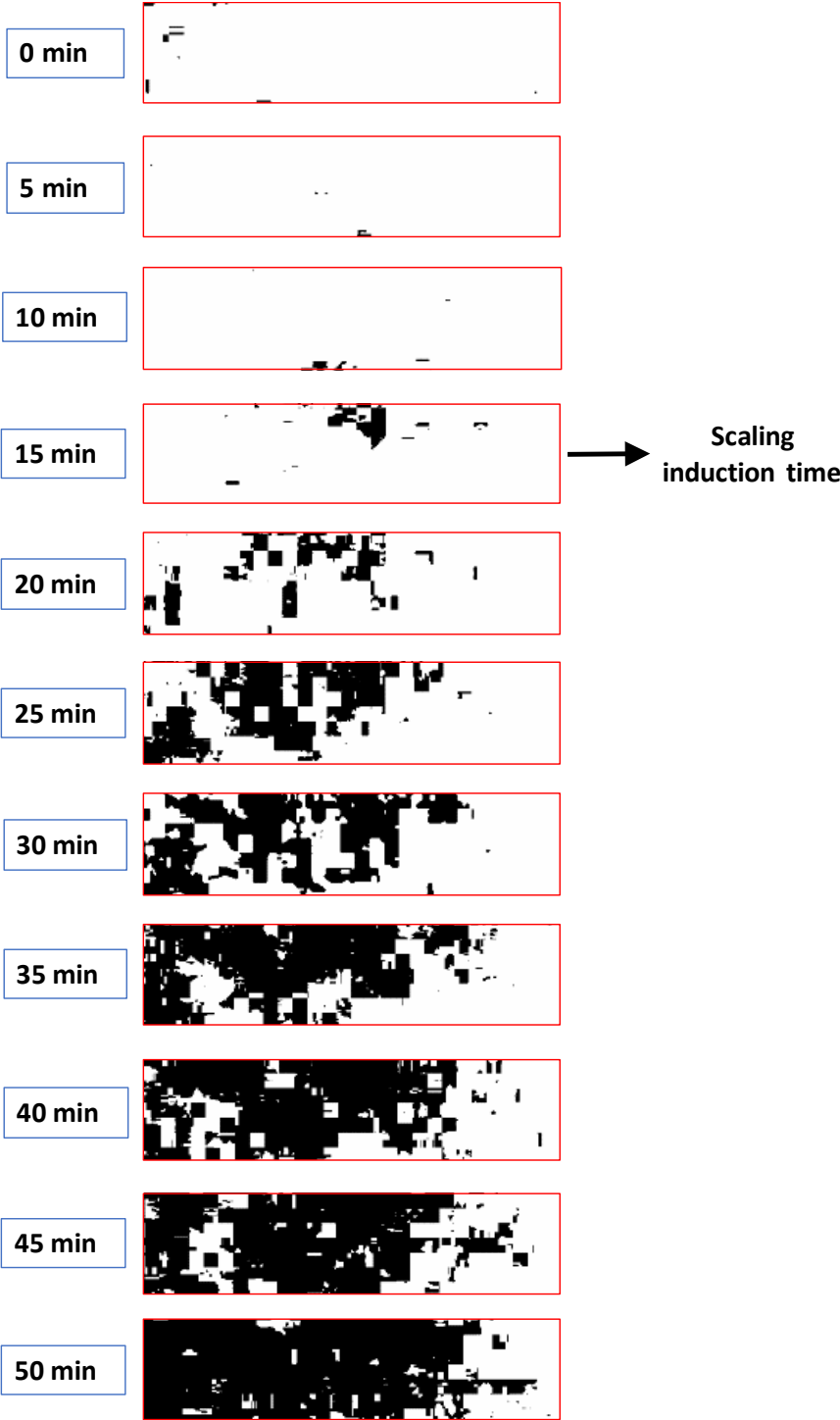


Figure S 4. Representative example of the scaling evolution on a PVDF-St membrane during a crystallisation test conducted at a Reynold of 105. White area represents the membrane surface and black area represents the surface covered by solid particles.

S5. Preferential heterogeneous nucleation on a porous membrane

The probability for preferential heterogeneous nucleation aided by a solid surface has been estimated in the literature based on the relation between the Gibbs free energy of the primary heterogeneous and homogeneous nucleation (ΔG_{het} and ΔG_{hom} , respectively). This relation can be described with the following model [1,2]:

$$\frac{\Delta G_{\text{het}}}{\Delta G_{\text{hom}}} = 0.25(2 + \cos \theta)(1 - \cos \theta)^2 \left[1 - \epsilon \frac{(1 + \cos \theta)^2}{(1 - \cos \theta)^2} \right]^3 \quad (\text{S } 13)$$

where θ is the contact angle of a nucleus on the substrate [3] and ϵ is the fractional porosity of the membrane ($\epsilon = \varepsilon / 100$). This model has been widely accepted in the literature for different membrane crystallisation systems to determine the influence of the membrane surface in promoting heterogeneous primary nucleation [1,4–6]. The model infers that heterogeneous nucleation tends to increase as porosity increases. Therefore, porosity can contribute to improved micromixing and the reduction in the energy barrier for nucleation. The energy barrier tends to decrease as WCA rises at a constant membrane porosity [4,5], thereby reducing the bulk induction time [4]. From data of this work as an example, the non-modified PVDF-Ds (WCA = $103 \pm 2^\circ$) presented a higher induction time than the hydrophobized Fun_PVDF-Ds (Figure 5a in main paper) with a higher WCA ($144 \pm 2^\circ$) and a similar porosity ($\sim 60\%$), indicating that Fun_PVDF-Ds promotes the vivianite crystallisation rather than PVDF-Ds. However, the bulk induction time obtained with the hydrophilised Act_PVDF-Ds (WCA = $87 \pm 3^\circ$) was similar to that obtained with PVDF-Ds. Furthermore, PTFE-1 and PTFE-3 with similar WCA ($\sim 148^\circ$) and porosities ($\sim 90\%$) presented different induction times. While instructive for membrane design, the model cannot provide a unified perspective on the probability for heterogeneous nucleation on porous surfaces. This may be due to competing

factors in material design, that can similarly modify Gibbs free energy requirement for nucleation through competing mechanisms (e.g. solute entrapment) [7].

S6. Solid particles collected at the end of the crystallisation tests



Figure S 5. Representative example of the collected solid particles onto the 0.025 μm filter at the end of the crystallisation tests.

References

- [1] E. Curcio, E. Fontananova, G. Di Profio, E. Drioli, Influence of the structural properties of poly(vinylidene fluoride) membranes on the heterogeneous nucleation rate of protein crystals, *J. Phys. Chem. B.* 110 (2006) 12438–12445. <https://doi.org/10.1021/jp061531y>.
- [2] G. Di Profio, E. Curcio, E. Drioli, Supersaturation control and heterogeneous nucleation in membrane crystallizers: Facts and perspectives, *Ind. Eng. Chem. Res.* 49 (2010) 11878–11889. <https://doi.org/10.1021/ie100418z>.
- [3] T. Horseman, Y. Yin, K.S. Christie, Z. Wang, T. Tong, S. Lin, Wetting, Scaling, and Fouling in Membrane Distillation: State-of-the-Art Insights on Fundamental Mechanisms and Mitigation Strategies, *ACS ES&T Eng.* 1 (2021) 117–140. <https://doi.org/10.1021/acsestengg.0c00025>.
- [4] S. Bavarella, M. Hermassi, A. Brookes, A. Moore, P. Vale, G. Di Profio, E. Curcio, P. Hart, M. Pidou, E.J. McAdam, Is Chemically Reactive Membrane Crystallization Facilitated by Heterogeneous Primary Nucleation? Comparison with Conventional Gas-Liquid Crystallization for Ammonium Bicarbonate Precipitation in a CO₂-NH₃-H₂O System, *Cryst. Growth Des.* 20 (2020) 1552–1564. <https://doi.org/10.1021/acs.cgd.9b01276>.
- [5] A. McLeod, P. Buzatu, O. Autin, B. Jefferson, E. McAdam, Controlling shell-side crystal nucleation in a gas-liquid membrane contactor for simultaneous ammonium bicarbonate recovery and biogas upgrading, *J. Membr. Sci.* 473 (2015) 146–156. <https://doi.org/10.1016/j.memsci.2014.07.063>.
- [6] C.J. Davey, M. Hermassi, E. Allard, M. Amine, N. Sweet, T.S. Gaité, A. McLeod, E.J. McAdam, Integrating crystallisation into transmembrane chemical absorption: Process intensification for ammonia separation from anaerobic digestate, *J. Membr. Sci.* 611 (2020) 118236. <https://doi.org/10.1016/j.memsci.2020.118236>.
- [7] E. Chabanon, D. Mangin, C. Charcosset, Membranes and crystallization processes: State of the art and prospects, *J. Membr. Sci.* 509 (2016) 57–67. <https://doi.org/10.1016/j.memsci.2016.02.051>.

